Smart Sensors, Measurement and Instrumentation 15

Subhas Chandra Mukhopadhyay *Editor*

Wearable Electronics Sensors

For Safe and Healthy Living

Springer

Smart Sensors, Measurement and Instrumentation

Volume 15

Series editor

Subhas Chandra Mukhopadhyay
School of Engineering and Advanced Technology (SEAT)
Massey University (Manawatu)
Palmerston North
New Zealand
E-mail: S.C.Mukhopadhyay@massey.ac.nz

More information about this series at http://www.springer.com/series/10617

Subhas Chandra Mukhopadhyay
Editor

Wearable Electronics Sensors

For Safe and Healthy Living

Springer

Editor

Subhas Chandra Mukhopadhyay
Massey University (Manawatu)
Palmerston North
New Zealand

ISSN 2194-8402 ISSN 2194-8410 (electronic)
Smart Sensors, Measurement and Instrumentation
ISBN 978-3-319-18190-5 ISBN 978-3-319-18191-2 (eBook)
DOI 10.1007/978-3-319-18191-2

Library of Congress Control Number: 2015937733

Springer Cham Heidelberg New York Dordrecht London

Printed on acid-free paper

Springer International Publishing AG Switzerland is part of Springer Science+Business Media (www.springer.com)

Editorial

The increase in world population along with a significant ageing portion forces rapid rise in healthcare cost. The healthcare system is going through a transformation in which continuous monitoring of inhabitant is possible even without hospitalization. The advancement of sensing technology, embedded system, wireless communication technology, nano-technology, and miniaturization make it possible to develop smart wireless electronic systems to monitor activities of human beings continuously. The developed wearable sensors monitor physiological parameters along with other symptoms to decide whether any abnormal and/or unforeseen situation happened. The necessary help can be provided at the time of dire need. The physical and physiological activity monitoring of human based on wearable sensors are extremely important to provide necessary help before any unforeseen accidents happened as well as can predict the immediate future of the individual in terms of health condition.

This Special Issue titled "Wearable Electronics Sensors: for safe and healthy living" in the book series of "Smart Sensors, Measurement and Instrumentation" contains the invited papers from renowned experts working in the field. A total of 14 chapters have described the advancement in the area of Wearable Sensors, Wireless Sensors and Sensor Networks, Protocols, Topologies, Instrumentation architectures, Measurement techniques, Energy harvesting and scavenging, Signal processing, Design and Prototyping in recent times.

The first chapter by A. Nag and S. C. Mukhopadhyay has described the overview of the current and past means of wearable sensors with its associated protocols used for communication. It concludes with the ways the currently dealt wearable sensors can be improved in future. In Chapter 2, W. Xu and M. C. Huang has presented a concept of Total Health is which transforms the healthcare with an aims for complete 24/7 coverage. The challenges that come with bringing technology into widespread use have been discussed.

The design of a novel biometric algorithm which based on biometric feature Electrocardiogram (ECG) and Data Authentication Function (DAF) for the security of Body Sensor Network instead of utilizing traditional key generation procedure has been presented in chapter 3 by S. Pirbhulal, H. Zhang, W. Wu and Y.T. Zhang.

Wearable health monitoring systems face a number of hurdles to become a reality. The enabling processors and architectures demand a large amount of energy, requiring sizable batteries. In chapter 4, H. Ghasemzadeh and R. Jafari have discussed a granular decision making architectures for physical movement monitoring applications. Such modules can be viewed as tiered wake up circuitries. The signal processing based decision making, in combination with a low-power microcontroller, allows for significant power saving through an ultra-low-power processing architecture.

Falls are the single largest cause of injury for elderly people. Falls may lead to several major health problems for the elderly and immediate help need to be provided to reduce the risk of complications. An interrupt-driven fall detection algorithm has been proposed and implemented by J. Yuan and K.K. Tan in chapter 5 which consumes much less power because Wearable Devices (WD) only process upon hardware and timer interrupts, and stay in sleep mode to conserve power the rest of time. Since WDs do not stream massive data wirelessly, this algorithm also saves tremendous transmission power and network bandwidth.

Widespread adoption of smartphone based medical apps is opening new avenues for innovation, bringing mobile medical applications (MMAs) to the forefront of low cost healthcare delivery. The chapter 6 by P. Bagade, A. Banerjee and S. K. S. Gupta have focused on a novel app development methodology, where trustworthiness of a MMA can be objectively evaluated by generating evidences using automatic techniques.

K. Takei in chapter 7 has introduced a flexible and wearable healthcare devices with an emphasis on inorganic nanomaterials and printing techniques to be realized for medical purposes and even predict illness prior to the onset of symptoms. A resistive, fabric-based temperature sensor that can determine temperature between 25°C and 45°C by monitoring variations in the material's electrical resistance suitable for wearable devices has been presented by N. J. Blasdel and C. N. Monty in chapter 8. The chapter 9 by M. Farooq and E. Sazonov has discussed use of strain sensors in wearable devices. Strain sensors have been used to monitor deformation under applied load. Special focus has been placed on textile based and inkjet-printed strain sensors.

M. A. F. Pimentel, P. H. Charlton, and D. A. Clifton have described a novel technique for measuring Respiration rate (RR) using waveform data acquired from wearable sensors in chapter 10. The technique derives RR from a physiological signal which is routinely acquired by many mobile sensors: the photoplethysmogram (PPG). The goal of this method is to improve upon existing methods, which simply report RR values without probabilistic estimation, and which therefore suffer the lack of robustness that prevents their use in clinical practice.

The chapter 11 by C. Occhiuzzi, C. Vallese, S. Amendola, S. Manzari and G. Marrocco described a fully passive RFID Ambient Intelligence platform, hereafter denoted as NIGHTcare, for monitoring people during the night. Battery-less tags are integrated into clothes and dispersed in the environment. A long-range UHF RFID reader illuminates the scene and the collected tags' responses, arising from the interaction between the subject and surrounding environment, are real-time

processed. The goal is detecting the presence or the absence of the user in the bed, his jerky movements and his motion patterns, accidental falls, persisting absence from the bed and prolonged periods of inactivity as well as his instantaneous sleeping posture.

G. Li, T. Liu, and Y. Inoue have used six-axial force sensors and inertial sensors together to construct a wireless wearable sensor system for the successive and non-laboratory measurement of gait as reported in chapter 12. The system consists of the wearable sensor shoes and motion sensors. The experiment results showed that the wearable system is able to measure the ground reaction force (GRF), joint angles, joint forces and joint moments.

In chapter 13, K. Odame and V. Hanson have explored the feasibility of controlling a hearing aid with a brain-computer interface (BCI) that is based on auditory-evoked electroencephalography (EEG) responses to an open set of natural auditory stimuli. To address practical concerns about the size and latency of the BCI, the performance implications of using single-channel EEG, semi-dry electrodes and single trial detection of the EEG signal have been examined.

The last chapter by Y. Lin and D. Schmidt talked about wearable sensors to collect biological feedback. Biological feedback from an interacting human can be useful for robots during human interaction. The feedback can be used to increase the effectiveness and safety of a robot's actions during interaction, which in turn will make humans more comfortable with the interaction. The chapter has discussed varying types of interaction under development, and show how feedback from wearable sensors could greatly increase robot performance.

I do sincerely hope that the readers will find this special issue interesting and useful in their research as well as in practical engineering work in the area of wearable sensing technology. We are very happy to be able to offer the readers such a diverse special issue, both in terms of its topical coverage and geographic representation.

Finally, we would like to whole-heartedly thank all the authors for their contribution to this special issue.

Subhas Chandra Mukhopadhyay
School of Engineering and Advanced Technology (SEAT),
Massey University (Turitea Campus)
Palmerston North, New Zealand
S.C.Mukhopadhyay@massey.ac.nz

Contents

A Short Biography of Subhas Mukhopadhyay

Dr. Subhas Chandra Mukhopadhyay (M'97, SM'02, F'11) graduated from the Department of Electrical Engineering, Jadavpur University, Calcutta, India with a **Gold medal** and received the Master of Electrical Engineering degree from **Indian Institute of Science**, Bangalore, India. He has **PhD (Eng.)** degree from Jadavpur University, India and **Doctor of Engineering** degree from Kanazawa University, Japan.

Currently he is working as a **Professor of Sensing Technology** with the School of Engineering and Advanced Technology, Massey University, Palmerston North, New Zealand. He has over 25 years of teaching and research experiences.

His fields of interest include Sensors and Sensing Technology, Instrumentation, Wireless sensor networks, Electromagnetics, control, electrical machines and numerical field calculation etc.

He has authored/co-authored four books and over **300** papers in different international journals, conferences and book chapter. He has edited **twelve** conference proceedings. He has also edited **Eleven** special issues of international journals as lead guest editor and **nineteen** books out of which **seventeen** are with Springer-Verlag. He has delivered **229** seminars as keynote, invited, tutorial and special lectures in **24** countries.

He was awarded numerous awards throughout his career and attracted over NZ $4.1 M on different research projects.

He is a **Fellow** of IEEE (USA), a **Fellow** of IET (UK) and a **Fellow** of IETE (India). He is a **Topical Editor** of IEEE Sensors journal, an **Associate Editor** of IEEE Transactions on Instrumentation and Measurements and a **Technical Editor** of IEEE Transactions on Mechatronics. He is the co-Editor-in-chief of the International Journal on Smart Sensing and Intelligent Systems (www.s2is.org). He was the Technical Programme Chair of ICARA 2004, ICARA 2006 and ICARA 2009. He was the General chair/co-chair of ICST 2005, ICST 2007, IEEE ROSE 2007, IEEE EPSA 2008, ICST 2008, IEEE Sensors 2008, ICST 2010, IEEE Sensors 2010, ICST 2011, ICST 2012, ICST 2013 and ICST 2014. He has organized the IEEE Sensors conference 2009 at Christchurch, New Zealand during October 25 to 28, 2009 as General Chair. He is planning to organize the Ninth ICST in Auckland, New Zealand during December 8 to 10, 2015.

He was a Distinguished Lecturer of IEEE Sensors council from 2010 to 2013. He is the Founding and Ex**-Chair** of the IEEE Instrumentation and Measurement Society New Zealand Chapter. He chairs the IEEE IMS Technical Committee 18 on Environmental Measurements.

Wearable Electronics Sensors: Current Status and Future Opportunities

Anindya Nag and Subhas Chandra Mukhopadhyay

Massey University,
Palmerston North, New Zealand

Abstract. The technological advancement in the past three decades has impacted our lives and wellbeing significantly. Different aspects of monitoring our physiological parameters are considered. Wearable sensors are one of its most important areas that have an ongoing trend and have a huge tendency to rise in the future. The wearable sensors are the externally used devices attached to any individual to measure physiological parameters of interest. The range of wearable sensors varies from minuscule to large scaled devices physically fitted to the user operating on wired or wireless terms. Many common diseases affecting large number of people notably gait abnormalities, Parkinson's disease are analysed by the wearable sensors. The use of wearable sensors has got a better prospect with improved technical qualities and a better understanding of the currently used research methodologies. This chapter deals with the overview of the current and past means of wearable sensors with its associated protocols used for communication. It concludes with the ways the currently dealt wearable sensors can be improved in future.

1 Introduction

The betterment in the field of medical science has its adverse effect on the abhorrent increase in population in the last five decades. As per the ongoing trend, the current population is likely to reach 10 billion by next three decades [1]. This massive growth also tends to increase the people above the age of 65 double its present value [2]. To have a better treatment facility other than hospitable conditions, elderly people are looking for better options with certain prominent protocols. The smart homes, since its development, have always been a better choice for the monitoring of people of all ages. The research goes on ways to give a better life for the people who are incapable of doing day-to-day activities of their own. The smart homes are being used for monitoring the behavioural pattern and activities people for more than ten years. But there are some clauses that are followed by the people operating these automated homes, like 1. Use of video cameras intrude the privacy of the people living in these homes are avoided. 2. Minimum use of technological hardware to decrease the complexity of the overall

S.C. Mukhopadhyay (ed.), *Wearable Electronics Sensors*,
Smart Sensors, Measurement and Instrumentation 15, DOI: 10.1007/978-3-319-18191-2_1

system. 3. Maximizing the security of data regarding any individual. Different types of sensors are used in these homes to monitoring various activities in these homes. Wearable sensors are one of the externally close fitted sensors to an individual monitoring the activities of the connected person. The wearable sensors are operated in both wired and wireless manner. A single wearable sensor is used to measure more than one physiological parameter, for example, the wrist watch [3-5] measures the heart rate, blood pressure, body temperature [6] of the individual wearing it. Research works have also been done on the individualistic measurements of parameters of gait analysis [7-19], blood pressure [20, 21], respiration rate [22-25] at different intervals, heart beat [26-31], human posture [32], cigarette smoking [33], etc. One of the primary objectives of using these wearable sensors is to minimize the disturbance faced by the person being operated on. Some of the sensors are used in proximity like for measuring sweat [34-36], and some are worn on the hands or other body parts of the user [37-44]. Human activity recognition [45-47] is another aspect on which considerable work is done. Different wireless technologies are acquired to work along with these sensors for the real-time data collection.

2 Motivation

The amount of population in New Zealand grew from around 800,000 to 4,000,000 in the last century [2]. The number of people above the age of 65 is likely to increase to 230,000 in the next decade. So the need of smart homes is likely to increase in the future. The elderly people have a tendency to live independently or in their homes. They do not prefer to be monitored in every step or visualized doing any activity. Therefore, the smart homes are built on the residing home of the people so that they do not face a change in ambiance. The smart homes designed for the elderly people are customized to make sure that the caregiver is in a continuous touch with the people living in these homes so that any abnormality in the house can be notified. Different kind of alarm systems is installed in the smart homes to take immediate action. The sensors used in the smart homes can be categorized into wearable and non-wearable. Fig. 1 represents the estimated change of the elderly population for 100 years. The non-wearable sensors are the ones mainly used for the detection of usage of different electrical objects [48] or the position of the individuals residing in the house [45-47]. They are also used to keep a note of the ambient conditions of the people living in. The wearable sensors are attached to the clothes, accessories or bare body of the individual for the measurement of individualistic parameters.

Wearable sensors are in more need in future because they have a few distinct advantages over the non-wearable ones like 1.They can be placed dynamically and moved according to the need. 2. They can be turned on only when the measurement is to be taken. 3. They can be designed according to different parameters to be measured. 4. They are designed to be smaller in size in order to fit comfortably causing minimum disturbance to the person under consideration. So the increase in wearable sensors would help to detect number of measured parameters, as well as the actual physiological conditions of the person being monitored on real-time.

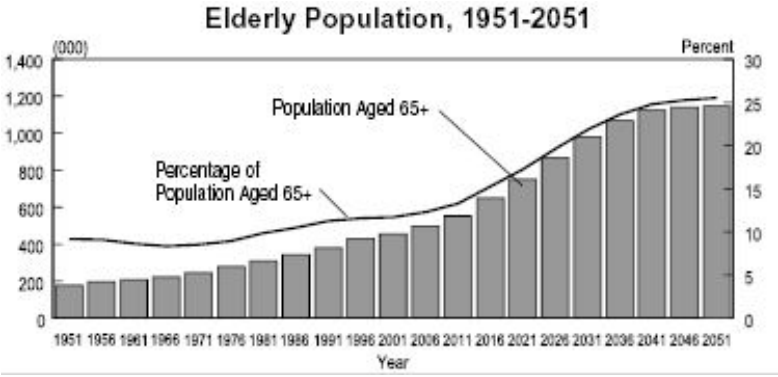

Fig. 1 Estimated change in population in 100 years [49]

3 Physiological Conditions That Are Measured by Wearable Sensors

With the current lifestyle, a person tends to face from number of problems in his/her body which needs attention. It is tough to experience the hospital conditions every time a person suffers from a minor or major disease. So, it is recommended to scrutinize every physiological parameter possible as soon as possible. Some of the typical physiological parameters need to be monitored on a regular basis are:

1. Body temperature – The temperature of a human body is one of the vital parameters to know the condition of a person. A normal body temperature ranges between 35^0C to 38^0C. Any aberration from this range indicates the abnormality of the person. In many cases, high rise of temperature causes death. Analogue or digital thermometers are used for the measurement of temperature. But they are only used when the patient is in need. Any deflection from the ideal temperature of a human body proves the person is already affected. In older persons, the temperature of the body tends to decrease with the typically defined temperature. This is due to the incapability of the body to control the temperature. This may increase (hyperthermia) or may decrease (hypothermia) the temperature of the body from a normalized temperature. So, in order to avoid any critical condition, it is better to use a temperature sensor to keep a note of the temperature at regular intervals. Now, there are various types of temperature sensors with different ranges [50]. Many of them have been used for the temperature monitoring of the rooms the elderly people reside in. The temperature sensors to be used for body temperature measurement need not be of higher range. It may not have to vary more than 20^0C, the field to be lying from 30^0C to 50^0C. The temperature sensors are constructed along with other measurement parameters in a complete wearable sensor. Only in few cases, the

temperature sensor, used as a wearable sensor is extensively classified for body temperature variation.

2. Heart rate- The heart rate (HR) is unarguably the most pivotal variable that matters in a human body. This needs to be working in perfect condition every time for the well-being of a person. The heart is responsible for pumping blood to all the parts of the body, so any change in the HR will also change the blood pressure and other parameters of the body. In earlier days, the HR is calculated by the auscultation process by a stethoscope, but that is manual which makes it prone to error and takes a long of time for the calculation of healthy number of patients. The HR of a healthy person is 72 times per minute. But the frequency of HR of any individual tends to change from that of a healthy value depending on activities and physiological state. As the age of an individual increases, the person experiences more abiotic pollution that degrades the condition of an individual's heart. The measurement for the HR of these affected people with an infection has been reported [27]. With the change in the heart beat rate, many kinds of cardiovascular diseases happen. Extensive work has been done on the monitoring of the HR of an elderly person [26-31]. The wearable sensors are connected to the person's chest to measure and analyse the HR of an individual. Like body temperature measurement, the HR of an individual is also calculated along with other parameters with different devices like accelerometers [26] connected to the human body. The measurement of HR is done in both wired [28] [30] and wireless way [26] where in later part, the nodes are connected to the chest and signals are wirelessly collected to a receiver connected to a computer.
3. Respiration rate- The respiration rate (RR) of a human being is the foremost external sign to verify if a person is healthy or not. The RR of a person at all ages tends to be constant. However, the elderly people sometimes find it difficult to breathe normally. Internal structures of lungs and breathing system changes in as the age progresses, causing it difficult for an elderly person to breathe. The rate of extraction and contraction of the lungs decreases that leads to forcible breathing of the individual. The extensive research works [22-25] have been done by monitoring the RR. It is favourable to use wearable sensors for continuous monitoring [22] of the respiration rate of a person. Miniaturized battery-operated devices [25] are used for the detection of rate of respiration. But it would be favourable to have a system of RR detection which can be operated wirelessly. This is because the connection of the wearable sensor wired into the monitoring system will cause uneasiness to the person and, as a result, change the rate of respiration.
4. Blood pressure- The blood pressure (BP) of a person signifies what the arterial pressure of the blood at which it is circulating in the body. The increase (hypertension) or decrease (hypotension) of BP in the body malfunction the system of the body. The real reason for the change in BP is still under research, but some of the causes might be stress, and overweight. Increase in BP leads to other problems especially in the heart. The change in BP is not very detrimental till the age of 45 for both men and women and then

gradually tends to become more prominent. The BP of a healthy person is said to be 120/80 [51, 52] where, the systole is 120, and the diastole is 80. Anything above 140/90 or below 120/80 is a matter of concern and should be checked. A number of work [20, 21] has been done on the monitoring of BP of a person. The wearable sensors are used; similar to the measurement of HR are connected to the body of the individual being monitored.

5. Gait Analysis- Gait analysis, even though is not ancient research has come up to the limelight in the past fifteen years [7-9] [11, 12] [19]. The gait and proper balance of an elderly person is one of the main consequences of being healthy. The problems are associated with a decreased speed of walking, abnormal walking stances leading to strokes and falls. Abnormality in gait is the primary reason for falls. One of the concerns regarding falling is that it will result in recurrent falls. The change in the gait posture among the elderly people also causes other associated problems like bend standing position, taking too much time to walk to reach a destination or standing on two feet. There could be many reasons for gait problems like cardiovascular diseases and psychiatric conditions. The cardiovascular diseases include fear of falling and sleeping disorders for the elderly people, and the cardiovascular diseases include arterial disease or congestive heart failure. Another reason for declining might be due to irregular habits and obesity. Due to the modernization of the technical world, the amount of physical activity has decreased in a substantial quantity. This has led to an increase in the cases of gait abnormalities. The amount of research work [7-19] for gait analysis is done on a significant number and is likely to increase in the future. Using wearable sensors for gait analysis is one beneficial way to make sure that the gait posture is nearly normalized. The elderly person wearing wearable sensor and walking might lead to the person walking in a slower pace but will decrease the chances of falling. The person would be under continuous monitoring while walking or standing.
6. Spinal posture- The spinal cord is the central platform on which human body rests. As the age increases, the bones of a person's body tend to become weaker. This leads to loss of weight and the change in the posture of an individual. The position of a person decides the way he/she stands, sits or walks. When the structured bones of the spinal cord called vertebrae tend to lose the fluid present in the inner spatial region of two bones, the structure tends to contract, and the overall shape becomes small. As a result of this, the overall height of the person decreases a bit. This causes a stooped like posture of the individual while standing or walking. The person tends to be more bent while standing or walking. The legs become weak and tend to experience more falls. The wearable sensor should be used to determine the degree of change of spinal posture of the person. Research work has been done on the determination of spinal posture [53] by integrating the sensor with the garment. But the person does not have to keep wearing the sensor on a continuous matter as the spinal cord posture would not change very rapidly. The testing of the position of the elderly person can be done once in a week or

two. In this manner, the wearable sensor would not have to put on all the time for its monitoring. A person, in general, will not be willing to put on a sensor fitted garment. So, particular clothing can be made with sensor fitted to it, but to be used on a weekly basis.

7. Sweat rate- The sweat is related to the physical activities of a person as well as the ambient conditions. When a person does rigorous exercise, too much of glucose content comes out his body in the form of sweat. Glucose is the primary energy source for human beings. The content of glucose is sugar that is a monosaccharide that is broken down in the body to provide energy. When any activity involves physical exhaustion, sweat comes out of the body. For example, when the athletes participate in any running activity, too much sweat comes out of the body. Now, in typical cases, the sweat does not come out when a person is not doing any activity. So, it preferable to use a wearable sensor to monitor the sweat rate of an individual when any activity, for example, jogging or cycling is done. A considerable amount of research work [34-36] has been regarding the monitoring of sweat rate has been done in the recent years. But if any wearable sensor is used, for example, like the one used detection of heart rate of respiration rate, the sensor, not being used separately can be integrated with the clothing that will be located in the close proximity to the skin or attached to any part of the body to determine the sweat rate during any physical activity.
8. Parkinson Disease- One of the common diseases in today's day world affecting over five million [8] people worldwide is Parkinson disease. These conditions are mostly seen in elderly persons with above over 60 years. The main reason for this disease is not entirely known yet but anatomically, the formation of proteins is caused in specified regions called 'Lewy bodies' [54]. These structures are formed in brains leading to abnormality. The elderly people face this disease with a small of young people affected by it. Some of the symptoms caused by this illness can be tremors to a part and gradually to the whole body, loss of willingness to show emotions, inability to maintain balance of the body. The cure for this disease is not known yet because of the lack of knowledge of the actual symptoms, but the initial stages can be treated with medications. Now, CT scans can be done by the doctors to detect the formation of protein bodies in the brain, but by that time, the disease would already have affected the body in a substantial amount. A considerable quantity of research work [55-57] regarding analysis of tremor of Parkinson's disease has done with the help of Markov's models. The wearable sensors have been used and the level of tremor has been analyzed. The wearable sensor in this disease would play a vital role as the checking of this neural disease in initial stages could prevent future worse symptoms.

9. Arm and limb motion- The degree of ease of movement of arm and legs of an elderly person decreases as the reflex of the muscles reduces. As the age progresses, the fat storing capability of the body reduces. So, due to decrease in fat content, the muscles contract and as a result of which, the inner spatial

gap between the bones reduces. So, any sudden jerk in the hand or leg can cause the bone to break. The elderly people find it very difficult to move their arms to do any physical activity. The joint between the two bones also becomes stiff as it loses the fluid between them. One of the ways to increase the flexibility of the arms and limbs is to do exercise, but still the possibility of the reduction in motion remains in a large percentage. Fig. 2 shows a wrist sensor used for detection of arm motion. The wearable sensors can be used here to note the degree of movement of arms and perform continuous monitoring to determine the change in movement gradually. One of the other benefits of continuous monitoring would help to develop the movement of the arms and limbs after a fall. Work regarding the arm and limb movement [59-62] has been done involving wearable sensors. Modelling concerning the movement of upper limb motion and accelerometer is used for the analysis of the arm motion. The wearable sensors might be well knitted to the garments worn everyday to know the ease at which the person can movement the operated part and can act accordingly in case of any anomaly. Fig. 3 depicts a wearable sensor on a patient's leg to detect the movements.

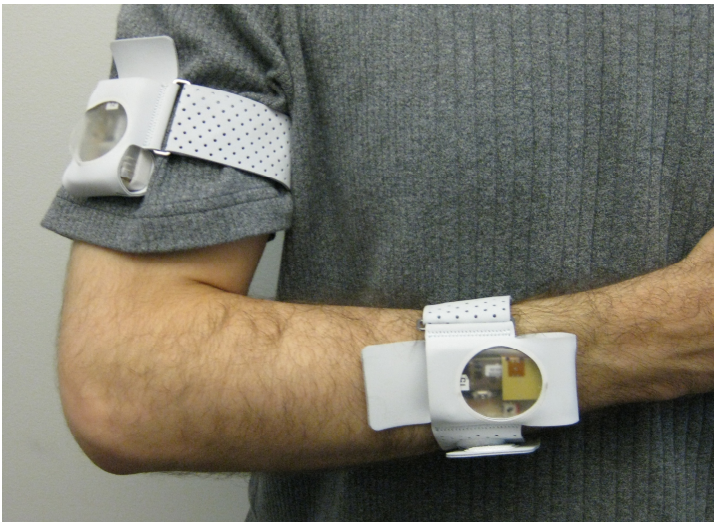

Fig. 2 Use of wrist sensors to detect its motion [58]

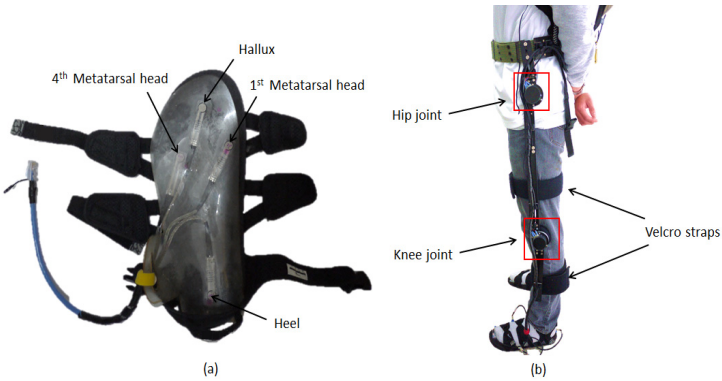

Fig. 3 Use of wearable sensors for the detection of knee and limbs [63]

10. Stress Monitoring- Stress is one of the common problems that people face in everyday life. Stress causes people to have all sorts of anxiety, hypertension, etc. The stress not only affects young people, but can also affect the elderly people. The old people tend to recapitulate the memories of their experience and can express a lot of emotions that includes stress. Persons in all age, especially from 35 can experience daily tensions that might lead to prolonged stress. The result of prolonged stress might result in nervous problems, heart attacks. The problem with the elderly people is even if they are under stress for any reason; they might not be able to or voluntarily show any emotions out of it. This can even cause more stress and even loss of sleep. The pressure monitoring is one of the important issues to be dealt with, especially in a smart home. It might look that the person being monitored on other aspects like heart rate, respiration rate, etc. Is healthy and thus ignoring the stress factor can be suffering from internal emotional problems that the person is not able to explain. Due to this, the person will eventually become weak and a result of which the person will start to face physiological problems. Research work [64, 65] regarding the stress monitoring has been done on in recent years on and off smart homes. One of the innovative ways [66] to determine the level of stress is to detect the respiratory pattern of the operated individual.

4 Sensors for Physiological Parameters Monitoring

Different types of sensors are being developed and used for the monitoring of physiological parameters in and out of smart homes. Some of the sensors are available in the market and used for the monitoring by improvising an algorithm to operate the sensor. A few of the sensors are:

1. **Piezoresistive Sensor:** These are the sensors used for force or pressure measurement of a particular type. They are used for force or pressure measurement in smart homes. When any pressure, is applied to it, the resultant voltage applied to it increases, as a result of which, the resistance of these sensors decreases. These sensors are placed beneath the legs of the chair, bed and sofa and beneath the brim of the toilet. These sensors are available in various ranges of resistances ranging from 0-1lb, 25lbs, 100lbs and 1000lbs. The construction of the piezoresistive sensors are simple [67] and is same for all the sensors constructed of this type. Two layers of polyester film are stuck on two sides with a conductive material like silver applied on top of it with a layer of pressure sensitive ink. An adhesive ink is also added to the two sides of the sensor. The central circular region of the sensor is the sensing area and the force exerted on the sensor has to be applied to this circular region. The conducting material, i.e., silver is extended forms the connected leads to making the sensor electrically conductive. The piezoresistive materials can also be integrated with other conducting materials for cardiopulmonary signs monitoring [68] and other parameters. A conditioning circuit is fabricated with the sensor to collect the data and send it wirelessly through one of the communication protocols to the receiver. The circuit is placed near the devices or person to be monitored, and the sensor is placed beneath the object.
2. **Sweat rate sensor:** Sweat is the form of an energy that goes out from the body. The main constituent of sweat is glucose. The glucose in the body is broken down into simpler constituents to provide energy. Any physical activity will lead to perspiration called sweat. The monitoring of sweat can help to detect the amount of body glucose that comes out. Fick's law of diffusion can be applied for the measurement of sweat. The sweat rate sensor can also be used as a wearable sensor by integrating it with the garment to measure both pH and sweat during any physical activity [36]. The pH measurement of sweat is important for the diagnosis of any diseases can be made from the nature of the sweat. One of the important factors for measuring sweat rate is the sensor should be placed in proximity to the skin. The water vapour evaporated from the skin is absorbed by the sensor to determine the constituents of the sweat. In many sports activities like football, rugby, the amount of sweat coming out from the body is too high. This leads to a high chance to dehydrate the body. In order to identify the characteristic condition of a person to sustain any activity with experiencing fatigue or too much tiredness, it would be better if the optimum level of work that a person can sustain is diagnosed beforehand.
3. **Shoe monitor sensor:** These sensors are used for monitoring of locomotion of individuals in smart homes. The shoe sensor is laboratory made shoes fitted with pressure sensors and accelerometers. The sensor can also be used in in smart homes where the motion is monitored by the wireless communication protocol from the sensor attached to the shoe. The shoe sensor is an important parameter to be monitored in an elderly smart home as the older people face

frequent falls. The athletes can also be monitored with shoe sensors to determine the speed or characteristic pattern of his/her running. The monitoring of other physiological parameters like gait analysis [7-19], condition of the foot. The range of parameters can even be increased by experimenting in a simulated condition to determine the change in running or walking pattern caused by the person due to fatigue experienced for a prolonged time for the activity. The shoe sensor can also be used in medical applications for determining other physiological parameters like heart conditions, blood pressure while walking or running at different paces. The complexity of shoe sensor is the positioning of the sensors on the heel, toes or the region between. Sometimes it might be possible that the person wearing the shoe sensor is not exerting enough pressure on the all the sensors connected to the shoe. Another issue related to the use of many homogenous sensors is the analyses of received data of different sensors. The application of shoe sensors might increase in future to deal with the medical conditions of people in a better way. Fig. 4 shows a common shoe sensor with its circuitry used for detection of any sports activity.

Fig. 4 Shoe sensors used for monitoring sports activity [69]

4. **Blood pressure sensor:** The indication of change of blood pressure grows to be an important factor for people above 50 years. The systolic and diastolic measurements determine the hypertension caused to an individual. There are four readings [70] for the blood pressure measurement, namely

prehypertension, high blood pressure- stage 1, high blood pressure- stage 2, hypertensive crisis, where the systolic and diastolic readings are 120-139/80-89, 140-159/90-99, 160 or higher/100 or higher and higher than 180/higher than 100 respectively. The mercury sphygmomanometer is replaced by other techniques [71] measuring the systolic and diastolic pressure with mean arterial pressure. The use of the traditional method for blood pressure measurement was done using cuffs strapped to the hand. Volume-Oscillometric techniques [20] are also used for the measurement of blood pressure based on the change in pressure caused by the rise and lowering of an individual's arm. The principle of oscillometry states that the difference between the mean internal arterial pressure and mean external cuff pressure is zero, the magnitude of arterial volume pulsations reaches its highest value. Hypertension is one of the major causes of coronary heart disease, stroke and other heart related diseases. Prehypertension is another concern that happens when the blood pressure of an individual reaches the higher end of the normal reading. Many research works [20, 21] has been done regarding the measurement of blood pressure through different techniques based on the same principle of calculation of blood pressure.

5. **Pulse oximetry sensor:** These types of sensors [72-75] are used for the measurement of oxygen saturation level in blood. The sensor is attached one part of the body, and the signal goes to the monitor with the cable attached to the sensor. One of the advantages of using this technique is that the process can be carried out anywhere without the blood samples taken from the body for measurement. In this process, two wavelengths are passed through the body calculating the absorbance caused by the arterial blood. The reason for passing two wavelengths is to measure the absorption coefficients due to the difference in concentration of haemoglobin and deoxyhaemoglobin level in blood. The signal is inverted and divided into AC and a DC component representing light absorption of the tissue and arterial blood. The disadvantage of this technique is that the signal cannot be collected wirelessly, even though the portability of the system is possible. The monitoring of the saturation level of oxygen is on a continuous matter is done in different situations to check ventilation and aircraft applications. The sensor is connected to any region where tissue is present. Reusable and non-reusable connecting regions are available where the former is more expensive, and the latter is attached to the reusable region. The oximeters are normally attached to the finger for measurement. A big disadvantage of pulse oximeters is that, even if there is insufficient flow of oxygen in the blood, the saturation level of blood might be high, so it would be insignificant to use these devices to measure the amount of oxygen.
6. **Personal Digital Assistant (PDA):** PDA can be described the combination of computer and smart homes. Some of the features of smart homes, like touch pad, may not be available in PDA, but it the earlier version of smart homes that is portable and consists of many features of the computer. The PDA is used a lot in monitoring of different physiological parameters nowadays [76, 77] where

the patients can be continuously monitored by the sensor connected to him/her and sending the data wirelessly to the receiving end through the PDA. The also usually consists of a memory card that can store the data monitored, or the data downloaded for PDA used for other applications. It can also be used a phone or to send a fax. The use of PDA might go down with the invention of smart phones, but still it is largely used for monitoring purposes. One of the advantages of using a PDA instead of a USB is that the data can be immediately sent the receiving station wired or wirelessly. Many operating systems like Windows, Linux, EPOC, Newton, etc. can be used on PDAs. Other applications with the PDAs are in medical applications, navigation monitoring and since the device can be connected to internet both wired and wirelessly, it can also be used for entertainment purposes.

7. **Accelerometer:** Accelerometers or acceleration sensors are devices that are used to determine the speed or to be precise, the acceleration of a person experienced in a fall position. In other words, it is used to measure the relative acceleration. The presence of accelerometer in any given frame determines the relative acceleration relative to that frame. Four kinds of accelerometers are available, namely piezoelectric, piezoresistive, capacitive and servo type sensors. They work on the principle of generation of electricity, change in resistance, change in capacitive effect, and change in heat induction respectively. The use of accelerometers has increased to a large extent for the monitoring of movements in [26] [47] and out [78] of smart homes. The accelerometers are mainly used in smart homes for continuous monitoring for posture recognition, physical activity [79] and monitoring of movements [80]. The use of accelerometers has greatly increased due to the falls [81, 82] faced by the elderly people in smart homes. The use of accelerometers has also grown to be in other applications like medical, transport, industry, engineering, etc. The uses of accelerometers are expanded by integrated with the garments for continuous monitoring of the movements. This would help to determine the average speed a person moves in the house and also the cause and time of the fall. The uses of accelerometers will increase in the future with the betterment is size, power requirement, portability. Fig. 5 shows a shoe sensor connected with Zigbee for wireless monitoring of movements.
8. **ECG:** This is a very common technique for the measurement of heart signals. The electrodes are connected to the heart for the detection of the rhythm of the heart. Heart is divided into four chambers, namely two arteries and two ventricles. Ten electrodes are connected to the body with the machine reading the signals, even though the number might vary. Twelve leads are attached to the electrodes, namely augmented, standard and chest leads. A proper connection between the electrode and the skin is made by applying a gel in between them. The phenomenon can be divided into two categories, depolarization and repolarization. The change in heart beats causes changes in the conduction properties of the skin. The cell being at rest are negatively charged and is known as repolarization. When the membranes pump blood, the heart muscles contracts and lose the charge, known as depolarization. The change in the muscle's travels

from one cell to another which is detected by the electrodes connected to the skin. The ECG of a person is done to detect the abnormality in breathing, heart problems and emergency situations. The smart homes have been using wearable sensors [84-89] for the monitoring of heart signals by integrating the electrodes with the garments. The continuous monitoring of the heart rhythm of the elderly has to be performed to determine any sudden heart attack. Portable ECG [84-86] systems are also being developed to be carried to avoid the electrodes being integrated with the garments. It might be cases that the system developed for performing ECG would also include the devices for the measurement of other physiological parameters. Extensive research work [84-89] has also been done on the use of internet for the performance of this process. Fig. 6 depicts the rhythm of the heart beat being monitored.

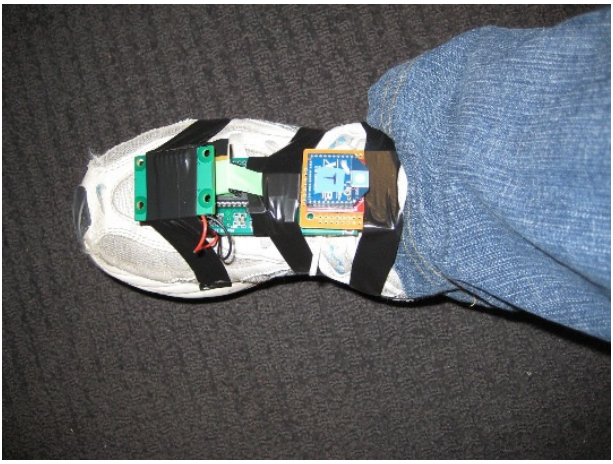

Fig. 5 Use of accelerometers used gait analysis [83]

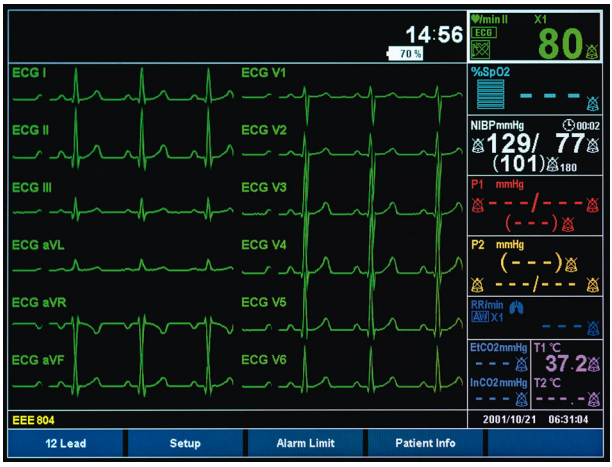

Fig. 6 Representation of rhythm of heart beat by ECG [90]

9. **Light sensor:** The light sensors are the ones that show a change in their properties on exposure to light. They are used in a wide range of applications like navigation, medical, military, home monitoring. They are used for generation of electricity from light energy. The range of light sensors can be divided roughly into four categories namely photo-emissive, photo-voltaic, photo-junction and photoconductive sensors. The photo-emissive are the ones that release free electrons on exposure to light. The photons are emitted from the device hitting the surface of the sensor. It then emits the electrons. The number of electrons emitted from the surface of the sensor depends on the frequency of the photons smacking on the sensor. The photovoltaic sensors generate a voltage on reception of energy in terms of photons. These types of materials are used for solar cookers where the light energy is converted into electrical energy. Semiconductor materials like silicon and germanium are used for the fabrication of these sensors. The cut-off voltage has to be crossed for the generation of voltage. The photoconductive sensors are the ones where the conductivity of the material changes on reception of light. The material with the absence of light on it has high resistance to it. Elements like lead sulphide, lead selenide are used to make photoconductive materials. The continuous use of non-renewable sources will lead the increase in the use of light sensors is likely to increase in the future due to its renewable nature. Fig. 7 shows a light sensor commonly used for security purposes.

Fig. 7 Light sensors used for security purpose [91]

5 Types of Activities

As the impact of wearable sensor increases, the types of activities to be monitored are also increasing. The wearable sensor, depending upon its size, shape, durability, can be used in a lot of applications in today's world. Some of them can be categorized as:

1. Physical activities: Normally, the use of wearable sensors is much associated with the activities performed inside the smart homes. Even though some of the activities like human navigation, monitoring of physical activities of the elderly at home can be performed with the wearable sensor, most of the physical activities are to be performed outside the smart homes. Some of them can be categorized as:
   a. **Jogging/running:** This is one of the common uses of wearable sensor where it is normally seen that a sensor is strapped around the arm of the runner to monitor different attributes like number of steps, breathing rate, body temperature. The size of the wearable sensor used in this activity is compact and is self-operated. The sensor can also be used to collect the data wirelessly to monitor the running or walking of patients with asthma or dementia. Even the sensor can be integrated into the clothing of the elderly people, and monitoring can be done for their movements. The wearable sensors to be used in the smart homes are needed to be operated wirelessly as the use of this sensor will reduce the use of passive infrared sensors that is normally used for movement monitoring. Now, the parameters of the sensor monitoring a runner can also be increased like including the GPRS and the stress factor or emotional condition of the person so that any difficulty faced by that person performing the activity can be addressed immediately. The person can also be monitored while walking so that any mismatch of the way to the destination of that person can be dealt with without the use of cell phones or trackers. Without the use of wearable sensors attached to the garments, other sensors like accelerometers can also be used to know the pace of the person while running or walking. The person can attached the accelerometer working on a modelled algorithm to analyze the speed of that person. Fig. 5 shows another shoe sensor connected with an accelerometer for detection of movement.
   b. **Driving:** In today's fast pacing world, driving is an everyday activity. People drive cars every day to go to different places like work, home, parties. Professional people drive buses, trucks and other bigger automobiles. To have a better view and understanding of the position and condition of a person driving a vehicle, wearable sensors can be used with that person. It might be difficult for a person to use a wearable sensor on his arm while driving, especially that of professional vehicle, but the wearable sensor can be attached to other parts of the body for its monitoring. One of the bigger reason for the use of wearable sensor is to reduce the fatality rate. In today's technologically progressing world, every person almost owns a care in towns and cities. The number of vehicles has increased to around 1.5 million in this world. As a result, the number of accidents has also increased considerably. Sometimes, it is heard in the news that a car or bus has faced an accident, and it has been founded in two days. The problem was with the location of the accident where normally not too many people visit. To avoid these type of

circumstances, a sensor can be used to monitor the position of the vehicle. One possible option might be to contact sensor to the vehicle. But, it might be possible that the person who is supposed to drive the vehicle may not be within it at a particular moment when the vehicle is parked or other people to be monitored may not be present in the vehicle at particular circumstance, even if the car is monitored, it will be of no use. A sensor can be connected to the person or people monitored individually that can be operated wirelessly in order to locate the position of those people. A wearable sensor can be fitted to the garment as the activity of running or jogging for the ease of the person to be monitored. This is because it might be very difficult for the person, especially the one who is driving, to wear externally fitted wearable sensor to be inspected while driving. There might be some situations where it will be needed continuously to monitor more than one person in a vehicle. It would be better to introduce a one-to-many transceiver where the signal can be captured from different nodes connected to different people and identified according to the identification number. There might be situations where the vehicle might be located at places where it might be difficult for receiving the signals from remote locations. The mobile phone can be one of the probable options for the communication in which the data can be sent to the mobile phones of the receiving station in a continuous manner. The older people, even though, may early drive can face a lot of problems while driving. Due to the problems with their eyesight, loss of reflexes, there is a high probability of accidents while they are driving. The wearable sensors can be attached to their body parts for determining their mental condition while driving.

Fig. 8 Sensors attached to shoes to monitor the activity [92]

c. **Playing any sport/athlete:** Wearable sensors can be a big advantage for any sport played. The sensor can be connected to the athlete or player performing any activity, and the level of emotion, anxiety, excitement can be monitored. Sometimes, it happens that the player is undergoing through an emotional turmoil before or during a match, the wearable sensor connected to the player can detect the exact emotional state of the player. The physical injuries among players can also be reduced by the use of the sensors as the connected sensors can continuously monitor the change in physical state of the person. Monitoring of a lot of characteristics of the human body like body temperature, heart rate, sweat rate can be done during the sports activity with the wearable sensor. For example, in football, it is seen that some players become tired of playing for the stipulated time. The connected wearable sensor can detect the tiredness of a person can generate a pattern for different players in the game. One of the disadvantages of using a separately connected wearable sensor during any sport is, the sensor might get damaged by harsh physical contact in some of the activities like football, karate, etc. The sensors can be wrapped with a strap around the person's body part that is to be least exposed to physical contact. Some sports like sky diving, water rafting will require a high degree of dauntless that might not be present in few people. This will lead to an increase in adrenaline level and eventually cause heart and neural problems. The use of sensors can detect the change in hormonal levels and determine the extreme condition of the person. This might also happen to a person getting involved with any sport or adventurous activity for the first time. The person will have some fear about the upcoming experience of the sport and will have tension. Recently, prominent amount of work [45] [93] has been done regarding the monitoring of sports activities by designed sensors. Sports have become one of the common reasons to increase the interaction among different countries of the world. Every five years, more and number of athletes participate from different countries in Olympics [94]. In order of scrutinize the condition of every player, checking if they are on steroids or not, sensors can be used for the activity or sport they perform. The sensor has to detect the energy level of that athlete compared to others to verify the absence of drugs in that person. The wearable sensors can be designed in such a way that the person finds it least difficult to perform wearing that sensor.

d. **Writing/Reading:** Even though performing these activities is not so strenuous compared to playing sports or driving, but it can still be considered one of the physical activities, especially when a high degree of performance is required in this field for a long period. Writing or reading may be considered as a physical activity that is done sitting or lying. But performing these activities also creates pressure in the brain causing nervous fluctuations. In today's competitive world, every student has to remain at his/her peak in terms of performance. The students taking exams

on a regular basis are under pressure to perform well. This happens with the research scholars and people working the administration section as well. The constant pressure of performing well especially in written and oral exams brings a person under a lot of pressure. A sensor connected to electrodes can be attached to the person's brain to determine the mental condition of the person. It might be the case that the person is under tremendous pressure of dealing with the exam. These situations on long-term cause sleeplessness and heart related problems. The use of sensors can also help the universities and companies to choose a person as their candidature whose can hold his/her nerve in critical conditions. The use of wearable sensor might be a bit difficult in this activity especially when giving an exam or oral presentation as the concentration of the person might be defocused due to the sensor. Even if the testing is done in laboratory conditions, it is still different from the laboratory conditions. Another aspect to be noted in this activity is that the data collected during the monitoring of the neural conditions to determine stress should be kept highly confidential to avoid any future problems for that person. The data from the nodes has to be collected wirelessly and away from the subject. It may be possible to determine the stress condition of that person on simulated conditions perfecting to the original one, but may be avoiding the original condition avoid the conundrums faced by the person with the sensor fitted.

Fig. 9 Wrist worn sensor used for hand motion detection [95]

2. Non-physical activities: Maximum of the activities that takes place in an elderly smart home is non-physical. Due to the lack of many movements of the older people, they perform most of their activities from one position. Some of the non-physical activities that can be considered within and outside the smart homes for the use of wearable and non-wearable sensors are:

a. **Sleeping:** One of the most common activities, especially for older people is sleeping. A normal person, before the age of 60, requires at least 8 hours of sleep a day. The older people need at least 10 hours sleep a day. An elderly person might face a lot of problems during the sleep of which he/she might be unaware of. Some of these problems might be breathing problems, heart related problems. In order to monitor any anomaly during the sleeping periods, sensor can be connected to the bed, or the person being operated. In some of the works [96-98], a piezoresistive sensor is used beneath the legs of the bed or the mattress to determine the sleeping position and the timings of the sleep. The sensors also monitor the timing of the sleep at which it is most effective during the night. Even the wearable sensors can be considered for the monitoring of sleeping pattern. If an elderly person faces any respiratory problems during sleep, the sensor can immediate defect it and steps can be taken accordingly. The wearable sensor has to be fitted to the person is such a way that the person does not face any discomfort while sleeping. The consistency of the heart rate can also be checked during the sleep by fitting the sensor to the garment the person wears during the sleep. The sensor can also analyse the position or changes in position that the person makes during the sleep. Non-wearable sensors can include the monitoring of emotional condition of the person when he is sleeping. It might be possible in some cases that the person is experiencing a bad dream that causing stress and tension that might permanently imprint that image into his dream. Monitoring can be done to analyse the fluctuation of emotion a person experiences during his dream. This might be particularly helpful for elderly people as their anatomical conditions are weaker than that of a healthy person. The wearable sensors can also be tested in simulated conditions to determine the health conditions like tremors, too much thirstiness during the sleep.
b. **Talking:** This is one of the important characteristics that drastically reduce in old age. The older people tend to talk less due to some reason. They stay quick most of their time. This might be normal in maximum circumstances, but in certain cases, they might be going through an emotional turmoil that they are unable to share with anybody and as a result of which their health deteriorates more. Both wearable and non-wearable sensors can be used for monitoring the emotional condition of the elderly person while talking about different subjects. A normal healthy person with age between 25 and 50 would take on various topics that affect him/her in daily life. In might be possible in certain cases that the person is not willing to talk about things that bother in his/her life. This might be affecting him/her emotionally in a long-term, which, as a result, would not be good both for her heart and brain. It would be useful to have a sensor to identify the emotional condition of the person when the person is not willing to talk. But there would certainly be cases where the person will not be willing to experience their emotional state as they are not ready to open up. The experiments can also be performed at simulated

conditions to differentiate between the responses in emotional characteristic between two persons talking on the same topic. This would also lead to analyse the way a person tries to think a particular topic.

c. **Watching television/ playing computer games:** It is seen that a person is highly entertained while watching television or playing computer games. The children normally remain excited to watch their favourite programmes on television or play computer games at particular stipulated times. It would be useful to use a sensor to determine the excitement level of a person while performing these activities. The elderly people in smart homes can also be monitored when they watch television determine the tiredness they face or sleepiness that feel. It may also be useful to use a wearable sensor to determine the effect in eyes of watching television or playing computer games for people of every age. The sensor can be used in a simulated condition of people with different age, gender with different intervals of time performing these activities to diagnose the level of effects that are taking place on two separate individuals. In today's world, using computer for professional and personal work has become a common task. Almost everyone uses the computer every day to do some work. Use of computer for longer periods of time will cause adverse effects on eyes. The wearable sensors can be used to detect the rate of adversity in the eyes with continuous use of computer on a daily basis. It can be seen [99] that watching television causes obesity among children. The children of age between 10 to around 20 watch television almost every day for watching some specified programmes. This might also affect the posture at which they watch television and simultaneously gaining weight on the body. It might be useful to use a sensor that might detect the change in weight with every posture they watch television. Watching television among kids might also affect their psychological thinking, tending to act more the way they watch the programmes in the television. It might be helpful to detect the thought process of the children to determine the way they think to act.

d. **Different activities in a smart home:** We have been running a continuous system for more than one year dealing with the different activities and issues encountered in a smart home. Daily activities that include both physical and non-physical are monitored in a continuous manner. Different types of sensors that include passive infrared (PIR), electrical sensors, force sensors and temperature sensors, are connected at different locations of the house and electrical objects to parameterize the readings at different intervals of time. Solar temperature sensors are connected outside the house to keep a note of the ambiance temperature. Extensive research work [100-119] has been carried regarding the designing and functioning of a smart home. Real-time data collection and analysis is done to decrease the complexity of the system and deal with the integral parameters like power management, cost effectiveness and to make the system more user friendly. The future work is to make the system more compact and developing it to a larger scale.

6 Wireless Technologies

Wireless technology has recently [120-122] gained a lot of popularity in electronics and electrical sector. The use of wireless communication has increased the degree of interaction between two or more nodes. The wireless technology has led the formation of networks involving the transmission of data between nodes simultaneously. The sensors used in smart homes can be conveniently operated via wireless technology. Some of them which are commonly used are:

1. **Wi-Fi:** This is the most common technology in recent days in almost every institute, company and home. The Wi-Fi is a serial standard if IEEE 802.11. The applications with Wi-Fi are continuously growing and are making the use of internet in an efficient way. Wi0fi makes the use of broadband access. Some of the advantages of using Wi-Fi are marked by its speed, coverage of transmission of data and security. The Wi-Fi is also gaining its popularity [123, 124] in local area network and private area network. The heterogeneous sensors used in smart homes can be connected at different locations in the house, and the data can be simultaneously collected from all the nodes to the receiving node via separate identification number of nodes. The wearable sensor can also be collected by the person being monitored, and the data can be received wirelessly to avoid the use of disturbance caused to the person by the use of wires. The use of Wi-Fi is also being used in telemedicine [125] to measure the heart rate, blood pressure of the patient more quickly. The use of this technology also ranges to games, entertainment, telephone, photos and videos. The future of Wi-Fi is foreseen to be brighter with the involvement of this technology in wider range of applications.

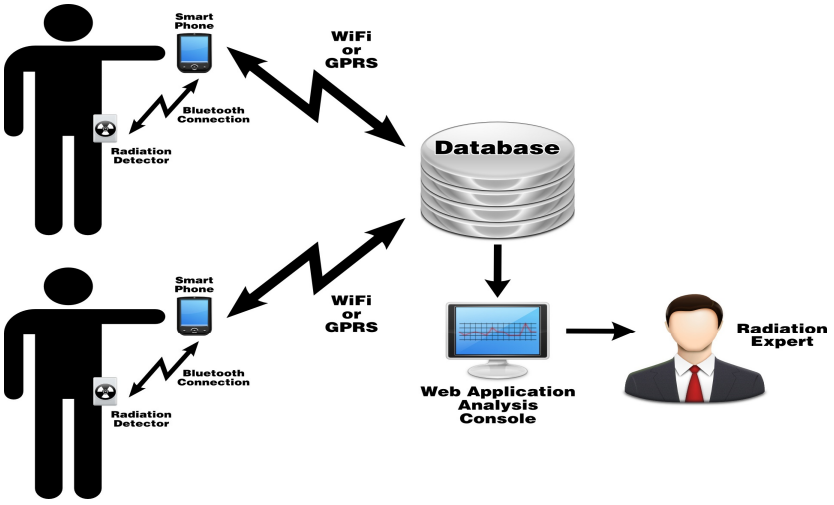

Fig. 10 Wi-Fi and Bluetooth used for data transfer [126]

2. **Bluetooth:** This is similar wireless technology to Wi-Fi specially used for low range communications. The security issue of Bluetooth is better as compared to Wi-Fi. A security key has to be provided by both the users in order to transfer any data. The authentication key is scripted so that any intruder injected virus will not be able to hack it. The variation of types of data send through Bluetooth is very much similar as compared to Wi-Fi through which text, multimedia messages could be exchanged. One of the most common uses of Bluetooth is the transmission of data between cell phones where the data is simultaneously sent from different phones to one, but not vice-versa. This technology uses Frequency-hopping spread spectrum in the 2.4 GHz ISM frequency band with the transfer of data at 1 Mbps. The use of Bluetooth is significant if the monitoring of different activities both inside [123,127] and outside smart homes. One of the disadvantages of this technology is the limitation of range between the transmitter and receiver. The distance upon which is the communication via Bluetooth between two devices can take place is around 10 metres that do not have to be necessarily in line of sight. The blue is rather used as wireless personal area network whereas the Wi-Fi is used a wireless local area network.

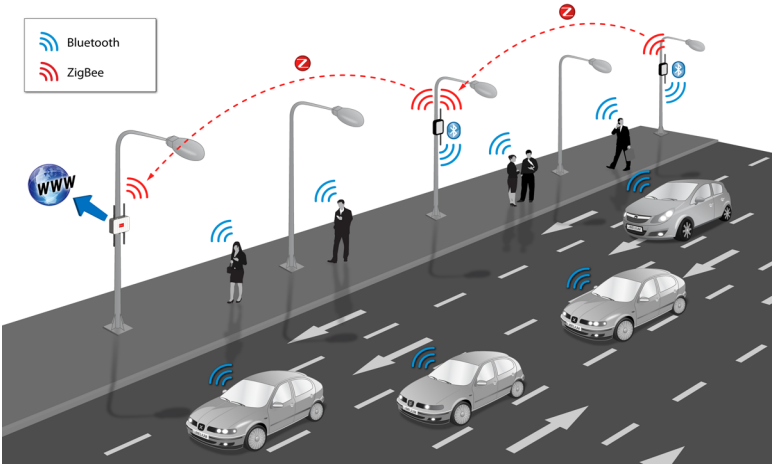

Fig. 11 Bluetooth and Zigbee functioned in daily life [128]

3. **Zigbee:** This is a very popular technology for low power application. It is based on the IEEE standard 802.15.4. It also works on short range, almost up to 30 metres [129]. The working principle of Zigbee is very simple making it one of the best choices for the transmission of data in smart homes. The Zigbee works ideally between 2.8V to 3.9V. It is also highly secured like Bluetooth as the transfer of data takes place after the matching of identification number between the end devices connected to the sensor and the receiving node. Zigbee is smart homes is used [130] as routers and end

devices with the formation of different networks collecting data from the end devices to the coordinator connected to the computer via routers. The application of Zigbee also includes medical science [131], industrial sectors [132] and environmental monitoring [133, 134]. The application with short-range, low power, highly secured data transfer is ideal for Zigbee. The nodes operating on the principle of Zigbee should have a high battery life. There is a slight time delay between the transmission and reception of the data between the nodes. This principle works on unslotted CSMA/CA principle that is different from the Bluetooth that uses a slotted one. The main advantage of Zigbee over another communication protocol is that it requires very low power for transmission of data from heterogeneous sensors.

4. **NFC:** Near-field communication (NFC) is similar to Zigbee protocol with the exception that the communication range decreases to 10cms. It uses 13.56MHz frequency bands with the speed ranging from 106 to 424 Kbits/second. RFID is used for communication by this technology. Active or passive modes are used in this phenomenon for transmission. The rate of transmission is chosen by the main device providing the RF field while the receiving node uses load modulation technique to receive the data from the transmitting node. Three modes named target, initiator and peer to peer are available to work with this technology. A lot of medical applications [135] are using NFC as their communication protocol for monitoring of blood pressure, heart rate. Alzheimer patients, as well as other medication monitoring, are well monitored with NFC technology. Smartphones [136], security [137] gaming and other common applications [138-143] are the reasons of popularity NFC. The communication between smartphones takes place with tags attached to it. One other advantage of using NFC is the availability of sending and receiving the data simultaneously, apart from the fact that the power required for exchange of data is the least in this protocol compared to Bluetooth, Zigbee and Wi-Fi. There is a major disadvantage of using NFC than Bluetooth and Wi-Fi other than the range of communication is the security. Since, no pairing between devices is required for this technology; malware can be introduced in the data transmitted between two nodes.

7 Current Status and Future Opportunities

Though there are many wearable sensors available in the market, most of them are still not universally accepted by the general public. There are many reasons, and the sensor/system's manufacturers face a lot of challenges. In order to make wearable devices common item of our daily lives, there is a need for overcoming several major technological cum social challenges. The most important challenge being the drastic reduction of the cost of fabrication of wearable sensors. The total cost of the wearable system should be affordable to low income earners. To make it feasible there us a need of breakthrough in sensor hardware such as the sensing

elements, signal processing and computational parts and communication system should be small in size and consume less amount of battery power [144]. There should be a trade-off between user comfort, long-term wearability and reliable measurement and communication. It is a general social condition that most people do not want to wear uncomfortable sensors to monitor their health unless they have serious health problems [144]. The wearable system should be light in design and will be worn at a place of the body so that it is not uncomfortable to wear 24/7 for 365 days. To make the wearable devices more acceptable to society, there is a need for more widespread clinical trials, and they should be robust for long-term monitoring of people for real-life conditions [145]. So far wrist watch, bangle or necklaces are such devices that are comfortable to many people. Another important requirement is continuity of high quality of service. The wearable devices should be waterproof and is robust so that it is safe from physical damage due to fall or any such incident. The same type of devices may not be suitable for everyone, so there is a need of understanding the requirement and to address that. The wearable devices should be interoperable so that the devices are compatible with other existing devices manufactured by different companies [146]. This means that the device can be easily replaced when they become damaged or stops satisfactory operation. The wearable devices will be battery fed so the design of electronics including communication should be sympathetic to energy consumption. There are many chronic illnesses, neurological disorders, and mental health issues including diabetes, autism spectrum disorder (ASD), depression, drug addiction, and anxiety disorders for which wearable devices will be extremely useful [147]. Another challenge is faced to convince people about the usage of personal data for privacy consideration. It is to be ensured that the collected data will not be misused at any cost.

Even though, there are some challenges on the design issues, usages and acceptability of the wearable sensors but the market and development is at full swing. The continuous research and developmental works are going on to address the issues faced by the wearable electronic sensors and continue to do so in the future. The growth of the wearable electronics and fitness monitoring market will, in turn, provide good revenue opportunities for MEMS motion sensor manufacturers [148]. The revenue for MEMS motion sensors in wearable electronics and fitness monitoring climb to $31.0 million in 2013 from $20.0 million range in 2012, and then jump 33 percent to $41.3 million in 2014 [148]. It is expected even a larger increase, equivalent to 47 percent, will occur in 2015 when takings amount to $60.8 million and continue to grow in 2016 and beyond. The figure 12 presents the forecast of global MEMS shipments for wearable electronics and fitness monitoring devices.

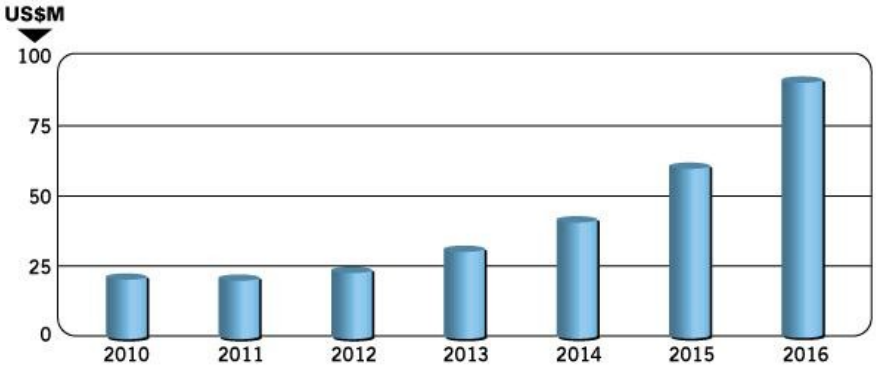

Fig. 12 The market of MEMS sensors for wearable electronics [148]

Though there may be some issues in terms of long-term monitoring using wearable sensors but that sensors and wireless technology had advanced to a point where they could bring amazing experiences to fitness and health for a short-duration use [149]. Use of intelligent armbands for tracking physical activities, wearable electronics and fitness monitoring devices are attracting increased attention from health-conscious consumers. One of the very interesting developments of wearable electronics in recent times is the Google Glass [150]. Google Glass is an attempt to free data from desktop computers and portable devices like phones and tablets, and place it right in front of the eyes of the viewer. Google Glass is a camera, display, touchpad, battery and microphone built into spectacle frames so that a display is perched in the wearer's field of vision, allowing him to film, take pictures and search and so on. Wearable electronics could open up new applications such as memory aids and navigational tools [151,152]. There are a lot of developments taking place in the area of smart watches [153] which can provide a significant amount of physiological information, as well as physical activities. In the future the data measured by the wearable sensors may be collected by IoT (Internet of Things) based system and will be available to be visible to everyone through a secured access may be necessary. It may also be possible to use all the measured data of daily activities to find the model the lifestyle of human. One interesting opportunity to the manufacturers will be to looks into ways of reduction of the electronic-waste by developing new types of materials which will not be hazardous to the environment.

8 Conclusion

The use of wearable sensors has recently gained a popular trend for continuous monitoring of different physiological parameters related to an individual. The sensors connected externally to different parts of the body as well as to the garments can specifically detect the parameter it is used for. Some of the sensors are designed in a way to the diagnosis of more than one physiological parameter.

The chapter lists some of the applications that can be considered for the use of sensor, both wearable and non-wearable, some of which as mentioned are already in use. It also briefly explains some of the wireless technologies currently used for operating the different sensors related to its application. The technologies explained cover most of the applications in the field of home monitoring system. It also reviewed some the signal processing techniques used for the monitored parameters. Lastly, it provides the current market condition of electronics with its probable future possibilities.

References

1. Lutz, W., Samir, K.C.: Dimensions of global population projections: what do we know about future population trends and structures? Philosophical Transactions of the Royal Society B: Biological Sciences 365(1554), 2779–2791 (2010)
2. http://www2.stats.govt.nz/domino/external/web/prod_serv.nsf/092edeb76ed5aa6bcc256afe0081d84e/5977c54210e1abc7cc256dd600030457?OpenDocument
3. Kang, J.M., Yoo, T., Kim, H.C.: A wrist-worn integrated health monitoring instrument with a tele-reporting device for telemedicine and telecare. IEEE Transactions on Instrumentation and Measurement 55(5), 1655–1661 (2006)
4. Kim, D., Hilliges, O., Izadi, S., Butler, A.D., Chen, J., Oikonomidis, I., Olivier, P.: Digits: freehand 3D interactions anywhere using a wrist-worn gloveless sensor. In: Proceedings of the 25th Annual ACM Symposium on User Interface Software and Technology, pp. 167–176. ACM (2012)
5. Pittman, S.D., Ayas, N.T., MacDonald, M.M., Malhotra, A., Fogel, R.B., White, D.P.: Using a wrist-worn device based on peripheral arterial tonometry to diagnose obstructive sleep apnea: in-laboratory and ambulatory validation. Sleep 27(5), 923 (2004)
6. Sung, M., DeVaul, R., Jimenez, S., Gips, J., Pentland, A.: Shiver motion and core body temperature classification for wearable soldier health monitoring systems. In: Eighth International Symposium on Wearable Computers, ISWC 2004, vol. 1, pp. 192-193. IEEE (2004)
7. Goulermas, J.Y., Findlow, A.H., Nester, C.J., Liatsis, P., Zeng, X.-J., Kenney, L.P., Tresadern, P., Thies, S.B., Howard, D.: An instance-based algorithm with auxiliary similarity information for the estimation of gait kinematics from wearable sensors. IEEE Transactions on Neural Networks 19(9), 1574–1582 (2008)
8. Mariani, B., Jiménez, M.C., Vingerhoets, F.J.G., Aminian, K.: On-shoe wearable sensors for gait and turning assessment of patients with Parkinson's disease. IEEE Transactions on Biomedical Engineering 60(1), 155–158 (2013)
9. Chelius, G., Braillon, C., Pasquier, M., Horvais, N., Gibollet, R.P., Espiau, B., Coste, C.A.: A wearable sensor network for gait analysis: A six-day experiment of running through the desert. IEEE/ASME Transactions on Mechatronics 16(5), 878–883 (2011)
10. Winter, D.A., Patla, A.E., Frank, J.S., Walt, S.E.: Biomechanical walking pattern changes in the fit and healthy elderly. Physical Therapy 70(6), 340–347 (1990)

11. Mariani, B., Jiménez, M.C., Vingerhoets, F.J.G., Aminian, K.: On-shoe wearable sensors for gait and turning assessment of patients with Parkinson's disease. IEEE Transactions on Biomedical Engineering 60(1), 155–158 (2013)
12. Kurihara, Y., Watanabe, K., Yoneyama, M.: Estimation of walking exercise intensity using 3-D acceleration sensor. IEEE Transactions on Systems, Man, and Cybernetics, Part C: Applications and Reviews 42(4), 495–500 (2012)
13. Bloem, B.R., Haan, J., Lagaay, A.M., van Beek, W., Wintzen, A.R., Roos, R.A.C.: Investigation of gait in elderly subjects over 88 years of age. Journal of Geriatric Psychiatry and Neurology 5(2), 78–84 (1992)
14. Colledge, N.: Gait Disorders of Aging. Falls and Therapeutic Strategies. Journal of Neurology, Neurosurgery, and Psychiatry 64(4), 566 (1998)
15. Sudarsky, L.: Clinical approach to gait disorders of aging: an overview. Gait disorders of aging. Lippincott-Raven, Philadelphia (1997)
16. Shaban, H.A., El-Nasr, M.A., Buehrer, R.M.: Toward a highly accurate ambulatory system for clinical gait analysis via UWB radios. IEEE Transactions on Information Technology in Biomedicine 14(2), 284–291 (2010)
17. Elble, R.J., Sienko Thomas, S., Higgins, C., Colliver, J.: Stride-dependent changes in gait of older people. Journal of Neurology 238(1), 1–5 (1991)
18. Hough, J.C., McHenry, M.P., Kammer, L.M.: Gait disorders in the elderly. American Family Physician 35(6), 191–196 (1987)
19. Alexander, N.B.: Differential diagnosis of gait disorders in older adults. Clinics in Geriatric Medicine 12(4), 689–703 (1996)
20. Shaltis, P.A., Reisner, A.T., Asada, H.H.: Cuffless blood pressure monitoring using hydrostatic pressure changes. IEEE Transactions on Bio-Medical Engineering 55(6), 1775–1777 (2008)
21. Rotariu, C., Pasarica, A., Costin, H., Adochiei, F., Ciobotariu, R.: Telemedicine system for remote blood pressure and heart rate monitoring. In: E-Health and Bioengineering Conference (EHB), 2011, pp. 1–4. IEEE (2011)
22. Guo, L., Berglin, L., Li, Y.J., Mattila, H., Mehrjerdi, A.K., Skrifvars, M.: 'Disappearing Sensor'-Textile Based Sensor for Monitoring Breathing. In: 2011 International Conference on Control, Automation and Systems Engineering (CASE), pp. 1–4. IEEE (2011)
23. Zito, D., Pepe, D., Mincica, M., Zito, F., Tognetti, A., Lanata, A., De Rossi, D.: SoC CMOS UWB pulse radar sensor for contactless respiratory rate monitoring. IEEE Transactions on Biomedical Circuits and Systems 5(6), 503–510 (2011)
24. Wilhelm, F.H., Roth, W.T., Sackner, M.A.: The LifeShirt An Advanced System for Ambulatory Measurement of Respiratory and Cardiac Function. Behavior Modification 27(5), 671–691 (2003)
25. Corbishley, P., Rodríguez-Villegas, E.: Breathing detection: towards a miniaturized, wearable, battery-operated monitoring system. IEEE Transactions on Biomedical Engineering 55(1), 196–204 (2008)
26. Tapia, E.M., Intille, S.S., Haskell, W., Larson, K., Wright, J., King, A., Friedman, R.: Real-time recognition of physical activities and their intensities using wireless accelerometers and a heart rate monitor. In: 2007 11th IEEE International Symposium on Wearable Computers, pp. 37–40. IEEE (2007)
27. Devlin, R.B., Ghio, A.J., Kehrl, H., Sanders, G., Cascio, W.: Elderly humans exposed to concentrated air pollution particles have decreased heart rate variability. European Respiratory Journal 21(40 suppl.), 76s–80s (2003)

28. Yan, L., Bae, J., Lee, S., Roh, T., Song, K., Yoo, H.-J.: A 3.9 mW 25-electrode reconfigured sensor for wearable cardiac monitoring system. IEEE Journal of Solid-State Circuits 46(1), 353–364 (2011)
29. Zhang, T.T., Ser, W., Daniel, G.Y.T., Zhang, J., Yu, J., Chua, C., Louis, I.M.: Sound based heart rate monitoring for wearable systems. In: 2010 International Conference on Body Sensor Networks (BSN), pp. 139–143. IEEE (2010)
30. Kastner, P., Morak, J., Modre, R., Kollmann, A., Ebner, C., Fruhwald, F.M., Schreier, G.: Innovative telemonitoring system for cardiology: from science to routine operation. Appl. Clin. Inf. 1(2), 165–176 (2010)
31. Buske, O., Neils, C., Regnier, M.: Heartbeat: Design and Development of a Headphone
32. Tang, W., Sazonov, E.S.: Highly accurate recognition of human postures and activities through classification with rejection. IEEE Journal of Biomedical and Health Informatics 18(1), 309–315 (2014)
33. Lopez-Meyer, P., Tiffany, S., Patil, Y., Sazonov, E.: Monitoring of cigarette smoking using wearable sensors and Support Vector Machines. IEEE Transactions on Biomedical Engineering 60(7), 1867–1872 (2013)
34. Morris, D., Coyle, S., Wu, Y., Lau, K.T., Wallace, G., Diamond, D.: Bio-sensing textile based patch with integrated optical detection system for sweat monitoring. Sensors and Actuators B: Chemical 139(1), 231–236 (2009)
35. Salvo, P., Di Francesco, F., Costanzo, D., Ferrari, C., Trivella, M.G., De Rossi, D.: A wearable sensor for measuring sweat rate. IEEE Sensors Journal 10(10), 1557–1558 (2010)
36. Coyle, S., Morris, D., Lau, K.-T., Diamond, D., Di Francesco, F., Taccini, N., Trivella, M.G., et al.: Textile sensors to measure sweat pH and sweat-rate during exercise. In: 3rd International Conference on Pervasive Computing Technologies for Healthcare, PervasiveHealth 2009, pp. 1–6. IEEE (2009)
37. Pantelopoulos, A., Bourbakis, N.: A survey on wearable biosensor systems for health monitoring. In: 30th Annual International Conference of the IEEE Engineering in Medicine and Biology Society, EMBS 2008, pp. 4887–4890. IEEE (2008)
38. Anliker, U., Ward, J.A., Lukowicz, P., Troster, G., Dolveck, F., Baer, M., Keita, F., et al.: AMON: a wearable multiparameter medical monitoring and alert system. IEEE Transactions on Information Technology in Biomedicine 8(4), 415–427 (2004)
39. Axisa, F., Dittmar, A., Delhomme, G.: Smart clothes for the monitoring in real time and conditions of physiological, emotional and sensorial reactions of human. In: Proceedings of the 25th Annual International Conference of the IEEE Engineering in Medicine and Biology Society, vol. 4, pp. 3744–3747. IEEE (2003)
40. Pandian, P.S., Mohanavelu, K., Safeer, K.P., Kotresh, T.M., Shakunthala, D.T., Gopal, P., Padaki, V.C.: Smart Vest: Wearable multi-parameter remote physiological monitoring system. Medical Engineering & Physics 30(4), 466–477 (2008)
41. Gatzoulis, L., Iakovidis, I.: Wearable and portable eHealth systems. IEEE Engineering in Medicine and Biology Magazine 26(5), 51–56 (2007)
42. Lukowicz, P., Anliker, U., Ward, J., Tröster, G., Hirt, E., Neufelt, C.: Amon: A wearable medical computer for high risk patients. In: 2012 16th International Symposium on Wearable Computers, pp. 133–133. IEEE Computer Society (2002)
43. Ma, Y.-C., Chao, Y.-P., Tsai, T.-Y.: Smart-clothes—Prototyping of a health monitoring platform. In: IEEE Third International Conference on Consumer Electronics?? Berlin (ICCE-Berlin), pp. 60–63. IEEE (2013)

44. Paradiso, R., Alonso, A., Cianflone, D., Milsis, A., Vavouras, T., Malliopoulos, C.: Remote health monitoring with wearable non-invasive mobile system: the healthwear project. In: 30th Annual International Conference of the IEEE Engineering in Medicine and Biology Society, EMBS 2008, pp. 1699–1702. IEEE (2008)
45. Ermes, M., Parkka, J., Mantyjarvi, J., Korhonen, I.: Detection of daily activities and sports with wearable sensors in controlled and uncontrolled conditions. IEEE Transactions on Information Technology in Biomedicine 12(1), 20–26 (2008)
46. Lee, S.-W., Mase, K.: Activity and location recognition using wearable sensors. IEEE Pervasive Computing 1(3), 24–32 (2002)
47. Atallah, L., Lo, B., King, R., Yang, G.-Z.: Sensor positioning for activity recognition using wearable accelerometers. IEEE Transactions on Biomedical Circuits and Systems 5(4), 320–329 (2011)
48. Ricquebourg, V., Menga, D., Durand, D., Marhic, B., Delahoche, L., Loge, C.: The smart home concept: our immediate future. In: 2006 1st IEEE International Conference on E-Learning in Industrial Electronics, pp. 23–28. IEEE (2006)
49. http://www.stats.govt.nz/browse_for_stats/people_and_communities/older_people/pop-ageing-in-nz.aspx
50. Souri, K., Chae, Y., Makinwa, K.A.A.: A CMOS Temperature Sensor With a Voltage-Calibrated Inaccuracy of 0.15 C (3) From 55 C to 125 C. IEEE Journal of Solid-State Circuits 48(1), 292–301 (2013)
51. http://www2.stats.govt.nz/domino/external/web/prod_serv.nsf/092edeb76ed5aa6bcc256afe0081d84e/5977c54210e1abc7cc256dd600030457?OpenDocument
52. http://www.agingcare.com/Articles/What-is-normal-blood-pressure-for-elders-108019.htm
53. Dunne, L.E., Walsh, P., Hermann, S., Smyth, B., Caulfield, B.: Wearable monitoring of seated spinal posture. IEEE Transactions on Biomedical Circuits and Systems 2(2), 97–105 (2008)
54. Gibb, W.R., Lees, A.J.: The relevance of the Lewy body to the pathogenesis of idiopathic Parkinson's disease. Journal of Neurology, Neurosurgery & Psychiatry 51(6), 745–752 (1988)
55. Patel, S., Lorincz, K., Hughes, R., Huggins, N., Growdon, J., Standaert, D., Akay, M., Dy, J., Welsh, M., Bonato, P.: Monitoring motor fluctuations in patients with Parkinson's disease using wearable sensors. IEEE Transactions on Information Technology in Biomedicine 13(6), 864–873 (2009)
56. Chen, B.-R., Patel, S., Buckley, T., Rednic, R., McClure, D.J., Shih, L., Tarsy, D., Welsh, M., Bonato, P.: A web-based system for home monitoring of patients with Parkinson's disease using wearable sensors. IEEE Transactions on Biomedical Engineering 58(3), 831–836 (2011)
57. Rigas, G., Tzallas, A.T., Tsipouras, M.G., Bougia, P., Tripoliti, E.E., Baga, D., Fotiadis, D.I., Tsouli, S.G., Konitsiotis, S.: Assessment of tremor activity in the Parkinson's disease using a set of wearable sensors. IEEE Transactions on Information Technology in Biomedicine 16(3), 478–487 (2012)
58. http://fiji.eecs.harvard.edu/Mercury
59. Shyr, T.-W., Shie, J.-W., Jiang, C.-H., Li, J.-J.: A Textile-Based Wearable Sensing Device Designed for Monitoring the Flexion Angle of Elbow and Knee Movements. Sensors 14(3), 4050–4059 (2014)

60. Lee, G.X., Low, K.S., Taher, T.: Unrestrained measurement of arm motion based on a wearable wireless sensor network. IEEE Transactions on Instrumentation and Measurement 59(5), 1309–1317 (2010)
61. Stupar, D.Z., Bajic, J.S., Manojlovic, L.M., Slankamenac, M.P., Joza, A.V., Zivanov, M.B.: Wearable low-cost system for human joint movements monitoring based on fiber-optic curvature sensor. IEEE Sensors Journal 12(12), 3424–3431 (2012)
62. Zhang, Z.-Q., Wong, W.-C., Wu, J.-K.: Ubiquitous human upper-limb motion estimation using wearable sensors. IEEE Transactions on Information Technology in Biomedicine 15(4), 513–521 (2011)
63. http://robinhsieh.com/?p=1115
64. Choi, J., Gutierrez-Osuna, R.: Removal of respiratory influences from heart rate variability in stress monitoring. IEEE Sensors Journal 11(11), 2649–2656 (2011)
65. Jovanov, E., Lords, A.O., Raskovic, D., Cox, P.G., Adhami, R., Andrasik, F.: Stress monitoring using a distributed wireless intelligent sensor system. IEEE Engineering in Medicine and Biology Magazine 22(3), 49–55 (2003)
66. Choi, J., Gutierrez-Osuna, R.: Removal of respiratory influences from heart rate variability in stress monitoring. IEEE Sensors Journal 11(11), 2649–2656 (2011)
67. http://www.trossenrobotics.com/flexiforce-1lb-resistive-force-sensor.aspx
68. Loriga, G., Taccini, N., De Rossi, D., Paradiso, R.: Textile sensing interfaces for cardiopulmonary signs monitoring. In: 27th Annual International Conference of the Engineering in Medicine and Biology Society, IEEE-EMBS 2005, pp. 7349–7352. IEEE (2006)
69. http://www.sciencedaily.com/releases/2012/11/121108140845.htm
70. http://www.heart.org/HEARTORG/Conditions/HighBloodPressure/AboutHighBloodPressure/Understanding-Blood-Pressure-Readings_UCM_301764_Article.jsp
71. Cappuccio, F.P., Kerry, S.M., Forbes, L., Donald, A.: Blood pressure control by home monitoring: meta-analysis of randomised trials. BMJ 329(7458), 145 (2004)
72. Rafert, S.C., Marble, D.R., Pelikan, G.W., Kahn, A.: Conformal pulse oximetry sensor and monitor. U.S. Patent 5,817,008 (issued October 6, 1998)
73. Haahr, R.G., Duun, S.B., Toft, M.H., Belhage, B., Larsen, J., Birkelund, K., Thomsen, E.V.: An electronic patch for wearable health monitoring by reflectance pulse oximetry. Biomedical Circuits and Systems 6(1), 45–53 (2012)
74. Duun, S.B., Haahr, R.G., Birkelund, K., Thomsen, E.V.: A ring-shaped photodiode designed for use in a reflectance pulse oximetry sensor in wireless health monitoring applications. IEEE Sensors Journal 10(2), 261–268 (2010)
75. Yan, Y.-S., Zhang, Y.-T.: An efficient motion-resistant method for wearable pulse oximeter. IEEE Transactions on Information Technology in Biomedicine 12(3), 399–405 (2008)
76. Ahn, H.S., Sa, I.-K., Choi, J.-Y.: PDA-based mobile robot system with remote monitoring for home environment. IEEE Transactions on Consumer Electronics 55(3), 1487–1495 (2009)
77. Korhonen, I., Parkka, J., Van Gils, M.: Health monitoring in the home of the future. IEEE Engineering in Medicine and Biology Magazine 22(3), 66–73 (2003)
78. Mehta, D.D., Zanartu, M., Feng, S.W., Cheyne, H.A., Hillman, R.E.: Mobile voice health monitoring using a wearable accelerometer sensor and a smartphone platform. IEEE Transactions on Biomedical Engineering 59(11), 3090–3096 (2012)

79. Tapia, E.M., Intille, S.S., Haskell, W., Larson, K., Wright, J., King, A., Friedman, R.: Real-time recognition of physical activities and their intensities using wireless accelerometers and a heart rate monitor. In: 2007 11th IEEE International Symposium on Wearable Computers, pp. 37–40. IEEE (2007)
80. Atallah, L., Lo, B., King, R., Yang, G.-Z.: Sensor positioning for activity recognition using wearable accelerometers. IEEE Transactions on Biomedical Circuits and Systems 5(4), 320–329 (2011)
81. http://link.springer.com/article/10.1007/BF02351026
82. http://journals.plos.org/plosone/article?id=10.1371/journal.pone.0037062#pone-0037062-g004
83. https://courses.cit.cornell.edu/ee476/FinalProjects/s2009/vlc6_ljs62/vlc6_ljs62/images/working/IMG_1941.JPG
84. Chi, Y.M., Cauwenberghs, G.: Wireless non-contact EEG/ECG electrodes for body sensor networks. In: 2010 International Conference on Body Sensor Networks (BSN), pp. 297–301. IEEE (2010)
85. Alzaidi, A., Zhang, L., Bajwa, H.: Smart textiles based wireless ECG system. In: 2012 IEEE Long Island Systems, Applications and Technology Conference (LISAT), pp. 1–5. IEEE (2012)
86. Taji, B., Shirmohammadi, S., Groza, V., Bolic, M.: An ECG monitoring system using conductive fabric. In: 2013 IEEE International Symposium on Medical Measurements and Applications Proceedings (MeMeA), pp. 309–314. IEEE (2013)
87. Hoffmann, K.-P., Ruff, R.: Flexible dry surface-electrodes for ECG long-term monitoring. In: 29th Annual International Conference of the IEEE Engineering in Medicine and Biology Society, EMBS 2007, pp. 5739–5742. IEEE (2007)
88. Ravanshad, N., Rezaee-Dehsorkh, H., Lotfi, R., Lian, Y.: A Level-Crossing Based QRS-Detection Algorithm for Wearable ECG Sensors. IEEE Journal of Biomedical and Health Informatics 18(1), 183–192 (2014)
89. Biel, L., Pettersson, O., Philipson, L., Wide, P.: ECG analysis: a new approach in human identification. IEEE Transactions on Instrumentation and Measurement 50(3), 808–812 (2001)
90. http://www.primedic.com/cms/upload/produkte/DefiMonitor-EVO_Optionen-1.jpg
91. http://www.google.co.nz/imgres?imgurl=http://www.usc.edu/dept/engineering/summerprograms/assets/001/75386.jpg&imgrefurl=http://www.usc.edu/dept/engineering/summerprograms/anti-theft-device/group-3/anti-theft-device/important-concepts-and-ideas/&h=370&w=452&tbnid=YtwA_0vHgUmprM:&zoom=1&docid=vaJVRl5fTDr7gM&ei=IhL5VJymNYTemAXbzoGICg&tbm=isch&ved=0CB4QMygDMAM&biw=1920&bih=956
92. http://www.intelligent-systems.info/biofeedback/biofeedback.htm
93. Avci, A., Bosch, S., Marin-Perianu, M., Marin-Perianu, R., Havinga, P.: Activity recognition using inertial sensing for healthcare, wellbeing and sports applications: A survey. In: 2010 23rd International Conference on Architecture of Computing Systems (ARCS), pp. 1–10. VDE (2010)
94. http://www.olympic.org/national-olympic-committees
95. http://www.engadget.com/2009/05/26/sensaris-wearable-sensor-promises-to-track-noise-and-air-quality/

96. Suryadevara, N.K., Mukhopadhyay, S.C.: Wireless sensor network based home monitoring system for wellness determination of elderly. IEEE Sensors Journal 12(6), 1965–1972 (2012)
97. Baker, C.R., Armijo, K., Belka, S., Benhabib, M., Bhargava, V., Burkhart, N., Der Minassians, A., et al.: Wireless sensor networks for home health care. In: 21st International Conference on Advanced Information Networking and Applications Workshops, AINAW 2007, vol. 2, pp. 832–837. IEEE (2007)
98. Axisa, F., Schmitt, P.M., Gehin, C., Delhomme, G., McAdams, E., Dittmar, A.: Flexible technologies and smart clothing for citizen medicine, home healthcare, and disease prevention. IEEE Transactions on Information Technology in Biomedicine 9(3), 325–336 (2005)
99. Quigley, R., Taylor, R.: Does watching TV contribute to increased body weight and obesity in children?
100. Suryadevara, N.K., Mukhopadhyay, S.C.: Smart Homes: Design, Implementation and Issues. SIST, vol. 14. Springer, Heidelberg (2015)
101. Mukhopadhyay, S.: Wearable Sensors for Human Activity Monitoring: A Review (2015)
102. Suryadevara, N.K., Mukhopadhyay, S.C., Barrack, L.: Towards a Smart Non-Invasive Fluid Loss Measurement System. Journal of Medical Systems 39(4), 1–10 (2015)
103. Suryadevara, N., Mukhopadhyay, S.: Determination of Wellness of an Elderly in an Ambient Assisted Living Environment, p. 1 (2014)
104. Suryadevara, N.K., Mukhopadhyay, S.C., Wang, R., Rayudu, R.K.: Forecasting the behavior of an elderly using wireless sensors data in a smart home. Engineering Applications of Artificial Intelligence 26(10), 2641–2652 (2013)
105. Suryadevara, N.K., Gaddam, A., Rayudu, R.K., Mukhopadhyay, S.C.: Wireless sensors network based safe home to care elderly people: Behaviour detection. Sensors and Actuators A: Physical 186, 277–283 (2012)
106. Malhi, K., Mukhopadhyay, S.C., Schnepper, J., Haefke, M., Ewald, H.: A Zigbee-based wearable physiological parameters monitoring system. IEEE Sensors Journal 12(3), 423–430 (2012)
107. Bhardwaj, S., Lee, D.-S., Mukhopadhyay, S.C., Chung, W.-Y.: Ubiquitous healthcare data analysis and monitoring using multiple wireless sensors for elderly person. Sensor & Transducer Journal 90, 87–99 (2008)
108. Mukhopadhyay, S.C., Gaddam, A., Gupta, G.S.: Wireless sensors for home monitoring-a review. Recent Patents on Electrical & Electronic Engineering (Formerly Recent Patents on Electrical Engineering) 1(1), 32–39 (2008)
109. Suryadevara, N.K., Kelly, S., Mukhopadhyay, S.C.: Ambient Assisted Living Environment Towards Internet of Things Using Multifarious Sensors Integrated with XBee Platform. In: Mukhopadhyay, S.C. (ed.) Internet of Things. SSMI, vol. 9, pp. 217–231. Springer, Heidelberg (2014)
110. Gaddam, A., Sen Gupta, G., Mukhopadhyay, S.C.: Human Behavior Recognition Technologies: Intelligent Applications for Monitoring and Security. In: Guesgen, H., Marsland, S. (eds.) Sensors for Smart Home, vol. 5, pp. 130–156. IGI Global (2013) ISBN 978-1-4666-3683-5

111. Mukhopadhyay, S.C., Suryadevara, N.K., Rayudu, R.K.: Are Technologies Assisted Homes Safer for the Elderly? In: Mukhopadhyay, S.C., Postolache, O.A. (eds.) Pervasive & Mob. Sens. & Comput. for Healthcare. SSMI, vol. 2, pp. 51–68. Springer, Heidelberg (2012)
112. Nag, A., Mukhopadhyay, S.C.: Smart Home: Recognition of activities of elderly for 24/7; Coverage issues. In: Proceedings of the 2014 International Conference on Sensing Technology, Liverpool, UK, vol. 2, pp. 480–489 (2014)
113. Mukhopadhyay, S.C., Suryadevara, N.K.: Homes for Assisted Living: Smart Sensors, Instrumentation, Energy, Control and Communication Perspective. In: Proceedings of IEEE International Conference on Control, Instrumentation, Energy & Communication (CIEC), Kolkata, India, pp. 9–14 (2014)
114. Suryadevara, N.K., Mukhopadhyay, S.C., Wang, R., Rayudu, R.K., Huang, Y.M.: Reliable measurement of Wireless Sensor Network data for forecasting wellness of elderly at smart home. In: 2013 IEEE International Instrumentation and Measurement Technology Conference (I2MTC), pp. 16–21. IEEE (2013)
115. Survadevara, N.K., Mukhopadhyay, S.C., Rayudu, R.K.: Applying SARIMA time series to forecast sleeping activity for wellness model of elderly monitoring in smart home. In: 2012 Sixth International Conference on Sensing Technology (ICST), pp. 157–162. IEEE (2012)
116. Suryadevara, N.K., Quazi, M.T., Mukhopadhyay, S.C.: Intelligent sensing systems for measuring wellness indices of the daily activities for the elderly. In: 2012 8th International Conference on Intelligent Environments (IE), pp. 347–350. IEEE (2012)
117. Suryadevara, N.K., Mukhopadhyay, S.C., Rayudu, R.K., Huang, Y.M.: Sensor data fusion to determine wellness of an elderly in intelligent home monitoring environment. In: 2012 IEEE International Instrumentation and Measurement Technology Conference (I2MTC), pp. 947–952. IEEE (2012)
118. Quazi, M.T., Mukhopadhyay, S.C., Suryadevara, N.K., Huang, Y.M.: Towards the smart sensors based human emotion recognition. In: 2012 IEEE International Instrumentation and Measurement Technology Conference (I2MTC), pp. 2365–2370. IEEE (2012)
119. Devlin, B.S., Mukhopadhyay, S.C., Sen Gupta, G.: Remote Medical Monitoring Unit. In: Proceedings of ENZCon Conference, Christchurch, New Zealand, November 13-14, pp. 110–115 (2006) ISBN-13: 978-0-473-11779-5, ISBN-10:0-473-11779-7
120. Kim, T., Lee, H., Chung, Y.: Advanced universal remote controller for home automation and security. IEEE Transactions on Consumer Electronics 56(4), 2537–2542 (2010)
121. Lubecke, V.M., Boric-Lubecke, O., Host-Madsen, A., Fathy, A.E.: Through-the-wall radar life detection and monitoring. In: IEEE/MTT-S International Microwave Symposium, pp. 769–772. IEEE (2007)
122. Berezdivin, R., Breinig, R., Topp, R.: Next-generation wireless communications concepts and technologies. IEEE Communications Magazine 40(3), 108–116 (2002)
123. Yu, S.-N., Cheng, J.-C.: A wireless physiological signal monitoring system with integrated bluetooth and WiFi technologies. In: 27th Annual International Conference of the Engineering in Medicine and Biology Society, IEEE-EMBS 2005, pp. 2203–2206. IEEE (2006)
124. Radu, V., Kriara, L., Marina, M.K.: Pazl: A mobile crowdsensing based indoor WiFi monitoring system. In: CNSM, pp. 75–83 (2013)

125. Qu, H., Cheng, J., Cheng, Q., Wang, L.Y.: WiFi-based telemedicine system: signal accuracy and security. In: International Conference on Computational Science and Engineering, CSE 2009, vol. 2, pp. 1081–1085. IEEE (2009)
126. http://www.gammawatch.com/images/Bluetooth-Detector-Concept-Diagram.jpeg
127. http://www.libelium.com/vehicle_traffic_monitoring_bluetooth_sensors_over_zigbee/#prettyPhoto-img9052/0/
128. Haartsen, J.: Bluetooth-The universal radio interface for ad hoc, wireless connectivity. Ericsson Review 3(1), 110–117 (1998)
129. Song, J.-H., Lee, N.-S., Yoon, S.-W., Kwon, S.-W., Chin, S., Kim, Y.-S.: Material tracker for construction logistics. In: Proceedings of the ISARC 2007, Kochi, Kerala, India, pp. 63–67 (2007)
130. Lee, H.J., Lee, S.H., Ha, K.-S., Jang, H.C., Chung, W.-Y., Kim, J.Y., Chang, Y.-S., Yoo, D.H.: Ubiquitous healthcare service using Zigbee and mobile phone for elderly patients. International Journal of Medical Informatics 78(3), 193–198 (2009)
131. Frehill, P., Chambers, D., Rotariu, C.: Using Zigbee to integrate medical devices. In: 29th Annual International Conference of the IEEE Engineering in Medicine and Biology Society, EMBS 2007, pp. 6717–6720. IEEE (2007)
132. Baker, N.: ZigBee and Bluetooth: Strengths and weaknesses for industrial applications. Computing and Control Engineering 16(2), 20–25 (2005)
133. Valente, A., Morais, R., Serôdio, C., Mestre, P., Pinto, S., Cabral, M.: A zigbee sensor element for distributed monitoring of soil parameters in environmental monitoring. In: 2007 IEEE Sensors, pp. 135–138. IEEE (2007)
134. Zhang, Q., Yang, X.-L., Zhou, Y.-M., Wang, L.-R., Guo, X.-S.: A wireless solution for greenhouse monitoring and control system based on ZigBee technology. Journal of Zhejiang University Science A 8(10), 1584–1587 (2007)
135. Lahtela, A., Hassinen, M., Jylha, V.: RFID and NFC in healthcare: Safety of hospitals medication care. In: Second International Conference on Pervasive Computing Technologies for Healthcare, PervasiveHealth 2008, pp. 241–244. IEEE (2008)
136. Korostelev, M., Bai, L., Wu, J., Tan, C.C., Mastrogiannis, D.: Body sensor networks in fetal monitoring with NFC enabled Android devices. In: Proceedings of the 7th International Conference on Body Area Networks, pp. 9–12. ICST (Institute for Computer Sciences, Social-Informatics and Telecommunications Engineering) (2012)
137. Haselsteiner, E., Breitfuß, K.: Security in near field communication (NFC). In: Workshop on RFID Security, pp. 12–14 (2006)
138. Morak, J., Kumpusch, H., Hayn, D., Modre-Osprian, R., Schreier, G.: Design and evaluation of a telemonitoring concept based on NFC-enabled mobile phones and sensor devices. IEEE Transactions on Information Technology in Biomedicine 16(1), 17–23 (2012)
139. Miranda, S., Pastorelly, N.: NFC mobiquitous information service prototyping at the University of Nice Sophia Antipolis and multi-mode NFC application proposal. In: 2011 3rd International Workshop on Near Field Communication (NFC), pp. 3–8. IEEE (2011)
140. Timalsina, S.K., Bhusal, R., Moh, S.: NFC and its application to mobile payment: Overview and comparison. In: 2012 8th International Conference on Information Science and Digital Content Technology (ICIDT), vol. 1, pp. 203–206. IEEE (2012)

141. Opperman, C.A., Hancke, G.P.: A generic NFC-enabled measurement system for remote monitoring and control of client-side equipment. In: 2011 3rd International Workshop on Near Field Communication (NFC), pp. 44–49. IEEE (2011)
142. Yamashita, K., Izumi, S., Nakano, M., Fujii, T., Konishi, T., Kawaguchi, H., Kimura, H., et al.: A 38 μA wearable biosignal monitoring system with near field communication. In: 2013 IEEE 11th International New Circuits and Systems Conference (NEWCAS), pp. 1–4. IEEE (2013)
143. Aziza, H.: NFC Technology in mobile phone next-generation services. In: 2010 Second International Workshop on Near Field Communication (NFC), pp. 21–26. IEEE (2010)
144. Kim, I., Lai, P.-H., Lobo, R., Gluckman, B.J.: Challenges in wearable personal health monitoring systems. In: 2014 36th Annual International Conference of the IEEE Engineering in Medicine and Biology Society (EMBC), August 26-30, pp. 5264–5267 (2014), doi:10.1109/EMBC.2014.6944813
145. McAdams, E., Krupaviciute, A., Gehin, C., Grenier, E., Massot, B., Dittmar, A., Rubel, P., Fayn, J.: Wearable sensor systems: the challenges. In: Conf. Proc. IEEE Eng. Med. Biol. Soc. 2011, pp. 3648–3651 (2011), doi:10.1109/IEMBS.2011.6090614
146. McAdams, E., Gehin, C., Massot, B., McLaughlin, J.: The challenges facing wearable sensor systems. Stud. Health Technol. Inform. 177, 196–202 (2012)
147. Fletcher, R.R., Poh, M.Z., Eydgahi, H.: Wearable sensors: opportunities and challenges for low-cost health care. In: Conf. Proc. IEEE Eng. Med. Biol. Soc. 2010, pp. 1763–1766 (2010), doi:10.1109/IEMBS.2010.5626734
148. http://electroiq.com/blog/2013/04/health-awareness-spurs-quadrupling-in-mems-sensor-market-for-wea/
149. http://www.fitbit.com/nz/about#i.1x3oxveo9hfqu1
150. https://www.google.com/glass/start/
151. http://www.technologyreview.com/featuredstory/532691/google-glass-is-dead-long-live-smart-glasses/
152. http://techcrunch.com/2015/03/04/google-glass-is-alive-and-well-and-living-in-the-enterprise/
153. http://www.tomsguide.com/us/best-smartwatches,review-2156.html

TOTAL HEALTH: Toward Continuous Personal Monitoring

Wenyao Xu[1] and Ming-Chun Huang[2]

[1] Department of Computer Science and Engineering University at Buffalo, The State University of New York (SUNY), NY 14260-2500, USA
wenyaoxu@buffalo.edu
[2] Department of Electrical Engineering and Computer Science at Case Western Reserve University, OH 44106, USA
ming-chun.huang@case.edu

Abstract. Ubiquitous personal monitoring of health is being rapidly developed in recent years. However the concept of pervasive computing in healthcare focuses on individual systems. We propose that Total Health is the transformation of healthcare that aims for complete 24/7 coverage in which no one system can provide. We discuss what are the challenges that come with bringing technology into widespread use. Following this discussion, a selection of current applications in healthcare is presented. These applications use state-of-the-art systems that relate to personal health monitoring with the goal of providing a 24/7 picture of one's health. The key requirements of these systems is that they provide continuous available monitoring, must be as unobtrusive as possible, require as little human intervention as possible, identify and alert health risks, and be cost effective.

1 The Total Health Concept

We begin by defining a number of important concepts and then we describe what Total Health means.

Firstly, Eysenbach [1] defined e-health as:

> *An emerging field in the intersection of medical informatics, public health and business, referring to health services and information delivered or enhanced through the Internet and related technologies. In a broader sense, the term characterizes not only a technical development, but also a state-of-mind, a way of thinking, an attitude, and a commitment for networked, global thinking, to improve health care locally, regionally, and worldwide by using information and communication technology.*

This definition of e-health places the practice of healthcare in-line with the use of electronic systems that is not just limited to Internet technology. For example, e-health can mean the application of electronic health record systems in hospitals, i.e. hospital information systems (HIS), radiological information systems (RIS), picture archive and communications systems (PACS). It in-

S.C. Mukhopadhyay (ed.), *Wearable Electronics Sensors*,
Smart Sensors, Measurement and Instrumentation 15, DOI: 10.1007/978-3-319-18191-2_2

cludes primary care office computerized systems, electronic prescriptions and order entry, and even email systems. Furthermore, telemedicine has been developed significantly such as in teleradiology and telepathology [2], and new applications for remote vital signs monitoring are now seeing increasing favor.

Secondly, we discuss ubiquitous computing, also known as pervasive computing. Mark Weiser first coined the term ubiquitous computing and states the following at the beginning of his influential work [3]:

> *The most profound technologies are those that disappear. They weave themselves into the fabric of everyday life until they are indistinguishable from it.*

His vision listed a number of properties which are summarized here. *Service is present everywhere.* This is the idea of ubiquity, meaning everywhere. A device can either be wearable, or other devices can be available wherever you go. *It is not the device but an environment.* It is not a single device, but a collection of devices that work together to form a service and create the system environment. *The user is not conscious of the device being used.* In contrast with smartphones or laptops that demand the attention of the user, ubiquitous computing devices work for the user in the background. The user, although aware that nearby devices exist, need not actively interact with the devices nor need to worry that the services of the devices are running.

So we are now in a position to state what Total Health means:

> *Total Health strives for complete 24/7 coverage of well-being through the use of ubiquitous computing that focuses on e-Health monitoring, diagnosis, alerting, and action.*

It is the round-the-clock environment of health management and technology utilization with as little human intervention as possible. Devices are required to be as unobtrusive as possible. This means that wireless solutions are preferable over wired solutions. Non-contact sensing is preferred over contact sensing. It is as if technology is not present at all, yet information is gathered and analyzed, results concluded, and a plan of action advised. No one system can provide complete 24-hour coverage, however, the Total Health concept strives for this using complementary systems. Total Health aims for anytime and anywhere health assurance. In later sections, we describe current technology and innovation related to wireless healthcare. Since continuous coverage of personal monitoring requires multiple systems, we identify the issues and gaps between systems, and we describe how Total Health could be achieved.

2 Why Total Health Is Important?

Healthcare costs are a major portion of the US gross domestic product, current estimates by OECD are approximately 17% of GDP [4]. This is the highest in the world; most developed nations have their healthcare spending between 7 - 11% of GDP. Not only is the US healthcare spending at a very

high level, it has been increasing since the beginning of the recorded data in 1960's. There are many reasons why this is so: the population is aging, utilization of health services is increasing, more advanced technology is used, labor resources are not increasing at the same rate as usage, insurance costs escalates with liability issues, and so healthcare is getting more expensive [5].

Chronic illness accounts for 78% of the total US healthcare spending [6]. From the 2004 US in-patient cost estimates on Medicare by the Agency for Health Quality Research, Healthcare Cost and Utilization Project, the five most costly of the chronic diseases in the US are: coronary artery disease ($39.6 billion), heart failure ($19.8 billion), mental health disorders ($11.4 billion), chronic obstructive pulmonary disease ($8.2 billion), and diabetes ($7.4 billion) [6]. These staggering amounts lead many to believe that much of the costs are preventable.

> *Approximately 95% of the $1.4 trillion that we spend as a nation on health goes to direct medical services, while approximately 5% is allocated to preventing disease and promoting health.* [7]

The vast majority of the expenses is being incurred on prolonged hospital stays and managed care after which the chronic conditions have progressed past any turning point. Only 5% is spent on prevention. If many of these conditions are prevented earlier in the cycle by detecting occurrences of key indicators or proactively monitoring high-risk patients, then a major portion of the healthcare costs will be eliminated. It is clear that chronic conditions currently are not being managed correctly. Even treatment at any earlier stage will reduce some of the costs.

Unfortunately, the current medical environment is one of reactive action and it is too late in many cases. By that point, the costs have escalated into the hundreds of thousands of dollars per patient. Some studies have shown up to 40% reduction in hospital admissions, 67% reduction in mortality and 62% reduction in bed days of care [8].

One solution is to provide as much out of hospital care as possible. This could be in the form of trained health care providers that operate outside of the hospital and are focused on personalized home-based care. Unfortunately this would not address the ever increasing health bill, since the current labor force would be stretched thin and in turn require more and more people to be trained in healthcare. By adding more people, the total expense for healthcare would increase.

The other and more reasonable solution would be relying on technology. Technology can provide monitoring services not only within hospital environments but also at home. Current research has focused on many approaches to home-based remote monitoring. User initiated measurement devices such as weight scales and blood pressure monitors are one form of technology that have been wirelessly connected to monitoring systems. More ubiquitous systems such as those that are smartphone-based are also included in these solutions. These types of systems are not location dependent and professional

medical help can be contacted when needed or, ideally, professional medical help will contact the patient when pending danger occurs.

Such Total Health systems are complementary to the traditional forms of healthcare services and are not intended to replace them. The overall goal is to improve the quality of healthcare while reducing the costs. To this end, the strategy of moving the healthcare process toward the patient for in-home care, relying more on the patient's own personal needs and control, actually promotes active, healthy living style. In the end, Total Health improves the overall quality of life.

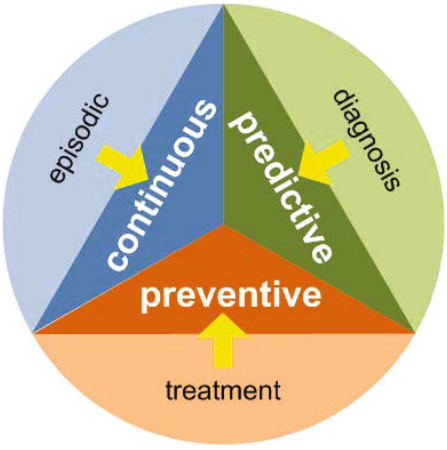

Fig. 1 Transformation of Healthcare Environment

Not only are there cost benefits and reductions in the need for ongoing medical interventions, but also these continuous systems improve the compliance of medical condition management. It is estimated that up to $100 billion is wasted due to poor medical adherence [9]. Continuous health management systems can address some of the problems with non-compliance. With automatic analysis tools, pertinent data can also be presented to the user about health issues. Furthermore, mobile communication with healthcare providers can provide current monitored data as well as important alerts.

So, the goals of Total Health are:

- Use ubiquitous technology for sensing, monitoring, analyzing, and communicating to effectively manage healthy living.
- Be available 24/7.
- Be as unobtrusive as possible. Be as comfortable as possible.
- Require as little human intervention as possible.
- Identify important indicators of possible health risk.
- Provide information to the user or medical providers about health alerts.
- Be cost effective. Reduce costly and unnecessary medical services that are common with current healthcare practices.

3 What Is the Impact?

It is important to realize that the change to Total Health is a cultural and sociological change. It requires a change in people's thinking, a change in one's idea of healthcare control, and a change in responsibility. The current landscape of healthcare has a limited supply of healthcare providers and they are usally overwhelmed by the process of information collection. It is a reactive environment in which action is taken after significant events occur. However, a shift in the process will allow physicians to concentrate on providing the medical expert care at the right time [5]. Continuous remote monitoring of the patient takes much of the load away from doctors. The focus toward patient monitoring will relieve much of the work of the healthcare professional. It requires a paradigm change toward user responsibility and pre-emptive action. Continuous and ubiquitous healthcare systems provide a promising answer to today's medical questions.

The impact of Total Health is a three-fold transformation in the healthcare environment: (1) from episodic examination to continuous monitoring; (2) from disease diagnosis to disease prediction; (3) from reactive treatment to pre-emptive prevention. Figure 1 summarizes this change in healthcare. Currently episodic patient examination only captures snapshots of the health status of individuals. Total Health aims for continuous coverage of healthcare. Currently, a disease is only diagnosed if a patient has a health complaint and makes a visit to a healthcare professional. The focus of healthcare change aims to move the analysis toward prediction. Once conditions have been diagnosed in patients, reactive treatment plans are prescribed. However, often this is too late. We must strive for pre-emptive prevention of medical condition. There are existing steps toward pre-emptive prevention, such as early screenings for breast cancer and prostate cancer, however there is more that can be done.

4 What Are the Challenges of Total Health?

The goals of Total Health are ambitious and there are many factors that contribute to its future success. Bott et al. describe some of the challenges in bringing ubiquitous computing to healthcare [10]. Adams and Brown note some ethical issues involved in continuous monitoring of patients [11]. Little and Briggs discuss real survey responses about the main concerns of shared personal data [12]. In this section, we summarize some of the challenges of bringing Total Health to all, with the focus on technological issues.

Continuous patient monitoring generates a considerable amount of raw data which leads to storage problems and information overload. If the data is stored in the device, then it creates an issue of memory storage. If the data is to be sent remotely to physicians, then there is a huge demand on the communication process. Data size can be reduced by periodic sampling; however,

this requires to be balanced with the continuous monitoring requirements of the system. Periodic sample will reduce both the local storage requirements of the device as well as communication requirements.

Other types of applications do not require raw data at all; instead, an analysis or summary of the data is used. In other applications, anomaly detection is done. In these situations, local device processing of the data is performed, and then the results are logged or transmitted.

Questions that are raised about data management are about how reliable and accurate the data process can be. Certainly errors do creep into systems, but how tolerant of errors should systems be? Issues such as the reliability of data and even of data transmission to physicians need to be considered by implementers and users of these systems. During medical emergencies, it is critical that systems can communicate with medical providers and also with time constraints. There are issues with mobility of systems. Ideal systems should work indoors and outdoors, as well as moving between mobile network cells.

One issue that could severely hamper the widespread adoption of remote monitoring is the health risk associated with the radiation effects of wireless technology. The World Health Organization and the International Agency for Research on Cancer has recognized that "radiofrequency electromagnetic fields as possibly carcinogenic to humans" [13]. To this end, wireless technology aims at lowering the power consumption of mobile communication and has the benefit of improving the battery life of the mobile devices.

One of the major challenges in remote mobile devices is the use of conventional batteries which are heavy, rigid, and do not last long. More research needs to be done in developing batteries which are light, flexible, and easily chargeable [14]. The transformation toward pro-active monitoring requires better power supply management and longer battery life.

In all of the above situations, there is always the consideration of costs to implement and costs to maintain. We have discussed the need to reduce the overall healthcare spending, but it mandates that the change in technology and labor will be low cost. This is the assumption, however, there is no up-to-date reports on real financial improvements.

The rate of adoption to change in technology is remarkably slow in the medical industry. Compared to banking, such as in online account management, electronic medical records have been slow to gain widespread use. Healthcare has lagged behind other industries in electronic records keeping. There are many reasons for this. The cost of moving to electronic data management is high and only larger institutions are able to absorb the costs. Private practices and small communities cannot justify the expenditure. Healthcare workflow is not easily standardized or amenable to electronic formats. So, the healthcare environment is possibly set for a dramatic change in lifestyle.

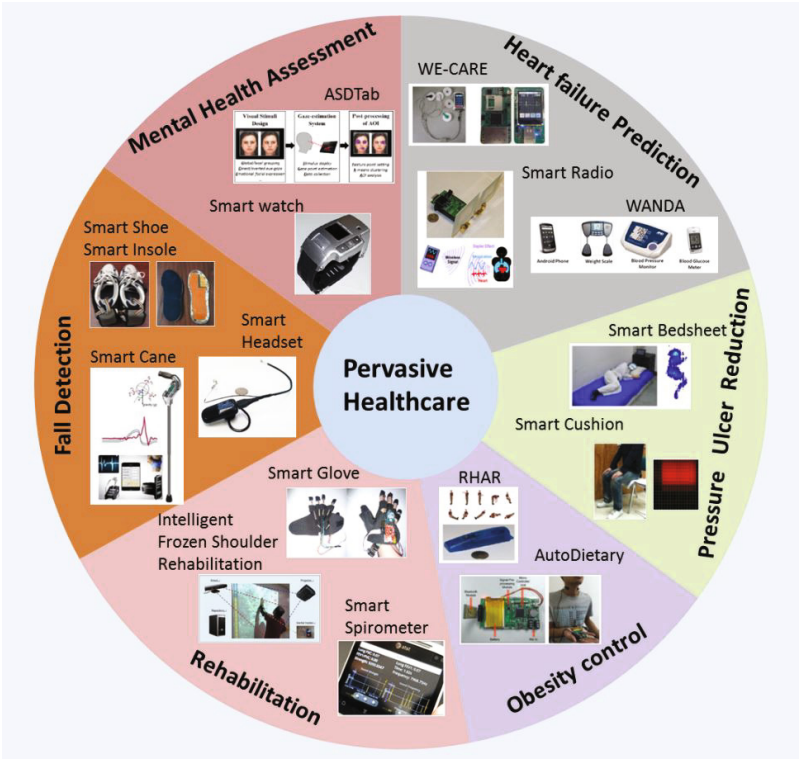

Fig. 2 Applications of Total Health

5 Total Health Applications

In this section, we detail a selection of medical applications where continuous monitoring systems will affect the change toward better human health. There are many more applications that will see huge benefits that are not described here. Figure 2 shows five applications that have seen promising system developments: heart failure, pressure monitoring, fall detection, mental health assessment, and applications for rehabilitation.

Within each application, there could be a number of systems that work together to provide complete coverage. Each of the systems can be broadly categorized [15] into:

- Mobile devices: devices that are portable such as smart phones, tablets, PDAs, and even laptops.
- Wearable items: devices that can be a part of clothing or e-textile, or devices that are strapped to the body.
- Stationary devices: devices such as sensors embedded or mounted in furniture, building walls, or fixed structures.

Although there has been a lot of development and good applications for implantable devices, such as pacemakers, defibrillators, diabetic implants, we shall not include such devices in this paper due to their invasiveness.

The following subsections introduce current development as well as relevant applications for the technology. We also identify the challenges in bringing the systems to widespread use. No one system can effectively satisfy all the requirements of Total Health. A combination of systems would work to complement each other. We also discuss the gaps and overlaps in the systems.

5.1 Heart Failure Prediction

Cardiopulmonary signals are the most important human biomarkers and have many important medical implications, especially for chronic health conditions such as heart diseases, chronic obtrusive pulmonary disorders (COPD) disease and diabetes. A significant portion of that cost comes from the expense of monitoring patients and transferring the recorded data to physicians.

A technology that is currently being investigated is a Doppler radar to measure human vital signs [16]. It is a non-contact autonomous vital sign monitoring system, called Smart Radio (Figure 3). Based on Doppler theory, this economic and lightweight Doppler-radar system senses chest wall movement and heartbeat, which are highly correlated to respiratory rate and heart rate. This enables wireless vital sign measurements that are completely unobtrusive and can pass through clothing. Compared to traditional vital sign measurement instruments, Smart Radio is easier to deploy and more convenient to use due to the non-contact sensing and auto-calibration scheme.

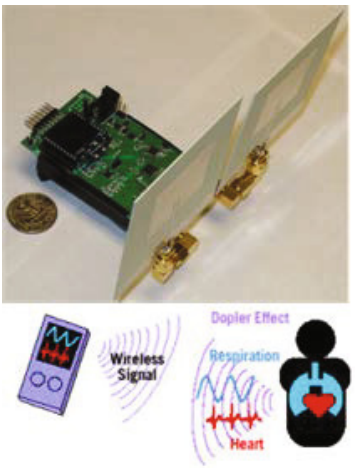

Fig. 3 Smart Radio [16]

Cardiovascular disease is the No. 1 cause of death in the past 30 years. Longitudinal monitoring on heart status is important for heart failure patients. WE-CARE [17](see Figure 4) is an online risk-monitoring systems which measures ECG signals to offer real-time risk monitoring. For the sake of the sustainability of use, a compressed sensing based technique is fed into the system to reduce power consumption. This research product has been approved by Ministry of Health (MOH) in China and under evaluation by thousands of heart failure patients.

Fig. 4 WE-CARE [17]

Suh *et al.* developed a remote patient monitoring system called WANDA to monitor subjects post-surgically who had suffered congestive heart failure [18]. The system integrates weight scales, blood pressure monitors, blood glucose meters, and cell phones via Bluetooth (Figure 5). Once all patient data has been measured, the information is communicated automatically over cell phone networks to servers located on the Internet where the data is analyzed by health professionals. Complete history of the patients is stored in databases and any anomalies can be detected and the patient notified immediately. Many of the large medical device companies are offering their own versions of remote patient monitoring such as Philips' Telestation, Bosch's Health Buddy, and Honeywell's Genesis DM.

The systems do rely on daily action by the patient, but give them reminders to use the monitors when overdue. The cost benefit is realized when a single medical provider can monitor a group of patients under their care. Early detection of problems is referred to specialized care before major problems

Fig. 5 WANDA [18]

occur and avoid expensive re-hospitalizations. The process of remote patient monitoring is becoming increasingly used and the range of applications is expanding from heart monitoring (e.g. chronic heart disease) to diabetes, hypertension, and lung disease (e.g. chronic obstructive pulmonary disease).

An important part of these systems is feedback and education. It is generally known that feedback of progress is a good method of continued encouragement. These systems also provide education through multimedia and online coaching. The current trend is availability of information. All of the above systems have methods to communicate data into cloud networks typically through cell phone networks to the Internet. Data can be stored in personalized electronic health record systems that can provide a complete longitudinal record of the patient's medical history. Medical professionals to provide the best ongoing healthcare can access this information, if they obtain required authorization.

5.2 Pressure Ulcer Reduction

E-textile sensors can record biometric data during the day while patients wear such devices as WE-CARE, and at night they are monitored by Doppler technology in their beds, this would be a good step toward Total Health. The gaps could be the current ECG recording requires direct skin contact sensors, so further research needs to be done in finding non-contact ECG recording. In fact, non-skin contact sensors have been developed [19]. These sensors can be attached to clothing and can detect changes in the electrical field around the patient. The sensors need not be attached directly to the skin. This one significant advance toward Total Health since placing sensors on clothes is less obtrusive that directly on the skin.

E-Textile sensors applied in Smart Cushion system for dedicated underhip pressure analysis while sitting. Xu *et al.* [20] developed a dynamic time warping based algorithm to recognize different sitting postures base on Smart Cushion.

Sleep plays a pivotal role in the quality of life, and sleep posture is related to many medical conditions such as pressure ulcers. A pressure-sensitive bed sheet system provides an unobtrusive method for sleep posture monitoring and sleep analysis [21]. Further application is on-bed physical rehabilitation for those who are recovering from surgery or for the bed prone.

Although this system is not mobile, it is hoped to be cost effective enough for it to be widely distributed, less than $1,000. For comfort the bed sheet feels like a regular bed sheet, and does not require wearable devices for monitoring. The combination of radar-based vital sign measurement, Smart Radio, and pressure sensitive bed sheet enables comprehensive monitoring of patients during their sleep.

Fig. 6 Smart Cushion

Fig. 7 Smart Bedsheet

5.3 Fall Detection

Annually, 1.8 million older adults are treated for falls, which results in $20 billion in direct costs in 2008 [22, 23]. A lightweight smart shoe and supporting infrastructure aims at gait and human balance monitoring. This system comprises accelerometers, compass, and pressure sensors mounted within shoe insoles with built-in Bluetooth communication to cell phones [24, 25, 26]. This system monitors walking behavior and uses instability assessment to classify various types of activity. Due to the challenge power consumption, an energy-efficient adaptive sensing was proposed which can effectively reduce the number of samples required per frame and still keep good signal quality

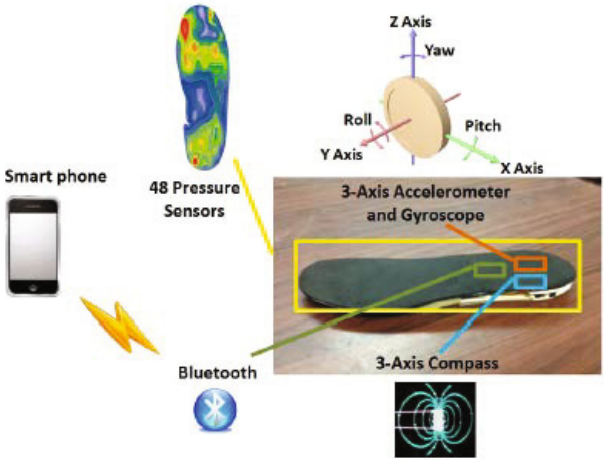

Fig. 8 Smart Insole

and gait parameters [26]. An important application of this technology is to determine fall risk and identification of episodes as precursors to instability. For mainstream use, the cost of smart insoles need to be viable, currently the estimated manufacturing cost is under $200 with further research being continued.

For applications, such as activity monitoring, the smart insole captures a record of a person's activity. This is beneficial for obesity analysis and general fitness. Other applications are pressure ulcers that develop especially for diabetics. The smart insole can analyze the pressure distribution of a person's foot and generate alerts for prolonged pressure points.

Smart Headset is a lightweight EEG signal sensing and analysis devices, and it can calculate the level of concentration of users while walking. Intelligence also has been built into an assistive device like the smart cane [27]. The smart cane is design to monitor and predict situations of high falling risk. The same technology is employed in smart crutches. Having to use crutches does not occur frequently for most people, and the proper use of crutches requires a balanced amount of pressure. Pressure sensors can give the best feedback to the user.

5.4 Mental Health Assessment

Autism spectrum disorder (ASD) is a neurodevelopmental disorder defined by atypicalities in three major symptom domains: communication, social interaction and behavior [28]. Children with ASD have impaired social interaction, impaired verbal and non-verbal communication, and restricted, repetitive or stereotyped behavior, which may result in lifelong disabilities. These disorders

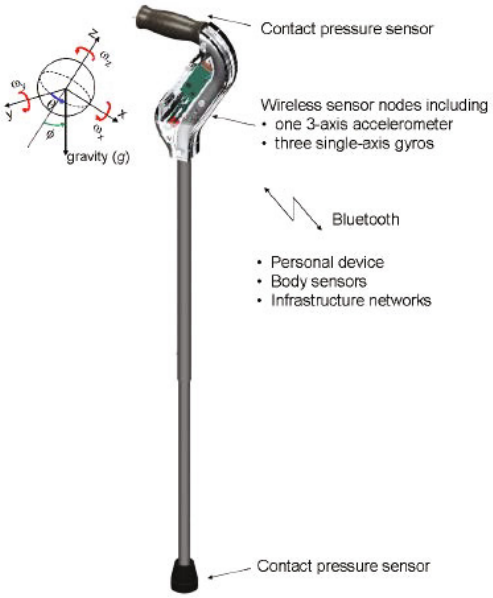

Fig. 9 Smart Cane [27]

both across and within individuals present particular challenges for autism diagnosis and treatment. ASDTab, a novel in-home ASD assessment tool, mainly comprises three parts, as show in Figure 15: (1) Visual Stimuli Design, (2) Gaze Estimation System and (3) Data Post-processing. ASDTab implements a highly-accurate eye-tracking and collects the gaze points of the child which means the impression of the interest areas of the child, it is important for ASD diagnosis.

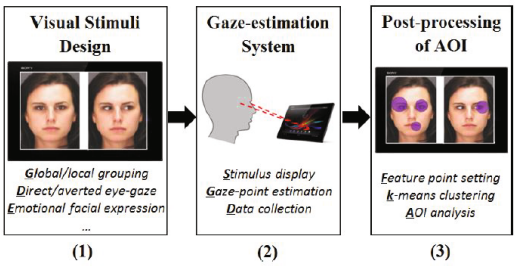

Fig. 10 ASDTab system mainly involves three parts: (1) Visual Stimuli Design; (2) Gaze-point Estimation; (3) AOI (area-of-interest) Detection

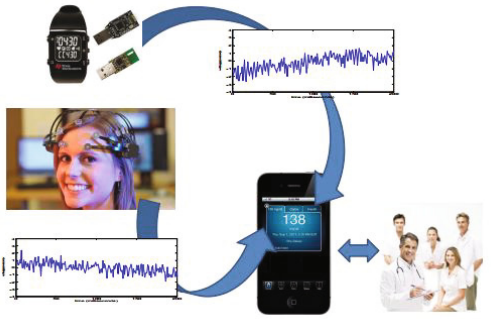

Fig. 11 Smartphone Monitoring for Management of Parkinson's Disease [29]

Fig. 12 Smart Watch for Dementia Patients [30]

Parkinson's Disease (PD) is a disabling neurodegenerative disease affecting millions of people worldwide. Teresa *et al.* [29] developed a system for portable monitoring of Parkinsonism based on EEG signal features and advanced techniques for monitoring human movement from gyroscopes and accelerometers.

Dementia means cognitive impairment that makes functioning in daily life more difficult in the older population. A Smart Watch System was developed for dementia patients to improve their health and safety [30]. The smart watch system includes a wristwatch-type device and server system. The device includes a built-in GPS, ambient light sensor, acceleration sensor, and to communicate with the server system. The system can create a personal profile for patients and monitor the location, motion through the amount of light and step count.

5.5 Obesity Control

Nutrition-related diseases are nowadays a main threat to human health and pose great challenges to medical care. A crucial step to solve the problems

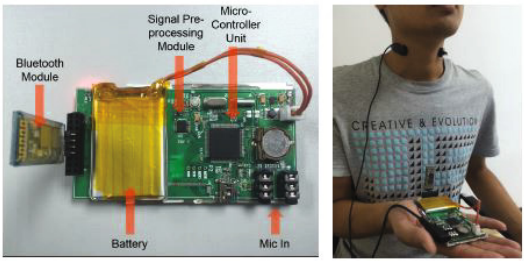

Fig. 13 AutoDietary [31]

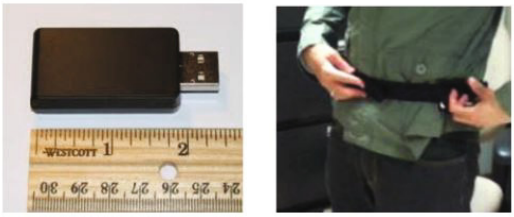

Fig. 14 Motion sensor for Activity Recognition [32]

is to monitor the daily food intake of a person precisely and conveniently. AutoDietary [31](see Figure 13), a wearable system to monitor and recognize food intakes in daily life, is developed to collect food intake sensor data, which is highlighted by a high-fidelity microphone worn on the subject's neck to precisely record acoustic signals during eating in a non-invasive manner. The corresponding application on the smartphone which aggregates the food intake recognition results in a user-friendly way and provides suggestions on healthier eating, such as better eating habits or nutrition balance.

Wearable sensors, specifically inertial sensors, continue to be used in activity recognition systems and devices. Alshurafa *et al.* [32] designed a robust activity recognition framework for health and exergaming using wearable sensors. The application is a novel exergaming environment aimed at using games to reward physical activity performed throughout the day, to encourage a healthy lifestyle.

5.6 Rehabilitation

People with stroke often need physical therapy services to improve stroke symptoms or retain functionality and independence with daily activities. SmartGlove consists of five-finger bending sensors and is a finger angle extraction device which is packaged in an easy-to-wear and adjustable manner for a patient with an upper extremity rehabilitation progress [33].

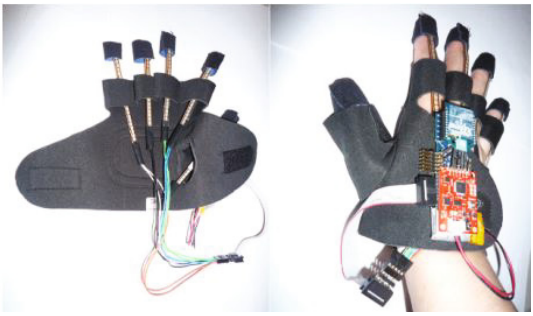

Fig. 15 Smart Glove [33]

Fig. 16 Smart Spirometer [34]

Smart Spirometer (See Figure 16) is a mobile-phone based platform to measure lung function parameters (FEV1, FVC, PEF), which are critical clinic evidences for CPOD, asthma, and cystic fibrosis diagnosis. Taking advantage of the existing built-in microphone in every phone, this system modeled the microphone frequency-domain response on airflows and has the function of accurate lung function measurement. Moreover, to increase patient-compliance for breathing exercise, this system has a phone video game for daily respiration exercise and training [34].

Frozen shoulder is a common condition characterized by painful and limited range of motion. Using interactive technologies can help patients complete the exercises crucial to their rehabilitation. Huang *et al.* [35] created a virtual reality game-based treatment system that encourages patients to participate in regular rehabilitation. Vision and inertial sensors are used to collects patient ROM data during the game tasks for further analysis.

For people with imbalance and vestibular dysfunction issues, this study used VR video games that adopted Cawthorne&Cooksey exercises and machine learning-based classifiers as a balance assessment tool [36]. The objective of this

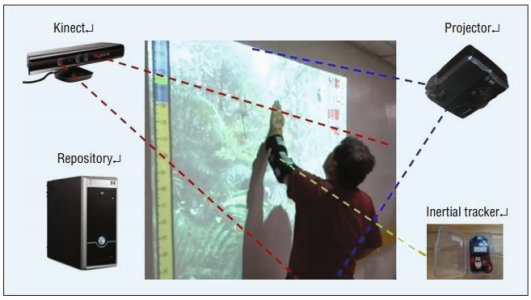

Fig. 17 Intelligent Frozen Shoulder Rehabilitation System [35]

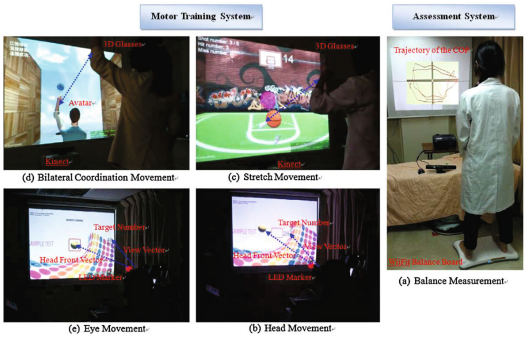

Fig. 18 Imbalance and Vestibular Dysfunction Rehabilitation System [36]

study is to validate a VR system that can be used for balance rehabilitation. The consistent findings between the performance data and balance assessment measurements suggest that this VR game-based exercise may be applicable to the clinical assessment and rehabilitation of people with vestibular dysfunction.

6 Conclusion

This paper presented the concept of Total Health. It is clear that complete health monitoring is the way forward. In fact, remote patient monitoring devices had the fastest growth in yearly revenue of any medical device sectors and the US market will be worth $20 billion in 2016 [37]. The future of healthcare will see a boom in patient-controlled out-of-hospital monitoring, with personal health data shared with the patient's healthcare provider. There is much hope that continuous and ubiquitous healthcare systems will supply a solution for today's healthcare situation. However, this will require a transformation of the current concept of healthcare.

References

1. Eysenbach, G.: What is e-health? J. Med. Internet Res. 3(2), 20 (2001)
2. Krupinski, E., Nypaver, M., Poropatich, R.: Telemedicine/telehealth: An international perspective. clinical applications in telemedicine/telehealth. Telemed. J. E Health 8(1), 13–34 (2001)
3. Weiser, M.: The computer for the 21st century. SIGMOBILE Mob. Comput. Commun. Rev. 3(3) (July 1999)
4. Organisation for economic co-operation and development (2012), http://www.oecd.org/
5. Enabling ubiquitous patient monitoring: Model, decision protocols, opportunities and challenges. Decision Support Systems 46(3), 606–619 (2009)
6. I. E.-H. Committee, Chronic care improvement: How medicare transformation can save lives, save money, and stimulate an emerging technology industry. ITAA E-Health White paper (2004)
7. Steps to a healthier u.s. washington (dc): Office of public health promotion. U.S. Department of Health and Human Services (2001), http://www.healthierus.gov/steps/steps_brochure.pdf
8. Dang, S., Dimmick, S., Kelkar, G.: Evaluating the evidence base for the use of home telehealth remote monitoring in elderly with heart failure. Telemedicine and e-Health 15, v (2009)
9. Cocosila, M., Archer, N., Yuan, Y.: Mobile healthcare for adherence: Business considerations. Mednet, Toronto, Canada, pp. 13–20 (October 2006)
10. Bott, O., Ammenwerth, E., Brigl, B., Knaup, P., Lang, E., Pilgram, R., Pfeifer, B., Ruderich, F., Wolff, A., Haux, R., Kulikowski, C.: The challenge of ubiquitous computing in health care: technology, concepts and solutions. findings from the imia yearbook of medical informatics. Methods Inf. Med. 44(3), 473–479 (2005)
11. Adams, A.A., Brown, I.: The ethical challenges of ubiquitous healthcare. International Review of Information Ethics 8, 53–60 (2007)
12. Little, L., Briggs, P.: Ubiquitous healthcare: do we want it? In: Proceedings of the 22nd British HCI Group Annual Conference on People and Computers: Culture, Creativity, Interaction, BCS-HCI 2008, Liverpool, United Kingdom, vol. 2, pp. 53–56 (2008)
13. World health organization/iarc (2011), http://www.iarc.fr/en/media-centre/pr/2011/pdfs/pr208_E.pdf
14. Khosla, A.: Smart garments in chronic disease management: progress and challenges. In: Proc. SPIE 8548, Nanosystems in Engineering and Medicine, pp. 85 482O–85 482O–8 (2012)
15. Orwat, C., Graefe, A., Faulwasser, T.: Towards pervasive computing in health care - a literature review. BMC Medical Informatics and Decision Making 8(1), 26 (2008)
16. Huang, M.-C., Liu, J.J., Xu, W., Gu, C., Li, C., Sarrafzadeh, M.: A self-calibrating radar sensor system for measuring vital signs. IEEE Transactions on Biomedical Circuits and Systems (2015)
17. Huang, A., Xu, W., Li, Z., Xie, L., Sarrafzadeh, M., Li, X., Cong, J.: System light-loading technology for mhealth: Manifold-learning based medical data cleansing and clinical trials in we-care project. IEEE Journal of Biomedical and Health Informatics (JBHI) 18(5), 1581–1589 (2014)

18. Suh, M.-K., Chen, C.-A., Woodbridge, J., Tu, M., Kim, J., Nahapetian, A., Evangelista, L., Sarrafzadeh, M.: A remote patient monitoring system for congestive heart failure. Journal of Medical Systems 35, 1165–1179 (2011)
19. Chi, Y., Cauwenberghs, G.: Wireless non-contact eeg/ecg electrodes for body sensor networks. In: 2010 International Conference on Body Sensor Networks (BSN), pp. 297–301 (June 2010)
20. Xu, W., Huang, M.-C., Amini, N., He, L., Sarrafzadeh, M.: ecushion: A textile pressure sensor array design and calibration for sitting posture analysis. IEEE Sensors Journal 13(10), 3926–3934 (2013)
21. Liu, J.J., Xu, W., Huang, M.-C., Alshurafa, N., Sarrafzadeh, M.: A dense pressure sensitive bedsheet design for unobtrusive sleep posture monitoring. under review IEEE International Conference on Pervasive Computing and Communications (2013)
22. Centers for disease control and prevention, `http://www.cdc.gov/HomeandRecreationalSafety/Falls/fallcost.html`
23. Stevens, J., Corso, P., Finkelstein, E., Miller, T.: The costs of fatal and nonfatal falls among older adults. Injury Prevention 12, 290–295 (2006)
24. Noshadi, H., Ahmadian, S., Hagopian, H., Woodbridge, J., Dabiri, F., Amini, N., Sarrafzadeh, M., Terrafranca, N.: Hermes - Mobile Balance and Instability Assessment System. In: Proc. BIOSIGNALS, pp. 264–270 (2010)
25. Xu, W., Huang, M., Amini, N., Liu, J., He, L., Sarrafzadeh, M.: Smart insole: A wearable system for gait analysis. In: PETRAE (2012)
26. Xu, W., Wu, Y., Liu, J., Huang, M., Luan, S., Lee, Y.: An energy-efficient adaptive sensing framework for gait monitoring using smart insole
27. Wu, W., Au, L., Jordan, B., Stathopoulos, T., Batalin, M., Kaiser, W., Vahdatpour, A., Sarrafzadeh, M., Fang, M., Chodosh, J.: The smartcane system: an assistive device for geriatrics. In: Proceedings of the ICST 3rd International Conference on Body Area Networks, BodyNets 2008 (2008)
28. Wing, L., Gould, J.: Severe impairments of social interaction and associated abnormalities in children: Epidemiology and classification. Journal of Autism and Developmental Disorders 9(1), 11–29 (1979)
29. Sanders, T.H., Devergnas, A., Wichmann, T., Clements, M.A.: Remote smartphone monitoring for management of parkinson's disease. In: Proceedings of the 6th International Conference on PErvasive Technologies Related to Assistive Environments, p. 42. ACM (2013)
30. Shin, D.-M., Shin, D., Shin, D.: Smart watch and monitoring system for dementia patients. In: Park, J.J.(J.H.), Arabnia, H.R., Kim, C., Shi, W., Gil, J.-M. (eds.) GPC 2013. LNCS, vol. 7861, pp. 577–584. Springer, Heidelberg (2013)
31. Bi, Y., Xu, W., Guan, N., Wei, Y., Yi, W.: Pervasive eating habits monitoring and recognition through a wearable acoustic sensor. In: 8th International Conference on Pervasive Computing Technologies for Healthcare (PervasiveHealth 2014), Oldenburg, Germany, pp. 1–4 (May 2014)
32. Alshurafa, N., Xu, W., Liu, J.J., Huang, M.-C., Mortazavi, B.J., Sarrafzadeh, M.: Designing a robust activity recognition framework for health and exergaming using wearable sensors. IEEE Journal of Biomedical and Health Informatics (JBHI) 18(5), 1636–1646 (2014)
33. Huang, M.-C., Xu, W., Su, Y., Lange, B., Chang, C.-Y., Sarrafzadeh, M.: Smartglove for upper extremities rehabilitative gaming assessment. In: Proceedings of the 5th International Conference on Pervasive Technologies Related to Assistive Environments, p. 20. ACM (2012)

34. Xu, W., Huang, M.-C., Liu, J.J., Ren, F., Shen, X., Liu, X., Sarrafzadeh, M.: Microphone-based spirometer for copd diagnosis and exergame design. In: International Conference on Pervasive Technologies Related to Assistive Environments (PETRA 2013), Rhodes Island, Greece, pp. 45–52 (May 2013)
35. Huang, M.-C., Lee, S.-H., Yeh, S.-C., Chan, R.-C., Rizzo, A., Xu, W.: Intelligent frozen shoulder rehabilitation using virtual reality
36. Machine learning-based assessment tool for imbalance and vestibular dysfunction with virtual reality rehabilitation system. Computer Methods and Programs in Biomedicine 116(3), 311–318 (2014)
37. Kalorama information, http://www.kaloramainformation.com/Remote-Wireless-Patient-6487095/

A Novel Biometric Algorithm to Body Sensor Networks

Sandeep Pirbhulal[1,2], Heye Zhang[1,2], Wanqing Wu[1,2,*], and Yuan Ting Zhang[1,2,3]

[1] Institute of Biomedical and Health Engineering, Shenzhen Institutes of Advanced Technology, Chinese Academy of Sciences, Shenzhen, China
[2] The Key Laboratory for Health Informatics of the Chinese Academy of Sciences at Shenzhen Institutes of Advanced Technology, Shenzhen, China
[3] Research Centre for Biomedical Engineering, Chinese University of Hong Kong, Hong Kong
{sandeep,wq.wu,hy.zhang}@siat.ac.cn

Abstract. In Body Sensor Networks (BSN) several sensor nodes are attached on, inside or around human body to monitor vital sign signals such as, Electrocardiogram (ECG), Electroencephalogram (EEG), Blood pressure etc. The information from each sensor node is very significant; therefore privacy and security is very important during data transmission in BSN. The conventional cryptographic approaches make use of cryptographic keys to achieve authentication, and use of these keys not only require high resource utilization and computation time, but also consume large amount of energy, power and memory in BSN. Therefore, it is necessary to develop power efficient and less computational complex authentication technique for BSN. In this paper we design a novel biometric algorithm which is based on biometric feature Electrocardiogram (ECG) and uses Data Authentication Function (DAF) for the security of BSN instead of utilizing traditional key generation procedure. Our proposed algorithm is compared with two cryptographic authentication techniques, Data Encryption Standard (DES) which is symmetric or private-key based encryption technique and RSA (Rivest Shamir Adleman) which is asymmetric or public-key based encryption scheme. Simulation is performed in MATLAB and results explain that our algorithm is efficient in terms of transmission time utilization and average remaining energy.

Keywords: Body Sensor Network, Biometric, Electrocardiogram (ECG), Heart Rate Variability (HRV), Security.

1 Introduction

These days Wireless Sensor Networks (WSNs) technology has attracted vast attention in different domains. Wireless Body Area Networks (WBANs) or BSN is

* Corresponding author.

S.C. Mukhopadhyay (ed.), *Wearable Electronics Sensors*,
Smart Sensors, Measurement and Instrumentation 15, DOI: 10.1007/978-3-319-18191-2_3

very important application of WSNs for healthcare monitoring, which is the wireless network of different in-body, on-body and around-body associated sensor nodes. The general BSN architecture is demonstrated in Fig.1, it contains three parts as presented in S. D. Bao, et.al [1]. In the first part, BAN-Coordinator receives the vital and unique information from each sensor node, that data is the real time information of human body such as heart rate, Electrocardiogram (ECG), temperature,blood pressure, etc. That physiological data from all subjects is stored at sink (may be cellular device or PDA) and deliver that information to remote server in second part. The third part allows access to the concerned doctor or authorized person from server.

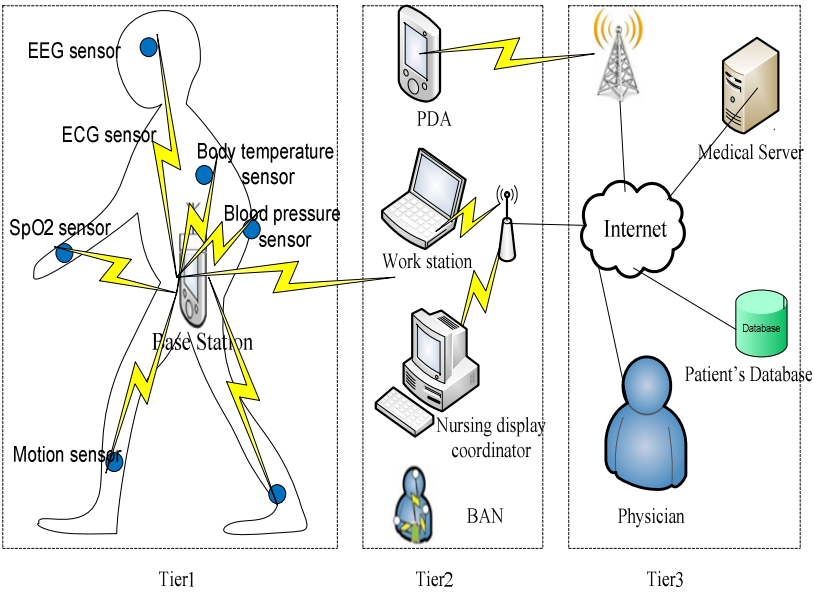

Fig. 1 Body Sensor Network Architecture [9]

The BSN is the best way for telemedicine and m-health but as sensor nodes carry very vital information, therefore data privacy is one of the major aspects in these networks. Along with privacy, data security is also the important factor. Only authorized person should access the information generated by nodes, therefore security should be implemented in all aforementioned parts of system. However, due to small size and their energy constrained nature security is very important in BSN as discussed in H. Wang, et.al [2]. Whereas, each human body has different behavior, that is why it will be difficult for attacker to hack the data. Therefore features of human body can be used to implement security in BSN.

Biometric technology is automatic detection of persons in the behavioral or physiological traits. In our research we used electrocardiogram (ECG) as a biometric characteristics. The heart beats of human body produce electrical signals

continuously and collection of these electrical currents are termed as ECG. The ECG is a unique individual trait, whereas its properties completely depend on human body and heart beats. To become ensure about ECG as a biometric feature, it is essential to know ideal biometric characteristics [3-5], as shown in Table.1.

In sensor networks many security protocols with symmetric as well as asymmetric keys are employed to obtain privacy, reliability and accuracy during data transmission C. S. lang, et.al [6]. Whereas, the BSN is the different from other ad-hoc networks because of interference in body mobility and inadequate computing resources of human body, therefore simple and efficient authentication and confidentiality techniques are very important in BSN.

Several symmetric key-based encryptions techniques have been introduced in last decade for BSN. S.D.Bao,et.al in [7], designed a symmetric key based approach , they claim that their approach is efficient to secure BSN during data transmission, but only one private key is used in whole BSN, therefore if any sensor node is compromised then private information will no more be secure as presented in C. William, et.al [8]. One solution to overcome that problem is to use multiple keys in BSN, if any one key is disclosed it will not affect the security of network. By introducing multiple keys, key management is very complex during encryption and decryption. Therefore many protocol such as; SSL (Secure Sockets Layer) utilizes private key approach during data transmission.

Table 1 Ideal biometric trait properties [16]

Property Name	**Detail**
Universal	Almost acquired by all or major portion of population hold
Unique	Two individuals have enough difference for identification
Everlasting	Having ability to not to change with respect to time
Measurable	convenient to obtain for an individual technically
Efficient	provide high-quality performance in terms of speed, accuracy with limited resource utilization
Adequate	acceptable to human i.e. patient as well as organization to utilize as an identifier
Unassailable	quite complicated to recreate by fake acts

In asymmetric public key encryption different keys are used for both encryption and decryption. On the one hand, it has advantage over symmetric cipher of multiple keys utilization, through this way level of security and privacy can be increased. However, on other hand these techniques are resource constrained as explained in C. C. Y. Poon, et.al [4]. Therefore asymmetric cipher is not

cost-efficient and feasible solution for BSN. Whereas, some researchers introduce the hybrid approach for symmetric and asymmetric to increase the security and privacy in BSN. C. S. lang, et.al [6], presents a hybrid technique in a more effective way to implement authentication, integrity and confidentiality, all these conventional approaches are based on public or private keys to secure human body information in BSN.

However, wavelet-domain HMM (Hidden Markov Model) based approach to secure BSN in H. Wang, et.al [2], increases the performance of network because it does not require synchronization and generation of external keys. When physiological and behavioral characteristics are used instead of external keys to implement security in WBAN is referred as biometric based authentication [10][11], they used human body features as generation of multiple keys for entity identification to implement security and privacy in WBAN during data transmission. This biometric based security increases reliability, provides rapid action and cost efficient solution as compared to conventional cryptographic key-based authentication. Therefore in modern research biometric characteristics are utilized for implementing security in WBAN.

In [12], S.D.Bao, et.al designed architecture of BSN and model to implement security by using physiological feature of human body. They used collective approach of wireless channel as well as bio-channel for data authentication. F.Miao, et.al in [13] used ECG as biometric triat to secure BSN, they used AES (Advanced Encryption standard) to generate keys from ECG for data integrity, data authentication and privacy between source and destination. The major drawback of their research was that their technique was based on asymmetric key based, which is not energy efficient and cost-effective solution.

The Physiological Signal based Key Agreement (PSKA) scheme is proposed in K. K. Venkat, et.al [14]; it uses Fuzzy vault logic between source and destination for key synchronization. In their research encoding of key is done with polynomial on source and at destination decoding procedure is utilized based on chaff points to restructure the key. There are two problems associated with that technique i) if key size is small, hacker can guess key by brute force attacks, ii) if key size is large, destination will require high computational cost for polynomial due to availability of used chaff points. In [15], GH Zhang, et.al introduced fast method to generate key from biometric feature ECG, hamming distance is used to find interval between any two generated keys. The randomness and uniqueness of keys are measured to check the accuracy of theses keys. In S. Cherukuri, et.al [16], the authors put forward a security strategy for BSN; their approach provides inexpensive and easy method for data transmission. According to S. D. Bao, et.al in [1], the IPI (Inter Pulse Interval) can be used as biometric trait for entity identification to obtain security in BSN. Lin Yao,et.al in [17], develop a data integrity and data confidentiality technique for BSN in which ECG is utilized as a biometric trait for key generation and encryption. Their research presents Syverson-van Oorschot (SVO) logic for correction and verification of results, as that technique performs well in security implementation, but is less power efficient and requires a lot of time for data authentication due to computational

complexity. Shu-Di-Bao, et.al [18], proposes Inter-pulse intervals (IPI) from ECG and Photo-plethysmogram (PPG) as biometric characteristics to accomplish security in WBAN. They support the performance of their protocol with false rejection rate and false acceptance rate. Their research claims accurate security model for WBAN, but due to complexity involved during key generation process in their designed scheme it does not provide cost efficient and energy efficient solution for data authentication in BSN.

The IPI of biometric feature PPG is used for generation of distinctive keys is studied by G. H. Zhang, et.al [19], furthermore; these keys were applied for synchronization between source and destination to execute security in WBAN. The matchless and difficult algorithm used for key generation in this paper, guarantees that accurate authentication can be obtained. However, computational complexity is the major drawback of their research, because high cost, energy and power are required to implement this technique in WBAN. S. N. Ramli, et.al [20], designs a biometric based model; it uses Message Authentication Protocol (MAC) as a key for authentication between source and destination, and omits complex key generation methods for implementing authentication in BSN. The MAC is based on R-Peak detection and Heart Rate Variability (HRV) calculation of physiological feature ECG. Their work does not discuss energy efficiency as well as power efficiency.

One of the major problem in all aforementioned research is that they used different security techniques, algorithms and models such as, PSKA based fuzzy logic, SVO etc, these all are based on key generation mechanism, which is complex and time consuming procedure, also their research do not discuss energy efficient and power efficient security approach for BSN. To remedy all these problems, we propose a novel unique algorithm based on ECG as biometric trait in which Data Authentication Function (DAF) is presented and difficult key generation procedures are excluded to secure BSN. DAF consists three basic parts; detection of QRS-complex, HRV calculation and authentication protocol. The authentication protocol is the ratio of Low Frequency-to-High Frequency ratio, and it is acting as key between source and destination to implement security in BSN. However, to further increase the security hashing algorithm SHA1 is used to hide original message before its transmission.

Rest of the paper is organized as follows. In section 2 motivation is presented, section 3 presents proposed algorithm, section 4, section 5 and section 6 include performance analysis, simulation environment and simulation and results respectively, finally paper is concluded in section 7.

2 Motivation

Body area networks (BANs) seamlessly connect miniaturized and low-power devices and biosensors that are worn on or implanted in human body. The development of BANs is emerging as one of the main research trends, particularly to collect and jointly process biological data for continuous and long-term

monitoring of health conditions. Since medical and health data are private and sensitive information that are protected by law in many countries, for example, by the Health Information and Portability Accountability Act (HIPAA) in the USA, the European Union Directive 2002/58/EC in Europe, and Law of the People's Republic of China on Medical Practitioners in China, the security of data transmission within BANs must be addressed in order for them to be widely used in real-life health applications. Although BANs share some common features with generic wireless sensor networks (WSNs), it is anticipated that the two networks should have very different security schemes [21]. WSNs have many constraints, such as low computation capability, small memory, and limited energy resources, and the security issues of them have been previously addressed in literatures. SPINS is a suite of security protocols optimized for sensor networks, where the base station accesses nodes using source routing. Differed from SPINS, Undercoffer et al. [22] proposed another protocol that relies upon broadcasts and provides a mechanism for detecting certain types of aberrant behaviours. TinySec is the first fully implemented link layer security architecture for WSNs. It generated secure packets by encrypting data using a group key shared among sensor nodes and calculating a message integrity code (MIC) for the whole packet, including the header. These security methods those were proposed or implemented for WSNs are not optimal, if not impractical, for BANs, which require a security solution that consumes even less energy and memory space than generic WSNs [21].

A unique feature of this solution is the generation of random keys by physiological data (i.e. a biometric approach) for securing communication. Our research aims to produce cost efficient (by offering less computational complexity and low resources utilization), time efficient (by requiring less transmission time for processing as complex keys are being omitted), energy and power efficient (by demanding less energy and power consumption) as well as accurate authentication model for BSN. The beauty of our algorithm is that it eradicates conventional procedure of key generation and uses biometric feature i.e. ECG as authentication protocol to secure transmission between nodes in BSNs.

3 Proposed Algorithm

In our research, we extended the work of S. N. Ramli, et.al [20], the block diagram of our proposed algorithm for data authentication in BSN is shown in Fig. 2. The authentication protocol mentioned in Data Authentication Function (DAF), is acting as a key, once this key matches between source and destination than message can be transmitted. In case receiver does not match statistically, transmission will not get start and message will be discarded as shown in demonstrated in Fig. 2.

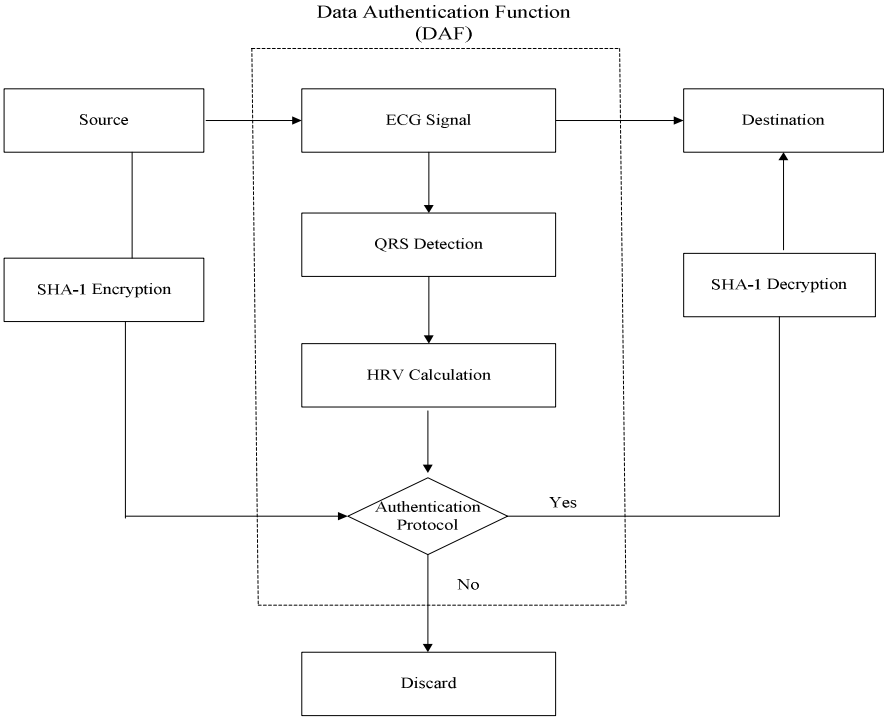

Fig. 2 Block diagram of Biometric-based Proposed Algorithm

Our proposed algorithm is simple because it eliminates the use of complex key-based techniques. As in BSN those methods not only require high computational cost for keys management and its distribution, but also consume a lot of time, energy and power during data transmission. Although by using DAF, data reliability and accuracy can be achieved, but to increase the level of security before sending patient's data to DAF for authentication, our proposed algorithm utilizes SHA-1 hashing scheme for encryption of original message. This hashing technique is very simple, easy to apply and less complex in managing keys, therefore it provides low cost encryption.

3.1 Data Authentication Function (DAF)

The Data Authentication Function (DAF) is shown in Fig.2, which includes three main parts; QRS detection; HRV calculation; and authentication protocol. The authentication protocol used in DAF is responsible to make decision either to transmit data to destination or discard the message initiated from source. ECG is used as biometric trait for authentication in our proposed algorithm.

3.1.1 Wearable System for Biosignal Collection

Electrical considerations for the system platform are driven by its use model. It must perform at least as well as commercially available devices, with a small and comfortable form factor. It must be able to record ECG continuously for at least one week. Dry noncontact electrodes work based on the capacitive coupling between the skin and the conductive disc which leads to the polarization of the electrode, causing displacement current to flow for a while. The proposed capacitive coupling based is composed of a conductive textile fabric electrode, clothes and the skin of the subject, as shown in Fig.3. To achieve strong capacitive coupling, we can increase the area of contact, use a thin insulator layer or include an insulator with a high dielectric constant. Dry noncontact electrodes are sensitive to motion artifacts, but show better behavior in terms of decreased skin irritation.

We design a measuring device to extract ECG signal from a textile electrode (Fig. 1). The measuring device of ECG and breathing signal is constructed using filtering and amplification circuit, and its block diagram as shown in Fig.1. The device consisted of a common part and a differential separation filter for sensing ECG signal and breathing activity respectively. The common part was composed of two buffers, which functioned as an impedance of the capacitive coupling with low impedance required by the subsequent circuitry. Operational amplifier ICs with high input resistance were used in the present study. The differential separation filter described in the subsection A and a driven-right-leg (DRL) circuit. The differential separation filter separated the input signal into high frequency component containing ECG signal (>1Hz) and low frequency component including breathing signal (<1Hz). The separation filter was constructed of two sets of subtracter, amplifiers and integrators. The book diagram in circuit was employed in order to reduce common mode noise mainly due to power line interference.

The differential separation filter separated the input signal into sets of subtracters, amplifiers and integrators according to DC suppression circuit. The part for sensing ECG signal consisted of an instrumentation amplifier, a high-pass filter(HPF), a low pass filter(LPF) and two inverting amplifiers. The circuit elements of the HPF and the LPF were designed in order to obtain a cutoff frequency of 5 and 40Hz, respectively. Although electrocardiograph for diagnostic purpose requires a bandwidth from 0.01 to 100Hz, we narrowed the bandwidth of the developed part for obtaining breathing activity. And the part for sensing breathing signal is constructed of a high-pass filter (HPF of 0.1Hz).

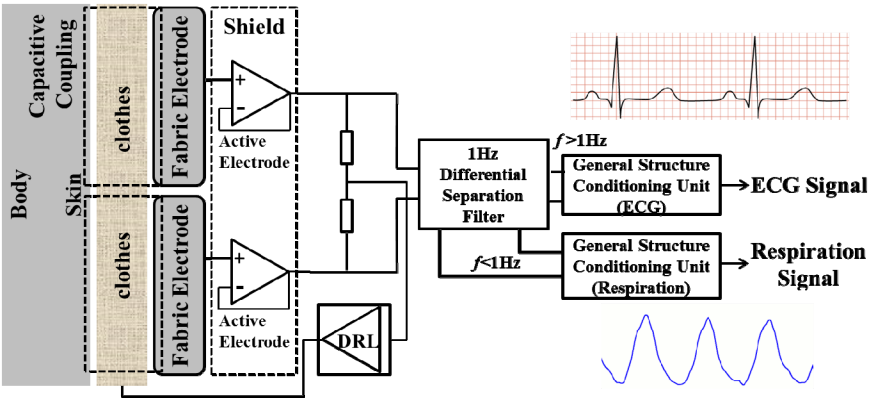

Fig. 3 Block diagram of capacitive measurement system

3.1.2 HRV-Calculation

Software platform is responsible for extracting bio-information from raw data and for calculating the corresponding characteristic parameters of the bio-signal to provide HRV based key for the proposed algorithm. Physiological signals are usually weak and easily corrupted by various kinds of noise (power line interference, electrode contact noise, baseline drift, instrumentation noise, motion artifacts, electrosurgical noise, and other less significant noise sources), which cannot be filtered completely by the hardware platform. Therefore, a digital 60-Hz notch filter for minimizing the power line interference, a finite impulse response (FIR) band-pass filter for correcting baseline wander, a multi-scale mathematical morphology (3M) filter for eliminating motion artifacts and power line interference, and a differential operation method (DOM) for smoothing and normalizing have been integrated into the software. In order to measure the HRV, an adaptive QRS detect algorithm, which was easy to implement on a simple, real-time device developed by our laboratory in a previous study, has been adopted to extract RR interval series for HRV analysis, with 99.3% detection rate. The calculated time domain(Mean RR, SDNN, rMSSD, pNN50), frequency domains (VLF, absolute and normalized LF, HF, total power), geometric (TINN, HRV TI) and nonlinear measures (Poincare plot, Detrended fluctuation analysis) of HRV are obtained according to the standards of measurement, proposed by the Task Force of the European Society of Cardiology and the North American Society of Pacing and Electrophysiology, which describes the detail of physiological correlates of HRV and calculation methods.

3.1.3 Autentication Protocol

The LF/HF ratio approach is used for decision either data transmission will be carried out or not. It will act as key, if source and destination both matches by authentication protocol then original information generated from sender can be

transmitted to receiver. But before sending data to DAF, this data is encrypted by using low cost hashing algorithm to increase the level of security.

There are two methods to evaluate HRV. The first one is evaluation of HRV in time domain by investigating ECG's RR intervals chain. However, second method is based on frequency domain analysis of ECG, in which same spectrum of identical RR intervals are analyzed. The frequency domain approach has following benefits in comparison with time domain approach

i) Their results could be presented with the absolute value (magnitude) of variability as power spectrum function.
ii) Same spectrum of identical RR intervals is analyzed, and it decomposes chain of successive RR intervals as addition of functions of sinusoidal with different frequencies and amplitudes.
iii) The frequency specific fluctuations of signals can be studied by analyzing its power spectrum or frequency
iv) The spectral analysis displays fluctuations of heart rate at different frequencies, Fast Fourier Transformation (FFT) and Autoregressive modelings (AR) are renowned methods for its analyzing.

Due to these advantages, we prefer to use frequency domain approach to measure efficiency of our proposed algorithm. For conventional HRV measurements, there are three spectral components are explained [23]; a) Very Low Frequency (VLF) b) Low Frequency (LF) c) High Frequency (HF). The VLF component has range of 0.0 to 0.04 Hz and it is related to not fast regulatory methods. The range of LF component is 0.04 to 0.15 Hz; it is useful for reflecting sympathetic activity. The reflecting vagal activity is performed at HF components having range of 0.15 to 0.4Hz. The ratio between LF and HF is utilized to specify steadiness between both components of Autonomic Nervous System (ANS) action; the sympathetic and parasympathetic. The heart rate is increased and decreased by sympathetic and parasympathetic respectively. Further, statically calculated index of LF and HF can be used to calculate which factors are important for autonomic misbalance. Therefore, this ratio is utilized as authentication protocol in our proposed algorithm to reduce the computational complexity so to provide efficient approach to secure BSN.

3.1.4 DAF Algorithm

The algorithm 1 explains how DAF (Data Autentication Function) is generated by using MATLAB. It involves three basic parts QRS detection, HRV calculation and authentication protocol. In our algorithm, Pan and Tompkins approach [24-25] is used for QRS detection based on three steps: Linear filtering, non-linear transformation and threshold detection. The linear filtering is based on differentiation which is basically high-pass filtering process. It amplifies higher frequencies that are characteristic for the QRS- complex and attenuates lower

frequencies that are characteristic for P and T deflections. Consider $r[n]$ is the input raw ECG signal, and $O[n]$ is the output of linear filtering, which is the linear combination of $d_1[n]$ and $d_2[n]$, first derivative and second derivative of $r[n]$ respectively. The non-linear transformation is achieved by the combination of squaring operator and moving windows integration .The squaring operator $s[n]$ as shown in eq. (4) gives optimal output by squaring $O[n]$. In QRS complex, it performs suppression, if any difference arises due to P and T deflections and also enhances amplitude of high frequency components. The $y(n)$ represents moving window integration, it helps to make output from squaring operator further smooth. The threshold detection is essential step to discover the QRS-complex. For all value of i, where i is the number of heart beats or ECG signals involved in the ECG waveform, if outputs of non-linear transformation $y[n]$ is greater than or equal to the predetermined threshold all these outputs will be termed as QRS-complex. Once the QRS-complex is detected, next step is to determine the R-Peak, just by finding the absolute value or index of QRS-complex. In ECG, Q-to-Q intervals are the time intervals between successive heart beats during whole QRS-complex; they are also normally termed as RR intervals. However, FFT is used to determine power density spectrum by using a hanning windows (H), then we can find VLF, LF and HF. Finally, LF/HF ratio is used as authentication protocol.

3.2 Low Cost Encryption

In our research, we use SHA-1 as low cost encryption technique to increase level of authentication. Although DAF can provide authentication but for extra security, less expensive and flexible encryption technique is used in proposed algorithm as shown in Fig.2. The SHA-1 stands for Secure Hash Algorithim-1. It produces 20 bytes or 40 hexadecimal digits hash value, because it implements security in many applications and protocols, few are enlisted here Secure Sockets Layer (SSL), Internet Protocol Security (IPSec), Secure Shell (SSH) and Transport Layer Security (TLS). It is very simple and cost-effective because it does not require high resources for encryption and decryption. The proposed algorithm provides unique, accurate and efficient technique to secure BSN and its authentication is verified twice; i) by using DAF, and ii) by low cost encryption. Our designed algorithm is simple and effective and based on LF/HF ratio, as authentication protocol for implementing security in BSN.

Algorithm 1. Data Authentication Function

$$
\begin{aligned}
&Algorithm\ Parameters\\
&r[n] \rightarrow raw\ ECG\ signal\\
&d_1[n] \rightarrow first\ derivative\ of\ r[n]\\
&d_2[n] \rightarrow second\ derivative\ of\ r[n]\\
&O[n] \rightarrow output\ linear\ filter(r[n])\\
&s[n] \rightarrow squaring\ operator\\
&y(n) \rightarrow moving\ window\ integeration\ output\\
&F \rightarrow output\ of\ FFT\\
&PSD \rightarrow Power\ Spectral\ Denisty\\
&HF \rightarrow High\ Frequency\\
&LF \rightarrow Low\ Frequency\\
&VLF \rightarrow Very\ Low\ Frequency\\
&a_p \rightarrow authentication\ protocol\\
&Step\ \#\ 1: Linear\ filtering\\
&d_1[n] \rightarrow diff(r[n])\\
&d_2[n] \rightarrow diff(d_1[n])\\
&O[n] \rightarrow d_1[n] + d_2[n]\\
&Step\ \#\ 2: Non-linear\ transformation\\
&s[n] \rightarrow \{O[n]\}^2 \rightarrow apply\ squaring\ operator\\
&y(n) \rightarrow \frac{1}{N}[s(n-(N-1)) + s(n-(N-2)) + \ldots\ldots\ldots + s(n)]\\
&(perform\ moving\ window\ integeration)\\
&Step\ \#\ 3: Threshold\ Detection\\
&Thershold \rightarrow \{max(y[n]) - mean(y[n])\} / 2\\
&For \rightarrow i = 1:1:b\\
&(whereas\ "b"\ is\ nunber\ of\ heartbeats\ or\ ECG\ signal\ sin\ ECG\ waveform)\\
&if \rightarrow y[n] >= Thershold\\
&QRS \rightarrow y[n]\\
&end\\
&end\\
&R-Peak\ Detection\\
&R = index(QRS)\\
&whereas R \rightarrow R-Peak\\
&For \rightarrow i = 1:1:QRS\\
&RR \rightarrow RR_{i+1} - RR_i, whereas\ RR \rightarrow RR\ interval\\
&end\\
&end\\
&Step\ \#\ 4: HRV\ Calculation\\
&i)\ Apply\ FFT\\
&F \rightarrow fft(N, H)\\
&whereas N \rightarrow index\ of\ RR, H \rightarrow hanning\ windows\\
&A = absolute(F)\\
&ii)\ Calculate\ PSD\\
&PSD \rightarrow autocorrelation(A)\\
&iii)\ output\ of\ PSD, will\ be \rightarrow VLF, LF\ and\ HF\\
&Step\ \#\ 5: Autentication\ protocol\\
&Determine \rightarrow a_p\\
&a_p \rightarrow LF\ /\ HF
\end{aligned}
$$

4 Performance Analysis

The block diagram of our proposed algorithm is shown in Fig.2, uses authentication protocol in DAF as key to achieve security in BSN, no external keys are required for data authentication; this advantage leads our algorithm toward simplicity in comparison with other traditional cryptographic approaches. However, key management and its distribution make conventional methods more complex and ineffective.

In symmetric encryption conventional schemes, only single key is used for both encryption and decryption; there are two main reasons to cause high transmission time in these approaches. Firstly, unique keys are generated for different rounds from initial key such as in 64bits DES original key, from which other 8 different keys of size 56 bits are generated. Secondly, they support only fix block size of data such as 64 bits for DES. If data is more than 64 bits, it must be divided into multiples of 64, and data is transmitted in multiple rounds.

However, for asymmetric encryption process, even more complex and time consuming algorithm is utilized for key generation and data transmission. RSA is one of the examples of public-key encryption, which uses public and private keys for encryption and decryption respectively.

To explain the efficiency of our proposed algorithm for data authentication in BSN, simulation environment with real-time data of several patients was created and parameters used in performance analysis are shown in Table 2. We used real time ECG data of 20 years old female patient, which is received by associated sensor on his body. The length of this ECG data is 258decimal values in different matrix format, and each decimal value is equal to 36 bits which means overall length in binary is 9216 bits.

In our proposed algorithm, if authentication protocol i.e. ratio of LF/HF ratio, matches between source and destination then all 9216bits will be transmitted in one round, this is the main reason to make our proposed protocol efficient. Whereas, this is not true for DES and RSA, because DES only support block size of 64bits and in RSA message of one decimal (i.e. 36 bits) value can be transmitted at a time.

a) Transmission Time

The transmission time is the amount of time required for data transmission from source to destination. It depends upon the number of rounds involved during transmission. As number of rounds increases; transmission time will increase as shown in eq. (1).

$$t = N_r \times k \tag{1}$$

Whereas t represents total transmission time, and N_r demonstrates number of rounds and complexity involved per round is denoted by k. For our proposed algorithm , $N_r = 1$ because all data is transmitted in one round, if key matches between source and destination, authentication protocol in DAF is acting as key. Due to this reason proposed algorithm requires less transmission time in data transmission, so is simple and cost-effective for implementing security in BSN.

For DES, number of rounds depends upon the initial key size and length of data generated from source. The number of rounds is directly proportional to length of data and inversely proportional to initial key size. In eq. (2) L_b, K_i represents length of data in bits and initial key size in bits, respectively.

$$N_r = \frac{L_b}{K_i} \tag{2}$$

In our simulation L_b is 9216 bits and K_i is 64 bits for DES, therefore N_r will be 144 rounds

$$N_r = \frac{L_b}{K_i} = \frac{9216}{64} = 144$$

The overall number of keys required for all rounds (N_k) depends upon N_r and keys required per round (Kr) as shown in eq. (3).

$$N_K = N_r \times Kr \tag{3}$$
$$N_K = 144 \times 8 = 1152$$

It can be visualized that DES uses 144 rounds and 1152 keys in order to achieve authentication, also this complex calculation takes longer transmission time as compared to our proposed algorithm. For RSA, number of rounds N_r equal to the length of data in decimal (L_d), in our simulation L_d is 258, therefore N_r is also 258. As transmission time depends upon number of rounds and complexity involved per round, in both conditions RSA requires more time to process complete data than our proposed algorithm and DES. Because for our proposed algorithm. DES and RSA N_r =1, N_r =144 and N_r =258, respectively.

b) Average Remaining Energy

Let E_i is the initial energy of source and destination for data transmission. The amount of energy consumed is proportional to the transmission time, larger the time required for processing; more the energy consumed. To check whether our proposed algorithm is energy efficient or not, it is necessary to determine the average remaining energy of nodes. The eq. (6) calculates average remaining energy of nodes; where, E_{rs} and E_{rd} represents remaining energy of source and destination, respectively; which depends upon data length (L_d), data rate (D) and transmitting /receiving power (T_x / R_x) as shown in eq. (4) and eq. (5).

$$E_{rs} = \sum_{j=1}^{N} [(E_i)_{(j-1)} - (T_x \times L_d / D)] \quad (4)$$

$$E_{rd} = \sum_{j=1}^{N} [(E_i)_{(j-1)} - (R_x \times L_d / D)] \quad (5)$$

$$E_{ar} = (E_{rs} + E_{rd}) / 2 \quad (6)$$

The value of E_{ar} is high for our proposed algorithm, because it requires less time for processing. Therefore, it can be said that proposed algorithm consumes less energy than DES and RSA, because it requires less transmission time than conventional methods.

c) Power Utilization

Our proposed algorithm is also power efficient, because utilization of power depends upon energy consumption and transmission time. As we explained earlier that our proposed algorithm utilizes less energy and time for data transmission, hence it can be stated that less power will be utilized to secure BSN. The amount of power utilized (P_u) can be measured by any one of following equations

$$P_u = \frac{1}{t} \sum_{i=1}^{N} [2 \times E_{(i-1)} - \frac{L_d}{D}(T_x + R_x)] \quad (7)$$

The algorithm 2 represents the performance analysis of our proposed algorithm, in which M represents the original transmitted from source, C is the cipher text generated after applying low cost encryption, where as S and D are the source and destination respectively. The authentication protocol a_p is the ratio between LF and HF, if it matches between S and D, then transmission will be started. After data transmission, total transmission time, average remaining energy and power utilization, t , E_{ar}, P_u are calculated to evaluate the performance of proposed algorithm.

5 Simulation Environment

MATLAB is used in our simulation. It is assumed that initial energy is 1 joule for both source and destination. It is considered that transmission power, receiving power and data rate as -25dbm, -95dbm and 256Kbps, respectively. A comparative analysis of proposed algorithm based on ECG as biometric trait and two conventional cryptographic security approaches; Data Encryption Standard (DES) which is symmetric or private-key based encryption technique and RSA (Rivest Shamir Adleman) which is an asymmetric or public-key based encryption method. In this research real time data of ECG from physioNet including two data bases; MIT-BIH Normal Sinus Rhythm Database (nsrdb) and MIT-BIH long-Term ECG Database (ltdb) was used. Overall we have analyzed ECG data of 20 patients in between age of 20 to 80.

Table 2 List of abbreviations used in performance analysis

Abbreviation	Detail	Abbreviation	Detail
t	total simulation time	L_b	data length in binary
k	complexity per round	E_i	Initial energy
N_r	number of rounds	E_{rs}	Remaining energy from source
N_k	overall keys required for all rounds	E_{rd}	remaining energy for destination
Kr	number of keys required per round	E_{ar}	average remaining energy
K_i	initial key size	T_x	transmission power
L_d	data length in decimal	R_x	reception power
D	data rate	P_u	Power utilized

Algorithm 2. Performance Analysis

```
Alg orithm parameters
M → orignal message
C → ciephertext
S → sourcenode
D → destinationnode
a_p → autenticationprotocol
LF / HF → LowFrequencytoHighFrequencyRatio
Ear → Average Remaining Energy
P_tr → TotalPower Required
t → TransmissionTime
Step # 1 : Low cost Encryption
C → E(M)
Step # 2 : DataTransmissionand Reception
i) Stranmits → C
ii) if → S.a_p = D.a_p
whereas, a_p → LF / HF
Drecieves → C
DdecryptsCtogetback → M, whereasM = D(C)
end
Step # 3 : PerformanceEvaluation
i) Determine → t
ii) Determine → E_ar
iii) Determine → P_tr
```

6 Experimental Results

The Fig.4 represents ECG waveform of 20 years old subject (female). The grid interval used in this waveform is 0.2 seconds and amplitude is 0.5 mV, a 12-bit Analog-to-Digital converter sampling at 128Hz frequency is used to get digital signal. The RR-interval representation at different time durations of mentioned subject is shown in Fig. 5, this time interval is distance between two consecutive R-peaks. The Figs.5 (a), 5(b) and 5(c) exploit the RR-interval for time duration of 1minute, 1hour and for complete wave respectively. The Fig.6 demonstrates histogram of RR-interval for different time durations. The Figs.6 (a), 6(b) and 6(c) explain histogram for RR-interval representation for time duration of 1minute, 1hour and for complete wave, respectively.

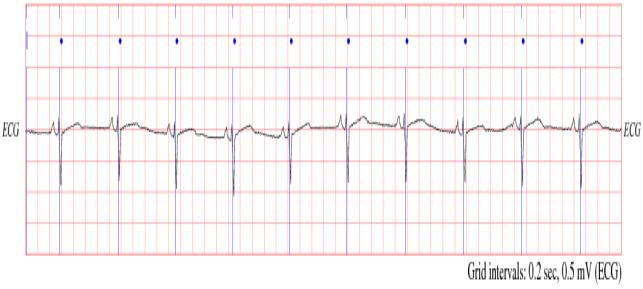

Fig. 4 ECG waveform of 20years female patient

The RR-intervals are further used to determine HRV by using different time domain as well as frequency domain approaches. The ratio LF/HF is used as authentication protocol between source and destination in our proposed algorithm to provide efficient solution to secure BSN as shown in Figs. 7, 8 and 9. Our proposed algorithm eliminates the need of complex key generation procedure, which is more cost-effective and efficient approach that existing techniques for data authentication in BSN as shown in Table 3. Fig.7 shows total amount of transmission time required for proposed algorithm, DES and RSA is 0.214 ms, 3.40ms and 6.40 ms respectively. From results it can be analyzed that proposed algorithm consumes less time than traditional cryptographic techniques during transmission. In parallel with more transmission time consumption, the key generation procedure for two cryptographic techniques consumes more resources, such as, transmission time execution. Fig.8, shows the average remaining energy of our proposed algorithm, DES and RSA of 0.998 joules, 0.963 joules and 0.932 joules respectively. The implementation of proposed algorithm is simple and easy than DES and RSA, therefore it requires less time and energy than both conventional techniques. Total power consumed by proposed algorithm, DES and RSA during data transmission is 9.64mW, 10.05mW and 10.10mW respectively, as shown in Fig.9. Hence, we can say that our proposed algorithm is power-efficient than DES, and RSA.

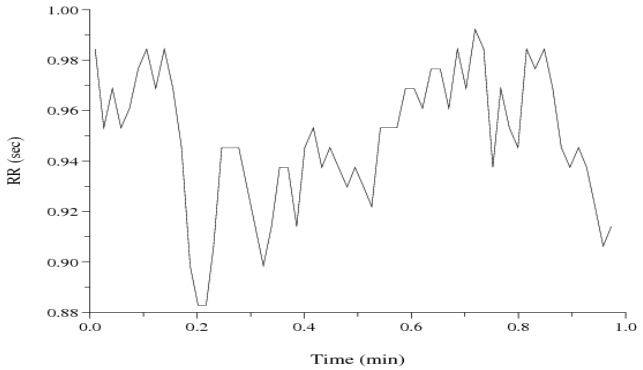

(a)

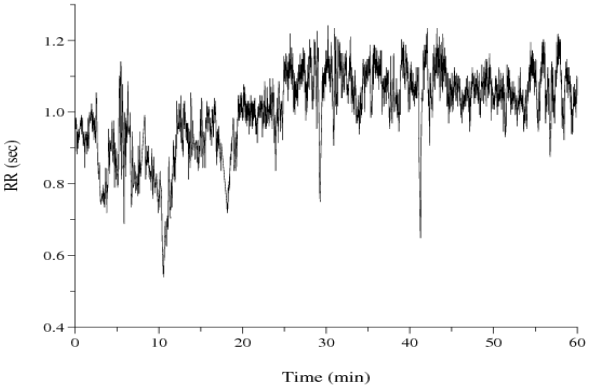

(b)

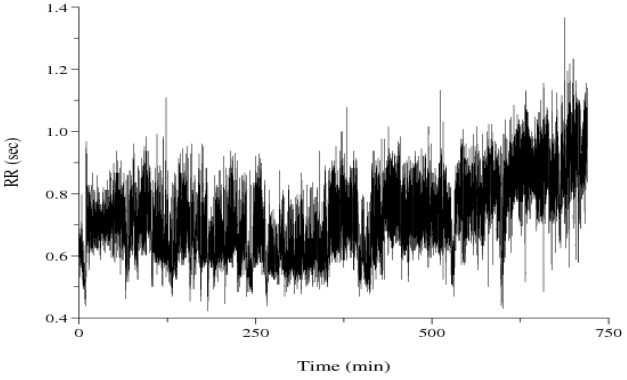

(c)

Fig. 5 RR-Interval representation (a) RR-interval for 1minute, (b) RR-interval for 1hour, and (c) RR-interval for complete wave

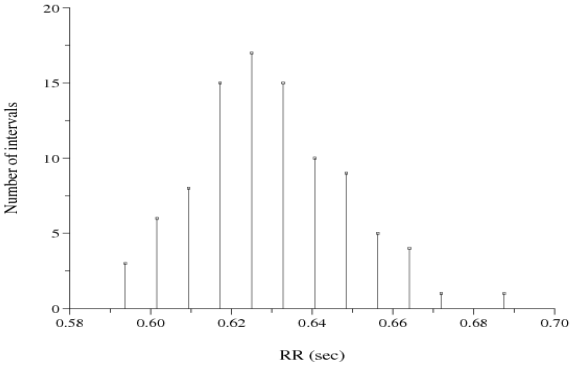

(a)

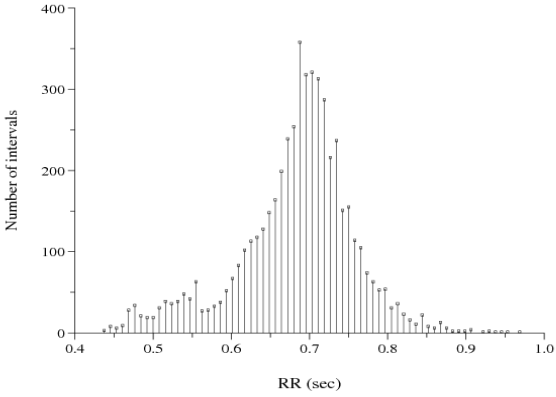

(b)

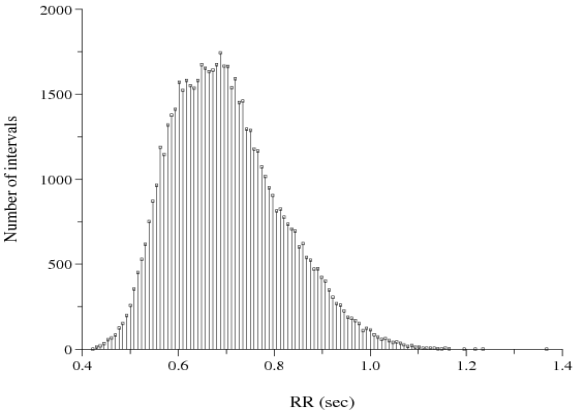

(c)

Fig. 6 Histogram representation of RR-interval (a) Histogram representation of RR-interval for 1minute, (b) Histogram representation of RR-interval for 1hour and (c) Histogram representation of RR-interval for complete wave

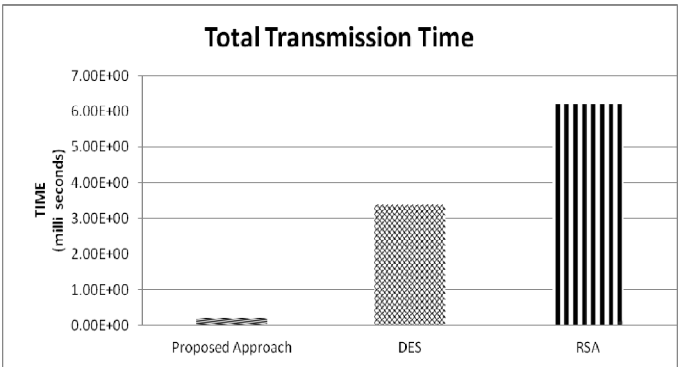

Fig. 7 Total transmission time

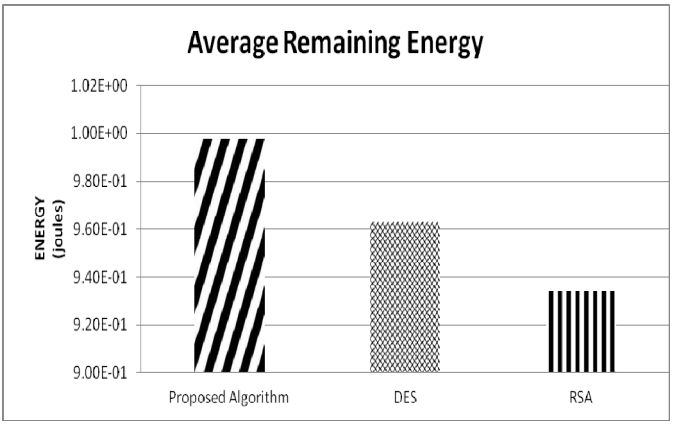

Fig. 8 Average Remaining Energy

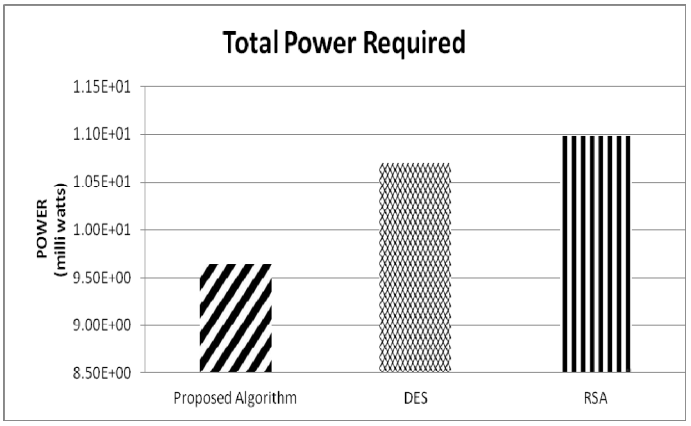

Fig. 9 Total Power required

Table 3 Comparison between proposed algorithm, DES and RSA

	Transmission Time (ms)	Average Remaining Energy(Joules)	Power Utilization (mW)
Proposed Algorithm (Biometric-based)	0.214	0.998	9.64
DES(Symmetric Encryption Approach)	3.40	0.963	10.07
RSA(Asymmetric-Encryption Approach)	6.20	0.934	10.10

7 Conclusion

This paper presents one efficient and cost-effective algorithm based on ECG as biometric characteristics to attain security and privacy in BSN, whereas ECG is used as biometric feature. The real-time data of ECG from physiobank is used in simulation; we utilized two data bases namely MIT-BIH Normal Sinus Rhythm Database (nsrdb) and MIT-BIH long-Term ECG Database (ltdb) to carry out experiments. The real-time ECG data of 20 patients of the age in between 20 to 80 is received from both databases. The aim of our research is to minimize time consumption during key generation mechanism in conventional methods. Therefore, we utilize the ECG as biometric feature to implement security; the Data Authentication Function (DAF) is applied in our proposed algorithm instead of generation of complex keys. The DAF involves three major steps i) detection of QRS-complex iii) to calculate Heart Rate Variability v)the LF/HF ratio is used as authentication protocol, the output of authentication protocol is acting as key between source and destination in our research paper. Transmission between source and destination will only begin if this ratio LF/HF matches, otherwise message will be discarded. Although DAF provides the authentication, but to raise the further level of security, we added low cost hashing encryption scheme in our research. The source performs encryption of message by SHA1, before processing to DAF. Simulation results show that our proposed scheme outperforms symmetric encryption based technique DES and asymmetric encryption based algorithm RSA. Finally, it can be concluded by simulation results that our proposed algorithm requires less transmission time than DES and RSA as, 0.214 ms, 3.40ms and 6.40 ms, respectively. Average remaining energy of our proposed algorithm, DES and RSA is 0.998 joules, 0.963 joules and 0.932 joules respectively. Total power required by proposed algorithm is 9.64mW which is lower than DES and RSA with total power consumption of 10.05mW and 10.10mW respectively. As fewer resources are required during data transmission, therefore our proposed algorithm claims to offer cost-efficient solution than conventional approaches for security of BSN.

References

[1] Bao, S.D., Zhang, Y.T., Shen, L.F.: Physiological signal based entity authentication for body area sensor networks and mobile healthcare systems. In: Proc. 27th Annual Conf. IEEE-EMBS, Shanghai, China (September 2005)

[2] Wang, H., Fang, H., Xing, L., Chen, M.: An Integrated Biometric-Based Security Framework Using Wavelet- Domain HMM in Wireless Body Area Networks (WBAN). In: 2011 IICC, pp. 1–5 (June 2011)

[3] Challa, N., Cam, H., Sikri, M.: Secure and Efficient Data Transmission over Body Sensor and Wireless Networks. Eurasip Journal on Advances in Signal Processing (2008)

[4] Poon, C.C.Y., Bao, S.D., Zhang, Y.T.: A Novel Biometrics Method to Secure Wireless Body Area Sensor Networks for Telemedicine and M-health. To appear in IEEE Communications Magazine (April 2006)

[5] Uludag, U., et al.: Biometric Cryptosystems: Issues and Challenges. Proc. IEEE 92(6), 948–960 (2004)

[6] Lang, C.S., Lee, D.G., Han, L.-W., Park, L.H.: Hybrid security protocol for wireless body area networks. Wireless Communications and Mobile Computing, 277–288 (2011)

[7] Bao, S.-D., Shen, L.-F., Zhang, Y.-T.: A Novel Key Distribution of Body Area Networks for Telemedicine. In: IEEE International Workshop on Biomedical Circuits & Systems (2004)

[8] William, C., Tan, C.C., Wang, H.: Body Sensor Network Security: An Identity-Based Cryptography Approach. Security, 148–153 (2008)

[9] Chen, M., Gonzalez, S.: Body area networks: A survey. MONET (2010)

[10] Jain, A.K., Ross, A., Prabhakar, S.: An introduction to biometric recognition. IEEE Trans. Circ. Syst. Video Technol. 14(1), 4–20 (2004)

[11] Reid, P.: Biometrics for Network Security, pp. 4–5. Prentice-Hall, Englewood Cliffs (2004)

[12] Bao, S.-D., Zhang, Y.-T., Shen, L.-F.: A Design Proposal of Security Architecture for MedicalBody Sensor Networks. In: Proceedings of the International Workshop on Wearable and Implantable Body Sensor Networks (2006)

[13] Miao, F., Jiang, L., Li, Y., Zhang, Y.-T.: A Novel Biometrics Based Security Solution for Body Sensor Networks. In: 2nd International Conference on Biomedical Engineering and Informatics, BMEI (2009)

[14] Venkatasubramanian, K.K., Banerjee, A., Gupta, S.K.S.: PSKA: usable and secure key agreement scheme for body area networks. IEEE Transactions on Information Technology in Biomedicine 14(1), 60–68 (2010)

[15] Zhang, G.H., Poon, C.C.Y., Zhang, Y.T.: A Fast Key Generation Method based on Dynamic Biometrics to Secure Wireless Body Sensor Networks for p-Health. In: 32nd Annual International Conference of the IEEE EMBS (2010)

[16] Cherukuri, S., Venkatasubramanian, K.K., Gupta, S.K.S.: BioSec: A Biometric Based Approach for Securing Communication in Wireless Networks of Biosensors Implanted in the Human Body. In: Proc. IEEE Int'l. Conf. Parallel Processing Wksp., October 6-9, pp. 432–439 (2003)

[17] Yao, L., Liu, B., Wu, G., Yao, K., Wang, J.: A Biometric Key Establishment Protocol for Body Area Networks. Hindawi Publishing Corporation International Journal of Distributed Sensor Networks 2011, 1–10

[18] Bao, S.-D., Poon, C.C.Y., Zhang, Y.-T., Shen, L.-F.: Using the Timing Information of Heartbeats as an Entity Identifier to Secure Body Sensor Network. IEEE Transaction on Information Technology in Biomedicine 12(6) (November 2008)
[19] Zhang, G.H., Poon, C.C.Y., Li, Y., Zhang, Y.T.: A Biometric Method to Secure Telemedicine Systems. In: 31st Annual International Conference of the IEEE EMBS, Minneapolis, Minnesota, USA, September 2-6 (2009)
[20] Ramila, S.N., Ahmed, R., Abdollah, M.F., Dutkiewicz, E.: A Biometric-based Security for Data Authentication in Wireless Body Area Network (WBAN) (2013)
[21] Zhang, G.H., Poon, C.C.Y., Zhang, Y.T.: A Review on Body Area Networks Security for Healthcare. ISRN Communications and Networking 2011, 1–8 (2011)
[22] Undercoffer, J., Avancha, S., Joshi, A., Pinkston, J.: Security for sensor networks. In: Proceedings of the CADIP Research Symposium (2002)
[23] Jovic, A., Bogunovic, N.: Feature set extension for heart rate variability analysis by using non-linear, statistical and geometric measures. In: Proceedings of the ITI 2009 31st International Conference on Information Technology Interfaces, pp. 35–40 (June 2009)
[24] Pan, J., Tompkins, W.J.: A real-time QRS detection algorithm. IEEE Trans. Biomed. Eng. 32(3), 230–236 (1985)
[25] Hamilton, P.S., Tompkins, W.J.: Quantitative investigation of Qrs detection rules using the Mit/Bih arrhythmia database. IEEE Trans. Biomed. Eng. 33(12), 1157–1165 (1986)

Ultra Low-Power Hardware-Assisted Signal Screening in Wearable Systems

Hassan Ghasemzadeh[1] and Roozbeh Jafari[2]

[1] Washigton State University, Pullman, WA 99164, USA
hassan@eecs.wsu.edu
[2] University of Texas at Dallas, Richardson, TX 75083, USA
rjafari@utdallas.edu

Abstract. Advances in technology have led to development of wearable sensing, computing and communication devices that can be woven into the physical environment of our daily lives, enabling a large variety of new applications in several domains including wellness and health care. Despite their tremendous potential to impact our lives, wearable health monitoring systems face a number of hurdles to become a reality. The enabling processors and architectures demand a large amount of energy, requiring sizable batteries. In this chapter, we discuss granular decision making architectures for physical movement monitoring applications. Such modules can be viewed as tiered wake up circuitries. The signal processing based decision making, in combination with a low-power microcontroller, allows for significant power saving through an ultra low-power processing architecture. The significant power saving can be obtained by performing a preliminary ultra low-power signal processing and hence, keeping the microcontroller off when the incoming signal is not of interest. The preliminary signal processing is performed by a set of special purpose functional units, also called screening blocks, that implement template matching functions. Furthermore, an optimization problem is presented, in this chapter, to select screening blocks such that the accuracy requirements of the signal processing are accommodated while the total amount of power is minimized. Finally, this chapter concludes with experimental results on real data from wearable motion sensors. These results show that granular decision making modules fine tuned for signal pre-screening can achieve 63.2% energy saving while maintaining a sensitivity of 94.3% in recognizing physical activities.

1 Introduction

Long-term pervasive sensing and monitoring can aid in diagnosis and tracking of many medical conditions such as Parkinson's [21, 29] and in extracting biokinematic characteristics of human body such as gait parameters [23, 14].

S.C. Mukhopadhyay (ed.), *Wearable Electronics Sensors,*
Smart Sensors, Measurement and Instrumentation 15, DOI: 10.1007/978-3-319-18191-2_4

Advances in technology have led to development of wearable sensing, computing and communication devices that can be woven into the physical environment of our daily lives, enabling a large variety of new applications in several domains including wellness and health care. These systems, also called Body Sensor Networks (BSNs), enable real-time monitoring of the human body. A BSN consists of several nodes placed on the human body that provide sensing, processing and communication capabilities. BSNs offer the unprecedented ability to monitor patients in a natural setting for an extended period of time.

Despite their tremendous potential to impact our lives, wearable health monitoring systems face a number of hurdles to become a reality. In particular, the enabling processors and architectures demand a large amount of energy, requiring sizable batteries. This creates challenges for further miniaturization of the wearable units.

In addressing energy concerns in wearable monitoring platforms, this chapter presents an ultra low-power *granular decision making* methodology based on coarse-to-fine grained signal processing techniques requiring low to slightly higher power. This architecture is presented in the context of physical movement monitoring which aims at detecting target physical activities/actions such as 'walking', 'sit to stand', 'kneeling', or 'lie to sit'. The granular decision making module (GDMM) will remove actions that are *not of interest* as early as possible from the signal processing chain, deactivating all remaining signal processing modules, including the microcontroller. The granular decision making module can be viewed as a tiered wake up circuitry. It is composed of hundreds or thousands of choices of screening blocks, although this chapter considers only a specific case where bit resolution of sensor readings is used to optimize power consumption of decision making architecture. Each screening block is essentially a classifier with several tunable parameters, by which power versus classification accuracy can be adjusted.

Emerging applications of health care monitoring have unique properties motivating a granular decision making architecture: signals and events observed from the human body are slowly changing [25]. They are governed by the physics of the human body (e.g., kinematics, dynamics) which constrains the variations and reduces the randomness in the signals. In addition, *events of interest*, which may require the microcontroller's attention, often occur with a low duty cycle [7]. This chapter attemts to exploit these properties and introduce programmable multi-level information driven decision making techniques that are highly power optimized.

2 Preliminaries

The problem discussed in this chapter is energy savings in BSNs through a preliminary signal screening block, called granular decision making module. Before going into more details of the ultra low-power architecture, several

Table 1 Notations

Term/Abbreviation	Description
BSN	Body Sensor Network
GDMM	Granular Decision Making Module
MSPC	Main Signal Processing Chain
MCSP	Minimum Cost Screening Path
$\hat{a}$	target action
A	set of m non-target actions
T	template generated for target action $\hat{a}$
$\gamma(T, S)$	similarity score between template T and signal segment S
n	maximum number of quantization bits provided by ADC
B_i	i-th screening block
thr_i	threshold value for screening block B_i
b_i	bit resolution of screening block B_i
tp_i	true positive rate, percentage of target actions accepted by B_i
fp_i	false positive rate, percentage of non-target actions accepted by B_i
λ	desired true positive rate
w_i	per-action energy consumption of B_i

preliminary discussions are needed to provide sufficient background on wearable systems and related low-power design approaches. Throughout this chapter, the notations listed in Table 1 are used.

2.1 Wearable Sensor Unit

A BSN is composed of several sensor nodes mounted on the patient's body, embedded with the clothing, or implanted in the human body. Physical movement monitoring uses inertial information acquired by motion sensors such as accelerometers, gyroscopes, and magnetometers. An example of a sensor node platform is TelosB mote [30] from XBow, with several analog-to-digital (ADC) channels responsible for acquiring and digitizing analog signals. It allows for integration of external sensors such as motion sensors within the TelosB sensor board. The ADC (Analog to Digital Convertor) unit within the microcontroller can sample sensor data with a specific resolution. For instance, a MSP430 microcontroller embedded with TelosB may have an ADC unit with 12-bit resolution. The sensor node has also a radio module for communication with other nodes in the network or with a gateway such as a cell phone. Ideally, a granular decision making can be a screening module fully integrated with the microcontroller. For the purpose of simplicity and evaluation in this chapter, however, we assume that a wearable sensor unit is used only to collect data in order to design the high level architecture of the granular decision making module. In other words, in Section 5, the data collected from such a wearable sensing platform will be used to validate the architecture presented in Section 3.2.

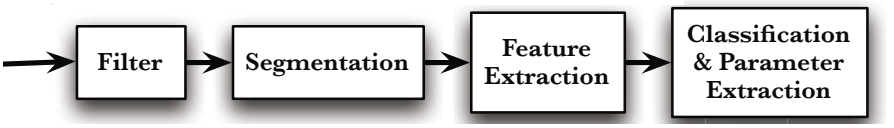

Fig. 1 MSPC (Main Signal Processing Chain) for action recognition.

2.2 Main Signal Processing Chain

The goal of main signal processing chain (MSPC) is to extract useful information from sensor data. Frequently, this data is a high-level observation, such as "Is the subject running?" or "What is the stride length when the subject is walking?". In other words, the purpose of main signal processing is to provide a 'fully' SW programmable environment for development of 'highly' reliable signal processing technique for action detection/verification and extracting details from the signals (e.g., balance during 'sit to stand' when it occurs).

Out of all possible actions, mostly only a few are of interest to the main signal processing, for example 'walking' or 'sit to stand'. Therefore, the main signal processing needs to classify actions of interest prior to extracting any further details about actions. The overall goal of the classifier is labeling actions of interest, also called target actions. Figure 1 shows a typical signal processing model commonly used for movement monitoring applications and algorithms appearing in literature [42]. In this model, signals are processed in real time by a series of processing blocks to arrive at a classification result. These processing blocks include filtering, segmentation, feature extraction, and classification and parameter extraction. The filtering is generally applied to remove sensor artifacts and noise. In the context of action recognition, segmentation determines portions of the signal that represents a complete action, segregating activity versus rest. Features are functions run on the segmented data to decrease dimensionality of the signal without significantly reducing the relevant information. Statistical features are frequently used for action recognition [12]. Finally, each node uses the feature vector generated during feature extraction to determine the most likely action by utilizing some classification algorithm such as k-Nearest Neighbor (k-NN) [10].

2.3 Low-Power Wearable System Design

Several ultra low-power wearable systems, with power budget of less than 1 mW, with signal processing capabilities have been proposed. These systems, however, are either not programmable (except that they may provide a few tunable parameters), or the programmability is handled completely by a microcontroller. An intraocular CMOS pressure sensor system implant was proposed which contains an on-chip micro mechanical pressure sensor array, a temperature sensor, a microcontroller-based digital control unit, and an RF

transponder [37]. An interface chip for implantable neural recording was proposed with tunable band-pass filters and adjustable gain [18]. A batteryless accelerometer system, with 3D loop antenna, was proposed that utilizes the radio wave for power feeding and signal communication as RFID. However, the control unit of the system is a microcontroller and is unclear how it can be powered up by energy scavenging [34].

Several other systems were suggested that are primarily tailored towards specific applications. Examples include a machine-learning based patient-specific seizure detector [36], an implantable blood pressure, ECG sensing micro-system with adaptive RF powering [4, 5, 2, 6], an implantable batteryless telemetric micro-system for EMG recording [28] and a batteryless MEMS implant for cardiovascular applications [24]. An ultra low power sensing device for measuring pulse oximetry was presented in [38]. The work in [20, 33] introduces a battery-free sensing device with radio frequency energy-harvesting from wireless module.

There has been efforts towards creating ultra low-power semiconductor components. Multi-threshold CMOS (MTCMOS) circuits is an example [8]. A wireless system with MTCMOS/SOI circuit technology was suggested which lowers the supply voltage of the LSIs 0.5 V and reduces the power dissipation to 1 mW [9]. 1 mW, however, is still larger than the energy budget of the energy harvesting circuits. The power budget of energy harvesting circuits is often tens of μWs. For example, a batteryless vibration-based energy harvesting system was proposed for ultra low-power ubiquitous applications that can generated 36.79 μW [3].

The ultra low-power processing model presented in this chapter employs a sequence of lightweight built-in classifiers and operates in a chain. The idea of using a cascade of simple classifiers for performance enhancement is studied in a variety of image processing subfields including detection of handwritten digits [44], face detection [27], and many other object detection areas [39]. The approach proposed by Viola and Jones for object detection [39] is a widely used technique in which a cascade architecture is proposed to boost the classification performance. This object detection framework is primarily used for face detection applications [40] and employs an AdaBoost-like scheme to perform both feature selection and classifier training. A set of classifiers are arranged in a cascade in order of complexity, where each successive classifier is trained only on those selected samples which pass through the preceding classifiers. If at any stage in the cascade a classifier rejects the current sub-window, no further processing is performed and continues on searching the next sub-window [41]. The idea of combining simple classifiers to achieve higher accuracy is also discussed in [31] where authors suggest to use a single accelerometer for activity monitoring and combining classifiers using plurality voting. Much work has been done on selecting only relevant pieces of information for classification. Selecting only individual features for each activity can improve the performance as demonstrated in [15]. In [17] AdaBoost is used to select a small number of features in order to ensure fast

classification. The algorithm automatically selects the best features and ranks them based on their classification performance. Given the maximum number of features that the activity recognition system can use, the system automatically chooses the most discriminative sub-set of features and uses them to learn an ensemble of discriminative static classifiers for activity recognition.

As stated previously, the idea of granular decision making for wearable systems is motivated by sparsity of the events that occur in health monitoring applications. Sparsity of events has inspired many studies in the past in other monitoring applications. An example of these studies is Lucid Dreaming [16] that is proposed for use in structural crack monitoring. The system performs high resolution sampling of sensor data in bursts upon occurrence of an event of interest. This wake-up circuit consumes only 16.5 μW. CargoNet [19] is another system aimed at environmental monitoring and is capable of asynchronous wake-up upon occurrence of exceptional events. The wake-up module uses adjustable thresholds to adapt to dynamic environments. The power consumption of the system is reported to be less than 25 μW. The work in [1] employes a decision tree model to activate sensor nodes and adjust their sampling rates. The performance of the decision tree classifier is comparable with that of the support vector machines while the decision tree consumes significantly less energy. Another example is the system presented in [32] which uses an ultra low power front-end analog circuitry to enable/disable digital component of the system by examining the power spectrum of the signal. Furthermore, an acoustic surveillance system is presented in [13] which implements a digital VLSI periodicity detector (with a core power consumption of 835nW) to wake up the system. The detection criterion is based on the degree of low-frequency periodicity in the acoustic signal.

3 Signal Screening for Power Saving

This section presents different components of the signal screening architecture. The section starts with a describtion of the motivation for signal screening first, and presents a high-level view of the system followed by more detailed information on each component.

3.1 Motivation

Most BSN applications are only concerned with a very small subset of human actions. For instance, gait analysis only is concerned with 'walking', fall detection with 'falls', Parkinson's disease monitoring with certain movements such as 'tremors' [29], sleep apnea with 'restless leg syndrome' and 'periodic limb movements' [26]. In real-time continuous patient monitoring, these target actions occur infrequently. Considerable energy is wasted processing non-target actions. As a result, efficiently rejecting non-target actions with a screening classifier could lead to a significant increase in system lifetime through

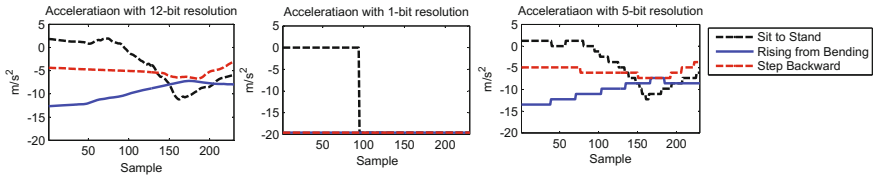

Fig. 2 Motivation

deactivating the main processor which provides the full signal processing for classification. This way, an ultra low-power screening block activates the MSPC only when a target action is observed. Clearly, one requirement of such screening classifier is to achieve a significantly high precision, *true positive rate*, in detecting target actions (activating main processor due to occurrence of a target action). To obtain high true positive rates, the screening architecture may accept some non-target actions. Such actions determine the *false positive rate*. For the actions that the screening block cannot reject reliably, the MSPC will be activated. The main advantage of this method is the power saving due to removing non-target actions from the signal processing chain, deactivating the remaining modules in the signal processing chain. Note that the false positives may not result in inaccurate activity monitoring because they can be rejected by the MSPC through more intenstive signal processing. Furthermore, a chain of classifiers, which perform coarse to fine grained preliminary processing, can be used. In this chapter, we focus on using a sequence of classifiers that differ in the level of bit resolution of sensor readings. Lower level classifiers operate at lower precision and consume less power while higher level classifiers have higher percision at the cost of higher power consumption.

Figure 2 illustrates motivation behind using a sequence of screening blocks with low-to-high bit resolution. This figure shows real signals collected with our wearable sensors where only three actions are used for visualization. The graphs show raw sensor readings from Z-axis accelerometer of a node placed on the 'waist' of a subject. Assume 'Rising from Bending' (bold blue plot) is the action of interest and the other two actions, 'Sit to Stand' (dashed black plot) and 'Step Backward' (dashed red plot) may occur as non-target. The graph on the left shows sensor readings with 12 bits of ADC resolution. Clearly, the target action ('Rising from Bending') can be distinguished from the two other actions on the 12-bit graph. This can be accomplished by a template matching function as will be discussed in Section 4.1. Let us assume that all actions are equally likely. Therefore, a 12-bit template matching needs to be active all the time monitoring incoming signals. It would activate the main signal processing chain only when a target action occurs (33.3% of the time). Now assume that two classifiers with 1-bit and 5-bit resolutions are used, as shown in middle and right graphs, instead of a 12-bit classifier.

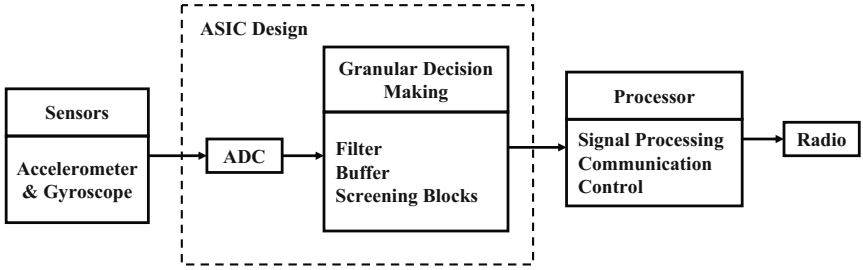

Fig. 3 Architecture of the wearable system with GDMM.

As shown in the figure, a 1-bit resolution classifier can reject 'Sit to Stand' as not being the target action. However, it cannot reject a 'Step Backward' action as the signal has the same value as the target action (see blue and red graphs in the 1-bit resolution scenario). A not-rejected action, however, can be further processed by the next classifier in the chain (a 5-bit resolution classifier) where 'Step Backward' and 'Rising from Bending' actions are distinguishable. Therefore, an incoming signal can be reliably classified as either 'target' or 'non-target' after passing through a sequence of two classifiers with lower bit resolutions than the 12-bit classifier. In this example, a 1-bit resolution classifier is active all the time while a 5-bit classifier is active only 66.7% of the time. Note that a sequence of lower resolution classifiers can potentially consume a lot less power than a classifier with full scale quantization.

3.2 Architecture of Wearable Unit with Signal Screening

An overview of the system architecture for low-power signal processing is shown in Figure 3. There are four main components of the platform: the sensors, the special purpose functional unit or granular decision making module (GDMM), a low-power general purpose processor, and the radio. Human actions can be examined using motion sensors such as accelerometers and gyroscopes. The sensor readings are sent through an ASIC architecture including an analog-to-digital converter (ADC) and GDMM, which digitizes the reading and performs screening tests. The ADC is an essential component which acquires and digitizes analog signals for further analysis. The MSP430 microcontroller used for the experiments presented in this chapter has an ADC unit with 12-bit resolution. Any action accepted by the GDMM will be forwarded to the MSPC for further processing. The following two subsections present details of the signal screening architecture. The MSPC presented in Section 2.2 is implemented on the main processor where the results can be transmitted through the radio.

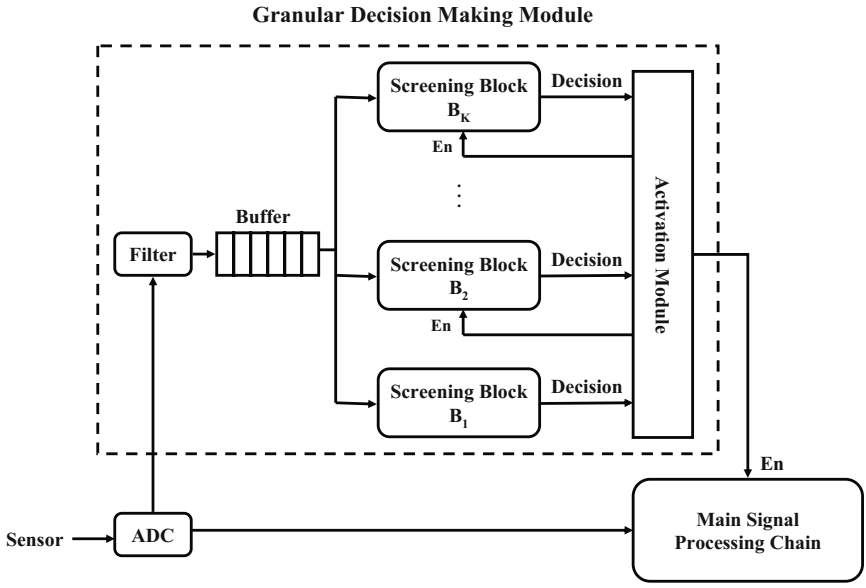

Fig. 4 GDMM (Granular Decision Making Module) composed of several screening blocks, each having a different bit resolution

3.3 Granular Decision Making

The power saving model operates based on a set of screening blocks performing template matching on incoming signal. Each screening block can be adjusted to perform preliminary signal processing at different precision rates at the cost of power usage. An example of tunable parameters is the number of quantization bits or bit resolution of the sampled data. Specifically, optimizing the screening architecture with respect to bit resolution is the main focus of this chapter. Figure 4 illustrates GDMM in connection with other components of the system where screening blocks operate at different bit resolutions. The module includes digital pre-filtering, a buffer, and a chain of screening classifiers as described previously. The data from body-mounted motion sensors is frequently noisy. A moving average filter is enough to filter the signal and remove high frequency noise [11].

Each screening block in the chain is applied in a sequence that will be detailed in Section 4. The processing stops as soon as a screening block in the chain rejects the incoming action. Activating screening blocks in serial introduces a time delay for each subsequent block. In order to allow each block to operate on the proper signal segment, a single buffer is used.

The lowest level screening block (i.e., B_1) has the lowest precision (e.g., 1-bit resolution) but is also the least energy consuming block. An active screening block makes a preliminary binary decision (Accept/Reject) on

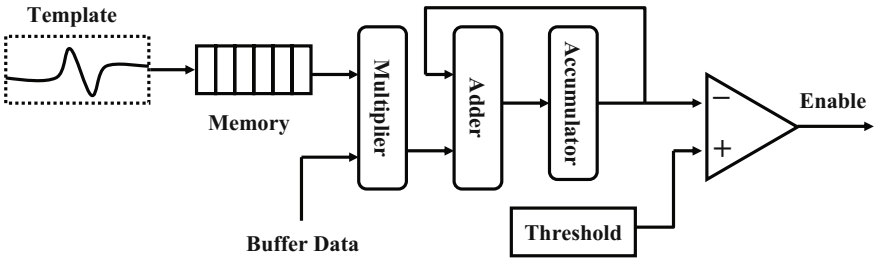

Fig. 5 Screening block performing template matching operations

incoming signal. A higher level block (e.g., B_2) is activated only if the incoming action is accepted by the preceding block (e.g., B_1). Clearly, the block at the lowest processing level (e.g., B_1) needs to be active all the time, processing incoming signals. In Section 4, an optimization problem aiming to find the optimal sequence of the screening blocks is presented where quantization bit is considered as the tunable parameter.

The *Activation Module* is responsible for turning on the next screening block or the MSPC. In other words, activation of the screening blocks and the main processor are programmable thought the activation module. A higher-level screening block is activated only if the current action is accepted by its preceding block.

3.4 Screening Blocks

Each screening block compares the incoming signal against a predefined template over a fixed window. The comparison is made using template matching operations. The template matching, shown in Figure 5, is based on Normalized Cross Correlation (NCC) [43] which will be discussed in Section 4.1. Template matching is implemented using a multiplier-accumulator (MAC) circuit. Real-time signal processing requires high speed and high throughput MAC units that consume low energy, which is always a key to achieving a high performance low-power computing system.

Each screening block is a binary template classifier based on the cross correlation score obtained by comparing the incoming action with a precomputed template of the target action. This comparison assigns a score value, γ, based on a similarity measure between the signal segment and the template. For classification decision, γ is compared against a threshold value, thr_i, and the action is classified as either *accept* or *reject*. A rejection causes processing to stop for that action.

4 Optimization of Granular Decision Making Module

The GDMM in Figure 4 is composed of several screening blocks that form a decision path for classification. Each block is associated with a quantization bit level which affects performance of the classification. Finding minimum set of screening blocks and their ordering is challenging because each block has a different operating point depending on the bit resolution and the threshold used for classification. In this section, an optimization problem is formulated to find the optimal decision path forming the best sequence of screening blocks for examining each incoming action.

4.1 Template Matching

Given a target action $\hat{a}$ and $A = \{a_1, a_2, \ldots, a_m\}$ a set of m non-target actions, template T, associated with $\hat{a}$, is generated from a set of training trials. Templates are generated as shown in Definition 1 using a set of training trials. During real-time operation of the system, a classification decision is made by comparing the incoming action to the predefined template. The comparison is made based on the similarity score defined in Definition 2.

Definition 1 (Template). Given an action a_i with L number of training trials, a template T_i for a_i is the best representative trial with respect to the similarity score γ between all pairs of the trials. The trial with the highest summed similarity score between itself and the other trials is selected, as shown in (1).

$$T_i = \arg\max_{a_i^l} \sum_r \gamma(a_i^l, a_i^r) \tag{1}$$

Definition 2 (Similarity Score). Given two time series signals f and g of length N, the similarity score $\gamma(f,g)$ between the two signals is defined based on their normalized cross correlation by

$$\gamma(f,g) = \frac{\sum_{t=1}^{N}[f(t)-\bar{f}][g(t)-\bar{g}]}{\sqrt{\sum_{t=1}^{N}[f(t)-\bar{f}]^2 \sum_{t=1}^{N}[g-\bar{g}]^2}} \tag{2}$$

where $\bar{f}$ and $\bar{g}$ denote mean values of f and g.

4.2 Performance of Screening Blocks

Each screening block performs preliminary classification based on the score associated with cross correlation between the template and the incoming action. A screening block B_i rejects the incoming action if the score is smaller than a certain threshold thr_i. Classification performance of a screening block B_i depends on thr_i and the bit resolution of the block, b_i. The threshold is set during the training to obtain a pre-specified precision associated with

a desired performance criterion. The larger the threshold is the higher the likelihood of rejecting an incoming action. Therefore, the threshold value directly affects the true positive rates (tp_i) and false positive rates (fp_i). The granular decision making architecture aims to minimize power consumption of the system while maintaining a given lower bound on the true positive rate (λ). The module introduces a decision path including a sequence of the screening blocks. The power consumption of the module is determined by the *acceptance rate* of the screening blocks on the path (r_i) and the energy consumption of each block (w_i). Let us call this problem *Minimum Cost Screening Path* (MCSP). In the remainder of this section, we study this problem by mapping the entire set of screening paths onto a graph model and formally formulating the problem on the proposed graph.

Definition 3 (Block Acceptance Rate). For each screening block B_i on a decision path, an acceptance rate r_i is defined by

$$r_i = tp_i + fp_i \tag{3}$$

where tp_i and fp_i refer to true positive rate and false positive rate of the block B_i. The acceptance rate r_i is clearly determining percentage of the actions (including target and non-target) accepted by B_i.

Note that true positive rate and false positive rate concepts are absolute measures and do not carry the effect of one screening block on the other. That is, tp_i and fp_i values are calculated while all actions are fed to B_i. Similarly, the resulting acceptance rate, r_i, represents percentage of the actions that pass through a block if all actions are used as input to that block.

4.3 Problem Formulation

In order to present the minimum cost screening path (MCSP) problem, all possible decision paths are mapped onto a graph model called *screening graph*. This model is then used to find the optimal path including a subset of screening blocks and their ordering for preliminary signal screening.

Definition 4 (Screening Graph). Given a set of screening blocks $\{B_1, \ldots, B_n\}$ with $b_i < b_{i+1}$, the screening graph $G=\{V,E,W\}$ is a direct acyclic graph defined by a set of vertices, V, a set of edges, E, and sets of weights, W associated with vertex set. The set of vertices, V, is $\{s, v_1, \ldots, v_n, t\}$ where s is a dummy node connected to all other nodes, and t is the destination node associated with the main signal processing chain. Thus, $|V|=n+2$. Furthermore, each vertex v_i $(1 \leq i \leq n)$ is associated with a screening block B_i. An edge e_{ij} $(i < j)$ connects a vertex v_i (corresponding to a lower level block B_i) to vertex v_j (corresponding to higher level block B_j). Thus, $|E|=\frac{(n+1)(n+2)}{2}$. The set $W=\{w_1, \ldots, w_n\}$ denotes cost of each vertex for processing a single incoming action, and is associated with the energy consumption of corresponding screening blocks.

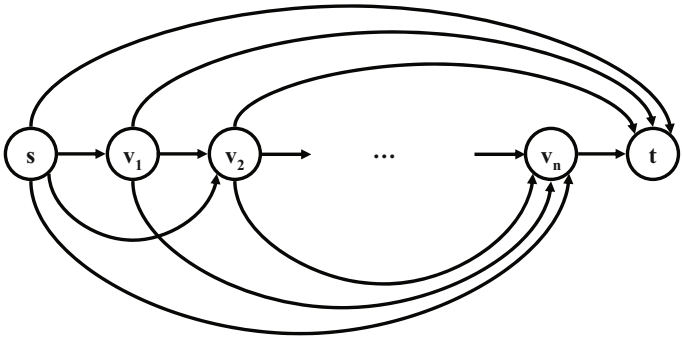

Fig. 6 An example of a screening graph with four vertices.

Definition 5 (Outgoing Flow). For each vertex $u_i \in V$ on a path P={s, u_1, ..., u_l, t} of length l from s to t, define an outgoing flow (f_i) representing percentage of actions that are passed through the corresponding block B_i. The set of outgoing flows for vertices on the path P is denoted by F={f_1, ..., f_l}.

Note that the outgoing flow, f_i, associated with B_i is different from the acceptance rate, r_i. Acceptance rates define percentage of actions that can be accepted by individual screening blocks, independent of how they are connected to other blocks. Outgoing flows, however, represent percentage of actions that are accepted by a particular block while considered as part of the screening graph. Each f_i is a function of r_i and acceptance rate of the preceding blocks on the path as discussed later in this section.

For the dummy node s, f_s=1 resulting in an outgoing flow of 1. The idea is to feed all actions to the dummy node first. A path from s to t determines what screening blocks are activated during preliminary classification. Furthermore, w_s=0 because the dummy node does not represent a physical component of the system. Also, a zero outgoing flow is assigned to the destination node (f_t=0) because MSPC is the last processing component of the system and does not convey actions to any subsequent module. The energy consumption of the destination node, w_t, is the amount of energy required for running MSPC on the main processor.

Figure 6 shows the screening graph with v_1 to v_n corresponding to n screening blocks. As mentioned previously, the energy cost of a screening block B_i is denoted by w_i per incoming action. Therefore, the overall cost of each screening block depends on the percentage of the incoming actions that are passed through the decision path to the screening block B_i. This is directly defined by the outgoing flows. The objective is to find the decision path with minimum overall cost.

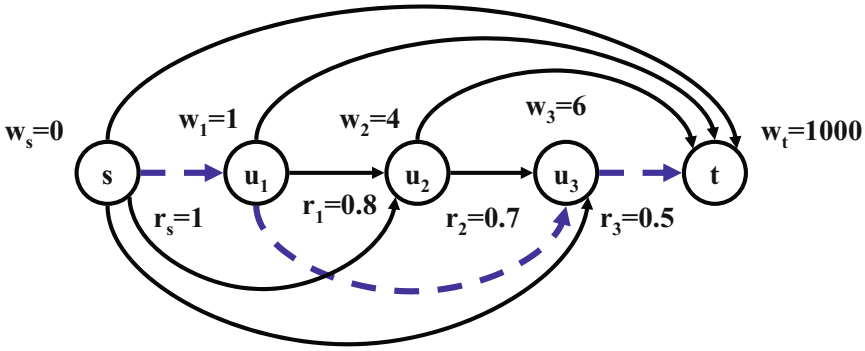

Fig. 7 A minimum cost decision path is P={s, u_1, u_3, t} with a total cost of 505 nW

To better describe how the overall cost for a path from s to t is calculated ,a synthetic screening graph (Figure 7) with three screening blocks indicated by u_1, u_2, and u_3 is presented. Each vertex has an outgoing flow, f_i and a weight denoted by w_i. The weights are shown in nW with destination node (t) having a significantly larger amount of power consumption (e.g., w_t=1000) as it corresponds to the main signal processing chain. A path P={s, u_1, u_3, t} which is the minimum cost path has a cost of 505 nW. The edge (s,u_1) has a cost of $f_s \times w_1$=1 nW. The next edge, (u_1,u_3) has a cost of $f_1 \times w_3$=4.8 nW. Note that f_1 is the minimum rate among all previously traversed vertices (s and u_1). The cost for the edge (u_3,t) is $f_3 \times w_t$=500 nW. Similarly, f_t is the smallest acceptance rate among previously traversed nodes (s, u_1, u_3). In general, however, if r_i is not the smallest rate among all preceding nodes, the cost for an edge e_{ij} is a function of acceptance rates on all traversed nodes. In this example, acceptance rates are monotonically decreasing. Thus, the cost for each edge e_{ij} can be computed based on the rate and weight of adjacent vertices (i.e., r_i and w_j). In order to formally define the MCSP problem, let us define the cost for each decision path on a given screening graph.

Definition 6 (Decision Path Cost). Given a screening graph G, the total cost for a decision path P={s, u_1, ..., u_l, t} of length l is given by

$$\mathbf{w}^P = f_s w_1 + f_1 w_2 + f_2 w_3 + \ldots + f_l w_t \quad (4)$$

$$= r_s w_1 + min(r_s, r_1) w_2 + min(r_s, r_1, r_2) w_3 + \ldots + min(r_s, r_1, \ldots, r_l) w_t \quad (5)$$

where $u_i \in V$, r_i is the acceptance rate for vertex u_i, and r_s=1. Furthermore, each term $f_i w_j = min(r_s, r_1 \ldots, r_i) w_j$ represents the cost associated with the edge e_{ij}=(u_i,u_j) on the path.

The intuition behind using *min* function in the above formulation is that the acceptance rates, r_i, are all calculated with respect to the source node,

s, rather than the adjacent node in the graph. Therefore, each r_i denotes the percentage of the actions that can pass through B_i if the node is placed adjacent to s (i.e., all actions are fed to the block). As it can be observed from Definition 6, the cost for each edge e_{ij} on the path depends on the cost of u_j and acceptance rate of all previously traversed nodes.

Problem 1. Given a screening graph G, the MCSP problem is to find a decision path, $\hat{P}$, with minimum cost.

Definition 7 (Path Acceptance Rate). For a decision path P from s to t on the screening graph G, the acceptance rate R_P is defined as the percentage of actions that are accepted by all the nodes on the path, and is given by

$$R_P = min_{u_i \in P}(r_i) \tag{6}$$

4.4 Shortest Path Solution

The problem presented in Section 4.3 is different from the traditional shortest path problem because the contribution of an edge to path cost depends not only on the cost of that edge but also on the costs of the edges already traversed. A special case of this problem with applications in multimedia data transmission has been studied in [35].

The MCSP problem can be transformed to the traditional shortest path by simplifying some of the assumptions on acceptance rate of our screening blocks. It can be shown that under these realistic assumptions, the problem can be solved with computationally simple shortest path algorithms. In fact, the classifiers under consideration in this chapter use the same template and signal, but linearly quantized at different bit levels. From this model, several basic assumptions can be inferred.

1. The target actions are rejected in approximately the same order by all the screening blocks on the decision path. Equivalently, if a target action is rejected by B_i, it is also rejected by B_j while $j > i$. In other words, a higher level block B_j may reject some target actions that are accepted by B_i. Therefore, compared to a lower level block, a higher level block may have smaller or equal true positive rate ($tp_j \leq tp_i$).
2. Similarly, the non-target events are rejected in approximately the same order by all the classifiers. Thus, a higher level block B_j may reject some non-target actions that are accepted by a lower level block B_i. Therefore, compared to a lower level block, a higher level block may have smaller or equal false positive rate ($fp_j \leq fp_i$).
3. Classifiers at higher quantization bit levels perform better or equal to classifiers at lower bit levels. That is to say, for two screening blocks with equal true positive rates $tp_i = tp_j = F$ and $j > i$, then $r_j \leq r_i$. In fact, in order to achieve the lower bound λ on true positive of the entire granular decision making, we set the threshold thr_i on each screening block such that the fixed true positive rate of λ is obtained.

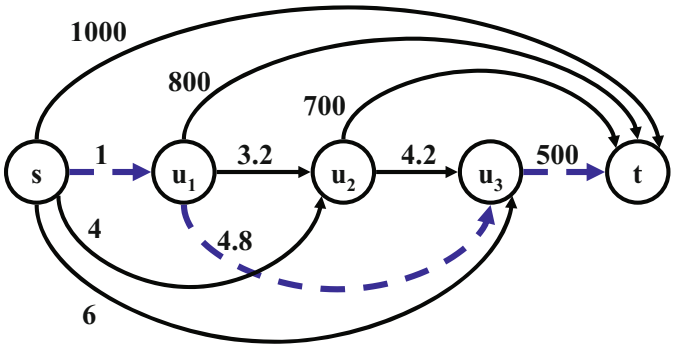

Fig. 8 Example of shortest path calculation

Theorem 1. *If u_1, u_2, ..., u_k (associated with screening blocks $B_1 \ldots B_k$) form an optimal decision path, the cost of an edge e_{ij} is a function of w_j and r_i.*

Proof. As shown in (4), the total cost associated with edge e_{ij} on path P is given by

$$w_{ij}^e = min(r_s, r_1, \ldots, r_i) w_j \tag{7}$$

The assumptions on monotonically decreasing acceptance rate would result in u_i having smallest acceptance rate among all preceding nodes. That is $min(r_s, r_1, \ldots, r_i)$=$r_i$. Therefore,

$$w_{ij}^e = r_i w_j \tag{8}$$

An immediate implication of Theorem 1 is that the cost of each edge on the decision path is deterministic and can be computed before running any algorithm for computing the path. Therefore, the problem is transformed into a simple shortest path problem [22].

Calculating shortest path on Directed Acyclic Graphs (DAGs) is computationally less expensive than general graphs, based on the principal of topological ordering. It can be done by processing the vertices in a topological order and computing the path cost from each vertex to be the minimum cost obtained via any of its incoming links. Each screening graph in our modeling is a DAG with a unique topological ordering. This ordering is specified by the directed path that contains all the vertices. In the example shown in Figure 8, the topological ordering is $\{s, u_1, u_2, u_3, t\}$. In this example, costs associated with edges are calculated by applying (8) on the graph in Figure 7. The shortest path from s to t is $\{s, u_1, u_3, t\}$, which is calculated as follows. Vertex u_1 has only one incoming edge. Thus, there is only one path from s to u_1 with the cost of 1. The next vertex in the topological ordering is u_2 which has two incoming edges associated with two paths ($\{s, u_1, u_2\}$ and $\{s, u_2\}$ with the costs of 4.2 and 4 respectively. Therefore, minimum cost

Table 2 Experimental Actions

No.	Action
1	Stand to Sit
2	Sit to Stand
3	Sit to Lie
4	Lie to Sit
5	Bend and grasp
6	Rise from Bending
7	Kneel
8	Rise from Kneeling
9	Look Back
10	Return from look back
11	Turn clockwise
12	Step forward
13	Step Backward
14	Jump

path from s to u_2 is $\{s, u_2\}$. Similarly, u_3 has three incoming edges which indicate three paths $\{s, u_2, u_3\}$, $\{s, u_1, u_3\}$, and $\{s, u_3\}$ introducing costs of 8.2, 5.8, and 6. Consequently, $\{s, u_1, u_3\}$ is the minimum cost path from s to u_3. And finally, destination t has four incoming edges representing four candidates for the shortest path. These paths include $\{s, u_1, u_3, t\}$, $\{s, u_2, t\}$, $\{s, u_1, t\}$, and $\{s, t\}$ with the costs values of 505.8, 704, 801, and 1000 respectively. Thus, $\{s, u_1, u_3, t\}$ is the overall shortest decision path from s to t with a cost of 505.8.

5 Performance Analysis

This section presents an assessment of the discussed power saving model using real data collected from motion sensors duirng daily physical activities. The evaluation is done for identifying each one of the 14 target actions listed in Table 2. In each phase, one of the actions is considered as target action and the rest as non-target. The analysis uses data collected through a set of experiments with three male subjects, all between the ages of 25 to 35 and in good health condition.

5.1 Datase

The dataset used for analysis contains data from nine motion sensor nodes. Each sensor node has a 3-axis accelerometer and a 2-axis gyroscope. For simplicity, only one sensor/node is used for detecting each target action (e.g., Z-axis of the node placed one the 'waist' for 'sit to stand'). For actions that require multiple sensors, the same methodology can be used. That is, the template matching on multiple nodes/axes can be utilized to activate MSPC.

In this case, a data fusion algorithm will be used to combine decisions made by different sensors and decide if the microcontroller needs to be turned on/off.

5.2 Parameter Setting

As discussed in Section 4, a screening graph has two set of parameters which are used for constructing optimal decision path. These parameters include weights (W) and incoming rates (R) associated with different screening blocks. Both parameters are calculated using training trials. Weights are calculated based on the amount of energy consumed by corresponding screening blocks. Incoming rates are calculated by examining percentage of training trials that are accepted by each screening block.

To estimate the energy consumption of each screening block, the screening blocks are implemented using template matching units as described previously. Template matching function is modeled using Verilog. The cross-correlation is implemented by a series of MAC steps depending on the number of incoming samples. At each clock instant, the digitized template data and the incoming signal data are multiplied and added to the previous MAC value. The multiply-add operation repeats depending on the length of the template, to calculate the cross correlation function. All the operations are carried out at a low frequency of 20 Hz. The design is synthesized using Synopsys with the 45nm NanGate Open Cell library. The switching activity is then considered and the power numbers are computed in Synopsys. The power values ranges between 0.34 nW for the 1-bit block (w_1=0.34) and 1.45 nW for the 12-bit screening block (w_{12}=1.45).

In order to calculate the incoming rates (R) on individual vertices of the screening graph, the threshold (thr_i) is set on each screening block such that the desired true positive rate (λ) is obtained. In fact, the threshold is set to guarantee the lower bound λ on the overall true positive rate of the system. Therefore, the threshold on each screening block B_i is given by

$$\hat{thr}_i = \arg\max_{thr_i} \quad tp_i \geq F \tag{9}$$

Note that tp_i (sensitivity) decreases as thr_i grows. Thus, thr_i is set to the largest possible value that meet the desired sensitivity requirement. Thus, once can start with a small value (e.g., close to '0' which would result in 100% sensitivity) and increase this value as long as the sensitivity rate is above the desirable rate.

5.3 Decision Paths

Table 3 shows decision path reported by the optimization technique while the desired true positive rate (λ) varies from 50% to 100%. In this table, a node 's' denotes the source and a 't' represents the destination node (associated

Table 3 Shortest paths for detecting 'sit to stand'

Sensitivity (%)	Decision Path	Path Activation (%)	Classifier Threshold
50	$s \to B_1 \to B_{12} \to t$	4.76	0.95
55	$s \to B_1 \to B_{12} \to t$	5.71	0.94
60	$s \to B_1 \to B_{12} \to t$	5.71	0.94
65	$s \to B_1 \to B_{12} \to t$	7.62	0.93
70	$s \to B_1 \to B_{12} \to t$	9.05	0.92
75	$s \to B_2 \to B_{12} \to t$	12.9	0.86
80	$s \to B_2 \to B_{12} \to t$	12.9	0.86
85	$s \to B_2 \to B_{12} \to t$	14.3	0.85
90	$s \to B_2 \to B_{12} \to t$	16.7	0.84
95	$s \to B_2 \to B_{12} \to t$	22.9	0.80
100	$s \to B_2 \to B_{12} \to t$	22.9	0.80

with the main processor). In all cases, only two screening blocks are chosen by the algorithm. Note, however, that the total energy depends also on the bit resolution of the individual screening blocks. For example, B_{12} consumes more power than B_1 and B_2. An interesting observation is that more power hungry blocks (e.g., B_2) are chosen as the desirable sensitivity increases. This observation can be interpreted as follows. When sensitivity rate increases, lower quality blocks (e.g., B_1 in this example) may not be able to provide the amount of granularity required for obtaining the desirable sensitivity. Thus, higher level blocks (i.e., B_2) get activated to provide sufficient performance.

The third column in Table 3 shows path acceptance rate, percentage of the time that the main signal processing chain (MSPC) is activated by the algorithm. The first screening block (e.g., 3-bit or 4-bit template matching block) is active all the time. However, the second screening block is activated based to the outcome of the previous template matching.

The last column in Table 3 shows the threshold values assigned to the last screening block (i.e., B_{12}) on the path. These values determine how similar an incoming signal and the target template need to be in order to classify the signal as target. Correspondingly, this indicates the amount of difference between a non-target action and the target action in order to properly classify them. We recall that the classification is based on the similarity score in Definition 2. If the similarity score between an incoming signal and the template exceeds the threshold, the signal is classified as target. Otherwise, the signal is classified as non-target, resulting in the main processor remaining inactive. Clearly, the threshold value for a particular GDMM depends on the sensitivity of the system, which is a design parameter. Higher sensitivities incur smaller thresholds, allowing more actions to be classified as target.

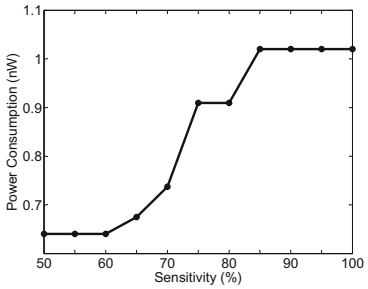

(a) Power Consumption of the GDMM

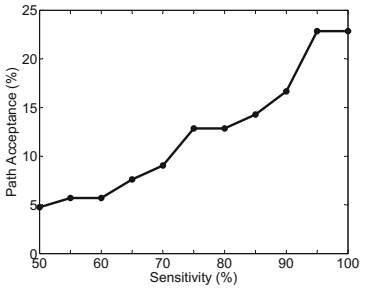

(b) Path Acceptance Rate

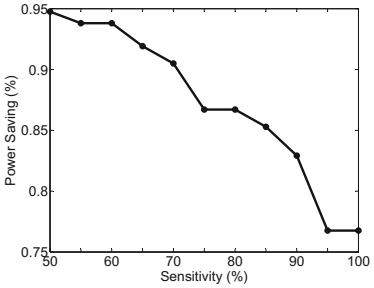

(c) Power Saving

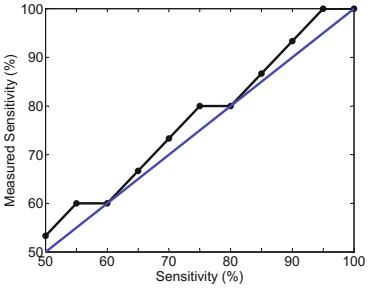

(d) Measured Sensitivity

Fig. 9 Results for detecting 'Sit to Stand'.

5.4 Power Analysis

The power optimization problem with a desired true positive rate would lead to a shortest path problem as explained in Section 4.4. Power and accuracy results for detecting 'sit to stand' through the granular decision making module (GDMM) are shown in Figure 9. Figure 9(a) shows the power consumption of the GDMM. The power consumption ranges from 0.64 nW to 1.02 nW with an average of 0.84 nW.

As expected, Figure 9(b) confirms that MSPC is activated more often when a higher sensitivity is desired. The value of path activation ranges from 4.8% for the case of 50% sensitivity to 22.9% for the case of 100% sensitivity.

The power consumption of the decision making module can be compared with that of an MSP430 microcontroller which consumes 3 mW in active mode. Figure 9(c) shows the amount of power savings obtained by our system compared to a system with the microcontroller being instantly active (a direct connection between node s and t in the screening graph). As expected, the higher the true positive rate is, the lower energy saving that can be achieved. Depending on the desired sensitivity, the percentage of power saving ranges from 76.8% to 94.8%.

Once the optimal decision path is constructed, it can be used to measure its actual precision when test trials are applied. This simulates a real-time scenario where incoming signals are examined by the decision making module for identification of a specific target action. For this purpose, the sensor data are fed to the optimal decision paths shown in Table 3. The actual measured sensitivities are shown in Figure 9(d). The values range from 53.3% to 100% with an average of 77.6%. Note that all values on the graph in Figure 9(d) are above the dashed line, which implies that the measured sensitivity is always higher than the desired lower bound (λ).

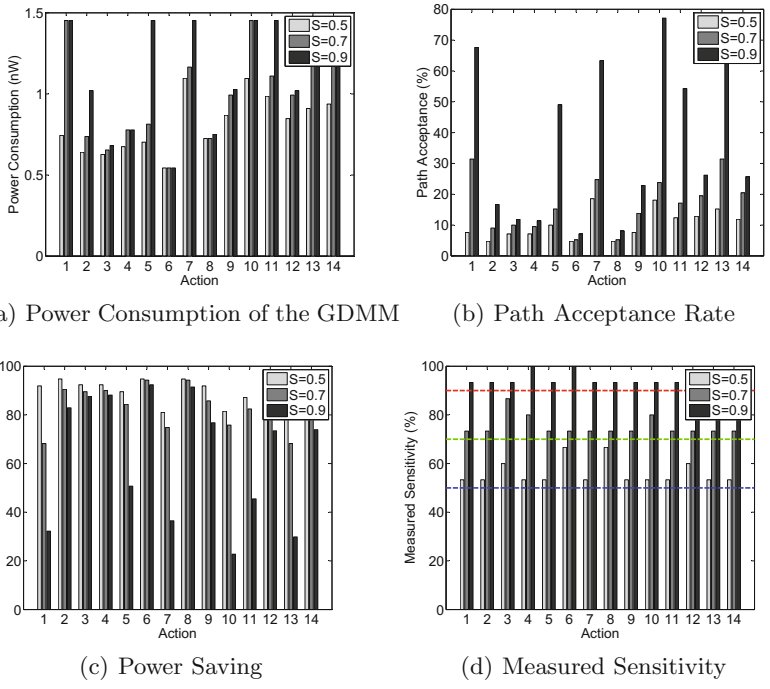

(a) Power Consumption of the GDMM (b) Path Acceptance Rate

(c) Power Saving (d) Measured Sensitivity

Fig. 10 Results when each action is considered as target action. Results are shown for three different values of desired sensitivity (S=50%, S=70%, S=90%).

5.5 Single Action Detection

In order to establish the robustness of our granular decision making architecture with respect to different target actions, the data are used and each action in Table 2 is considered to be the target action. In each case, appropriate template can be chosen and the specific action can be considered as the target. For each target action, the optimal decision path is then constructed from the screening graph as discussed in Section 4. For extracting each decision path,

Table 4 Power consumption and savings for detecting multiple actions

	S=0.5	S=0.7	S=0.9
Power Consumption (mW)	2.7	3.6	3.9
Power Saving (%)	71.5	38.3	20.9

the thresholds are set on each template matching block to meet the desired true positive rate. The sequence of the screening blocks on the decision path is used to accept/reject each incoming signal and activate MSPC. The set of screening blocks is then employed to classify the target movement. The results obtained from this analysis are shown in Figure 10(a)-Figure 10(d) for three different sensitivity rates. In particular, the discussed system achieves an average power saving of 63.1% while maintaining a sensitivity of 92.7%.

Figure 10 shows the details of this analysis. Figure 10(a) shows power consumption of GDMM for detecting each one of the 14 target actions. For the case of a 90% sensitivity, the power consumption of the GDMM veries depending on the target action. It ranges from 0.543 nW for 'Rise from Bending' to 1.45 nW for 'Stand to Sit' and 'Kneel'. On average, the screening path consumes 1.14 nW. The amount of power saving ranges from 22.7% to 92.4% with an average of 63.1% while maintaining a minimum sensitivity of 90%.

5.6 Detecting Multiple Actions

Thus far, the presented performance analysis considers the case where the granular decision making module is trained to monitor only one particular action (associated with the template) and the analysis is presented accordingly to wake the main processor up upon occurrence of the target action. Yet, this methodology can be extended to detect a group of target actions. In case of multiple target actions, one can use one of the following approaches: 1) The most straightforward, but not essentially optimal, approach is to replicate the decision making module for each action of interest where each module classifies one target template and activates the main processor independent of the others. This approach may result in less power saving because similarity among target actions is not taken into consideration and therefore, some of the modules might be redundant; 2) Another approach is to generate a unique template that represents all actions of interest and use that template as target template. This method is more efficient, but may not be feasible if actions of interest are significantly different in terms of structural patterns, which makes generation of a common template challenging; 3) If a large number of target actions with significant structural variations are given, a combination of the two aforementioned approaches can be used. Similar actions can be grouped together to generate a unique template, and one granular decision making module can be constructed per action group.

Table 5 Similarity scores for irregular walking (a_1 is 'touch right side' and a_2 is 'touch left side')

	$\gamma(a_1, a_1)$	$\gamma(a_2, a_2)$	$\gamma(a_1, a_2)$
Mean Value	0.81	0.79	0.68
Standard Deviation	0.17	0.18	0.10

In order to provide insight into how detection of multiple actions can be addressed using the GDMM, the first approach (using one GDMM for each target action) is used in this chapter to detect the first four actions in Table 2. The results are illustrated in Table 4 for different sensitivity values.

6 Conclusion

This chapter presented a light-weight signal processing methodology for Body Sensor Networks applications by early rejection of non-target actions. The discussed hardware-assisted algorithm uses template matching blocks at different bit levels and finds an optimal order for their execution. The results demonstrate the effectiveness of this architecture in reducing the power consumption of the system. In particular, it achieves an average energy saving of 63.1% while maintaining 94.3% true positive rates in detecting actions of interest.

References

1. Benbasat, A.Y., Paradiso, J.A.: A framework for the automated generation of power-efficient classifiers for embedded sensor nodes. In: Proceedings of the 5th International Conference on Embedded Networked Sensor Systems, SenSys 2007, pp. 219–232. ACM, New York (2007)
2. Chaimanonart, N., Young, D.J.: A wireless batteryless in vivo EKG and body temperature sensing microsystem with adaptive RF powering for genetically engineered mice monitoring, pp. 1473–1476 (2009)
3. Chao, L., Tsui, C.-Y., Ki, W.-H.: A batteryless vibration-based energy harvesting system for ultra low power ubiquitous applications. In: Proceedings - IEEE International Symposium on Circuits and Systems, pp. 1349–1352 (2007)
4. Cong, P., Chaimanonart, N., Ko, W.H., Young, D.J.: A wireless and batteryless 10-bit implantable blood pressure sensing microsystem with adaptive RF powering for real-time laboratory mice monitoring. IEEE Journal of Solid-State Circuits 44(12), 3631–3644 (2009)
5. Cong, P., Chaimanonart, N., Ko, W.H., Young, D.J.: A wireless and batteryless 130mg 300w 10b implantable blood-pressure-sensing microsystem for real-time genetically engineered mice monitoring. In: Digest of Technical Papers - IEEE International Solid-State Circuits Conference (2009)
6. Cong, P., Ko, W.H., Young, D.J.: Wireless batteryless implantable blood pressure monitoring microsystem for small laboratory animals. IEEE Sensors Journal 10(2), 243–254 (2010)

7. Cuddihy, P., Weisenberg, J., Graichen, C., Ganesh, M.: Algorithm to automatically detect abnormally long periods of inactivity in a home. In: Proceedings of the 1st ACM SIGMOBILE International Workshop on Systems and Networking Support for Healthcare and Assisted Living Environments, p. 94. ACM (2007)
8. Douseki, T.: Ultralow-voltage MTCMOS/SOI technology for batteryless mobile system. In: International Conference on Solid-State and Integrated Circuits Technology Proceedings, ICSICT, vol. 2, pp. 1242–1247 (2004)
9. Douseki, T., Tsukahara, T., Yoshida, Y., Utsunomiya, F., Hama, N.: A batteryless wireless system with MTCMOS/SOI circuit technology. In: Proceedings of the Custom Integrated Circuits Conference, pp. 163–168 (2003)
10. Duda, R.O., Hart, P.E., Stork, D.G.: Pattern Classification. Wiley-Interscience Publication (2000)
11. Ghasemzadeh, H., Barnes, J., Guenterberg, E., Jafari, R.: A phonological expression for physical movement monitoring in body sensor networks. In: 5th IEEE International Conference on Mobile Ad Hoc and Sensor Systems, MASS 2008, pp. 58–68 (2008)
12. Ghasemzadeh, H., Guenterberg, E., Jafari, R.: Energy-Efficient Information-Driven Coverage for Physical Movement Monitoring in Body Sensor Networks. IEEE Journal on Selected Areas in Communications 27, 58–69 (2009)
13. Goldberg, D.H., Andreou, A.G., Julián, P., Pouliquen, P.O., Riddle, L., Rosasco, R.: A wake-up detector for an acoustic surveillance sensor network: algorithm and VLSI implementation. In: Proceedings of the 3rd International Symposium on Information Processing in Sensor Networks, IPSN 2004, pp. 134–141. ACM, New York (2004)
14. Hagler, S., Austin, D., Hayes, T.L., Kaye, J., Pavel, M.: Unobtrusive and ubiquitous in-home monitoring: A methodology for continuous assessment of gait velocity in elders. IEEE Transactions on Biomedical Engineering 57(4), 813–820 (2010)
15. Huynh, T., Schiele, B.: Analyzing features for activity recognition. In: Proceedings of the 2005 Joint Conference on Smart Objects and Ambient Intelligence: Innovative Context-Aware Services: Usages and Technologies, pp. 159–163. ACM (2005)
16. Jevtic, S., Kotowsky, M., Dick, R.P., Dinda, P.A., Dowding, C.: Lucid dreaming: reliable analog event detection for energy-constrained applications. In: Proceedings of the 6th International Conference on Information Processing in Sensor Networks, IPSN 2007, pp. 350–359. ACM, New York (2007)
17. Lester, J., Choudhury, T., Borriello, G.: A practical approach to recognizing physical activities. In: Fishkin, K.P., Schiele, B., Nixon, P., Quigley, A. (eds.) PERVASIVE 2006. LNCS, vol. 3968, pp. 1–16. Springer, Heidelberg (2006)
18. Liew, W.-S., Zou, L., abd Yao, X., Lian, Y.: A 1-v 60-uw 16-channel interface chip for implantable neural recording. In: Proceedings of the Custom Integrated Circuits Conference, pp. 507–510 (2009)
19. Malinowski, M., Moskwa, M., Feldmeier, M., Laibowitz, M., Paradiso, J.A.: Cargonet: a low-cost micropower sensor node exploiting quasi-passive wakeup for adaptive asychronous monitoring of exceptional events. In: Proceedings of the 5th International Conference on Embedded Networked Sensor Systems, SenSys 2007, pp. 145–159. ACM, New York (2007)
20. Mandal, S., Turicchia, L., Sarpeshkar, R.: A low-power, battery-free tag for body sensor networks. IEEE Pervasive Computing 9(1), 71–77 (2010)

21. Mitchell, S.L., Collin, J.J., De Luca, C.J., Burrows, A., Lipsitz, L.A.: Open-loop and closed-loop postural control mechanisms in Parkinson's disease: increased mediolateral activity during quiet standing. Neuroscience Letters 197(2), 133–136 (1995)
22. Moore, E.F.: The shortest path through a maze. In: Proceedings of the International Symposium on the Theory of Switching, vol. 2, pp. 285–292 (1959)
23. Morris, S.J., Paradiso, J.A.: Shoe-integrated sensor system for wireless gait analysis and real-time feedback. In: Proceedings of the Second Joint 24th Annual Conference Engineering in Medicine and Biology and the Annual Fall Meeting of the Biomedical Engineering Society, EMBS/BMES Conference, vol. 3, pp. 2468–2469 (October 2002)
24. Najafi, N., Ludomirsky, A.: Initial animal studies of a wireless, batteryless, MEMS implant for cardiovascular applications. Biomedical Microdevices 6(1), 61–65 (2004)
25. Nelson, R.C.: Qualitative detection of motion by a moving observer. International Journal of Computer Vision 7, 33–46 (1991), doi:10.1007/BF00130488
26. Ohayon, M.M., Roth, T.: Prevalence of restless legs syndrome and periodic limb movement disorder in the general population. Journal of Psychosomatic Research 53(1), 547–554 (2002)
27. Ou, Z., Tang, X., Su, T., Zhao, P.-F.: Cascade adaBoost classifiers with stage optimization for face detection. In: Zhang, D., Jain, A.K. (eds.) ICB 2005. LNCS, vol. 3832, pp. 121–128. Springer, Heidelberg (2005)
28. Parramon, J., Doguet, P., Marin, D., Verleyssen, M., Munoz, R., Leija, L., Valderrama, E.: ASIC-based batteryless implantable telemetry microsystem for recording purposes. In: Annual International Conference of the IEEE Engineering in Medicine and Biology - Proceedings, vol. 5, pp. 2225–2228 (1997)
29. Patel, S., Lorincz, K., Hughes, R., Huggins, N., Growdon, J.H., Welsh, M., Bonato, P.: Analysis of feature space for monitoring persons with Parkinson's Disease with application to a wireless wearable sensor system. In: 29th Annual International Conference of the IEEE Engineering in Medicine and Biology Society, EMBS 2007, pp. 6290–6293. IEEE (2007)
30. Polastre, J., Szewczyk, R., Culler, D.: Telos: enabling ultra-low power wireless research. In: Fourth International Symposium on Information Processing in Sensor Networks, IPSN 2005, pp. 364–369 (April 2005)
31. Ravi, N., Dandekar, N., Mysore, P., Littman, M.L.: Activity recognition from accelerometer data. In: Proceedings of the National Conference on Artificial Intelligence, vol. 20, p. 1541. AAAI Press; MIT Press, Menlo Park, Cambridge (2005)
32. Rumberg, B., Graham, D.W., Kulathumani, V.: Hibernets: energy-efficient sensor networks using analog signal processing. In: Proceedings of the 9th ACM/IEEE International Conference on Information Processing in Sensor Networks, IPSN 2010, pp. 129–139. ACM, New York (2010)
33. Sarpeshkar, R.: Ultra low power electronics for medicine. In: International Workshop on Wearable and Implantable Body Sensor Networks, BSN 2006, pp. 1–37 (2006)
34. Sasaki, S., Seki, T., Sugiyama, S.: Batteryless accelerometer using power feeding system of RFID. In: 2006 SICE-ICASE International Joint Conference, pp. 3567–3570 (2006)

35. Sen, A., Candan, K., Ferreira, A., Beauquier, B., Perennes, S.: On shortest path problems with "non-Markovian" link contribution to path lengths. In: Networking 2000 Broadband Communications, High Performance Networking, and Performance of Communication Networks, pp. 859–870 (2000)
36. Shoeb, A., Carlson, D., Panken, E., Denison, T.: A micropower support vector machine based seizure detection architecture for embedded medical devices. In: Proceedings of the 31st Annual International Conference of the IEEE Engineering in Medicine and Biology Society: Engineering the Future of Biomedicine, EMBC 2009, pp. 4202–4205 (2009)
37. Stangel, K., Kolnsberg, S., Hammerschmidt, D., Hosticka, B.J., Trieu, H.K., Mokwa, W.: A programmable intraocular CMOS pressure sensor system implant. IEEE Journal of Solid-State Circuits 36(7), 1094–1100 (2001)
38. Tavakoli, M., Turicchia, L., Sarpeshkar, R.: An ultra-low-power pulse oximeter implemented with an energy-efficient transimpedance amplifier. IEEE Transactions on Biomedical Circuits and Systems 4(1), 27–38 (2010)
39. Viola, P., Jones, M.: Rapid object detection using a boosted cascade of simple features. In: Proceedings of the 2001 IEEE Computer Society Conference on Computer Vision and Pattern Recognition, CVPR 2001, vol. 1, I-511–I-518 (2001)
40. Viola, P., Jones, M.J.: Robust real-time face detection. International Journal of Computer Vision 57(2), 137–154 (2004)
41. Viola, P., Jones, M.J.: Robust real-time face detection. Int. J. Comput. Vision 57, 137–154 (2004)
42. Yang, G.Z., Yacoub, M.: Body sensor networks. Springer-Verlag New York Inc. (2006)
43. Yang, Z.: Fast template matching based on normalized cross correlation with centroid bounding. In: 2010 International Conference on Measuring Technology and Mechatronics Automation (ICMTMA), March 13-14, vol. 2, pp. 224–227 (2010)
44. Zhang, P., Bui, T.D., Suen, C.Y.: A novel cascade ensemble classifier system with a high recognition performance on handwritten digits. Pattern Recognition 40(12), 3415–3429 (2007)

Inexpensive and Power-Efficient Wireless Health Monitoring System for the Aging Population

Jian Yuan[1] and Kok Kiong Tan[2]

[1] NUS Graduate School for Integrative Sciences and Engineering, Singapore
imyuanjian@gmail.com
[2] Department of Electrical and Computer Engineering,
National University of Singapore, Singapore
eletankk@nus.edu.sg

1 Introduction

As people age, many people experience health problems like heart attacks, strokes, accidental falls. When such events occur, immediate help is crucial to reduce the risk of complications or even deaths and greatly increase the likelihood of a return to independent living. To offer a sense of security to seniors and bring peace to their family members, automatic health monitoring is needed to detect such emergencies and raise timely alerts to family members. Currently, this need is remedied by Personal Emergency Response Systems (PERS). With PERS, seniors wear a pendant/watch which is wirelessly connected to a base unit with a built-in telephone. When needing help, they press a button to speak to an emergency response centre. Modern PERS offer more functionalities such as fall detection and heart rate monitoring. Notable examples are Philips Lifeline with AutoAlert and myHalo monitoring. However, PERS typically use point-to-point wireless technologies which impose a hard limit on the reception range. PERS typically works well within 100 meters, preferably with line-of-sight. In addition, PERS charge expensive monthly fees (e.g. US$53 for Lifeline [1] and US$59 for myHalo [2]), which are heavy financial burdens for seniors.

2 Related Research

2.1 Heal Monitoring Using Wireless Sensor Networks

Since the emergence of wireless sensor networks (WSN), numerous health monitoring systems based on WSN have been proposed. Malan *et al.* [3] designed a multi-hop WSN called CodeBlue for emergency and disaster responses. Sensor nodes periodically transmit packets containing heart rate, oxygen saturation (SpO2) in multiple hops to a PC or a PDA. [4] implemented a multi-hop WSN called AlarmNet for assisted living and 24/7 monitoring of temperature, activity, luminosity, electrocardiography (ECG) and oxygen saturation (SaO2) in a residential environment.

S.C. Mukhopadhyay (ed.), *Wearable Electronics Sensors,*
Smart Sensors, Measurement and Instrumentation 15, DOI: 10.1007/978-3-319-18191-2_5

AlarmNet also integrates a WBAN (Wireless Body Area Network) called SATIRE for classifications of activities of daily living. SATIRE logs and caches accelerometer data in flash memory and upload when close to a remote processing unit.

2.2 Fall Detection Using MEMS Sensors

In recent years, there is an increasing trend in utilizing MEMS accelerometers to detect falls. Some [5, 6, 7, 8, 9, 10, 11] used a single triaxial accelerometer attached to torso (e.g. waist, chest or pelvic). Others such as Kangas *et al.* [12] used more than one accelerometer to study waist, wrist and head simultaneously. Researchers at MIT [13] use multiple miniature and low-cost devices called Wockets to collect human motion data using accelerometers at various parts of the human body so as to increase accuracy and detect a wide range of activities. MEMS accelerometers are capable of generating massive amount of data within short periods. As pointed out by [7], in studies of falls using accelerometers, a sampling frequency ranging from 50 Hz to 250 Hz is typically required so as not to miss high frequency components which might contain a fall. Processing massive accelerometer data in real-time is too expensive for a resource-constrained device thus most researchers choose to stream data wirelessly to a remote processing unit instead. However, continuous wireless transmission consumes bandwidth and drains battery life quickly. This approach is acceptable for research studies but impractical in real applications.

3 Motivation

Aforementioned reasons and technologies motivate the development of a low-cost and scalable wireless health monitoring system, *e-Guardian*, for the lone elderly. It aims to transform elder-care into a collaborative effort mainly involving people who live with the elderly, rather than a private company that provides service at subscription charges. *e-Guardian* takes advantage of recent advances in wireless sensor networks (WSN), hardware miniaturization, MEMS (microelectromechanical systems) sensors, mobile computing and machine learning.

In an *e-Guardian* system, a base station (BS) starts a local wireless network and a number of range extenders (RE) extend the network to cover a much larger area. The highlight of *e-Guardian* is a set of small, light weight and low-power wearable devices (WD). A WD consists of a micro-controller unit (MCU), a RF (radio frequency) transceiver and several miniaturized sensors. It can be used to summon help and automatically detect accidental falls, monitor simple activities such as walking, casual movement and inactivity.

e-Guardian is simple and low-cost, yet still capable of alerting caregivers at life-critical moments. Its scalability allows sharing of a single system (together with SMS and data subscriptions) among multiple seniors, which reduces cost per capita significantly.

4 Challenges

e-Guardian employs multi-hop WSN which is essential for achieving scalability but it usually suffer from limited bandwidth. As the number of wearable nodes increases, network at the remote processing unit will be easily congested. To deal with this problem, *e-Guardian* takes a decentralized approach to process raw sensor data locally in WDs. WDs are based on low-power 8-bit MCU with limited clock speed and memory so they cannot handle expensive computations. *e-Guardian* avoids this by utilizing advanced digital sensors which support hardware interrupts as well as data buffering. An interrupt-driven fall detection algorithm has been proposed and implemented which consumes much less power because WDs only process upon hardware and timer interrupts, and stay in sleep mode to conserve power the rest of time. Since WDs do not stream massive data wirelessly, this algorithm also saves tremendous transmission power and network bandwidth.

5 System Architecture

Fig. 1 shows the system architecture of *e-Guardian*. Essentially, *e-Guardian* embodies a wireless infrastructure which provides a wireless link between caregivers and seniors wearing WDs. Inter-device communications are enabled by ZigBee, which

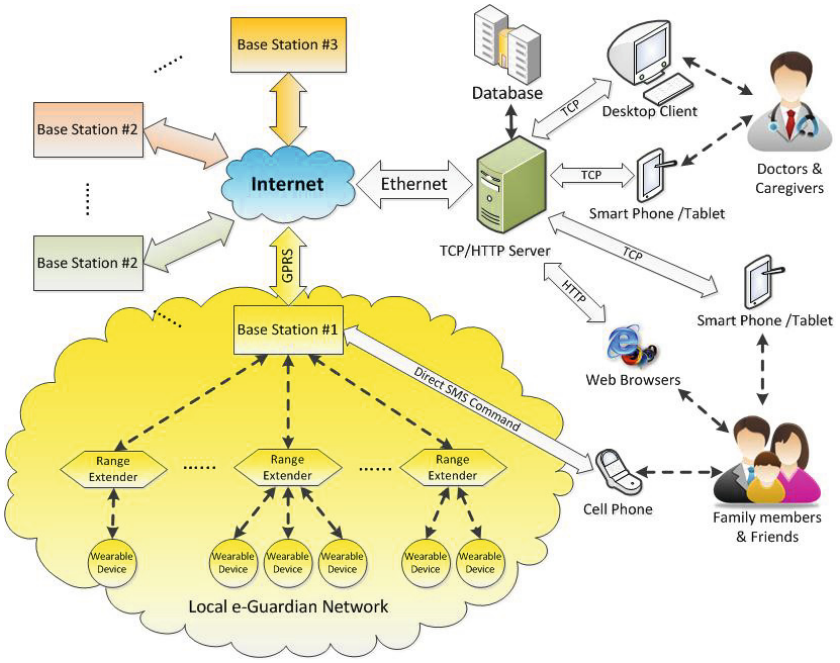

Fig. 1 *e-Guardian*'s System Architecture

is a low-cost, low-power and secure wireless mesh network standard. ZigBee is self-organizing and self-healing. If an existing route is broken, a route discovery will be initiated automatically and a new route will be established. In this way, *e-Guardian* can cover a single household with its surroundings or an entire village/community area.

BS is the gateway device between ZigBee and cellular networks. It integrates a GSM/GPRS module which is used to implement two alternative channels, SMS and Internet, for commanding and accessing information. *e-Guardian* can be implemented to connect to a TCP (Transmission Control Protocol) server. On top of that, an HTTP (Hypertext Transfer Protocol) server can be configured to allow users to access *e-Guardian* anywhere via a web browser.

In *e-Guardian*, BS and REs are mains-powered with fixed locations. WDs are battery-powered and can move freely in a local *e-Guardian* network. To achieve long battery life, WDs only incorporate sensors which support duty-cycling or hardware interrupts. Example sensors include digital MEMS accelerometers, body temperature sensors, light sensors and heart rate sensors.

6 Realization

6.1 e-Guardian Devices

An *e-Guardian* prototype has been developed to show the concept and various features of *e-Guardian*. Fig. 2(a) shows a BS prototype which consists of a ZigBee module CC2430 from Texas Instruments and a GSM/GPRS module GM862 from Telit. BS is configured as a ZigBee Coordinator, responsible for starting up the network. A command parser has been implemented to allow users to interact via either SMS or Internet. Fig. 2(b) shows an RE prototype. It routes data packets for other devices and is powered by the mains supply. Whenever there is any dead spot, a RE is all that is needed. Fig. 2(c) shows a prototype of a WD which consists of a CC2430 chip and a digital MEMS accelerometer (ADXL345 from Analog Devices). It is configured as a sleeping ZigBee End Device. The design philosophy of WD is that seniors are only expected to press a panic button to summon help and all other features are automatic.

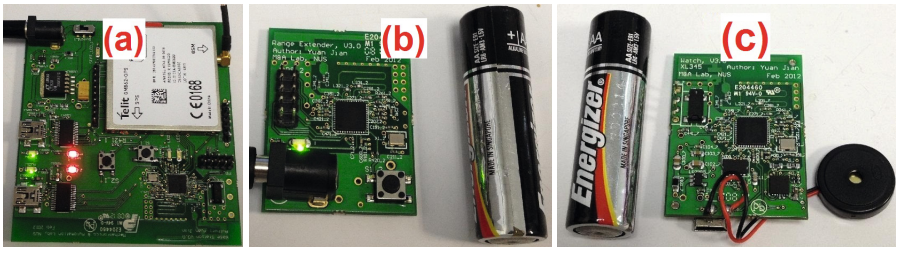

Fig. 2 (a) Base Station, (b) Range Extender, (c) Wearable Device

6.2 TCP/HTTP Server

A TCP/HTTP server allows caregivers to access *e-Guardian* via a web browser. A prototype TCP server is developed using Twisted, an event-driven asynchronous network framework for Python. The TCP server accepts connections from an *e-Guardian* system and the HTTP server on behalf of a client connection from a web browser. Upon a client connection, the TCP server will populate all online *e-Guardian* systems so a client could choose one to communicate with. A WebSocket application has been developed using Python, HTML and Javascript, and is hosted using a small standalone WebSocket server called pywebsocket. WebSocket, as standardized in HTML5, is a web technology which allows a web browser to exchange messages with a HTTP server in real-time without periodic polling. Fig. 3 shows a web connection from a Safari browser in an iPhone 4S.

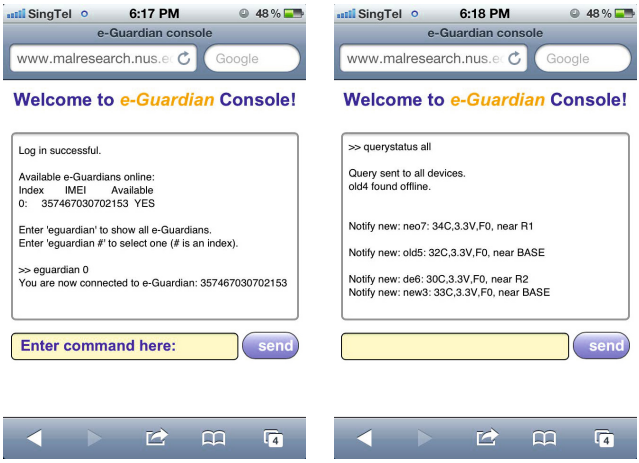

Fig. 3 *e-Guardian* Web Application

7 Fall Detection

7.1 MEMS Accelerometers

In recent years, MEMS (microelectromechanical systems) inertial sensors have sparked an intense interest in studying falls. [14] and [15] separately implemented fall detection algorithms right within Android phones, taking advantage of their built-in accelerometers and high-level APIs (application programming interface). [5, 16, 6, 7, 17, 8, 18, 10, 11] used a single triaxial accelerometer attached to certain parts of the torso (waist, chest, back or pelvic) to study falls. Some used more than one accelerometer. For example, [12] studied accelerometers on waist, wrist and head simultaneously. Some others [19, 20] used gyroscopes in addition to accelerometers. [19] used a triaxial accelerometer on waist and a bi-axial gyroscope

on thigh. [20] studied a triaxial accelerometer and a triaxial gyroscope on both chest and thigh.

MEMS accelerometers have also been used to study activities of daily livings (ADLs) [21, 22, 23, 24]. In this field, Wockets [13] is a notable open source project which aims to build hardware and software that permits automatic, 24/7 physical activity and context detection on mobile phones. Wockets are miniature and low-cost devices that collect human motion using accelerometers, and send raw data via Blue-tooth to users' mobile phones for further processing. Wockets are placed at various positions of the human body to increase robustness and accuracy thus detecting a wide range of activities.

MEMS accelerometers, small and low-power, are well-suited for battery-powered wearable devices. However, they can generate a huge amount of data quickly. In studies of falls using accelerometers, a sampling rate ranging from 50 Hz to 250 Hz is typically required [7], in order not to miss critical high frequency components (e.g., a sudden fall). Assuming a sampling rate of 50 Hz, even if each axis is represented by a single byte, there will be 150 bytes of information per second for a triaxial accelerometer. Analyzing each piece of data is no easy task for a resource-constrained device which typically has limited processing power. For practical implementation of fall detection and ADL classification algorithms, a design can take one of the three approaches below.

I. Remote Processing: Stream accelerometer data wirelessly to a base unit which has more processing power or,
II. Local Processing: Implement an algorithm completely within a wearable unit which is typically resource and power constrained or,
III. Heterogeneous: Pre-process raw accelerometer data (e.g., run-length encoding, feature selection, dimensionality reduction) so as to compress it into smaller size, and then transmit wirelessly to a base unit for further processing.

Approach I consume tremendous bandwidth and power due to continuous wireless transmission. Approach II drains batteries quickly due to continuous processing of accelerometer data and classification algorithms. Approach III seems most promising. However, it remains a challenge to design a preprocessing algorithm that is lightweight and capable of transforming raw data effectively into much smaller feature sets.

In studies of falls or ADLs evaluated above, except for a few which chose to store data on an SD card [17, 10, 12] for off-line processing, all took a remote processing approach to stream raw accelerometer data wirelessly to a remote unit via either Blue-tooth [8, 18, 9, 25] or ZigBee [5, 11, 19]. This approach is acceptable and usually the most convenient for research studies. However, it is challenging to make practical use of algorithms designed this way in a small wearable device while achieving long battery life. For instance, Wockets continuously stream raw accelerometer data via Blue-tooth which is very power consuming for both Wockets and mobile phones. In fact, Wockets were designed only to meet a goal of 24-hour performance on one charge.

People become increasingly forgetful as they age so charging/replacing batteries should be as infrequent as possible. A practical fall detector should have a battery life of several months in order to make it appealing to the elderly. For instance, a senior might fall once a year. If a fall detector needs recharge once every two days, this will translate to $365/2 = 182.5$ charges per fall. As a result, the senior will probably be reluctant to wear one on a 24/7 basis. Therefore, a practical fall detector should have a battery life of several months in order to make it appealing to the elderly.

This paper approaches fall detection and ADL classification from a practical point of view. A fall detection algorithm and an ADL classification algorithm are proposed, both of which are very power-efficient and can be implemented in most 8-bit MCUs (micro-controller unit) with limited RAM (random access memory) and clock speed. Both algorithms are based on a digital MEMS accelerometer which supports interrupts and data buffering. They take an interrupt-driven approach which is completely different from conventional approaches where an algorithm must examine and process every piece of data sampled at high frequencies. The interrupt-driven approach allows a host MCU to examine significantly less data and only process upon an accelerometer interrupt or a timer interrupt. Thus, it conserves both power and bandwidth.

7.2 Analog vs. Digital Accelerometer

An analog tri-axial MEMS accelerometer requires three dedicated ADC (analog-to-digital converter) channels on the host MCU to continuously convert accelerometer signals into digital representations. Currently, MEMS accelerometers are shifting from conventional analog types to digital types. A digital accelerometer typically features a serial interface which is either SPI (Serial Peripheral Interface) or I^2C (Inter-Integrated Circuit). It is less susceptible to noise than its analog counterpart. Digital accelerometers often have a FIFO (first-in/first-out) memory block for buffering data and various interrupt features such as data-ready, free-fall, inactivity, activity, wake-up, single-tap, double-tap and orientation. Some have built-in low/high-pass filters. Some has taken even bigger steps by incorporating advanced technologies into a single MEMS chip. For instance, InvenSense released a family of MEMS chips that combine several inertial sensors with an on-chip low-power Digital Motion Processor (DMP) [26]. This DMP can carry out simple processing and calculations so as to offload the host MCU and thus reduces overall power consumption.

Digital accelerometers are gaining popularity as they are used in many battery-powered devices where there is a strong need to relieve burdens on host MCUs. Depending on MEMS vendors, each digital accelerometer offers slightly different sets of features. Nevertheless, most digital accelerometers support FIFO and common interrupt features including activity, inactivity, free fall. Creative use of these features can save tremendous amount of computational resource. For instance, acceleration data can be queued in FIFO and when it reaches certain amount, an interrupt will be generated to notify the host MCU to retrieve all data at once. If an accelerometer

is stationary, an inactivity interrupt will be asserted and the host MCUs could go to sleep without examining any data. However, taking advantage of such advanced features does come at a price which is the lack of portability. If an algorithm exploits a particular feature of an accelerometer which is not available elsewhere, it cannot be ported to other accelerometers without tweaking the algorithm. In contrast, analog accelerometers are free from such concerns.

It is noticeable that in the pstudies of falls and ADLs evaluated above, all used an analog accelerometer except for [5, 11]. However, [5, 11] used it in a way no different than analog accelerometers, i.e., raw accelerometer data was simply read and streamed to a remote base unit for processing.

Despite the lack of portability in algorithms designed for digital accelerometers, a digital accelerometer outperforms its analog counterpart by several orders in term of power saving. In this paper, a digital MEMS accelerometer, ADXL345 from Analog Devices, is used to implement a fall detection algorithm and an ADL classification algorithm.

7.3 ADXL345 Basics

ADXL345 supports various interrupts, of which INACTIVITY, ACTIVITY, FREE_FALL are important for the proposed algorithms. For both ACTIVITY and INACTIVITY interrupts, there are two modes, DC mode and AC mode respectively. In DC mode, the current acceleration magnitude is directly compared with THRESH_ACT and THRESH_INACT, threshold values for ACTIVITY and INACTIVITY respectively. In AC mode, for ACTIVITY detection, a reference value is taken as the acceleration value at the start of activity detection. New samples of acceleration are compared to this reference value and ACTIVITY is triggered if the difference exceeds THRESH_ACT. For INACTIVITY detection, a reference value is used for comparison and is updated whenever the device exceeds THRESH_INACT. Subsequent samples are compared against this reference value.

To reduce the number of ACTIVITY and INACTIVITY interrupts, ADXL345 provides a link mode functionality. Link mode delays the start of ACTIVITY detection after an INACTIVITY is detected. Only after ACTIVITY is detected, INACTIVITY detection then begins, preventing the detection of ACTIVITY. Link mode makes it possible that when an accelerometer is static, no repeated INACTIVITY interrupts will ever be generated.

ADXL345 offers an FIFO of 32 sets of accelerometer data. FIFO has four modes, of which TRIGGER mode is important for the two algorithms. A trigger evepnt refers to interrupts assigned to either INT1 or INT2, which is configurable. A trigger level for FIFO can be set to a number n, which can be anywhere between 0 to 31 (inclusive). Upon a trigger event, the FIFO will discard all accelerometer data in FIFO except the latest n samples. The FIFO will continue to fill up till it is full. This feature allows FIFO to retain a window of 32 samples around a trigger event and the host MCU can choose to run a relatively complex algorithm on these 32 samples.

Interrupts together with FIFO allow both algorithms to skip the majority of accelerometer data and only examine a tiny portion which is of interest.

7.4 Embedded Software Environment

CC2430 in WD runs a ZigBee software stack called Z-Stack. Z-Stack is built on a cooperative, round-robin scheduler called OSAL (Operating System Abstraction Layer) which provides timers, memory allocation, inter-task communication, interrupt handling, and power management, etc. At the low level, OSAL interfaces with ISR and board hardware. OSAL has a high level software timer implemented on top of one of the on-chip hardware timers. This high level timer is used to implement a flexible recurrent timer routine that can be enabled and disabled any time the program wishes.

Besides the timer routine, CC2430 also implements two hardware ISRs for INT1 and INT2 pins respectively. These three routines will be placed where the code for both algorithm resides.

7.5 Accelerometer Placement

Currently, most fall detection algorithms and ADL classifiers are based on accelerometers attached to parts of a torso. Accelerometer data collected at wrists are typically used to complement accelerometers attached to torsos. [12] evaluated accelerometers placed at waist, wrist and head and concluded that wrist was not optimal for fall detection. [27] argued that a wrist-worn accelerometer could not reliably distinguish falling and sitting down.

Placing accelerometers at the center of gravity is the most reliable means, but also the least comfortable on a daily basis. A wrist-watch type would be the most acceptable as it can remove social stigma associated with wearing a medical or health care device. Another advantage of a wrist device is high acceptability for wearing at night and during bathing. The proposed algorithms are based on wrist-worn accelerometers despite higher false positive rates due to complicated movements of wrists in daily activities.

7.6 Fall Detection Algorithm

The proposed fall detection algorithm is derived from an algorithm [28] proposed in an application note by Analog Devices. The original algorithm characterizes a fall by examining four phases of a fall – INITIAL STATUS, WEIGHTLESS, IMPACT and MOTIONLESS. In a valid fall, WEIGHTLESS, IMPACT and MOTIONLESS must occur in succession within predefined time intervals. A fall is finally qualified if vector difference between final orientation and initial orientation surpasses a threshold, which indicates a significant orientation change.

The original algorithm has three major limitations.

1. It relies heavily on the host MCU to check the accelerometer's interrupt status every 20ms using a recurrent timer interrupt, even if seniors may be sleeping through the whole night. This approach wastes the majority of processor time doing useless checking.
2. It assumes a fixed initial status of gravity orientation (x = 0, y = -g, z = 0). Immediately after the wearer falls, the final orientation will be significantly different than the fixed initial orientation. This assumption only makes sense if an accelerometer is worn with one axis parallel to the gravity, (e.g. when the accelerometer is embedded within a belt worn by a standing human subject). The assumption is totally invalid if the accelerometer is wrist-worn.
3. The proposed FREE_FALL threshold will lead to continuous assertions when an accelerometer is positioned in certain orientations, even though the wearer is not falling. This will be explained thoroughly in Section 7.6.2 below.

The proposed algorithm has made significant improvements in terms of power saving by removing its timing dependency on the host MCU as much as possible. As sleeping is an instinct of a ZigBee End Device, this algorithm spares the host MCU from periodical polling and allows the host MCU to stay in deep sleep mode completely when there is no interrupt.

7.6.1 Output Data Rate (ODR)

Conventional fall detection algorithms require sampling rates of no less than 50Hz. ADXL345 provides lower ODR by decimating a common sampling frequency. Frequency components higher than an ODR such as a sudden and short impact are likely not to be present in sampled data. However, ACTIVITY and FREE_FALL are based on undecimated accelerometer data so frequencies up to 1600Hz are always captured. Thus, ADXL345 can be safely set to a lower ODR without worrying that high frequency components such as a fall will ever be missed.

The proposed ODR is 25Hz. At this rate, FIFO will be able to hold $32/25 = 1.28$ seconds of data. As FIFO TRIGGER mode is used, only the latest 16 samples are kept upon a trigger. These 16 samples, corresponding to 0.64 seconds of accelerometer data, will be used for estimation of initial postures of a wrist.

7.6.2 Threshold of Falling

During a fall, a wrist typically falls from a high level to a low level within a very short time. During this time, the accelerometer attached to the wrist will experience some gravity loss, which is reflected in the accelerometer reading by all axes converging towards zero. This pattern can be exactly captured by using FREE_FALL interrupt.

[28] proposed 0.75g and 30ms for THRESH_FF and TIME_FF which are threshold and time windows of FREE_FALL interrupt respectively. There is a serious flaw with this threshold. ADXL345 asserts FREE_FALL when all axes are smaller than

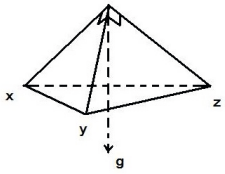

Fig. 4 All Axes with Equal Angles with the Gravity

THRESH_FF for a time longer than TIME_FF. This assertion is not based on the vector sum of all axes which is $sv = \sqrt{x^2 + y^2 + z^2}$. There is a possibility that the accelerometer is positioned such that all axes have equal angles with the gravity vector, as shown in Fig. 4.

The projection of the gravity vector onto each axis can be calculated by using volume of the triangular pyramid. Assuming that the three sides on the top all have a length of 1, the height h can be calculated to be $\frac{\sqrt{3}}{3}$ and the projection angle is $\theta = sin^{-1}(\frac{\sqrt{3}}{3})$. Thus, the projection of the gravity into each axis will be $\frac{\sqrt{3}}{3}g \approx 0.57735g$. When the accelerometer is positioned as in Fig. 4, FREE_FALL interrupts will be continuously asserted as all axes are smaller than THRESH_FF ($0.75g$). This will be inaccurately detected as a long free-fall in the original algorithm.

The new threshold proposed is $0.5625g$ which is the largest configurable value under $0.57735g$. The TIME_FF is correspondingly smaller, which is set to $20ms$ instead. This setting has been tested to be responsive enough when wrists lower down relatively quickly in experiments.

7.6.3 Threshold of Impact

During a fall, a wrist will typically hit something. The impact can be detected by using ACTIVITY interrupt. However, during ADLs, there are occasional movements leading to relatively high impacts. Impacts caused by ADLs are normally smaller than impacts caused by falls but there is a region of overlap between the two, as studied by [29]. A threshold must be set to differentiate fall impacts from ADL impacts. From extensive experiments, during a fall, this impact will easily exceed 4g while ADLs only occasionally exceed this value.

The ACTIVITY interrupt is asserted when any of the axes exceeds THRESH_ACT. Due to a problem similar to that in Section 7.6.2, during an impact, the vector sum of the impact could have a direction with the same angles with all axes. Thus, this impact will be projected equally to each axis, leading to smaller values detected at each axis. This scaling factor is still $\frac{\sqrt{3}}{3}$. Therefore, THRESH_ACT is set to be 2.25g, the largest configurable value under $\frac{\sqrt{3}}{3} \times 4g \approx 2.31g$.

7.6.4 Assumption of Orientation Change

Most fall detections using accelerometers around torsos could easily assume that before and after a fall, there will be significant change in orientation [20, 18, 30, 11].

For wrists, it is less certain to assume an orientation change. However, extensive experiments performed by human test subjects show that during an actual fall, the orientation or posture of wrist will almost certainly change. This is due to the fact that, most falls occur when seniors are upright (walking or standing). As a result, their lower arms usually point roughly downwards. After falls, their lower arms will be typically horizontal. Therefore, after a fall, at least a slight orientation change could be legitimately assumed.

The assumption of slight change in orientation will help eliminate the majority of ADLs. As discussed in Section 7.6.3, there is an overlap between impacts due to falls and impacts due to ADLs. During ADLs such as sitting down and resting arms on chairs, wrists will typically hit things, thus leading to impacts, which can be relatively high sometimes. However, most conscious human actions usually do not result in much change in orientation before and after impacts. This is certainly not always true. Nevertheless, the assumption of slight change in orientation is able to filter out quite a lot of ADLs while it is less likely to filter out a fall mistakenly.

The slight change in orientation is quantitatively defined as a relatively small vector difference of 0.5g between the gravity vector measured in the accelerometer before and after a fall.

7.7 Algorithm Description

The proposed algorithm is modeled as a finite-state machine. A flow chart shown in Fig. 5 is used to illustrate the algorithm. It essentially consists of six states, from F0 to F5. The details of this algorithm are described as below.

(F0) F0 is the initial state as well as reset state. ADXL345 is initialized as follows:

a. Data rate: 25Hz.
b. ACTIVITY, INACTIVITY are enabled and mapped to INT1. ACTIVITY threshold is 2.25g. INACTIVITY threshold is 0.5g and its detection time window is 1 second.
c. Link mode is enabled. By enabling link mode in the state F0, INACTIVITY will not be asserted repeatedly if seniors are not moving (e.g. sleeping).
d. FREE_FALL is enabled and mapped to INT2. FREE_FALL threshold is 0.5625g and its detection window is 20ms.
e. FIFO is initialized to TRIGGER mode and is triggered by FREE_FALL. When triggered, FIFO will hold the latest 16 samples before the trigger, discard earlier ones, continue to collect until full.
f. When returning from other states, CC2430 timer ticks (started in F1) will be stopped and the system is reinitialized.

(F1) When FREE_FALL is asserted, the algorithm enters F1.

a. FIFO is triggered and will hold latest 16 samples.
b. CC2430 starts a 100ms timer. This timer is recurrent, which means it will start another 100ms timer when the previous one expires.

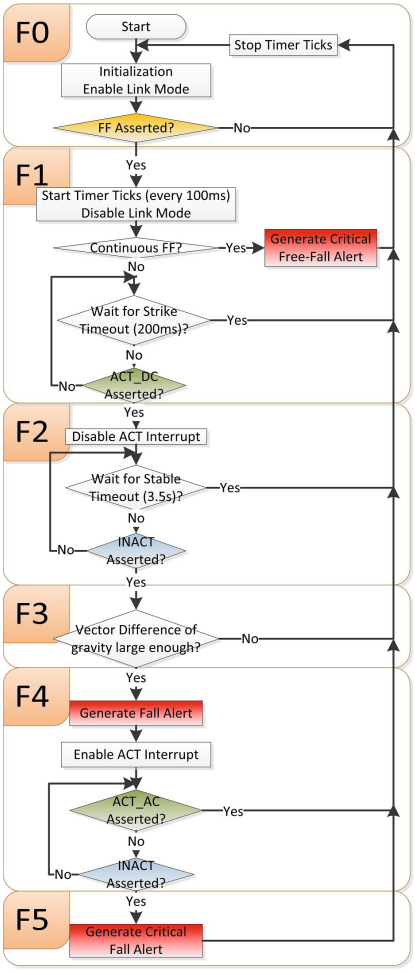

Fig. 5 Flow Chart of the Proposed Fall Detection Algorithm

c. Link mode is disabled, so both ACTIVITY and INACTIVITY are ready to be detected.
d. If FREE_FALL is asserted for more than 300ms (i.e. 3 timer ticks), a critical free-fall alert will be generated.

(F2) If ACTIVITY is asserted within 200ms after FREE_FALL was asserted, the algorithm enters F2, otherwise F0.

a. ACTIVITY is disabled. During an impact, ACTIVITY might be asserted multiple times since link mode is disabled in state F1. One assertion is enough for judging an impact and subsequent assertions are inhibited by disabling ACTIVITY.

b. CC2430 retrieves 16 data samples in FIFO, averaging the first 10 samples as the initial posture of wrist. At a data rate of 25Hz, 10 samples equal to 0.4 (10/25) seconds of data, 0.24 ((6-6)/25) seconds before FREE_FALL. This initial status will be useful in F3.

(F3) If INACTIVITY is asserted within 3.5s after ACTIVITY, the algorithm enters F3, otherwise F0. In F3, CC2430 retrieves the latest 10 samples and does an average on them as the final posture of wrist. The vector difference between the final and initial postures is calculated.

(F4) If the difference exceeds 0.5g which suggests a slight change in orientation, a fall alert is generated and the algorithm enters F4.

a. ACTIVITY is enabled again.
b. INACTIVITY detection time window is set to 10s to determine if there is a long fall (long motionless).
c. If ACTIVITY is asserted in F4, the system goes to F0 and gets ready for another round of detection.

(F5) If INACTIVITY is asserted after 10s, this indicates long motionless and the system goes to F5. A critical fall alert is raised and the system goes to F0 immediately.

7.8 Experimental Studies

7.8.1 Trial Study

A trial study has been carried out to evaluate fall detection accuracies in real world scenarios at Jurong Central Daycare Centre, which is a typical elder-care center in Singapore. It takes care of seniors from 9 a.m. to 6 p.m., Monday to Friday. The trial started from 9th July to 9th August, 2012. There were altogether 24 week days during the whole trial period. Three senior volunteers were willing to participate in this study. They wore WDs when they arrived at 9 a.m. and took them off before they left at 6 p.m..

During the period of this trial study, no real fall occurred. However, this study still provided valuable information about one important factor of a fall detection algorithm - false positives. A total number of 83 false positives were registered. This means that, on average, each WD had a false positive rate of $83/(24 \times 3) \approx 1.153$ times per day. For comparison, the best false positive rate in all fall detection algorithms for measurement at parts of a torso is 0.6 false positive per day, as evaluated by [7]. Considering that wrists are more difficult to study than parts of a torso, this rate of false positives is encouraging.

7.8.2 Simulated Falls

As it is difficult to obtain real-world falls, tests of the proposed fall detection algorithm were simulated by four young subjects. Each of them wore a WD on his/her

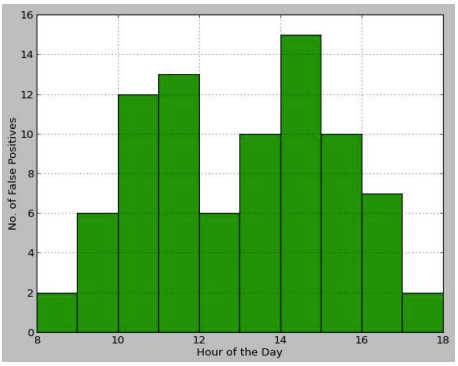

Fig. 6 Total False Positives in the Trial

left wrist and performed 4 types of activities: (1) walking, (2) walking upstairs, (3) walking downstairs, (4) walking some distance away, sitting down in a chair beside a desk and doing things such as writing, picking up and putting down random objects. Each person performed each activity five times for two minutes each time. Then activities (1), (2), (3) were performed again for five times, but each with a fall in the middle. Test results are shown in Table 1.

Table 1 Simulated Fall Results

Activity type	With a fall	Falls detected
(1)	yes	19/20
(1)	no	0/20
(2)	yes	19/20
(2)	no	0/20
(3)	yes	17/20
(3)	no	0/20
(4)	no	3/20

It is observed that during continuous walking, falls were never be falsely triggered as INACTIVITY interrupt did not have a chance to assert. While sitting down, wrists occasionally hit the desk with high impact, a false positive fall will be accidentally triggered. It can also be observed that young subjects easily created false positives (3/20). In contrast, seniors in their real daily lives only creates 1.153 times per day as evaluated in Section 7.8.1. A very probable reason is that young stronger subjects create large impacts in their ADLs which were easily confused with a fall in the fall detection algorithm, as discussed in Section 7.6.3

7.9 Power Improvement and Battery Life Analysis

To simplify the estimation of improvement in power consumption compared to the original algorithm, a WD is assumed to be static so it never triggers FREE_FALL and ACTIVITY interrupts. This will be true the majority of the time considering that seniors are relatively inactive. The original algorithm requires CC2430 to trigger a timer event every 20 ms. CC2430 consumes 492 μA current in the active mode (with radio off) and 0.9 μA in the sleep mode. It takes at least 54 μs to switch from sleep mode to active mode and vice versa. Context switch due to interrupt handling, calculations and serial communications with ADXL345 are all assumed to be quick and thus neglected for the convenience of estimation. The duty cycle of the 20 ms timer interrupt will be $54\mu s \times 2/20ms = 0.54\%$. The average current consumption will be $0.54\% \times 492\mu A + (1 - 0.54\%) \times 0.9\mu A \approx 3.55\mu A$. Compared to the new algorithm which never uses this 20 ms timer when static, the power consumption is nearly four times ($3.55/0.9 \approx 3.94$). In reality, interrupt handling, calculations and serial communications will take quite some time. Therefore, the actual power saving is much more than four times.

The total current consumption of a WD is measured by connecting a 7.5Ω resistor in series with it. The WD polls message from its parent range extender once every 5 seconds. Fig. 7 shows a measurement of power consumption of the WD when statically placed. It can be clearly seen that two current peaks are spaced by 5 seconds. Each current peak corresponds to CC2430 waking up from sleep mode for polling. The magnitude of the current peak is approximately $4.4 \times 50mV/7.5\Omega = 29.33mA$. The sleep current appears to be noisy and is too small to be visible. Instead, it was measured by a multimeter to be $69\mu A$. Within the $69\mu A$ sleeping current, $40\mu A$ is attributed to the current consumption of ADXL345 at an ODR (output data rate) of 25Hz. The remaining $29\mu A$ is consumed by CC2430 in sleep mode and its peripherals.

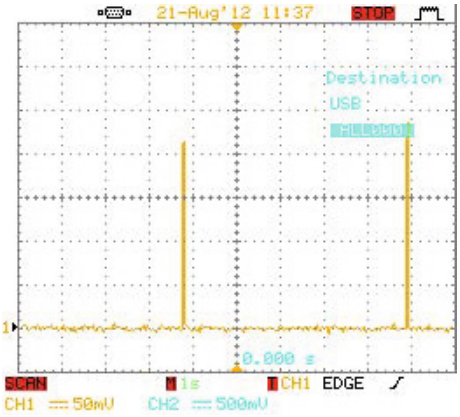

Fig. 7 Current Consumption Measured by an Oscilloscope (duration of 10 seconds)

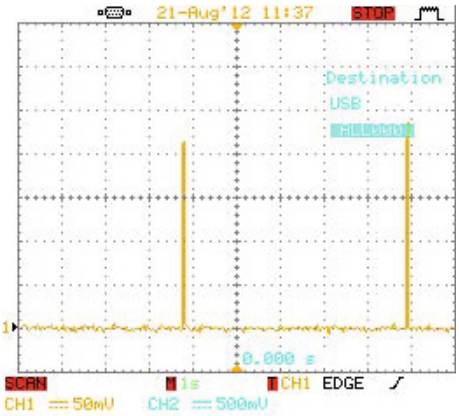

Fig. 8 Current Consumption Measured by an Oscilloscope (duration of 50 milliseconds)

Zooming in to a current peak reveals more details. Fig. 8 shows the same current peak for a duration of 50 milliseconds. Equation 1 estimates the power consumption during a single current peak by evaluating the area of the current peak. The bottom of the current peak spans a time frame of approximately 2.1 horizontal divisions. Then the 2.1 division is subdivided into 0.9, 0.5, 0.2 and 0.5. The total area is calculated by summing the four approximately rectangular blocks.

$$P_{peak} \approx \frac{(1.7 \cdot 0.9 + 4.6 \cdot 0.5 + 4.3 \cdot 0.2 + 1.7 \cdot 0.5) \cdot 50mV \cdot 5ms}{7.5\Omega} \approx 0.1847mA \cdot s \quad (1)$$

The power consumption during sleep in a 5-second time frame is $69\mu A \times 5s = 0.345mA \cdot s$. Therefore, the total current consumption within 5 seconds is $0.1847 + 0.345 = 0.5297mA \cdot s$. Then, it follows that the current consumption of a day is $0.5297 \times (12 \cdot 60 \cdot 24) = 9153.2mA \cdot s = 2.5426mAh$. Assuming a button cell battery with a nominal capacity of 200 mAh, it could power a WD continuously for $200/2.5426 \approx 78.7$ days.

8 Activities of Daily Living

In the proposed fall detection algorithm, depending on the wrist's movement, the algorithm flows dynamically among the six states. The time it spends in each state gives a lot of information about activities of a wearer.

Traditionally, studies of ADLs such as Wockets aim to identify a number of activities including walking, climbing stairs, sitting, sleeping, bathing, cooking, using multiple sensors. In this paper, since only one accelerometer is used, only a few simple activities can be inferred from accelerometer data. The identifiable activities are

"Walk", "Random"(random wrist movements), and "Quiet" (no movement at all). These activities are purely inferred from accelerometer information. However, it is possible to categorize these activities into more specific activities or even abnormalities by using accelerometer data along with additional contextual information such as time and location. For instance, "Quiet" at mid night most likely means sleeping. Too many "Random" incidences during night might indicate poor sleeping quality. "Quiet" in bath rooms longer than certain time (e.g ., 30 minutes) is abnormal and an alert can be raised.

8.1 Feature Extraction

The features used to study ADL are extracted from the fall detection algorithm. However, a minor change is necessary, which does not affect the correctness of the proposed fall detection algorithm but will increase the number of interrupts generated when the wrist is doing "Random" activities. This change is made to state F0. Originally, in state F0, ACTIVITY threshold is set to 2.25g while INACTIVITY threshold is 0.5g, as shown in Fig. 5. Even though these two thresholds are initialized in state F0, they are not used until state F2 and state F4. To capture ADL, a change needed is to set both thresholds to 0.75g in state F0, an empirical threshold obtained by experiments. Both interrupts need to operate in AC mode and link mode is still enabled. By setting both thresholds to the same small value, when a wrist moves a small amount, ACTIVITY will be asserted, and when the wrist is relatively static, INACTIVITY will be asserted in 1 second. This setting only lives within state F0. Whenever the fall detection algorithm transits to state F1, both thresholds will be immediately configured to 2.25g and 0.5g for ACTIVITY and INACTIVITY respectively.

With above hardware settings, four types of events can be identified from the fall detection algorithm and they are named with the following conventions:

$E0$: generated whenever an INACTIVITY interrupt asserts in state F0
$E1$: generated whenever an ACTIVITY interrupt asserts in state F1
$E3$: generated whenever the fall detection algorithm transits from state F1 to F2

There are underlining physical meanings associated with these four events. $E0$ is generated whenever a wrist changes from active movements to motionless. $E1$ is generated when the wrist slightly moves or changes orientation. This corresponds to casual movements human makes during ADLs. $E2$ corresponds to weightlessness at the wrist, which is generated when the wrist is lowered from a higher level. This happens when the subject falls, walks (swings arms) and sits down. During ADLs, accelerometer values will typically fluctuate around the gravity value. Capturing only the weightless part is good enough to estimate the activity level. $E3$ is typically generated during drastic movements such as a fall, suddenly sitting down and putting down arms onto desks.

Along with above events, directions of Y-axis during the occurrence of these events are also taken as a feature. Fig. 9 shows the alignment of axes of the accelerometer when worn by a human subject on his left wrist. Y-axis is always aligned

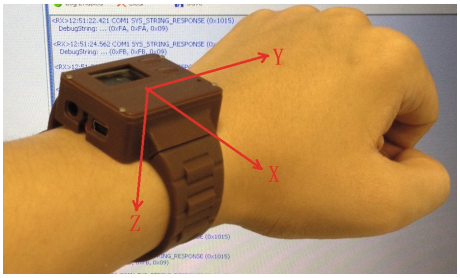

Fig. 9 Alignment of Accelerometer Axes when worn by a Human Subject

with the subject's lower arm. Y-axis information is critically important for estimating ADL as Y-axis is typically pointing approximately downwards when the human subject is standing or walking. During sleeping, Y-axis is usually approximately horizontal.

8.2 Preprocessing

Fig. 10 shows raw data collected from a WD worn by a human subject who performed two actions including "Walk" and "Random" ("Quiet" is not shown as it basically contains no events). Each action lasted exactly a minute. Below is a list of intuitions based on the raw data.

- During "Random", only $E0$ and $E1$ are generated in alternating manners (as the accelerometer's link mode is enabled).
- During "Walk", as the arm swings, FREE_FALL interrupt will be generated and the fall detection algorithm moves from state F0 to state F1. As there is no impact following FREE_FALL during walking, the fall detection algorithm returns to state F0 shortly. This pattern repeats and generates a lot of $E2$ as well as $E0$ and $E1$ along the way. Also observe that Y-axis values are always positive as Y-axis typically points downwards during walking.
- During "Quiet", no events will be generated.

An ADL classifier is to be designed to differentiate these actions automatically.

It is to be noted that events can be generated at any time depending on wearers' activity. These events are asynchronous and non-uniform with respect to time, as opposed to typical uniform time series accelerometer data sampled at constant rates. Thus, the proposed ADL classifier is an asynchronous event-driven classification algorithm that only computes upon occurrence of an event.

The ADL classifier is designed to be run completely inside a WD, similar to the fall detection algorithm. When a new event occurs, the classifier needs to determine the type of ADL based on the current event as well as events in the past few seconds. Currently, the "past" of an event has been defined as a time window of 10 seconds before and including this event. To take the past into consideration, a classification algorithm can take one of the two approaches below:

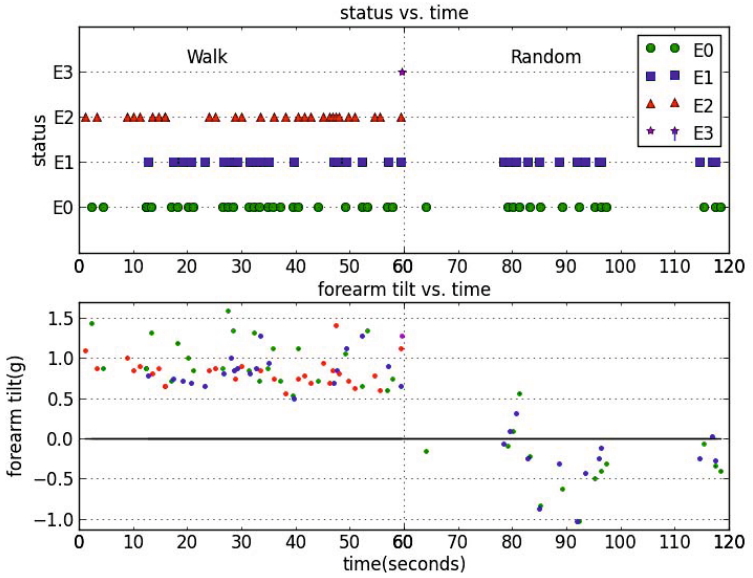

Fig. 10 Four Events and Corresponding Y-Axis Values

1. Upon occurrence of an event, the host MCU retrieves all events in the past 10 seconds it stored earlier, together with their time stamps, and determine the current ADL based on these events.
2. The classification algorithm can construct an energy function for each event which records this event's activeness in the paPst 10 seconds. This energy function decays according to time. Thus, an event just occurred recently leaves more energy at the present time than an event which occurred a long time ago. The host MCU could tell if an event has just occurred recently by evaluating current energy level of this event.

The proposed ADL classifier takes the second approach. The first approach requires uncertain amount of memory space to keep track of all events in the past 10 seconds, which should be avoided in an 8-bit MCU. In addition, it will compute the same event multiple times as the 10-second time-window shifts by one each time. The second approach can be easily implemented and requires less computational resources. For each of the four events ($E0$, $E1$, $E2$ and $E3$), an energy function is proposed to keep track of the activeness of this event in the recent past.

The contribution of an event to its energy function decays with time. An exponential decay function is proposed in Equation 2.

$$\eta(t) = e^{-t/\tau}. \tag{2}$$

where t is the elapsed time and $\tau = 10$ seconds which means that an event's energy decays to $e^{-1} \approx 0.37$ of its original value after 10 seconds.

Upon the occurrence of an event, energy of all events in the past are reduced by a factor η ($0 < \eta \leq 1$) which is related to the elapsed time of the previous event. The energy of the occurred event will be incremented correspondingly. The exponential function for computing the decay factor can be efficiently approximated by using a look-up table and interpolation in host MCUs.

The proposed ADL classifier is completely event-driven as it only computes upon occurrence of an event. This leads to a problem when a WD is "Quiet". Consider a human subject is walking initially and suddenly keeps still. An event $E0$ will be generated one second after he keeps still. At this point, the classification of his action over the past 10 second could be "Walk". As no event will be generated after this $E0$, the algorithm will not compute at all thereafter and the classification result remains as "Walk" which does not reflect the fact. To resolve this issue caused due to no events ever being generated during "Quiet", an artificial event is created and named as E_{-1} to signify its special purpose. Upon occurrence of an E_0 event, after which might follow a long "Quiet" period, a dummy check event is scheduled to be set in 5 seconds using a timer. Any other event which occurs before this timer expires will cancel this timer. If no other event cancels, the algorithm, upon seeing this dummy event, will reset energy functions of all events to zero.

The proposed energy function is in fact a modified exponential smoothing algorithm for non-uniform time series. It is elaborated in Algorithm 1.

Algorithm 1. Exponential Smoothing for Non-uniform Time Series

Data: $D = \left\{d^0, d^1, ..., d^i, ..., d^n\right\}$ is a non-uniform time series, where
$d^i = (t^i, e^i)$ is a time-and-event pair at time t^i and $e^i \in \{-1, 0, 1, 2, 3\}$.
Result: Energy value ${A_j}^i$ for each event E_j where $j \in \{0, 1, 2, 3\}$.
begin
  ${A_j}^0 \longleftarrow 1$ for $j = e^i$
  ${A_j}^0 \longleftarrow 0$ for all $j \in \{0, 1, 2, 3\}$ where $j \neq e^i$.
  $\alpha \longleftarrow 0.6$
  for $i \in \{1, 2, ..., n\}$ **do**
    $\Delta t \longleftarrow t^i - t^{i-1}$
    $\eta \longleftarrow e^{\left(-\frac{\Delta t}{10}\right)}$
    if $\Delta t \geq 5$ **then**
      ${A_j}^i \longleftarrow 0$ for all $j \in \{0, 1, 2, 3\}$
    else
      for $j \in \{0, 1, 2, 3\}$ **do**
        ${A_j}^i \longleftarrow \eta \times {A_j}^{i-1}$
        if $e^i \geq 0$ **then**
          ${A_{e^i}}^i \longleftarrow (1 - \alpha) \times {A_{e^i}}^i + \alpha/\eta$

The effect of an energy function is analogous to a leaky bucket with a hole on the bottom. Such a bucket leaks faster when there is more water in it due to higher pressure difference. In about 10 seconds, a full bucket will retain only 37% of its original capacity. Each event has a corresponding leaky bucket. Upon seeing an event, the proposed smoothing algorithm adds a fixed amount of water into the event's corresponding bucket. By looking at the amount of water in all buckets at any given time, the algorithm can tell which event has just recently occurred.

Applying the proposed smoothing algorithm to the non-uniform series in Fig. 10 yields energy levels for all four events, as shown in Fig. 11. Upon occurrence of any event, energy functions for all events will be evaluated. Thus, at any time instant when an event occurs, there are four energy values corresponding to four events. Together with Y-axis value at this instant, there are totally 5 features which can be fed into a classifier.

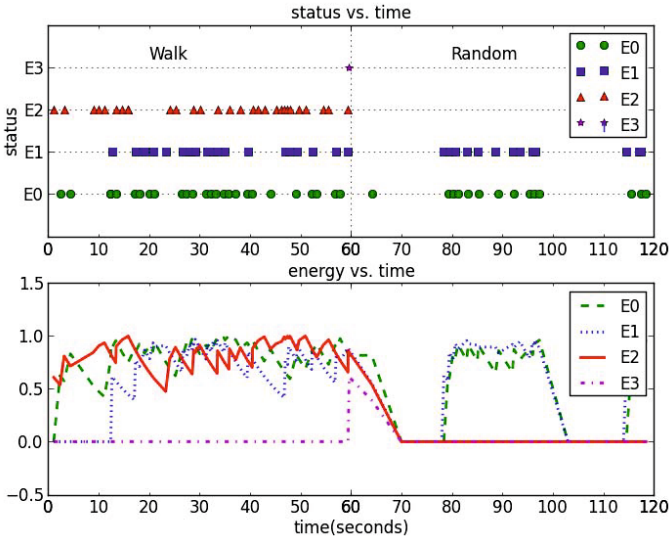

Fig. 11 Energy Values for All Four Events

8.3 Decision Tree Training

ADL classifications using analog accelerometers typically use classifiers such as LDA (linear discriminant analysis), naive Bayes, SVM (support vector machine), ANN (artificial neural network), decision tree classifier, etc, which have been compared by [22, 31, 32]. The proposed ADL classification employs decision tree learning as decision trees can be efficiently implemented as a number of if-else or switch statements. In contrast, ANN and SVM classifiers involve multiplications of floating point numbers which can not be efficiently calculated in an 8-bit MCU.

Decision tree learning has been extensively used in statistics, data mining and machine learning. C4.5, developed by Ross Quinlan, is a well-known learning algorithm for generating decision trees. As it accepts numerical attributes, data obtained from the Algorithm 1 can be conveniently fed into a C4.5 training algorithm. This paper uses a C4.5 implementation in Weka (Waikato Environment for Knowledge Analysis), a data mining suite developed at the University of Waikato.

As there is no event data generated during a "Quiet" period, the training data will be biased towards "Walk" and "Random" as they have more training samples. To prevent this, artificial data is injected into the training data every 1 second during "Quiet" periods. These artificial data has $E0$, $E1$, $E2$ and $E3$ all equal to zero, to indicate that none of the interrupts will be generated during a "Quiet" period. Y-Axis values are random values between $-g$ and $+g$, which is based on an assumption that tilt level of an arm can form any angle with the gravity vector during "Quiet".

Listing 1 Part of the Training Data in ARFF

```
@RELATION ADL
@ATTRIBUTE E0 NUMERIC
@ATTRIBUTE E1 NUMERIC
@ATTRIBUTE E2 NUMERIC
@ATTRIBUTE E3 NUMERIC
@ATTRIBUTE YAXIS NUMERIC
@ATTRIBUTE TARGET {Random, Walk, Quiet}
@DATA
0.594445866751,0.605606027623,0.0,0.0,0.7176,Random
0.874125264632,0.55309493264,0.0,0.0,0.0312,Random
...
0,0,0,0,0.725084125307,Quiet
0,0,0,0,-0.218702173083,Quiet
...
0.650817753982,0.618025460739,0.0,0.0,-0.2184,Walk
0.591658526558,0.884732100327,0.0,0.0,0.0624,Walk
```

8.4 Classification Algorithm

Six groups of ADL data have been collected from six young human subjects. Each subject performed 4 minutes of "Walk", 4 minutes of "Quiet" and 5 minutes of "Random". Four out of the six groups of ADL data are used training data and the other two are used as testing data.

Running the decision tree algorithm on the training data (with reduced error pruning enabled and the number of folds set to 3) leads to the following decision tree shown in Fig. 12.

The resultant decision tree accords well with human intuitions. It selects energy values of $E0$ as the root split, which is the most obvious feature that differentiates "Quiet" from other ADLs. Between "Walk" and "Random", it determines that

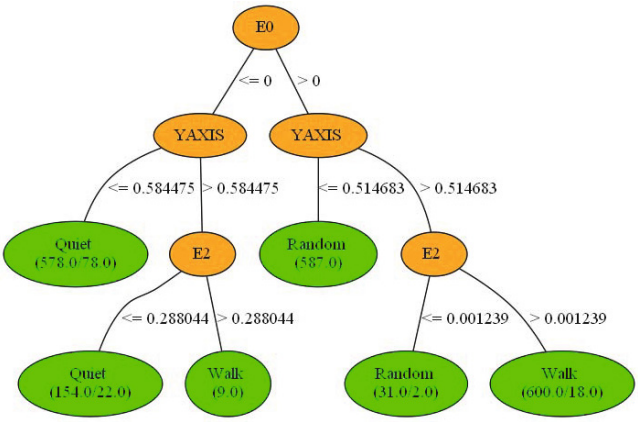

Fig. 12 Decision Tree After Training

$YAXIS$ values are the best to differentiate them. It is also to be noticed that, two other features $E1$ and $E3$ do not appear in the decision tree. $E1$ has a strong correlation‘ with $E0$ because link mode of ADXL345 makes them always appear in alternating manners. $E3$, corresponding to impacts, which seldom appears in the training data, thus is not shown in the decision tree as a dominant factor. The resultant decision tree suggests that feature $E1$ and $E3$ could be removed from the feature set as they either has little effect or is redundant.

8.5 Classification Accuracies

The confusion matrix in Table 2 only shows classification accuracies in terms of events. Due to bias in the number of sampled events, events occur frequently during “Walk” period while rarely during “Quiet” period. A better representation of the classification accuracy should be based on time instead of events. Fig. 13 show the details of the classification results for one of the testing subjects along the time line. Activity of the first 240 seconds is “Walk”, followed by another 240 seconds of “Quiet” and ended by 300 seconds of “Random”. It can be seen that the classifier performs fairly well. In fact, it is robust enough that in the “Random” period, the subject pauses a few seconds in between. Thus, the labels for that interval is actually incorrect. Nevertheless, the classifier is robust enough to capture those and correctly identify it as “Quiet” segments.

Table 2 Confusion Matrix of Two Testing Sets

	Classification Outcome		
Number of Events	Random	Walk	Quiet
Random(492)	0.945	0.154	0.024
Walk(475)	0.053	0.846	0.026
Quiet(496)	0.002	0.000	0.950

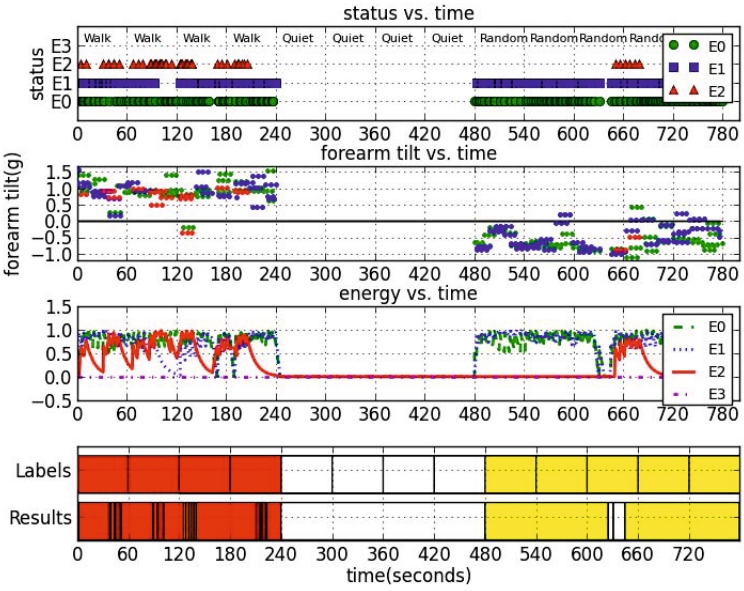

Fig. 13 ADL Classification of a Human Testing Subject

Fig. 13 shows the classification accuracies along the time-line. Within a total period of 780 seconds, the correctly classified time is 740.76 seconds. As a result, the classifier is accurate 94.97% of the time for this test set.

9 Conclusions

e-Guardian is a simple, low-cost, low-power and scalable health monitoring system for the lone elderly. In the event of accidental falls, wearable devices worn by seniors will automatically notify caregivers. A fall detection algorithm and an ADL classification algorithm for the wearable device have been proposed. Both algorithms are interrupt-driven and can be efficiently implemented in small MCUs by taking advantage of interrupt and FIFO features in modern digital sensors. They are more power-efficient than conventional algorithms which must examine and process each sample of accelerometer data. By processing data locally, a WD does not have to wirelessly stream massive sensor data out thus saving both power and bandwidth. Less bandwidth consumption results in better scalability which allows a single system to accommodate more WDs, thus reducing the cost of use per senior greatly.

References

1. Product review: Philips lifeline with auto alert, `theseniorlist.com/2011/10/product-review-philips-lifeline-with-auto-alert`
2. Halo Monitoring Independence Redefined, `http://myhalomonitor.com/order`

3. Malan, D., Jones, T.F., Welsh, M., Moulton, S.: CodeBlue: an ad hoc sensor network infrastructure for emergency medical care. In: International Workshop on Wearable and Implantable Body Sensor Networks (2004)
4. Wood, A., Virone, G., Doan, T., Cao, Q., Selavo, L., Wu, Y., Fang, L., He, Z., Lin, S., Stankovic, J.: Alarm-net: Wireless sensor networks for assisted-living and residential monitoring. Tech. Rep. (2006)
5. Benocci, M., Tacconi, C., Farella, E., Benini, L., Chiari, L., Vanzago, L.: Accelerometer-based fall detection using optimized zigbee data streaming. Microelectronics Journal 41(11), 703–710 (2010); IEEE International Workshop on Advances in Sensors and Interfaces 2009
6. van de Ven, P., Bourke, A., Nelson, J., O'Brien, H.: Design and integration of fall and mobility monitors in health monitoring platforms. In: Lay-Ekuakille, A., Mukhopadhyay, S.C. (eds.) Wearable and Autonomous Biomedical Devices and Systems for Smart Environment. LNEE, vol. 75, pp. 1–29. Springer, Heidelberg (2010)
7. Bagala, F., et al.: Evaluation of accelerometer-based fall detection algorithms on real-world falls. PLoS ONE 7(5), e37062 (2012)
8. Bourke, A., et al.: Assessment of waist-worn tri-axial accelerometer based fall-detection algorithms using continuous unsupervised activities. In: 2010 Annual International Conference of the IEEE Engineering in Medicine and Biology Society (EMBC), August 8-September 4, pp. 2782–2785 (2010)
9. Van Wieringen, M., Eklund, J.M.: Real-time signal processing of accelerometer data for wearable medical patient monitoring devices. In: 30th Annual International Conference of the IEEE Engineering in Medicine and Biology Society, EMBS 2008, pp. 2397–2400 (August 2008)
10. Lee, M.-S., Lim, J.-G., Park, K.-R., Kwon, D.-S.: Unsupervised clustering for abnormality detection based on the tri-axial accelerometer. In: ICCAS-SICE 2009, pp. 134–137 (August 2009)
11. Lombardi, A., Ferri, M., Rescio, G., Grassi, M., Malcovati, P.: Wearable wireless accelerometer with embedded fall-detection logic for multi-sensor ambient assisted living applications. In: 2009 IEEE Sensors, pp. 1967–1970 (October 2009)
12. Kangas, M., Konttila, A., Lindgren, P., Winblad, I., Jamsa, T.: Comparison of low-complexity fall detection algorithms for body attached accelerometers. Gait & Posture 28, 285–291 (2008)
13. Open source accelerometers for phones, `http://web.mit.edu/wockets/index.html` (online accessed July 14, 2013)
14. Sposaro, F., Tyson, G.: ifall: An android application for fall monitoring and response. In: Annual International Conference of the IEEE Engineering in Medicine and Biology Society, EMBC 2009, pp. 6119–6122 (September 2009)
15. Yavuz, G.R., Kocak, M.E., Ergun, G., Alemdar, E., Yalcin, H., Incel, O.D., Akarun, L., Ersoy, C.: A smartphone based fall detector with online location support
16. Nguyen, T.-T., Cho, M.-C., Lee, T.-S.: Automatic fall detection using wearable biomedical signal measurement terminal. In: Annual International Conference of the IEEE Engineering in Medicine and Biology Society, EMBC 2009, pp. 5203–5206 (September 2009)
17. Jantaraprim, P., Phukpattaranont, P., Limsakul, C., Wongkittisuksa, B.: Evaluation of fall detection for the elderly on a variety of subject groups. In: Proceedings of the 3rd International Convention on Rehabilitation Engineering & Assistive Technology, i-CREATe 2009, pp. 11:1–11:4. ACM, New York (2009)

18. Narayanan, M., Lord, S., Budge, M., Celler, B., Lovell, N.: Falls management: Detection and prevention, using a waist-mounted triaxial accelerometer. In: 29th Annual International Conference of the IEEE Engineering in Medicine and Biology Society, EMBS 2007, pp. 4037–4040 (August 2007)
19. Nyan, M.N., Tay, F.E.H., Murugasu, E.: A wearable system for pre-impact fall detection. Journal of Biomechanics 41(16), 3475–3481 (2008)
20. Li, Q., Stankovic, J., Hanson, M., Barth, A., Lach, J., Zhou, G.: Accurate, fast fall detection using gyroscopes and accelerometer-derived posture information. In: Sixth International Workshop on Wearable and Implantable Body Sensor Networks, BSN 2009, pp. 138–143 (June 2009)
21. Curone, D., Tognetti, A., Secco, E., Anania, G., Carbonaro, N., De Rossi, D., Magenes, G.: Heart rate and accelerometer data fusion for activity assessment of rescuers during emergency interventions. IEEE Transactions on Information Technology in Biomedicine 14(3), 702–710 (2010)
22. Gyllensten, I., Bonomi, A.: Identifying types of physical activity with a single accelerometer: Evaluating laboratory-trained algorithms in daily life. IEEE Transactions on Biomedical Engineering 58(9), 2656–2663 (2011)
23. Hong, Y.-J., Kim, I.-J., Ahn, S.C., Kim, H.-G.: Mobile health monitoring system based on activity recognition using accelerometer. Simulation Modelling Practice and Theory 18(4), 446–455 (2010); Modeling and Simulation Techniques for Future Generation Communication Networks
24. Yang, S.-I., Cho, S.-B.: Recognizing human activities from accelerometer and physiological sensors. In: IEEE International Conference on Multisensor Fusion and Integration for Intelligent Systems, MFI 2008, pp. 100–105 (August 2008)
25. Lan, M., Nahapetian, A., Vahdatpour, A., Au, L., Kaiser, W., Sarrafzadeh, M.: SmartFall: An Automatic Fall Detection System Based on Subsequence Matching for the SmartCane. In: Fourth International Conference on Body Area Networks, BodyNets (2009)
26. MPU-6000/6050 Six-Axis (Gyro + Accelerometer) MEMS MotionTracking^{TM} Devices, `www.invensense.com/mems/gyro/mpu6050.html` (Online; accessed July 14, 2013)
27. Bersch, S., Chislett, C., Azzi, D., Khusainov, R., Briggs, J.: Activity detection using frequency analysis and off-the-shelf devices: Fall detection from accelerometer data. In: 2011 5th International Conference on Pervasive Computing Technologies for Healthcare (PervasiveHealth), pp. 362–365 (May 2011)
28. Ning, J.: Fall detection application by using 3-axis accelerometer ADXL345. Application Note AN-1023 from Analog Devices (2009) (Online; accessed July 14, 2013)
29. Kangas, M., Konttila, A., Winblad, I., Jamsa, T.: Determination of simple thresholds for accelerometry-based parameters for fall detection. In: 29th Annual International Conference of the IEEE Engineering in Medicine and Biology Society, EMBS 2007, pp. 1367–1370 (August 2007)
30. Jantaraprim, P., et al.: Improving the accuracy of a fall detection algorithm using free fall characteristics. In: 2010 International Conference on Electrical Engineering/Electronics Computer Telecommunications and Information Technology (ECTI-CON), pp. 501–504 (May 2010)
31. Altun, K., Barshan, B., Tunçel, O.: Comparative study on classifying human activities with miniature inertial and magnetic sensors. Pattern Recogn. 43(10), 3605–3620 (2010)
32. Park, C., Kim, J., Choi, H.-J.: A watch-type human activity detector for the aged care. In: 2012 14th International Conference on Advanced Communication Technology (ICACT), pp. 648–652 (February 2012)

Evidence-Based Development Approach for Safe, Sustainable and Secure Mobile Medical App

Priyanka Bagade, Ayan Banerjee, and Sandeep K.S. Gupta

Arizona State University
{pbagade,abanerj3,sandeep.gupta}@asu.edu

Abstract. According to industry surveys, by 2018, more than 1.7 billion smartphone and tablet users will have downloaded at least one mobile medical app (MMA) [40]. Such widespread adoption of smartphone based medical apps is opening new avenues for innovation, bringing MMAs to the forefront of low cost healthcare delivery. These apps often control human physiology and work on sensitive health data, thus it is necessary to have evidences of their trustworthiness before actual marketing. The key challenges in ensuring trustworthiness of MMAs are maintaining privacy of health data, long term operation of wearable sensors and ensuring no physical harm to the user. Traditionally, clinical studies are used to generate evidences of trustworthiness of medical systems. However, they can take a long time and could potentially harm the user during studies. Thus it is essential to establish trustworthiness of MMAs before their actual use. One way to generate such evidences can be using simulations and mathematical analysis. These methods involve estimating the MMA interactions with human physiology. However, the nonlinear nature of human physiology makes the estimation challenging.

Thus, it is required to *analyze and develop MMA software while taking into account its interactions with human physiology to assure trustworthiness*. This chapter focuses emerging app development methodologies, which support automatic evaluation of trustworthiness of MMAs by supporting automatic generation of evidences. This methodology involves, a) evidence generation to assure trustworthiness i.e. safety, security and sustainability of MMAs and b) requirement assured code generation for vulnerable components of the MMA without hindering the app development process. These methods are intended to expedite the design to marketing process of MMAs. In this regard, this chapter discusses example models, tools and theory for evidence generation with the following themes:

- **Software design configuration estimation of MMAs:** Using an optimization framework which can generate sustainable and safe sensor configurations while considering interactions of the MMA with the environment.
- **Requirements verification of the MMA design:** Using models and tools to verify safety properties of the MMA design which can ensure the verified design will not cause any harm to the human physiology.

S.C. Mukhopadhyay (ed.), *Wearable Electronics Sensors,*
Smart Sensors, Measurement and Instrumentation 15, DOI: 10.1007/978-3-319-18191-2_6

- **Automatic code generation for MMAs:** Investigating methods for automatically generating safety, sustainability and security assured software for vulnerable components of a MMA.
- **Performance analysis of MMA software developed using evidence-based approach:** Evaluating quality and response time of MMA software developed using evidence-based approach .

1 Introduction

Use of mobile medical apps (MMAs) in healthcare is becoming prevalent as they provide low cost healthcare delivery [40]. These apps often control human physiology by acting as a controller to wearable and implanted medical devices such as artificial pancreas which automatically controls the blood glucose level by infusing insulin. They also provide diagnosis using physiological data collected by implanted sensors. Such close interaction of MMAs with human physiology make them critical. Thus, despite their ability to provide low cost healthcare delivery, getting these apps in the market is a tedious process e.g. design for the automated artificial pancreas came in 1999s [28]. However the actual app is marketed in 2014, which is a first generation app and capable of only predicting hypoglycemia (low blood glucose level) [65]. Due to involvement of human physiology, MMAs are technically challenging to implement and get market approval which requires to establish trustworthiness of these apps. Trustworthiness of MMAs can be viewed as having properties such as interaction safety, communication and storage security and wearables sustainability [44]. Assuring these trustworthy properties in MMAs is challenging due to difficulty in extracting their interactions with human physiology, which leads to lack of mathematical structure to objectively provide evidences of the MMAs. The evidence can be defined as a set of observations on certain properties of MMA software and its effects on the human body, generated through the usage of scientifically sound emulations, clinical studies, simulations and mathematical proofs. Traditionally, emulations and clinical studies are used to generate evidences of trustworthiness of MMAs. However they can be difficult and costly to be comprehensive due to the requirement of approval from institutional review board (IRB) and patient availability. These techniques can also potentially harm the user and may take long time to establish their trustworthiness. Simulation and mathematical proofs can generate evidences before the actual use of the MMAs on the user. However, developing such techniques might increase app development time and may require higher skills set from the developer. Thus, this chapter focuses on discussing,
tools and techniques to enable evidence-based design and development of trustworthy MMAs without hindering the app development process.

Simulating the MMA involves estimating its interactions with human physiology. It uses models of MMA software and human physiology to appraise the values of continuous variables of the system over certain time. These values are then used to estimate resource requirements, cost and verify the design against requirements which can provide evidence for the trustworthiness of a MMA design. The nonlin-

ear and spatio-temporal nature of the human physiology makes its models difficult to simulate. Further, the events generated in controller software and human physiology changes the system configurations. Thus inaccurate handling of such events might end up in getting sub-optimal design. Accurate handling of the events require infinitely small time step in current simulators, which leads to increased simulation time. Thus to overcome these challenges in accurately simulating MMAs, the chapter gives an overview of an example simulator with a time refinement approach which predicts the event timing and accordingly modify the time step to handle the event.

Formal methods, which provide mathematical proofs to show correctness of the software, can be used to obtain the evidence of the trustworthy properties of MMAs. Formal methods encompasses several techniques such as equivalence checking, symbolic execution, model checking, theorem proving etc. This chapter uses model checking approach for generating evidence of trustworthiness of MMAs. It uses a state based abstraction of the MMA software. The discrete states of the abstraction represent the operating conditions of the software, while the transitions in the state are governed by changes in the human physiology variables. An execution of this state based model results in valuations of the system variables. If the set of all possible valuations intersects with the unsafe set, then the system will not satisfy the trustworthy properties. This analysis is typically called *reachability analysis*. It requires solving non-linear, spatio-temporal differential equations of human physiology to accurately estimate values of system variables. The available solutions for reachability analysis are for linear systems. Thus they cannot be directly applicable to the human physiology based systems which are non-linear in nature. There has been many efforts to reachability analysis of non-linear systems such as piecewise linearization [14, 15], polynomial approximation using Bezier curves [33] etc. This chapter discusses one of such technique to perform rechability analysis of nonlinear systems using exponential box splines, which are traditionally being used for curve fitting in geometric modeling.

Simulations and mathematical proofs can be used to develop trustworthy MMAs as well as to generate evidences. The verified MMA design obtained using these techniques can be used to develop MMA using automated code generator to reduce manual implementation errors which is a main cause of software failures. Such automated techniques can be used, if the implementation follows a standard model. However, the standard model may lead to generate similar types of MMAs and might limit the functionalities of the smartphone that can be exploited by the developers e.g. different graphical user interfaces, data displaying techniques. Thus, to avoid such limitations, the app developer should be responsible for developing GUI and processing algorithms on smartphone end and the critical interfaces such as data communication, sensor/actuator code should be generated and handled by the trustworthy entity. Thus, the chapter hypothesizes that trustworthy mobile medical applications should have an operating model, where every instance of data communication to the sensor, data storage in the smartphone, control inputs to the actuator, interaction with the user, data communication to the Electronic Health Record (EHR) and even EHR access by physician has to pass through a certification entity, Trustworthy Data Manager (TDM).

1.1 Overview of the Chapter

To ensure the trustworthiness of MMAs, the MMA software development process should provide evidences at every step of its life cycle. Such evidence-based MMA development process (Figure 1) can be divided into four parts, a) Design, b) Verify if design meets requirements, c) MMA Implementation, and d) Verification and Validation of implemented MMA. The process starts with obtaining MMA design which should satisfy trustworthy requirements of MMA. It is then followed by providing evidence to check if the obtained design meets the trustworthy requirements of MMAs. This verified design is then used for implementation which includes sensor code and smartphone app development. Two types of evidences are required for implemented code to verify if the implementation follows the design and to validate if the implementation ensures trustworthy requirements of MMAs. Traditional app development method uses only controller software simulator which does not estimate interactions with human physiology. Further, manual implementation method is used for MMA software development which it does not provide any evidence for correctness of the design. The implemented code is generally validated using experiments such as clinical study which is time consuming and might lead to user safety hazards due to wrong design or implementation. The chapter focuses on filling the gap by providing example models, tools and methodologies to generate evidences with theoretical guarantees for ensuring correct working of MMAs before their experimental studies. The research topics and their example solutions in MMA development process are discussed as follows:

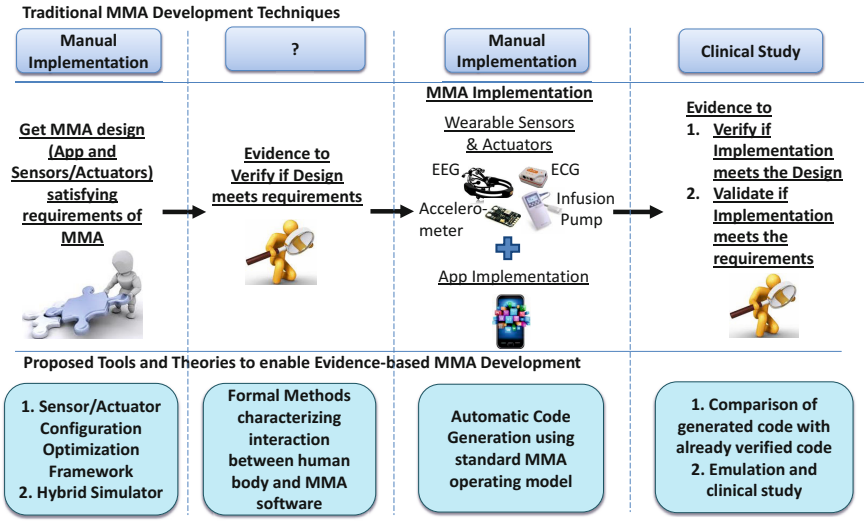

Fig. 1 Overview of evidence-based MMA development approach

- **MMA Design:** MMAs interact with environment through wearable devices, e.g. wearable devices scavenge energy from unpredictable sources such as human heat, sun light etc. Also as they are implanted on human body, they interact with human physiology by controlling it using actuators or by heating the human skin at the sensor worn spot. Thus to assure sustainable and safe working of the MMAs, the design of the wearable devices should consider the interaction effects [70]. Traditional MMA design techniques fail to consider these interactions, which might result in an unsafe and power hungry design. Thus, it is important to address following research question while configuring the wearable sensor/actuators in MMAs:

  How to incorporate interactions of MMA with its environment while configuring the sensor/actuator?

  Available Solutions: Typically optimization frameworks are used to obtain sensor configuration for given requirements. One of the example solution discussed in Section4 is the use of an optimization framework to get sensor configuration that supports privacy ensured continuous monitoring powered by energy scavenged from human body or sun light and does not cause any harm to the human physiology [17]. It takes hardware and software requirements of the sensor/actuator to generate the optimal design. The framework uses hybrid simulator to simulate human physiology and controller algorithm to obtain the safe design. Researchers have proposed many such hybrid simulators [11, 39, 42]. This chapter discusses one example hybrid simulation method in Section 5 to accurately handle events from human physiology and controller algorithm to get realistic system behavior.
- **Design Verification:** This step acts as an evidence for the design obtained in previous step follows the requirements. The software design verification usually involves logical reasoning by giving a mathematical proof of correctness of the design. In case of MMAs, as they directly interact with human physiology, considering the effect of MMA operation on human physiology is the important part in the reasoning process. Traditional MMA development techniques do not provide any of such method for the reasoning. Thus, following research question needs to be answered:

  How to generate evidence for the MMA design using models of human physiology?

  Available Solutions: Formal techniques can be used to perform MMA design verification. In the example technique incorporated in this chapter, the combined analysis of continuous dynamics of human physiology and discrete dynamics of the MMA controller software is done using reachability analysis. Reachability analysis computes the values of continuous variables of the system with a given controller at any point in time. These values are further used to check instability in controller design. There has been many methods proposed by researchers to do reachability analysis of non-linear systems such piece-wise linearization [14, 15], polynomial approximation using Bezier curves [33]. One of such technique discussed in this chapter in Section 6 uses exponential box splines to represent

the trajectory of these continuous variables of nonlinear systems. Exponential box splines are being traditionally used for curve fitting in geometric modeling. Their curve fitting property will be applied to express the nonlinear variation of the continuous variables in the system.

- **MMA Implementation:** Traditional app development process uses manual implementation which might result in software bugs. These errors can lead to safety and security issues such as bug in the infusion pump controller software can lead to excess drug infusion in the blood which can lead to distress, error in security algorithm can cause leakage of health data. In order to avoid these issues the app software should be bug-free. Thus, the chapter focuses on following research question:

  How to reduce manual implementation errors in MMAs?

  Available Solutions: Automated code generation can be used to reduce manual implementation errors [23,26,57]. This chapter discusses the example of Health-Dev tool [23], a model based automatic code generator for sensors and smartphones. The chapter explains how Health-Dev tool can be extended to generate TDM with safe, secure and sustainable sensor and smartphone code. In the extended tool, customizable code for sensor communication, data storage in smartphone and communication to the EHR will be automatically generated from high level descriptions using a parameterized code frame data-base. The visualization software (Graphical User Interface) can be independently developed by a manufacturer. The extended Health-Dev tool, referred as Health-Dev β tool will be equipped with a data-base of security enabled communication protocol code frames such as password based and physiological value based security.
- **Verification and Validation of implemented code**: To check if the implemented code conforms to the requirements and design of the MMA, the use of clinical studies in traditional app development methods can be hazardous to human physiology. Thus, the implemented code can be compared with already verified code such as BSNBench [61] to verify if the implemented code satisfies the MMA design. Further, emulation platform can be used to validate the MMA requirements of safety from MMA operation before actual use of the app. Such emulation platform can use field-programmable analog arrays (FPAAs) to implement sensor design. The ability of FPAAs to emulate the operation of human physiology represented by differential equations enables them to test power consumption and adverse effects on human physiology.

2 Related Works

Mobile medical apps (MMAs) are involved in critical healthcare operations which might lead to risks or hazards to human physiology. The risks addressed in this chapter are categorized as: a) safety violations, a user is not harmed due to the operation of the smartphone app (the controller app might harm user physiology), b) security violations, user's data is always kept private and free from unauthorized access (unauthorized access to the health data), and c) sustainability violations, lack

of availability of apps due to resource constraints such as power, CPU, and memory. These are the trustworthy properties of MMAs which need to be evaluated before the actual use of the app to have dependable healthcare system..

Traditionally, static analysis, complexity analysis of the source code, functional testing, structural testing are used to check errors in the developed software [13,36]. These techniques may not ensure that the program is totally bug-free as they check for particular types of errors or requirements only e.g. static analysis focuses on buffer overflows, null pointer detection, dead code detection but fail to consider the interactions of system with environment. Further, system monitoring approach is used to establish trust in software working which relies on specified operating conditions of the system and detects anomaly in system behavior such as component failure, memory corruption, change in environment [45]. However, the monitoring of the system can be used after the system deployment which can lead to testing certain requirements only and fixing any critical error might lead to redeveloping the product or dealing with potential harm to the software environment. Considering the critical nature of the MMAs, the trustworthiness should be established before the actual use of the system to ensure no harm to the user when being tested in clinical studies.

To avoid, the software testing flaws after development, process based methods are used to establish software trustworthiness where the trustworthy properties of the software are tested at every step of the development life cycle [12,59,64]. They are mainly focused on converting the trustworthy requirements in finite state machines (FSM) and then testing the automata to check if the design satisfies the requirements as well as developed software functions according to the FSM. In case of MMAs, the interactions between discrete system i.e. MMA software and continuous system i.e. human physiology need to be studied to establish trustworthiness. However, FSM provides limited support to represent such hybrid system. Thus these methods cannot be used to verify the MMA design to check the trustworthy properties.

There has been several frameworks proposed for developing MMAs to reduce development time. UPHIAC application [54] framework provides interfaces for networking, storage, measurement devices and user interface for data visualization. However, it does not include any discussion on how trustworthy properties of the MMA will be handled. It uses smartphone sensors only, not the external ones or use external proprietary sensors which may not support any modifications in parameter configurations. Further, secure data communication, sharing data with other apps, storage in cloud is one of the main concerns in MMAs. Researchers have extensively addressed the issue of data sharing in mobile apps and cloud while considering the pervasive monitoring systems [8,27,43,60]. Open mHealth architecture [38] promotes the use of having single framework which can collect data from various apps used by the patient/user and share with the physician instead of asking each app to upload data separately. It mainly focuses on data transfer from apps to cloud. However it does not check for security vulnerabilities during the data transfer. bHealthy [60] promotes the use of data sharing between apps to give better feedback to the user. Mobius [27], a middleware for interfacing with complex data management, supports unified data messaging and abstraction for mobile apps. Another interface (Simba) [8] interfaces the complexities of synchronizing data to the cloud

with minimal work from the developer. A Service-Oriented Context-Aware Middleware (SOCAM) has been proposed [43] to enable rapid prototyping of context-aware services in pervasive computing environments. SOCAM provides a middleware of components to define context providers, interpreters, and the interaction between different components. All of these approaches use APIs to provide the interfaces and require an app to change structural design to adapt to the interface. Configuration of the APIs is tedious and inaccuracy in setting the API parameters correctly can result in failure of the system. Thus, to reduce development effort a non-invasive interface provider framework is needed which requires very less configuration. In this regard, TDM app can be used to provide critical interfaces for MMAs. It allows developer to use the interfaces in the same way as communicating with other app on the smartphone and avoids possible configuration issues.

Several individual efforts are taken to assure trustworthy properties in MMAs. The safety violation of the apps can be caused by compromising health data by sharing it with non-legitimate app. To combat this issue, Android uses sandboxing to secure direct data access between apps. Inaccurate control input to actuator computed by MMA can cause serious harm to human physiology. This issue can be viewed as verification hybrid model and existing techniques such as reachability analysis can be used to verify the control algorithm before implementation [16,18]. Further, there has been many efforts taken to secure data communication over wireless channel for in body implanted sensors and smartphone [20,41,48,49,73]. The availability of the sensors can be jeopardized by low battery capacity. This issue is mainly addressed by using schemes such as throttling, duty cycling, sustainable sensing [66]. All these efforts to combat safety, security and sustainability issues focus independently on each issue and try to find solution for it. However in case of MMAs, a technique is needed which should consider the inter-effect of these issues on each other.

This creates a need to have a MMA development framework which can ensure trustworthy properties while generating the evidences at every step of the development process. This leads to develop a framework which can specifically focus on trustworthy properties in MMAs.

3 Mobile Medical Apps Examples

MMAs communicate with physiological sensors worn by the user and use the collected physiological data for further processing such as diagnosis, controlling actuator operation, displaying data in user readable format. The apps also communicate with a cloud server to upload the health data to an electronic health record (EHR) which is a health data storage.

Since, MMAs control medical grade actuators and monitor health, they need to meet safety, security and sustainability requirements. Indeed, Food and Drug's Administration (FDA) classify smartphone health apps as medical devices. According to the definition of the MMAs published by FDA in September 2012, the healthcare apps can be classified in three types, a) *displaying app* - which displays the sensor data in graphical format, b) *diagnostic app* - which processes the collected physiological data and provides diagnostic feedback to the user, and c) *controlling*

app which controls the actions of the body implanted actuator device depending the sensed physiological signals.

Following MMA examples are used throughout the chapter to explain the example solutions. The example MMAs are classified according to the FDA definition of smartphone medical apps.

Example 1 PETPeeves: Display app: *PETPeeves is an app aimed to help users alter their lifestyle to be healthier by presenting the user with a virtual pet whose mood changes based on the amount of exercise the user performs a week. The app uses accelerometer and ECG sensor to monitor the user's heart rate and accordingly calculates calories burned during exercise.*

Example 2 BrainHealth: Diagnostic app: *The app consists of three activities-focus, mood change, and relaxation. Focus is aimed towards users who suffer from learning disabilities and need a boost in mental performance, motivation, and focus. Mood change is aimed towards users whom are not satisfied with their mood and want to achieve a more positive mood. Lastly, relaxation is aimed at any user who wants to learn how to relax in any situation. The app consists of a visual feedback system which uses a glob of goop. When the user is performing well in an activity, the glob is very structured and dense, however when the user's performance degrades, the glob breaks apart and the goop drifts to the edges of the screen. Neurofeedback or phsychostimulants are found to be an effective method for encouraging healthy behavior [69]. PETPeeves app uses this neurofeedback as additional input to give reward points to the user which acts as the bonus to pet's mood modifier.*

Example 3 Artificial Pancreas/Infusion Pump App: Controller App *Automated control of blood glucose levels in human are often obtained using artificial pancreas. Artificial pancreas are distributed systems consisting of an infusion pump, glucose meter, and a controller implemented in a mobile device such as smartphone. These distributed components are networked through the wireless communication channel and operate in a close loop to keep the drug concentration in the human blood within recommended limits. The different components of the automated control system may have skews in the clock rates as well as data transfer rates. This results in transport delays in the sensed values of glucose meter and actuation delay in infusion. Thus, the continuous dynamic equation that represents the blood glucose level in the blood sensed by the glucose meter due to infusion from the pump is given by equation 1.*

$$\begin{aligned} \dot{y_1} &= A_p y_1 + B_p \dot{Q} z_2 + B_p u(t - T_i), \\ z_1 &= C_p y_1(t - T_p), \\ \dot{y_2} &= A_s y_2 + B_s \dot{Q} z_1, \\ z_2 &= C_s y_2(t - T_r). \end{aligned} \tag{1}$$

Here y_1 and y_2 are the state space variables of the equation. y_1 consists of vectors of left heart, lung blood, lung tissue and right heart compartments through which infused drug passes. Newly infused drug merges with recirculated drug from Vessel Rich Group, Muscle, Fat and Residual drug which is represented by y_2 state space

variable vectors. A_p, A_s, B_p, $\dot{Q}$, C_s, and C_p are constants. z_1 is the drug concentration in the blood while z_2 is the arterial drug concentration. The initial infusion rate $u = x_0$ is the input to the model and the output is the drug concentration in the blood. The time delays related to the infusion input ($Taya_i$) is due to the delay in actuation, the cardio-pulmonary transport delay T_p and the arterial, capillary and venous transport delays T_r manifest the delay in sensing the blood glucose level by the glucose meter.

The discrete controller of the infusion pump has five states: a) basal, where infusion rate is I_0 and the blood glucose rate is between 120 ug/dl and 70 ug/dl, b) braking, where infusion rate is a fraction f of I_0, and blood glucose level goes below 70 ug/dl but is still above 20 ug/dl, c) correction bolus, where infusion rate is incremented by I_{cb}, and the blood glucose level is between 120 ug/dl and 180 ug/dl, d) bolus, where the infusion rate is incremented by $I_b > I_{cb}$, and the blood glucose level is above 180 ug/dl, and e) stop, when the infusion is stopped i.e., $I_b = 0$, since the blood glucose level drops below 20 ug/dl.

Example 4 Body sensor Networks: *This example considers a network of implanted sensors, which communicate in a cluster protocol. The implanted sensors form a cluster, where a cluster head collects all communication packets from the participating sensors and sends it out to a base station.*

Example 5 Medical Ventilator: Controller *Medical ventilators provide critical life support to the patients when they are unable to breathe properly. Due to diseased or injured lungs, respiratory system of the patient stops functioning correctly. In such a scenario, ventilator develops the required pressure for air flow through the patient's respiratory system as well as it supplies air with appropriate amount of oxygen concentration. The percentage of oxygen concentration in the ventilator supplied air is referred as F_IO_2 which is basically a fraction of inspired oxygen in the air. Ventilator system calculates F_IO_2 by measuring oxygen saturation, S_PO_2 , in the blood. Ventilators use non-invasive method to measure S_PO_2 using pulse-oximeter. If the blood oxygen saturation level drops below certain level, the patient suffers from hypoxemia and if it goes above the higher limit of target oxygen saturation, the patient suffers from hyperoxia. Ventilator needs to adjust F_IO_2 to maintain S_PO_2 in desired level. Blood cells are oxygenated in the lungs. Inhaled oxygen and patient physiology decides the oxygen saturation in the blood. Thus, to avoid development of hypoxemia or hyperoxia in the patient improper oxygen saturation, ventilator's control algorithm uses S_PO_2 as feedback to determine appropriate value of F_IO_2.*

For ventilators, initially the input oxygen level is set to some default value or a value decided by a physician as per the patient need. Then depending on the saturation level of oxygen in the lungs, the input oxygen level should change. To accommodate this control in ventilators, the oxygen level in the lungs is being measured using pulse-oximeter after predefined time interval. The output of pulse-oximeter acts as an input to the ventilator control algorithm. Next input oxygen level is decided depending on this feedback.

The patient model (patient physiology) gives the relation between the input oxygen level and the saturation oxygen level. The non-linear patient model is used from [24] as defined in equation 2.

$$\frac{\Delta S_aO_2(s)}{\Delta F_IO_2} = \frac{G_sG_Pe^{-T_ds}}{1+\tau_ps}, \tag{2}$$

Here,
S_aO_2 : *arterial oxygen saturation*
F_IO_2 : *input oxygen level*
T_d : *system transport lag (sec)*
G_p : *sensitivity of* P_aO_2 *to* F_IO_2
τ_p : *time constant (sec)*
G_s : *linearised sensitivity of the* O_2 *dissociation curve.*
S_aO_2 *measured using pulse-oximeter is referred as* S_PO_2. *The patient model in equation 2 is in Laplace transform. Hybrid Automata is used to represent the ventilator system and it cannot compute the equations in Laplace transform format. Thus, it is converted in a differential equation in order to represent continuous dynamics of the system (equation (3)).*

$$\frac{dS_PO_2}{dt} = G_sG_PF_IO_2e^{t/T_d}, \tag{3}$$

4 MMA Configuration Optimization Framework

4.1 Motivating Examples

Single sensor thermal safety: Thermal effects of a sensor on the human body follows a complex pattern and varies with the location and placement of the sensor. Sensors worn on the arm or on the chest, where the skin is not very sensitive to the heat energy, for short periods of time does not cause severe heat related problems. Sensors such as Shimmer, TelosB, with power consumption around 50 mW, cause negligible temperature rise in the human body ($\approx$ 0.01 °C) for a prolong operating time of 24 - 48 hours [62]. Symbiotic sensors on the other hand will have a power cap of 5 μW [56], but can have a higher thermal effect due to their location. A simulation study is conducted that shows a non-intuitive result as depicted in Figure 2. The skin temperature rise of a sensor with 1 mW power dissipation installed on the cornea is greater than that of a sensor with 50 mW power worn on the human arm for 24 hrs by almost 0.2 °C. Another interesting fact is that the reduction of sensor power does not significantly change the temperature rise. As shown in Figure 2, if power of the sensor is reduced to 5 μW [56] from 1 mW, the skin temperature reduces only by 0.01 °C. This result is due to the fact that the average temperature rise of the human tissue around a sensor is not only a function of the power consumption of the sensor, the frequency of sensing, the data transmission rate but is also a function of the blood perfusion rate and hence varies based on the location of installation.

Networked Infusion Pump: In a networked autonomous infusion pump, a controller wirelessly samples the blood glucose levels from a glucose meter and computes the future infusion rate to stabilize blood glucose concentration in the human body. The interaction between insulin and glucose can be modeled as the spatio-temporal differential equation [50].

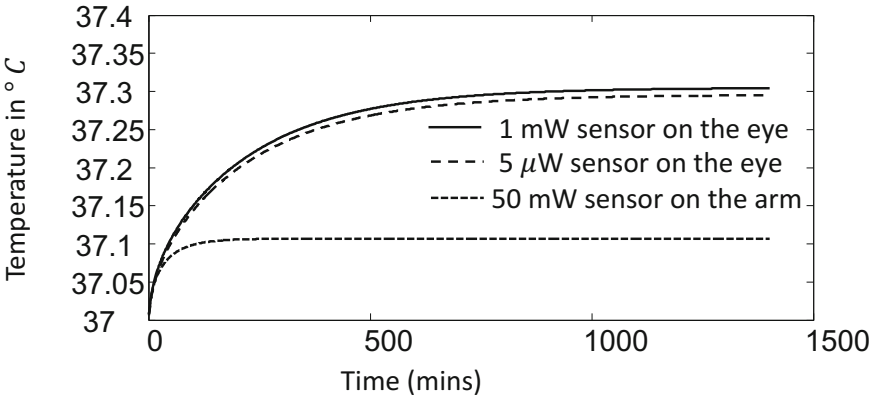

Fig. 2 Skin temperature rise depending on sensor location

$$\frac{\partial d}{\partial t} = \nabla(D \nabla d) + \Gamma(d_B(t) - d) - \lambda d, \tag{4}$$

where $d(x, t)$ is the tissue drug concentration at time t and distance x from the infusion site, D is the diffusion coefficient of the blood, Γ is the blood to tissue drug transfer coefficient, $d_B(t)$ is the prescribed infusion rate at time t, and λ is the drug decay coefficient. The design of the controller involves finding five parameters, the optimal sampling rate of glucose sensor, infusion change or increment step by which the controller increases infusion, allowable bolus rate, the set point $d_B(t)$, and the delay in taking control decisions.

4.2 Problem Formulation

Authors in [17] have tried to answer following research problem -

Given a set of design requirements expressed in the form of a set of favorable states, find a sensor design that always keeps the system in one of the favorable states.

Optimization approach: The problem of finding the sensor design is framed that satisfies regulatory requirements in an optimization framework. Let us consider a contact lens glucose sensor placed on the retina which consumes P_s power for sensing, P_c for data transmission, P_{sec} for executing security protocol. The sensor has an energy storage device of capacity B_c and its stored power at time t is denoted by $P_b(t)$. The energy available from the scavenging source is denoted by $E(t)$ at time t. There will be constraints on the frequency at which the sensor can sense and communicate data. Let us consider that the sensing frequency is f_s and the communication frequency is f_c. The aim is to determine P_s, P_c, P_{sec}, B_c, f_s and f_c from an optimization formulation that minimizes the temperature rise of the human body part and also never depletes the storage device.

Let us consider that the specific absorption rate of the tissue is SAR, which is directly proportional to the radio power and inversely proportional to the square of the distance between the sensor and the point at which temperature is to be calculated. The change in temperature of the tissue is represented using Penne's bioheat equation [67] as follows,

$$\rho C_p \frac{dT}{dt} = K \bigtriangledown^2 T - b(T - T_b) + \rho \text{SAR} + P_{avg}, \tag{5}$$

where ρ is the mass density, C_p is the specific heat, K is the thermal conductance, and T is the temperature of the body part, A is the surface area of contact with the device, T_r is its temperature, b is the blood perfusion constant, T_b is the blood temperature, and P_{avg} is the average power required by the sensor.

The Penne's bioheat equation can be written as a temporal differential equation by discretizing it over $N \times N$ space grid. It is discretized over time and space using the finite difference time domain (FDTD) technique [67].

At grid points (i, j), the temperature $T(i, j)$ is:

$$\begin{aligned} \frac{dT(i,j)}{dt} &= \left[-\tfrac{(b\delta^2+4K)}{\rho C_p \delta^2}\right] T(i,j) + \tfrac{SAR}{C_p} + \tfrac{b}{\rho C_p} T_b + \tfrac{P_{avg}}{\rho C_p} \\ &+ \tfrac{K}{\rho C_p \delta^2}[T(i+1,j) + T(i,j+1) + T(i-1,j) \\ &+ T(i,j-1)]. \end{aligned} \tag{6}$$

If $\boldsymbol{T}$ is considered to be a vector consisting of the temperatures at each grid point, then Equation 6 is analogous to Equation 7, which is in the form of linear time invariant differential equation.

$$\dot{\boldsymbol{T}} = A\boldsymbol{T} + B, \tag{7}$$

where, matrix A will have dimensions $N^2 \times N^2$ and its each row will be as,

$$A = \begin{array}{c} \begin{array}{ccccccccc} \cdot\cdot & X_1 & X_2 & X_3 & X_4 & X_5 & X_6 & X_7 & \cdot\cdot \end{array} \\ \begin{pmatrix} \cdot\cdot & \alpha & \cdot\cdot & \alpha & \beta & \alpha & \cdot\cdot & \alpha & \cdot\cdot \end{pmatrix} \end{array} \tag{8}$$

where, $\alpha = \frac{K}{\rho C_p \delta^2}, \beta = -\frac{(b\delta^2+4K)}{\rho C_p \delta^2}$, $X_1 = N(j-1)+i$, $X_2 = N-2$ zeros, $X_3 = N(j+1)+i$, $X_4 = Nj + i$, $X_5 = Nj + (i-1)$, $X_6 = N - 2$ zeros, $X_7 = Nj + (i+1)$. The dotted elements of matrix A are all zero. The computed matrix B of dimension $N^2 \times 1$ is as follows,

$$B = \begin{array}{c} \\ 1 \\ \vdots \\ N^2 \end{array} \begin{array}{c} 1 \\ \begin{pmatrix} \frac{SAR}{C_p} + \frac{b}{\rho C_p} T_b + \frac{P_{avg}}{\rho C_p} \\ \vdots \\ \frac{SAR}{C_p} + \frac{b}{\rho C_p} T_b + \frac{P_{avg}}{\rho C_p} \end{pmatrix} \end{array}. \tag{9}$$

The solution to Equation 7 is a non linear function of time given by,

$$\boldsymbol{T}(t) = e^{A(t-t_0)}\boldsymbol{T}(0) + e^{At}A^{-1}(e^{At} - e^{At_0})B, \tag{10}$$

where t_0 is the starting time.

The average power consumption of the sensor over a time τ can be obtained using Equation 11,

$$P_{avg} = (P_s f_s + (P_c + P_{sec}) f_c). \tag{11}$$

A principal requirement of the sensor to operate is the energy neutrality constraint. A system is energy neutral for a time τ if the storage device level remains unchanged after the execution, i.e., $P_b(0) = P_b(\tau)$. Thus, effectively all the power required for computation comes from scavenging sources (Equation 12),

$$(P_s f_s + (P_c + P_{sec}) f_c)(\tau - t_0) \leq \int_{t_0}^{\tau} E(t)dt. \tag{12}$$

The power from the scavenging sources are not directly provided to the sensor but has to be stored in a storage device. The storage device should have a capacity greater than the peak power consumption of the sensor. Also, the available charge at any time should be greater than the power requirements of the sensor,

$$P_b(t) \geq P_{avg} \text{ and } B_c \geq max\{P_s, P_c, P_{sec}\} \tag{13}$$

The aim of the optimization analysis is to find P_s, P_c, P_{sec}, B_c, f_s and f_c such the temperature rise is maximized without violating dangerous levels. In order to frame

---

Find $P_s, P_c, P_{sec}, f_s, f_c,$ and B_c that minimizes
$abs(\epsilon - max(\boldsymbol{T}(t) - \boldsymbol{T}(0)))\forall t \in [t_0 \ldots \tau]$
such that
[Penne's Equation] , $\forall t : \boldsymbol{T}(t) = e^{A(t-t_0)}\boldsymbol{T}(0) + e^{At}A^{-1}(e^{At} - e^{At_0})B$, (14)
[Energy Neutrality], $(P_s f_s + (P_c + P_{sec}) f_c)\tau \leq \int_0^{\tau} E(t)dt$,
[Storage Constraint], $\forall t : P_b(t) \geq P_{avg}$,
[Capacity Constraint], $\forall t : B_c \geq max\{P_s, P_c, P_{sec}\}$.

---

it as an optimization problem as shown in Equation 14, the above requirement has to be converted in an objective function. Let us assume that $\boldsymbol{T}$ should not increase by more than ϵ°C. In such a case, the objective function can be framed as minimization of the quantity, $abs(\epsilon - max(\boldsymbol{T}(t) - \boldsymbol{T}(0)))\forall t \in [t_0 \ldots \tau]$, where τ is the final time.

For the energy scavenging unit the energy $E(t)$ can be given by the linear model $E(t) = \alpha(max(\boldsymbol{T}) - T_{amb})$, where α is the thermal resistance of the human body and T_{amb} is the ambient temperature.

4.3 Validation

The optimization problem is solved in Matlab using *fmincon*, which starts with initial values of variables and minimizes the scalar function within the specified

constraints. The usage of the optimization technique is demonstrated using three examples: a) single sensor operation, b) cluster head scheduling for implanted sensor networks, and c) designing infusion control algorithm.

Single Sensor Example. The problem formulation of Subsection 4.2 is utilized. The objective function of Equation 14 is used as a scalar function for *fmincon*. ϵ is considered as 0.1 °C. Energy sustainability of sensors are described by the battery constraints and energy neutrality constraints.

The initial values of design parameters are considered as, sensing power P_s = 7.1μW, data transmission power P_c = 50 mW, power for executing security protocol P_{sec} = 12 mW, sampling frequency f_s = 100 Hz, and frequency of data transmission f_c = 6/3600 Hz. For forming the complete optimization problem, feasible design considerations are set for aforementioned parameters as P_s = 5 μW, P_c = 1 mW, P_{sec} = 5 mW, f_s = 10 Hz, and f_c = 0.001 Hz. These are minimum values of design parameters for currently available sensors. Using these values, the optimization problem is solved and optimized design parameters are obtained as P_s = 8.3 μW, P_c = 61 mW, P_{sec} = 13.3 mW, f_s = 112 Hz, and f_c = 1/360 Hz which satisfied all the constraints.

To implement and experimentally validate the optimization design, commercially available sensing platforms TelosB, Shimmer, Imote2, and BSN v3 are benchmarked. Table 1 enlists the power consumption of respective platform for sensing once. We measured sensing power and radio power while both plain data and encrypted data are being sent. Table 2 shows the bench-marking results for the radio power.

From Tables 1 and 2, the Shimmer platform is the best match for the given optimized power consumption constraint, thus used for validation.

Table 1 Power consumption of sensor query task

Platform	Consumed Power	Time
TelosB	5.46 mW	500 ms
Imote2 (13 MHz)	156.15 mW	286 ms
BSN v3	6.586 mW	235 ms
SHIMMER 2R	7.145 mW	452.8 ms

Table 2 Radio power consumption results with plaintext packets and encrypted packets

Platform	Consumed Power Encrypted data(mW)	Consumed Power Plain data(mW)
TelosB	58.2	47.6
Imote2	209.4	198.3
BSN v3	70.7	59.7
SHIMMER 2R	72.4	60.1

After obtaining optimal design for sensors and choosing testing platform as Shimmer, the sensor software code has to be written for the given obtained optimized design. For code development, automated code generator, Health-Dev [23] can be used. It takes requirements of wearable sensors in the form of models in Advanced Architectural Description language (AADL) and generates downloadable code for them. The automated code generation reduces manual implementation errors.

Input sampling frequency is used as 112 Hz, data transmission frequency of once every 6 mins, and choice of sensor as ECG sensor to Health-Dev [23]. Then, the generated code is downloaded in Shimmer platform and wore it to measure ECG signal continuously for 12 hours. Two sets of experiments are conducted: a) without any radio duty cycling and b) with the optimize sensing frequency and duty cycle. At the end of the testing period, the energy required and rise in temperature of the body part are measured. With no duty cycling and at a sampling rate of 250 Hz, the energy consumption was 432 J and the temperature rise was (≤ 0.167 °C) on the arm. With the optimized design, the sensor consumed 11 J of energy and there was no measurable temperature rise. The power available from body heat was 9 J and an energy storage unit with initial energy 4 J is considered.

Networked Implanted Sensors. In this example, a network of implanted sensors is used, which communicate in a cluster protocol. The implanted sensors form a cluster, where a cluster head collects all communication packets from the participating sensors and sends it out to a base station. Here, for each sensor, the sensing power P_s is fixed to 3 μW, communication power P_c is fixed at 5 μW and there is no security protocol, hence $P_{sec} = 0$. The sensing frequency is set at 10 Hz while the communication frequency is set at 0.5 Hz. Since the cluster head has to collect data from all other sensors, it has the most power consumption and the tissue around the cluster head is heated the most. To keep the temperature of the surrounding tissue within limits, the cluster head has to be frequently rotated. This example found the optimal cluster head rotation scheme that can keep the temperature within thresholds at different parts of the body.

It is observed that as the location within the body changes, different leader rotation schemes are needed to keep the temperature within thresholds as shown in Figure 3. In the arm where the blood perfusion is the lowest, the leader can be changed every 600 s to keep the temperature below 37.8 °C. However, for the same threshold a cluster in the tongue will have to have its leader power reduced to half, every time the temperature is greater than 37.6 °C in addition to changing its leader every 600 s. If the implant is in the eye, the leader has to be changed every 300 s.

Designing Infusion Pump Control Algorithm. For the infusion pump case study, a requirement of the drug concentration should not be above 1300 μg/min is considered. The aim of this study was to derive the design parameters discussed in Section 4.1 such that this requirement is satisfied. In addition to the five design parameters, the packet delivery ratio as a measure of the wireless channel characteristics is also used. Equation 4 is of the same form as the Penne's bioheat equation and hence can be solved using FDTD. The form of the objective function will thus

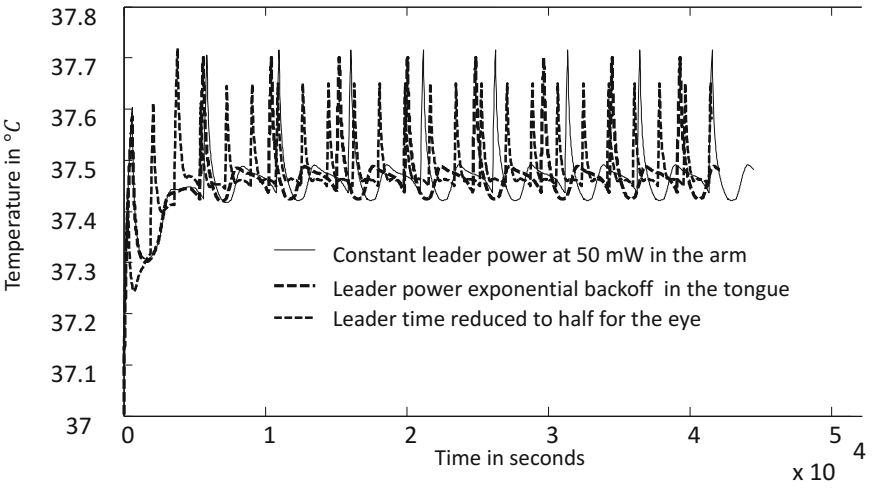

Fig. 3 Cluster scheduling schemes for implanted sensors

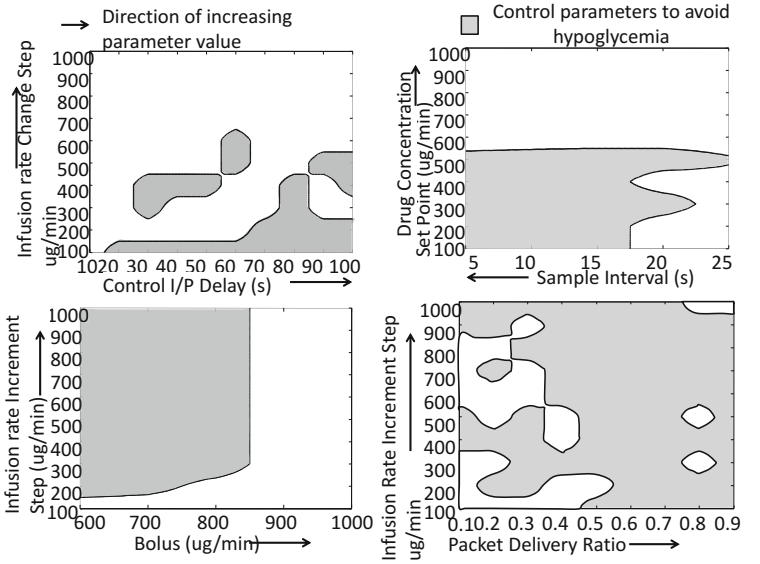

Fig. 4 Infusion pump parameters for avoiding hypoglycemia

be the same as that in Equation 14. Figure 4 shows the results of 10000 optimization runs. Since several local minimums are possible, a set of design parameters (within the gray bounded region) are obtained that satisfy the requirements.

5 Hybrid Simulator

The sensor configuration framework described in Section 4 uses hybrid simulator only to simulate continuous dynamics of the human physiology. However, to simulate the MMA system design with controller app software, sensors and human physiology, events from both continuous dynamics of human physiology as well as events from discrete system (controller software) need to be considered. One of the example hybrid simulator to accurately simulate events from both continuous and discrete domains is discussed in this section.

In MMAs, controller algorithm in smartphone which is a computing system and physical dynamics form a closed loop control system, which is a cyber-physical system. The interactions between these two systems are guided by two types of events: a) *random discrete computing events*, that arise from the interaction of a user with the MMA, and b) *physical events*, that arise due to threshold crossing of continuous system variables of human physiology system. These events reconfigure the computing and physical system parameters. This example hybrid simulator has focused on accurate simulation of cooperation between computing and physical systems, their interactions, through a unified hybrid simulation approach.

Simulations play an important role in: a) estimating resource requirements and designing their organization, b) estimating cost, c) comparing strategies, and d) verifying the design against requirements. While analytical techniques such as model checking and formal requirements verification may provide more rigorous evaluation framework, they often have limited solutions for complex systems including delayed differential dynamics. For such cases, simulation provides a time efficient and scalable solution. Lack of accurate simulation of MMA interactions with human physiology may result in sub-optimal design. This can cause significant hazards to the physical environment e.g., wrong infusion of insulin can cause hypo or hyperglycemia problems [74], burning of the skin due to over-heating of the wearable sensors. Simulation of MMA interactions with human physiology are challenging and traditional approaches of interfacing domain specific simulators may have simplifying assumptions that adversely affect efficient MMA design.

Traditionally there are two different paradigms of simulation: a) event driven (ED), that progresses by processing events that can change system variables and generate new events, and b) finite horizon time stepped (FHT), that progresses by increasing time by a small fixed amount and evaluating the dynamics of system variables. ED simulators operate in discrete time and hence cannot simulate continuous dynamics of human physiology while FHT operate in continuous time and can only process events at the start of a time slot. For MMAs, a hybrid approach is the most optimal where computing events are handled by ED at exact event times while continuous physical system is handled by FHT.

5.1 Challenges of Hybrid Simulation

Co-simulation of computing and physical events: In MMAs, random discrete computing events originating from the networked computing systems may result in

change in controller configuration or may also induce mode transition for a given controller. Events in computing domain can be efficiently handled by discrete event simulators such as ns2 or OMNET++ [42] (first row in Table 3). Changes in the physical system variables due to a random discrete computing event in control algorithms is a property unique to MMAs. For cyber-physical systems (CPS), researchers have tackled this problem by interfacing a discrete event simulator such as ns2 with a physical simulator such as Matlab, second row in Table 3). These techniques can be applied to MMAs as they also form a CPS.

Table 3 Summary of existing CPS simulation tools

Existing CPS simulation tools	**Discrete computing events**	**Physical system**	**Physical events & time adjustment to reduce error**	**Event time prediction**
Omnet++ [42], Situation Calculus based simulator [71]	✓	×	×	×
GISOO [11], PiccSIM [53], iSEE [75], Matlab+EPANET [58]	✓	✓	×	×
NCSWT [39], Modelica [46], WCPS [55], Truetime [25]	✓	✓	✓	×
HyrefSim	✓	✓	✓	✓

Time step adjustment problem: Simulating MMAs require accurate estimation of: a) solutions of differential equations using a time stepped approach, and b) physical event timings. Existing hybrid simulators (third row Table 3) use tools such as Simulink to estimate physical dynamics and state change in controllers due to physical events. Such simulators dynamically adjust simulation time step in order to reduce error in estimation of differential dynamics. However, they have an inherent assumption that a time step that ensures accuracy in differential dynamics can also accurately estimate physical event timings, which is often not the case as shown in Section 5.2. A slight difference in event processing times can have long lasting impact in MMA simulation, by progressively increasing error in estimating the physical system variables.

Artifacts of wrong time step adjustment: Wrong estimation of physical event timings may lead to: a) event delays, when an event scheduled to be processed within a time slot of an FHT is pushed towards the end of a time slot, b) event loss, when events scheduled to occur within a time slot of an FHT is lost at the end of a time slot since the differential dynamics fails to satisfy threshold crossing conditions, and c) false clustering of events, when multiple events scheduled to occur at different times within a time slot of an FHT are grouped at the end of a time slot, often resulting in conflicting control requests. Examples of such effects are shown in Section 5.2.

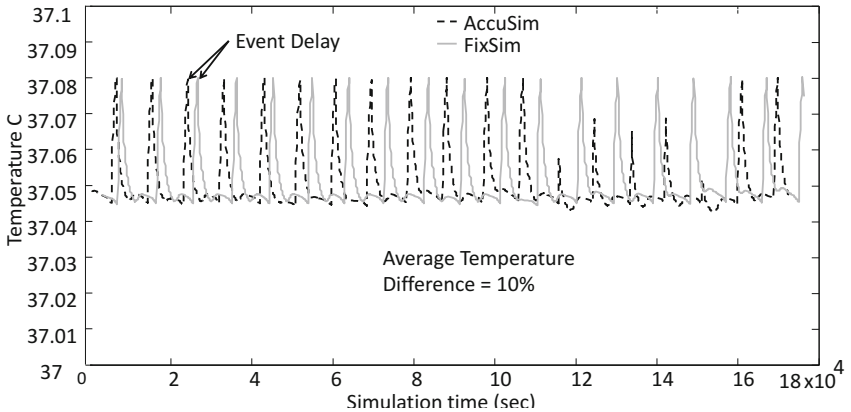

Fig. 5 Difference in temperature profile for *FixSim* type simulation and *AccuSim* with exact event times

A way to avoid such errors is to have an arbitrarily small time step, however, that will drastically increase the simulation time. Hence, simulation approaches that combine physical simulators such as Simulink and discrete event simulators such as ns2, are either limited in their capabilities to process events at accurate times or take a prohibitively long processing time. This is due to a lack of a method for refining simulation time step to reduce error in predicting physical event timings. An associated side-effect of this gap is that a time efficient unified simulator that can process random events from computing domain and physical events from continuous domain is difficult to develop.

5.2 Practical Need for Processing Events at Accurate Time

Let us consider a example of network of implanted sensors (example 4) from Section 3 that sense physiological signals from different parts of the human body and send it back to the smartphone outside the body for storage, processing and diagnosis. The sensors form a cluster where a cluster head is randomly chosen to communicate with the smartphone. All other sensors are slaves and they only communicate with the cluster head. Communication of sensors with the cluster head leads to power consumption. Since the cluster head is the most power hungry sensor, it has to be periodically re-selected or rotated i.e., some other slave sensor takes up the task of a cluster head.

As these sensors operate inside the human body, power dissipation causes temperature rise of the tissue. This can be modeled using the Penne's bioheat equation [67]. The rotation of cluster head can also be triggered by tissue temperature rise. This is an example of physical event triggered action in the computing domain. Let us further assume that the implanted network has to be designed such that it lasts at least a year without the need for recharging. Hence, another strategy is employed

such that a cluster head with energy less than 30% of initial energy has to be rotated (low energy events). A cluster head rotation scheme has to be designed that never causes a temperature rise of 0.15 °C above the normal body temperature and can have at most one sensor that is not capable of being a cluster head after an year of operation. The design parameters are placement, power consumption, and energy storage size of the sensors.

The aim is to consider the simulation paradigm of existing CPS simulators and evaluate if event loss, delay, and false clustering can cause any significant difference in design cost or operation of the system. Existing CPS simulators interface physical simulator with computing or network simulators, which use fix time step. Here, existing simulators are referred as *FixSim*. *FixSim* is compared with a hypothetical simulator that has infinitesimally small time step and can process physical events at their exact times of occurrence.

Event Delay

FixSim results in a different temperature profile with a higher temperature rise on an average and also predicts 10% higher energy consumption of the sensors (Figures 5 and 6). FixSim will always process a physical event at the end of a time slot. Hence cluster head rotations due to temperature rise above a certain threshold are always delayed. Hence, *FixSim* estimates that sensors remain cluster head for a longer period of time. This error in estimation leads to an error in computing the thermal profile of the sensors and also their energy consumption. Hence, if the sensor network is designed using the estimations of *FixSim*, following things are needed to be done: a) over provision energy storage for the sensors, and b) reduce the power consumption of sensors to prevent higher temperature rise. Based on fuel cell cost [72], $ 3 extra are needed to be spent on sensors to accommodate for 10 % more fuel cell capacity, and also have to reduce the power consumption to keep the temperature within the safety threshold of 37.15 °C.

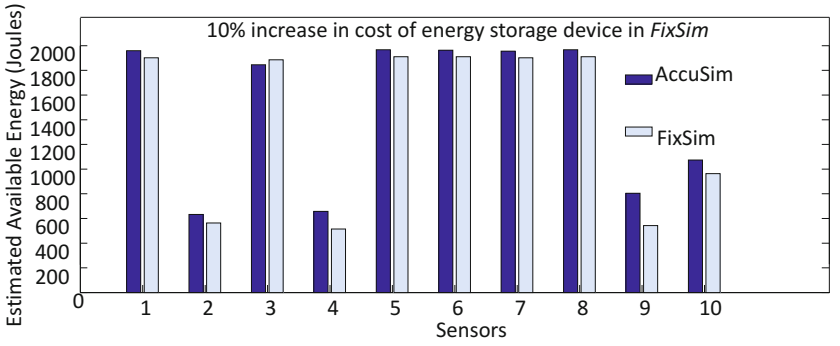

Fig. 6 Difference in energy consumption of sensors for *FixSim* type simulation and *AccuSim* with exact event times

Event Loss

FixSim fails to process three critical low energy events over a period of 24 hours. Error due to event delay accumulates over time, which eventually leads to loss of events in *FixSim*. From experiments it is observed that for a period of 1 day *FixSim* missed three times more low energy events and predicted that only one cluster head will be out of energy. However, if the events are processed at the exact time of occurrence, *AccuSim* predicts that three cluster heads will be out of energy and non-operational. Hence, if the system is designed using the estimation given by *FixSim* then it can jeopardize the system performance.

False Clustering of Events

False Clustering of events in FixSim induces loss of events or renders events meaningless.

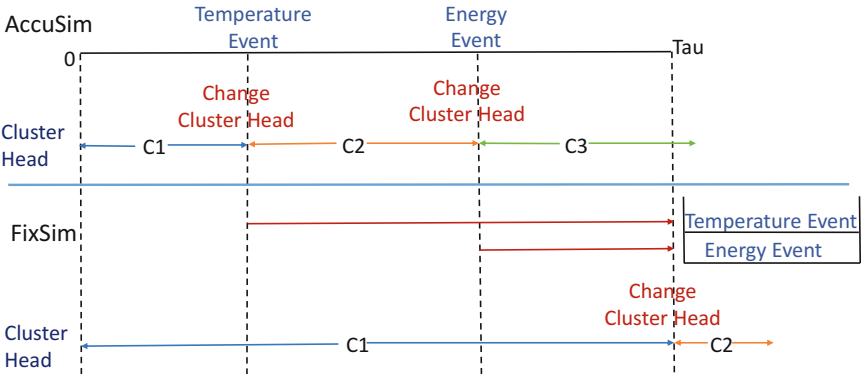

Fig. 7 False Clustering of Events

A case of event clustering is as shown in Figure 7, where within a time slot first the cluster head $C1$ has to be rotated due to temperature rise then $C2$ is selected, which had to be rotated due to a low energy event. In *FixSim*, these two events will occur at the same time slot. The simulator will consider the events in the order that they arrived at the event queue. Hence, rotation of $C1$ will be handled first. However, the low energy event for $C2$ will not make sense to the simulator since $C2$ has not yet served as cluster head and hence its energy is not reduced yet. Thus, the low energy event will not be processed and hence for the next slot cluster head $C2$ will be drained of energy. If the energy drain occurs within a time slot then *FixSim* will have an in-feasible solution.

A case for further concern is that the errors from the above-mentioned artifacts are unbounded. Figure 8 plots the difference between the energy estimation by *FixSim* and that by *AccuSim* that has exact event times. The error increases with respect to simulation steps t without bounds and at a rate of $O(t^5)$ (determined experimentally).

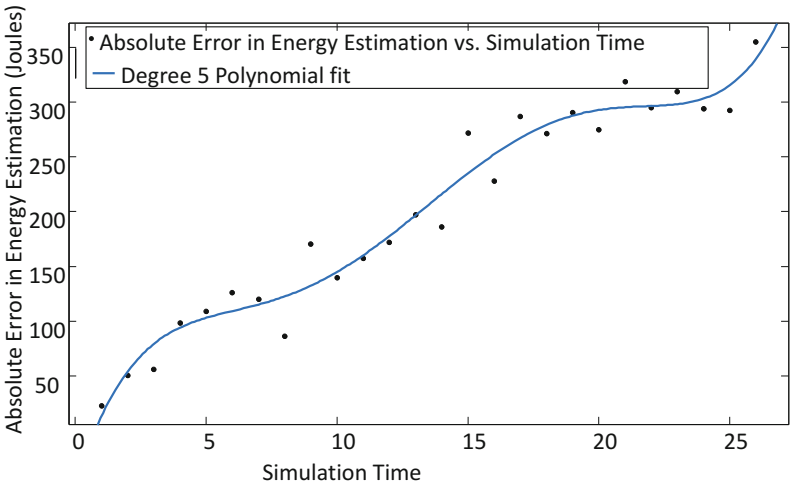

Fig. 8 Error in estimation of stored energy by *FixSim* increases with increase in simulation time without bounds

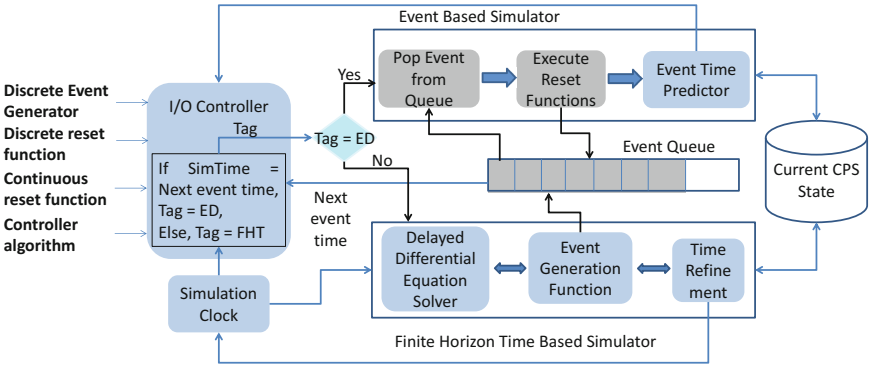

Fig. 9 The *HyrefSim* execution model in its Matlab implementation

5.3 *HyrefSim* Simulation Approach

HyrefSim employs a time refinement approach towards hybrid simulation of MMAs. The primary simulator is ED and it processes events from both computing and physical operation (Figure 9). After an event is processed, the ED passes control to the FHT until the next event is generated. For each time step in FHT, it not only evaluates the continuous system variables but also uses sophisticated predictive models of physical systems to determine the exact time of occurrence of physical events within one step in the future. The time step is then dynamically adjusted to account for the predicted physical event at the correct time within an user specified error margin. This time refinement strategy not only minimizes event delay, event loss,

and false clustering of events, but also ensures that the simulation progresses over time. However, before going to the details of the simulator, let us first consider an example and determine whether simulation errors related to event loss, event delay and false clustering can cause significant sub-optimality in the MMA design.

6 Design Verification

Mobile medical apps (MMAs) work closely with human physiology which might lead to safety hazards such as heating of human skin or hypoglycemia due to low insulin dose in case of infusion pump app. To avoid these issues, the design of the MMA should be verified before its actual implementation. Typically a model based approach is taken to verify safety of a MMA design. In this regard, the chapter considers verification of MMA design using formal methods which incorporates models of human physiology and MMA control algorithms. This method is based on theoretical safety verification of the MMA controller software. It is more rigorous and time consuming than simulation method for system design verification, however it provides eternal safety guarantees.

6.1 Model Checking Using Reachability Analysis

When the smartphone acts as a controller to an actuator device, it obtains feedback from physiological signals to determine the control inputs to the actuator. Thus, it directly interacts with the human physiology typically in a complex non-linear manner. In this regard, poor controller design can cause instabilities in the human physiology leading to hazardous conditions such as hypo-glycemia. Thus the combined analysis should be done on continuous dynamics of human physiology and discrete dynamics of controller software. Hybrid Automata (HA) is able to represent both continuous and discrete dynamics of the system. Reachability analysis on hybrid automata computes the values of continuous variables of the system with a given controller at any point in time. These values are further used to check instability in controller design which is used to perform safety checks in MMAs. However, a hybrid automata representation of the interaction between smartphone and physiology will be non-linear and have multiple independent dimensions. Current hybrid system research have given limited focus on non-linear hybrid automata (discussed in Related works). This section gives an example technique to perform reachability analysis of non-linear system using exponential box splines.

Related Works: To compute the reach set of nonlinear systems, the approach of linearizing the nonlinear equations has widely been accepted [14–16]. In these methods, due to linearization of systems, the available linear solutions are directly applicable. However, the reach set computing methods for linear systems are already approximated and if they get applied to approximated nonlinear system, the error becomes very large. These approximation errors are nonlinear in terms of discretization and increase exponentially with increase in simulation time. To improve the

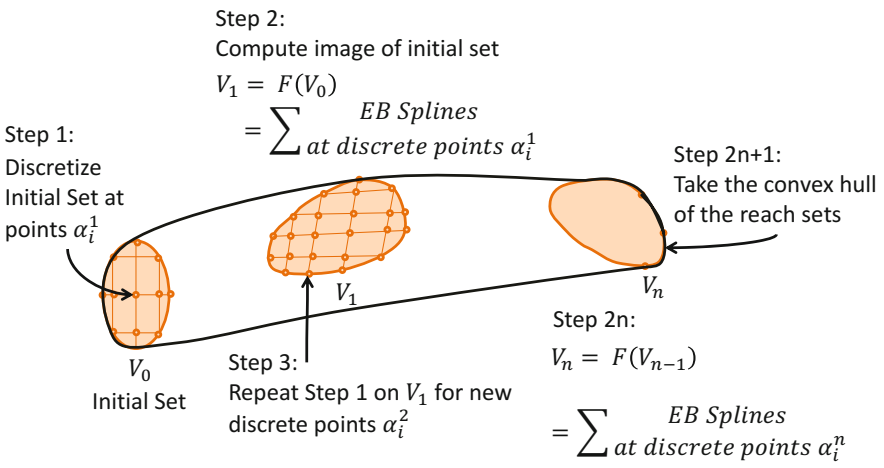

Fig. 10 Approach for reach set computation of nonlinear hybrid system using Exponential box splines

reachability analysis with linearized systems, the state space is decomposed in linearization
domains and considered overlapping linear regions [34, 35]. This method increases the number of state variables, increasing the computation complexity. Also the reach set approximation error increases with increase in size of linearization domains. HyperTech [47] proposes the use of interval numerical method to approximate the reach set for nonlinear Hybrid system. It uses rectangular shape to represent the non-rectangular region shape, resulting in increased wrapping error, which is a result of fitting nonrectangular region using the rectangular shape. Also this error keeps on growing with each iteration as reachability analysis considers sets from previous time, which adds the errors from previous time step as well. To avoid these linearization errors, recently few methods have been proposed which compute reachable sets of non-linear system without linearizing them. One of the method proposes polynomial Zonotope to capture nonlinearity of the system [10]. It converts nonlinear system equations in polynomial differential equations which do not have closed form solutions. This approach introduces error while converting nonlinear system equations in polynomial differential equations by adding uncertainty. However, this methodology will not be useful for nonlinear system having closed form solution.

Research Approach: The un-intentional interactions in human physiology and controller in medical app are usually non-linear in nature. This study considers nonlinear interactions directly in reachability analysis without linearizing them. In reachability analysis, the reach set computation requires to estimate trajectory of continuous variables and discrete state transition. Exponential box splines can be used to represent the trajectory of these continuous variables of nonlinear systems. Exponential box splines are being traditionally used for curve fitting in geometric

modeling [37,68]. Their curve fitting property will be applied to express the nonlinear variation of the continuous variables in the system. Figure 10 gives an overview of computing reach set using exponential box splines. Starting with the initial set V_0, the time will be discretized in small intervals. From each discrete point, the image of the set V_1 will be computed using continuous equations of system. While computing image V_1, the trajectory of discrete points from set V_0 to V_1 will be represented as exponential box splines. The set V_1 will again be discretized in small time intervals and compute image V_2. This process will be repeated of computation of image until simulations ends or discrete transition occurs. It is expected that this approach will reduce the error in reachability analysis of nonlinear systems occurred due to the linearization used in traditional methods.

7 Implementation - Automated Code Generation Using Standard MMA Operating Model

This section focuses on details on the standard operating model to enable use of automatic techniques to design and develop evidence-based trustworthy MMAs. Further, an example framework is discussed which uses techniques mentioned in Sections 5 and 6.

7.1 App Model

It is hypothesized that trustworthy mobile medical applications should have an operating model as shown in Figure 11, where every instance of data communication to the sensor, data storage in the smartphone, control inputs to the actuator, interaction

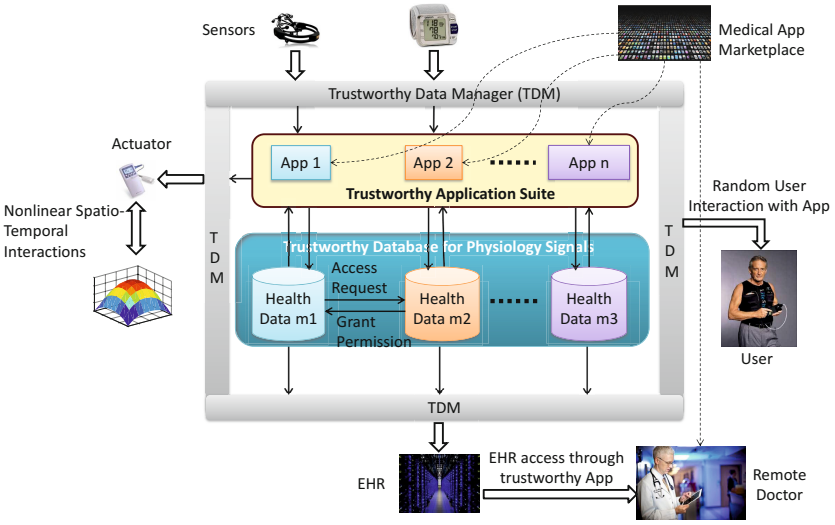

Fig. 11 Operating Model for a suite of applications sharing data and inferences to provide better diagnosis and treatment

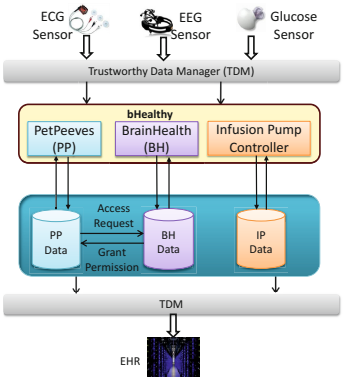

Fig. 12 bHealthy Application suite

with the user and data communication through a certification entity, Trustworthy Data Manager (TDM).

In this new model of applications, the smartphone software itself is in charge of only the graphical and algorithmic aspects of the application. Any form of data communication is privacy ensured by TDM and any form of control input is tested for patient safety. Further, data collected by the different applications are kept in secured databases (similar in principal to application sandboxing). Two applications can share data if they are both certified and have proper access permissions. The TDM can employ different security protocols including public key infrastructure as well as safety assurance techniques such as hybrid automata based model checking.

The app model enables the development of health apps in the form of a suite, where participating apps are certified by the regulatory agencies against safety, sustainability and security. The app model registry will provide guidelines to other apps to become a part of the application suite e.g. the types of sensors being used by currently available apps in the application suite, sensor sampling frequency, energy management algorithms. If any app wants to enter in already existing application suite, the app needs to follow these guidelines if it requires sensors which are being used in that suite. If any app does not follow the registry guidelines of existing application suite and it utilizes sensor data from one of the sensors being currently used in application suite, the new app should be able to modify its requirements or consider re-developing those. If any app is not able to follow the registry guidelines due to its mandatory requirements, it can create new application suite.

As an example of app model with multiple apps working together, interacting with sensors through trustworthy interface, an application suite is developed, bHealthy [60] (Figure 12). It consists of PetPeeves (example 1), BrainHealth (example 2) and infusion pump controller apps (example 3) as discussed in Section 3. These apps use physiological data collected by ECG, EEG and glucose sensors to monitor and control human health. PetPeeves uses processed data from BrainHealth as well to motivate the user by rewarding bonus points.

7.2 *Framework for Developing Trustworthy MMAs*

As an example Health-Dev [23] tool is extended, referred as *Health-Dev β* framework to allow the developer to implement MMAs following the app model in Figure 11 and automatically ensuring safety from interactions, sustainability in sensor and security of data.

The *Health-Dev β* tool for trustworthy development of MMAs may have the architecture as shown in Figure 13. A developer can use such an architecture to either verify whether the developed MMA satisfies trustworthiness requirements or automatically generate critical parts of the code that can impose safety, sustainability or security vulnerabilities. As an input, Health-Dev *β* requires a high level specification of the MMA. Architectural Analysis and Description Language (AADL) can be used as specification language since it is industry standard and is generic enough to describe computational methods of smartphone apps as well as physiological aspects of human body [21]. The high level design can be further optimized and tested using the toolset which has three modules:

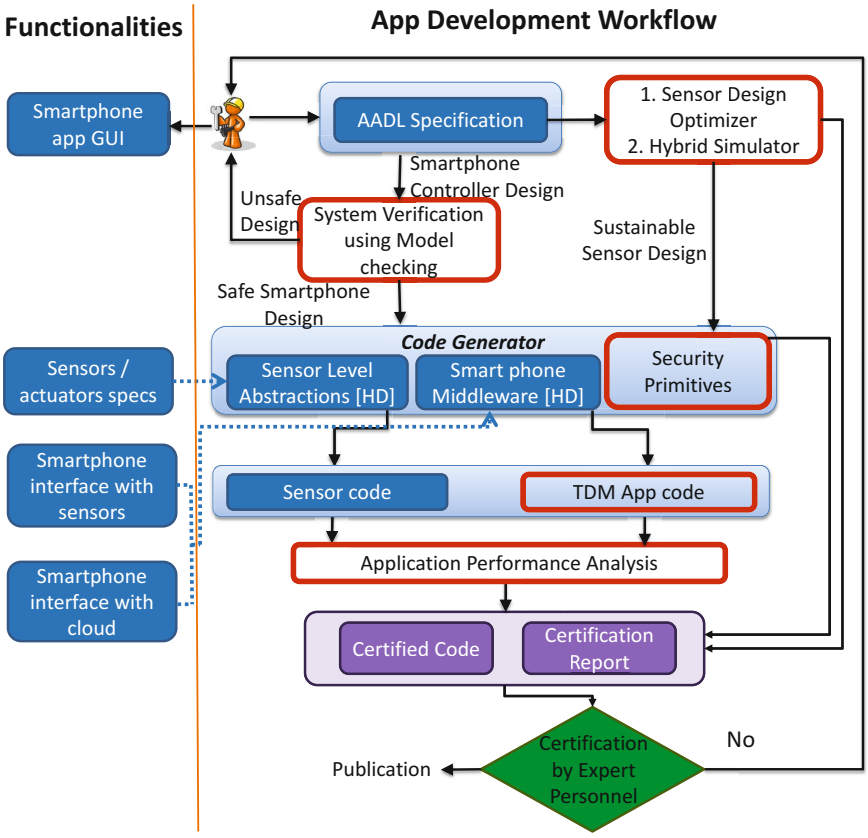

Fig. 13 Architecture for development of trustworthy mobile medical applications

a) sustainable sensor design optimization module: The specified sensor configuration can be optimized for energy neutrality. It is assumed that sensor operates on battery as well as scavenges energy from sources such as sunlight, body heat etc. The energy neutrality problem is modeled as a multi-objective optimization problem as discussed in Section 4. The hybrid simulator discussed in Section 5 can be used to estimate resource requirements and designing their organization for MMAs.

b) MMA system verification: For the verification of the controller of MMA, model checking using reachability analysis as explained in Section 6 can be used. It is a theoretical safety verification technique which represents MMA system using hybrid automata and uses reachability analysis to determine patient safety.

c) security-enabled for sensor code and TDM app generation module: The interface specification can be used by the automatic code generator to generate sensor interface and communication code for the health app. Health-Dev [23] can convert an AADL design in sensor and smartphone implementations. In addition to using the standard software primitives, Health-Dev is extended to have security plug-in, which contains pre-verified code for data communication security algorithms such as physiology value based security [20], AES encryption [32] and private-public key infrastructure [9].

The generated sensor and smartphone code can then be also passed through performance analyzers to validate the code against type and memory related errors. The performance analyzer, the MMA simulation, the reachability analysis, sustainable optimized sensor design and the security primitives generate a certification report stating their findings. The code and the certification report can then be reviewed by an expert personnel in the field to certify the application which can then be uploaded to a dedicated medical app store. If the MMA fails certification, the developer can redesign and again use the same architecture. The key feature of this architecture is that it will be implemented in a modular fashion so that the user can use different modules individually and generate only partial reports.

7.3 Security-Enabled MMA Implementation and TDA Generation

MMA security vulnerabilities arise from three main sources: a) poor configuration management of APIs when developing smartphone applications, b) poor sensor code with common software errors such as unreachable code, array overflow, and inadequate input validation, and c) insecure wireless communication between smartphone and sensor. The problem is not in the technique since there are robust algorithms to avoid these security vulnerabilities. The problem is an implementation problem ([22]) arising from two aspects: a) mis-configuration of APIs in smartphone, and b) scarcity of resources in a sensors. These two factors coupled with the real time requirements of MMAs make it extremely non-intuitive to implement a secure MMA.

One of the typical hypothesis is that models of health apps can be optimized to obtain the correct configurations of implementation modules and then an automatic code generator can be used to reduce software errors. There are two parts of the Health-Dev β code generator: sensor code generator and the TDM app generator.

Both the code generators consist of three parts: a) high level specification module, b) a meta model consisting of code frames that can be filled by functions with appropriate attributes, and c) a database of template code with attributes that can be appropriately parameterized to fit the security needs of the application.

High-level specification. The high-level specification allows user to specify sensor and TDM app specification and translate it to respective models. In this regard, Health-Dev β tool uses Architecture Analysis and Design Language (AADL). It has been shown that the usage of AADL to specify a sensor construct defined with input and output ports [19]. The instance of that sensor consists of identifier, algorithm and communication components. It also allows to specify routing of the data through algorithms.

Meta-Model. Meta-model highlights the information content in a model. It is an abstraction of a model which is itself an abstraction of real-life system. Meta-modeling provides method to analyze, create constructs, frames, rules to model a given set of problems. The high-level specification is written under such regulation that allows parser to create a meta-model of a given model. The parser extracts out all the relevant information from the model which is further used in code generation. Figure 14 shows meta-model containing enough information to allow code generation.

Template code with attribute. Template codes are platform specific code which are used as a base to generate required code. It contains reference entities or attributes which helps parser to inject required frame (piece of a code) and brings modularity in generation. This also makes template code light-weight and generic by storing the functionalities away from it. Based upon the information obtained from meta-model, generator calls an appropriate template code and replaces its attributes by respective frames. The frame can be an algorithm or a function.

Code frame. Code frames are generic implementation of a function which could be used by generator after it is instantiated and parametrized. They are used for specifying and sequencing of algorithms. The generator injects the frame in the specific location making the generation more modular. The Figure 15 shows repository of

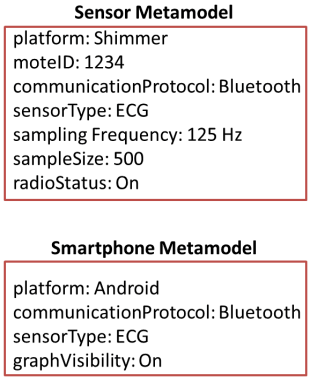

Fig. 14 Sensor and smart phone metal-model are input to generator

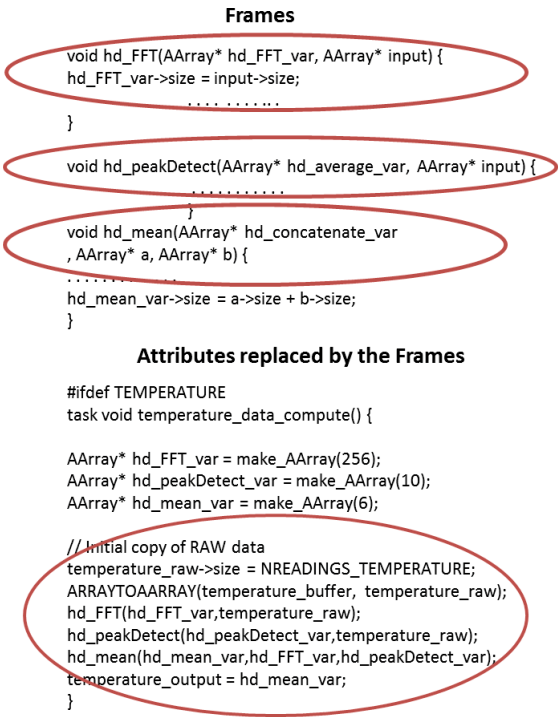

Fig. 15 Declaration and sequencing of algorithm frame in TinyOS template code

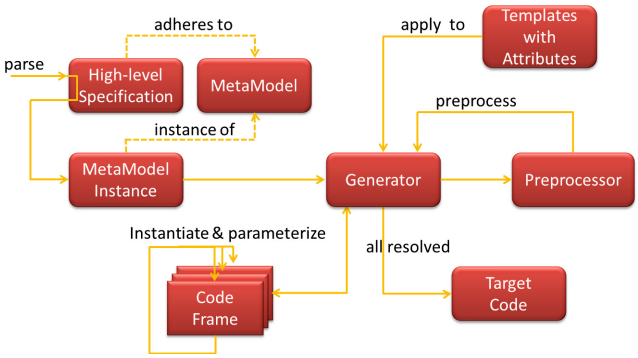

Fig. 16 Code generator

algorithm frames namely, peak detection, Fast Fourier Transform (FFT) and Mean. These frames are declared and sequenced in a copy of a template code by generator.

Given these three components the code generator operates in a manner shown in Figure 16. The high level specification adheres to meta-model is parsed to create an instance of meta-model and is fed to generator as an input. Based upon the given

meta-model generator pulls a copy of a platform specific template code with attributes. It applies preprocessing technique to template file, defining and expanding the required expressions. Appropriate code frames are instantiated and parametrized before getting injected in a specific location in template file.

TDM app generation: The code generator also generates a TDM app which ensures the secure wireless communication. It includes the security algorithm specified by the user in the input. The code generator maintains a code template for generating TDM app. On getting the specification of the security algorithm, it pulls the algorithm from database and inserts in the code. It contains encryption-decryption algorithms such as PEES [20], Advanced Encryption Algorithm (AES) to secure the physiological data over vulnerable wireless channel. In TDM code generation, code generator uses the Application Programming Interfaces (APIs) to allow communication between external wireless mote and an Android smartphone via Bluetooth. It consists of two components, Bluetooth API and sensor handler. Bluetooth API ensures connection establishment and data communication between mote and smartphone while sensor handler acts as a manager and registers all user assigned sensor, different algorithms associated with each sensor and handling of data received from the particular sensor. For each of the wireless communication calls the generator appends the security protocol.

8 Performance Analysis

The performance of the MMAs can be decided by two factors: a) quality of the code and b) latency in serving the app request. To check the quality of the smartphone and sensor code in the health app, static analysis tools are used to check software errors in generated code. Perform interference analysis should be performed on MMAs in the app model to check the latency in serving requests from the apps.

8.1 Quality of the Code

As software plays a major role in safer operation of Mobile Medical apps, there is a need to have a metric to measure the quality and efficiency of the generated code for sensor and smart phone for a personalized health monitoring system. In this regard, to validate the software of mobile medical apps, static analysis tools can be used for both smartphone and sensors code.

Static Analysis for Smartphone

The software for the smartphone apps typically use high level languages such as java, C#, objective C. The compilers for these languages include advanced features to find bugs or errors in the code as compared to compilation features provided by low level languages such as C, nesC. However, the complexity involved in high level languages such as multithreading, methods, classes, various design types make available compilers inefficient to capture all the bugs. Thus, static analysis tools are recommended to use along with the usual compiler feedback to make code more robust.

There are many static analysis tools available such as Dexter [3], FlowDroid [5], Lint [6], Find Bugs [4], CodePro Analytics [1], PMD [7] for Android. These tools are plugins with the Android framework, which makes them easy to use. Dexter [3] and FlowDroid [5] mainly deals with security issues in Android apps such as information leakage. Lint [6] is a inbuilt static analysis tool for Eclipse which captures layout performance problems, manifest and icon problems, translation issues etc. Find Bugs [4], CodePro Analytics [1] and PMD [7] report duplicate code, generate unit test cases, computes code metrics, dead code, well explained defect reports, misunderstood API methods etc.

As an example the results from CodePro Analytics used with Health-Dev generated smartphone code. Figure 17 shows the audit report generated using CodePro Analytix tool. The report includes typecast errors, efficient ways to copy arrays as well as all the unnecessary parts added in the code such as imports, variables, return statements etc. The report also puts flags in front of each reported bug to show its severity. The audit report helps developers to reduce these errors to improve code quality and efficiency. The tool also points out the dead code sections and their exact location in all the classes using tree hierarchy.

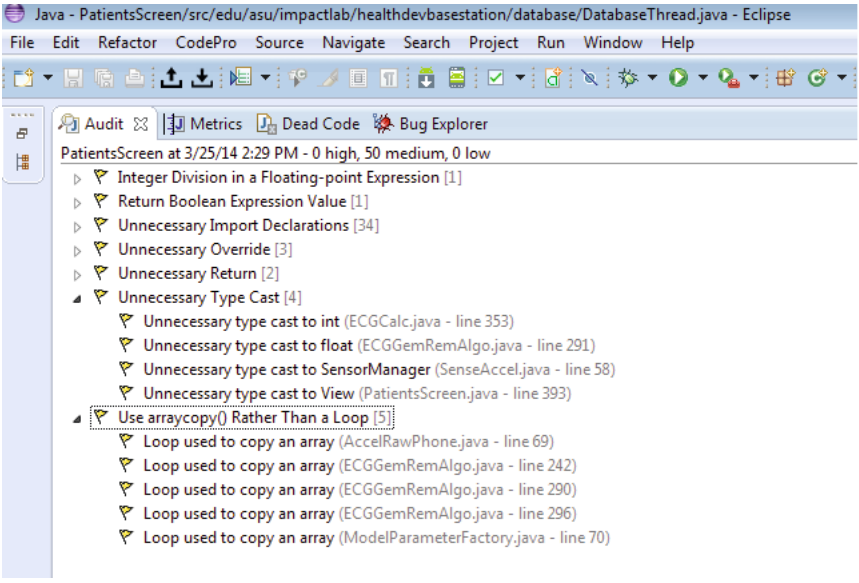

Fig. 17 CodePro Analytix audit report

Static Analysis for Sensors

The wearable sensors used in health apps typically do not have a good runtime exception capture support. For example, in TinyOS which is used by most commercially available sensors there is absolutely no support to capture array out of bound errors, null pointer errors, or race conditions in runtime. Hence safety of sensor code from runtime errors has to be ensured during the implementation and compilation

phase. To avoid these errors, static analysis should be done on the developed code. There are number of such tools available for sensor code validation. Since TinyOS is a popular operating system designed for low-power wireless sensor networks, it is considered as an example to perform static analysis on Health-Dev [23] generated TinyOS-based sensor code.

TinyOS Compiler: It is a widely used compiler for TinyOS applications but often regarded as unsafe because it does not check for array and pointer related errors which can corrupt memory during runtime operation of sensor software.

cXprop: cXprop is static analyzer and source to source optimizer for embedded C programs such as nesC [30]. It tracks data-flow in values through scalars, pointers, structure fields, arrays, and global scope.

Safe TinyOS: Safe TinyOS [30] is built on the top of TinyOS and uses cXprop to optimize code and Deputy [2,29], a source-to-source compiler for ensuring type and memory safety. It adds safety checks, ensures interrupt driven concurrency for these checks, compresses safety violation information and performs optimization of the program.

"Frama-c" (static code analyzer): Frama-c analyses the code using forward data-flow analysis based on the principles of abstract representation [31]. It checks for array and pointer related errors in the code.

The Table 4 shows percentage change in the code size observed when Safe TinyOS and cXprop were applied on Health-Dev generated code. The change code size observed with respect to the code of size found using ordinary TinyOS tool chain. It is observed that, in each case there is an increase in the code size when Safe TinyOS is applied. This is because it uses safety annotation and stores error messages in ROM (stores code) of a micro-controller. However, cXprop used in Safe TinyOS reduces average code size cost. In order to include safety checks code size is increased and can be seen as a trade-off between safety and code size. Whereas cXprop only performs optimization without safety checks and hence the code size is found to be reduced.

Table 4 Change in code size observed with respect to code produced by ordinary TinyOS tool chain

Task	**Safe TinyOS**	**cXprop**
FFT*	+32.3%	-8.2%
Peak detect*	+32%	-8.8%
FIR*	+31.4%	-8.16%
Differential encoding*	+38.02%	-9.1%
Out of range*	+34.2%	-8.88%
Statistics*	+31.2%	-8%

8.2 Performance Analysis of TDM App

The app model explained in Section 7.1 can increase the number of Inter Process Communication (IPC) calls since all the required memory access, sensor access, and communication radio access occur through the TDM. Processes in an application can use all three types of IPC (intend, broadcast and content provider) to communicate with apps, sensors, and actuators. Estimating the total number of IPC at a given time and computing its effect on the response time of apps is non-trivial task given the randomness of IPC generation, the scheduling policy of the operating system and the bandwidth limitations of the connectors.

To estimate the effect of number of IPC calls and increased payload size of request on response time of TDM app, one possible approach is to consider the model of Android IPC communication scheduling and derive analytical expressions for the response time. Each type of IPC call have their own overheads. In a smartphone there can be several combinations of IPC calls. Following three different conditions are considered for experimental purpose:

Condition 1: An applications A_1 communicates with the TDM through a broadcast receiver. A_1 receives X bytes of data every t seconds from the TDM while TDM receives data at the same rate from the sensor. The IPC mechanism is synchronous such that a broadcast receiver order is followed and each app receives the broadcast in order from Sensor Interface.

Condition 2: An application A_1 is accessing a system file through the TDM using the Content Provider interface. A_1 has to first use a Binder interface to establish contact with the TDM. The TDM uses Content Provider to read the file. The content provider is enabled with appropriate read write permissions. The TDM then issues broadcasts to the app A_1 with the file information. There are 3 broadcasts and 1 Content Provider IPC call for data sharing. Like Condition 1, X bytes are received every t seconds from synchronous Sensor Interface broadcasts.

Condition 3: Condition 3 models apps A_1 and A_2 where A_2 is sharing data with A_1 through the TDM. One registration broadcast is made from A_2 to the TDM, TDM then initiates a content provider with A_1 and two broadcasts are made from app A_2 to app A_1.

Latency is dependent upon the scheduling of tasks (IPC calls) by the underlying scheduler of Android. Android is based on Linux 2.6 kernel and uses *Complete Fairness Scheduler* (CFS), which is an implementation of a well-studied algorithm, weighted fair queuing (WFQ). WFQ is a data packet scheduling technique allowing different scheduling priorities to statistically multiplex data flows. The scheduler must balance the queues each time slice so that no process is neglected. Bearing payload size in mind and considering the working of CFS, the latency model is defined as:

$$L = \frac{\sum_{i=1}^{N} payload\_size_i + overhead}{R} \tag{15}$$

where R is the bandwidth of the communication medium.

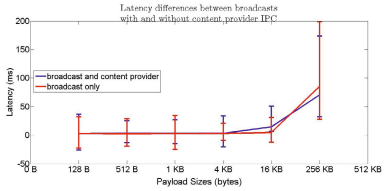

Fig. 18 Broadcast latency differences between inter-app communication with and without content provider

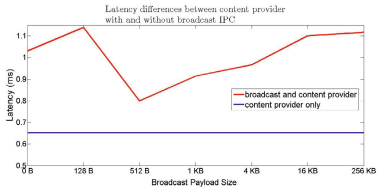

Fig. 19 Content Provider latency differences between inter-app communication with and without broadcast IPC

Table 5 Summary of evidences for trustworthy MMAs

Types of evidences	Method of generation	Available Tools	Examples
Clinical Studies	Deploy the system in a practical scenario	N/A	GeMREM [63], Artificial Pancreas, Ventilators
Emulation	Lab testing on a dummy system	Cadence	Virtual Heart Model [51]
Simulation	Use computer model and execute it for specified input	Hybrid Simulators, BAND-AiDe [21], NS2	bHealthy [60]
Mathematical proofs	Generate theoretical proof	Formal methods, STHA [18]	Infusion Pump [18,52]

In Android, broadcasts that are not serviced within 1 second are prompted for killing. Thus, L should be less than or equal to 1 seconds. The response time degradation of apps heavily depends on the type of IPC chosen and the size of the payload in the IPC. Results of preliminary experiments (Figures 18 and 19) show that the response time degradation of apps vary with the type of IPC, combination of IPCs and its payload. Content Providers typically have low overheads while broadcasts have higher latencies. Regardless it is found that after a payload size of 4 KB, the latencies begin rising and starts affecting the response time. At 512 KB, the latency is greater for broadcast and content provider than with only broadcast.

9 Conclusions

This chapter discussed various techniques and tools to enable evidence-based design and development of mobile medical apps. Different types of evidences required to assure trustworthiness in MMAs and their generation methods are summarized in Table 5. Clinical studies require deployment of MMAs on users to validate their trustworthiness. It is a time consuming process due to patient availability and approval from the institutional review board. Also this type of study can potentially harm the user. To avoid possible injuries to the user during the study, emulation can be used which emulates human physiology. However, emulation technique requires the system to be developed completely. Thus any system flaw obtained during emulation can lead to redesigning and redeveloping the whole system. Thus for rapid

development of trustworthy MMAs, methods such as simulation and mathematical proofs can be used which can give early feedback on MMA design before the actual system development. However, the available tools for evidence generation (few are discussed in the chapter and also enlisted in Table 5) work independently. Thus, there is a need to get such tools working together as a single tool to enable rapid and evidence-based design and development of trustworthy mobile medical apps.

References

1. Codeproanalytics, https://marketplace.eclipse.org/content/codepro-analytix
2. Deputy manual, http://ivy.cs.berkeley.edu/ivywiki/uploads/deputy-manual.html
3. Dexter, http://dexter.dexlabs.org/
4. Findbugs, http://findbugs.sourceforge.net/
5. Flowdroid, http://sseblog.ec-spride.de/tools/flowdroid/
6. Lint, http://developer.android.com/tools/help/lint.html
7. Pmd, http://pmd.sourceforge.net/
8. Agrawal, N., Aranya, A., Ungureanu, C.: Mobile data sync in a blink. Presented as part of the 5th USENIX Workshop on Hot Topics in Storage and File Systems, San Jose, CA. USENIX (2013)
9. Al-Riyami, S.S., Paterson, K.G.: Certificateless public key cryptography. In: Laih, C.-S. (ed.) ASIACRYPT 2003. LNCS, vol. 2894, pp. 452–473. Springer, Heidelberg (2003)
10. Althoff, M.: Reachability analysis of nonlinear systems using conservative polynomialization and non-convex sets. In: Proceedings of the 16th International Conference on Hybrid Systems: Computation and Control, pp. 173–182. ACM (2013)
11. Aminian, B., Araújo, J., Johansson, M., Johansson, K.H.: Gisoo: a virtual testbed for wireless cyber-physical systems. In: 39th Annual Conference of the IEEE Industrial Electronics Society, IECON 2013, pp. 5588–5593. IEEE (2013)
12. Amoroso, E., Taylor, C., Watson, J., Weiss, J.: A process-oriented methodology for assessing and improving software trustworthiness. In: Proceedings of the 2nd ACM Conference on Computer and Communications Security, pp. 39–50. ACM (1994)
13. Anderson, P.: The use and limitations of static-analysis tools to improve software quality. CrossTalk: The Journal of Defense Software Engineering 21(6), 18–21 (2008)
14. Asarin, E., Dang, T., Girard, A.: Reachability analysis of nonlinear systems using conservative approximation. In: Maler, O., Pnueli, A. (eds.) HSCC 2003. LNCS, vol. 2623, pp. 20–35. Springer, Heidelberg (2003)
15. Asarin, E., Dang, T., Girard, A.: Hybridization methods for the analysis of nonlinear systems. Acta Informatica 43(7), 451–476 (2007)
16. Bagade, P., Banerjee, A., Gupta, S.K.S.: Safety assurance of medical cyber-physical systems using hybrid automata: A case study on analgesic infusion pump (2013)
17. Bagade, P., Banerjee, A., Gupta, S.K.S.: Optimal design for symbiotic wearable wireless sensors. In: 2014 11th International Conference on Wearable and Implantable Body Sensor Networks (BSN), pp. 132–137. IEEE (2014)
18. Banerjee, A., Gupta, S.K.S.: Spatio-temporal hybrid automata for safe cyber-physical systems: A medical case study. In: Intl.-Conf.-on Cyber-Physical Systems (2013)
19. Banerjee, A., Gupta, S.K.S.: Analysis of smart mobile applications for healthcare under dynamic context changes (2014)
20. Banerjee, A., Gupta, S.K.S., Venkatasubramanian, K.K.: PEES: physiology-based end-to-end security for mhealth. In: Wireless Health, p. 2. Citeseer (2013)

21. Banerjee, A., Kandula, S., Mukherjee, T., Gupta, S.K.S.: BAND-AiDe: A tool for cyber-physical oriented analysis and design of body area networks and devices. ACM Trans. on Embedded Computing Systems, Special issue on Wireless Health Systems (2010)
22. Banerjee, A., Venkatasubramanian, K., Gupta, S.K.S.: Challenges of implementing cyber-physical security solutions in body area networks. In: Proceedings of the Fourth International Conference on Body Area Networks, BodyNets 2009, pp. 1–18. ICST (Institute for Computer Sciences, Social-Informatics and Telecommunications Engineering), Brussels (2009)
23. Banerjee, A., Verma, S., Bagade, P., Gupta, S.K.S.: Health-dev: Model based development pervasive health monitoring systems. In: 2012 Nineth International Conference on Wearable and Implantable Body Sensor Networks (BSN), pp. 85–90 (May 2012)
24. Borrello, M.: Modeling and control of systems for critical care ventilation. In: Proceedings of the 2005 American Control Conference, pp. 2166–2180. IEEE (2005)
25. Cervin, A., Henriksson, D., Lincoln, B., Eker, J., Årzén, K.-E.: How does control timing affect performance? IEEE Control Systems Magazine 23(3), 16–30 (2003)
26. Cheong, E., Lee, E.A., Zhao, Y.: Viptos: a graphical development and simulation environment for tinyos-based wireless sensor networks. In: Proceedings of the 3rd International Conference on Embedded Networked Sensor Systems, SenSys 2005, p. 302. ACM, New York (2005)
27. Chun, B.-G., Curino, C., Sears, R., Shraer, A., Madden, S., Ramakrishnan, R.: Mobius: unified messaging and data serving for mobile apps. In: Proceedings of the 10th International Conference on Mobile Systems, Applications, and Services, pp. 141–154. ACM (2012)
28. Cobelli, C., Renard, E., Kovatchev, B.: Artificial pancreas: past, present, future. Diabetes 60(11), 2672–2682 (2011)
29. Condit, J., Harren, M., Anderson, Z., Gay, D.M., Necula, G.C.: Dependent types for low-level programming. In: De Nicola, R. (ed.) ESOP 2007. LNCS, vol. 4421, pp. 520–535. Springer, Heidelberg (2007)
30. Cooprider, N., Archer, W., Eide, E., Gay, D., Regehr, J.: Efficient memory safety for TinyOS. In: Proceedings of the 5th International Conference on Embedded Networked Sensor Systems, SenSys 2007, pp. 205–218. ACM, New York (2007)
31. Cousot, P., Cousot, R.: Abstract interpretation: a unified lattice model for static analysis of programs by construction or approximation of fixpoints. In: Conference Record of the Fourth Annual ACM SIGPLAN-SIGACT Symposium on Principles of Programming Languages, Los Angeles, California, pp. 238–252. ACM Press, New York (1977)
32. Daemen, J., Rijmen, V.: The design of Rijndael: AES-the advanced encryption standard. Springer (2002)
33. Dang, T.: Approximate reachability computation for polynomial systems. In: Hespanha, J.P., Tiwari, A. (eds.) HSCC 2006. LNCS, vol. 3927, pp. 138–152. Springer, Heidelberg (2006)
34. Dang, T., Le Guernic, C., Maler, O.: Computing reachable states for nonlinear biological models. In: Degano, P., Gorrieri, R. (eds.) CMSB 2009. LNCS, vol. 5688, pp. 126–141. Springer, Heidelberg (2009)
35. Dang, T., Maler, O., Testylier, R.: Accurate hybridization of nonlinear systems. In: Proceedings of the 13th ACM International Conference on Hybrid Systems: Computation and Control, pp. 11–20. ACM (2010)
36. D'silva, V., Kroening, D., Weissenbacher, G.: A survey of automated techniques for formal software verification. IEEE Transactions on Computer-Aided Design of Integrated Circuits and Systems 27(7), 1165–1178 (2008)
37. Dyn, N., Ron, A.: Local approximation by certain spaces of exponential polynomials, approximation order of exponential box splines, and related interpolation problems. Transactions of the American Mathematical Society 319(1), 381–403 (1990)

38. Estrin, D., Sim, I.: Open mhealth architecture: an engine for health care innovation. Science(Washington) 330(6005), 759–760 (2010)
39. Eyisi, E., Bai, J., Riley, D., Weng, J., Yan, W., Xue, Y., Koutsoukos, X., Sztipanovits, J.: Ncswt: An integrated modeling and simulation tool for networked control systems. Simulation Modelling Practice and Theory 27, 90–111 (2012)
40. FDA. Mobile medical applications, http://www.fda.gov/medicaldevices/productsandmedicalprocedures/connectedhealth/mobilemedicalapplications/default.htm
41. Garawi, S., Istepanian, R.S., Abu-Rgheff, M.A.: 3g wireless communications for mobile robotic tele-ultrasonography systems. IEEE Communications Magazine 44(4), 91–96 (2006)
42. Gavrilescu, M., Magureanu, G., Pescaru, D., Doboli, A.: A simulation framework for psoc based cyber physical systems. In: 2010 International Joint Conference on Computational Cybernetics and Technical Informatics (ICCC-CONTI), pp. 137–142. IEEE (2010)
43. Gu, T., Pung, H.K., Zhang, D.Q.: A middleware for building context-aware mobile services. In: 2004 IEEE 59th Vehicular Technology Conference, VTC 2004-Spring, vol. 5, pp. 2656–2660. IEEE (2004)
44. Gupta, S.K.S., Mukherjee, T., Venkatasubramanian, K.K.: Body Area Networks: Safety, Security, and Sustainability. Cambridge University Press (2013)
45. Harauz, J., Voas, J., Hurlburt, G.F.: Trustworthiness in software environments. IT Professional 11(5), 35–40 (2009)
46. Henriksson, D., Elmqvist, H.: et al. Cyber-physical systems modeling and simulation with modelica. In: International Modelica Conference, Modelica Association, vol. 9 (2011)
47. Henzinger, T.A., Horowitz, B., Majumdar, R., Howard, W.-T.: Beyond HYTECH: Hybrid systems analysis using interval numerical methods. In: Lynch, N.A., Krogh, B.H. (eds.) HSCC 2000. LNCS, vol. 1790, pp. 130–144. Springer, Heidelberg (2000)
48. Hu, F., Hao, Q., Lukowiak, M., Sun, Q., Wilhelm, K., Radziszowski, S., Wu, Y.: Trustworthy data collection from implantable medical devices via high-speed security implementation based on ieee 1363. IEEE Transactions on Information Technology in Biomedicine 14(6), 1397–1404 (2010)
49. Istepanian, R.S., Jovanov, E., Zhang, Y.: Guest editorial introduction to the special section on m-health: Beyond seamless mobility and global wireless health-care connectivity. IEEE Transactions on Information Technology in Biomedicine 8(4), 405–414 (2004)
50. Jackson, T.L., Byrne, H.M.: A mathematical model to study the effects of drug resistance and vasculature on the response of solid tumors to chemotherapy. Mathematical Biosciences 164(1), 17–38 (2000)
51. Jiang, Z., Pajic, M., Mangharam, R.: Cyber–physical modeling of implantable cardiac medical devices. Proceedings of the IEEE 100(1), 122–137 (2012)
52. Kim, B., Ayoub, A., Sokolsky, O., Lee, I., Jones, P., Zhang, Y., Jetley, R.: Safety-assured development of the gpca infusion pump software. In: Proceedings of the Ninth ACM International Conference on Embedded Software, pp. 155–164. ACM (2011)
53. Kohtamaki, T., Pohjola, M., Brand, J., Eriksson, L.M.: Piccsim toolchain-design, simulation and automatic implementation of wireless networked control systems. In: International Conference on Networking, Sensing and Control, ICNSC 2009, pp. 49–54. IEEE (2009)
54. Laakko, T., Leppanen, J., Lahteenmaki, J., Nummiaho, A.: Mobile health and wellness application framework. Methods of Information in Medicine 47(3), 217–222 (2008)
55. Li, B., Sun, Z., Mechitov, K., Hackmann, G., Lu, C., Dyke, S.J., Agha, G., Spencer Jr., B.F.: Realistic case studies of wireless structural control. In: Proceedings of the ACM/IEEE 4th International Conference on Cyber-Physical Systems, pp. 179–188. ACM (2013)

56. Liao, Y.-T., Yao, H., Lingley, A., Parviz, B., Otis, B.: A 3- μ W cmos glucose sensor for wireless contact-lens tear glucose monitoring. IEEE Journal of Solid-State Circuits 47(1), 335–344 (2012)
57. Lim, J.B., Jang, B., Yoon, S., Sichitiu, M.L., Dean, A.G.: Raptex: Rapid prototyping tool for embedded communication systems. ACM Trans. Sen. Netw. 7, 7:1–7:40 (2010)
58. Lin, J., Sedigh, S., Miller, A.: Integratedcyber-physical simulation of intelligent water distribution networks. In: Leite, E.P. (ed.) Matlab/Book2. Intech (2011)
59. Michael, J.B., Drusinsky, D., Otani, T.W., Shing, M.-T.: Verification and validation for trustworthy software systems. IEEE Software 28(6), 86–92 (2011)
60. Milazzo, J., Bagade, P., Banerjee, A., Gupta, S.K.S.: bhealthy: A physiological feedback-based mobile wellness application suite. In: Proceedings of the Conference on Wireless Health. ACM (2013)
61. Nabar, S., Banerjee, A., Gupta, S.K.S., Poovendran, R.: Evaluation of body sensor network platforms: a design space and benchmarking analysis. In: Wireless Health 2010, ACM (2010)
62. Nabar, S., Banerjee, A., Gupta, S.K.S., Poovendran, R.: Evaluation of Body Sensor Network Platforms: A Design Space and Benchmarking Analysis (October 2010)
63. Nabar, S., Banerjee, A., Gupta, S.K.S., Poovendran, R.: GeM-REM: Generative model-driven resource efficient ecg monitoring in body sensor networks. In: 2011 International Conference on Body Sensor Networks (BSN), pp. 1–6 (May 2011)
64. Nami, M., Suryn, W.: Software trustworthiness: Past, present and future. In: Yuan, Y., Wu, X., Lu, Y. (eds.) ISCTCS 2012. Communications in Computer and Information Science, vol. 320, pp. 1–12. Springer, Heidelberg (2013)
65. Pancreas, A.: The artificial pancreas aces new tests, `http://www.diabetesforecast.org/2014/mar/the-artificial-pancreas-aces.html`
66. Park, G., Rosing, T., Todd, M.D., Farrar, C.R., Hodgkiss, W.: Energy harvesting for structural health monitoring sensor networks. Journal of Infrastructure Systems 14(1), 64–79 (2008)
67. Pennes, H.H.: Analysis of tissue and arterial blood temperature in the resting human forearm. Journal of Applied Physiology 1(1), 93–122 (1948)
68. Ron, A.: Exponential box splines. Constructive Approximation 4(1), 357–378 (1988)
69. Rossiter, T.R., LaVaque, T.J.: A comparison of eeg biofeedback and. Journal of Neurotherapy (1995)
70. Schwiebert, L., Gupta, S.K.S., Weinmann, J.: Research challenges in wireless networks of biomedical sensors. In: MobiCom 2001: Proceedings of the 7th Annual International Conference on Mobile Computing and Networking, pp. 151–165. ACM, New York (2001)
71. Singh, V.K., Jain, R.: Situation based control for cyber-physical environments. In: IEEE Military Communications Conference, MILCOM 2009, pp. 1–7. IEEE (2009)
72. Tsuchiya, H., Kobayashi, O.: Mass production cost of pem fuel cell by learning curve. International Journal of Hydrogen Energy (2004)
73. Venkatasubramanian, K.K., Banerjee, A., Gupta, S.K.S.: PSKA: usable and secure key agreement scheme for body area networks. IEEE Transactions on Information Technology in Biomedicine 14(1), 60–68 (2010)
74. Wada, D.R., Ward, D.S.: The hybrid model: a new pharmacokinetic model for computer-controlled infusion pumps. IEEE Transactions on Biomedical Engineering 41(2), 134–142 (1994)
75. Yan, W., Xue, Y., Li, X., Weng, J., Busch, T., Sztipanovits, J.: Integrated simulation and emulation platform for cyber-physical system security experimentation. In: Proceedings of the 1st International Conference on High Confidence Networked Systems, pp. 81–88. ACM (2012)

Wearable and Fexible Sensor Sheets toward Periodic Health Monitoring

Kuniharu Takei

Department of Physics and Electronics, Osaka Prefecture University, Sakai, Osaka, Japan
takei@pe.osakafu-u.ac.jp

Abstract. Recent progress of flexible and wearable health-monitoring devices is introduced by showing examples of flexible sensor components (e.g., strain sensors for heartbeat monitoring and temperature sensors) with an emphasis on printing techniques using inorganic materials to form flexible sensor components on flexible substrates for high performance and low-cost flexible electronics. Printing methods create flexible sensors, which are the next class of economical and disposable wearable health-monitoring devices that will allow people to use these devices without awareness similar to a bandage and a sanitary environment. For commercial applications, flexible sensor devices need to be further developed and signal processing circuits must be integrated on flexible substrates. However, the concept may significantly contribute to comfortable, convenient, secure, and healthy human lives. Periodic health condition monitoring using flexible and wearable health-monitoring devices should allow data to be gathered for medical purposes and even predict illness prior to the onset of symptoms.

1 Introduction

Wearable devices are greatly impacting the market of next-generation electronics. Widely available commercial wearable devices include those that sense human conditions such as activity and heartbeat monitoring for athletes. However, current commercial devices employ conventional rigid sensors, but differ from conventional electronics because the device is assembled with a sensor and a signal processing circuit in a conventional wearable tool (e.g., watch or glasses) by shrinking the device size and considering a human interface. A big contribution of these wearable devices is the development of informatics technology based on a human interface.

Although the present wearable devices are of great interest, there is still room for dramatic improvement. These devices are (1) expensive like a conventional rigid electronic device, (2) perceived as unfashionable, (3) uncomfortable due to their rigidity, and (4) for a single purpose (e.g., one sensor for a specific purpose such as motion or heartbeat). Thus, flexible and wearable health-monitoring

S.C. Mukhopadhyay (ed.), *Wearable Electronics Sensors*,
Smart Sensors, Measurement and Instrumentation 15, DOI: 10.1007/978-3-319-18191-2_7

systems should be of great interest as electronics that interact with humans more closely and precisely. These devices should also attract attention from people interested in their health since the device can be attached on the human body without awareness. If the device behaves like a bandage, the number of products should dramatically increase, and the device price should be low-cost like a bandage. For sanitary reasons, the device should also be disposable.

If periodic health monitoring under comfortable conditions is realized, changes in a health condition can be detected by periodic measurements. For example, a severe illness may be detected before noticeable systems appear and can be cured before it becomes acute. There are some reports about the relation between periodic health condition monitoring and the rate of illness. They found that those who monitored blood pressure periodically had improved medical compliance compared to those who did not [1,2,3]. Compliance should eventually suppress most medical conditions, and good health condition makes people happy[4]. However, it is important that people's happiness and activity are unaffected by the wearable device because this creates a comfortable human life with less stress. In addition, happiness tends to result in better health conditions, creating a positive cycle that can help maintain health and quality of life. In addition, if the device can collect more periodic statistics about health trends before and after illness, this information can be applied to future medical care and may even predict future illness.

Because future wearable devices must realize comfortable, convenient, secure, and healthy human lives, mechanically flexible devices have been widely developed using organic and/or inorganic materials [5,6,7,8,9,10,11,12,13,14, 15,16,17,18,19]. The concept of a flexible and wearable device is to place it on the human skin or clothes without awareness like a bandage. To realize such flexible and wearable devices, a key technique is the formation of mechanically flexible electrical materials and components on a flexible substrate. However, flexibility cannot be trade-off of electrical performance of the integrated devices even on a flexible substrate.

Because thin organic materials are usually mechanically flexible and readily formed on flexible substrates, they are often used as the flexible device [11,13,15]. On the other hand, inorganic materials are rigid when they are tens of micrometers in thickness, but their performance and stability as electrical devices are much better than those of organic materials [8,10,12,20]. Each material system has advantages and disadvantages. However, a practical device requires mechanical flexibility, affordability, stability, and high performance. To address these important issues, inorganic nanomaterials have been proposed for the electrical device components by developing uniform printing techniques on a macroscale flexible substrate. Although inorganic materials are rigid on the macroscale, shrinking them down to the nanoscale can provide mechanical flexibility within the bending radius of a wearable device [20]. In this chapter, flexible and wearable healthcare devices are introduced with an emphasis on inorganic nanomaterials and printing techniques to realize the aforementioned requirements.

2 Future Flexible and Wearable Devices

Periodic statistics on a health condition are important to predict illness and improve medical compliance [1,2,3]. However, none of the currently available healthcare-monitoring devices can monitor periodic statistics without awareness due to solid-based electronics, which are uncomfortable in daily life. This section introduces the concept of future flexible and wearable bandage-type health-monitoring devices. We propose a multi-functional flexible healthcare-monitoring and curing system, which we call a "*smart bandage*" [16].

Figure 1 exhibits the concept of the smart bandage [21]. By developing a device fabrication method on a flexible substrate, multi-function sensors, circuits, actuators, and probably a display can be integrated economically to build an affordable and disposable smart bandage that monitors real-time periodic health conditions. By monitoring small change in health conditions and analyzing all data such as skin temperature, heartbeat, and blood pressure with motion sensing, the device can notify the person or send the diagnostic results to a doctor via a cell phone. Furthermore, a diffusion-type drug can probably be delivered via the smart bandage, depending on the health condition measured by the integrated sensors. Due to medical ethical issues, a noninvasive device is necessary as well as a drug that diffuses and does not require a penetrating needle.

For wide use of flexible and wearable health-monitoring devices, "low-cost", "disposable", and "multi-sensing" are necessary features. In addition, the flexible device may only be applied to health monitoring (i.e., not a medical device application) due to reliability issues of a flexible device compared to a solid-based device (e.g., tearing). Below economical fabrication methods and multi-sensing integration, which are reported mainly by my group, are discussed to realize a disposable multi-functional smart bandage.

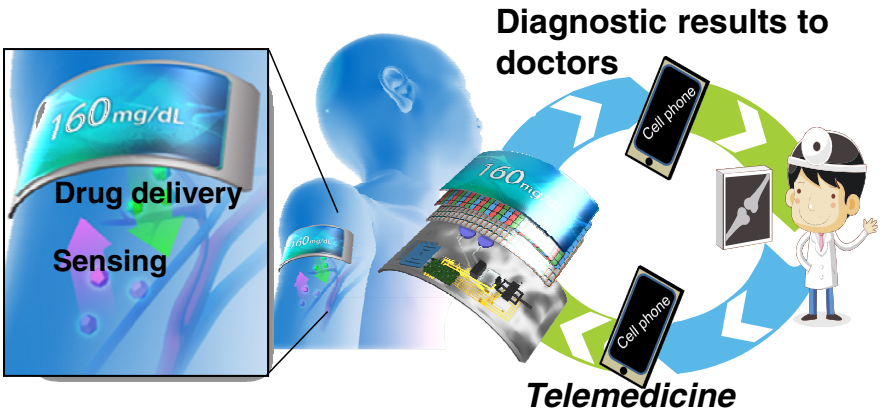

Fig. 1 Concept of a flexible and wearable smart bandage. Reproduced with permission [21]. Copyright 2014, John Wiley and Sons.

3 Printing Methods for Sensor Fabrication

Inorganic nanomaterial printing methods realize economic macroscale flexible devices with a high performance [14,16,19 ,22 ,23 ,24 ,25]. This printing technology allows flexible devices to incorporate active components such as sensors and transistors by developing printing inks, which is one of the challenges to realize truly flexible electronics.

Figure 2 shows the screen printer used to pattern the sensor components and electrodes [16,19]. This technique has diverse applications and can readily be scaled up without increasing the printing costs. For example, it used to print graphics on T-shirts.

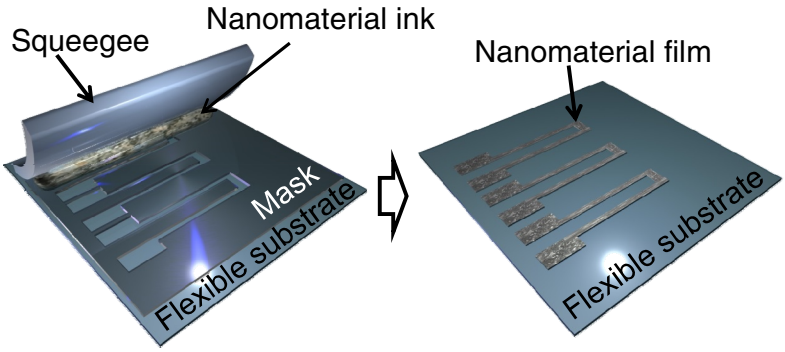

Fig. 2 Screen-printing of nanomaterial-based sensor materials for economic macroscale electronics. Reproduced with permission [19]. Copyright 2014, American Chemical Society.

In the case of strain sensor patterning via a screen printer, first, nanomaterial-based ink, which consists of a mixture of silver (Ag) nanoparticle (NP) ink and carbon nanotube (CNT) ink, is prepared [19]. Then the mixed ink is printed on a flexible plastic substrate and subsequently cured. The low-temperature process and printing method allow any plastic substrate to be used. Either after or before strain sensor printing, a Ag interconnection is screen-printed with alignment of the strain sensor. More details of the printing condition are described later in this chapter.

The printing method explained here is only one such example. Although many printing methods (e.g., ink-jet printing [26], gravure printing [22,25], and flexographic printing [27,28]) have been developed, each printing technique has unique ink conditions, such as the viscosity of inks. The most suitable printing method depends on the ink condition, resolution of patterning, and throughput of the fabrication process. In addition, inks for active components such as sensors, transistors, and actuators must be further developed because few printing inks for the active components have been reported.

4 Toward a Smart Bandage from Each Sensor Component

4.1 Overview of a Smart Bandage

The first proof-of-concept of the proposed health-monitoring device, a smart bandage, is integrated with a temperature sensor to monitor human skin temperature, a touch sensor with a wireless coil, and a drug delivery pump for a curing function (Figure 3) [16]. The important features are that only printing methods are used to fabricate the device on flexible substrates without conventional semiconductor infrastructures (e.g., lithography and vacuum systems). These features drastically reduce the device cost; in fact, a disposable device similar to a conventional bandage may be realized, allowing a sanitary environment to be maintained. Furthermore, all the flexible components of sensors and drug delivery system on a flexible substrate should be comfortable even when placed on the human skin. The goal of this flexible and wearable health-monitoring device is to simultaneously monitor a lot of information in order to analyze the health condition (i.e., "one system"="multi-sensing results") by just attaching the device to the skin (Figure 3).

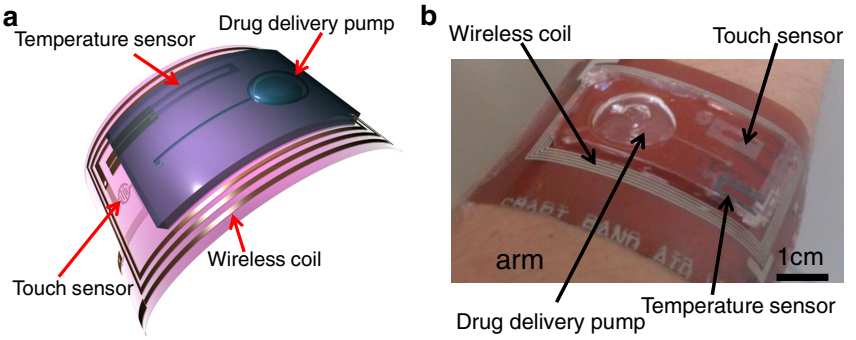

Fig. 3 Schematic and photo of the proposed smart bandage fabricated by printing methods. Reproduced with permission [16]. Copyright 2014, John Wiley and Sons.

4.2 Temperature Sensor

Simple but important information about health is body temperature. If the daily and real-time human body temperature can be monitored along with other information such as activity, heartbeat, and blood pressure, it may be possible to predict a human body condition and illness before the onset of symptoms. This trend is also important to improve medical care. This section introduces a temperature sensor formed by a shadow printing method using a hard mask on a flexible substrate [16,19,29].

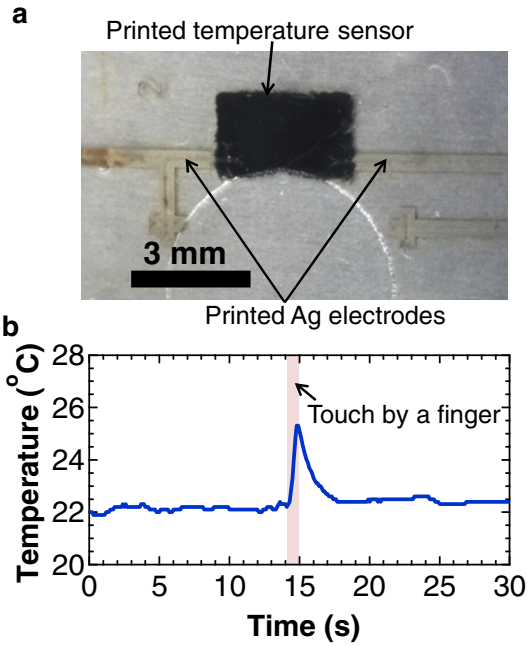

Fig. 4 (a) Printed temperature sensor on a PET substrate. (b) Real-time temperature monitoring of a human touch. Reproduced with permission [29]. Copyright 2014, American Chemical Society

First, to form a highly sensitive temperature sensor, a printing ink is developed. Utilizing electron hopping at the interface between two materials to increase the sensitivity, carbon nanotube (CNT) ink (SWeNT, USA) and poly(3,4-ethylenedioxythiophene) polystyrene sulfonate (PEDOT:PSS) in water (Sigma-Aldrich, USA) are mixed with a weight ratio of 1:3 [29]. The mixed ink is then printed on a flexible substrate (e.g., Kapton, polyethylene terephthalate (PET), or other plastic substrates). Finally, the printed film is cured at 70 °C for at least an hour. Because a printing method is used to pattern the temperature sensor, any material and size for substrates can be used.

This temperature sensor shows the resistance change as a function of temperature due to mostly electron hopping at the interface of CNT and PEDOT:PSS. The temperature sensitivity is ~0.78%/°C for the electrical resistance change of the temperature sensor. To read out the electrical resistance change, a silver (Ag) interconnection is also printed with alignment of the temperature sensor (Figure 4a). The resistance linearly changes as a function of temperature. Based on the calibration of the electrical resistance and temperature, the temperature of the target can be extracted from the measured resistance change. Consequently, temperature can be monitored in real-time (Fig. 4b).

Due to the low thermal conductivity of a plastic substrate [in this case, PET], the response time when a finger is removed from the sensor is relatively slow (~3 sec). However, the response time should be sufficient for a wearable device application. More importantly, the temperature resolution should be suitable to monitor a change in body temperature precisely. This temperature sensor has a ~0.1 °C resolution, which should be appropriate for body temperature measurements based on human activity.

In addition to the human body temperature monitoring based on activity, precise temperature monitoring allows a tumor or some other illness to be detected. To find an illness by monitoring temperature change via skin, a ~0.01 °C resolution is required [30,31]. To monitor such a small temperature change, an amplifier and good environment to measure precise temperature must be realized on a flexible substrate, which is the next step in flexible and wearable device applications.

4.3 Heartbeat Strain Sensor

The heartbeat trend is also important information to understand health conditions. In general, there are two types of heartbeat sensors: an optical measurement [32] and a mechanical deformation measurement [33,34]. Due to the simple structure needed to form a strain sensor to observe mechanical deformation caused by heartbeat, a highly sensitive flexible strain sensor [19] is introduced here. First, a printing ink for a strain sensor is formed by mixing a CNT ink (SWeNT, USA) and Ag nanoparticle (AgNP) ink (Paru, Korea) with 5:3 weight percent ratio. This ink is screen-printed on a flexible substrate and subsequently cured at 70 °C for at least an hour. Ag electrodes are also screen-printed to form interconnections to read out the strain change.

This strain sensor shows an electrical resistance change when the stress corresponding to the structural deformation is applied. Figure 5 exhibits a strain sensor attached on the wrist a 34-year-old male and a result of heartbeat measurement. On the basis of the peaks for the resistance change, $\Delta R(=R-R_0)/R_0$, ~0.8 sec heartbeat (~75 beats per minute) is extracted, where R_0 and R are the strain sensor resistance at zero force and under some force applied to the strain sensor, respectively. Figure 5b shows that this printed strain sensor can monitor a human heartbeat, suggesting that this may be applicable to a wearable health-monitoring device. One concern about heartbeat sensing using a strain sensor is that the sensor also detects human motion, which is detrimental when measuring precise information. To prevent this issue, a structural design based on strain engineering or a different method (e.g., optical measurement) should be applied.

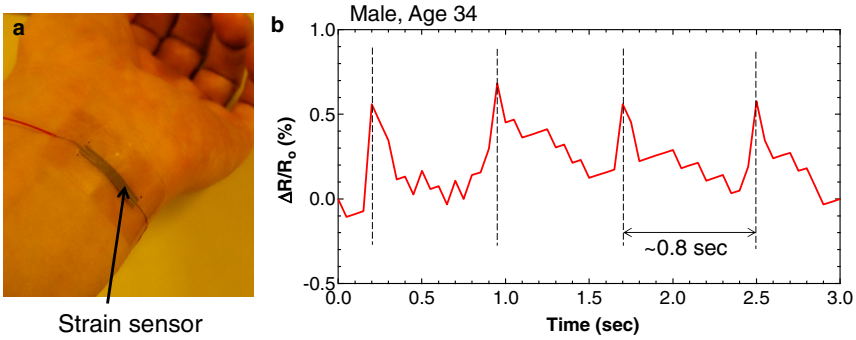

Fig. 5 (a) Photo and (b) real-time resistance change of heartbeat monitoring using a printed strain sensor

4.4 Other Strain Sensor Applications

Strain sensors on flexible substrates should realize other applications such as macroscale tactile sensor sheets. One example is to imitate functions of a human skin. Human skin can detect "tactile force", "friction force", and "temperature". Mimicking these functionalities may realize a prosthetic application as an artificial electronic skin or a cursor to operate a wearable health-monitoring device like a joystick. Figures 6a and 6b show examples of three-axis force measurements integrated with strain and temperature sensors fabricated by a full printing method [29]. In particular, each pixel has four strain sensors surrounding a three-dimensional prong, which is called a "fingerprint-like" structure, and a temperature sensor. When a tactile force is applied, the strain is identically applied to the four-strain sensors, resulting in the same output strain values (Figure 6c, left). In contrast, when a frictional force is applied on the fingerprint-like structure, a nonuniform strain distribution is observed (Figure 6c, right). By reading this strain distribution, the friction force and direction can be extracted. As a proof-of-concept, a 3×3 array three-axis force sensor and a temperature sensor have been demonstrated by touching fingerprint-like structures. Figure 6d confirms that two-dimensional tactile, friction, and temperature distributions are successfully monitored. However, this is only one of the demonstrations to monitor multi-stimuli as an artificial skin application using a fully printed sensor device. Applying this technique to different structures and applications should realize other flexible and wearable electronics (e.g., joystick).

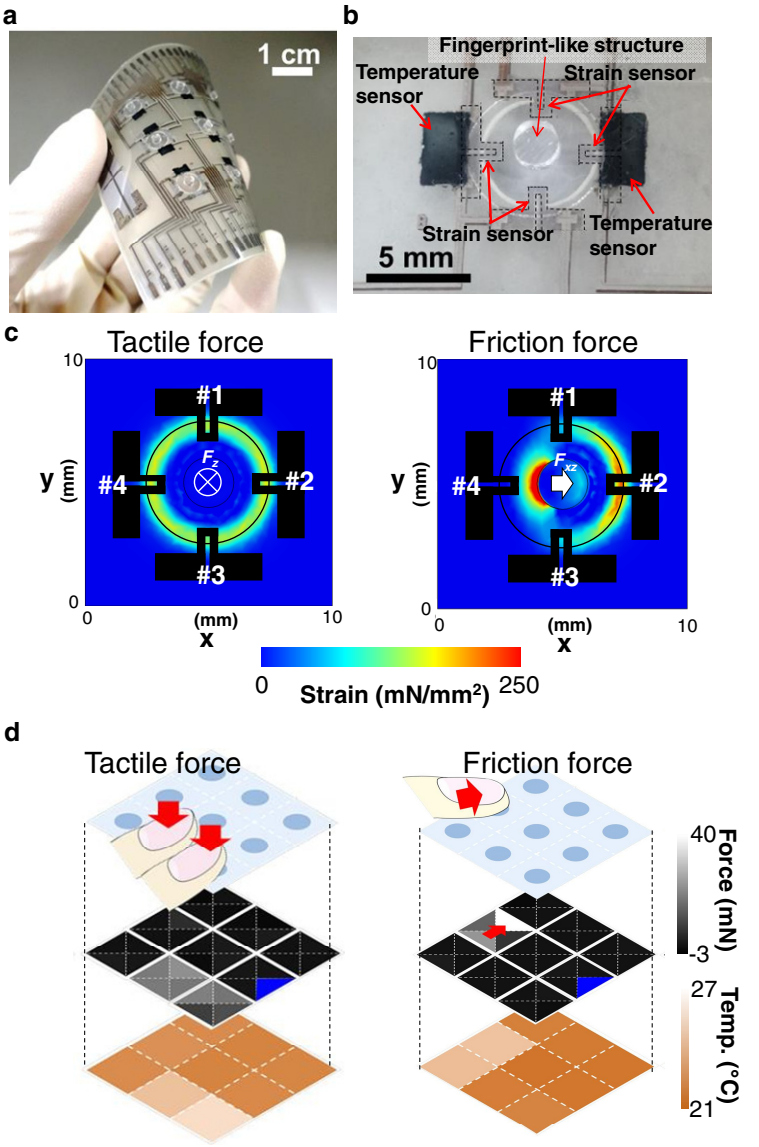

Fig. 6 (a) Photo of a 3×3 array flexible three-axis force and temperature sensor sheet. (b) Enlarged photo of one pixel. (c) Finite element method simulation results when a tactile force (left) and a friction force (right) are applied. (d) Two-dimensional force and temperature distributions measured by a 3×3 array three-axis force and temperature sensor device when a tactile force (left) or a friction force (right) is applied. Reproduced with permission [29]. Copyright 2014, American Chemical Society.

4.5 *Wireless Detection*

Two concerns for flexible and wearable devices are how to detect the signal and how to supply power without using a wired connection. One possible solution is to use wireless technology with signal transmission via wireless coils. This technology allows the device to supply electrical power and wirelessly read the measured sensing results [9,15,16,35 ,36]; however, complicated circuits and systems are required. Since a flexible device including circuits and sensor integration is still under development, this technology needs to be developed stepwise from silicon-based wireless systems.

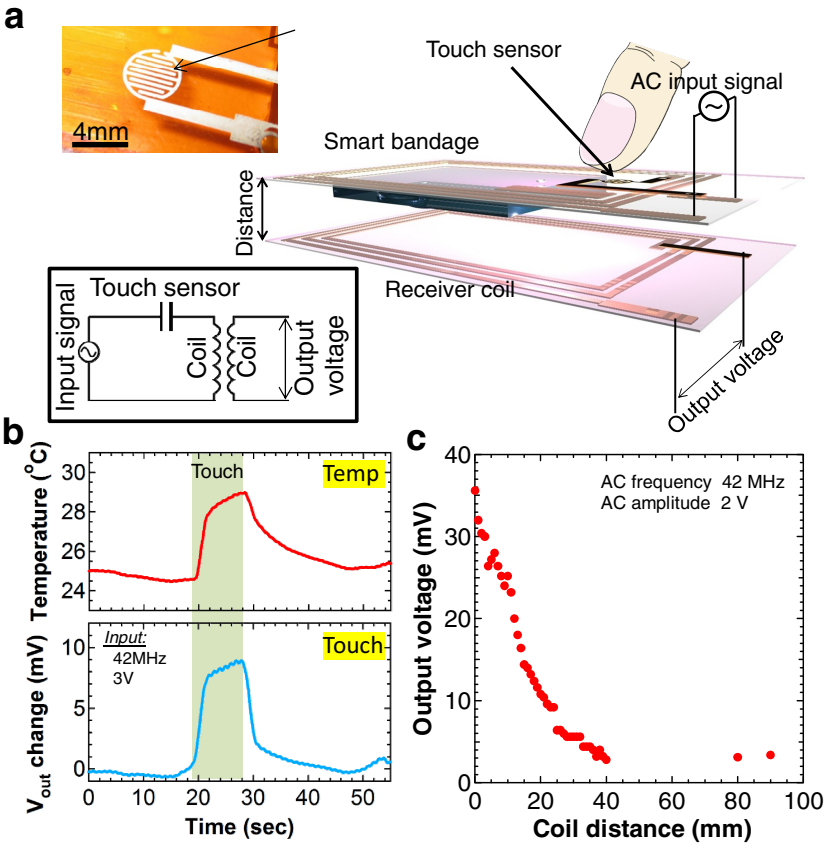

Fig. 7 (a) Schematic of the wireless touch sensor with coils, photo of a capacitive touch sensor, and equivalent circuit diagram. (b) Real-time temperature and wireless touch detections by touching the sensors with a human finger. (c) Wireless transmitted output voltage as a function of coil distance. Reproduced with permission [16]. Copyright 2014, John Wiley and Sons.

As the first step, a printed wireless coil integrated with a capacitive touch sensor on a flexible substrate has been introduced [16]. Two coils formed by Ag electrodes are fabricated by a screen printer. Then a capacitive touch sensor is connected in series with a coil. Due to changes in the capacitance of the touch sensor by touching the sensor, the resonance frequency, which is mainly determined by a capacitance and an inductance, changes. By reading this frequency shift and the amplitude change of the transmitted signal, the output signal of the touch sensor can be read wirelessly (Figure 7a). The resonant frequency of this setup is ~42 MHz.

Figure 7b shows a real-time measurement of temperature and touch wirelessly at ~42 MHz and a 3 V input signal. The results indicate that the output of the touch sensor can be transmitted through the wireless coils. In addition, by integrating with temperature sensor as a health-monitoring sensor, two results are obtained simultaneously. However, the distance that the signal can be transmitted is relatively short (Figure 7c). The output signal is attenuated at the rate of 1.2 mV/mm (~3.3 %/mm). Although several items need to be developed and improved (e.g., integration of circuits and transmitted distance), this demonstration shows the potential as a future flexible and wearable wireless system.

It should be noted that several advanced approaches to develop wireless devices on flexible substrates have been reported previously (e.g., a sensor tag [25], a wireless integrated liquid sensor and circuit [15], and a power transmission [35]). By combining these techniques and developing further integration techniques, a flexible wireless system should be realized in the near future.

4.6 Drug Delivery

Another potential function of a wearable device is a curing system. Many people feel that taking a medicine, especially multiple times per a day, is inconvenient. A previous study has shown that patient compliance decreases as the dosage frequency increases [37,38]. If an automatic drug delivery can be realized, it may be able to realize a convenient, comfortable, and healthy human life. For a wearable device, the curing function, especially drug delivery device, should be noninvasive due to medical ethical issues and to support a secure life. For noninvasive drug delivery, a diffusion type of drug through the skin may be required. Probably, one of the most interesting developments of a diffusive type drug is insulin for a diabetic patient who usually takes the drug by him/herself using a penetrating type syringe. Realization of this device should dramatically decrease the patient load as well as infection risk from a needle. Of course, this device is controversial because it is for a medical application.

Some recent examples of such a system include a flexible and wearable thermally enhanced diffusive drug delivery system [39] and a mechanical pump delivery system. Figure 8 shows an example of a drug delivery pump that can

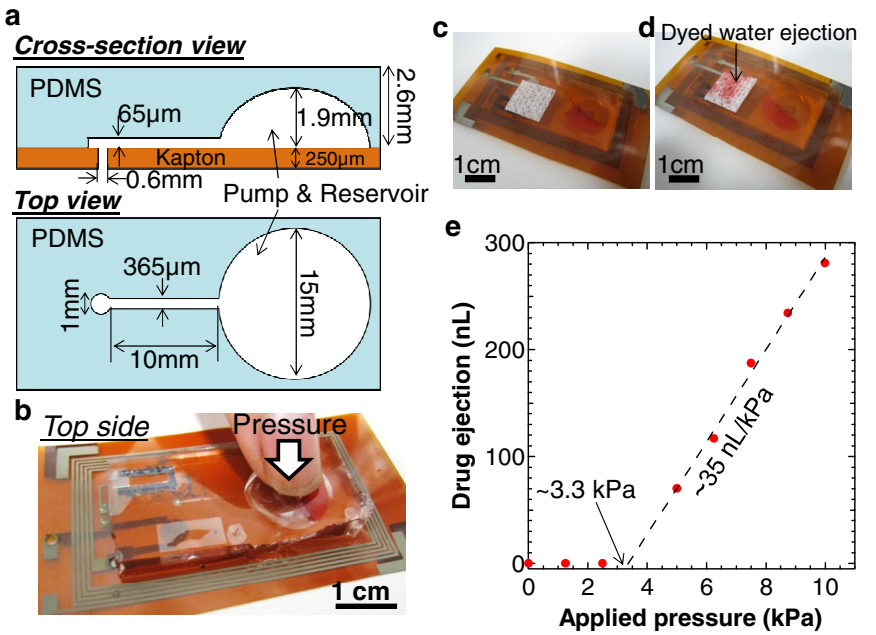

Fig. 8 (a) Cross-section and top view schematics of a drug delivery pump. (b) Photo of a fabricated smart bandage with a drug delivery pump. Photos of (c) before and (d) after dyed water ejection by pushing the drug delivery pump. (e) Drug ejection as a function of applied pressure onto the drug delivery pump. Reproduced with permission [16]. Copyright 2014, John Wiley and Sons.

eject a drug by manually pushing the pump [16]. To eject a drug at a low applied pressure, the pump is fabricated from an elastomer polymer of polydimethylsiloxane (PDMS), which has a low Young modulus (~700 kPa). The structure is deformed by applying pressure to push out the drug from the reservoir chamber (Figures 8a–d). This PDMS structure is easily fabricated using a soft lithography technique. With the structural dimension and material shown in Figure 8a, the drug ejection rate and threshold applied pressure are ~35 nL/kPa and ~3.3 kPa, respectively (Figure 8e). This threshold pressure of ~3.3 kPa is like a gentle human touch; hence, anyone (even a child) can operate this pump. This particular pump does not have a function to control the amount of drug ejection, which is crucial for a curing function as a drug delivery system. A sub-chamber to control the amount or another concept must be integrated for practical applications by learning from the lab-on-chip device fabrication technology. This should be addressed in the next step of wearable health-monitoring devices.

4.7 Other Functional Devices

Above some potential devices for flexible and wearable devices are introduced. However, additional sensors and actuators for the health-monitoring devices should be added as long as the added functions are useful to monitor the human condition. Examples include cuff-less blood pressure monitoring [40,41,42], noninvasive glucose sensors [43,44], electrophysiological signal sensors [45,46], and signal processing circuits [47,48]. To realize these sensors and circuits, many researchers and engineers have devoted much effort. Since health-monitoring devices are often for a specific condition, flexibility of device integration without increasing the device cost is an important factor. Future developments toward flexible and wearable healthcare devices may include using new fabrication methods (e.g., other printing methods) and employing low-cost materials unlike conventional high-performance electronics. It may also be necessary to create separate layers where some are disposable (low-cost layer) and others are reusable (expensive layer) to reduce the total cost of the system. Because at least one layer must come in direct contact with the skin, this layer should be a sanitary clean environment. The best way is to replace the layer often (i.e., a disposable layer should be in contact with the skin).

5 Flexible and Wearable Device Demonstration

As a proof-of-concept of a wearable flexible device, real-time skin temperature monitoring has been demonstrated by attaching a flexible temperature sensor onto a human arm with medical tape to realize a stable and good contact between the sensor and skin. Figure 9 shows the skin temperature while eating spicy soup and short-duration exercise [16]. The average temperature of the skin while resting is ~29 – 31 °C. The skin temperature while eating the spicy soup increases up to ~33 °C likely due to the release of heat to control body temperature. On the other hand, the temperature change while exercising is small compared to eating soup. This is most likely because the exercise period (~12 min) was too short to increase the skin temperature. Additional studies are necessary.

To realize a practical flexible health-monitoring system, many issues must be addressed (e.g., signal processing, more functionality for health monitoring, and a power supply that does not sacrifice mechanical flexibility). Additionally, the reliability of the measured results is another issue for medical applications. For flexible devices, it might be better to start with a health-monitoring “toy” for daily use without a relationship with medical diagnostic results.

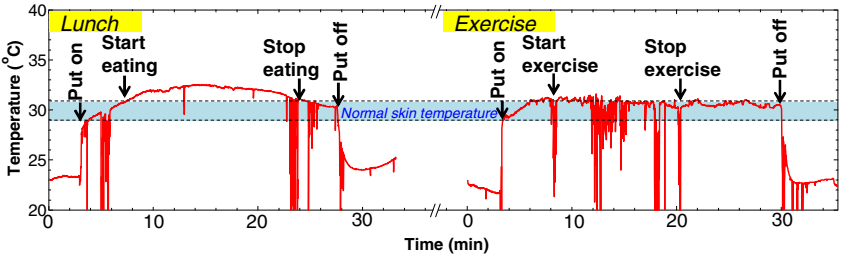

Fig. 9 Real-time human skin temperature monitoring while eating spicy soup and exercising by attaching the smart bandage on a wrist. Reproduced with permission [16]. Copyright 2014, John Wiley and Sons.

6 Conclusion

This chapter introduces several approaches toward flexible health-monitoring devices on the basis of flexible sensor components reported previously with a focus on the economical fabrication techniques using a printing method to realize multi-functional sensors on a flexible substrate. Flexible and wearable health-monitoring systems should be macroscale like a bandage and economically available. By developing printing methods to fabricate sensor components, the device cost should be reduced dramatically, increasing commercial viability in the future. For practical, flexible, and wearable health-monitoring devices, a lot of developments and improvements such as refining the sensing functionalities, power supply and consumption, signal processing circuits including a wireless system, and device costs must be addressed. These topics should be one of the top priorities to develop not only health-monitoring applications but also for other flexible device applications.

Acknowledgements. The author acknowledges financial support from Osaka Prefecture University.

References

[1] Ashida, T., Sugiyama, T., Okuno, S., Ebihara, A., Fujii, J.: Relationship between home blood pressure measurement and medication compliance and name recognition of antihypertensive drugs. Hypertens. Res. 23, 21–24 (2000)
[2] Edmonds, D., Foerster, E., Groth, H., Greminger, P., Siegenthaler, W., Vetter, W.: Does self-measurement of blood pressure improve patient compliance in hypertension? J. Hypertens. Suppl. 3, S31–S34 (1985)
[3] Bobrie, G., Postel-Vinay, N., Delonca, J., Corvol, P.: Self-measurement and self-titration in hypertension. Am. J. Hypertens. 20, 1314–1320 (2007)
[4] Easterlin, R.A.: Explaining happiness. Proc. Natl. Acad. Sci. USA 100, 11176–11183 (2003)

[5] Takei, K., Honda, W., Harada, S., Arie, T., Akita, S.: Toward flexible and wearable human-interactive health monitoring devices. Adv. Healthcare Mater. 4, 487–500 (2015)
[6] Kim, D.-H., Lu, N., Ghaffari, R., Kim, Y.-S., Lee, S.P., Xu, L., Wu, J., Kim, R.-H., Song, J., Liu, Z., Viventi, J., Graff, B., Elolampi, B., Mansour, M., Slepian, M.J., Hwang, S., Moss, J.D., Won, S.-M., Huang, Y., Litt, B., Rogers, J.A.: Materials for multifunctional ballon catheters with capabilities in cardiac electrophysiological mapping and ablation therapy. Nat. Mater. 10, 316–323 (2011)
[7] Hu, L., Choi, J.W., Yang, Y., Jeong, S., Mantia, F.L., Cui, L.-F., Cui, Y.: Highly conductive paper for energy-storage devices. Proc. Natl. Acad. Sci. USA 106, 21490–21494 (2009)
[8] Takei, K., Takahashi, T., Ho, J.C., Ko, H., Gillies, A.G., Leu, P.W., Fearing, R.S., Javey, A.: Nanowire active matrix circuitry for low-voltage macro-scale artificial skin. Nat. Mater. 9, 821–826 (2010)
[9] Liao, Y.-T., Yao, H., Lingley, A., Parviz, B., Otis, B.P.: A 3-μW CMOS glucose sensor for wireless contact-lens tear glucose monitoring. IEEE J. Solid-State Circuits 47, 335–344 (2012)
[10] Webb, R.C., Bonifas, A.P., Behnaz, A., Zhang, Y., Yu, K.J., Cheng, H., Shi, M., Bian, Z., Liu, Z., Kim, Y.-S., Yeo, W.-H., Park, J.S., Song, J., Li, Y., Huang, Y., Gorbach, A.M., Rogers, J.A.: Ultrathin conformal devices for precise and continuous thermal characterization of human skin. Nat. Mater. 12, 938–944 (2013)
[11] Liang, J., Niu, X., Yu, Z., Pei, Q.: Elastomeric polymer light-emitting devices and displays. Nat. Photon. 7, 817–824 (2013)
[12] Wang, C., Hwang, D., Yu, Z., Takei, K., Park, J., Chen, T., Ma, B., Javey, A.: User-interactive electronic-skin for instantaneous pressure visualization. Nat. Mater. 12, 899–904 (2013)
[13] Kaltenbrunner, M., Sekitani, T., Reeder, J., Yokota, T., Kuribara, K., Tokuhara, T., Drack, M., Schwodiauer, R., Graz, I., Bauer-Gogonea, S., Bauer, S., Someya, T.: An ultra-lightweight design for imperceptible plastic electronics. Nature 499, 458–463 (2013)
[14] Takei, K., Yu, Z., Zheng, M., Ota, H., Takahashi, T., Javey, A.: Highly sensitive electronic whiskers based on patterned carbon nanotube and silver nanoparticle composite films. Proc. Natl. Acad. Sci. USA 111, 1703–1707 (2014)
[15] Fuketa, H., Yoshioka, K., Yokoto, T., Yukita, W., Koizumi, M., Sekino, M., Sekitani, T., Takamiya, M., Someya, T., Sakurai, T.: Organic-transistor-based 2kV ESD-tolerant flexible wet sensor sheet for biomedical applications with wireless power and data transmission using 13.56MHz magnetic resonance. In: Proc. 2014 IEEE Int. Solid-State Circuits Conf., pp. 490–492 (2014)
[16] Honda, W., Harada, S., Arie, T., Akita, S., Takei, K.: Wearable human-interactive health-monitoring wireless devices fabricated by macroscale printing techniques. Adv. Funct. Mater. 24, 3299–3304 (2014)
[17] Wang, Y., Wang, L., Yang, T., Li, X., Zang, X., Zhu, M., Wang, K., Wu, D., Zhu, H.: Wearable and highly sensitive graphene strain sensors for human motion monitoring. Adv. Funct. Mater. 24, 4666–4670 (2014)
[18] Jung, S., Kim, J.H., Kim, J., Choi, S., Lee, J., Park, I., Hyeon, T., Kim, D.-H.: Reverse-micelle-induced porous pressure-sensitive rubber for wearable human-machine interfaces. Adv. Mater. 26, 4825–4830 (2014)

[19] Harada, S., Honda, W., Arie, T., Akita, S., Takei, K.: Fully printed, highly sensitive multi-functional artificial electronic whisker arrays integrated with strain and temperature sensors. ACS Nano 8, 3921–3927 (2014)
[20] Rogers, J.A., Lagally, M.G., Nuzzo, R.G.: Synthesis, assembly and applications of semiconductor nanomembranes. Nature 477, 45–53 (2011)
[21] Honda, W., Harada, S., Arie, T., Akita, S., Takei, K.: Flexible electronics: Wearable, human-interactive, health-monitoring, wireless devices fabricated by macroscale printing techniques. Adv. Funct. Mater. 24, 3298 (2014)
[22] Lau, P.H., Takei, K., Wang, C., Ju, Y., Kim, J., Yu, Z., Takahashi, T., Cho, G., Javey, A.: Fully printed, high performance carbon nanotube thin-film transistors on flexible substrates. Nano Lett. 13, 3864–3869 (2013)
[23] Liu, X., Gu, L., Zhang, Q., Wu, J., Long, Y., Fan, Z.: All-printable band-edge modulated ZnO nanowire photodetectors with ultra-high detectivity. Nat. Commun. 5, 4007 (2014)
[24] Honda, W., Arie, T., Akita, S., Takei, K.: Printable and foldable electrodes based on a carbon nanotube-polymer composition. Physical Status Solidi A 11, 2631–2634 (2014)
[25] Jung, Y., Park, H., Park, J.-A., Noh, J., Choi, Y., Jung, M., Jung, K., Pyo, M., Chen, K., Javey, A., Cho, G.: Fully printed flexible and disposable wireless cyclic voltammetry tag. Sci. Rep. 5, 8105 (2015)
[26] Lu, Z., Layani, M., Zhao, X., Tan, L.P., Sun, T., Fan, S., Yan, Q., Magdassi, S., Hng, H.H.: Fabrication of flexible thermoelectric thin film devices by inkjet printing. Small 10, 3551–3554 (2014)
[27] Gupta, R., Walia, S., Hosel, M., Jensen, J., Angmo, D., Krebs, F.C., Kulkarni, G.U.: Solution processed large area fabrication of Ag patterns as electrodes for flexible heaters, electrochromics and organic solar cells. J. Mater. Chem. A 2, 10930–10937 (2014)
[28] Hosel, M., Krebs, F.C.: Large-scale roll-to-roll photonic sintering of flexo printed silver nanoparticle electrodes. J. Mater. Chem. 22, 15683–15688 (2012)
[29] Harada, S., Kanao, K., Yamamoto, Y., Arie, T., Akita, S., Takei, K.: Fully printed flexible fingerprint-like three-axis tactile and slip force and temperature sensors for artificial skin. ACS Nano 8, 12851–12857 (2014)
[30] Chamberlain, D.P., Chir, B., Chamberlain, B.D.: Changes in the skin temperature of the trunk and their relation ship to sympathetic blockade during spinal anesthesia. Anesthesiology 65, 139–143 (1986)
[31] Gao, L., Zhang, Y., Malyarchuk, V., Jia, L., Jang, K.-I., Webb, R.C., Fu, H., Shi, Y., Zhou, G., Shi, L., Shah, D., Huang, X., Xu, B., Yu, C., Huang, Y., Rogers, J.A.: Epidermal photonic devices for quantitative imaging of temperature and thermal transport characteristics of the skin. Nat. Commun. 5, 4938 (2014)
[32] Lochner, C.M., Khan, Y., Piere, A., Arias, A.C.: All-organic optoelectronic sensor for pulse oximetry. Nat. Commun. 5, 5745 (2014)
[33] Dagdeviren, C., Su, Y., Joe, P., Yona, R., Liu, Y., Kim, Y.-S., Huang, Y., Damadoran, A.R., Xia, J., Martin, L.W., Huang, Y., Rogers, J.A.: Conformable amplified lead zirconate titanate sensors with enhanced piezoelectric response for cutaneous pressure monitoring. Nat. Commun. 5, 4496 (2014)
[34] Schwartz, G., Tee, B.C.-K., Mei, J., Appleton, A.L., Kim, D.H., Wang, H., Bao, Z.: Flexible polymer transistors with high pressure sensitivity for application in electronic skin and health monitoring. Nat. Commun. 2013, 4 (1859)

[35] Sekitani, T., Takamiya, M., Noguchi, Y., Nakano, S., Kato, Y., Sakurai, T., Someya, T.: A large-area wireless power-transmission sheet using printed organic transistors and plastic MEMS switches. Nat. Mater. 6, 413–417 (2007)
[36] Kim, D.-H., Lu, N., Ma, R., Kim, Y.-S., Kim, R.-H., Wang, S., Wu, J., Won, S.M., Tao, H., Islam, A., Yu, K.J., Kim, T.-I., Chowdhury, R., Ying, M., Xu, L., Li, M., Chung, H.-J., Kuen, H., McCormick, M., Liu, P., Zhang, Y.-W., Omenetto, F.G., Huang, Y., Coleman, T., Rogers, J.A.: Epidermal electronics. Science 333, 838–843 (2011)
[37] Paes, A.H., Bakker, A., Soe-Agnie, C.J.: Impact of dosage frequency on patient compliance. Diabetes Care 20, 1512–1517 (1997)
[38] Eisen, S.A., Miller, D.K., Woodward, R.S., Spitznagel, E., Przybeck, T.R.: The effect of prescribed daily dose frequency on patient medication compliance. Arch. Intern. Med. 150, 1881–1884 (1990)
[39] Son, D., Lee, J., Qiao, S., Ghaffari, R., Kim, J., Lee, J.E., Song, C., Kim, S.J., Lee, D.J., Jun, S.W., Yang, S., Park, M., Shin, J., Do, K., Lee, M., Kang, K., Hwang, C.S., Lu, N., Hyeon, T., Kim, D.-H.: Multifunctional wearable devices for diagnosis and therapy of movement disorders. Nat. Nanotech. 9, 397–404 (2014)
[40] Lee, S.-S., Nam, D.-H., Hong, Y.-S., Lee, W.-B., Son, I.-H., Kim, K.-H., Choi, J.-G.: Measurement of blood pressure using an arterial pulsimeter equipped with a hall device. Sensors 11, 1784–1793 (2011)
[41] Espina, J., Falck, T., Muehlsteff, J., Yilin, J., Adan, M.A., Aubert, X.: Wearable body sensor network towards continuous cuff-less blood pressure monitoring. In: Proc. Medical Devices and Biosensors, pp. 28–32 (2008)
[42] Islam, M.M., Rafi, F.H.M., Mitul, A.F., Ahmad, M., Rashid, M.A., Bin Abd Malek, M.F.: Development of a noninvasive continuous blood pressure measurement and monitoring system. In: IEEE Int. Conf. Informatics, Electronic & Vision, p. 1085 (2012)
[43] Tamada, J.A., Garg, S., Jovanovic, L., Pitzer, K.R., Fermi, S., Potts, R.O.: Noninvasive glucose monitoring. JAMA 282, 1839–1844 (1999)
[44] Tierney, M.J., Kim, H.L., Burns, M.D., Tamada, J.A., Potts, R.O.: Electroanalysis of glucose in transcutaneously extracted samples. Electroanalysis 12, 666–671 (2000)
[45] Jeong, J.-W., Kim, M.K., Cheng, H., Yeo, W.-H., Huang, X., Liu, Y., Zhang, Y., Huang, Y., Rogers, J.A.: Capactive epidermal electronics for electrically safe, long-term, electrophysiological measurements. Adv. Healthcare Mater. 3, 642–648 (2014)
[46] Myers, A.C., Huang, H., Zhu, Y.: Wearable silver nanowire dry electrodes for electrophysiological sensing. RSC Advances 5, 11627–11632 (2015)
[47] Cao, Q., Kim, H.-S., Pimparkar, N., Kulkarni, J.P., Wang, C., Shim, M., Roy, K., Alam, M.A., Rogers, J.A.: Medium-scale carbon nanotube thin-film integrated circuits on flexible plastic substrates. Nature 454, 495–500 (2008)
[48] Pantelopoulos, A., Bourbakis, N.G.: A survey on wearable sensor-based systems for health monitoring and prognosis. IEEE Trans. Sys., Man Cybern.-Part C: Appl. Rev. 40, 1–12 (2010)

Temperature Sensitive Fabric for Monitoring Dermal Temperature Variations

Nathaniel J. Blasdel and Chelsea N. Monty

The University of Akron, Akron, Ohio 44325-3906, USA

Abstract. Electronic fabrics and smart textiles are advancing biomedical research for use in a variety of ambulatory, diagnostic, and therapeutic devices. New materials and technologies are making it possible to continuously monitor important parameters for health and wellness applications. This chapter will discuss a resistive, fabric-based temperature sensor that can determine temperature between 25ºC and 45ºC by monitoring variations in the material's electrical resistance. The measured resistance of the material decreases with increasing temperature, indicating that this fabric sensor has a negative temperature coefficient of resistance, or α and sometimes called the TCR, which is approximately -0.228 ± 0.03%/ºC averaged over three separate sensors. These results indicate that this material's electronic conductivity behaves analogous to semiconductor materials and would classify this device as a thermistor.

1 Introduction

Biomedical monitoring through nanostructured fabric materials is becoming important for the diagnosis, prevention, and maintenance of a variety of human conditions and diseases. In general, biomedical monitoring encompasses the measurement of a range of physiological and biological properties of the human body to diagnose diseases, prevent worsening conditions, and perform daily health maintenance. Biomedical monitoring is performed both by medical professionals and patients, depending on the complexity of the procedure and the effective availability of methods and devices. Medical monitoring technologies are becoming more available to patients due to lower costs of manufacturing, patient education, and the emergence of newer materials and technologies.

Electronic fabrics or smart textiles are finding use in biomedical research for a variety of ambulatory, diagnostic, and therapeutic devices[1–5]. These technologies seek to fulfill important medical needs for their users, while maintaining comfort and efficiency. For example, A.H. Reynolds at MIT developed a therapeutic sweater for treating the painful symptoms of rheumatoid and other arthritic diseases[2]. This device heats a specified area using three small button sized batteries and a conductive woven fabric. This conductive fabric gently heats when a small current is applied and shows potential for use in other heat treatment therapies or situations of extreme cold to warm the body.

S.C. Mukhopadhyay (ed.), *Wearable Electronics Sensors*,
Smart Sensors, Measurement and Instrumentation 15, DOI: 10.1007/978-3-319-18191-2_8

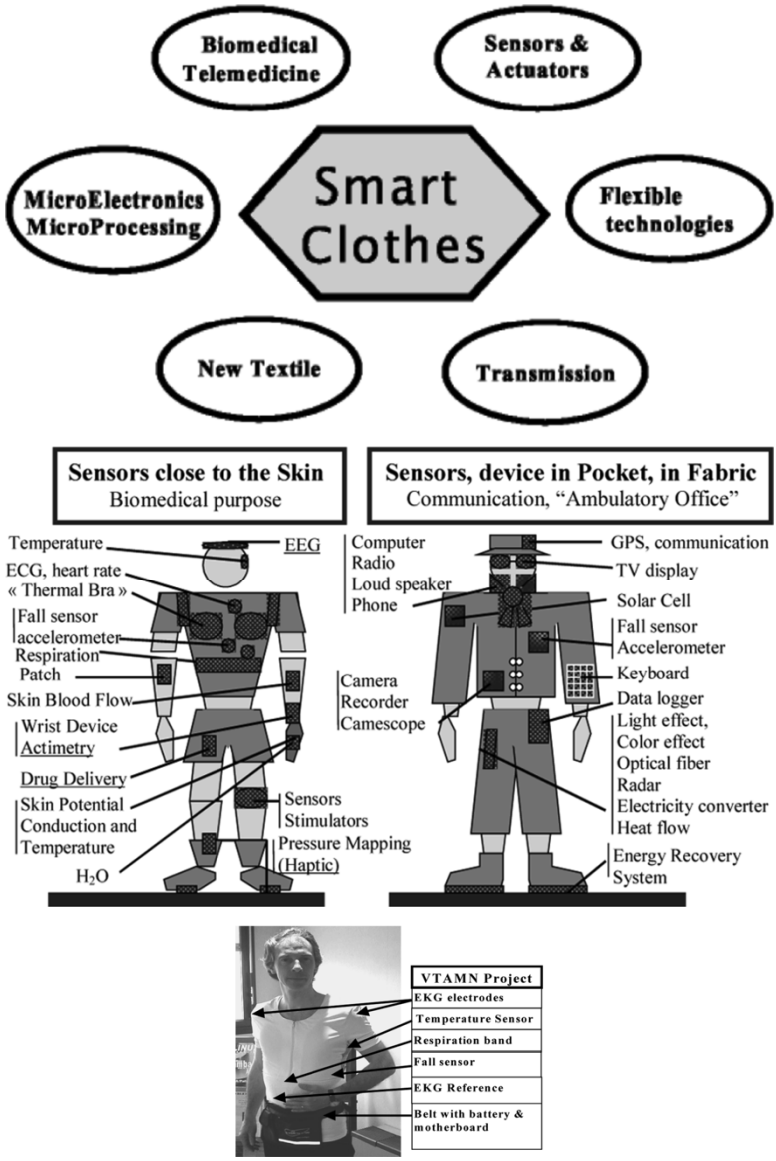

Fig. 1 General overview of smart textiles for biomedical monitoring applications including a conceptual description as well as an actual smart clothing example, i.e. the VTAMN Project, which is a shirt designed to wirelessly monitor important physiological parameters such as heart rate, temperature, respiration rate, and whether or not the person has fallen, which is intended for Alzheimer's patients. *Reprinted with permission from IEEE Transactions*[1].

Additional work evaluated the viability of a noninvasive electrocardiographic shirt[5]. When this shirt is worn, a special textile electrode monitors the user's heart rate and a GPS unit and accelerometer record the user's relative positioning. The device wirelessly communicates the recorded information to a computer and software package, which illustrates the data as the user's active condition. This device is important to patients dealing with cardiac diseases as it allows the patient ease of access to vital information about their daily cardiac rhythms in a comfortable way. These technological advances are just two practical examples of the importance of electronic fabrics in our lives.

Temperature detection close to the skin in load bearing or constricted applications is one example of biomedical monitoring that could be performed using a temperature sensitive electronic fabric. For example, diabetic patients could monitor the temperature difference between their right and left feet to determine if they are at risk for ulceration [6–10]. Amputees could also benefit from monitoring the temperature and humidity inside their prosthetic sockets to maintain a comfortable and hygienic stump-socket environment [11–14]. A temperature sensor used in load bearing or constricted applications would have to be thin and durable, reducing the potential for pressure points against the body. However, the majority of accurate temperature detectors are made from rigid materials. One solution to this problem is to design a thin, flexible thermal sensor that could be worn close to the skin in load bearing situations.

The following chapter will include an overview of nanomaterials for biomedical sensor applications, resistive temperature detection in metals and semiconductors, and a discussion on relevant state-of-the-art for carbon nanotube (CNT) temperature sensors. Specific focus will be placed on the design and development of a fabric-based, functionalized nanomaterial that can resistively determine temperature between 25ºC and 45ºC for its practical use in biomedical monitoring technologies. A schematic representation of the fabric temperature sensor described in this chapter is shown in Figure 2. This sensor is constructed using randomly oriented nylon 6, nanofiber mats that are surface functionalized with multiwalled CNTs. Finally, the sensor materials are coated with an oxidant, and polymerized with conductive polypyrrole (PPy). Sensor material conductivity can be tailored from $1x10^{-7}$ to $1x10^{-3}$ S/cm by varying the amount of multiwalled carbon nanotubes (MWCNTs) on the substrate surface. The measured resistance of the material decreases with increasing temperature, indicating that this fabric sensor has a negative TCR (-0.228 ± 0.03%). The sensor sensitivity, or dR/dT, was consistent for a single sensor over 100 cycles between 25ºC and 45ºC. The initial resistance, or R_0, drifted 300 Ohms over the 100 cycles to stabilize at approximately 6850 Ohms at 25ºC.

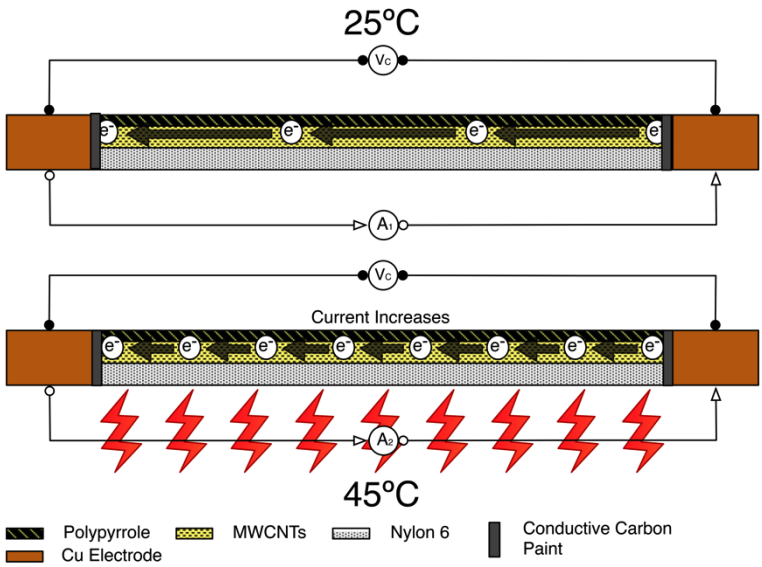

Fig. 2 Schematic representation of the temperature sensor constructed for this work, showing the basic materials of construction. In addition, semiconductor behavior is represented as an increasing electrical conductivity with increasing temperature *Reprinted with permission from IEEE Sensors Journal* [15].

2 Overview of the Electrical Properties of Materials

A material's conductivity, σ, is the reciprocal of its resistivity, ρ, and is a measure of the material's capacity to conduct electrons, or electrical current, I. Conversely, the resistivity is a measure of a material's opposition to current conduction. These intrinsic properties depend upon the material's number of charge carriers, n, the charge on a charge carrier, e' and the electron mobility, μ. Eq. (1) describes the relationship between the intrinsic electrical properties[16, 17]. In general, there are three main electrical classes of materials: conductors, semiconductors, and insulators. Conductor and semiconductor behavior will be discussed in this chapter, leaving the topic of insulators alone.

$$\sigma = \frac{1}{\rho} = ne'\mu \tag{1}$$

Practically, a material's conductivity or resistivity cannot be measured directly. Instead, potential, V, and current, I, are measured. These independent variables are related through a material's resistance, R, which is calculated utilizing Ohm's law in eq. (2).

$$R = \frac{V}{I} \tag{2}$$

Resistance, *R*, is a function of a material's resistivity, cross sectional area (perpendicular to the flow of current), and distance between electrodes as seen in eq. (3) and illustrated in Fig. 3 [16, 17].

$$R = \frac{\rho l}{a} = \frac{l}{\sigma a} \tag{3}$$

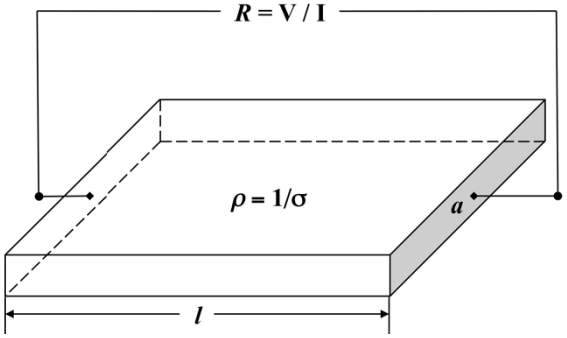

Fig. 3 Schematic illustrating the Resistivity-Resistance relationship

Figure 4 illustrates the affect of interatomic spacing on conductivity for each of the three material classifications. It is seen that metals are inherently conductive, because their valence and conduction energy bands are crossed. In contrast to metals, the conduction and valence bands for semiconductor materials are not crossed. This is due to increased interatomic spacing that results in an energy gap between the valence and conduction bands called the band gap. In general the band gap for materials gets slightly smaller with increasing temperature, is drastically reduced with the introduction of charge carriers, and can act as a switch at the interface of two materials with different band gap energies[16].

Metals generally have high conductivities in the ranges 10^5, 10^6 S/m, with silver having the highest at approximately 6.3×10^7 S/m ($\rho \cong 1.6\times10^{-8}$ Ohm-m) [16, 18]. These high conductivities result from the small interatomic spacing that allows the valence and conduction energy bands to cross. The valence electrons from the *s* and *p* orbitals are therefore completely delocalized and free to move around in the conduction band, resulting in a relatively constant number of charge carriers. This phenomenon, called the electron sea model, is illustrated in Figure 5 [16].

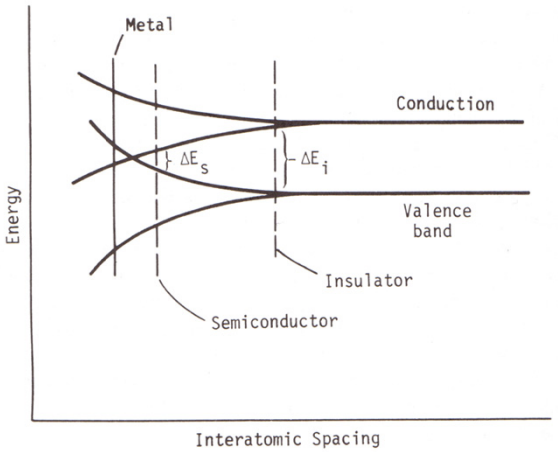

Fig. 4 The interatomic spacing affects the electron orbital energies of materials. For metals, the valence electrons are already in the conduction band due to the close-packed atomic structure. Semiconductor and insulator materials have an energy gap between their valence and conduction bands that requires an energy input, i.e. thermal, electrical, optical, and/or mechanical, for their electrons to pass from the valence band to the conduction band. *Reprinted with permission from John Wiley & Sons, Inc.* [16].

When the temperature of a metal increases, its overall conductivity decreases due to distortions in the metal's crystal lattice, which affect the localized electron mobility. These distortions arise from thermally induced inter-atomic vibrations in the crystal lattice and result in electron scattering, which in turn reduces the overall conduction throughout[16, 17]. This reduction in conduction current, or increase in resistance as it is typically described, is the measureable phenomenon that makes metals useful as resistance temperature detectors or Positive Temperature Coefficient (PTC) materials[19].

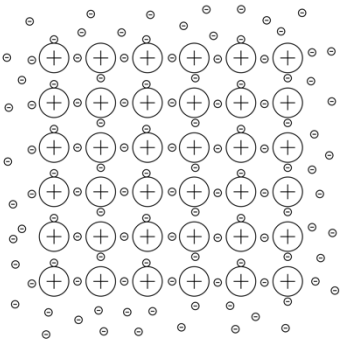

Fig. 5 Generic illustration showing delocalization of electrons surrounding positive nuclei in a metal crystal lattice

In comparison to metals, semiconductor materials have higher resistivities (10^{-3} Ω-cm to 10^{-6} Ω-cm), giving them much greater accuracy for temperature measurement[16]. Until 1955, semiconductor materials were considered as Negative Temperature Coefficient materials, or NTCs; however, a German patent was issued in 1955 for the production of semiconductor materials with a high PTC[19]. Additionally, in 1958 the first U.S. patent was issued for the production of high PTC semiconducting materials[20].

Semiconductor material also differ from metals in that their charge carriers are not solely electrons and n, is approximated by the Boltzmann equation,

$$n = n_0 e^{-\Delta E/kT} \tag{4}$$

where n_0 is the potential number of electrons that could be excited, ΔE is the energy difference between the valence and conduction bands, k is the Boltzmann constant, and T is the absolute temperature[16]. Although, the Boltzmann equation is a sufficient approximation, more sophisticated equations and theories are required in practice[16, 21–24].

At 0 Kelvin, all the electrons in the semiconductor material reside in the valence band. For elemental semiconductors the band gap (ΔE_S in Fig. 4) is approximately equal to kT at 298 K[16]. As temperature increases the electrons gain enough energy to cross the energy gap and start to leave the valence band and enter the conduction band, leaving holes in their place. As the number of charge carriers is dependent on temperature for semiconductors, the conductivity in eq. (5), must be expanded to include a term incorporating the contribution of holes to the overall conductivity,

$$\sigma = e'\left(n_e \mu_e + n_h \mu_h\right) \tag{5}$$

where the subscripts e and h refer to electrons and holes respectively. In elemental semiconductors n_e equals n_h, but for doped, compound, and junction semiconductors n_e rarely equals n_h.

Semiconductor materials are further classified into three different categories: elemental, compound, or junction semiconductors [16]. Elemental semiconductor materials are either intrinsically or extrinsically conductive. Intrinsically conductive materials are pure; while, extrinsically conductive materials are doped with other elements to add conductivity or other electronic functions to the material[16, 21–24]. Elemental semiconductor materials reside in groups IV and VI of the periodic table. Silicon and gallium arsenide are two of the most common, extensively studied semiconductor materials, and are widely used in the electronics industry[24].

Dopants can increase the conductivity of an elemental semiconductor by adding charge carriers to the crystal lattice. These elements are found in groups III and V of the periodic table and are classified as donors or acceptors. When doping silicon (Fig. 6), group III elements like boron and gallium add holes to the crystal

lattice by accepting a fourth electron into their unfilled valence shells. Conversely, group V elements like phosphorous and arsenic have five valence electrons and can contribute an electron for each atom added to the lattice. In both cases new classes of semiconductor materials, p-type and n-type, respectively, result.

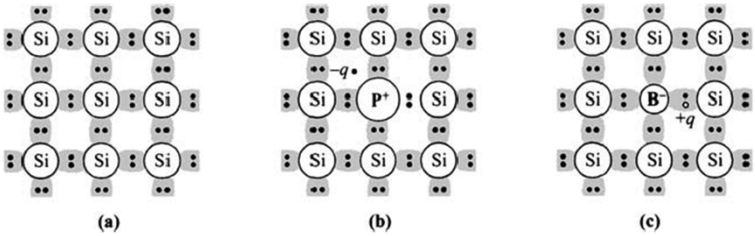

Fig. 6 Basic atomic bonding and doping in semiconductor materials. (a) Intrinsic Si with no impurity; (b) n-type Si with a phosphorous donor atom; (c) p-type Si with a boron acceptor atom. *Reprinted with permission from John Wiley & Sons, Inc.* [24].

In summary, metallic and semiconductor materials are important for resistance temperature detection. Metals and semiconductors have opposite resistance-temperature characteristic relationships, PTC or NTC, which can be ascribed to their different quantum phenomena. These differences stem from the variation in their interatomic spacing, their respective crystal lattices, and the affect of energy from their surroundings on electrons and their movement throughout the bulk material. The following section will describe devices developed using metallic and semiconductor materials for the determination of temperature.

3 Resistance Temperature Detection

Resistance temperature detection is a highly utilized natural material property that makes use of the temperature dependent change in the resistance of metals and semiconductors. Many researchers have studied different materials for their thermal sensing abilities and successfully applied those materials to a wide variety of systems requiring temperature measurement. As previously discussed, there are two main types of materials used as the sensing elements of "resistance thermometers": metallic conductors and semiconductors. Metallic materials make up the classification called Resistance Temperature Detectors, or RTDs, and are most commonly made from platinum, and sometimes palladium, nickel, copper, and other alloys[16]. Semiconductor materials, like semiconducting ceramics and polycrystalline metal oxides, make up the classification called thermistors[19].

Sir Humphrey Davy first studied the electrical resistance of metals as a function of temperature in 1821[16] and the relationship was put to practical use for temperature determination in the mid 19th century by C.W. Siemens[16, 25].

Resistance temperature detection has since become the most widely utilized phenomenon for laboratory and everyday temperature measurement applications [16].

In 1887, Hugh Callendar, greatly improved upon Siemen's methods and equipment designs using experiments to model the relationship between the changing electrical resistance of platinum and air thermometer temperature measurements[16]. The Callendar equation, shown in eq. (6), allowed him to perform quick numerical calculations for accurate temperature measurements, usually only requiring one to two iterations. His groundbreaking work was published in 1887 in the *Philosophical Transactions* of the Royal Society[16].

$$t = \left(\frac{R_t - R_0}{R_{100} - R_0}\right)100 - \delta\left(\frac{t}{100}\right)\left(\frac{t}{100} - 1\right) \tag{6}$$

where t is temperature in degrees Celsius, R is the measured electrical resistance at temperatures, t, 0ºC, and 100ºC, respectively. In addition, Callendar described the deviation from linearity due to differences between the sensing elements, using the empirical correction factor δ[16]. In 1925, Van Dusen expanded on eq. (6) to increase the accuracy of the platinum resistance thermometer in the range from the boiling point of oxygen to the ice point of water (eq. (7)). The Callendar-Van Dusen equation was used for over forty years as the standard equation for IPTS measurements[16].

$$t = \left(\frac{R_t - R_0}{R_{100} - R_0}\right)100 - \delta\left(\frac{t}{100}\right)\left(\frac{t}{100} - 1\right) + \beta\left(\frac{t}{100} - 1\right)\left(\frac{t}{100}\right)^3 \tag{7}$$

The earliest platinum "resistance thermometers" were used to standardize the International Practical Temperature Scale (IPTS), which is the standard list of single point temperatures used to calibrate devices and materials. The IPTS was developed over a period of approximately 60 years by the International Committee of Weights and Measures into the current list of thermodynamic triple-point temperatures to be used for standard device calibrations[16, 25].

Eqs. (6) and (7) are used for accurate determination of temperatures using very pure platinum RTDs. Ultimately the resistance of metals is a complex function of temperature, but above the Debye temperature (θ_D), a metal's resistance-temperature relationship, generally follows a 3rd order polynomial described by eq. (8).

$$R = R_0(1 + AT + BT^2 + CT^3) \tag{8}$$

where R_0 is the initial resistance value of the device in Ohms, A, B, and C are constants associated with the metal and its purity, and T is temperature in ºC[16]. For practical accuracy in most situations, eq. (8) can be rewritten very simply in a first order linear form,

$$R = R_0(1 + \alpha T) \tag{9}$$

The TCR, α, is characteristic of a material's ability to detect temperature resistively, and generally describes the material's percent change in resistance per degree Celsius change in temperature.

$$\alpha = \frac{1}{R}\frac{dR}{dT} \tag{10}$$

It is most usually taken in the material's linear range of temperature-dependent resistance with the highest sensitivity (S)[16], or

$$S = \frac{dR}{dT} \tag{11}$$

Because metallic RTDs generally respond linearly to temperature changes, integrating eq. (9). over the desired temperature range gives the general equation for a RTD's TCR, or

$$\alpha = \int_{R_0@T_0}^{R@T} \frac{1}{R}\frac{dR}{dT} = \frac{1}{R_0}\frac{\Delta R}{\Delta T} = \frac{1}{R_0}\left(\frac{R - R_0}{T - T_0}\right) \tag{12}$$

The resistance of a thermistor as a function of temperature, on the other hand, is generally written as a complex exponential function[16].

$$R = R_0 e^{\beta\left(\frac{1}{T} - \frac{1}{T_0}\right)} \tag{13}$$

where β is a constant for the device in units of Kelvin or degree Celsius and R_0 is the resistance in Ohms at temperature, T_0. For a thermistor, α is calculated similarly to the RTD. By taking the integral of eq. (13), and rearranging, the TCR becomes[16],

$$\alpha = -\frac{\beta}{T^2 - T_0^2} \tag{14}$$

RTDs generally have larger linear ranges than that of thermistors, which make them easier to calibrate and more practical for some situations. However, because many thermistors are more accurate and can generally withstand higher temperatures than traditional RTDs, they are highly attractive for certain applications. The main drawback of thermistors is that their resistance-temperature relationships are complex with non-linear temperature ranges. For these reasons, many materials that display linear resistance-temperature relationships in defined temperature ranges are chosen to construct the sensing elements necessary for defined applications.

RTDs and thermistors are typically constructed using rigid materials. They require protection from environmental factors that could lead to oxidation or material deformation, so that the sensing elements are not damaged. These devices work well in many different applications requiring temperature measurement, but can be problematic when trying to integrate them into biomedical technologies where a soft sensor may be better suited. Due to the rigidity of common RTD and thermistor materials, there are geometric constraints when attempting to make flexible temperature detectors for use in smart textiles for close to the skin applications. As they are easily damaged and rendered useless when any kind of plastic deformation, such as bending, stretching, or even breaking, occurs[16], these constraints make them unsuitable for load bearing situations where flexibility and durability are required.

4 Functional Nanostructured Materials For Temperature Detection

Functionalized nanomaterials have been extensively studied over the past two decades, due to the property enhancement that occurs at the molecular level through the addition of various bulk fillers and fibers to polymer melts or solutions in composite materials[26]. Molecular interactions between the polymer and particle are enhanced due to the small size of the particle and its ability to intermingle with the polymer chains. Functionalized polymer materials are important because many pure polymers lack the desired properties to function as sensors. Functionalized nanomaterials, on the other hand, have shown interesting shifts in mechanical, electrical/electronic, barrier, membrane and thermal properties over that of their pure bulk polymeric materials, including flammability resistance and polymer blend compatibilization[27].

Polymers and CNTs have been studied together extensively based on the interesting electrical[28–32], mechanical[33, 34], and thermal[26, 27, 35] behavior of CNTs themselves. Xiong et al., for example, found that just 2 weight percent CNTs added to polyurethane increases the thermal stability and enhances the mechanical properties over pristine polyurethane[35]. Bouhofer and Kovacs provide an extensive overview of the literature pertaining to the enhancement of electrical and electronic properties of many different polymers using CNTs[36]. It was determined that the electrical percolation in these nanocomposites related to dispersion types, properties, and methods, percolation thresholds and maximum composite conductivities, nanotube entanglement, nanotube aspect ratios, and theoretical and experimental comparisons[28]. Additionally, Han and Fina reviewed the thermal properties of CNT polymer nanomaterials and determined that these carbon allotropes are one of the most promising polymer additives for enhancing the thermal properties of polymer products[27].

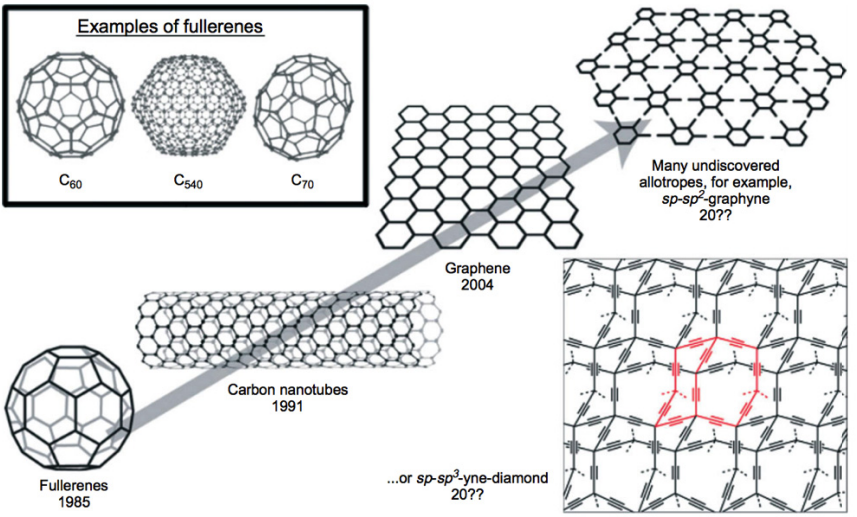

Fig. 7 Timeline of the discovery and development of structures of nanostructured carbon allotropes. *Reprinted with permission from John Wiley & Sons, Inc.*[37]

Since the discovery of Buckminsterfullerene (C60) in 1985 by Kroto et al., research on carbon nanomaterials has increased significantly. This discovery shed light into carbon nanostructures, which gave way to the discoveries of CNTs in 1991, and graphene in 2004. These discoveries gave the research community materials with especially interesting electrical properties and sparked new life into functional material research. It is proposed that future research will lead to graphyne and nanodiamond meshes or other potential carbon allotropes[37]. Fig. 7 illustrates the chronology of these efforts.

CNTs have unique semiconducting and metallic conducting properties, high strength, and high electrical breakdown, as well as their nano size and structure. Extensive research on CNTs started in 1993 with groups at NEC in Japan and IBM – Almaden[38, 39]. Since these discoveries, much effort has gone into characterization of CNTs using Raman spectroscopy and scattering,[40, 41] scanning electron microscopy (SEM), transmission electron microscopy (TEM), X-ray diffraction (XRD), thermal-gravimetric analysis (TGA), electrical, and electrochemical methods to better understand the various attractive electrical, thermal, and mechanical properties. CNTs are currently finding great use in application research and development. There is a large potential for CNTs in many different industries including biomedical, food, fishing and agriculture, environmental monitoring, manufacturing, security, and ultimately electronics, both flexible and solid state.[42]

CNTs are found in several different forms, depending on how they are produced and purified, single-walled CNTs (SWCNTs), double-walled CNTs (DWCNTs), and MWCNTs. SWCNTs have the ability to be metallically conducting or semiconducting, based on their tube diameter and the chirality of

the carbon atoms. The conductivity of CNTs increases with decreasing tube diameter, and CNTs have three different chirality's[43–47]. Figure 8 shows the different types of SWCNTs rolled from a single sheet of graphene, where T is the rolling vector and C_h is the chiral vector describing the axial direction down the length of the tube[48]. Armchair and zigzag tubes are metallically conducting and the many different chiral tubes are semiconducting. DWNTs and MWNTs are semiconducting in nature and considerably less expensive to produce than SWCNTs as they have higher yields and less complicated separation techniques[43, 44]. Ultimately, MWCNTs have gained the most attention as they are the cheapest to produce and they are able to provide adequate functionality to the systems in which they are employed.

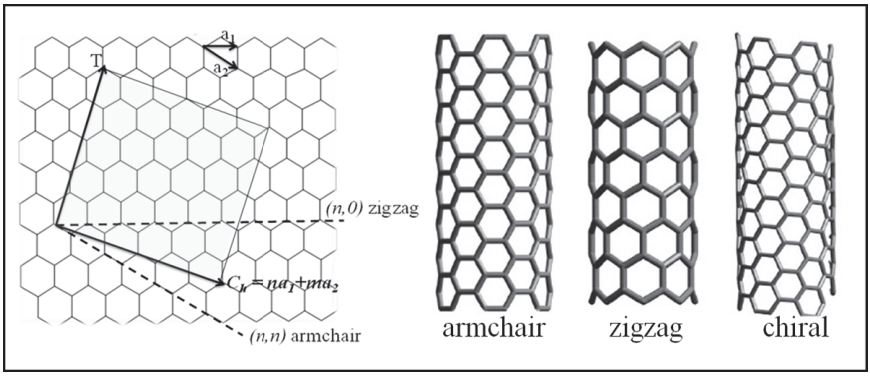

Fig. 8 Different types of SWCNTs rolled from a single graphene sheet to illustrate metallic and semiconducting CNTs. *Reprinted with permission from InTechOpen*[48].

With regards to temperature sensing, CNTs have also been studied for use in thermal sensors[15, 49–63] and were evaluated for their thermal sensing properties. Fung and Li, for example, developed polymer encapsulated CNT thermal sensors. The thermal sensors were made by electrophoretic alignment and then encapsulation in Parylene C. These sensors showed a linear response from about 25ºC to 60ºC and their TCR ranged from -0.15%/ºC to -0.18%/ºC. Many other groups have studied CNTs for their thermal sensing abilities and have found a wide variety of TCRs, which most likely results from differences in the CNTs used and the device structures.

Table 1 shows a brief review of these works. It is seen that carbon nanostructured devices display both NTC and PTC behavior, indicating the metallic and semiconducting electronic conduction mechanisms of these materials. CNTs can display both behaviors, because as previously stated CNTs are either metallically conducting or semiconducting depending on the type of CNT and carbon atom configuration around the tube. The semiconducting CNT temperature sensors varied in TCR from -0.08%/ºC to -2.8%/ºC with a very wide variety of resistance ranges (less than 1 kΩ to almost 1 MΩ) and temperature ranges (most extreme of -123ºC to 177ºC in DiBartolomeo et al., and most generally from the 20's to less than 100ºC

Table 1 Review of CNT thermal sensors and their operating parameters [15, 49–63].

Description	Reported TCR (%/°C)	*~ΔR Range (kOhms)	**ΔT Range (°C)	Reference
MWCNTs dispersed in SEBS, drop cast onto gold electrodes on polyimide	-2.8	3 to 4	20 to 60	Matzeu et al., 2012
MWCNT powder deposited on adhesive elastic polymer between Al foil electrodes	-1.26	11 to 8	20 to 70	Karimov et al., 2012
SWCNTs dielectrophoretically bundled between Cr/Au//parylene C//Cr/Au stacked electrodes, encapsulated in parylene C	-0.57	0.0432 to 0.0295	25 to 65	Selvarasah et al., 2007
MWCNTs dispersed in PVBC_Et_3N and sandwiched between Al plate electrodes	-0.4	95.0 to 92.6	20 to 40	Giuliani et al., 2014
SWCNT network spray deposited between Cr/Au interdigitated electrodes	-0.2954	***8.4516 to 6.4232	0 to 80	Cagatay et al., 2014
MWCNT powder deposited and pressed on glue on paper with silver paste electrodes	-0.24	0.115 to 0.096	20 to 75	Karimov et al., 2011
MWCNT dispersion vacuum filtered over nylon 6 nanofiber membrane with PPy overcoat	-0.204	6.6 to 6.85	25 to 45	Blasdel et al., 2015
MWCNTs dielectrophoretically bundled between Cr/Au electrodes, encapsulated in parylene C	-0.18	97 to 91	25 to 60	Fung and Li, 2004
MWCNTs dispersed in PMMA paste, dried onto yarn fiber, and encapsulated in thin silicon paste	-0.13	320.75 to 317.53	30 to 45	Sibinski et al., 2010
MWCNTs ODEP assisted self assembly between Au electrodes on hydrogenated amorphous silicon on ITO glass	-0.109	840 to 770	26 to 102	Hsu and Lee, 2014
Solvent assisted capillary self-assembly of microbridge made from CCVD grown MWCNTs on TiN electrodes	-0.1	1.43 to 1.22	27 to 147	De Volder et al., 2010
MWCNTs grown by CCVD on Co/Fe-Al_2O_3 from ethylene in helium, dispersed and vacuum filtered over a membrane and removed as variable thickness freestanding films	-0.08	1.15 to 0.94	-123 to 177	Di Bartolomeo et al., 2009
Graphene Nano Platelets (GNPs) drop cast onto silver paste/silicon rubber IDE on polyimide sheet	0.0371	125 to 500	10 to 60	Tian et al., 2014
PECVD CNTs grown on Y:Fe catalyst sol-gel spin coated onto silicon	0.0421	2.5 to 25	20 to 150	Ali and Hafez., 2013
Long SWNT (10's of μm) array grown between Cr/Pt electrodes on silicon by CCVD of EtOH and $FeCl_3$	0.601	1150 to 2500	0 to 100	Yang et al., 2010
Metallic SWNT CMOS compatible between Pt electrodes on SiO_2	0.9	7 to 25	20 to 400	Mohsin et al., 2014

*Most usually read from the graph and not explicitly stated throughout the text

**Most usually explicitly stated in the text, but sometimes taken from the the graph when best suited

***Calculated based on tabulated R_0 values and % changes from the graph

for the other studies). The metallic CNT temperature sensors varied in TCR from 0.0371%/ºC to 0.9%/ºC with resistances ranging from a few kΩ to 1 to 2 MΩ, and temperature ranges anywhere from 0ºC to 400ºC. It should be noted the majority of NTC materials (semiconductors) were constructed using MWCNTs, which are generally semiconducting in nature. All of this research shows the viability of using CNTs as thermal sensing materials.

5 Sensor Construction

Nylon 6 was selected for this work as nylon 6 nanocomposites formed with CNTs have been shown to enhance properties over pristine nylon 6. Lala et al., for example, researched the effect of surface functionalized MWCNTs versus impregnated nanofibers on material properties. They found that the surface functionalized nanofibers had a higher conductivity over the impregnated nanofibers, although the enhancement in mechanical properties was higher for the impregnated nanofibers[64]. Mahmood et al. also showed increased thermal properties for nylon 6 nanocomposites made with multiwalled CNTs, reporting that the thermal degradation temperature of the nanocomposite increased by approximately 70ºC[65]. Nanocomposites formed with nylon 6 and multiwalled CNTs have the additional advantage for use as sensors as CNTs are easily functionalized[66–70].

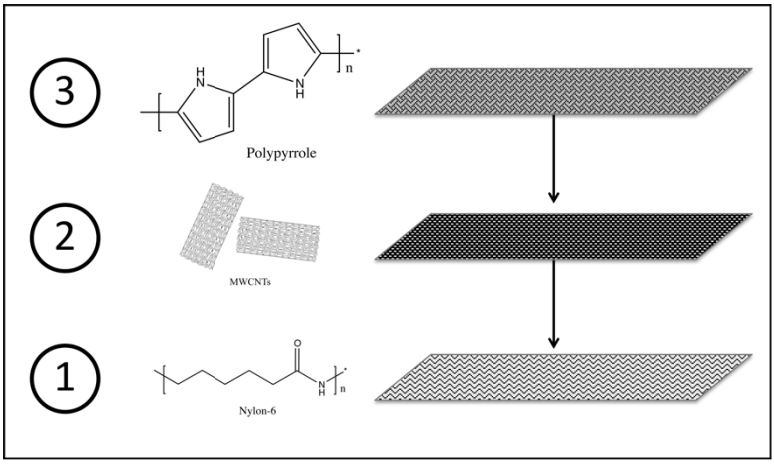

Fig. 9 Schematic illustrating the materials used for construction of the fabric temperature detector

PPy was selected for this work as it is an intrinsically electrically conductive polymer of the heterocyclic compound pyrrole and is easily synthesized directly onto the nylon/MWCNT substrate. Characteristically, PPy is a bluish-black compound and is insoluble without functionalization or the addition of chemical

solubilizers[71–74]. It is electrically conductive due to the conjugated, or alternating double and single, bonds around the carbon atoms in the polymer backbone. The electrical conductivity of PPy is controlled through ion doping and polymerization conditions[75]. For example, PPy has shown metallic behavior when polymerized in lower temperatures, and when polymerized at room temperature or higher it can act as an insulator[75]. PPy has been chemically synthesized using chemical oxidants like $FeCl_3$[76], $K_2S_2O_8$[77], and ozone[78] using chemical vapor deposition using chemical oxidants[79] either in template or non-template synthesis. PPy has crystallinity dependent electrical conductivity and electrons move through the bulk material by the range hopping mechanism[75] and it has relatively low thermal conductivity[80]. PPy has also been functionalized and used for bio and immunosensors[81–85] as well as to detect NO_2[86] and methanol[87]. Mahadeva et al., for example, developed a temperature and humidity sensor using PPy coated cellulose. This sensor is interesting as it illustrates the viability of using PPy for conductive connections for the individual MWCNTs.

All chemicals and materials were used without further purification. Nylon-6 was acquired from Scientific Polymers Inc. (U.S.A.) and had a viscosity-averaged molecular weight of 10,000 grams per mole. MWCNTs were obtained from Nanostructured and Amorphous Materials Inc. (U.S.A.) and had diameters in the range of 10 to 20-nanometers, with lengths in the range of 0.5 to 2-micrometers. Triton X-114 (TX-114) surfactant was purchased directly from Acros Organics (U.S.A). Iron chloride hexahydrate is from Flynn Scientific Inc. (U.S.A.). Pyrrole (≥99%, extra pure), formic acid (98%), and acetic acid (≥99%) were acquired through Sigma Aldrich (U.S.A)[15].

The nylon-6 substrate was electrospun using a homemade cabinet with rotating drum. A World Precision Instruments Inc. (U.S.A.) SP101I syringe pump and a Gamma High Voltage Research (U.S.A.) ES30P-5W voltage source were used. The fibers were spun using a 20% by weight solution of nylon-6 in a 1:1 by weight mixture of formic and acetic acid[88]. The syringe pump flow rate was 9.1-microliters per minute. 25-kilovolts were applied between the needle and collector. The needle to collector distance was 9-centimeters. The collector was a copper sheet encased in a paper towel. It was attached to the rotating drum, which was powered by a variac at a setting of 30-volts to give approximately 7-revolutions per minute. The fiber mats were spun for 4-hours[15]. A schematic representation of the electrospinning process is seen in Fig. 10.

The nylon-6 fiber mat was cut into 47-millimeter diameter disc-shaped membrane style filters. Each one was placed into a Fisherbrand™ membrane vacuum filtration funnel. It was then wet with a small amount of 0.3% TX-114 solution. A 1-gram per liter MWCNT stock solution was made in 0.3% TX-114 and diluted to desired MWCNT concentrations for filtration. TX-114 was used because of the reported enhanced adsorption efficiency of TX-114 for MWCNTs [89]. 250-300 milliliters of this solution were vacuum filtered through the nylon-6 membranes using approximately 17-kilopascals of vacuum. The membranes were

washed with deionized water and acetone and allowed to dry before application of 25-millimolar iron chloride hexahydrate solutions. 1 milliliter of the iron chloride solution was applied to the membrane by pipette to fully cover the membrane in solution and left to dry overnight in a desiccator[15].

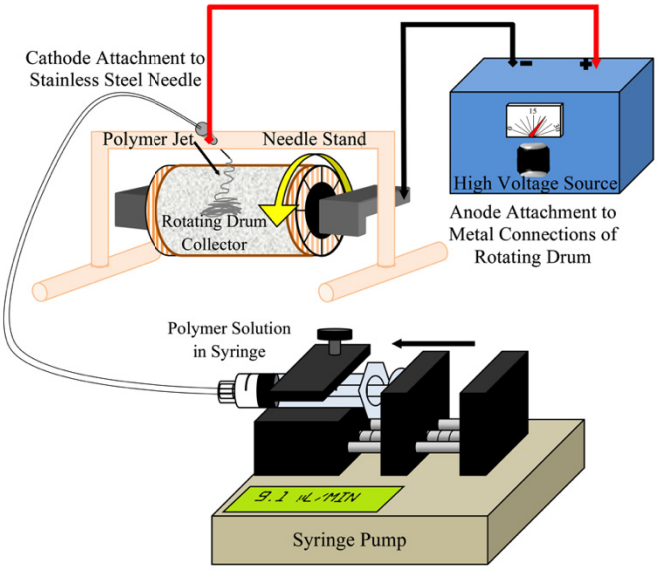

Fig. 10 Schematic illustrating the basic concept of electrospinning used to develop the detector substrate.

The membranes were then placed into plastic weigh boats and placed into the polymerization chamber with 1 to 2-milliliters of pyrrole. 100-kilopascals of vacuum was applied to the chamber to facilitate pyrrole vaporization. The membranes were exposed to pyrrole vapor for 48 hours to complete the polymerization. After polymerization of pyrrole to PPy, the detectors were allowed to sit covered, in air until testing. The material was connected to two copper electrodes using conductive carbon paint. These devices were vacuum-sealed using kitchen grade vacuum sealing bags cut down to the final dimensions of approximately 80 millimeters by 20 millimeters[15].

6 Sensor Material Characterization and Testing

Detector testing and characterization included SEM imaging, TGA, and DC electrical measurements of the polymer nanocomposite in a humidity and temperature-controlled box. SEM imaging was accomplished on a JEOL JSM-7401F (Japan) field emission scanning electron microscope with an accelerating

voltage of 1.5-kilovolts and a 13-millimeter working distance. TGA thermographs were obtained using a TA Instruments Q500 thermogravimetric analyzer with a platinum boat at a ramp rate of 10-ºC per minute up to 600-ºC. DC electrical measurements were obtained on a Solartron 1470E (UK) multichannel potentiostat/galvanostat, by applying a 0.7-volt potential and measuring the current while changing the testing box temperature. The box conditions were controlled using a J-KEM Apollo temperature controller and Omega Engineering HX15 (USA) humidity probe with OM-CP-QUADPROCESS-25MA data logger. The humidity of the box, labeled 2 in Fig. 11, was controlled at 0% RH. The box humidity was measured using the data acquisition system labeled 1 in Fig. 11 in conjunction with the humidity probe inside the box labeled 2 in Fig. 11. Dried air flows through the box at a rate of 400-ccm from the flow meters labeled 4 in Fig. 11 to maintain 0%RH during the tests. The temperature cycles were conducted by the J-KEM temperature controller, labeled 3 in Fig. 11, at 30ºC per hour from 25ºC to 45ºC and back down to 25ºC at 15ºC per hour[15].

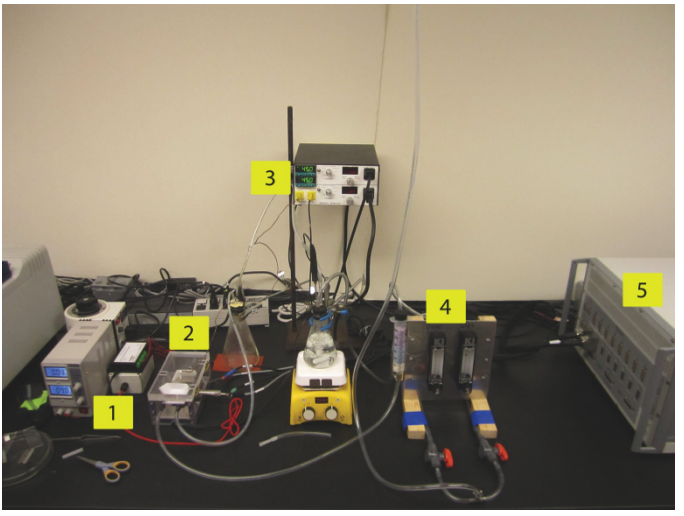

Fig. 11 Temperature/humidity controlled sensor-testing system: 1) Omega Engineering HX15 humidity probe with OM-CP-QUADPROCESS-25MA data logger; 2) Testing box, a 75 Watt silicon heating pad adhered to the aluminum bottom of the polycarbonate box with humidity control air ports; 3) JKEM temperature controller and K-Type thermocouple; 4) Humidity control flow meters; 5) Solartron 1470E multichannel potentiostat/galvanostat. *Reprinted with permission from IEEE Sensors Journal[15].*

7 Preliminary Results

The morphology of the nylon-6/MWCNT/PPy nanocomposite is shown in Fig. 12, as taken by SEM. Fig. 3a shows the bare nylon-6 fibers before functionalization. The nylon-6 fibers range in diameter from 123 to 180-nanometers and the fiber

mat porosity ranges from 0.86 to 0.89. Fig. 12b shows the nylon-6 fibers after functionalization with MWCNTs. Notice many of the nanotubes agglomerate into bundles and lay individually on the nanofibers, creating a disconnected network that leads to high resistances of the matrix before pyrrole polymerization. Fig. 12c shows the PPy coated composite. PPy polymerization integrates the MWCNT network and allows for higher conductivity and responses that are more sensitive to changing temperature[15].

Thermal gravimetric analysis (TGA) was performed on nanocomposite samples prepared using various concentrations of MWCNTs in the filtration solution, as well as on neat nylon samples, to examine the amount of MWCNTs adsorbed on the nylon nanofiber surface. As hypothesized, the nanocomposites prepared at higher MWCNT filtration concentrations show a higher weight percent of carbon, seen in Fig. 13. This figure shows a characteristic value for the neat nylon samples, as well as normalized (neat nylon baseline subtracted out) values of samples prepared under various filtration conditions. The thermograms in Fig. 13 illustrate that the loading of MWCNTs can be varied during the construction process to ultimately tailor the device resistance[15].

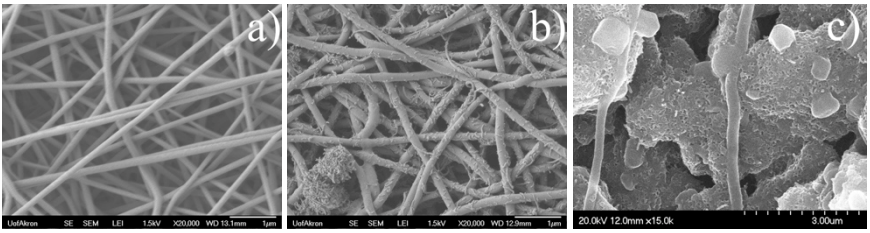

Fig. 12 SEM images showing the nanocomposite sensing material. a) neat nylon-6 nanofibers, b) MWCNT functionalized nylon nanofibers, and c) PPy coated composite material. *Reprinted with permission from IEEE Sensors Journal [15].*

A typical I-V curve for the nanocomposite material is shown in Fig. 14. The linearity of the I-V curve demonstrates that the material acts as an ideal resistor over the experimental range tested and that there should be very little noise in the resistance data. The linearity of these graphs, along with resistance, sensitivity, and stability data were used to choose the optimum material for device construction[15]. The resistance of the functionalized nanomaterial can be tailored (0.9 kΩ to over 20 MΩ) by varying MWCNT loading through the detector construction process. Resistances of devices from the same batch can vary due to inconsistencies in the conductive network, but as long as the oxidant layer is uniform, these inconsistencies were minimal. In this work, the optimum loading was found by determining the alpha values of the fabric sensors with increasing MWCNT loadings. Optimum MWCNT loading was determined to be approximately 6.6 weight percent MWCNTs resulting in α of –0.228 ± 0.03%/ºC. This TCR value was calculated as the average of three fabric sensors[15].

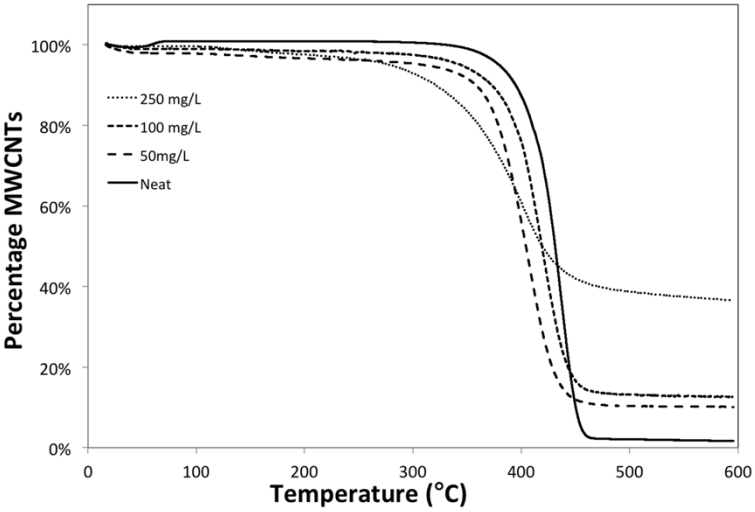

Fig. 13 Example TGA thermogram showing how changing the MWCNT concentration in the filtration solution affects the weight percent of nanotubes on the membrane surface. *Reprinted with permission from IEEE Sensors Journal* [15].

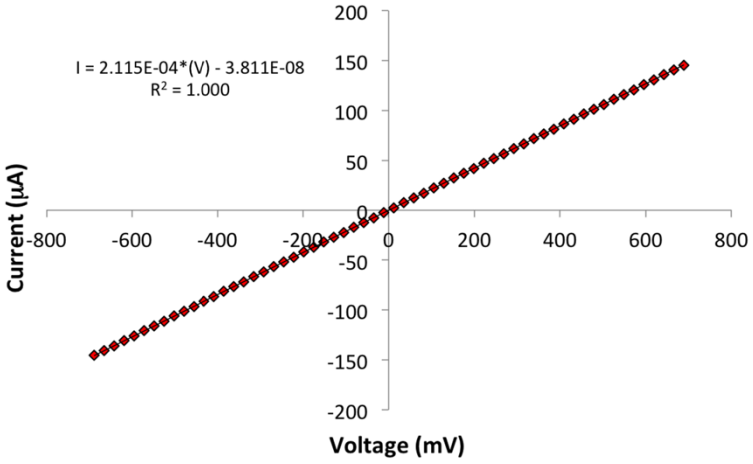

Fig. 14 Linear current-voltage characteristic curve of the sensor material from -0.7V to 0.7V. *Reprinted with permission from IEEE Sensors Journal* [15].

Initial data shows the ability of a nylon-6/MWCNT/PPy nanomaterial to determine changes in temperature. Fig. 6 shows the changing resistance of the fabric temperature detector when the temperature is changed in 4-degree increments, from 25ºC to 45ºC, with three-hour hold times at each temperature.

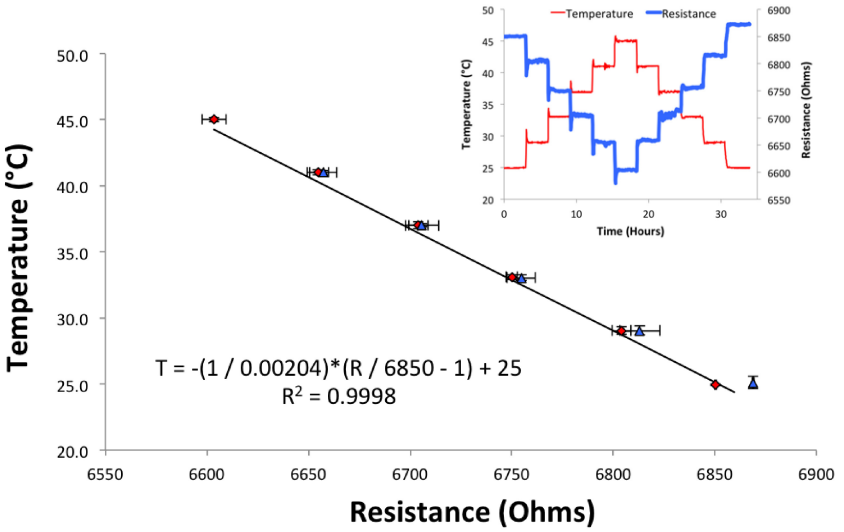

Fig. 15 Graph showing the steady state calibration curve data. Red diamonds indicate the up ramp and the blue triangles indicate the down ramp. Inset graph shows the raw data used to calculate the calibrated data points. *Reprinted with permission from IEEE Sensors Journal* [15].

Detector testing was limited to this range based on temperatures typically seen at the surface of the skin for a variety of conditions [6, 8, 13, 14]. The diamonds denote the up ramp and the triangles denote the down ramp. The detector resistance is sensitive towards temperature changes and a response is seen immediately upon changing temperature (see inset). This graph shows that the resistance-temperature relationship is highly linear over the temperature testing range indicating that the functionalized nanomaterial is a viable thermal sensor candidate[15].

The average of 100 steady state temperature cycles, as shown in Fig. 6, was used to determine TCR value (–0.204 ± 0.008%/C) of the optimized sensor material. This TCR value corresponds to previously reported values for CNTs and CNT devices, which can range from – 2.8 to 0.9%/°C (Table 1) [15, 49–63] Because the relationship between resistance and temperature is linear in the practical temperature range, dR/dT in eq. (10) becomes $\Delta R/\Delta T$. This equation is then rearranged to predict temperature, T, from a measured resistance, R:

$$T = -\frac{1}{\alpha}\left(\frac{R}{R_0} - 1\right) + T_0 \qquad (15),$$

where R_0 and T_0 are the baseline resistance and temperature established during a calibration process. Temperature was predicted using (15) based on the measured resistance of the optimized nanomaterial sensor during 100 temperature cycles,

and compared with a thermocouple control. The results of this comparison are shown in Figs. 16 and 17[15].

Fig. 16 illustrates the actual and predicted (sensor response) temperatures in time for cycling between 25ºC and 45ºC. This graph is an example of 5-cycles taken from the 100-cycle set of data. The temperature was ramped up at 30ºC per hour and down at 15ºC per hour. The solid (black) line in this graph depicts the temperature calculated from the measured resistance over the 5-cycles. The red symbols correspond to the actual temperature as measured by a K-Type thermocouple control. This analysis shows the close fit of the calculated temperature, based on the resistance of the fabric sensor, with the directly measured actual temperature, and verifies the ability of the empirically determined (15) to determine temperatures accurately from calculated resistances[15].

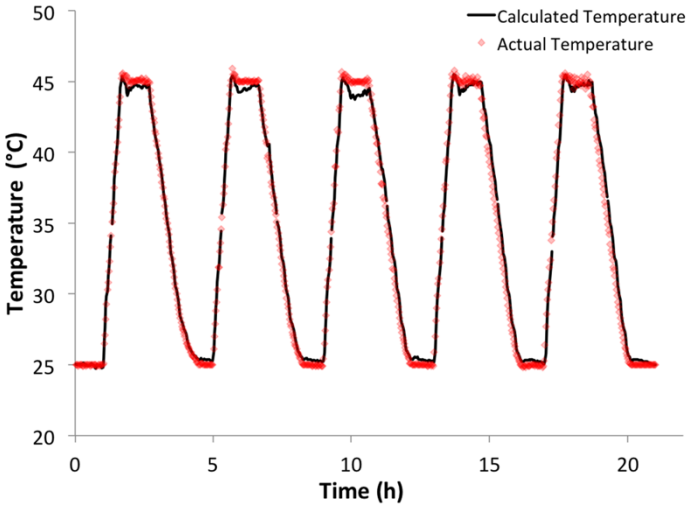

Fig. 16 Comparison of the actual temperature and the calculated temperature from (4) using α = -0.204 %/ºC. *Reprinted with permission from IEEE Sensors Journal* [15].

Fig. 17 plots temperature as predicted from the sensor response compared to the actual temperature for the data collected during one hundred temperature cycles of the sensor material. After one hundred cycles, the average percent error in the calculated temperature of the sensor material is approximately 4.29% ± 6.33%. The data displayed no appreciable hysteresis, but over 100 cycles there was approximately 300 Ohms of drift in the initial resistance, which stabilized overall. The sensitivity, or *dR/dT*[16], was consistent over the entire 100 cycle set (–13.49 ± 0.33 Ohms/ºC). This data demonstrates the success of the fabric-based, nanomaterial sensor at determining temperature in an accurate and reproducible manner [15].

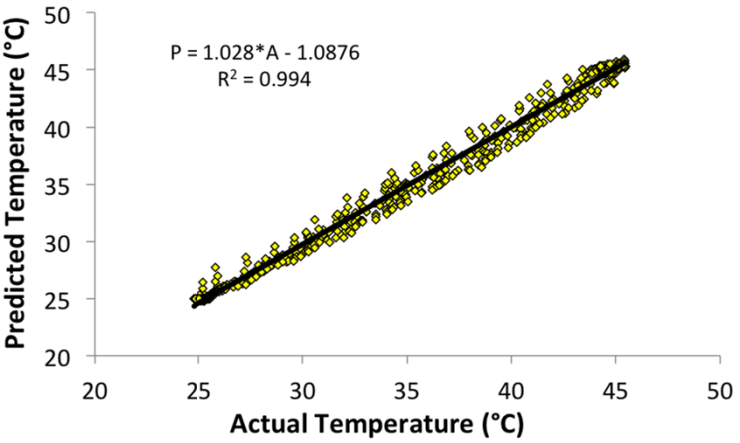

Fig. 17 Comparison of the temperature predicted by (4) to the actual recorded temperature. *Reprinted with permission from IEEE Sensors Journal*[15].

8 Conclusions

This chapter discussed the development and testing of a fabric-based temperature detector in the range of 25ºC to 45ºC, for the purpose of monitoring temperature variations near or at the dermis. Characterization of the nanomaterial sensor shows percolation behavior at the material surface; with 6.6 weight percent MWCNTs being the optimal loading. A PPy coating was used to enhance the electrical conductivity of the material by forming electrical interconnections between the MWCNTs. The fabric-based thermal sensor has an average negative TCR value of -0.204 ± 0.008 %/ºC, which is in line with previously studied CNTs and devices. The material displayed no appreciable hysteresis and the average percent error of the calculated temperature from the recorded temperature was 4.29% ± 6.33% over 100 cycles. This material shows promise for use in monitoring prosthetic socket environments or for other smart clothing applications; however, more research is required to develop this material into a robust sensing device for circuit integration[15].

Future work must include factors, such as better control of the PPy film formation through temperature control of the pyrrole vapor atmosphere during the polymerization reaction Encapsulation with a water vapor impermeable layer will most likely be required to reduce undesirable environmental effects on the sensor response. Imaging the increase in surface conductivity with increasing temperature using Conductive Atomic Force Microscopy (CAFM) to verify the sensing mechanism must also be completed. Imaging the material's surface at different temperatures should elucidate the electronic pathways across the fabric and will result in an in depth understanding of which nanostructures and construction procedures are paramount to the sensitivity of the fabric sensor. Ultimately, this

fabric sensor will be integrated into a useful device and tested for its efficacy on humans. The knowledge gained will then be adapted for use with other functional fabrics for wearable electronic technologies.

References

1. Axisa, F., Schmitt, P.M., Gehin, C., Delhomme, G., McAdams, E., Dittmar, A.: Flexible technologies and smart clothing for citizen medicine, home healthcare, and disease prevention. IEEE Trans. on Inf. Technol. Biomed. 9, 325–336 (2005), doi:10.1109/TITB.2005.854505
2. Reynolds, A.H.: Resistively heated fabrics for use in wearable therapeutic devices. Bachelor of Science in Mechanical Engineering, Massachusetts Institute of Technology (2010)
3. Berzowska, J.: Electronic textiles: Wearable computers, reactive fashion, and soft computation. Text J. Cloth. Cult. 3, 58–75 (2005)
4. Ciluffo, G.: Therapeutic "smart" fabric garment including support hose, body garments, and athletic wear (2004)
5. Perez de Isla, L., Lennie, V., Quezada, M., Guinea, J., Arce, C., Abad, P., Saltijeral, A., Campos, N.C., Crespo, J., Gonzálvez, B., Macia, A., Zamorano, J.: New generation dynamic, wireless and remote cardiac monitorization platform: A feasibility study. Int. J. Cardiol. 153, 83–85 (2011), doi:10.1016/j.ijcard.2011.08.074
6. Armstrong, D.G., Holtz-Neiderer, K., Wendel, C., Mohler, M.J., Kimbriel, H.R., Lavery, L.A.: Skin Temperature Monitoring Reduces the Risk for Diabetic Foot Ulceration in High-risk Patients. Am. J. Med. 120, 1042–1046 (2007), doi:10.1016/j.amjmed.2007.06.028
7. Armstrong, D.G., Lavery, L.A., Liswood, P.J., Todd, W.F., Tredwell, J.A.: Infrared dermal thermometry for the high-risk diabetic foot. Phys. Ther. 77, 169–175 (1997)
8. Benbow, S.J., Chan, A.W., Bowsher, D.R., Williams, G., Macfarlane, I.A.: The prediction of diabetic neuropathic plantar foot ulceration by liquid-crystal contact thermography. Diabetes Care 17, 835–839 (1994)
9. Bharara, M., Cobb, J.E., Claremont, D.J.: Thermography and Thermometry in the Assessment of Diabetic Neuropathic Foot: A Case for Furthering the Role of Thermal Techniques. Int. J. Low Extrem Wounds 5, 250–260 (2006), doi:10.1177/1534734606293481
10. Stess, R.M., Sisney, P.C., Moss, K.M., Graf, P.M., Louie, K.S., Gooding, G.A., Grunfeld, C.: Use of liquid crystal thermography in the evaluation of the diabetic foot. Diabetes Care 9, 267–272 (1986)
11. Biddiss, E., Chau, T.: Upper-Limb Prosthetics Critical Factors in Device Abandonment. Am. J. Phys. Med. Rehabil. 86, 977–987 (2007)
12. Burger, H., Marincek, C.: Upper limb prosthetic use in Slovenia. Prosthet. Orthot. Int. 18, 25–33 (1994)
13. Huff, E.A., Ledoux, W.R., Berge, J.S., Klute, G.K.: Measuring residual limb skin temperatures at the skin-prosthesis interface. JPO J Prosthet. Orthot. 20, 170 (2008)
14. Peery, J.T., Ledoux, W.R., Klute, G.K.: Residual-limb skin temperature in transtibial sockets. J. Rehabil. Res. Dev. 42, 147–154 (2005)
15. Blasdel, N.J., Wujcik, E.K., Carletta, J.E., Lee, K.-S., Monty, C.N.: Fabric Nanocomposite Resistance Temperature Detector. IEEE Sens. J. 15, 300–306 (2015), doi:10.1109/JSEN.2014.2341915

16. McGee, T.D.: Principles and methods of temperature measurement. Wiley, New York (1988)
17. Suprynowicz, V.A.: Electrical and electronics fundamentals: an applied survey of electrical engineering. West, St. Paul (1987)
18. Rizzoni, G.: Principles and applications of electrical engineering, 5th edn. McGraw-Hill Higher Education, Boston (2007)
19. Sachse, H.: Semiconducting temperature sensors and their applications. Wiley, New York (1975)
20. Howling, D.H.: Positive temperature coefficient semiconductor device (1960)
21. Neamen, D.A.: Semiconductor physics and devices: basic principles. McGraw-Hill, Boston (2003)
22. Patterson, J.D., Bailey, B.C.: Solid-state physics. Springer, Berlin (2007)
23. Quinn, J.J., Yi, K.-S.: Solid State Physics. Springer, Heidelberg (2009)
24. Sze, S.M., Ng, K.K.: Physics of Semiconductor Devices. John Wiley & Sons, Inc. (2007)
25. Hunt, L.B.: The Origin of the Platinum Resistance Thermometer. Platin. Metals Rev. 24, 104–112 (1980)
26. Camargo, P.H.C., Satyanarayana, K.G., Wypych, F.: Nanocomposites: synthesis, structure, properties and new application opportunities. Mater. Res. 12, 1–39 (2009)
27. Paul, D.R., Robeson, L.M.: Polymer nanotechnology: Nanocomposites. Polymer 49, 3187–3204 (2008), doi:10.1016/j.polymer.2008.04.017
28. Cheung, W., Chiu, P.L., Parajuli, R.R., Ma, Y., Ali, S.R., He, H.: Fabrication of high performance conducting polymer nanocomposites for biosensors and flexible electronics: summary of the multiple roles of DNA dispersed and functionalized single walled carbon nanotubes. J. Mater. Chem. 19, 6465 (2009), doi:10.1039/b823065j
29. Hnaien, M., Lagarde, F., Bausells, J., Errachid, A., Jaffrezic-Renault, N.: A new bacterial biosensor for trichloroethylene detection based on a three-dimensional carbon nanotubes bioarchitecture. Anal. Bioanal. Chem. 400, 1083–1092 (2011), doi:10.1007/s00216-010-4336-x
30. Kahlweit, M.: Microemulsions. Annu. Rep. Prog. Chem. Sect. C Phys. Chem. 95, 89–116 (1999)
31. Lerner, M.B., Goldsmith, B.R., McMillon, R., Dailey, J., Pillai, S., Singh, S.R., Johnson, A.T.C.: A carbon nanotube immunosensor for Salmonella. AIP Adv. 1, 42127 (2011), doi:10.1063/1.3658573
32. Venturelli, E., Fabbro, C., Chaloin, O., Ménard-Moyon, C., Smulski, C.R., Da Ros, T., Kostarelos, K., Prato, M., Bianco, A.: Antibody Covalent Immobilization on Carbon Nanotubes and Assessment of Antigen Binding. Small 7, 2179–2187 (2011), doi:10.1002/smll.201100137
33. Kim, H.S., Jin, H.-J., Myung, S.J., Kang, M., Chin, I.-J.: Carbon Nanotube-Adsorbed Electrospun Nanofibrous Membranes of Nylon 6. Macromol. Rapid Commun. 27, 146–151 (2006), doi:10.1002/marc.200500617
34. Li, F., Scampicchio, M., Mannino, S.: Carbon Nanotube-Adsorbed Electrospun Nanofibrous Membranes as Coating for Electrochemical Sensors for Sulfhydryl Compounds. Electroanalysis 23, 1773–1775 (2011), doi:10.1002/elan.201100068
35. Jacobs, C.B., Peairs, M.J., Venton, B.J.: Review: Carbon nanotube based electrochemical sensors for biomolecules. Anal. Chim. Acta 662, 105–127 (2010), doi:10.1016/j.aca.2010.01.009
36. Bauhofer, W., Kovacs, J.Z.: A review and analysis of electrical percolation in carbon nanotube polymer composites. Compos. Sci. Technol. 69, 1486–1498 (2009), doi:10.1016/j.compscitech.2008.06.018

37. Wujcik, E.K., Monty, C.N.: Nanotechnology for implantable sensors: carbon nanotubes and graphene in medicine. Wiley Interdiscip. Rev. Nanomed. Nanobiotechnol. 5, 233–249 (2013), doi:10.1002/wnan.1213
38. Bethune, D.S., Klang, C.H., de Vries, M.S., Gorman, G., Savoy, R., Vazquez, J., Beyers, R.: Cobalt-catalysed growth of carbon nanotubes with single-atomic-layer walls. Nature 363, 605–607 (1993), doi:10.1038/363605a0
39. Iijima, S., Ichihashi, T.: Single-shell carbon nanotubes of 1-nm diameter. Nature 363, 603–605 (1993), doi:10.1038/363603a0
40. Jorio, A., Saito, R., Dresselhaus, G., Dresselhaus, M.S.: Determination of nanotubes properties by Raman spectroscopy. Philos. Trans. Math. Phys. Eng. Sci. 362, 2311–2336 (2004), doi:1J0Y9YKD70BCDJB0 [pii] 10.1098/rsta.2004.1443
41. Jorio, A., Saito, R., Hafner, J.H., Lieber, C.M., Hunter, M., McClure, T., Dresselhaus, G., Dresselhaus, M.S.: Structural (n, m) determination of isolated single-wall carbon nanotubes by resonant Raman scattering. Phys. Rev. Lett. 86, 1118–1121 (2001)
42. Sinha, N., Ma, J., Yeow, J.T.: Carbon nanotube-based sensors. J. Nanosci. Nanotechnol. 6, 573–590 (2006)
43. Dresselhaus, M.S., Dresselhaus, G., Eklund, P.C.: Science of fullerenes and carbon nanotubes. Academic Press, San Diego (1996)
44. Jorio, A., Dresselhaus, G., Dresselhaus, M.S.: Carbon nanotubes: advanced topics in the synthesis, structure, properties, and applications. Springer, Berlin (2008)
45. Rotkin, S.S.V., Subramoney, S.: Applied physics of carbon nanotubes. Springer (2005)
46. Saito, R., Dresselhaus, G., Dresselhaus, M.S.: Physical properties of carbon nanotubes. Imperial College Press, London (1998)
47. Carbon nanotubes: synthesis, structure, properties, and applications. Springer, Berlin (2001)
48. Choudhary, V., Gupta, A.: Polymer/carbon nanotube nanocomposites. Carbon Nanotub.-Polym. Nanocomposites, 65–90 (2011)
49. Ali, K., Hafez, M.: Growth and structure of carbon nanotubes based novel catalyst for ultrafast nano-temperature sensor application. Superlattices Microstruct. 54, 1–6 (2013), doi:10.1016/j.spmi.2012.10.007
50. Di Bartolomeo, A., Sarno, M., Giubileo, F., Altavilla, C., Iemmo, L., Piano, S., Bobba, F., Longobardi, M., Scarfato, A., Sannino, D., Cucolo, A.M., Ciambelli, P.: Multiwalled carbon nanotube films as small-sized temperature sensors. J. Appl. Phys. 105, 064518 (2009), doi:10.1063/1.3093680
51. Cagatay, E., Falco, A., Abdellah, A., Lugli, P.: Carbon nanotube based temperature sensors fabricated by large-scale spray deposition. Microelectron. In: Electron. PRIME 2014 10th Conf. Ph. Res., pp. 1–4. IEEE (2014)
52. Fung, C.K., Li, W.J.: Ultra-low-power polymer thin film encapsulated carbon nanotube thermal sensors. In: 2004 4th IEEE Conf. on Nanotechnol., pp. 158–160 (2004)
53. Giuliani, A., Placidi, M., Di Francesco, F., Pucci, A.: A new polystyrene-based ionomer/MWCNT nanocomposite for wearable skin temperature sensors. React. Funct. Polym. 76, 57–62 (2014), doi:10.1016/j.reactfunctpolym.2014.01.008
54. Hsu, M.-C., Lee, G.-B.: Carbon nanotube-based hot-film and temperature sensor assembled by optically-induced dielectrophoresis. IET Nanobiotechnol. 8, 44–50 (2014), doi:10.1049/iet-nbt.2013.0040
55. Karimov, K.S., Chani, M.T.S., Khalid, F.A.: Carbon nanotubes film based temperature sensors. Phys. E Low-Dimens. Syst. Nanostructures 43, 1701–1703 (2011), doi:10.1016/j.physe.2011.05.025

56. Karimov, K.S., Khalid, F.A., Chani, M.T.S., Mateen, A., Hussain, M.A., Maqbool, A., Ahn, J.: Carbon nanotubes based flexible temperature sensors. Optoelectron. Adv. Mater. 6, 194–196 (2012)
57. Matzeu, G., Pucci, A., Savi, S., Romanelli, M., Di Francesco, F.: A temperature sensor based on a MWCNT/SEBS nanocomposite. Sens. Actuators Phys. 178, 94–99 (2012), doi:10.1016/j.sna.2012.02.043
58. Mohsin, K.M., Banadaki, Y.M., Srivastava, A.: Metallic single-walled, carbon nanotube temperature sensor with self heating. SPIE Smart Struct. Mater. Nondestruct. Eval. Health Monit. International Society for Optics and Photonics, pp. 906003–906003 (2014)
59. Selvarasah, S., Chen, C.-L., Chao, S.-H., Makaram, P., Busnaina, A., Dokmeci, M.R.: A Three Dimensional Thermal Sensor Based on Single-Walled Carbon Nanotubes. In: Solid-State Sens. Actuators Microsyst. Conf, TRANSDUCERS, Int., pp. 1023–1026 (2007)
60. Sibinski, M., Jakubowska, M., Sloma, M.: Flexible Temperature Sensors on Fibers. Sensors 10, 7934–7946 (2010), doi:10.3390/s100907934
61. Tian, M., Huang, Y., Wang, W., Li, R., Liu, P., Liu, C., Zhang, Y.: Temperature-dependent electrical properties of graphene nanoplatelets film dropped on flexible substrates. J. Mater. Res. 29, 1288–1294 (2014), doi:10.1557/jmr.2014.109
62. De Volder, M., Reynaerts, D., Van Hoof, C., Tawfick, S., Hart, A.J.: A temperature sensor from a self-assembled carbon nanotube microbridge. In: 2010 IEEE Sens., pp. 2369–2372 (2010)
63. Yang, X., Zhou, Z., Zheng, F., Wu, Y.: High sensitivity temperature sensor based on a long, suspended single-walled carbon nanotube array. Micro Nano Lett. 5, 157 (2010), doi:10.1049/mnl.2010.0005
64. Lala, N., Thavasi, V., Ramakrishna, S.: Preparation of Surface Adsorbed and Impregnated Multi-walled Carbon Nanotube/Nylon-6 Nanofiber Composites and Investigation of their Gas Sensing Ability. Sensors 9, 86–101 (2009)
65. Mahmood, N., Islam, M., Hameed, A., Saeed, S.: Polyamide 6/Multiwalled Carbon Nanotubes Nanocomposites with Modified Morphology and Thermal Properties. Polymers 5, 1380–1391 (2013), doi:10.3390/polym5041380
66. Ramanathan, T., Fisher, F.T., Ruoff, R.S., Brinson, L.C.: Amino-Functionalized Carbon Nanotubes for Binding to Polymers and Biological Systems. Chem. Mater. 17, 1290–1295 (2005), doi:10.1021/cm048357f
67. Chang, C.M., Liu, Y.L.: Electrical Conductivity Enhancement of Polymer/Multi-walled Carbon Nanotube (MWCNT) Composites by Thermally-induced De-functionalization of MWCNTs. ACS Appl. Mater. Interfaces (2011)
68. Ryu, J.S.: Work Functions of Functionalized Single-Walled Carbon Nanotubes. Massachusetts Institute of Technology (2006)
69. Qi, P., Vermesh, O., Grecu, M., Javey, A., Wang, Q., Dai, H., Peng, S., Cho, K.J.: Toward Large Arrays of Multiplex Functionalized Carbon Nanotube Sensors for Highly Sensitive and Selective Molecular Detection. Nano Lett. 3, 347–351 (2003), doi:10.1021/nl034010k
70. Sahoo, N.G., Cheng, H.K.F., Cai, J., Li, L., Chan, S.H., Zhao, J., Yu, S.: Improvement of mechanical and thermal properties of carbon nanotube composites through nanotube functionalization and processing methods. Mater. Chem. Phys. 117, 313–320 (2009)
71. Lee, J.Y., Song, K.T., Kim, S.Y., Kim, Y.C., Kim, D.Y., Kim, C.Y.: Synthesis and characterization of soluble polypyrrole. Synth. Met. 84, 137–140 (1997)

72. Song, M.-K., Kim, Y.-T., Kim, B.-S., Kim, J., Char, K., Rhee, H.-W.: Synthesis and characterization of soluble polypyrrole doped with alkylbenzenesulfonic acids. Synth. Met. 141, 315–319 (2004), doi:10.1016/j.synthmet.2003.07.015
73. Jang, K.S., Lee, H., Moon, B.: Synthesis and characterization of water soluble polypyrrole doped with functional dopants. Synth. Met. 143, 289–294 (2004), doi:10.1016/j.synthmet.2003.12.013
74. Lee, J.Y., Kim, D.Y., Kim, C.Y.: Synthesis of soluble polypyrrole of the doped state in organic solvents. Synth. Met. 74, 103–106 (1995)
75. Skotheim, T.A., Elsenbaumer, R.L., Reynolds, J.R.: Handbook of conducting polymers. M. Dekker, New York (1998)
76. Brezoi, D.V.: Polypyrrole Films Prepared By Chemical Oxidation of Pyrrol. In: Aqueous FeCl3 Solution. J. Sci. Arts 12
77. Inzelt, G.: Conducting polymers. Springer, New York (2012)
78. Vetter, C.A., Suryawanshi, A., Lamb, J.R., Law, B., Gelling, V.J.: Novel Synthesis of Stable Polypyrrole Nanospheres Using Ozone. Langmuir 27, 13719–13728 (2011), doi:10.1021/la202947e
79. Mohammadi, A., Hasan, M.A., Liedberg, B., Lundström, I., Salaneck, W.R.: Chemical vapour deposition (CVD) of conducting polymers: polypyrrole. Synth. Met. 14, 189–197 (1986)
80. Lunn, B.A., Unsworth, J., Booth, N.G., Innis, P.C.: Determination of the thermal conductivity of polypyrrole over the temperature range 280–335 K. J. Mater. Sci. 28, 5092–5098 (1993)
81. Ramanavičius, A., Ramanavičienė, A., Malinauskas, A.: Electrochemical sensors based on conducting polymer—polypyrrole. Electrochimica Acta 51, 6025–6037 (2006), doi:10.1016/j.electacta.2005.11.052
82. Du, D., Ye, X., Cai, J., Liu, J., Zhang, A.: Acetylcholinesterase biosensor design based on carbon nanotube-encapsulated polypyrrole and polyaniline copolymer for amperometric detection of organophosphates. Biosens. Bioelectron. 25, 2503–2508 (2010), doi:10.1016/j.bios.2010.04.018
83. Tam, P.D., Hieu, N.V.: Conducting polymer film-based immunosensors using carbon nanotube/antibodies doped polypyrrole. Appl. Surf. Sci. (2011)
84. Ouerghi, O., Touhami, A., Jaffrezic-Renault, N., Martelet, C., BenOuada, H., Cosnier, S.: Electrodeposited Biotinylated Polypyrrole as an Immobilization Method for Impedimetric Immunosensors. IEEE Sens. J. 4, 559–567 (2004), doi:10.1109/JSEN.2004.832858
85. Vidal, J.C., García, E., Castillo, J.R.: In situ preparation of a cholesterol biosensor: entrapment of cholesterol oxidase in an overoxidized polypyrrole film electrodeposited in a flow system: Determination of total cholesterol in serum. Anal. Chim. Acta 385, 213–222 (1999)
86. An, K.H., Jeong, S.Y., Hwang, H.R., Lee, Y.H.: Enhanced Sensitivity of a Gas Sensor Incorporating Single-Walled Carbon Nanotube–Polypyrrole Nanocomposites. Adv. Mater. 16, 1005–1009 (2004), doi:10.1002/adma.200306176
87. Bartlett, P.N., Ling-Chung, S.K.: Conducting polymer gas sensors part II: response of polypyrrole to methanol vapour. Sens. Actuators 19, 141–150 (1989)
88. De Schoenmaker, B., Van der Schueren, L.: Wicking Properties of Various Polyamide Nanofibrous Structures with an Optimized Method. J. Appl. Polym. Sci. 120, 305–310 (2011)
89. Bai, Y., Lin, D., Wu, F., Wang, Z., Xing, B.: Adsorption of Triton X-series surfactants and its role in stabilizing multi-walled carbon nanotube suspensions. Chemosphere 79, 362–367 (2010), doi:S0045-6535(10)00169-4 [pii] 10.1016/j.chemosphere. 2010.02.023

Strain Sensors in Wearable Devices

M. Farooq and E. Sazonov

Department of Electrical Engineering, University of Alabama, Tuscaloosa 35401, USA
mfarooq@crimson.ua.edu, esazonov@eng.ua.edu

Abstract. This chapter discusses the use of strain sensors in wearable devices. Strain sensors are used to monitor deformation under applied load. Various techniques for the fabrication of strain sensors are discussed and some example applications are presented. Special focus is placed on textile based and inkjet-printed strain sensors. Textile based strain sensors open new frontiers for wearable systems by integrating sensors into garments which can be used for extended periods of time. Inkjet printing along with conductive inkjet inks provides low cost, efficient, and rapid prototyping solution for implementation of strain sensors in wearable devices. Applications in the area of remote monitoring of physiological signals, vital signs, and human activity are presented.

Keywords: Wearable devices, strain sensors, textile, inkjet printing, screen printing, activity recognition.

1 Introduction

Technology spans the modern lifestyle with applications ranging from neonatal care to improving quality of life of senior citizens through exploratory treatment and procedures. The rapid developments in sensor devices, computer, storage, communication systems and power technologies have been a driving force to the widespread emergence of wearable devices. Some of the recent applications of the wearable devices are in business operations (e.g. keeping track of logistic and event tracking etc.), security (hazard detection and identity recognition etc.), safety (e.g. remote monitoring and emergency services), clinical and wellness applications (such as vital sign monitoring, patient monitoring systems, sleep, diet and motion tracking etc.), sports and fitness applications (such as fitness monitoring, activity tracking, outdoor navigation, and tracking etc.). There are many sensors being used in wearable systems, but this work will mainly focus on strain sensors.

Strain is defined as the amount of deformation in a structure due to the applied force or load. Based on the nature of the applied force, strain can be tensile or compressive. Fig. 1 shows a bar under tensile strain, where the length of the bar changes by ΔL under an applied uni-axial force, where L is the length of the bar. In this case the girth of the bar, D, will contract in the transverse direction based on the material properties of the bar, which is defined by the Poisson's Ratio.

S.C. Mukhopadhyay (ed.), *Wearable Electronics Sensors*,
Smart Sensors, Measurement and Instrumentation 15, DOI: 10.1007/978-3-319-18191-2_9

In cases where the force tries to bend the structure instead of stretching or shrinking, the structure is said to be under bending stress. Bending forces produce both tensile and compressive components and are defined in terms of bending moment. Most of the sensors we discuss in this chapter are under bending strain. Strain can be measured with a strain sensor called strain gauge. A conventional strain sensor can be considered as a resistor on a substrate which exploits it piezo-resistive properties. Structural deformation in conductive materials under force/load can exhibit a change in the bulk resistivity of the material. This piezo-resistive property of the conductive material can be exploited as a sensing mechanism in the form of strain gauges in wearable devices. The variation in stress or strain under applied force can be recorded by the intrinsic changes in the resistance of the material. For example, a strain gauge attached to a joint will deform with joint motion; this motion can be monitored by the resultant changes in the resistance [1].

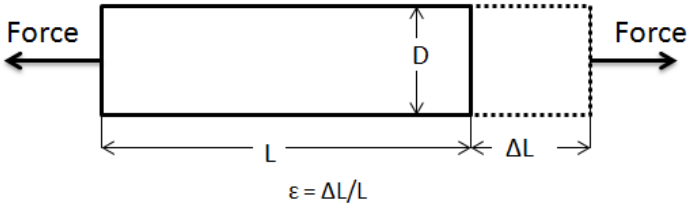

Fig. 1 Strain in a bar under the applied force

The goal of this chapter is to introduce recent research in the use of strain sensors in wearable devices and to discuss technologies which are used to make such sensors possible. Current wearable systems utilize commercially available strain sensors which may not be well suited for the intended applications. Some of the factors which limit their use are size, shape and other characteristics such as resistivity, flexibility of the sensor or incompatibility of the sensor, and the surface on which it is supposed to be used. Therefore, there is a need for technology to enable the design and fabrication of low-cost application specific strain sensors. The rest of the chapter focuses on various techniques for fabrication of wearable strain sensors and their applications: Section 1.2 provides a summary of the recent work in textile based strain gauges. Techniques used for the fabrication of textile based strain sensor are also discussed. Some applications are presented where emphasis is made on the use of textile based strain gauges for (i) monitoring of physiological signals and (ii) monitoring of gestures and joint motions. Example applications of both commercially available, as well as specially designed strain sensors are presented. There are other strain sensors which are wearable but not textile based. These sensors can be directly attached to the skin and a brief introduction to these is provided at the end of the section. Section 1.3 introduces the use of inkjet printers for printing strain sensors. Choice of inks and substrates is also discussed. Section 1.4 presents examples of strain sensors printed with inkjet printers for

both textile based wearable devices as well as skin attachable devices to show that inkjet printing can provide a viable solution to fabricate strain sensors for wearable devices. Section 1.5 introduces strain sensors which are primarily used on skin directly but the fabrication methods used are different than those used for textile based or inkjet-printed sensors. Section 1.6 concludes this chapter.

2 Textile Based Strain Sensors for Wearable Devices

Monitoring of human movement has been extensively studied using accelerometer, goniometers and cameras for motion capture systems [2–5]. Although accurate, such systems are not easy to use for extended periods of time because of their dependence on the individual's motion characteristics, the mechanisms involving their application to human body and the need for stationary installation (such as in case of the camera systems) [3, 6]. Textile based strain sensors provide a practical and wearable alternative to motion capture and monitoring of physiological signals such as respiration [6, 7]. Textiles instrumented with sensors need to be flexible and comfortable to the wearer so that they can be used for an extended period of time. Textile based strain sensors find their use in applications that need to register various types of body movement, such as joint flexion.

Strain sensors embedded in the textile works on a similar principle as the conventional strain gauges. Changes in stress or strain under applied force are converted into changes in resistance which is monitored over time. For example, breathing can be monitored by embedding two piezo-resistive fabric sensors on the chest and abdominal position as shown in Fig. 2 [8]. The circumference of the rib cage changes during breathing movements. During sensor elongation the resistance of the sensor increases. These variations in length are registered by the sensors as resistance changes and converted into voltage changes. The breathing patterns given by these sensors are similar to conventional techniques, such as respiratory inductive plethysmography. Changes in piezo-resistivity have also been used in textile-based wearable devices for monitoring of joint movements where strain sensors placed at the joints deform with movements [9–12].

A variety of options exist to integrate strain sensors into textile. One possibility is to use conventional strain sensors embedded in textile [9]. A potential problem with this approach is the limited availability of strain sensors in the desired form factor and with the electro-mechanical properties required by the intended application. To overcome these limitations, strain sensors in textile can be fabricated by using conductive threads [13], integrating conductive yarns in the textile structure such as weaving [14] and/or drawing patterns using conductive ink [15]. In all these cases, strain sensors are integrated into the garments but the manner in which the sensors are produced is different. In next subsection, we introduce some technologies which are used to realize these sensors on textile in contrast to using conventional strain sensors.

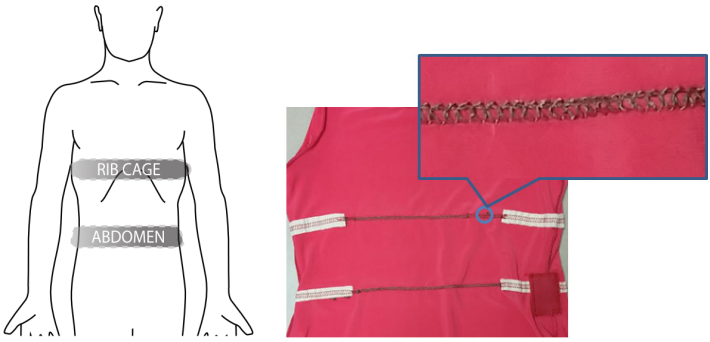

a) b)

Fig. 2 (a) A conceptual design of sensor placement for monitoring respiration. Two strain sensors are used; one is placed on the rib cage whereas the second is placed at the abdominal position. (b) A textile garment instrumented with two strain sensors placed at the chest and abdominal position. A zoomed in section of the strain sensor is also shown [Image courtesy of Dr. Lucy Dunne and Mary Ellen Berglund].

2.1 Fabrication of Textile Based Sensors

2.1.1 Conductive Fibers

In this process, conductive fiber based threads are twisted with the normal fibers to realize sensors. A mechanical production process called wire drawing is used for fabrication of the conductive fibers. The cross section of the wire is reduced by pulling the metal wire (conductive fiber) through a series of drawing dies. Steps involved in this process are shown in Fig. 3. A number of conductive materials such as copper, silver, brass, gold etc. can be used with this approach. Depending on the material used, the initial diameter of the conductive metal wire will be different. For example, for iron the initial diameter is 5mm, whereas for copper it is around 8mm. Wire drawing is followed by annealing the wire under high temperature [16]. The resultant fine metal wire can then be incorporated into base yarn like cotton, polyester, polyamides and aramids etc. Such fibers need to be lightweight as well as very fine. One thing to consider is that by using metal fiber, the elasticity of the textile will reduce, whereas the stiffness will increase. This approach has been used in making embedded strain sensors in textile [1].

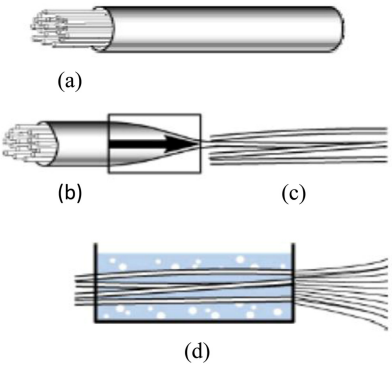

Fig. 3 (a) Coarse train: Iron tube containing metal wires. (b) Wire drawing to reduce the diameter of the wire. (c) Bundling of tubes together. (d) Leaching processing for realizing fibers [16].

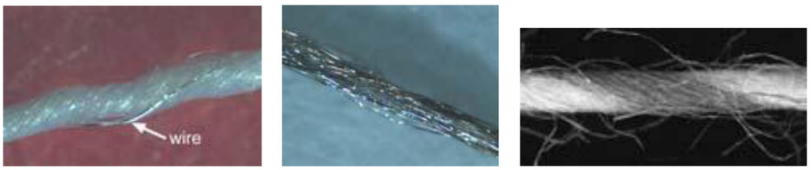

Fig. 4 (a) A polymer yarn with a twisted metal wire around it. (b) Metal coating: A polymer yarn coated with a metal layer. (c) Metal fibers: The conductive yarn made of metal multifilament [16].

2.1.2 Treated Conductive Fibers

Another method for producing conductive fibers is applying a conductive coating to the fiber. This can be achieved by using different coating processes such as sputtering, atomic layer deposition (ALD), evaporative deposition, polymer based and electroless plating, etc. [13, 16]. For coating, materials such as gold, silver, copper, nickel, conductive polymers and carbon are used. The coating process can be used with a large number of different fibers and the resulting conductivity is good, whereas properties of the substrate such as density and flexibility are minimally impacted. The coated fibers are integrated into the textile by weaving the fiber directly into the garments [17]. Fig. 4 shows examples of conductive metal fibers and fibers coated with metal layers.

2.1.3 Using Conductive Ink

Apart from using conductive metal fibers or coating fibers with a metal, there is also a possibility to draw or print textile sensors with a conductive ink directly on

the substrate using printing techniques. Conductive inks are based on silver, carbon, gold and conductive polymers. There are two widely used printing techniques i.e. inkjet printing and screen printing. In this section we will focus on screen printing only; inkjet printing is discussed in detail later. Screen printing is a fast, simple and cost effective printing technique. Screen printing uses a mask along with a roller to imprint conductive patterns on the substrates. Screen printing can be carried out on a number of substrates to implement strain sensors on textile [18, 19]. Parameters such as the conductivity of the tracks can be controlled by increasing the thickness of the tracks. Major drawback of screen printing is that it requires a mask and there is physical interaction between the roller mechanism and substrate.

2.2 Representative Applications of Textile Based Strain Sensors

The following subsections describe example applications of strain sensors integrated into textile. The focus is on the use of textile strain gauges in wearable devices for (i) monitoring of physiological signals and (ii) motion and gesture capturing. The first group of applications deals with cases where the movements are comparatively small and the sensors are supposed to be placed very close to the skin for the monitoring of vital signs such as breathing. The focus of the second group of presented applications is on larger movements such as opening or closing of hands or joint motions in the knee.

2.2.1 Textile-Based Strain Sensors for Monitoring of Physiological Signals

Wearable sensors that are able to capture vital health signals and are able to transmit them to a remote location will play an important role in the future health care system. The remote health monitoring system will be appealing to patients only if such a system is easy to use, comfortable and does not interfere with the daily routine of the patients and imposes minimum extra burden on them [20–22]. Therefore, integration of sensors into textile is a viable solution, which offers a low cost and flexible monitoring system which can be further customized based on the needs of the patient. Sensors embedded in the textile can provide information about respiration, ECG, temperature of the body and the activities performed by individuals [23].

Physiological signals such as rate of respiration can provide useful information about the health condition of a patient. For respiration monitoring, usually two sensors are used. One is placed over the rib cage and another over the abdominal area (Fig. 2(a)). During the respiratory cycle (inspiration and expiration), the rib cage will expand and contract and hence the circumference of the rib cage changes. This will result in the increase and decrease of the length of the strain sensor attached at those two locations; which in turn will produce a proportional output voltage during the respiratory cycle. An example of a wearable textile

instrumented with multiple sensors was proposed by researchers in [24, 25] called WEALTHY. The system consisted of sensors for monitoring of vital signs such as ECG and respiration/ breathing. Piezo-resistive sensors were made using lycra fabric coated with carbon-loaded rubber and commercial electro-conductive yarn (PAC 250 dtxx1, by Europa NCT, Poland) for monitoring of breathing [26]. The fabric acts as a strain gauge and is used for capturing respiration signals. According to the authors, their proposed method gave results comparable to a commercially available system (Biopac system) for detection of respiration. Similar sensor systems for monitoring breathing and other vital signs were proposed by other researchers as well [13, 27, 28].

2.2.2 Body Movements and Gesture Recognition with Textile Based Strain Sensors

This section deals with applications of strain gauges in monitoring body motion, posture and gesture. If a strain gauge is attached at a joint, the relative change in the output resistance of the strain gauge is proportional to the degree of motion at that joint. Some example applications include monitoring of flexion of fingers in the form of a glove [9–12], monitoring of movements in the knee, elbow etc. for motion capture and reconstruction [1, 12, 29–33], and monitoring movements in the upper body (trunk) [25, 34].

Hand gestures captured through gloves are used in many applications including robotics, virtual reality and the study of biomechanics. Strain gauges may also be used for monitoring the applied force/load. The force exerted by fingers while pressing a rubber ball can be measured by attaching a small steel blade on the thumb which is instrumented with two strain gauges, one on each side [9]. Strain gauge force sensors along with flex sensors (for finger position sensing) were attached to a cotton glove for monitoring the applied force.

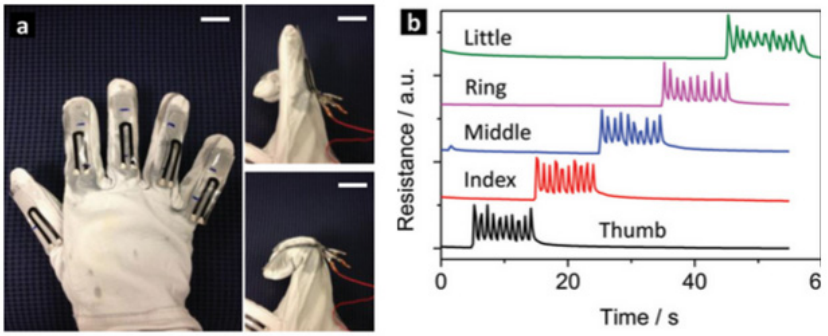

Fig. 5 (a) Glove instrumented with strain sensors for movement detection of the finger. Stretching and bending of a finger is also shown. (b) Relative resistance changes for independent strain sensors placed on fingers [35].

Apart from the force measurement, gloves instrumented with strain sensors can be used in monitoring hand gestures [10–12, 36]. The use of conventional strain gauges for hand gesture monitoring is complicated and uncomfortable because of the challenges involved in interfacing of the fabric with sensors. Recent technology development offers the possibility to directly spray conductive mixtures with piezo-resistive properties to implement strain sensors [11]. Authors in [11], used a commercially available conductive mixture (WACKER Ltd, ELASTOSIL LR 3162 A/B) to implement strain sensors on a glove made of Lycra fabric . Signals from strain sensors and the related signal processing algorithms were able to differentiate between 32 different hand gestures including basic grip and signs of American Sign Language. Fig. 5 shows a similar example application where graphene based strain sensors were used for monitoring finger movements [35]. Resistance changes with the stretching and bending of finger. These resistance variations can be used for recognizing gestures.

Like in gloves, strain sensors can be used to monitor upper and lower body movements. Textile integrated with conventional strain gauges, as well as strain sensors implemented using special conductive materials/polymers, have been proposed for this purpose [7, 12, 29–32]. Authors in [32] proposed the use of a wearable gesture sensing device which uses fabric based strain sensors (elastic webbing) for monitoring the flexion angle of elbow and knee movements (Fig. 6). The elastic conductive webbing has high resistance sensitivity, low tensile hysteresis, as well as high linearity. Resistance of elastic conductive webbing linearly changes with the flexion angle. A similar approach can be used for monitoring of lower body movements. In [1] a technique for adding conductive fibers into flexible, skin-tight garments is described, where the sensors on the garments are close to the joint. Such an approach can be used to monitor both single and multi-axis joint angles. These sensors were used to monitor joint movements both at hips and knee locations. Non-linear predictors were used to differentiate between the resistance changes caused by single or multi-axis joint angle movements.

The trunk part of the body provides control and stability to the upper part of the body and is critical for balancing the body posture in daily activities [37]. Trunk muscles are also critical in controlling the gait which is an important factor in motor and functional recovery of individuals going through functional rehabilitation [38]. Trunk movements can be monitored using wearable sensor systems containing strain sensors. The data captured from these sensors can be further analyzed by machine learning algorithms to track the improvements throughout the rehabilitation process. For this purpose a system was proposed in [25, 34] where strain sensors printed on textile were employed to capture trunk movements. Strain sensors were made with conductive elastomer, which is a polymer material with piezoelectric properties. The conductive elastomer is a lightweight and flexible material, and, therefore, can be integrated into the textile. Patterns for 13 strain sensors were drawn on a fabric using industrial printing process. Subjects were asked to perform a set of movements and the signals from all sensors were collected for each movement. This sensor system, coupled with machine learning techniques, has the ability to differentiate between different body postures and to

provide real time feedback to the users on their current postures. This information can also be transmitted to the clinicians to monitor progress of the patient. A similar system with 21 sensors is shown in Fig. 7.

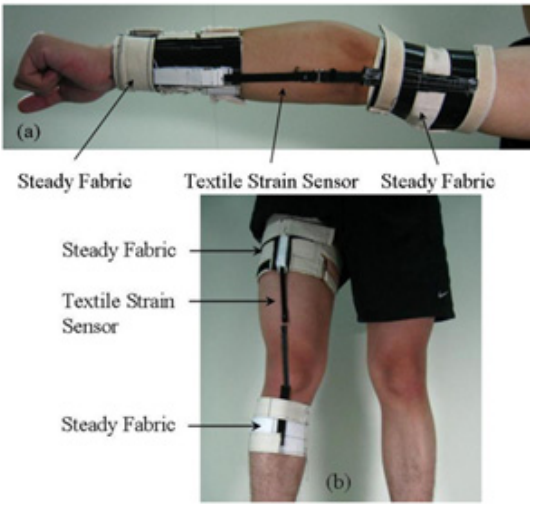

Fig. 6 The proposed wearable gesture sensing devices for monitoring the flexion angle during (a) elbow and (b) knee movements [32].This image is derivative of A textile-based wearable sensing device designed for monitoring the flexion angle of elbow and knee movements, published in Sensors.

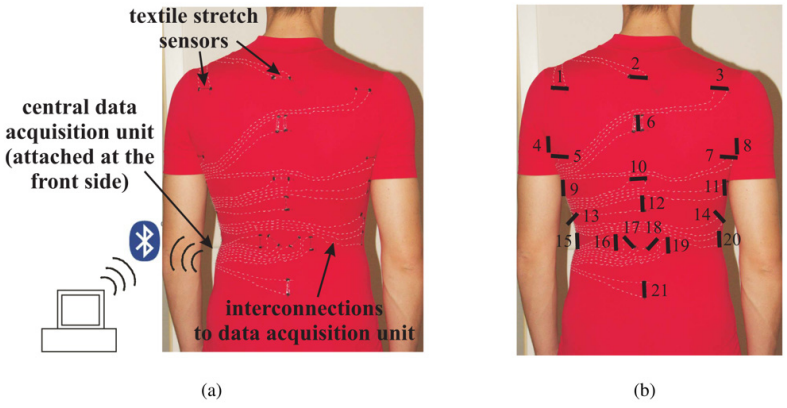

Fig. 7 A system for recognition upper body postures using 21 strain sensors [39]

3 Inkjet Printing of Strain Sensors

Conventional inkjet printing techniques with conductive inks can be used to print patterns of strain sensors on a substrate. With inkjet printers it is possible to use a variety of substrates with different flexibility and thickness. This makes inkjet printing an excellent candidate for printing sensor for wearable systems. Potentially, inkjet printing can provide a low cost and rapid prototyping technique for designing and fabrication of wearable sensors. This section introduces the working principle of inkjet printing as well as a variety of conductive inks which are available for the implementation of the printed strain gauges. We also discuss parameters to be considered for selection of inkjet printer and inks for printing electronic circuits.

3.1 Working Principle of Inkjet Printing

Inkjet printing techniques produces ink droplets with the diameter in the range of 10 to 150μm and the volume in the range of 1-100 pico-liters depending on the nozzle size [40]. For droplet generation, usually two techniques are used, namely continuous inkjet (CIJ) printing and drop on demand (DOD) inkjet printing. CIJ produces droplets in the range of 100μm whereas the DOD printing can produce droplets in the range of 20–50μm. CIJ technique produces a continuous stream of ink droplets and, therefore, this approach is not economical. In order to save the ink, the unused droplets are deflected to a gutter by an electric field and are recycled. This recycling can produce contamination of the ink (after the exposure to the environment) and therefore CIJ is not a good choice for printed electronics.

On the other hand, the DOD printing produces ink droplets when needed. Drop ejection is controlled in the chamber behind the printing nozzle by the use of a pressure pulse. Ink is held in the chamber by the surface tension and a droplet is ejected only when the pressure pulse generated is greater than a certain threshold. Both the velocity and size of the droplet can be controlled by the pressure pulse [40]. The formation of droplets in DOD printing can be further divided into three categories based on the techniques used. These categories include thermal inkjet, piezo inkjet, and electrostatic inkjet. In thermal DOD, printing droplet is generated by passing current through a small thin-film heater in the fluid chamber. This produces a small bubble which collapse on the removal of the heat. The process of bubble generation and collapse results in the pressure pulse mentioned above. In piezo inkjet printers a piezoelectric transducer actuated by a voltage pulse is used to form pressure (acoustic) waves which propagate through the ink chamber, generating droplets at the acoustic frequencies.

In literature, the use of different printers has been reported for printed electronics. In [41], the use of a piezoelectric Auto drop printer from Microdrop Technologies with a 68μm nozzle diameter was reported to study the effects of low temperature curing and thermal stability of printed silver tracks. Authors in [42] used a iTi industrial inkjet printing system for printing conductive traces of silver

ink on various substrates. Their printing system was equipped with a Dimatix Spectra SE piezoelectric print head that has 128 nozzles of 38μm diameter. In [43][44], the use of EPSON piezoelectric inkjet was suggested which has the ability of printing tracks with a width of 200μm and track spacing of 200μm. Some of the other printers reported in literature are Epson R210 [45], EPSON ME1+ [46], Canon BJC4550 [47], Fuji Dimatix DMP-2831 [48], HP Deskjet K7108 [49], Dimatix 2800 series printer [50] and Brother DCP–J140w [51].

When it comes to the selection of a printer, it is important to carefully consider nozzle size and viscosity of the ink. Nozzle size is related to the particle size of the ink as well as its viscosity. In general the inkjet printers require inks with low viscosity (in the range of 10 to 20 mPas) depending upon the printer nozzle used [51]. Using an ink whose viscosity is not compatible with the nozzle size will result in the clogging of the nozzle. The cost and performance of the printer is another factor to consider. One potential problem with low-cost inkjet printers is the resolution of the track that can be printed. For extremely thin lines/tracks, it is hard to achieve uniform thickness and conductivity. A possible solution is to use thick tracks or use printers with nozzle the can eject higher volumes of ink [51]. Another possibility is to use printers with multi-pass printing capability. These printers are able to achieve better conductivity and uniform track width, but they come with a higher price tag.

3.2 Conductive Inks

There are many commercially available metal-based conductive inkjet inks and the choice of selection depends upon the desired properties of the printed patterns. Some of the options include carbon nano-tubes and nano-fibers, silver and gold nano-particle and conductive polymer based inks [47, 52–57]. Each of these inks provides different particle sizes, conductivity and requires different sintering temperature. Silver nano-particle based ink is a common choice because of its high electrical conductivity, stability, and low sintering temperatures. Polymer based inks are used for providing extra flexibility of the printed patterns on flexible substrates [1, 12, 31]. Different solvents are used for ink to make it possible to pass through the printer head and then eject it via nozzle. The properties of printed patterns such as conductivity, resistivity and dielectricity can be controlled by these solvents. In general, for inkjet printing the conductive ink should have the following properties: high electrical conductivity, oxidation resistance, dry out without clogging the nozzle during printing, good adhesion to the substrate, lower particle aggregation and suitable viscosity and surface tension [58].

3.3 Substrates for Inkjet Printing

Inkjet printers can print on a large variety of substrates ranging from rigid substrates to flexible substrates. The selection of substrate for printed electronics depends on the application at hands and the type of interaction desired between the

ink and the surface of the substrate. To achieve better accuracy and long lasting printed structures, it is critical to ensure that both ink and substrates with matching properties are selected. For better adhesion of the ink to the substrate, the substrates may be processed prior to printing. Two of the most widely used options for pre-treatment are plasma treatment and corona treatment to achieve low roughness (this helps in keeping in-place the nano-scale conductive structures printed by the printer), improved ability to absorb ink, and suitable wetting [59]. Different commercially available substrates such as transparent PET films resin coated paper (available for Mitsubishi Paper Mill), glossy photo paper (such as Kodak Premium Photo Paper and Fujifilm Photo paper Kassai Pro) etc. can be used with inkjet printers. In [51] authors reported the use of several commercially available substrates such as canvas cloths, magnet sheets, iron-on transfer sheets, clear label seal, and clear transfer seal.

4 Inkjet-Printed Strain Sensors

Inkjet printers have been shown to be able to print strain sensors [55, 60, 61]. Electro-mechanical properties of the inkjet-printed strain sensors are comparable to the other commercially available strain gauges [62]. It is also possible to print sensor arrays (of strain gauges) using inkjet printing [56]. As mentioned earlier, with inkjet printers, complex patterns can be drawn on a variety of substrate. Inkjet printing technique may help in realizing cost effective and rapid prototyping of wearable systems. Electro-mechanical properties of the sensor can be controlled by selecting inks with different viscosity, conductivity, and flexibility. Wearable sensors which are embedded into the textile or in direct contact with skin can be realized using inkjet printing technology.

In [43][44], a piezo-resistive strain sensor with a track width of 200μm, track spacing of 200μm, and total length of 20mm were printed on the PET substrate with a thickness of 100μm. For printing, an EPSON piezo inkjet printer was used with the tracks printed using silver nano-particles solution “Metalon® JS-B15P” by Novacentrix. Authors in [56], demonstrated the fabrication of a single sensor and sensor arrays by using different conductive inks (ink based on PeDOT and silver ink) to achieve a track width of nearly 40μm. Such inkjet printer strain sensors can be integrated into wearable textile such as gloves to accurately track hand and finger movements [7].

Inkjet printing technology can also be used to print sensors which are directly place on the skin. For direct attachment of the sensor to the skin, it is critical for the printer to be able to print sensors patterns on biocompatible substrates such as Kapton [63–66]. Biocompatible materials can be used in wearable sensors/systems which can measure physiological signals from respiration rate, heart rate, EEG and body movements etc. [67, 68]. In [69], it was shown that the printed strain

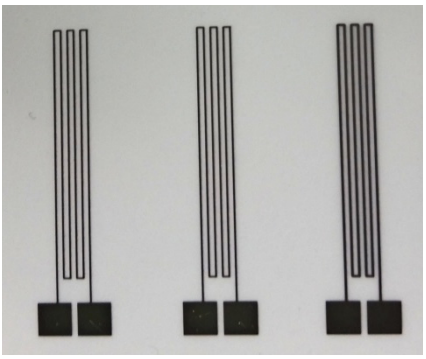

Fig. 8 Strain sensors printed with inkjet printer using silver ink. These sensors are used for monitoring of jaw movements.

gauges can be used for human motion identification such as knee and wrist movements. This strain gauge was made using silver based ink, printed on a flexible substrate using an inkjet printer. Similar to the case of wearable strain sensors, for a printed strain gauge attached to a joint, the resistance changes with joint movement. Fig. 8 shows an example of strain sensors printed with silver ink on a PET substrate using an inkjet printer. These sensors are used to monitor jaw movement during chewing.

5 Other Types of Wearable Strain Sensors

This section discusses a few representative examples of wearable strain sensors which provide similar functionality to the textile based strain sensors and inkjet-printed sensors, but are implemented using other fabrication techniques. For some wearable sensor applications, such as monitoring of the pulse rate, it may be necessary to attach the sensor directly to the skin. Such sensors need to be both flexible and sensitive while satisfying an extra requirement of biocompatibility. Therefore, biocompatible materials such as Kapton are commonly employed in fabrication [64]. Skin attachment is achieved by adhesive medical tape or a bandage. These sensors operate on the same principle as the other reported strain sensors i.e. with deformation of sensor material under the applied force, the resistance of the sensor changes, which produces voltage variations proportional to the applied force. For these sensors, a number of different fabrication techniques are used such as chemical vapor deposition (CVD) [70], dip coating and drying [71] and screen printing [19]. In [70], a flexible and extremely sensitive graphene-based strain sensor was proposed that can be directly attached to the skin. A combination of chemical vapor deposition (for growth of graphene on copper foil substrate) and etching was used to implement graphene-based sensors on a

medical tape. The proposed sensor is able to capture a variety of motions such as hand motions from stretch to clench (relatively large movements), muscle motions at the neck caused by speech, muscle motions during expressions and eye blinking and respiration (relatively small movements). Fig. 9(a) shows sensor response in terms of relative change in resistance to facial expression changes. Each spike represents an expression change such as from “poker face” to a smile or eye blink (Fig 9(b)). In [72] an extremely sensitive ultra-thin gold nano-wires based strain wearable sensor is introduced which is able to monitor the blood pressure of human radial artery in real-time. A dip coating and drying technique [71] was used for deposition of gold nano-wires on the substrate. Such a system can be used to monitor pulse rate in real time under different conditions and can provide vital information about the health conditions of the individual. This sensor was shown to be able to differentiate between pulse rate under normal conditions and after exercise. Similar sensors can be implemented by using conductive materials (for example silver nano-wires [19] deposited by screen printing).

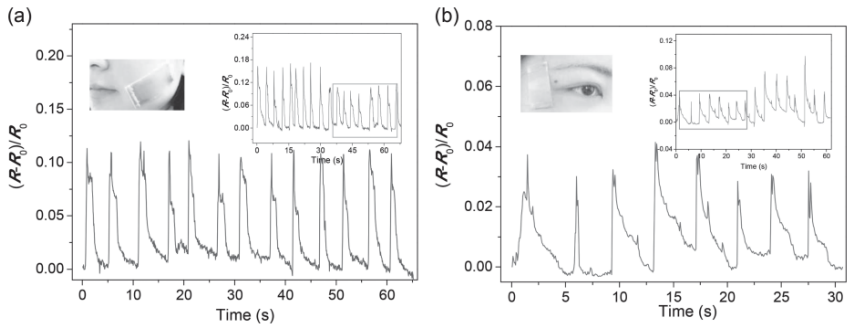

Fig. 9 Graphene based sensor for human movement capture. Relative change of resistance in muscle motions of expression changes and blinks, in (a) and (b), respectively [70].

6 Conclusion

This chapter introduces various techniques that can be used for fabrication of wearable strain sensors and example applications. Strain sensors are becoming an integral part of today's wearable systems. The chapter provides a summary of the state-of-the-art in wearable strain sensors, with a special focus on sensors integrated into textiles and inkjet-printed strain sensors. The described techniques pave the way for broader introduction of the strain sensors into various aspects of wearable technology, especially in the applications aimed at remote monitoring of physiological signals, vital signs, and activity of individuals.

References

1. Gibbs, P.T., Asada, H.H.: Wearable Conductive Fiber Sensors for Multi-Axis Human Joint Angle Measurements. J. NeuroEngineering Rehabil. 2, 7 (2005)
2. Wang, P.T., King, C.E., Do, A.H., Nenadic, Z.: A durable, low-cost electrogoniometer for dynamic measurement of joint trajectories. Med. Eng. Phys. 33, 546–552 (2011)
3. Cho, G., Jeong, K., Paik, M.J., Kwun, Y., Sung, M.: Performance Evalua-tion of Textile-Based Electrodes and Motion Sensors for Smart Clothing. IEEE Sens. J. 11, 3183–3193 (2011)
4. Hoshino, R., Arita, D., Yonemoto, S., Taniguchi, R.: Real-Time Human Motion Analysis Based on Analysis of Silhouette Contour and Color Blob. In: Perales, F.J., Hancock, E.R. (eds.) AMDO 2002. LNCS, vol. 2492, pp. 92–103. Springer, Heidelberg (2002)
5. Koyanagi, M., Shino, K., Yoshimoto, Y., Inoue, S., Sato, M., Nakata, K.: Ef-fects of changes in skiing posture on the kinetics of the knee joint. Knee Surg. Sports Traumatol. Arthrosc. Off. J. ESSKA 14, 88–93 (2006)
6. Tognetti, A., Lorussi, F., Bartalesi, R., Quaglini, S., Tesconi, M., Zupone, G., De Rossi, D.: Wearable kinesthetic system for capturing and classifying upper limb gesture in post-stroke rehabilitation. J. NeuroEngineering Rehabil. 2, 8 (2005)
7. Scilingo, E.P., Lorussi, F., Mazzoldi, A., De Rossi, D.: Strain-sensing fab-rics for wearable kinaesthetic-like systems. IEEE Sens. J. 3, 460–467 (2003)
8. Guo, L., Berglin, L., Wiklund, U., Mattila, H.: Design of a garment-based sensing system for breathing monitoring. Text Res. J. 83, 499–509 (2013)
9. Tarchanidis, K.N., Lygouras, J.N.: Data glove with a force sensor. IEEE Trans. Instrum. Meas. 52, 984–989 (2003)
10. Tognetti, A., Carbonaro, N., Zupone, G., De Rossi, D.: Characterization of a Novel Data Glove Based on Textile Integrated Sensors. In: 28th Annu. Int. Conf. IEEE Eng. Med. Biol. Soc., EMBS 2006, pp. 2510–2513 (2006)
11. Lorussi, F., Scilingo, E.P., Tesconi, M., Tognetti, A., De Rossi, D.: Strain sensing fabric for hand posture and gesture monitoring. IEEE Trans. Inf. Technol. Biomed. 9, 372–381 (2005)
12. Yamada, T., Hayamizu, Y., Yamamoto, Y., Yomogida, Y., Izadi-Najafabadi, A., Futaba, D.N., Hata, K.: A stretchable carbon nanotube strain sensor for human-motion detection. Nat. Nanotechnol. 6, 296–301 (2011)
13. Metcalf, C., Collie, S., Cranny, A., Hallett, G., James, C., Adams, J., Chappell, P., White, N., Burridge, J.: Fabric-based Strain Sensors for Measuring Movement in Wearable Telemonitoring Applications. The Institution of Engineering and Technology, pp. 1–4 (2009)
14. Parashkov, R., Becker, E., Riedl, T., Johannes, H., Kowalsky, W.: Large Area Electronics Using Printing Methods. Proc. IEEE 93, 1321–1329 (2005)
15. Tiberto, P., Barrera, G., Celegato, F., Coïsson, M., Chiolerio, A., Martino, P., Pandolfi, P., Allia, P.: Magnetic properties of jet-printer inks containing dispersed magnetite nanoparticles. Eur. Phys. J. B. 86, 1–6 (2013)
16. Stoppa, M., Chiolerio, A.: Wearable Electronics and Smart Textiles: A Critical Review. Sensors 14, 11957–11992 (2014)

17. Takamatsu, S., Kobayashi, T., Shibayama, N., Miyake, K., Itoh, T.: Fabric pressure sensor array fabricated with die-coating and weaving techniques. Sens. Actuators Phys. 184, 57–63 (2012)
18. Arshak, K.I., McDonagh, D., Durcan, M.A.: Development of new capacitive strain sensors based on thick film polymer and cermet technologies. Sens. Actuators Phys. 79, 102–114 (2000)
19. Yao, S., Zhu, Y.: Wearable multifunctional sensors using printed stretchable conductors made of silver nanowires. Nanoscale 6, 2345–2352 (2014)
20. Park, S., Jayaraman, S.: Enhancing the quality of life through wearable technology. IEEE Eng. Med. Biol. Mag. 22, 41–48 (2003)
21. Feys, H.M., De Weerdt, W.J., Selz, B.E., Cox Steck, G.A., Spichiger, R., Vereeck, L.E., Putman, K.D., Van Hoydonck, G.A.: Effect of a therapeutic inter-vention for the hemiplegic upper limb in the acute phase after stroke: a sin-gle-blind, randomized, controlled multicenter trial. Stroke J. Cereb. Circ. 29, 785–792 (1998)
22. Paolucci, S., Antonucci, G., Grasso, M.G., Morelli, D., Troisi, E., Coiro, P., Bragoni, M.: Early versus delayed inpatient stroke rehabilitation: a matched comparison conducted in Italy. Arch. Phys. Med. Rehabil. 81, 695–700 (2000)
23. Pacelli, M., Caldani, L., Paradiso, R.: Textile piezoresistive sensors for biomechanical variables monitoring. In: Conf. Proc. Annu. Int. Conf. IEEE Eng. Med. Biol. Soc. IEEE Eng. Med. Biol. Soc. Conf., vol. 1, pp. 5358–5361 (2006)
24. Paradiso, R., Loriga, G., Taccini, N.: A Wearable Health Care System Based on Knitted Integrated Sensors. Trans. Info. Tech. Biomed. 9, 337–344 (2005)
25. Giorgino, T., Tormene, P., Lorussi, F., De Rossi, D., Quaglini, S.: Sensor evaluation for wearable strain gauges in neurological rehabilitation. IEEE Trans. Neural Syst. Rehabil. Eng. Publ. IEEE Eng. Med. Biol. Soc. 17, 409–415 (2009)
26. Huang, C.-T., Shen, C.-L., Tang, C.-F., Chang, S.-H.: A wearable yarn-based piezoresistive sensor. Sens. Actuators Phys. 141, 396–403 (2008)
27. Pacelli, M., Loriga, G., Taccini, N., Paradiso, R.: Sensing Fabrics for Monitoring Physiological and Biomechanical Variables: E-textile solutions. In: 3rd IEEEEMBS Int. Summer Sch. Med. Devices Biosens., pp. 1–4 (2006)
28. Scilingo, E.P., Gemignani, A., Paradiso, R., Taccini, N., Ghelarducci, B., De Rossi, D.: Performance evaluation of sensing fabrics for monitoring physio-logical and biomechanical variables. IEEE Trans. Inf. Technol. Biomed. Publ. IEEE Eng. Med. Biol. Soc. 9, 345–352 (2005)
29. Menguc, Y., Park, Y.-L., Martinez-Villalpando, E., Aubin, P., Zisook, M., Stirling, L., Wood, R.J., Walsh, C.J.: Soft wearable motion sensing suit for lower limb biomechanics measurements. In: 2013 IEEE Int. Conf. Robot. Autom. ICRA, pp. 5309–5316 (2013)
30. Lorussi, F., Rocchia, W., Scilingo, E.P., Tognetti, A., De Rossi, D.: Wear-able, redundant fabric-based sensor arrays for reconstruction of body seg-ment posture. IEEE Sens. J. 4, 807–818 (2004)
31. Tognetti, A., Lorussi, F., Mura, G.D., Carbonaro, N., Pacelli, M., Paradiso, R., Ros-si, D.D.: New generation of wearable goniometers for motion capture systems. J. Neuroengineering Rehabil. 11, 56 (2014)
32. Shyr, T.-W., Shie, J.-W., Jiang, C.-H., Li, J.-J.: A textile-based wearable sensing device designed for monitoring the flexion angle of elbow and knee movements. Sensors 14, 4050–4059 (2014)

33. Mazzoldi, D.R.D., Lorussi, F., Scilingo, E.P., Paradiso, R., Paradiso, R.: Smart textiles for wearable motion capture systems. AUTEX Res. J. 2, 199–203 (2002)
34. Tormene, P., Bartolo, M., Nunzio, A.M.D., Fecchio, F., Quaglini, S., Tassorelli, C., Sandrini, G.: Estimation of human trunk movements by wearable strain sensors and improvement of sensor's placement on intelligent bio-medical clothes. Biomed. Eng. OnLine 11, 95 (2012)
35. Yan, C., Wang, J., Kang, W., Cui, M., Wang, X., Foo, C.Y., Chee, K.J., Lee, P.S.: Highly Stretchable Piezoresistive Graphene–Nanocellulose Nanopa-per for Strain Sensors. Adv. Mater. 26, 2022–2027 (2014)
36. Bae, S.-H., Lee, Y., Sharma, B.K., Lee, H.-J., Kim, J.-H., Ahn, J.-H.: Graphene-based transparent strain sensor. Carbon 51, 236–242 (2013)
37. Dickstein, R., Shefi, S., Marcovitz, E., Villa, Y.: Anticipatory postural ad-justment in selected trunk muscles in post stroke hemiparetic patients. Arch. Phys. Med. Rehabil. 85, 261–267 (2004)
38. Kwakkel, G., Wagenaar, R.C., Kollen, B.J., Lankhorst, G.J.: Predicting dis-ability in stroke–a critical review of the literature. Age Ageing 25, 479–489 (1996)
39. Mattmann, C., Clemens, F., Tröster, G.: Sensor for Measuring Strain in Textile. Sensors 8, 3719–3732 (2008)
40. Derby, B.: Inkjet Printing of Functional and Structural Materials: Fluid Property Requirements, Feature Stability, and Resolution. Annu. Rev. Mater. Res. 40, 395–414 (2010)
41. Perelaer, B.J., de Laat, A.W.M., Hendriks, C.E., Schubert, U.S.: Inkjet-printed silver tracks: low temperature curing and thermal stability investigation. J. Mater. Chem. 18, 3209 (2008)
42. Lee, Y., Choi, J., Lee, K.J., Stott, N.E., Kim, D.: Large-scale synthesis of copper nanoparticles by chemically controlled reduction for applications of inkjet-printed electronics. Nanotechnology 19, 415604 (2008)
43. Ando, B., Baglio, S., La Malfa, S., L'Episcopo, G.: All inkjet printed sys-tem for strain measurement. In: 2011 IEEE Sens., pp. 215–217 (2011)
44. Ando, B., Baglio, S.: All-Inkjet Printed Strain Sensors. IEEE Sens. J. 13, 4874–4879 (2013)
45. Lee, H.-H., Chou, K.-S., Huang, K.-C.: Inkjet printing of nanosized silver colloids. Nanotechnology 16, 2436 (2005)
46. Nie, X., Wang, H., Zou, J.: Inkjet printing of silver citrate conductive ink on PET substrate. Appl. Surf. Sci. 261, 554–560 (2012)
47. Kordás, K., Mustonen, T., Tóth, G., Jantunen, H., Lajunen, M., Soldano, C., Talapatra, S., Kar, S., Vajtai, R., Ajayan, P.M.: Inkjet Printing of Electrically Conductive Patterns of Carbon Nanotubes. Small 2, 1021–1025 (2006)
48. Lessing, J., Glavan, A.C., Walker, S.B., Keplinger, C., Lewis, J.A., Whitesides, G.M.: Inkjet Printing of Conductive Inks with High Lateral Resolution on Omniphobic "RF Paper" for Paper-Based Electronics and MEMS. Adv. Mater. 26, 4677–4682 (2014)
49. Huang, L., Huang, Y., Liang, J., Wan, X., Chen, Y.: Graphene-based con-ducting inks for direct inkjet printing of flexible conductive patterns and their applications in electric circuits and chemical sensors. Nano Res. 4, 675–684 (2011)
50. Dang, M.C., Dang, T.M.D., Fribourg-Blanc, E.: Inkjet printing technology and conductive inks synthesis for microfabrication techniques. Adv. Nat. Sci. Nanosci. Nanotechnol. 4, 15009 (2013)

51. Kawahara, Y., Hodges, S., Cook, B.S., Zhang, C., Abowd, G.D.: Instant Ink-jet Circuits: Lab-based Inkjet Printing to Support Rapid Prototyping of UbiComp Devices. In: Proc. 2013 ACM Int. Jt. Conf. Pervasive Ubiquitous Comput., pp. 363–372. ACM, New York (2013)
52. Mustonen, T., Kordás, K., Saukko, S., Tóth, G., Penttilä, J.S., Helistö, P., Seppä, H., Jantunen, H.: Inkjet printing of transparent and conductive patterns of single-walled carbon nanotubes and PEDOT-PSS composites. Phys. Status Solidi B 244, 4336–4340 (2007)
53. Huang, L., Huang, Y., Liang, J., Wan, X., Chen, Y.: Graphene-based con-ducting inks for direct inkjet printing of flexible conductive patterns and their applications in electric circuits and chemical sensors. Nano Res. 4, 675–684 (2011)
54. Tekin, E., Smith, P.J., Schubert, U.S.: Inkjet printing as a deposition and patterning tool for polymers and inorganic particles. Soft Matter 4, 703 (2008)
55. Al-Chami, H., Cretu, E.: Inkjet printing of microsensors. In: IEEE 15th Int. Mix.-Signals Sens. Syst. Test Workshop, IMS3TW 2009, pp. 1–6 (2009)
56. Correia, V., Caparros, C., Casellas, C., Francesch, L., Rocha, J.G., Lanceros-Mendez, S.: Development of inkjet printed strain sensors. Smart Mater. Struct. 22, 105028 (2013)
57. Cochrane, C., Koncar, V.: Design and Development of a Flexible Strain Sensor for Textile Structures Based on a Conductive Polymer Composite. Sensors 7, 473–492 (2007)
58. Bhushan, B., Luo, D., Schricker, S.R., Sigmund, W., Zauscher, S. (eds.): Handbook of Nanomaterials Properties. Springer, Heidelberg (2014)
59. Inkjet Printing as a Key Enabling Technology for Printed Electronics. In: Sigma-Aldrich, http://www.sigmaaldrich.com/technical-documents/articles/material-matters/inkjet-printing-as.html (accessed February 19, 2015)
60. Valeton, J.J.P., Hermans, K., Bastiaansen, C.W.M., Broer, D.J., Perelaer, J., Schubert, U.S., Crawford, G.P., Smith, P.J.: Room temperature preparation of conductive silver features using spin-coating and inkjet printing. J. Mater. Chem. 20, 543–546 (2009)
61. Sawhney, A., Agrawal, A., Patra, P., Calvert, P.: Piezoresistive Sensors on Textiles by Inkjet Printing and Electroless Plating. Symp. – Smart Nanotex-tiles (2006), doi:10.1557/PROC-0920-S05-04
62. Quintero, J.A.Q., Mancosu, R.D.: Comparison and characterization of a typical strain gage trace against another using the printed method, pp. 1–6 (2010)
63. Dionisi, A., Borghetti, M., Sardini, E., Serpelloni, M.: Biocompatible ink-jet resistive sensors for biomedical applications. In: Proc. 2014 IEEE Int. Instrum. Meas. Technol. Conf., I2MTC, pp. 1629–1633 (2014)
64. Sun, Y., Lacour, S.P., Brooks, R.A., Rushton, N., Fawcett, J., Cameron, R.E.: Assessment of the biocompatibility of photosensitive polyimide for im-plantable medical device use. J. Biomed. Mater. Res. A 90, 648–655 (2009)
65. Rustogi, R., Mill, J., Fraser, J.F., Kimble, R.M.: The use of Acticoat in neo-natal burns. Burns J. Int. Soc. Burn. Inj. 31, 878–882 (2005)
66. Borghetti, M., Sardini, E., Serpelloni, M.: Preliminary study of resistive sensors in inkjet technology for force measurements in biomedical applica-tions. In: 11th Int. Multi-Conf. Syst. Signals Devices, SSD 2014, pp. 1–4 (2014)

67. Borghetti, M., Sardini, E., Serpelloni, M.: Sensorized Glove for Measur-ing Hand Finger Flexion for Rehabilitation Purposes. IEEE Trans. Instrum. Meas. 62, 3308–3314 (2013)
68. Vaughn, C.M., Clemmons, P.: Piezoelectric belts as a method for meas-uring chest and abdominal movement for obstructive sleep apnea diagnosis. Neurodiagnostic J. 52, 275–280 (2012)
69. Calvert, P., Duggal, D., Patra, P., Agrawal, A., Sawhney, A.: Conducting Polymer and Conducting Composite Strain Sensors on Textiles. Mol. Cryst. Liq. Cryst. 484, 291/[657]–302/[668] (2008)
70. Wang, Y., Wang, L., Yang, T., Li, X., Zang, X., Zhu, M., Wang, K., Wu, D., Zhu, H.: Wearable and Highly Sensitive Graphene Strain Sensors for Human Motion Monitoring. Adv. Funct. Mater. 24, 4666–4670 (2014)
71. Brinker, C.J., Frye, G.C., Hurd, A.J., Ashley, C.S.: Fundamentals of sol-gel dip coating. Thin Solid Films 201, 97–108 (1991)
72. Gong, S., Schwalb, W., Wang, Y., Chen, Y., Tang, Y., Si, J., Shirinzadeh, B., Cheng, W.: A wearable and highly sensitive pressure sensor with ultrathin gold nanowires. Nat. Commun. (2014), doi:10.1038/ncomms4132

Probabilistic Estimation of Respiratory Rate from Wearable Sensors

Marco A.F. Pimentel[1], Peter H. Charlton[1,2], and David A. Clifton[1]

[1] Institute of Biomedical Engineering, Department of Engineering Science, Old Road Campus Research Building, University of Oxford, Roosevelt Drive, Oxford, OX3 7DQ, UK
{marco.pimentel,david.clifton}@eng.ox.ac.uk
[2] Department of Biomedical Engineering, King's College London, London, SE1 7EH, UK
peter.charlton@gstt.nhs.uk

Abstract. Respiration rate (RR) is a physiological parameter that is typically used in clinical settings for monitoring patient condition. Consequently, it is measured in a wide range of clinical scenarios, notably absent from which is measurement using wearable sensors. With increasing numbers of patients being monitored via wearable sensors, as described below, there is an urgent need to be able to estimate RR from such sensors in a robust manner. In this chapter, we describe a novel technique for measuring RR using waveform data acquired from wearable sensors.

The technique derives RR from a physiological signal which is routinely acquired by many mobile sensors: the photoplethysmogram (PPG). Each RR measurement from the proposed method is accompanied by a confidence measure, providing estimates of clinical quality that will allow the system to, for example, only report RR values when they exceed some probabilistic level of certainty. The goal of this method is to improve upon existing methods, which simply report RR values without probabilistic estimation, and which therefore suffer the lack of robustness that prevents their use in clinical practice.

1 Introduction

The value of measuring RR is demonstrated by its use in a wide range of clinical scenarios. It is routinely measured from acutely-ill patients in the emergency department [6], the intensive care unit [14], and in hospital ward settings [29]. Furthermore, RR is used to assist in the diagnosis of specific diseases, including pneumonia [13] and sepsis, [34], and with physiological conditions such as hypercarbia [5] and pulmonary embolism [9]. Measurement of RR using mobile sensors in hospitals would allow this clinically-significant quantity to be measured more frequently, allowing earlier identification of changes which may be indicative of acute deterioration. In the monitoring of patients in their own home, robust estimation of RR would assist with the

S.C. Mukhopadhyay (ed.), *Wearable Electronics Sensors,*
Smart Sensors, Measurement and Instrumentation 15, DOI: 10.1007/978-3-319-18191-2_10

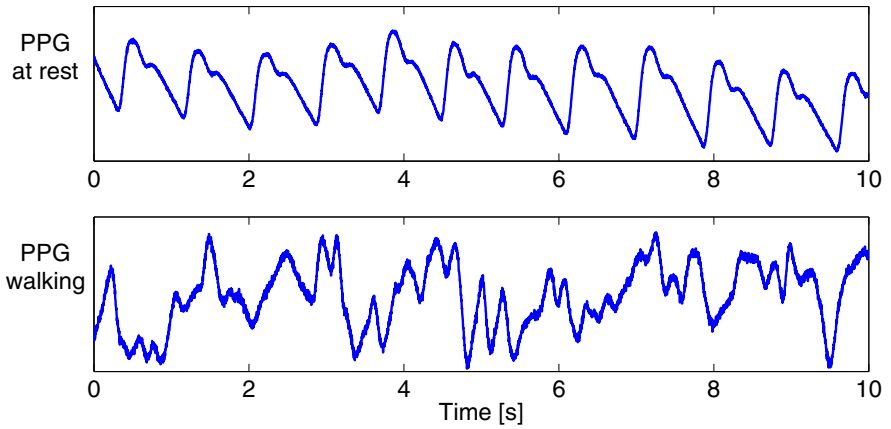

Fig. 1. PPG signals recorded from a healthy volunteer at rest and whilst walking, demonstrating the susceptibility of signals acquired using mobile sensors to movement artefact

management and monitoring of chronic diseases and postoperative rehabilitation [27]. Despite the importance of RR in assessing the physiological state of ambulatory patients, mobile sensors do not commonly measure RR.

A potential solution is to estimate RR from a physiological signal that is both routinely acquired by mobile sensors, and which is modulated by respiration. The electrocardiogram (ECG), PPG, and torso-mounted accelerometry signals are three such signals. All three signals are already acquired by mobile sensors for other purposes: (i) the ECG is used to monitor the heart rate, and to detect cardiac arrhythmias; (ii) the PPG is acquired during pulse-oximetry monitoring for measuring arterial blood oxygen saturation; and (iii) the accelerometry signal may be used for activity classification. In this paper, we consider the PPG signal for demonstrating the utility of our proposed probabilistic technique for estimating RR.

The strength of this probabilistic approach is that it provides RR estimates accompanied by a confidence measure. This is of particular utility for two reasons: firstly, a measure of the confidence of an RR estimate can be used to mitigate against the effect of noise on the final RR estimate. This is particularly relevant in the ambulatory setting where signals are highly susceptible to noise due to movement artefact, as illustrated in Figure 1, or to sensors becoming partially detached. Secondly, individual estimates from multiple sources or sensors can be subsequently *fused* according to their associated confidence measures, leading to a more robust final estimate. The latter is important for ensuring that the technique can be used widely, with varying patient groups, since the level of respiratory modulation of physiological signals may differ between those groups.

2 Extraction of Respiratory Rate from Wearable Sensors

A plethora of techniques have been developed to estimate RR from PPG, ECG and accelerometry signals. In this section, we firstly describe the physiological mechanisms by which these signals are modulated by respiration. Secondly, the structure of algorithms for estimation of RR from these signals is presented. Finally, techniques which have been commonly used in algorithms for the estimation of RR are described.

2.1 Physiological Basis of Respiratory Modulation

Accelerometers can be used to capture signals modulated by respiration when appropriately positioned over the diaphragm [10]. The accelerometer's orientation is changed by chest wall expansion and contraction during respiration. Thus, the direction of the force due to gravity acting on the accelerometer changes with respiration, modulating the signal.

In contrast, several different physiological mechanisms cause modulation of the PPG and ECG with respiration. We have previously described the mechanisms by which respiration modulates the PPG [21], although these are not fully understood. It is influenced by changes in venous return and stroke volume caused by changing intrathoracic pressure during respiration, changes in tissue volume due to varying arterial pressure, and respiratory sinus arrhythmia[1]. These result in amplitude modulation (AM), baseline wander (BW, also known as respiratory-induced intensity variation), and modulation of beat-to-beat intervals (frequency modulation, FM), respectively. The ECG is modulated by respiration [3] due to: (i) changing orientation of the electrical axis of the heart relative to the electrodes; (ii) changing thoracic impedance (although this is secondary to changes in axis orientation); and, (iii) RSA. The first two mechanisms result in AM and BW, while the latter results in FM. The respiratory modulations exhibited by ECG and PPG signals are illustrated in Figure 2.

The magnitude of each respiratory modulation may differ between patients. For instance, [17] evaluated the correlation of each modulation of the PPG with the respiratory cycle, and showed that no modulation is consistently optimal for respiratory monitoring across subjects. The correlation performance was found to be dependent on many factors including gender, age and body position. This finding suggests that, where multiple modulations are present in the PPG and ECG, more robust estimation of RR could be achieved by harnessing the information available provided by each modulation.

[1] RSA, which is variation in heart rate with respiration [15]

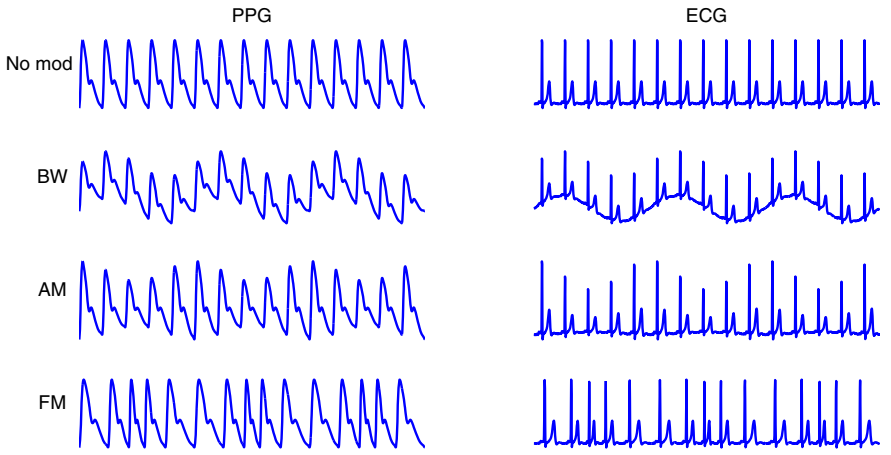

Fig. 2. Idealised respiratory modulations of the PPG (left hand side) and ECG (right hand side). During three respiratory cycles, from top: no modulation, baseline wander (BW), amplitude modulation (AM), and frequency modulation (FM). Adapted from [1].

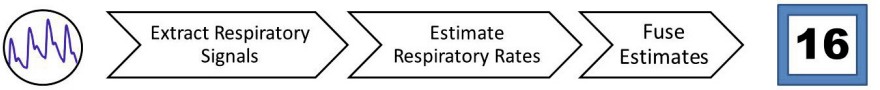

Fig. 3. The key components of an algorithm for estimating RR

2.2 The Structure of Algorithms for Estimating Respiratory Rate

Many algorithms for estimating RR from mobile sensor signals have been proposed in the literature. The algorithms consist of three key components, as illustrated in Figure 3. The role of each component is as follows:

- **Extract Respiratory Signals:** Time series exhibiting respiratory modulation are extracted from the raw physiological signal;
- **Estimate RRs:** Estimate a RR from each respiratory signal;
- **Fuse RR Estimates:** If multiple RR estimates are obtained, then these can be fused to obtain one estimate.

2.3 Extraction of Respiratory Signals

The first component of an algorithm for estimation of RR is extraction of a respiratory signal, or signals. This extracts the respiratory modulation from

the more complex, raw signal. For instance, a tri-axial accelerometer provides three measurements of the acceleration of a device using an orthogonal axis system. The component required for analysis is the direction of the acceleration due to gravity in the accelerometer's co-ordinate system, which is modulated by respiration. To obtain a respiratory signal, firstly a single, time-varying, acceleration vector is derived from the three measurements. Secondly, the rotation angle of the acceleration vector about the time-averaged predominant axis of rotation is calculated [4]. Lastly, the respiratory signal is given by the angular velocity - the rate of change of the rotation angle with respect to time. The predominant axis of rotation is calculated over an extended time period to reduce the effect of noise, which is of particular importance in mobile monitoring.

Several techniques have been proposed for extracting respiratory signals from the ECG and PPG. The techniques can often be applied to both signals since they are both primarily cardiac in origin, with secondary respiratory modulations of much lower magnitude. The techniques fall into two categories: feature- and filter-based extraction techniques. Feature-based extraction of a respiratory signal consists of the extraction of a time series of beat-by-beat feature measurements. Beat detection is typically performed using a segmentation algorithm (such as that proposed by [16] for PPG signals or that proposed by [26] for ECG signals). AM is commonly extracted by measuring the pulse peak-to-trough amplitude; FM is extracted by measuring beat-to-beat intervals (between consecutive fiducial points such as pulse peaks), and a composite of AM and BW is extracted by measuring pulse peak amplitudes. Filter-based extraction consists of filtering the raw signal to attenuate non-respiratory frequency components. BW is commonly extracted using band-pass filtering to eliminate frequencies outside the range of plausible respiratory frequencies. A respiratory signal influenced by all three modulations has been extracted by filtering using the centred correntropy function (CCF). This function incorporates information from both the time structure and statistical distribution of a signal. Exemplary signals extracted using feature- and filter-based approaches are shown in Figure 4.

2.4 Estimation of Respiratory Rate

Several methods have been proposed for estimating the RR from a window of data from a respiratory signal. This can be performed in both the time- and the frequency-domain, although frequency-domain techniques are most commonly used, four of which are now described.

Frequency-domain techniques typically require evenly sampled data. Consequently, respiratory signals derived using feature-based analysis must usually be re-sampled onto an even grid prior to frequency-domain analysis (see Figure 6).

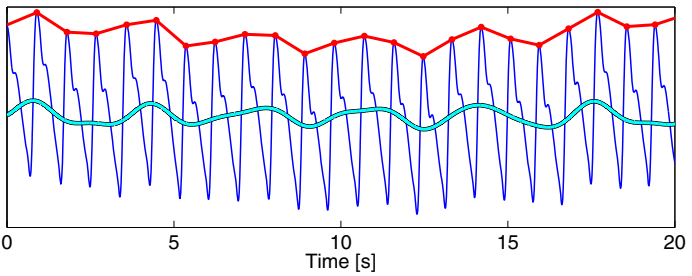

Fig. 4. Comparison of feature- and filter-based techniques for extraction of respiratory signals. Baseline wander (BW) signals have been extracted from the PPG using a feature-based technique (red) in which pulse peak amplitudes are extracted, and a filter-based technique (cyan) in which a band-pass filter with cut-off frequencies of 0.2 and 0.6 Hz (12 and 36 rpm).

Fourier analysis has been used to calculate the frequency spectra of respiratory signals, from which the RR can be estimated [8]. However, this technique does not perform well when RR is non-stationary across the window of data analysed. The short-time Fourier transform (STFT) has been proposed to improve the accuracy of RR estimation in the presence of non-stationarity [32]. In their application of the technique, Shelley *et al.* analysed the raw PPG signal using the STFT and a moving Hann window of 82 s duration. This approach is illustrated in Figure 5.

Autoregressive (AR) modelling has been used to identify the resonant frequencies contained within a respiratory signal. The poles generated by the ("all-pole" filter) model correspond to resonant frequencies, where the frequency is determined by the pole's phase angle. The respiratory pole (and accompanying frequency) can be identified as the pole with the greatest magnitude within the plausible range of respiratory frequencies. Alternatively, AR modelling can be used to calculate the power spectral density (PSD) of a respiratory signal. This is related to the analysis of the model's poles, since each pole provides a contribution to the PSD, centred on its resonant frequency [20]. The size of this contribution is determined by the pole's magnitude.

For all techniques except analysis of the poles of an AR model, a frequency spectrum is obtained. The respiratory frequency is typically identified from the spectrum as the frequency corresponding to the maximum spectral power.

2.5 Fusion of Respiratory Rate Estimates

The final step of estimating the RR from a physiological signal is to fuse estimates derived from multiple respiratory signals. Two recently proposed methods are considered here. The simplest method of fusing multiple RR estimates is to calculate the average. Karlen *et al.* used this approach,

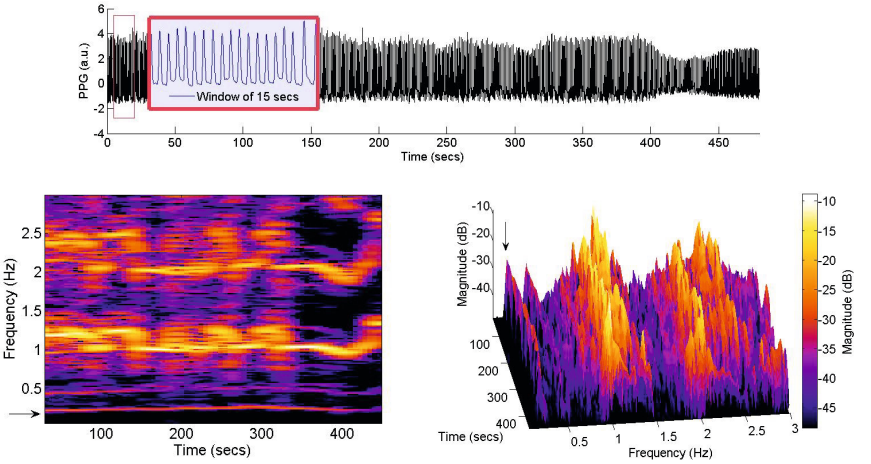

Fig. 5. Example of a full 8-minute record of PPG (on top) used for RR estimation (a 15-second segment of the signal is highlighted as indicated in the red box). The time-frequency spectrum, calculated using the short-time Fourier transform (STFT), is represented on the bottom-left. The frequency band corresponding to the respiratory rate (indicated by an arrow) is observed (at 0.18 Hz = 10.8 rpm), and is practically constant throughout the record. The corresponding magnitude of this band may be better observed in the 3D representation of the time-frequency spectrum on the bottom-right. This also shows the overwhelming signal strength for the heart rhythm at approximately 1.1 Hz.

obtaining the final estimate as the mean of the individual estimates [11]. They also extended this approach by including a quality assessment check. Any set of estimates with a standard deviation of more than 4 rpm was eliminated, and no RR estimate was obtained from that window of data.

A further method was proposed by Orphanidou *et al.* , which fuses RR estimates derived from the poles of an AR model [25]. Poles outside of 0.1 - 0.6 Hz (6 - 36 rpm) are excluded from the analysis. The remaining pole with the greatest magnitude is identified for each respiratory signal, and any poles which have a magnitude of less than 95% of this pole's magnitude are rejected. The candidate respiratory pole for each signal is then identified as the pole with the lowest corresponding frequency. The final RR estimate is the frequency corresponding to the candidate pole with the greatest magnitude.

3 A Probabilistic Approach

The main drawback of the approaches discussed above is that they provide a point estimate of the respiratory rate. The uncertainty associated with the

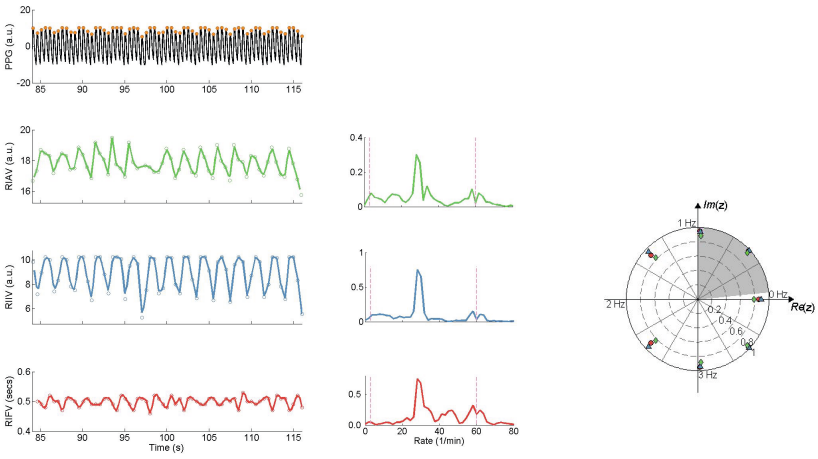

Fig. 6. Example of a 32 secs PPG sliding window (represented with black line on the top-left corner) used for RR estimation using two different methods. RIAV (top, in green), RIIV (middle, in blue), and RIFV (bottom, in red) are extracted and resampled to 4 Hz (left column). In the method proposed by [11], the power spectrum is calculated for each modulation using FFT (middle column), and the maximum power is selected within a physiologically expected RR range (dashed vertical lines). In the method proposed by [25], the poles from each modulation are determined using an autoregressive model, order $p = 7$ (right column), and the dominant pole within the possible range of RR (shown in grey) gives the "fused" estimate.

estimated value cannot be directly quantified, due to the nature of the algorithms employed. Specifically, the "fusion" approach of the estimates derived from the different modulations lack validity, and may reduce significantly the number of windows for which a final estimate of RR is computed [11, 8].

The failure of existing methods to estimate RR accurately using data from actual patients, rather than from healthy volunteers, motivates the use of a probabilistic approach. We propose a method that uses the framework of Gaussian process regression to extract RR from the different sources of modulation in the PPG signal. This brings all of the advantages of a principled, probabilistic approach: our uncertainty in the estimation may be directly quantified; incompleteness, noise, and artefact may be handled in a robust manner; and the output may consist of a predictive posterior distribution, rather than a single estimate - this is useful if the estimate of the respiratory rate is to be used as the input to a subsequent probabilistic inference system, where knowing the full distribution of the input is more informative than a point estimate. Finally, due to the generative nature of the approach, it is possible to generate data from the model, which can be useful for both

estimating the behaviour of RR during periods of missing data, and making predictions.

3.1 Gaussian Process Regression

In this section, we provide a brief summary of Gaussian processes for regression. It therefore makes a rather compressed introduction to the topic. A more thorough introduction is available in [28].

When performing a regression task we assume there exists some optimal prediction function $f \in \mathcal{X} \to \mathcal{Y}$, possibly with a noise distribution. In linear regression, we may assume that the outputs y are a linear function of the inputs $\mathbf{x}$, with some parameters θ, often much smaller than the number of training examples N, such that $|\theta| \ll N$. However, for many real-world data sets a simple parametric form, such as a linear form, is an unrealistic assumption. Therefore, we would like to have models that can learn general functions f. Since the functions may not be summarised by a small (fixed) number of parameters θ, maximum likelihood estimation of the parameters typically causes severe overfitting. Therefore, in order to perform inference and make predictions in a probabilistic framework, we must place a prior probability distribution on functions. We make predictions using our posterior on an underlying predictive function f given a set of training examples in the form of input-output pairs: $\mathcal{D} = \{(\mathbf{x}_i \in \mathbb{R}^D, y_i \in \mathbb{R})\}_{i=1}^N$.

Gaussian processes provide a distribution over real-valued functions which is widely used for non-linear regression and classification tasks [28]. By definition, a function $f : \mathcal{X} \to \mathbb{R}$ is distributed according to a Gaussian process if and only if $p(f(\mathbf{x}_1), ..., f(\mathbf{x}_N))$, the density of those function's values at any N points $\mathbf{x}_i \in \mathcal{X}$, is jointly Gaussian. This allows Gaussian processes to be tractably parameterised by a mean function $m(\mathbf{x})$ and a covariance kernel function giving the entries of matrix $\mathbf{K}(\mathbf{x}_i, \mathbf{x}_j)$ and which specifies the correlations within any finite point set. This yields

$$\mathbf{y} = f(\mathbf{x}) \sim \mathcal{GP}\Big(m(\mathbf{x}), \mathbf{K}(\mathbf{x}_i, \mathbf{x}_j)\Big), \tag{1}$$

with possibly some Gaussian observation noise. Note that the covariance matrix $\mathbf{K}$, or Gram matrix, whose entries $\mathbf{K}_{ij}$ are often thought of as the "similarity" between inputs $\mathbf{x}_i$ and $\mathbf{x}_j$, encodes our prior knowledge concerning the functional behaviour we wish to model.

Without loss of generality, the prior mean function is typically set to zero: $m(\mathbf{x}) = 0$. A commonly-used covariance function is the squared-exponential,

$$k_{SE}(\mathbf{x}_i, \mathbf{x}_j) = \sigma_0^2 \exp\left(-\frac{\| \mathbf{x}_i - \mathbf{x}_j \|^2}{2\ell^2}\right), \tag{2}$$

where σ_0 and ℓ are hyperparameters modelling the y-scaling and x-scaling (or time-scale if the data are timeseries), respectively, and where $\| \cdot \|$

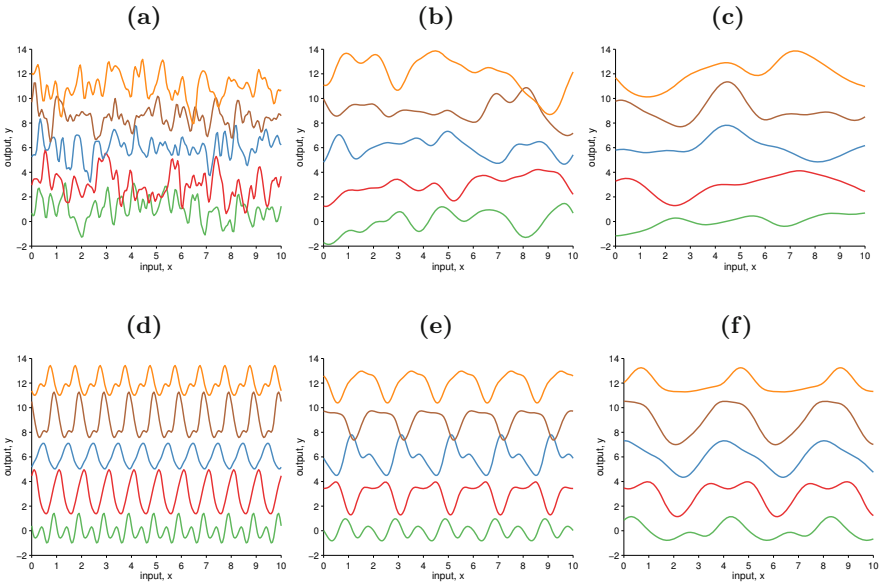

Fig. 7. (a-c) Functions drawn from a Gaussian process with a squared-exponential covariance function (zero-mean) with $\sigma_0 = 1$ and $\ell = 0.1$ (a), 0.5 (b), and 1 (c); (d-f) Functions drawn from a Gaussian process with a periodic covariance function (zero-mean) with $\sigma_0 = 1$, $\ell = 0.5$, and $T = 1$ (d), 2 (e), and 4 (f).

denotes the Euclidean norm. The squared-exponential covariance function is said to be *stationary* because it only depends on the difference between points $\mathbf{x}_i - \mathbf{x}_j$ (see Figure 7). In general, covariance functions have to fulfill Mercer's theorem, meaning that $\mathbf{K}(\mathbf{x}_i, \mathbf{x}_j)$ has to be symmetric and positive semidefinite, and therefore $k_{SE}(\cdot, \cdot)$ is a valid kernel. Many mathematical operations, such as the summation or the product, preserve positive definiteness and can therefore be used for combining "old kernels" to make "new kernels". Also, note that a valid covariance function under any arbitrary (smooth) map remains a valid covariance function. An interesting example of this mapping is given in [19], where the one-dimensional input variable x is mapped to the two-dimensional $\mathbf{u}(x) = (\cos(x), \sin(x))$ to give rise to a periodic random function of x. Using the squared-exponential kernel in $\mathbf{u}$-space, yields

$$k_{Per}(x_i, x_j) = \sigma_0^2 \exp\left(-\frac{1}{2\ell^2}\sin^2\left(\pi\left|\frac{x_i - x_j}{T}\right|\right)\right), \tag{3}$$

Here, the "extra" hyperparameter T corresponds to the period (see Figure 7). A survey of several covariance functions is given in [28, Chapter 4].

Given a training set $\mathcal{D}$, using the standard conditioning rules for a Gaussian distribution, we can obtain the predictive distribution on a new observation y_* at test input $\mathbf{x}_*$:

$$\begin{bmatrix} \mathbf{y} \\ y_* \end{bmatrix} = \mathcal{N}\left(\begin{bmatrix} 0 \\ 0 \end{bmatrix}, \begin{bmatrix} \mathbf{K} & \mathbf{K}_* \\ \mathbf{K}_*^\top & \mathbf{K}_{**} \end{bmatrix} \right) \tag{4}$$

implying

$$p(y_*|\mathbf{x}_*, \mathbf{X}, \mathbf{y}) \sim \mathcal{N}(\mu_*, \sigma_*^2), \text{ with} \tag{5}$$

$$\mu_* = \mathbf{K}_*^\top \mathbf{K}^{-1} \mathbf{y} \ \in \mathbb{R}, \tag{6}$$

$$\sigma_*^2 = \mathbf{K}_{**} - \mathbf{K}_*^\top \mathbf{K}^{-1} \mathbf{K}_* \ \in \mathbb{R}^+. \tag{7}$$

Here, $\mathbf{K}_* = k(\mathbf{X}, \mathbf{x}_*) \in \mathbb{R}^{N+1}$ is the cross-covariance between the test input $\mathbf{x}_*$ and the training inputs $\mathbf{X}$; $\mathbf{K}_{**} = k(\mathbf{x}_*, \mathbf{x}_*) \in \mathbb{R}^+$ is the prior variance of the test point.

The values of the hyperparameters $\boldsymbol{\theta}$ may be optimised by, for example, minimising the negative log marginal likelihood (NLML) which is defined as

$$\begin{aligned} \text{NLML} &= -\log p(\mathbf{y}|\mathbf{x}, \boldsymbol{\theta}) \\ &= \frac{1}{2}\log|\mathbf{K}| + \frac{1}{2}\mathbf{y}^\top \mathbf{K}^{-1}\mathbf{y} + \frac{N}{2}\log(2\pi) \end{aligned} \tag{8}$$

This is sometimes called the type-II maximum likelihood (if we remove the negative logarithm). Interpreting the NLML as a cost function reveals that the first term penalises model complexity and the second term penalises low data likelihood (i.e., low data fitness). Bias-variance trade-off is therefore performed by minimising the NLML, which is commonly achieved using gradient descent.

A full Bayesian treatment of GP regression requires integration over the posterior distribution of the hyperparameters. Even though most calculations in the GP regression framework are analytically tractable, the integral over the posterior of the hyperparameters often is not [28]. The integration over the posterior of the hyperparameters $p(\boldsymbol{\theta}|\mathcal{D})$, with $\boldsymbol{\theta} = \{\sigma_0, \lambda, P_L, \varepsilon\}$, can be approximated by a point via the *maximum a posteriori* (MAP) estimate

$$\begin{aligned} \hat{\boldsymbol{\theta}} &= \arg\max_{\boldsymbol{\theta}} p(\boldsymbol{\theta}|\mathcal{D}) \\ &= \arg\min_{\boldsymbol{\theta}} \Big[-\log p(\mathcal{D}|\boldsymbol{\theta}) - \log p(\boldsymbol{\theta}) \Big] \end{aligned}$$

In this approximation, the distribution over the hyperparameters is assigned a point mass at the mode of the posterior, allowing the marginal distribution of the latent function to be approximated by $p(f|\mathcal{D}) \approx p(f|\mathcal{D}, \hat{\boldsymbol{\theta}})$. This approach is computationally attractive. The grid search approximation

to the full integral over the posterior distributions of the hyperparameters follows the work of Rue *et al.* [30], in which the posterior mode $\hat{\theta}$ is first located by maximising the log-posterior distribution $\log p(\theta|y)$, and the shape of the log-posterior is approximated with a Gaussian, the covariance of which is the inverse of the negative Hessian at the mode (more details may be found in [28, 30]).

3.2 Proposed Method

Using the Gaussian process framework described above, we propose a method for "fusing" the estimates from the different modulations exhibited by the PPG. In the first step, for a given window of the signal, the (unevenly-sampled) time-series data corresponding to the BW, AM, and FM are extracted using a segmentation algorithm (note that no interpolation is performed). A Gaussian process with a periodic covariance function is then fitted to each of the timeseries, using the procedure described above to obtain an estimate of both the value and uncertainty of the respiratory rate value (which is determined directly from the distribution over the period, T). After converting the period T to RR ($60/T$), this results in three (uncertain) estimates of RR, given by $\mu_k \pm \sigma_k$, with $k = \{1, 2, 3\}$.

In order to combine the three estimates into a final RR estimate μ, a weighted average is employed (as described in [33]), as such

$$\mu = \mu_o \pm \left(\sum_{k=1}^{3} w_k \right)^{-1/2} \tag{9}$$

with

$$\mu_o = \sum_{k=1}^{3} w_k \mu_k \Big/ \sum_{k=1}^{3} w_k, \quad \text{where} \;\; w_k = \frac{1}{\sigma_k^2}. \tag{10}$$

Rather than the best estimate being given by the arithmetic mean of the RR estimates, the weighted average of the RR estimates is determined and taken as the final estimate of RR for that window. Less reliable estimates will have larger variances σ_k^2 and correspondingly smaller weights w_k.

4 Materials and Methods

In order to evaluate the performance of the proposed approach, described above, we have implemented state-of-the-art methods using the methods described according to each paper. The pre-processing stages are detailed be-

low. The source code of the implementations of the methods described in this study (as well as the data sets used) are available for download[2].

4.1 Datasets

For the analysis described in this experiment we used two independent, publicly available datasets: the Capnobase benchmark dataset[3], and a dataset extracted from the MIMIC II database[4].

4.1.1 CapnoBase Dataset

The CapnoBase dataset, described in [12], consists of ECG and PPG recordings, and capnometry data, all recorded using a sampling frequency of 300 Hz, from 59 children (median age: 8.7, range: 0.8-16.5 years) and 35 adults (median age: 52.4, range: 26.2-75.6 years). The cases in the dataset were randomly selected from a larger collection of physiological signals collected during elective surgery and routine anaesthesia. In the work reported in [11], the CapnoBase dataset was divided into a test set consisting of forty-two 8-minute segments (336 minutes in total) containing reliable recordings of spontaneous or controlled breathing, and a calibration set consisting of one hundred twenty-four 2-minute segments (248 minutes) from the remaining 52 cases. As in [11], the test dataset (forty-two 8-minute segments) was considered for analysis.

4.1.2 MIMIC II Dataset

The dataset extracted from the MIMIC II database [31] comprises PPG recordings and respiration signals acquired using the conventional impedance plethysmogram (IP), both sampled at 125 Hz, from 53 adults (median age: 64.8, range: [19-90+], 32 females). The cases in the dataset were extracted from a larger cohort of patients who were admitted to medical and surgical intensive care units at the Beth Israel Deaconess Medical Center, Boston, MA. As in the previous dataset, 8-minute segments containing reliable recordings of spontaneuous breathing were randomly selected.

4.2 Data Preparation

The recordings from both databases were grouped into different age groups, according to the age of the patient from which the recordings were taken (see Figure 8). Forty-one 8-minute recordings from the CapnoBase database and fifty-two 8-minute recordings from the MIMIC II database were included in

[2] To appear at `http://www.robots.ox.ac.uk/~davidc/`
[3] Available at `http://www.capnobase.org`
[4] Available at `https://mimic.physionet.org/`

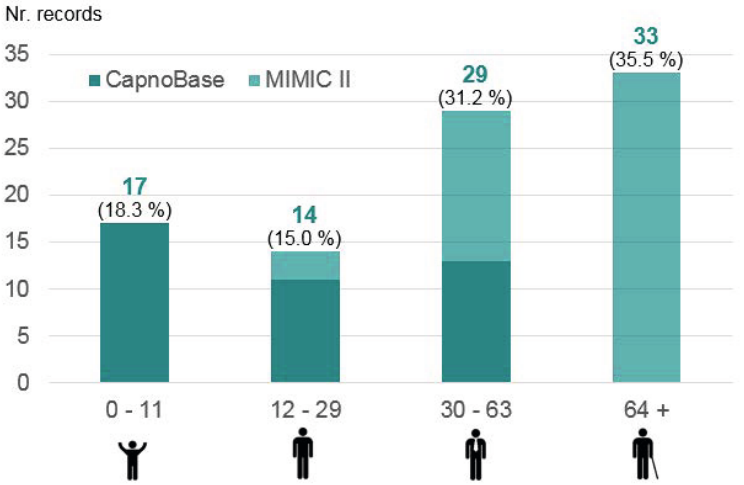

Fig. 8. Number of records available in the CapnoBase and MIMIC II databases for each age group

this analysis, as the age associated to two recordings (one from each database) was not available. All signals were re-sampled to 125 Hz. For the work described in this study, respiratory rate was computed for a single window size: 32-second windows, with successive windows having 29 seconds overlap. This window size was selected as it did not need zero padding (for frequency-based analysis) and was within reasonable physiological and clinical limits (as discussed in [7, 11]). For all methods described above, RR was estimated within the plausible range of respiratory frequencies set to 0.05-1 Hz, or 3-60 rpm. The estimated RR values from the PPG recordings were compared with the reference respiratory rate obtained from the reference gold standard recordings in each database.

In the CapnoBase dataset, the capnometric waveform was used as the reference gold standard recording for RR. Each breath in the capnogram has been manually labelled by a research assistant, and the annotations were used to derive the reference values. For each window, the time between consecutive exhalations and between consecutive inhalations was calculated. The median value was used to determine the reference RR for that window.

In the MIMIC II dataset, because of the absence of manually annotated data, we calculated the reference respiratory rate from the IP signal as follows. The respiration signal was first down-sampled to 4 Hz and then filtered using a 0.1-0.6 Hz finite-impulse response band-pass filter. For each window of the filtered signal, two RR estimates were calculated using two different algorithms. The first algorithm applied was a 3-point peak detector algorithm (outlined below), which was used to determine the first estimate of RR.

The second algorithm involved converting the filtered signal to the frequency domain using the fast Fourier transform. The resulting power spectrum was analysed for the frequency with maximum power within the expected respiratory frequency range, and the second RR estimate was obtained. Only those window sections of data for which the agreement between both estimates (provided by the two algorithms) was within 2 rpm were retained, and the mean value of the two estimates was taken as the reference RR. As a result, for a window size of 32 seconds, 93% of all available windows were deemed to be "valid". This approach ensured that only the highest quality reference values were considered by potentially eliminating regions of low IP signal quality.

4.3 Methodology

In our experiments, to extract the three respiratory-induced variations, PPG beat detection was performed using a segmentation algorithm proposed in [16], where a "beat" in this context corresponds to the pulse in the PPG associated with a heartbeat. This processing produces a series of maximum and minimum intensities for each pulse detected. The series of maximum intensities of the PPG pulses was used for extracting the BW timeseries. The amplitude of the resulting series of beats was determined (as the difference between the peaks and onsets of the beats) in order to derive the AM timeseries. The intervals between successive beats (which corresponds to the pulse period) was also calculated to extract the FM timeseries.

4.3.1 Methods

We compared the performance of the proposed approach with that of four other methods, which are described below.

Method 1. The first method is based on the approach proposed in [11], which, as described above, uses Fourier analysis to calculate the frequency spectra of the derived respiration signals. Because spectral analysis requires evenly sampled data, each timeseries (corresponding to BW, AM and FM) is first re-sampled onto an even 4-Hz grid using linear interpolation. The frequency at which the maximum intensity of each spectrum is obtained, is taken as the respiratory frequency. The final RR estimate is obtained as the mean of the three estimates, and any set of estimates with a standard deviation of more than 4 rpm is eliminated (i.e., no RR estimate is obtained from that window).

Method 2. This method is based on that described in [25]. After re-sampling the three timeseries onto an even 4-Hz grid using linear interpolation, an AR model (of order 7) is fitted to each timeseries. The resonant frequencies corresponding to the poles generated by the models are then evaluated, and

the respiratory is identified as that corresponding to the pole with the greatest magnitude within the plausible range of respiratory frequencies.

Method 3. In this method (based in [32]), the raw PPG signal is analysed using the STFT and a moving Hann window of 82 seconds, and the time-frequency spectrum is obtained. The frequency component (within the plausible range of respiratory frequencies) with the greatest magnitude in each window is identified as the RR.

Method 4. The fourth method implemented corresponds to the method used in [8], who proposed an algorithm based on the time-varying correntropy spectral density function applied (directly) to the PPG signal. From the correntropy spectral density applied to each signal segment, the heart rate is estimated by detecting the maximum frequency peak within the cardiac frequency band, and filtered from the signal (using a zero-phase 5^{th}-order low-pass filter with a cutoff frequency of 0.1 Hz below the cardiac frequency). The RR is finally estimated by detecting the maximum frequency peak within the respiratory frequency band.

4.3.2 Signal quality index

In order to remove windows of poor PPG signal quality, we employed a signal quality algorithm. Signal quality of the original PPG waveform was assessed using the same method as proposed by Li *et al.* [18]. The overall signal quality is assessed using four measures: three based upon template matching and a fourth based upon flat-line detection. For the template methods, the same beat detector [16] was applied to the PPG signal. The first 10 beats in each signal are assumed to be good quality, and a template is created by averaging windows centered on these 10 beats. For each subsequent beat, the signal quality is assessed using the correlation between the current beat and the template. This correlation is calculated for 1) the original unmodified beat, 2) the beat after a linear detrending, and 3) the beat after dynamic time warping (DTW) [18]. A rule-based approach for assigning signal quality using the above three signal qualities (SQIs 1-3) and the fourth signal quality based on flatline detection (SQI 4), as proposed by Li et al. [18], is used to aggregate the four metrics into a single estimate. The rule is as follows:

$$SQI = \begin{cases} \text{Excellent(E)} & \text{if } \textit{All } 4\ SQI \geq 0.9 \\ & \text{if } \textit{Any } 3\ SQI \geq 0.9 \\ \text{Acceptable(A)} & \text{if } \textit{All } 4\ SQI \geq 0.7 \\ & \text{if } median(SQI_1, SQI_2, SQI_3) \geq 0.8 \\ & \quad \textit{and } SQI_1 \geq 0.5 \textit{ and } SQI_4 \geq 0.7 \\ \text{Unacceptable(U)} & \textit{otherwise} \end{cases}$$

Windows with an "unacceptable" quality were removed, and no RR estimates were obtained for those windows (for any of the methods implemented in this experiment).

4.3.3 Methods Evaluation

The performances of the methods were assessed by calculating the mean absolute error (MAE) in breaths per minute (rpm), $\mathsf{MAE} = \frac{1}{n}\sum_{i=1}^{n} \mid \hat{y_i} - y_{ref,i} \mid$, where n is the number of valid windows over each patient in each age-group, $\hat{y_i}$ is the estimated respiratory rate (μ_o in the case of our proposed method) and $y_{ref,i}$ is the reference respiratory rate for window i.

5 Results

The results obtained with each method are shown in Figure 9. Results are displayed as the average of MAEs for the records included in each age-group. Also, the average number of windows considered in each method are displayed; i.e., the percentage of windows that were not rejected, and, hence, for which an estimate of RR was obtained.

6 Discussion

RR is a valuable physiological parameter which is used in a wide range of clinical scenarios. However, it is not yet commonly measured by wearable sensors. In this chapter we have presented a novel probabilistic technique for estimation of RR from physiological signals which are already acquired by wearable sensors. The technique is set in the framework of Gaussian process regression, whereby each RR estimate is accompanied by a measure of its associated uncertainty. The benefit of quantifying the uncertainty associated with RR estimates is that it allows multiple estimates obtained simultaneously to be fused in a principled manner. The performance of this technique was assessed using data acquired from patients spanning a wide range of ages. The results presented suggest that the technique may confer particular benefit in patients over 30 years old. Further work is required to determine whether use of this technique in mobile sensors would confer clinical benefit.

We have described a generalised structure which can be used to decompose algorithms for estimating RR into their constituent components, based that described in [11]. This structure allows algorithms to be adapted to estimate RR from any signal which is modulated by respiration. The first component, extraction of respiratory signals, should be adapted to the input signal. For instance, feature-based extraction methods should be tailored to the input signal to ensure correct beat detection and identification of fiducial points each cardiac cycle. However, once respiratory signals have been extracted, the remainder of an algorithm can be applied unchanged, regardless of the input

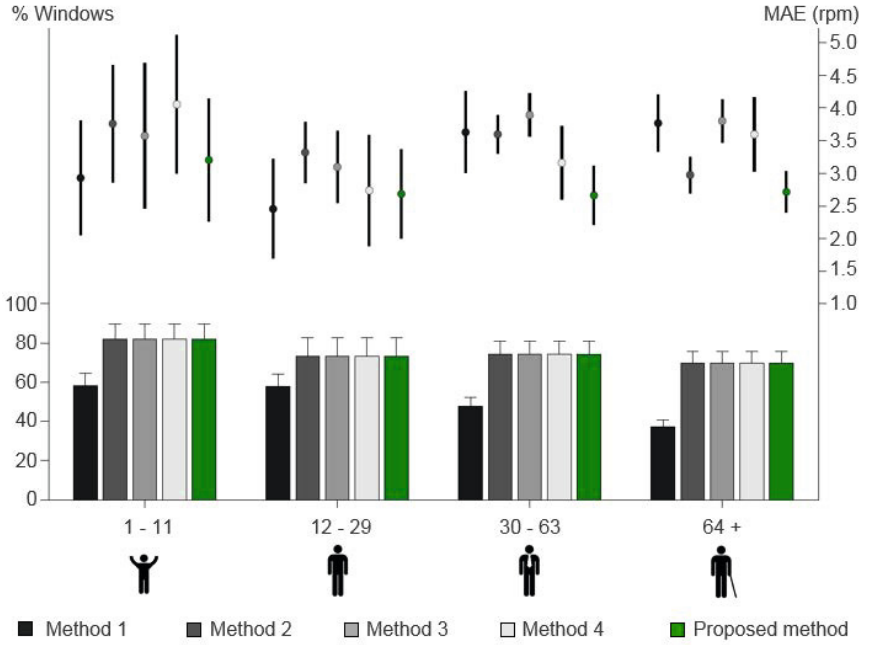

Fig. 9. Results obtained for the different methods: bars denote the average percentage of windows considered in each method (refer to axes on the left) and points denote the mean absolute error (refer to axes on the right). Error bars denote one standard error of the mean.

signal. The GP-based algorithm presented here uses a common approach for extraction of respiratory signals corresponding to BW, AM and FM, as described in [11]. The remainder of the algorithm, in which RR estimates are obtained from each respiratory signal, and multiple estimates are fused to provide a single estimate, could be applied to other signals acquired by wearable sensors such as ECG and accelerometry signals.

The proposed method of fusing multiple RR estimates based on their uncertainties has been designed to facilitate robust estimation of RR across a wide range of patient groups. The three respiratory modulations of the ECG and PPG are caused by physiological mechanisms which are likely to be affected by the physiological state of patients. Consequently, the magnitude of each modulation is likely to differ between patient groups. For instance, heart rate variability is known to diminish with age [24]. It may therefore be postulated that RSA, the physiological mechanism which causes FM, being closely linked to heart rate variability may also diminish with age. Furthermore, chest expansion is known to be affected by both age and gender [22]. Similarly, this physiological change may be expected to affect the magnitudes

of BW and AM. The effect of physiological factors on the magnitudes of respiratory modulations remains an open research question [23]. However, it is clear that if the magnitudes of modulations do vary between patients, then an adaptable method for fusing estimates derived from each modulation is required. Indeed, the results suggest that this novel technique confers greatest benefit in those patients aged over 30, which may be due to its ability to fuse RR estimates according to their associated uncertainties.

We see three potential directions for future work to translate this novel technique into clinical practice. Firstly, the approach to signal quality assessment, performed here using a signal quality algorithm, could be enhanced. Simply put, signal quality algorithms are designed to determine whether an input signal has a high signal to noise ratio. However, the signal investigated by the algorithm used with this technique is the cardiac, rather than respiratory, signal. An additional step may be required to exclude any signal in which there is insufficient respiratory modulation to estimate RR.

The second potential improvement lies in the methodology used to extract respiratory signals. This technique uses the feature-based methods for extraction of BW, AM and FM proposed in [11]. However, this results in respiratory signals of a low sampling frequency of one sample per cardiac cycle. Furthermore, they are calculated using one or two fiducial points in each cardiac cycle. Considering that signals are often acquired from mobile sensors at sampling frequencies of 75 Hz and above, much of the available information has not been included in the calculation of the respiratory signal. In addition, the cardiac frequency is approximately three to five times higher than the respiratory frequency. Therefore, relatively few samples of a single respiratory cycle are acquired. In contrast, the alternative category of methods, filter-based methods, uses all the available information and provides a respiratory signal at the sampling frequency of the original signal (as illustrated in Figure 4).

Thirdly, wearable sensors must be suitable for use by a wide range of patient groups. To this end the performance of wearable sensor technology must be tested across a heterogeneous patient cohort which is representative of the end users. In this study data collected from subjects with a wide range of ages was used, from paediatric to elderly patients. The only significant age cohort omitted was the neonatal cohort. This is in keeping with recent work by Addison *et al.* [2], who published a study of a RR algorithm for use with the PPG which was tested on data acquired from adult patients across the general care floor with a wide range of medical conditions and ages. This study is limited, however, by not including data from patients outside of the hospital setting, and by using data acquired from patients whilst being stationary, rather than truly ambulatory.

7 Conclusions

We proposed and evaluated a novel fusion algorithm for the extraction of respiratory rate from waveforms acquired by non-invasive wearable sensors; in this case, the PPG signal. This work has demonstrated that it is possible to enhance the capabilities of wearable devices (such as the pulse oximeter) by providing the possibility of incorporating important physiological parameters such as respiratory rate without significant added cost or complexity. Such devices are able to provide a better state of patients' health, as the respiratory rate is an important vital sign that is known to be correlated to other physiological conditions such as stress and obesity, and reduce the cost and time to assess the physiological status.

Acknowledgments. Marco A. F. Pimentel was supported by the RCUK Digital Economy Programme [Grant EP/G036861/1]; and *Fundação para a Ciência e Tecnologia* (FCT), Portugal [Grant SFRH/BD/79799/2011]. Peter H. Charlton acknowledges support from the EPSRC [Grant EP/F058845/1]; and the National Institute for Health Research (NIHR) Biomedical Research Centre based at Guys and St Thomas NHS Foundation Trust and Kings College London. David A. Clifton was supported by a Royal Academy of Engineering Research Fellowship; Balliol College, Oxford; and the Centre of Excellence in Personalised Healthcare funded by the Wellcome Trust and EPSRC [Grant WT 088877/Z/09/Z].

The views expressed are those of the authors and not necessarily those of the EPSRC, NHS, NIHR or Department of Health.

8 Conflicts of Interest

Peter H. Charlton has performed consultancy work for Philips Medical Systems (Böblingen, Germany) and OBS Medical Limited (Abingdon, UK).

References

1. Addison, P.S., Watson, J.N., Mestek, M.L., Mecca, R.S.: Developing an algorithm for pulse oximetry derived respiratory rate (RR(oxi)): a healthy volunteer study. Journal of Clinical Monitoring and Computing 26(1), 45–51 (2012)
2. Addison, P.S., Watson, J.N., Mestek, M.L., Ochs, J.P., Uribe, A.A., Bergese, S.D.: Pulse oximetry-derived respiratory rate in general care floor patients. Journal of Clinical Monitoring and Computing 29(1), 113–120 (2015)
3. Bailon, R., Sornmo, L., Laguna, P.: ECG-Derived Respiratory Frequency Estimation. In: Clifford, G.D., Azuaje, F., McSharry, P.E. (eds.) Advanced Methods and Tools for ECG Data Analysis, ch. 8, pp. 215–244. Artech House, London (2006)
4. Bates, A., Ling, M.J., Mann, J., Arvind, D.K.: Respiratory rate and flow waveform estimation from tri-axial accelerometer data. In: 2010 International Conference on Body Sensor Networks, pp. 144–150. IEEE, Singapore (2010)

5. Cretikos, M.A., Bellomo, R., Hillman, K., Chen, J., Finfer, S., Flabouris, A.: Respiratory rate: the neglected vital sign. The Medical Journal of Australia 188(11), 657–659 (2008)
6. Farrohknia, N., Castrén, M., Ehrenberg, A., Lind, L., Oredsson, S., Jonsson, H., Asplund, K., Göransson, K.E.: Emergency department triage scales and their components: a systematic review of the scientific evidence. Scandinavian Journal of Trauma, Resuscitation and Emergency Medicine 19(1), 42 (2011)
7. Fleming, S.G., Tarassenko, L.: A comparison of signal processing techniques for the extraction of breathing rate from the photoplethysmogram. International Journal of Biological and Medical Sciences 2(4), 232–236 (2007)
8. Garde, A., Karlen, W., Ansermino, J.M., Dumont, G.A.: Estimating respiratory and heart rates from the correntropy spectral density of the photoplethysmogram. PloS One 9(1), e86427 (2014)
9. Goldhaber, S.Z., Visani, L., De Rosa, M.: Acute pulmonary embolism: Clinical outcomes in the International Cooperative Pulmonary Embolism Registry (ICOPER). Lancet 353(2182), 1386–1389 (1999)
10. Jin, A., Yin, B., Morren, G., Duric, H., Aarts, R.M.: Performance evaluation of a tri-axial accelerometry-based respiration monitoring for ambient assisted living. In: Proceedings of the 31st Annual International Conference of the IEEE Engineering in Medicine and Biology Society, pp. 5677–5680 (2009)
11. Karlen, W., Raman, S., Ansermino, J.M., Dumont, G.A.: Multiparameter respiratory rate estimation from the photoplethysmogram. IEEE Transactions on Biomedical Engineering 60(7), 1946–1953 (2013)
12. Karlen, W., Turner, M., Cooke, E., Dumont, G., Ansermino, J.M.: Capnobase: Signal database and tools to collect, share and annotate respiratory signals. In: Annual Meeting of the Society for Technology in Anesthesia (STA), West Palm Beach (2010)
13. Khalil, A., Kelen, G., Rothman, R.E.: A simple screening tool for identification of community-acquired pneumonia in an inner city emergency department. Emergency Medicine Journal 24(5), 336–338 (2007)
14. Knaus, W.A., Wagner, D.P., Draper, E.A., Zimmerman, J.E., Bergner, M., Bastos, P.G., Sirio, C.A., Murphy, D.J., Lotring, T., Damiano, A.: The APACHE III prognostic system. Risk prediction of hospital mortality for critically ill hospitalized adults. Chest 100(6), 1619–1636 (1991)
15. Larsen, P.D., Tzeng, Y.C., Sin, P.Y.W., Galletly, D.C.: Respiratory sinus arrhythmia in conscious humans during spontaneous respiration. Respiratory Physiology & Neurobiology 174(1-2), 111–118 (2010)
16. Li, B.N., Dong, M.C., Vai, M.I.: On an automatic delineator for arterial blood pressure waveforms. Biomedical Signal Processing and Control 5(1), 76–81 (2010)
17. Li, J., Jin, J., Chen, X., Sun, W., Guo, P.: Comparison of respiratory-induced variations in photoplethysmographic signals. Physiological Measurement 31(3), 415 (2010)
18. Li, Q., Clifford, G.D.: Dynamic time warping and machine learning for signal quality assessment of pulsatile signals. Physiological Measurement 33(9), 1491 (2012)
19. Mackay, D.J.C.: Introduction to gaussian processes. In: NATO ASI Series F Computer and Systems Sciences, vol. 168, pp. 133–166 (1998)

20. Mason, L.: Signal Processing Methods for Non-Invasive Respiration Monitoring. PhD thesis, University of Oxford (2002)
21. Meredith, D.J., Clifton, D., Charlton, P., Brooks, J., Pugh, C.W., Tarassenko, L.: Photoplethysmographic derivation of respiratory rate: a review of relevant physiology. J. Med. Eng. Technol. 36(1), 1–7 (2012)
22. Moll, J.M., Wright, V.: An objective clinical study of chest expansion. Annals of the Rheumatic Diseases 31(1), 1–8 (1972)
23. Nilsson, L., Goscinski, T., Johansson, A., Lindberg, L.-G., Kalman, S.: Age and gender do not influence the ability to detect respiration by photoplethysmography. Journal of Clinical Monitoring and Computing 20(6), 431–436 (2006)
24. O'Brien, I.A., O'Hare, P., Corrall, R.J.: Heart rate variability in healthy subjects: effect of age and the derivation of normal ranges for tests of autonomic function. British Heart Journal 57(1), 109–110 (1986)
25. Orphanidou, C., Fleming, S., Shah, S.A., Tarassenko, L.: Data fusion for estimating respiratory rate from a single-lead ECG. Biomedical Signal Processing and Control 8(1), 98–105 (2013)
26. Pan, J., Tompkins, W.J.: A real-time qrs detection algorithm. IEEE Transactions on Biomedical Engineering 32(3), 230–236 (1985)
27. Pantelopoulos, A., Bourbakis, N.G.: Prognosis-a wearable health-monitoring system for people at risk: methodology and modeling. IEEE Transactions on Information Technology in Biomedicine 14(3), 613–621 (2010)
28. Rasmussen, C.E., Williams, C.K.I.: Gaussian Processes for Machine Learning. MIT Press (2006)
29. Royal College of Physicians. National Early Warning Score (NEWS): Standardising the assessment of acute-illness severity in the NHS. Technical Report July, Report of a working party. RCP, London (2012)
30. Rue, H., Martino, S., Chopin, N.: Approximate Bayesian inference for latent Gaussian models by using integrated nested Laplace approximations. Journal of the Royal Statistical Society: Series B (Statistical Methodology) 71(2), 319–392 (2009)
31. Saeed, M., Villarroel, M., Reisner, A.T., Clifford, G., Lehman, L., Moody, G., Heldt, T., Kyaw, T.H., Moody, B., Mark, R.G.: Multiparameter intelligent monitoring in intensive care II (MIMIC-II): A public-access intensive care unit database. Critical Care Medicine 39, 952–960 (2011)
32. Shelley, K.H., Awad, A.A., Stout, R.G., Silverman, D.G.: The use of joint time frequency analysis to quantify the effect of ventilation on the pulse oximeter waveform. Journal of Clinical Monitoring and Computing 20(2), 81–87 (2006)
33. Sivia, D.S., Skilling, J.: Data Analysis: A Bayesian Tutorial. Oxford University Press (2006)
34. The ACCP/SCCM Consensus Conference Committee. American College of Chest Physicians/Society of Critical Care Medicine Consensus Conference: definitions for sepsis and organ failure and guidelines for the use of innovative therapies in sepsis. Critical Care Medicine 20(6), 864–874 (1992)

Ambient Intelligence System for the Remote Monitoring and Control of Sleep Quality

C. Occhiuzzi, C. Vallese, S. Amendola, S. Manzari, and G. Marrocco

Pervasive Electromagnetic Lab – RADIO6ENSE
University of Rome Tor Vergata, Rome, Italy

Abstract. By applying one of the enabling technologies of the Internet of Things, an Ambient Intelligence platform is here described for application to the real-time remote monitoring and diagnostic of overnight living environments. The platform is fully based on the passive Radiofrequency Identification (RFID) tags spread around the bed and integrated into the user's clothes. The optimization of the electromagnetic set-up and the evaluation of the system compliance with electromagnetic exposure limits are performed by a Moment Method model of an anthropomorphic body phantom. The identification of the sleeper state (quiet sleep, out of bed, prolonged absence and fall) and the classification of sleep postures (prone, supine, left/right side) are obtained through a combined digital and analogue processing of the backscattered signals coming from the tags with accuracy close to 100%, as evaluated in both laboratory and real-life experimentations**.**

1 Introduction

The extension of the population age and the need to provide assistance to an increasing number of alone-living people in both large cities and in small towns are stimulating the interest for innovative healthcare infrastructures based on decentralized, pervasive and patient-centric methodologies [1], at the purpose to improve the human health with affordable costs for the community. Ambient Intelligence architectures [2], where people are empowered through a digital environment that is aware of their presence and sensitive, adaptive and responsive to their activities and needs, may provide useful support for remote monitoring and assistance. The environment is invested with the responsibility of continuously "sampling" the bio-physical activity of the user by means of sensors integrated in everyday objects [3] with the aim of supporting neurologic diagnostics and even of activating alarms in case of precursors of anomalous events.

Ambient Intelligence systems can benefit of the technologies currently being developed in the framework of the Internet of Things, and in particular of the Radio Frequency Identification (RFID) thanks to the low cost and the energy

S.C. Mukhopadhyay (ed.), *Wearable Electronics Sensors*,
Smart Sensors, Measurement and Instrumentation 15, DOI: 10.1007/978-3-319-18191-2_11

autonomy of its components. The elemental RFID sensor, the tag, is indeed definitely suitable to permanent integration within clothes, furniture, walls and everyday objects. Some experiments have already considered RFID tags placed on people [4] and onto some objects (medicine or food) to recognize activity and motion patterns of users by analyzing only their interaction with the objects [5,6,7,8]. Sensing-oriented UHF RFID tags, able to provide the physical state of tagged people and items such as the temperature, the humidity and the presence of toxic vapours, may further enrich the ambient monitoring [9,10].

This chapter is focused on the *sleep* that is definitively one of the most important behavioural parameters, since sleep disorders could sensibly affect the quality of life, leading to daytime sleepiness, spread weariness and even moodiness. Furthermore, especially for weak subjects such as elderly, children and neurologic patients, the night could be a source of several dangerous events (falls, disorientation, night-time wandering) demanding for early detection and prompt actions. These requirements are even more pressing in case of alone-living subjects or inside hospitals and nursing houses, where many patients need to be contemporarily monitored all along the night with the consequence of high personnel costs. Typical remote monitoring platforms comprise audio/video recording systems and active sensors directly connected to first-aid remote observation-centers [11]. However, their cost, complexity and intrusiveness have limited up to now their widespread diffusion and social acceptance by the end users [12]. Most innovative commercial devices propose the use of totally sensor-less wireless platforms to remotely and discretely monitor the sleep quality in term of posture and movements [13]. Their functioning rationale is similar to the one adopted by radar devices, e.g. for localizing persons buried under avalanche, but they suffer the possibility to contemporarily monitor more subjects (the electromagnetic field is in fact indiscriminately reflected by any subject presents in the monitoring area) and the limited operating distances (only 50-100 cm between the device and the sleeper). Other sensor-less systems recently proposed rely instead on the evaluation of the variation of communication link between personal wireless diagnostic devices (e.g. wearable pressure/heartbeat monitor) and fixed motes properly positioned in the environment to infer the subject position in the bed. They are mainly based on machine learning based classifiers [14] and hence they appear quite complex and not straightforwardly suited to be applied in clinical applications, especially when many subjects need to be contemporarily monitored during the night. Furthermore, they presuppose the use of active nodes integral with the body and a well-defined wireless architecture of the surrounding spaces.

RFID-based ambient intelligence systems look hence natural candidates to overcome at least part of such limitations. Recent applications of RFID technology to the sleep monitoring involved wearable or environmental tags loaded by active or passive accelerometers to detect pathological limbs movements [15] for mitigating the risk of nocturnal falls [16], for inferring postures and global

movements [17] or finally to automatically detect movements related to bed exit [18]. However, no attempts have been done, until now, to design an ambient intelligence platform suitable to simultaneously provide a knowledge tool for the analysis of the sleep as well as an effective scalable remote assistance infrastructure.

The chapter describes a fully passive RFID Ambient Intelligence platform, hereafter denoted as *NIGHTcare*, for monitoring people during the night. Battery-less tags are integrated into clothes and dispersed in the environment. A long-range UHF RFID reader illuminates the scene and the collected tags' responses, arising from the interaction between the subject and surrounding environment, are real-time processed. The goal is detecting the presence or the absence of the user in the bed, his jerky movements and his motion patterns, accidental falls, persisting absence from the bed and prolonged periods of inactivity as well as his instantaneous sleeping posture. The preliminary idea of the system has been very recently presented in [19] and [20] and will be now described in full details concerning the electromagnetic and signal-processing issues as well as the evaluation and the real-life experimentation.

2 The RFID Sensing System

A passive RFID system comprises one or more digital devices (tags), embedding an antenna and an IC-chip with a unique identification code (ID), and a radio scanner device (reader). The tags are completely passive and can be activated only by the radiofrequency energy coming from the reader. Once turned on, they reply to the interrogation by properly modulating the backscattered field.

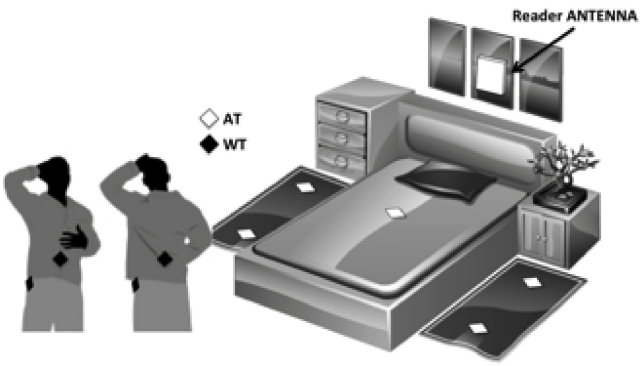

Fig. 1 NIGHTcare: Ambient intelligence system aimed to monitor and take care of the night sleep involving RFID tags placed over the body (WT: wearable tags) and in the surrounding environment (AT: ambient tags). A long-range UHF-RFID reader, properly placed in proximity of the bed headboard, scans the environment interrogating the tags.

Fig.1 shows a pictorial representation of the RFID data acquisition set-up for the *NIGHTcare* system**.** The patient, lying on the bed, wears four RFID tags (wearable tags - WT) sewn into his night-suit at the level of abdomen, back, left and right hip. A conventional dipole tag (Ambient tags - AT) is placed underneath the mattress so that it will be completely shadowed by the body when the subject lies on the bed, regardless its position along with the night. One or two additional ATs are finally placed at each side of the bed, eventually hidden by carpets or directly integrated in the floor (being totally passive and with a extremely simplified electronics, they do not require maintenance operation and are usually working for more than 50-year [21]) such to mitigate their visual impact or any possible fall hazard. The radio scanner device is placed in correspondence of the headboard, properly tilted and lifted in order to uniformly illuminate the entire bed and the surrounding floor.

The response of the tags to the reader's query is subjected to an ambient modulation, in the sense that the strength of the backscattered field is modified by the proximity of the human body with the tags themselves. Moreover, in case of specific body-environment configurations, a tag may be fully shadowed by the sleeper so that it will not be able to reply the reader's interrogation. For example, if the subject lies on the bed, the tag under the mattress will be totally shielded and it will be prevented from responding while the others on the floor will be free to communicate. Vice-versa if the subject falls.

The activity of the sleeper during the night may be therefore recognized by processing the signals received from the tags. More in details, the IDs of the responding tags can be used to recognize the *status* of the sleeper (whether he is in the bed, he is fallen down or instead he is outside), while the processing of the strength of the electromagnetic fields reflected by the responding tags can be used to extract information about motion and about specific *postures* during the sleep.

The selected components for the NIGHTcare setup are described below.

2.1 Components

The wearable RFID tag is a miniaturized UHF-RFID layout, already proposed by the authors in [22]. The lightweight and the small sizes (35mmx45mmx2mm) make this tag suitable to be integrated into plasters, wristbands or various clothes. The maximum measured realized gain of the tag when placed onto the human body is -7dB (at the European frequency 868MHz). Accordingly, when considering a linearly polarized reader antenna and an IC's power sensitivity P_{chip} =-18dBm, the estimated free-space maximum read range is about 5m (Fig.2).

The Ambient tag is a commercial AD-843 inlay (Fig.2) with external size of 94mm x 38mm x 0.2mm [23] suitable to be placed on the bed and on the ground thanks to its small size (only 0.2mm thick) and its proven good performances in a wide range of applications. The measured realized gain for the tag placed on the ground, with an IC's power sensitivity P_{chip} =-15dBm, is -4dB (at 868MHz), leading to a maximum read range longer than 5m. Even better performances are expected when the tag is placed under the mattress.

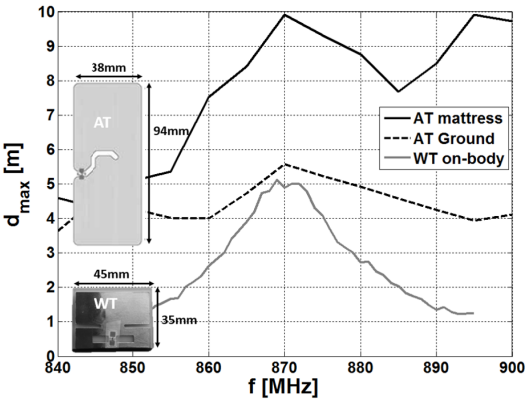

Fig. 2 Estimated maximum read ranges along the broadside direction of the ambient tag (AT) placed on the mattress and ground and of the miniaturized wearable tag (WT) placed on-body

Finally, the reader is the CAEN ION equipped with a broadband linear-polarized Stacked Planar Inverted-F Antenna (SPIFA) over Teflon substrate, having 130mm x 200mm x 12mm external size and 5.8dB maximum simulated gain evaluated at 868MHz along the broadside direction (Fig.3). The half-power beamwidth of the antenna (85° and 108° for the H-plane and the E-plane, respectively) enables a uniform illumination of the environment. The height and the angular tilt of the antenna are design parameters of the system to be optimized as shown later on in the next Section.

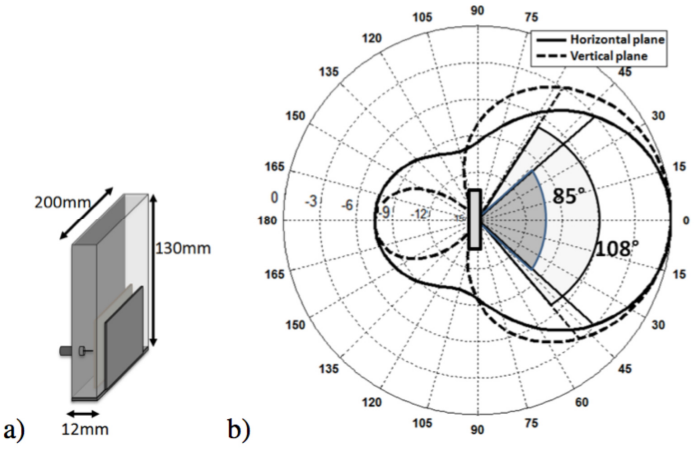

Fig. 3 a) Layout of the Stacked Planar Inverted-F Antenna (SPIFA) used for the interrogation; b) Normalized radiation patterns of the reader antenna for horizontal and vertical planes

3 Electromagnetic Analysis

In order to optimize some geometrical parameters of the monitoring system, and to take into account the electromagnetic emission and exposure issues, the *NIGHTcare* platform was preliminary analyzed by a three-dimensional computer model implementing the Method of Moment [24]. The model (fig. 5) comprises the reader antenna, that is accounted by means of its radiation pattern simulated in standalone configuration, the floor (represented by the Green function), the bed (with a conductive structure and a dielectric mattress) and the user, here emulated by considering an anthropomorphic homogeneous phantom (electromagnetic parameter at 868MHz ε_r =41.5 σ =0.94 S/m, ρ =1000Kg/ m^3).

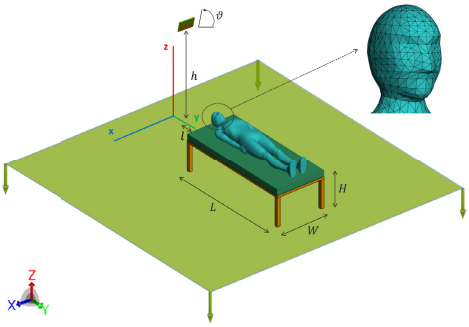

Fig. 4 Numerical Model of the *NIGHTcare* platform comprising the reader antenna, the bed and the human phantom. Geometrical parameters: *L*=190cm, *W*=80cm, *H*=52cm, *h*=180cm, *l*=40cm, θ =45°.

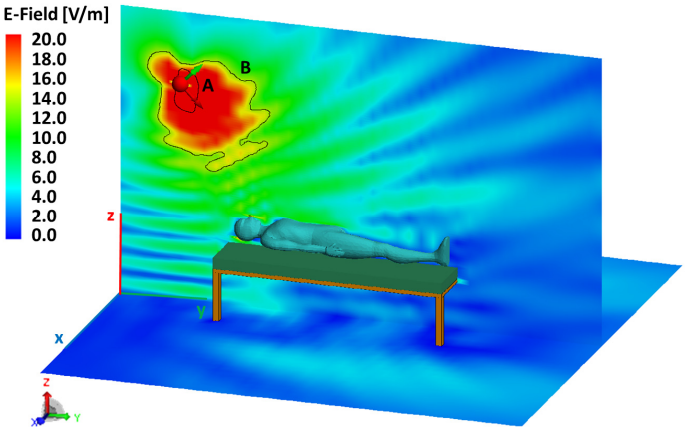

Fig. 5 Electromagnetic field on vertical and horizontal planes (the last one corresponding to the floor level) radiated by the reader antenna emitting 3.2 W EIRP. The highlighted isolines A and B correspond to the r.m.s. field $E(r)_{r.m.s.}$=20V/m and $E(r)_{r.m.s.}$=6V/m, respectively, when the communication duty cycle is d=0.2 (one interrogation per second).

Fig. 5 shows the computed electric field map for a realistic arrangement of the reader, placed at *h*=180cm height from the floor, at *l*=40cm distance from the bed and tilted by θ_0=45° with respect to the horizontal plane. The reader was assumed to emit 3.2W EIRP that is the maximum allowed value in Europe. The shadowing and diffractions from the bed and the body, as well as the reflections from the floor, produce a non uniform field distribution, with visible nulls on the floor, close to the bed, wherein ambient tag should be placed.

3.1 Communication Issues

The position and orientation of the antenna need to be selected so that all the tags could receive enough power to be activated in operative conditions. At this purpose, a parametric analysis over 1.5m<h<2.5m and 45°< θ_0 <80° allows evaluating the most appropriate system configuration. The minimum power P_{chip} that is required to activate the tags is related to the local field radiated by the reader and impinging on the tags

$$E_{min} = \sqrt{\frac{P_{chip} 4\pi z_0}{\eta G \tau \lambda^2}} \tag{1}$$

with z_0 the characteristic impedance of the medium, η the polarization mismatch between the reader and the tag and Gτ the realized gain of the tag. With reference to the setup in Fig. 4, the tags on the floor are assumed to be placed at each side of the bed, at y=170cm from the reader antenna and x=30cm from the sides of the bed, such to intercept the strongest field (see Fig.5) and to be fully overlaid by the user in case of falling. The wearable tags are assumed to be placed on abdomen, back, left and right hip. Thus, by introducing into (1) the tag realized gains indicated in Section II decreased by a 3dB safe margin, the estimated minimum fields required to activate the environmental and the wearable tags were found to be 3.5V/m and 3.7V/m respectively.

The bottleneck of the communication mostly concerns the tags placed on the floor since they are positioned at the longest distance from the reader antenna, and therefore the optimization will be referred only to the ground tags.

Fig. 6 shows the electric field isolines at the ground level versus {h, θ_0} parameters. In the shadowed area the field impinging the ground tags is lower than the minimum activation level E_{min}, and hence the antenna tilt must be kept between 45° and 68°, while the height is much more incisive and must be kept between 1.5 and 1.75 m.

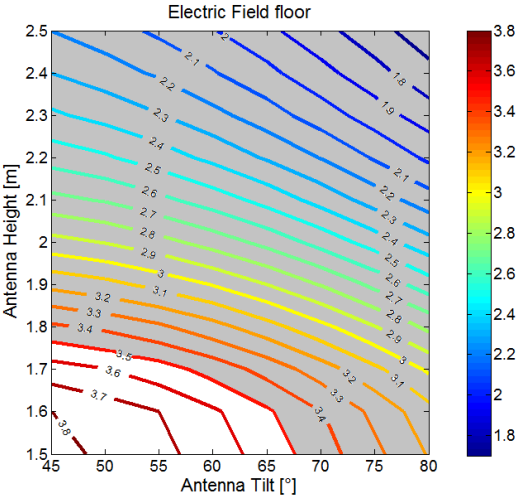

Fig. 6 Optimization of the reader antenna placement. Electric field isolines on the ground versus the height and the tilt of the reader's antenna.

3.2 Safety Compliance Issues

Constraints over electromagnetic field exposure and power absorbed by the human tissues are imposed by local Recommendations. In particular, the European rules [25] enforces requirements on the the r.m.s. emitted field averaged over a prescribed time interval T_{av}.

The reader interrogates the environment according to a given repetition period T_0. Denoted with T_{com} the time duration of a typical reader-tag communication, the duty-cycle is accordingly $d = {}^{T_{com}}/_{T_0}$. The averaged r.m.s electric field is hence

$$\langle E(r)_{r.m.s} \rangle T_{av} = \sqrt{d} E(r)_{r.m.s} \tag{2}$$

that is required to be less than $E_0 = 1.375\sqrt{f} = 41.3\ V/m$. Even more restrictive constraints may be found in some countries, as in the case of Italy where E_0 =6V/m. Some iso-lines of the simulated averaged r.m.s electric field are traced within Fig.5 and it is clearly visible how the user is placed in a fully compliant radiating region ($\langle E(r)_{r.m.s} \rangle < 4V/m$) if a duty cycle d=0.2, corresponding to an interrogation per second, is considered.

The Specific Absorption Rate (SAR)

$$\frac{SAR(r) = \sigma(r) \cdot d \cdot |E|^2_{r.m.s}}{\varrho(r)} \tag{3}$$

averaged on the entire body needs to be less than $SAR_{body,max}$ =0.08W/Kg and the SAR averaged over 10g of tissue less than $SAR_{10g,max}$ =2W/Kg. Fig.7 shows the estimated SAR profiles inside the body. Also in this case, the averaged values

SAR_{body} =0.6mW/Kg and SAR_{10g} =4mW/Kg (expected to arise in correspondence of the upper portion of the body) are greatly below the exposure limits.

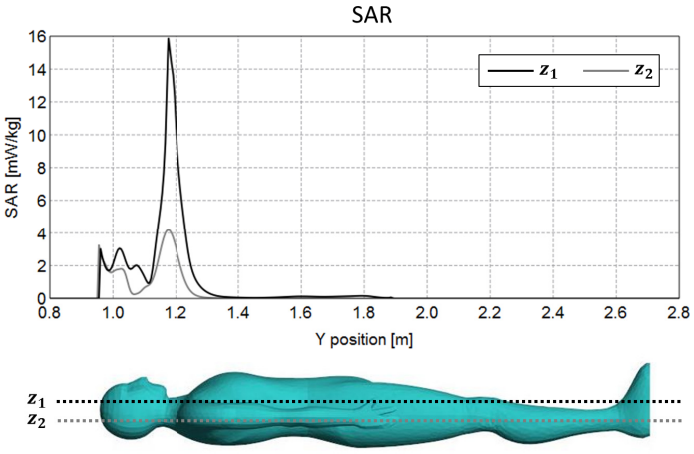

Fig. 7 Simulated values of SAR along the sagittal plane of the body exposed to the reader's radiation as in Fig.3 and Fig.4

4 Detection of Sleep Events

The detection of sleep events is performed by applying a threshold-based algorithm. The procedure comprises two parallel branches, the first one aiming at the detection of the user's state (presence/absence from the bed or accidental falls) and the second one aiming at the discrimination between activity and quite sleep condition and, in the latter case, at the classification of the sleeping postures (Fig.8)**.** The considered events, and their logical relationship, are summarized by the classification tree of Fig.9, to be walked from left to right.

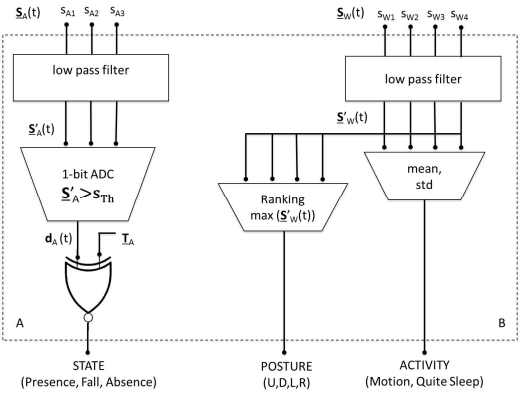

Fig. 8 Flow chart of the classification procedure for the discrimination of the sleeper state (left) and of his activity/posture (right)

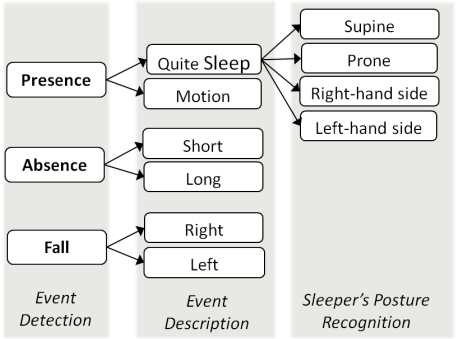

Fig. 9 Classification tree implemented into the *NIGHTcare* platform. The relevant sleep events are recognized starting from left to right.

The detection of the user's state relies on the processing of the signals coming from the three ambient tags (bed, left/right floor), forming a three-elements time-variant vector

$$\underline{S}_A(t) = [s_{A1}(t), s_{A2}(t), s_{A3}(t)] \tag{4}$$

while the estimation of activity rate and sleeper's posture requires the signals from the four wearable tags

$$\underline{S}_w(t) = [s_{w1}(t), s_{w2}(t), s_{w3}(t), s_{w4}(t)] \tag{5}$$

Such data stream is gathered by the reader in term of Received Signal Strength Indicator - RSSI [26]. As shown in Fig.10, RFID backscattered signal is characterized by low values (~ -50dBm) and high fluctuations, mainly due to the receiver internal noise, the limited stability of its components and above all the non-stationary communication channel. To overcome these drawbacks and ensure the reliability of the sleep monitoring system, the raw data are pre-processed before feeding the event-detection algorithm by low-pass filtering over a fixed temporal window. In doing so, the information about the user's state is inferred by analyzing a temporal record taking into account the past story of signals rather than the instantaneous noisy measurement. Furthermore, since the interrogation protocol could randomly fail because of environmental interferences and collisions, missed readings are dropped out the useful time series, in order to prevent false positive events detection. Finally, the proposed algorithm exploits a cross-validation between signals coming from the multiple channels and it relies on more robust on/off digital data for the detection of most dangerous events (e.g. fall or long absence).

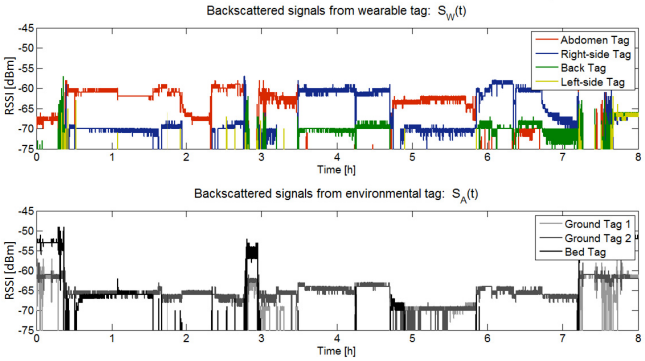

Fig. 10 Example of raw RSSI signals $S_W(t)$ and $S_A(t)$ collected by the reader from wearable and ambient tags during sleep events

4.1 Classification of the Sleeper's State

After a low-pass (LP) filtering to remove noise the resulting ambient signals $\boldsymbol{S'}_{\boldsymbol{A}}(t) = LP\{\boldsymbol{S_A}(t)\}$ undergo a 1-bit A/D conversion yielding the 3-bit data stream $\boldsymbol{d_A}(t)$, so that

$$d_{A,n}(t_m) = \begin{cases} 1 \; if \; S'_{A,n}(t_m) \geq s_{Th,n} \\ 0 \qquad otherwise \end{cases} \quad n = 1..3 \tag{6}$$

where $s_{Th} = [\, s_{Th1},\, s_{Th2},\, s_{Th3}]$ are predefined thresholds whose values can be a priori defined depending on the absolute range of RSSI values provided by the specific reader (for example if RSSI values for a detected tag range from 80 to 130, a RSSI value greater than 90 would ensure a reliable reading and consequently convert into digital signal as 1).

Let indicate with $T_{A\,[3\times4]}$ the *coding table* (see Fig. 11.a), a binary representation of the four meaningful states of the user, labelled as *STATE=[Presence, Absence, Left-fall, Right-fall],* with respect to the set of responding ambient tags. A *XNOR-like* gate is applied to $\boldsymbol{d_A}(t)$ and $T_{A\,[3\times4]}$ such to calculate the binary output matrix $\boldsymbol{out_A}(t_m)_{[3\times4]}$ at the time t_m:

$$\boldsymbol{out_A}(t_m)_{[3\times4]} = XNOR(\, \boldsymbol{d_A}(t_m), \boldsymbol{T_A}) \tag{7}$$

The column of $\boldsymbol{out_A}(t_m)$ having the maximum norm will yield the estimated user's state. An example of application of this last step is reported in Fig11.b.

Finally, a further state, the *Long-Absence,* is recognized when the *Absence* condition lasts for a period longer than a given threshold time accounting for physiological absences of the user. These temporal windows are set during the calibration phase (see Sec.6.1) and may be possibly adapted accordingly to the patient's own habits.

a) T_A

AT \ State	Pres.	Abs.	Fall (R)	Fall (L)
Bed	0	1	1	1
Floor (R)	1	1	0	1
Floor (L)	1	1	1	0

b)

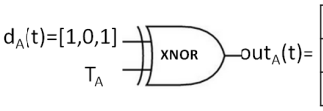

0	1	1	1
0	0	1	0
1	1	1	0

Right Fall

Fig. 11 a) Coding binary table T_A relating the set of responding ambient tags to the four considered states of the sleeper. b) An example of identification of the actual sleeper's state by means of the XNOR gate: the third (shadowed) column of $\boldsymbol{out_A}$ exhibits the maximum norm and hence the retrieved sleeper's state is the third label of the STATE vector, e.g. "*right fall*".

4.2 Classification of the Sleeper's Activity

The detection of the activity/posture relies instead on the simultaneous processing of the analogue signals coming from the wearable tags, and subjected to low-pass filter as before: $\boldsymbol{S'}_{\boldsymbol{W}}(t) = LP\{\boldsymbol{S_{WA}}(t)\}$.

The discrimination between motion and quite sleep is performed through the standard deviation of the signals. If the standard deviation exceeds a given threshold, then the sleeper is assumed to be moving. The threshold value, corresponding to the intrinsic signal fluctuations due to internal noise and environmental interferences, is empirically deduced by collecting a large amount of data during experimental sessions with volunteers having different ages and physiques. It is worth noticing that the threshold value turns out to be globally valid for each subject when the binary classification of the quiet/motion state is required, thus avoiding any ad-personam training of the system. However, more detailed information about the motion itself such as the classification of movements according to their intensity or the distinguish between physiological and pathological events may be inferred by defining thresholds on individual basis (motions strength strongly depends on the sleeper's age), possibly with the help of clinicians.

When the subject is instead in the rest condition his posture is retrieved by applying a maximum-value rule that is based on the assumption that the tag related to the maximum RSSI recorded by the reader is the closest to the reader's antenna. Since the user wears a tag on each side of the body, it is hence possible to introduce a classification table (Tab.1) univocally relating the tag having the highest backscattering power value to one of the four possible sleeper's postures.

Table 1 Classification table for the sleep's posture depending of the position of the tag that produces the maximum RSSI

Tag position	Posture
abdomen	**S**: supine
right hip	**R**: right side
left hip	**L**: left side
back	**P**: prone

Hence, at time t_m the elements of $\boldsymbol{S'}_W(t_m)$ are ranked according to their RSSI at the purpose to recognize the tag producing the highest signal. The sleep posture is finally estimated from the above classification table.

4.3 Representation of the Events

Fig.12a shows a typical trace of the night sleep when the user alternated periods of quite sleep (grey area), short absence (yellow area), physiological movements (green bars) and fall events (red bars). Each condition is classified according to its duration: a short absence from the bed could be considered as physiological, while a prolonged one (second yellow frame) could foresee a problem (for example illness in the bathroom) and thus an automatic alarm has to be generated, as well as in the case of a fall detection. The occurrence of events can be finally counted to produce statistics about the user's sleep quality and behaviour (Fig.12b and 12c), e.g. how many time he left the bed in the night, the number of movements and the time percentage spent in each position, as shown in the next experimental session.

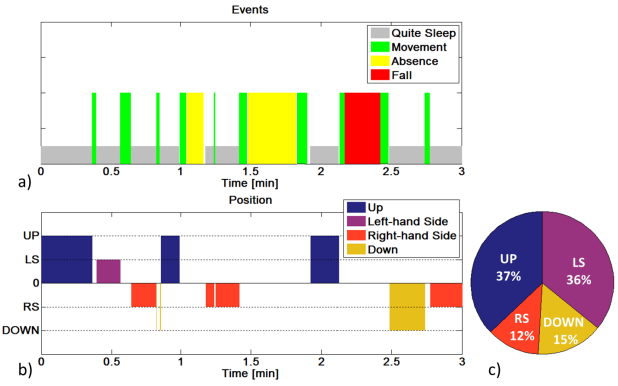

Fig. 12 a) Example of a recorded sleep activity trace. b) Classification of body postures for each quite sleep slots. c) Example of aggregated statistics.

5 Validation of the Systems

The accuracy of the algorithm for the detection of the sleeper's posture and state was evaluated by involving 20 volunteers (5 men and 15 women, whose ages span from 24 to 45 years {24, 26(x2), 27(x2), 28(x5), 29(x6), 30, 31, 32, 45}). Subjects were asked to take the four sleeping positions and the four states (presence, absence, left and right fall) separately, according to the indications randomly given by an acoustic pre-recorded "go-signal" phrase prompting for timing (e.g. "Prone Position", et similar). Each position was kept for about 20s (corresponding to the time interval between two consecutive audio commands) and it was repeated 8 times. The dataset hence consists of 32 positions to be recognized during 10 minutes and 40 seconds of recording session. Instruction labels were collected and synchronously stored together with the backscattered signal coming from wearable tags to keep track of the desired (asked) outputs as well as of the predicted ones. The statistic mode was calculated every 20 seconds of acquisition, and the predicted position was then compared with the real one.

Accuracy and error-rate were then estimated by means of the *confusion matrix* (Fig.13) that provides a graphical representation of classification accuracy. More in detail, denoting with $N=4$ the number of considered sleep positions and states, a confusion matrix (CM) is a $N \times N$ table whose columns correspond to the postures predicted by the algorithm, while each row represents the true ones. The fifth extra-column of the matrix in Fig.13 refers to the "abstention condition", namely the case in which the algorithm is not able to classify the posture in any of the four predetermined cases so that the "unclassified position" is assigned. The diagonal elements of the matrix give the number of correctly classified positions and state while the off-diagonal elements correspond to misclassified ones. The classification accuracy is finally the ratio between the sum of the diagonal elements and the sum of all the matrix elements.

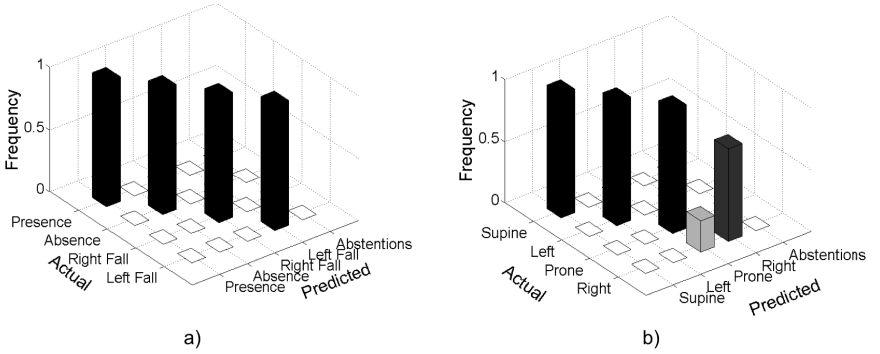

Fig. 13 Example of confusion matrices for the sleeper state (a) and the bed positions classification (b)

In the performed experiments, the estimated average accuracy of posture detection was 97% while accuracy of state detection was 100% for all the subjects confirming the robustness of the on/off -based algorithm. It worth noticing that the abstention condition never appears.

6 Example of Real-Life Recordings

The NIGHTcare system was finally experimented into two real scenarios without any supervision of technicians during the night. In both cases, the RFID data were corroborated by videocamera information or by annotations about the activity directly provided by the volunteer the morning after.

6.1 Installation Procedures

The installation procedure of the system is performed as follows:

1) The first step is to place the ambient tags on the carpets and mattress, making sure they are readable all the time, unless they are fully covered by the patient. Ambient tags on the floor are placed on both sides of the bed in the areas where the electric field is maximum (Fig.5) and the reader's antenna is slightly moved up or down and tilted according to Fig.6 up to obtain a stable and reliable value of RSSI of all the uncovered tags during the interrogations.
2) At this point, the patient wears the four wearable tags as in Fig.1. Interrogations of all the tags with the patient in the bed are then performed to register some profiles of the received signals.
3) From previous measurements and from analysis on patient behaviour time thresholds are finally set.

Less than twenty minutes are requested to complete the procedure and calibrate the system.

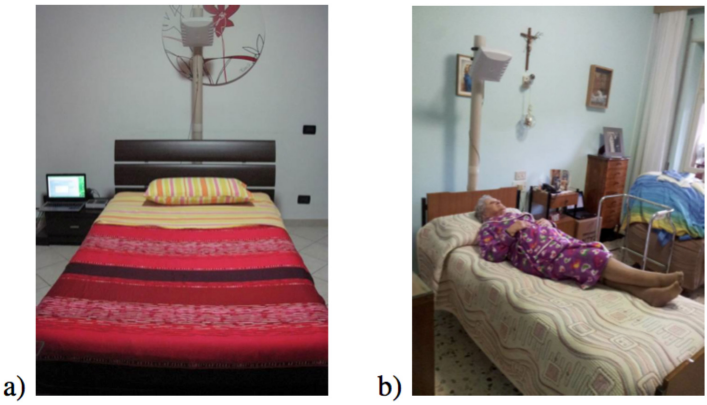

Fig. 14 NIGHTCare setup installed a) into a domestic room and b) into a nursing home for aged guests

Experiment 1: Young Subject in Domestic Environment

The first experiment was performed by applying the *NIGHTcare* system to a young volunteer (27 years old) during three consecutive nights. The set-up was installed into a domestic room (Fig.14a). A video recording system was positioned onto a support at 70 cm from the floor and at a distance of 30 cm from the bed so that all movements of the monitored subject were clearly visible.

Fig.15 shows the *NIGHTcare* response of one of the three nights. The user went to bed around 23:30 and slept approximately until 7:00 in the morning, with two short absences between 4:00 and 5:00, for going to the toilet. The sleep was peaceful, with only 7 small movements detected during the whole night, mainly related to the change of the sleep posture. The bottom of Fig.15 shows some snapshot taken by the video camera that fully agree with the *NIGHTcare* output. Aggregated statistics about the body posture, sleep duration, absence and movements are shown in Fig.16. The user mainly sleeps on the sides, while the prone position is never detected.

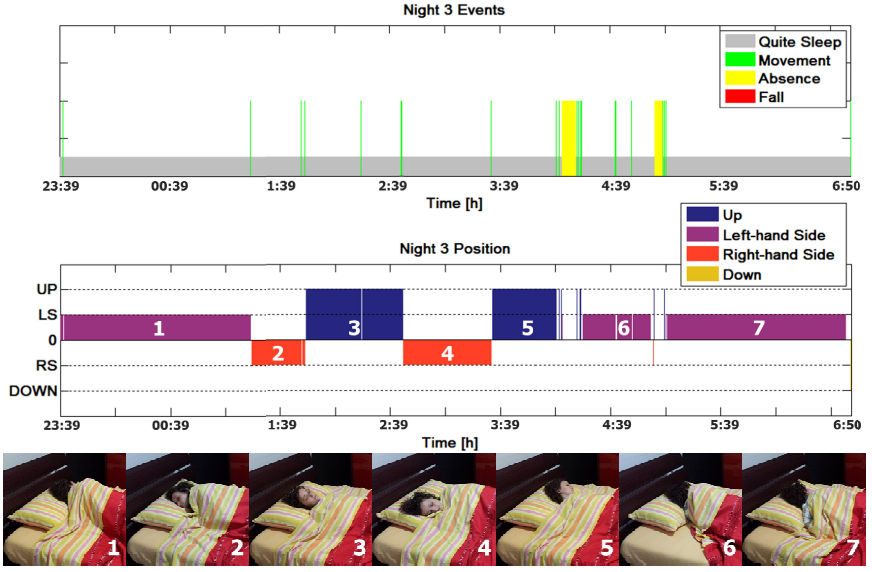

Fig. 15 Young volunteer. Up) traces from one of the three nights sleep activity and automatic classification of the body postures during the quiet sleep state. Bottom) Snapshots of body postures as recorded by a videocamera corresponding to the NIGHTcare profiles.

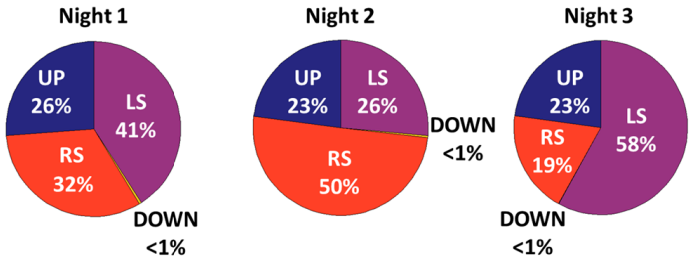

Fig. 16 Young volunteer. Overall percentages of time spent in each position by the user during the three monitored nights. The number of movements recorded during three nights was {12, 8, 7} respectively, while the number of absences from the bed was {3, 2, 2}.

Experiment 2: Elder Subject in Nursing Home

The second experimental campaign involved an elder subject (age 95) in good mental and physical conditions resident of a nursing home ("Residenza Maria Claràc, Monte Porzio Catone, Rome, Italy"). The setup has been optimized by considering the specific environment (spaces narrower that the domestic room ones). Particular attention has been devoted to the positioning of the environmental tag on the floor: in order to avoid any fall hazard, the carpets have been removed and the tags have been directly attached on the tiles. The volunteer (Fig.14b) was not fully aware of all the functionalities of the system, therefore providing a not-biased behaviour during the three nights.

Fig.17 shows the *NIGHTcare* responses over one of the three nights. The patient went to bed around 22:30 and slept approximately until 5:30, with a short absence around 1:00 for going to the toilet. The sleep was peaceful, with only 10 small movements detected over the entire night and a quite constant posture.

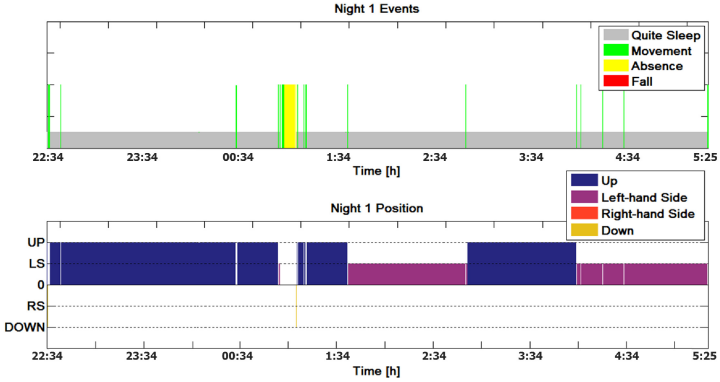

Fig. 17 Aged volunteer. NIGHTcare traces from one of the three nights sleep activity and automatic classification of the body postures during the quiet sleep state.

It is worth noticing that the elderly user changed position less frequently than the young volunteer, due to the slowness and difficulty in movement typical of the advanced age. The sleep appears well reproducible throughout the course of the three nights, as clearly demonstrated by the aggregated data about the body posture and the movements in Fig.18. Each night, the lady went to bed between the 22:15 and the 22:30 and slept until 5:15-5:30 in the morning. She went to the bathroom around 1:00 and took approximately 5-10 minutes to go back to bed.

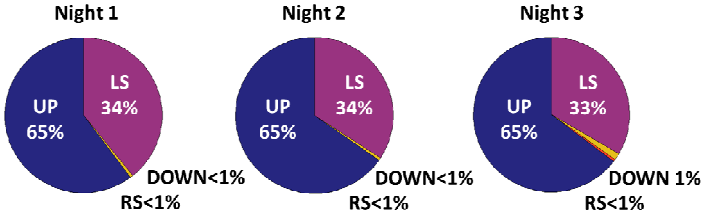

Fig. 18 Aged volunteer. Overall percentages of time spent in each position by the user during the three monitored nights. The number of body movements recorded during three night was{8, 6, 5} respectively, while the number of absences from the bed was {1, 1, 3}.

7 Conclusions

The results presented in the chapter demonstrated that by combining together wearable and ambient tags it is possible to develop a fully passive RFID system to remotely monitor the state and the activity of young and elderly people during the night. The sleep events (quiet sleep, absence from bed and falls) were recognized with 100% accuracy and the instantaneous posture with an accuracy higher than the 95% (within the 20-volunteers experimental campaign). It is worth noticing that the threshold-based algorithm here proposed does not require a starting ad-personam training phase as standard classification techniques [7,14] hence reducing the complexity and the duration of the installation procedures.

The platform is completely compliant with the EM exposure limits and hence it is suitable to be installed in both domestic and hospital environments. The system is scalable, in the sense that a single RFID reader connected to a set of antennas could monitor, in time division, a multiplicity of users and a network of readers could easily cover a large infrastructure. Real-time access to the data can be given from both fixed (desktop) and mobile devices (tablet, smart-phones) checked by qualified personnel, able to access the server if provided of security credentials. The personnel is therefore able to control the whole nursing home from any location.

Finally the platform permits not only to enable a remote observation of patients but also to produce statistical data about the individual sleep behaviour that can be useful to make correlation with pharmacologic therapies.

It is worth noticing that the system can be further simplified by reducing the number of tags worn by the subject. Without any wearable tag the system is still able to retrieve the status of the sleeper (presence, absence, fall) while early theoretical analysis demonstrated that it is possible to infer the sleeper posture and activity by considering only two wearable tags placed asymmetrically on the chest and on the back and by exploiting the shadowing effects of the human body on the communication link between floor tags and reader.

It is moreover possible to envisage a further improvement of the platform by augmenting the same infrastructure with wearable temperature sensor tags at the purpose to detect and follow fever events, as well as humidity sensor tags under the mattress to monitor incontinence and finally miniaturized tags placed over medicines and food to enrich the patients' behavioural analysis.

Acknowledgements. The authors wish to thank Mrs. Silvana and all the Sisters of the "Maria Claràc" nursing home (Monte Porzio Catone, RM) for their kind support during the experimental phase.

References

[1] Varshney, U.: Pervasive healthcare and wireless health monitoring. Mobile Networks and Applications 12, 113–127 (2007)
[2] Acampora, G., Cook, D., Rashidi, P., Vasilakos, A.: A survey on ambient intelligence in healthcare. Proceedings of the IEEE 101(12), 2470–2494 (2013)
[3] Bardram, J.: Pervasive healthcare as a scientific discipline. Methods of Information in Medicine 47(3), 178–185 (2008)
[4] Manzari, S., Occhiuzziand, C., Marrocco, G.: Feasibility of body-centric systems using passive textile RFID tags. IEEE Antennas and Propagation Magazine 54(4), 49–62 (2012)
[5] Pang, Z., Chen, Q., Zheng, L.: A pervasive and preventive health-care solution for medication noncompliance and daily monitoring. In: 2nd International Symposium on Applied Sciences in Biomedical and Communication Technologies, ISABEL 2009, pp. 1–6 (November 2009)
[6] Philipose, M., Fishkin, K., Perkowitz, M., Patterson, D., Fox, D., Kautz, H., Hahnel, D.: Inferring activities from interactions with objects. IEEE Pervasive Computing 3(4), 50–57 (2004)
[7] Amendola, S., Bianchi, L., Marrocco, G.: Combined passive radiofrequency identification and machine learning tecnique to recognize human motion. In: Proceedings of European Microwave Week, Rome, Italy (October 2014)
[8] Jiang, B., Fishkin, K., Roy, S., Philipose, M.: Unobtrusive long-range detection of passive rfid tag motion. IEEE Transactions on Instrumentation and Measurement 55(1), 187–196 (2006)
[9] Occhiuzzi, C., Caizzone, S., Marrocco, G.: Wireless sensing of things by passive rfid technology. IEEE Antennas and Propagation Magazine 55(6), 14–34 (2013)
[10] Marrocco, G.: Pervasive electromagnetics: sensing paradigms by passive RFID technology. IEEE Wireless Communications 17(6), 10–17 (2010)

[11] Alemdar, H., Ersoy, C.: Wireless sensor networks for healthcare: A survey. Computer Networks 54(15), 2688–2710 (2010), http://www.sciencedirect.com/science/article/pii/S1389128610001398

[12] Ranasinghe, D., Shinmoto Torres, R., Wickramasinghe, A.: Automated activity recognition and monitoring of elderly using wireless sensors: Research challenges. In: 2013 5th IEEE International Workshop on Advances in Sensors and Interfaces (IWASI), pp. 224–227 (June 2013)

[13] Omron hsl-101, http://www.engadget.com/2012/03/07/omron-sleep-monitoring-gadget/ and http://www.omron.co.jp/press/2012/02/h02292.html

[14] Barsocchi, P.: Position recognition to support bedsores prevention. IEEE Journal of Biomedical and Health Informatics 17(1), 53–59 (2013)

[15] Occhiuzzi, C., Marrocco, G.: The RFID technology for neurosciences: Feasibility of limbs' monitoring in sleep diseases. IEEE Transactions on Information Technology in Biomedicine 14(1), 37–43 (2010)

[16] Shinmoto Torres, R., Ranasinghe, D., Shi, Q., Sample, A.: Sensor enabled wearable rfid technology for mitigating the risk of falls near beds. In: 2013 IEEE International Conference on RFID (RFID), pp. 191–198 (April 2013)

[17] Hoque, E., Dickerson, R.F., Stankovic, J.A.: Monitoring body positions and movements during sleep using wisps. In: Wireless Health 2010, WH 2010, pp. 44–53. ACM, New York (2010), http://doi.acm.org/10.1145/1921081.1921088

[18] Ranasinghe, D.C., Shinmoto Torres, R.L., Hill, K., Visvanathan, R.: Low cost and batteryless sensor-enabled radio frequency identification tag based approaches to identify patient bed entry and exit posture transitions. Gait & Posture 39(1), 118–123 (2014)

[19] Amendola, S., Lodato, R., Manzari, S., Occhiuzzi, C., Marrocco, G.: Rfid technology for IOT-based personal healthcare in smart spaces. IEEE Internet of Things Journal 1(2), 144–152 (2014)

[20] Occhiuzzi, C., Vallese, C., Amendola, S., Manzari, S., Marrocco, G.: Night-care: A passive RFID system for remote monitoring and control of overnight living environment. Procedia Computer Science 32, 190–197 (2014); The 5th International Conference on Ambient Systems, Networks and Technologies (ANT 2014), The 4th International Conference on Sustainable Energy Information Technology (SEIT 2014), http://www.sciencedirect.com/science/article/pii/S1877050914006140

[21] Impinj, "Monza® 5 tag chip datasheet," Impinj, Inc., Tech. Rep. (2014)

[22] Manzari, S., Pettinari, S., Marrocco, G.: Miniaturised wearable uhf- rfid tag with tuning capability. Electronics Letters 48(21), 1325–1326 (2012)

[23] AD-843 UHF RFID inlay, http://rfid.averydennison.com/products/ad-843/

[24] FEKO 7.0 - EM Simulation Software, http://www.feko.info

[25] European council recommendation 1999/519/ec of 12 july 1999 on the limitation of exposure of the general public to electromagnetic fields (0 hz to 300 ghzs). Official Journal (1999)

[26] Nikitin, P.V., Rao, K.V.S.: Theory and Measurement of Backscattering from RFID tags. IEEE Antennas and Propagation Magazine, 212–218 (2006)

Measurement of Human Gait Using a Wearable System with Force Sensors and Inertial Sensors

Guangyi Li[1], Tao Liu[1], and Yoshio Inoue[2]

[1] The State Key Laboratory of Fluid Power Transmission and Control,
Department of Mechanical Engineering, Zhejiang University, 310027, Hangzhou, China
liutao@zju.edu.cn
[2] Research Institute, Kochi University of Technology, 185 Miyanokuchi,
Tosayamada-cho, Kami-city, 782-8502, Japan
inoue.yoshio@kochi-tech.ac.jp

Abstract. Six-axial force sensors and inertial sensors were used together to construct a wireless wearable sensor system for the successive and non-laboratory measurement of gait. The system consists of the wearable sensor shoes and motion sensors. In order to diminish the influence of motion acceleration in the measurements of accelerometers and the disturbance of surrounding magnetic field in the measurements of magnetic sensors, we modified the Extended Kalman Filter to check the values of the acceleration and magnetic field intensity before updating. And a reference system composed of high speed cameras and stationary force plates are used to validate the reliability of the wearable system. The experiment results showed that the wearable system is able to measure the ground reaction force (GRF), joint angles, joint forces and joint moments.

1 Introduction

In the past, the traditional gait analysis system is composed of the optical motion capture system with high speed cameras and stationary force plates [1,2,3]. The stationary force plate is quite heavy and bulky, and one force plate can only record one step of GRF in the walking. The optical motion capture system is sensitive to the light of sun and it costs too much to obtain a small motion capture volume. Some new low-cost optical motion analysis systems [4] and home video cameras [5] are considered to reduce the cost, but the application of this kind of systems are limited to the indoor environment. Nowadays, gait analysis is widely used in the rehabilitation and assessment of lower extremities, diagnosis in the clinics and healthy life. People now have a great demand for the unobstructed and successive ambulatory gait assessment in non-laboratory environments. Many researchers have proposed novel methods to evaluate variable gait parameters such as walking speed and gait events [6-9]. Inertial sensors such as gyroscopes [10,11], accelerometers [12,13] and magnetic sensors [14] are small and easy to be integrated in the portable and wearable devices for the measurement of orientations of human body.

S.C. Mukhopadhyay (ed.), *Wearable Electronics Sensors*,
Smart Sensors, Measurement and Instrumentation 15, DOI: 10.1007/978-3-319-18191-2_12

As for the analysis of kinetics of gait, instrumented shoes [15] or instrumented insoles [16,17] with varied special made force sensors are presented in the work of many researchers. But both instrumented shoes and instrumented insoles are made of special size for the certain subject and they are not suitable for common use. In our past research, we designed a series of wearable shoes to measure the GRF in walking with good performances [18,19]. In this paper, each wearable shoe is made up of three force sensors. We add the force sensors under the arch to acquire a better measurement accuracy of GRF. Moreover, the wearable sensor shoes and the motion sensors are connected together with WIFI communication to form a comprehensive wearable gait analysis system. The Extended Kalman Filter (EKF) is modified in a simple way to diminish the disturbances in accelerations and magnetic field intensities.

2 Wearable Sensor Shoes

In our research, we developed a kind of wearable sensor shoes to measure the ground reaction forces (GRFs) between the underside of foot and the ground. The wearable sensor shoes are an important part of the whole wearable gait analysis system. It can be used to estimate the joint forces and joint moments of the lower extremities besides detecting the variation of GRFs in walking. As we can see in Figure 1, each wearable shoe is consisted of a specific shoe with hollowed sole on the upper side, an insole, three six-axial force sensors and three WIFI communication/Power supply modules connected with the corresponding force sensors. The force sensors can measure the three axial forces and three axial force moments between their upper side and underside.

Fig. 1 Explosive view of a wearable shoe

According the magnitude of forces loaded on the different part of the underside of foot and the area of each part, we have designed the force sensors of different standards. It is known that the forefoot and the heel will support most of the body

weight while walking, so the force sensors mounted under the forefoot and heel have a great measuring range which is much bigger than the gravities of normal persons. And the forefoot also has a relative big supporting area for adjusting the attitude of lower extremities in walking, while the area of heel is relative narrow and small, so the size of these force sensors are different. As for the force sensor under the arch, both its size and measuring range are the smallest.

As shown in Figure 2, tiny inertial sensors units were mounted into the force plates of the forefoot and heel. Due to the flexibility of the foot and the motion of joint, the attitudes of force plates are changed all the time. These inertial sensors can measure the change of attitudes of the force plates which contain the force sensors inside. It means that the local coordinate system of the force sensors can be determinate to calculate the resultant force of GRF. But limited by the space of the hollowed sole and the size of the force sensors, there isn't enough room for the inertial sensors of force plate of arch. But the foot actually can be simplified into two parts connected with one joint if do not consider the deformation of mid-foot, so the force plate of arch can be considered as an extended part of the force plate of heel. We use the transformation matrices to transform the force of each sensor from its local coordinate system to the global coordinate system to acquire the resultant of GRF. The calculating process can be described as below:

$$GRF = R_{heel} \bullet F_{heel} + R_{heel} \bullet F_{arch} + R_{forefoot} \bullet F_{forefoot}$$

where R_{heel} and $R_{forefoot}$ are the transformation matrices of force sensors under the heel and forefoot respectively. F_{heel}, F_{arch} and $F_{forefoot}$ denote the forces measured by the force sensors under the heel, arch and forefoot respectively.

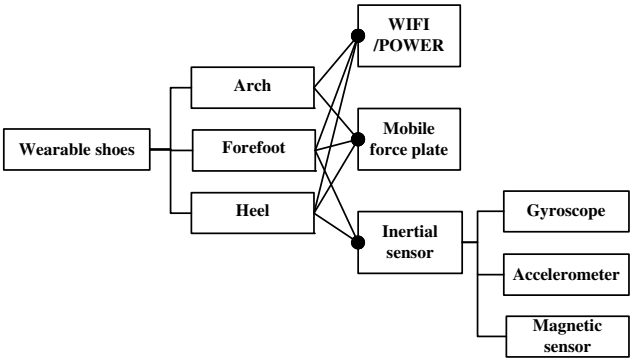

Fig. 2 Structure of the Wearable sensor shoes

Unlike most kinds of instrumented shoes, our wearable shoes embedded with thin and multi-axial force sensors in the hollowed sole and covered with insoles on the sensors. The soles are only a little thicker compared with normal shoes and the

sensors also are under good protection of the surroundings. Another advantage is that the specific shoes are designed easily to change the degree of tightness to suit most persons' foot. So the wearable shoes can be a used in the non-laboratory environments for most people.

3 Motion Sensors

As shown in Figure 3, five motion sensors were used to acquire the 3D orientation and attitude angle of lower limbs and waist. Accelerometer, gyroscope and magnetic sensor were integrated in the motion sensors. Sensor data were transmitted to the PC via a wireless local area network (WLAN). In our research, human lower limbs were simplified into nine rigid segments (pelvis, left thigh, left shank, left heel, left fore-foot, right thigh, right shank, right heel, right fore-foot) and eight global joints (left hip joint, left knee joint, left ankle joint, left foot joint, right hip joint, right knee joint, right ankle joint, right foot joint). We suppose that there is no relative movement between the motion sensors and human segments, so the transformation matrices measured by the motion sensors can represent the attitude of segments respectively. The transformation matrix R_0 can be calculated using the quaternions $q = [q_0 \quad q_1 \quad q_2 \quad q_3]$ and the equation is described as below:

$$R = \begin{bmatrix} q_0^2 + q_1^2 - q_2^2 - q_3^2 & 2(q_1 q_2 - q_0 q_3) & 2(q_1 q_3 + q_0 q_2) \\ 2(q_0 q_3 + q_1 q_2) & q_0^2 - q_1^2 + q_2^2 - q_3^2 & 2(q_2 q_3 - q_0 q_1) \\ 2(q_1 q_3 - q_0 q_2) & 2(q_0 q_1 + q_2 q_3) & q_0^2 - q_1^2 - q_2^2 + q_3^2 \end{bmatrix}$$

The angle of each joint can be acquired by transform the lower segment's attitude angle into its upper segment's coordinate system, so the transformation matrix of the joint can be described as:

$$R_j = R^{upper} \bullet R^{lower}$$

where R, R^{upper} and R^{lower} are the transformation matrices of the joint and the upper segment and lower segment respectively. Then, the triaxial joint angle can be calculated using the following equations:

$$Angle_x = \tan^{-1}\left(R_{j32} / R_{j33}\right)$$

$$Angle_y = -\sin^{-1} R_{j31}$$

$$Angle_z = \tan^{-1}\left(R_{j21} / R_{j11}\right)$$

where $Angle_x$, $Angle_y$ and $Angle_z$ represent the x-axial, y-axial and z-axial joint angle of the joint respectively.

Fig. 3 Structure of the Wearable sensor shoes

4 Design of Extended Kalman Filter

Accelerometers and magnetic sensors are widely used in the wearable devices and robotics to overcome the disadvantages of gyroscope. The measurement results of MEMS gyroscope are mixed with severe zero drifts and random errors. In many cases, acceleration and magnetic field intensity are used to update the Euler angles or quaternions without judgement that if the observation variables themselves are accurate enough. In fact, both the acceleration measured by the accelerometer and the magnetic field intensity measured by the magnetic sensor can be easily influenced in some common situations. The accelerometers measure both gravitational acceleration and motion acceleration of the human body. The disturbances are of large values when the body segment are striking on the ground especially the under the events of heel-strike and toe-off. As for the magnetic sensors, the measurement results are influenced by the surrounding magnetic field such as soft magnetic and many kinds of electronic instruments.

Our designed Extended Kalman Filter (EKF) [20] is improved by checking the reliabilities of the measurements of the accelerometer and magnetic sensor. A simple and practicable way is to set up the threshold values of acceleration and magnetic field intensity both. The quaternions are chose to be the state vector and the gravitational acceleration and the magnetic field intensity of the earth are chose to be the observation vector. As we can see in Figure 4, the main calculation procedure can be divided into three steps.

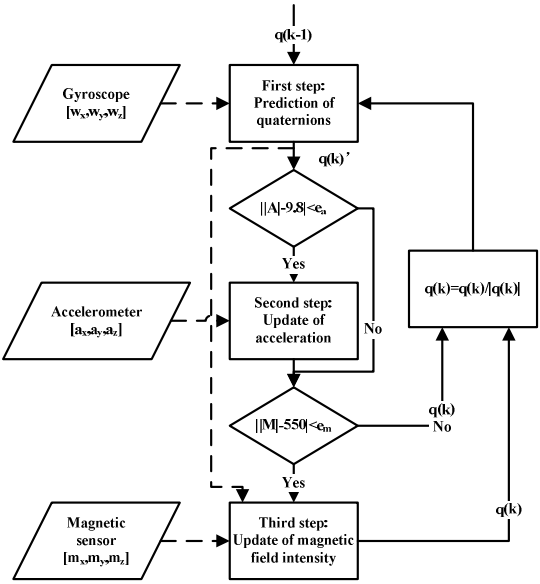

Fig. 4 Flow diagram of the Extended Kalman Filter

First step - Prediction of quaternions

We used the discrete state equation to calculate the quaternion in the next sample period. The state equation is described as:

$$q(k)' = \Phi_{k,k-1} \bullet q(k-1) + w_{k-1}$$

where $\Phi_{k,k-1}$ is the state transition matrix at $t = k \bullet \Delta t$ and w_{k-1} is the white noise of the state vector. And the state transition matrix can be calculated in the following equation:

$$\Phi_{k,k-1} = \begin{bmatrix} 1 & -\frac{1}{2}\omega_x T & -\frac{1}{2}\omega_y T & -\frac{1}{2}\omega_z T \\ \frac{1}{2}\omega_x T & 1 & \frac{1}{2}\omega_z T & -\frac{1}{2}\omega_y T \\ \frac{1}{2}\omega_y T & -\frac{1}{2}\omega_z T & 1 & \frac{1}{2}\omega_x T \\ \frac{1}{2}\omega_z T & \frac{1}{2}\omega_y T & -\frac{1}{2}\omega_z T & 1 \end{bmatrix}$$

where $\begin{bmatrix} \omega_x & \omega_y & \omega_z \end{bmatrix}$ is the triaxial angular velocity measured by the gyroscope and T is the sampling period. And the predicted covariance matrix $P_{k|k-1}$ can be calculated by the following equation.

$$P_{k|k-1} = \Phi_{k,k-1} \bullet P_{k-1} \bullet \Phi_{k,k-1}$$

Second step - Update of acceleration

Before the updating of gravitational acceleration, the computing program will check the value of the measured gravitational acceleration. If the measured value is closed enough to the real value, then the measured acceleration will be used to update the quaternions to reduce errors. Otherwise, the update of acceleration may cause bigger calculation error and the calculation procedure will jump to the third step. The threshold value of acceleration to exclude the motion acceleration is defined as $e_a = 0.1\, m/s^2$ and the criterion can be formulized as:

$$\left\| |A| - 9.8 \right| < e_a$$

where $A = \begin{bmatrix} a_x & a_y & a_z \end{bmatrix}^T$ is the measurement result of triaxial gravitational acceleration.

In this step, the observation vector is $\begin{bmatrix} A \end{bmatrix}$ and the observation function can be acquired by transforming the reference gravitational acceleration g from the global coordinate system to the local coordinate system of the motion sensor. The observation function of acceleration can be described as:

$$h^A(k) = R \bullet g$$

where $h^A(k)$ denotes the observation function and the value of gravitational acceleration is defined as $g = \begin{bmatrix} 0 & 0 & -9.8 \end{bmatrix}^T$.

Then, the observation matrix $H^A(k)$ can be described by calculating the Jacobian matrix of observation function $h^A(k)$ for $q(k)'$. The equation is described as below.

$$H^A(k) = \frac{dh^A(k)}{dq(k)'} = \begin{bmatrix} \frac{\partial h^A(k)}{\partial q_0} & \frac{\partial h^A(k)}{\partial q_1} & \frac{\partial h^A(k)}{\partial q_2} & \frac{\partial h^A(k)}{\partial q_3} \end{bmatrix}$$

And the observation equation can be described as $A(k) = H^A(k) \bullet q(k)'$ where $A(k)$ denotes the gravitational acceleration at $t = k \bullet \Delta t$. Finally, the measured acceleration will be used to update the quaternion in the following equation.

$$q_a(k) = q(k)' + K_k \left(A - H^A(k) \bullet q(k)' \right)$$

$q_a(k)$ denotes the quaternion updated by the acceleration and K_k denotes the gain matrix. The updates of gain matrix K_k and covariance matrix P_k can be described as below:

$$K_k = P_{k|k-1} \bullet H^A(k)^T \bullet \left(H^A(k) \bullet P_{k|k-1} \bullet H^A(k)^T + R_k \right)^{-1}$$

$$P_k = \left(I - K_k \bullet H^A(k) \right) \bullet P_{k|k-1}$$

where R_k denotes the covariance of the white noise of observation.

Third step - Update of magnetic field intensity

The calculation method in the third step is similar to the second step, but the observation vector is changed to the magnetic field intensity $M = \begin{bmatrix} m_x & m_y & m_z \end{bmatrix}$. Because of the influence of the magnetic fields generated by the electronic instruments or cables around the experiment subjects, some motion sensors may be disturbed at some moments more or less. The threshold value of magnetic field intensity $e_m = 80mGs$ can help us to find out the unavailable measurements and decrease the calculation errors caused by the magnetic field interference. The criterion can be described as below.

$$\left\| M \right| - 550 \left| < e_m \right.$$

In fact, the magnetic field intensity of earth is different at different locations and the magnetic field interference may be frequent. So the threshold value and the reference value of the magnetic field intensity m could be adjusted to the appropriate values. And the reference magnetic field intensities are also different for different motion sensors, because their locations and initial positions are changed in each experiment and we need to calibrate them for every motion sensors when the experiment started. The observation function of magnetic field intensity can be described as $h^M(k) = R \bullet m$. And the equation used to update the quaternion in this step is described as below.

$$q_m(k) = q_a(k) + K_k \left(M - H^M(k) \bullet q(k)' \right)$$

The quaternion is normalized to the unit quaternion before calculating the joint angle or going to the next circle.

5 Experiment Method of Dynamic Verification

As shown in Figure 5, the experimental setup is composed of the wearable system and the reference system. And the synchronization trigger is a linkage of the two systems to keep them working simultaneously. Both the wearable sensor shoes and motion sensors are the key components of the wearable system. Besides, a wireless router is necessary to provide a wireless local area network (WLAN) for the wearable system to transmit the sensor data. And the data acquisition software on the PC will reconstruct and analyse the sensor data received from the WLAN. A pair of trousers made of elastic materials with five small pockets can fasten the motion sensors tightly to the corresponding segments. As for the reference system, it consists of eight high speed cameras and three stationary force plates. The reference system is already commercialized and can be worked as the standard in the experiments.

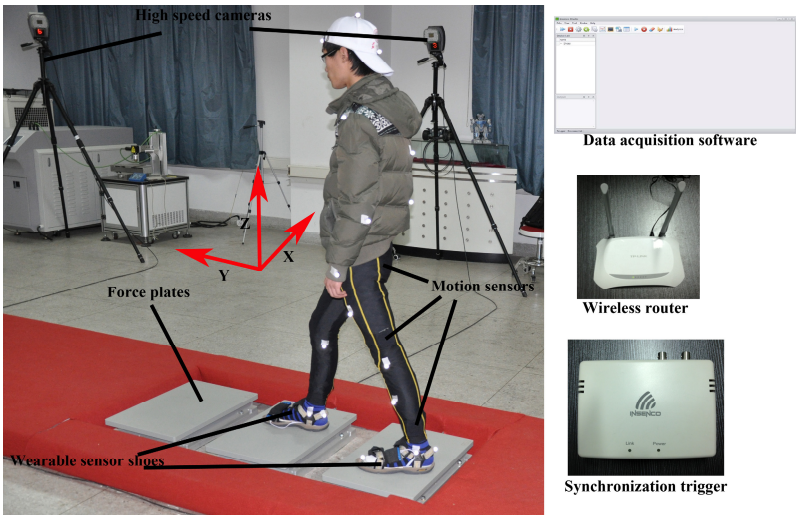

Fig. 5 Experimental setup

In order to make a comparison between the measurements of the wearable system and the reference system, the global coordinate system is defined. The x-axis positive direction is right of the body, the y-axis positive direction is aligned with the anterior direction of human motion, and the z-axis positive direction is vertical and upward. Five subjects without disability of lower extremity or history of injuries are consent to the experiment and signed up with moral and ethical agreements. Each subject was asked to repeat the experiment 10 times to keep a plenty of measurement results and verify the repeatability. The experiment procedure can be described in 6 steps:

Step 1: We put 29 markers on the subjects' body segments for the optical analysis system to rebuild the whole motion models of human body and make sure that the markers were all in the right place.

Step 2: Turn on the power of the optical analysis system and the wearable system. All the high speed cameras and stationary force plates should be available. And test the wearable sensors if they can transmit data to the PC.

Step 3: Before wearing the wearable system, all the motion sensors and the wearable shoes need to be reset. This step can eliminate the zero drift of the force sensors and rectify the orientation of the motion sensors. As shown in Figure 6(a), all the wearable sensors were put on their initial positions. The orientations of the sensors are corresponding to the orientations worn in the experiments. And due to the change of orientation in every experiment, the magnetic field intensities of the inertial sensors recorded in this step are used as references.

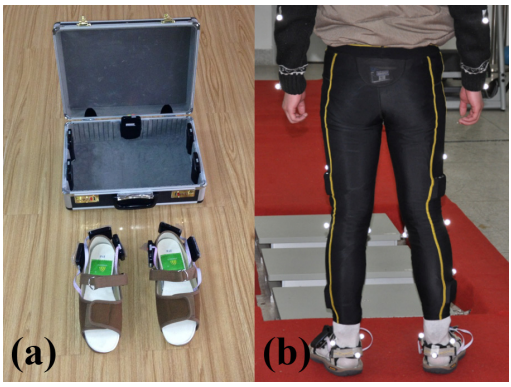

Fig. 6 Calibration of the wearable sensors

Step 4: Subjects are asked to wear the wearable sensors and stand still in front of the stationary force plates. As shown in Figure 6(b), when the motion sensors were carried in the elastic trousers, their orientations were all changed. Then, we calibrate the orientations of motion sensors again to record the initial orientations of body segments in lower extremities.

Step 5: Use the synchronization trigger to start the wearable system and reference system simultaneously. Then the subjects are allowed to walk normally through the stationary force plates.

Step 6: When the subjects passed the stationary force plates, stop recording and prepare for the next trial or turn off the systems.

6 Results of GRF

Table 1 shows the total comparison results of GRF between the two systems in the form of correlation coefficient (R) and root mean square error (RMSE). The RMSEs were normalized to body weight (N/kg). Figure 7 shows a group of representative measurement results to demonstrate the agreement between the wearable system and the reference system.

Table 1 The comparison results of GRF between the wearable system and the reference system

	GRF_x	GRF_y	GRF_z
R	0.63	0.80	0.95
RMSE	0.23	0.78	1.44

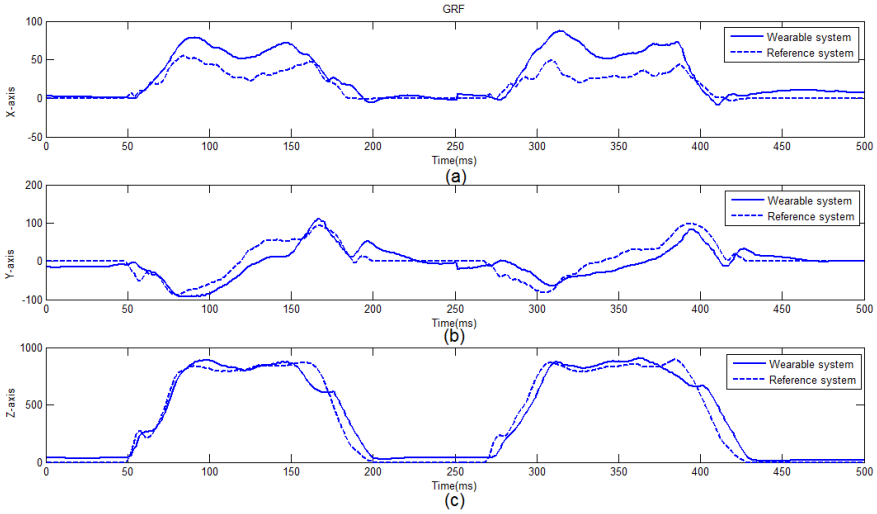

Fig. 7 Comparison results of GRF, (a): GRF_x; (b) GRF_y; (c) GRF_z

The measurement results of GRF_z showed a good agreement with average R of 0.95 and RMSE of 1.44 N/kg. However, the consistency of measurement results of GRF_x and GRF_y are not as good as GRF_z. The measurement results of GRF_y showed a reasonable agreement between the two systems with average R of 0.80 and RMSE of 0.78 N/kg. And the measurement results of GRF_x showed a low agreement with average R of 0.63 and RMSE of 0.23 N/kg. While walking with the shoes, the feet are unavoidable to touch the uppers and vamps of the shoes. But the force sensors were all mounted in the upper side of soles. So the x-axial and y-axial GRF in the horizontal plane can be influenced when the feet are in touch with the uppers and vamps. From Figure 7(c), we can see that the GRF_z remained 10~20 N in the swing phase. This phenomenon may be caused by the pretightening force to keep the shoes sticking to the feet.

7 Results of Joint Angles

Table 2 shows the comparison results of the joint angles, including the ankle joint angle, knee joint angle and hip joint angle. The A_x^{ankle}, A_y^{ankle} and A_z^{ankle} denote the x-axial, y-axial and z-axial joint angle of ankle respectively. The A_x^{knee}, A_y^{knee} and A_z^{knee} denote the x-axial, y-axial and z-axial joint angle of knee respectively. The A_x^{hip}, A_y^{hip} and A_z^{hip} denote the x-axial, y-axial and z-axial joint angle of hip respectively. Figure 8 shows a group of representative measurement results of ankle joint angle. Figure 9 shows a group of representative measurement results of knee joint angle. And Figure 10 shows a group of representative measurement results of hip joint angle.

Table 2 The comparison results of joint angles between the wearable system and the reference system

	A_x^{ankle}	A_y^{ankle}	A_z^{ankle}	A_x^{knee}	A_y^{knee}	A_z^{knee}	A_x^{hip}	A_y^{hip}	A_z^{hip}
R	0.75	0.37	0.62	0.96	0.68	0.56	0.94	0.73	0.52
RMSE	5.71°	4.73°	2.90°	6.20°	3.07°	7.18°	6.70°	2.28°	7.94°

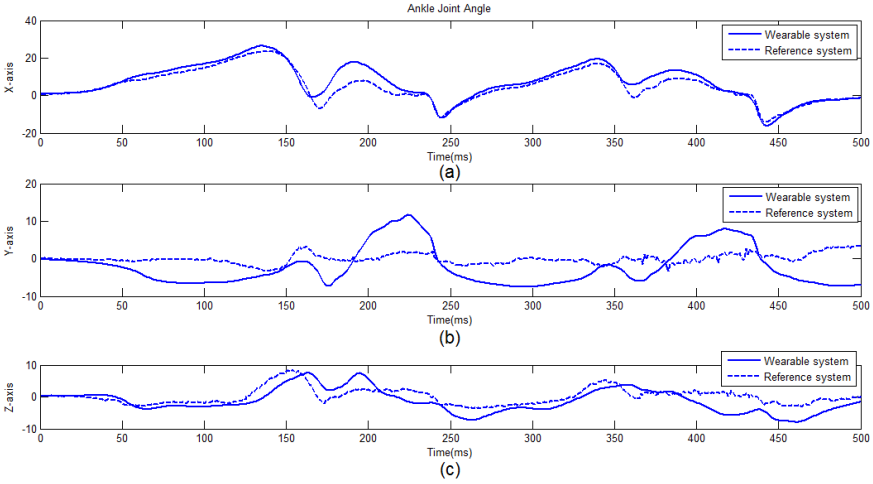

Fig. 8 Comparison results of ankle joint angle, (a): A_x^{ankle}; (b): A_y^{ankle}; (c): A_z^{ankle}

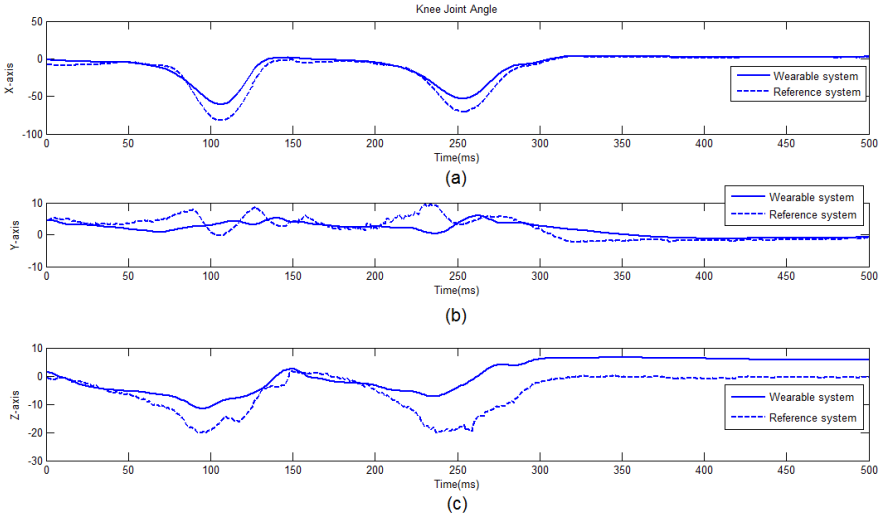

Fig. 9 Comparison results of knee joint angle, (a): A_x^{knee}; (b): A_y^{knee}; (c): A_z^{knee}

The measurement results of ankle joint angle showed an acceptable agreement of A_x^{ankle} with average R of 0.75 and RMSE of 5.71°, a low agreement of A_z^{ankle} with average R of 0.62 and RMSE of 2.90°. Contradiction was found between the measurement results of A_y^{ankle} of the wearable system and the reference system. We can see from Figure 8(b), the measurement results of the reference system are almost changeless while the measurement results of the wearable system are periodic and regular. So it's hardly to make a conclusion that the measurement results of the wearable system are undesirable. The wiggles of the shoes may cause inaccurate measurement of ankle joint angle, but it's still too hard to form a regular change of A_y^{ankle}.

The measurement results of knee joint angle showed a good agreement of A_x^{knee} with average R of 0.96 and RMSE of 6.20°, an acceptable agreement of A_y^{knee} with average R of 0.68 and RMSE of 3.07°, a low agreement of A_z^{knee} with average R of 0.56 and RMSE of 7.18°.

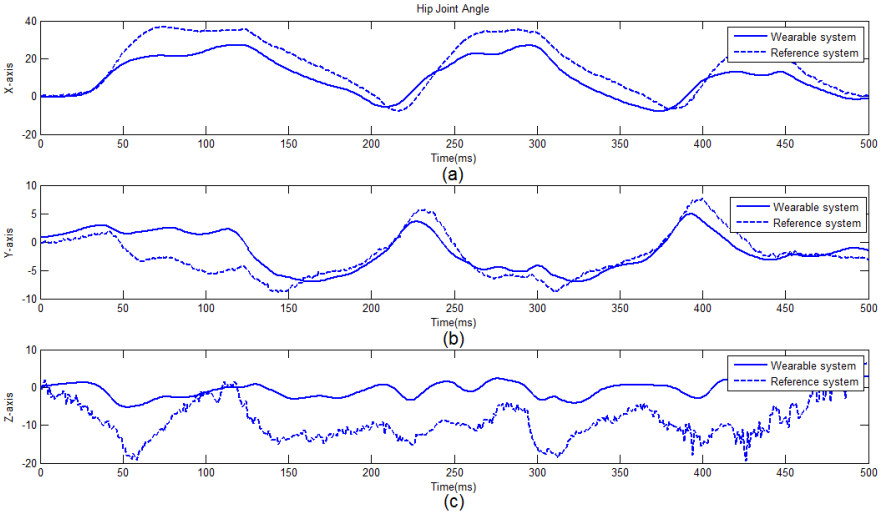

Fig. 10 Comparison results of hip joint angle, (a): A_x^{hip}; (b): A_y^{hip}; (c): A_z^{hip}

The measurement results of knee joint angle showed a good agreement of A_x^{knee} with average R of 0.94 and RMSE of 6.70°, an acceptable agreement of A_y^{knee} with average R of 0.73 and RMSE of 2.28°, a low agreement of A_z^{knee} with average R of 0.52 and RMSE of 7.94°.

8 Results of Joint Forces and Joint Moments

Table 3 shows the comparison results of z-axial joint forces and x-axial joint moments between the wearable system and the reference system. The RMSEs of joint forces and joint moments were normalized to the body weight (N/kg, Nm/kg). The

F_z^{ankle}, F_z^{knee} and F_z^{hip} denote the z-axial joint force of ankle, knee and hip respectively. The M_x^{ankle}, M_x^{knee} and M_x^{hip} denote the x-axial joint moment of ankle, knee and hip respectively. Figure 11 shows a group of representative measurement results of z-axial joint force of ankle, knee and hip. Figure 12 shows a group of representative measurement results of x-axial joint moment of ankle, knee and hip.

Table 3 The comparison results of z-axial joint forces and x-axial joint moments between the wearable system and the reference system

	F_z^{ankle}	F_z^{knee}	F_z^{hip}	M_x^{ankle}	M_x^{knee}	M_x^{hip}
R	0.85	0.90	0.90	0.64	0.79	0.72
RMSE	2.26	1.72	1.78	0.60	0.32	0.56

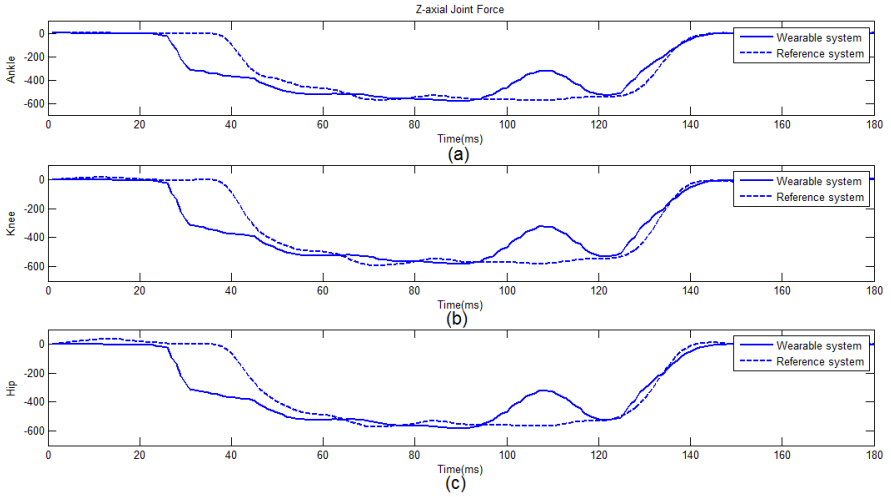

Fig. 11 Comparison results of z-axial joint forces, (a): ankle; (b): knee; (c): hip

The measurement results of z-axial joint forces showed a reasonable agreement of F_z^{ankle} with average R of 0.85 and RMSE of 2.26, good agreements of F_z^{knee} and F_z^{hip} with average R of 0.90 and RMSE of 1.72, average R of 0.90 and RMSE of 1.78 respectively.

The measurement results of x-axial joint moments showed a reasonable agreement of M_x^{knee} with average R of 0.79 and RMSE of 0.32, a low agreement of M_x^{ankle} with average R of 0.64 and RMSE of 0.60, an acceptable agreement of M_x^{hip} with average R of 0.72 and RMSE of 0.56. The calculation method of joint forces and joint moments in the wearable system are based on the rigid lower extremities model which take the human body as rigid segments and global joints to make the estimations. For now, the estimation of joint force and joint moment is still remaining a difficult problem. The difference in the calculation methods will lead to different values.

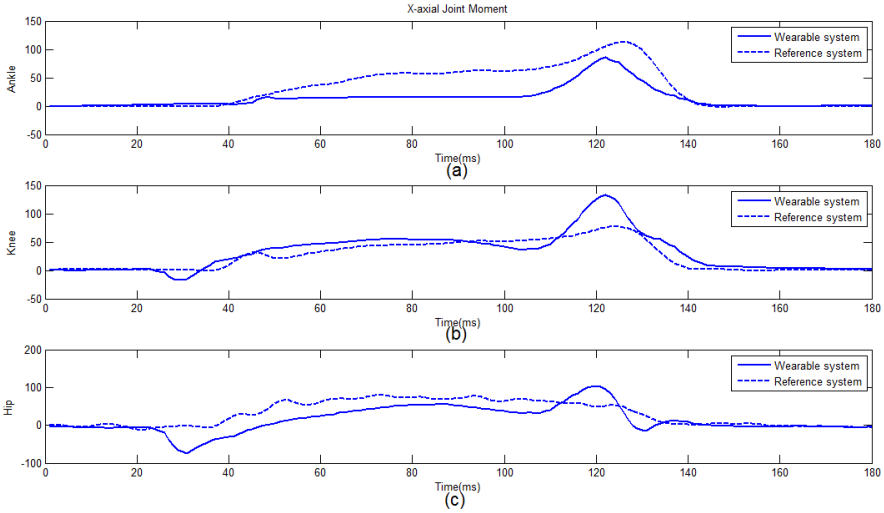

Fig. 12 Comparison results of x-axial joint moments, (a): ankle; (b): knee; (c): hip

9 Conclusion

We developed a wearable sensors system composed of wearable sensor shoes and motion sensors, and we accomplished the goal of successive measurement of walking gait in non-laboratory environment. A reference system composed of high speed cameras and stationary force plates was used to implement the dynamic verification of the wearable system. The experiment results support the feasibility and reliability of the developed system. The z-axial GRF, x-axial joint angles and z-axial joint forces can be measured with high accuracy. And the estimation of joint moments achieved an acceptable accuracy. But the measurement accuracy of the secondary axial components should be improved in our future work. And as the amount of sensors increased, the synchronization of wireless data communication is influenced slightly. The communication protocol used in this wireless wearable system should be modified to guarantee the high speed and low delay in data transmission.

References

[1] Passmore, E., Sangeux, M.: Improving repeatability of setting volume origin and coordinate system for 3D gait analysis. Gait & Posture 39, 831–833 (2014)
[2] Betker, A.L., Szturm, T., Moussavi, Z.M.K.: Estimation of 2-D center of mass movement during trunk flexion-extension movements using body accelerations. IEEE Trans. Neural Syst. Rehab. Eng. 17(6), 553–559 (2009)
[3] Tesio, L., Rota, V., Chessa, C., Perucca, L.: The 3-D path of body center of mass during adult human walking on force treadmill. J. Biomechan. 43(5), 938–944 (2010)

[4] Carse, B., Meadows, B., Bowers, R., Rowe, P.: Affordable clinical gait analysis: An assessment of the marker tracking accuracy of a new low-cost optical 3D motion analysis system. Physiotherapy 99, 347–351 (2013)
[5] Mihradi, S., Ferryanto, Dirgantara, T., Mahyuddin, A.I.: Tracking of makers for 2D and 3D gait analysis using home video cameras. International Journal of E-Health and Medical Communications 4(3), 36–52 (2013)
[6] Li, Q., Young, M., Naing, V., Donelan, J.M.: Walking speed estimation using a shank-mounted inertial measurement unit. J. Biomech. 43(8), 1640–1643 (2010)
[7] Hartmann, A., Murer, K., de Bie, R.A., de Bruin, E.D.: Reproducibility of spatio-temporal gait parameters under different conditions in older adults using a trunk tri-axial accelerometer system. Gait and Posture 30(3), 351–355 (2009)
[8] Galen, S.S., Clarke, C.J., Allan, D.B., Conway, B.A.: A portable gait assessment tool to record temporal gait parameters in SCI. Med. Eng. Phys. 33(5), 626–632 (2011)
[9] McGrath, D., Greene, B.R., Walsh, C., Caulfield, B.: Estimation of minimum ground clearance (MGC) using body-worn inertial sensors. J. Biomechan. 44(6), 1083–1088 (2011)
[10] Mayagoitia, R.E., Nene, A.V., Veltink, P.H.: Accelerometer and rate gyroscope measurement of kinematics: an inexpensive alternative to optical motion analysis systems. Journal of Biomechanics 35, 537–542 (2002)
[11] Wentink, E.C., Beijen, S.I., Hermens, H.J., Rietman, J.S., Veltink, P.H.: Intention detection of gait initiation using EMG and kinematic data. Gait & Posture 37, 223–228 (2013)
[12] Rueterbories, J., Spaich, E.G., Andersen, O.K.: Characterization of gait pattern by 3D angular accelerations in hemiparetic and healthy gait. Gait & Posture 37, 183–189 (2013)
[13] Lopez-Sanroman, F.J., Holmbak-Petersen, R., Santiago, I., Gomez de Segura, I.A., Barrey, E.: Gait analysis using 3D accelerometry in horses sedated with xylazine. The Veterinary Journal 193, 212–216 (2012)
[14] Liu, T., Inoue, Y., Shibata, K., Shiojima, K., Han, M.M.: Triaxial joint moment estimation using a wearable three-dimensional gait analysis system. Measurement 47, 125–129 (2014)
[15] Faivre, A., Dahan, M., Parratte, B., Monnier, G.: Instrumented shoes for pathological gait assessment. Mechanics Research Communications 31, 627–632 (2004)
[16] Galen, S.S., Clarke, C.J., Allan, D.B., Conway, B.A.: A portable gait assessment tool to record temporal gait parameters in SCI. Medical Engineering & Physics 33, 626–632 (2011)
[17] Macleod, C.A., Conway, B.A., Allan, D.B., Galen, S.S.: Development and validation of a low-cost, portable and wireless gait assessment tool. Medical Engineering & Physics 36, 541–546 (2014)
[18] Liu, T., Inoue, Y., Shibata, K.: A wearable force plate system for the continuous measurement of triaxial ground reaction force in biomechanical applications. Measurement Science and Technology 21(8), 085804–085813 (2010)
[19] Liu, T., Inoue, Y., Shibata, K., Shiojima, K.: A mobile force plate and three-dimensional motion analysis system for three-dimensional gait assessment. IEEE Sensors Journal 12(5), 1461–1467 (2012)
[20] Brookner, E.: Tracking and Kalman Filtering Made Easy. Wiley-Interscience, New York (1998)

Towards a Brain-Machine System for Auditory Scene Analysis

Valerie Hanson[2] and Kofi Odame[1]

[1] Dartmouth College, Hanover, NH, USA
odame@dartmouth.edu
[2] MC10 Inc. Cambridge, MA, USA

1 Introduction

In hearing aids, noise suppression algorithms that rely on spatial cues tend to improve the intelligibility of speech in noisy environments [1], [2], [3], [4]. Unfortunately, the location of target and noise sources can change rapidly in a natural, everyday acoustic environment. In fact, depending on what the listener is attending to, one source may be considered noise in one instant, and then considered the target in another instant. Adaptive filtering attempts to track the target source, but it is successful only under a set of simplifying constraints [5], [6]. It is much more effective to allow the user to determine the direction from which the target sound is coming.

A rudimentary way of doing this is for the algorithm to assume that the user's "look" or forward direction is also the direction from which the target sound is coming. In complex auditory environments, this scheme breaks down, and it is desirable for the user to have a wider and finer control of the direction of the target sound [7], [8]. Some hearing aid companies have addressed this problem by introducing a hand-operated controller. Unfortunately, such a solution increases the complication and obtrusiveness of the hearing aid, going against users' desire for a "wear and forget" device that requires no explicit operation [9]. In addition, use of a hand-operated controller may be encumbered by the user's having to hold or manipulate other objects [10], [11], [12].

The brain-computer interface (BCI) has been proposed as a means of unobtrusive human-computer interaction [13], [14], [15], [16], [17]. However, previous reported auditory-based BCIs, as would be used in a hearing aid application, have either relied on preset, dichotic pairs of stimuli [18], or have used simple, closed sets of stimuli [19], [20], [21]. These previous systems would not be suitable for a natural and uncontrolled listening situation.

In this chapter, we explore the feasiblity of controlling a hearing aid with a BCI that is based on auditory-evoked electroencephalography (EEG) responses to an open set of natural auditory stimuli, as would be encountered,

S.C. Mukhopadhyay (ed.), *Wearable Electronics Sensors,*
Smart Sensors, Measurement and Instrumentation 15, DOI: 10.1007/978-3-319-18191-2_13

for example, in a busy restaurant. To address practical concerns about the size and latency of the BCI, we also examine the performance implications of using single-channel EEG, semi-dry electrodes and also single trial detection of the EEG signal. Section 2 presents an overview of the system, and Section 3 describes our strategy for processing and analyzing the user's neural signals. We present and discuss preliminary experimental results in Sections 4 and 5.

2 System Overview

Figure 1 is a high-level diagram of the proposed system for hybrid brain-machine auditory scene analysis. It consists of a microphone array for sensing the auditory environment, scalp electrodes for measuring the user's electroencephalography (EEG) signals, as well as computational units (a beamsteerer, a binary mask algorithm implementation and a P300 detector) for processing the audio and EEG signals. When performing noise suppression, the system operates in either a scanning mode or a locked mode, depending on the cognitive state of the user.

In the scanning mode, the beamsteerer sweeps the direction of focus of the spatial filter's main lobe. If the incident angles of the primary sound sources are at least 30° apart, then the beamsteerer in combination with the binary masking algorithm is able to isolate the sound that is coming from different directions in the auditory environment in turn [22], playing it to the user via the hearing aid's loudspeaker. So, the hearing aid will effectively present interleaved, or non-overlapping speech to the user. (Note: any sound that bypasses the hearing aid molding and directly enters the user's ear canal will result in some level of overlapping speech, an effect that we did not model in our current experiments.)

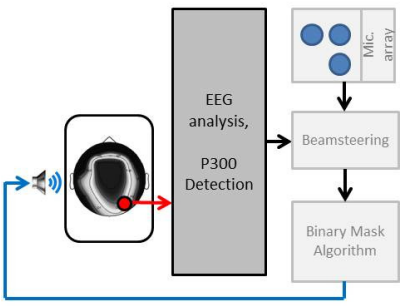

Fig. 1 Diagram showing the top level of the BCI system. Auditory scene information is input to the beamsteering unit. This unit takes as a second input the direction a user wishes to focus on, as obtained from the EEG analysis and P300 detection unit. The processed output of the beamsteerer/binary mask algorithm is then what the user hears through the device.

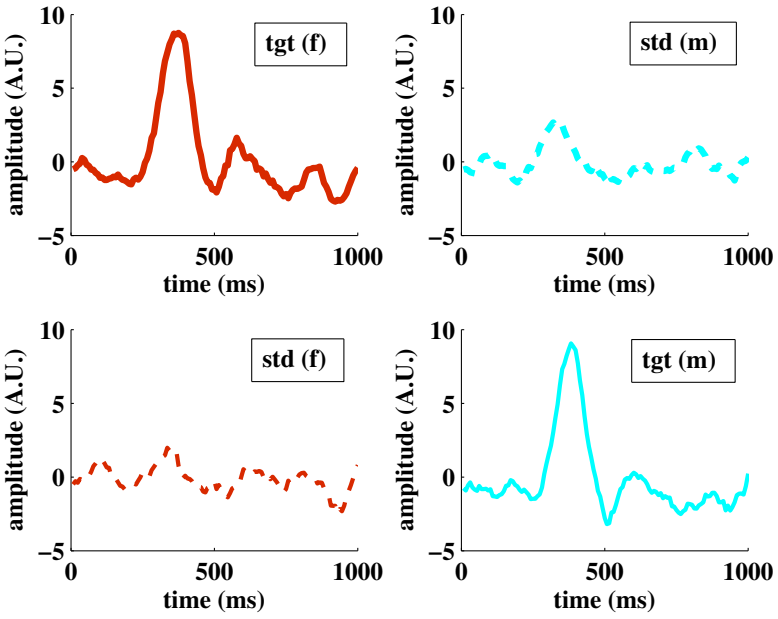

Fig. 2 Plots showing the averaged EEG response for four different stimulus conditions measured at the AF4 electrode after artifact rejection and filtering. In the top row, the target stimulus was a female voice, while in the bottom row, the target stimulus was a male voice. Presentation of the target stimulus elicits a P300 response in both cases. In addition, a P300 subcomponent appears in response to standard stimuli, but the latency and amplitude of this response are clearly distinguishable from those exhibited by the target condition P300.

For each direction of focus, the user's EEG signal is measured and analyzed for the presence of a P300 response. This is an involuntary and automatic neurological response to an anticipated stimulus. As shown in Fig. 2, the user's EEG will exhibit a P300 response when he hears a sound that he wants to pay attention to (this is the user's "target" stimulus). On the other hand, a sound that the user is not interested in listening to – known as a "standard stimulus" – will not elicit a P300 response. P300 habituation should not be a concern, because the stimuli presented to the user depends on the real-time auditory environment, which is constantly changing [23].

If the auditory scan results in a P300 response, the system enters the locked mode. Now, the beamsteerer remains trained on the direction of focus that elicited the P300 signal, and the binary mask algorithm isolates the corresponding target sound, exclusively playing this to the user via the loudspeaker (a potential improvement on this proposed locked mode would involve sound source tracking, in case the target were to move relative to the

user). During the locked mode, the user's EEG signal is continually measured and analyzed. Some indication from the EEG (e.g. increased cognitive load, or reduced correlation between the EEG response and the presented sound [24], [25], [26]) would cause the system to unlock and begin scanning the auditory environment again.

3 P300 Detection

The P300 detection algorithm is based on machine learning and classification methods, which are robust to the low signal-to-noise ratio (SNR) that is typical of scalp EEG [14]. The main tasks involved in P300 detection are signal preprocessing, feature extraction and classification. There is also an offline training step. Following are the details of each of these tasks.

3.1 Preprocessing

3.1.1 Artifact Rejection

Artifacts in the EEG signal are produced by changes in electrode contact impedance, as well as by eye blinks and other user movements. To avoid potential errors in P300 detection, the system performs some simple tests to detect and discard any EEG data that might contain these contaminating signals.

Large-amplitude artifacts, due for example to eye blinks, are detected by comparing the measured signal to a set threshold. Any EEG signal that exceeds this threshold is considered to contain artifacts and is discarded. Some artifacts do not cause large-amplitude disturbances, but might otherwise produce abnormal EEG signals. These are identified as those that have a mean and variance that is outside the 2 to 92 percentile range of all other readings made under the same stimulus conditions.

3.1.2 Bandpass Filtering

The P300 comprises multiple frequency components in the delta (1.5-4 Hz), theta (4-7.5 Hz), and alpha (7.5-12.5 Hz) bands. To retain as much of the P300 signal while suppressing any potential interference due to slow DC drifts or unrelated alpha band activity, the EEG data is band-pass filtered with a pass band of 0.8 Hz to 6 Hz. The filter is implemented as a linear phase FIR filter, in order to preserve the shape of the EEG response, and to allow for accurate time alignment with the audio stimulus.

3.1.3 Normalization

Our preliminary experiments have shown some variation in absolute P300 amplitude over time. However, for a given scanning period, the ratio of target P300 amplitude to that of non-target EEG signal remains fairly constant. Normalizing the EEG signal allows the system to be sensitive to relative, rather than absolute, changes in amplitude. The normalized EEG signal, x_i, is computed as

$$x_i = \frac{z_i - \overline{z}_{n \neq i}}{\sigma_i}, \tag{1}$$

where z_i is the raw EEG "epoch" that is recorded simultaneously as the i^{th} stimulus of a scan period is played. Also, $\overline{z}_{n \neq i}$ is the average of all epochs (except the i^{th} one) corresponding to the other stimuli that were presented during the same scan period. Finally, σ_i is the standard deviation of the z_i signal.

3.2 Feature Extraction

For each stimulus presentation, the simulataneously-measured epoch of EEG data is preprocessed, anti-aliased and down-sampled from 128 Hz to a rate of 32 Hz. This produces $n \times 32$ data points for an n-channel EEG device, but the system selects only 10 specific data points as features for the classifier.

Each EEG epochs is labelled according to the stimulus that produced it . Separation analysis is performed using the coefficient of determination, r^2 [27], computed from the labelled EEG epochs as

$$r^2 = \frac{\text{cov}(x, y)^2}{\text{var}(x)\text{var}(y)}, \tag{2}$$

where x is the value at an EEG data point, and $y \in (0, 1)$ is the class label of the EEG epoch ('0' denotes "produced by standard stimulus", and '1' denotes "produced by target stimulus"). Figure 3 shows a typical plot of r^2 coefficients that we generated. Feature selection is done by identifying the N electrode channels that produced the N largest r^2 values, and then selecting the $10/N$ strongest features from each of those channels. In our experiments, we chose $N = 5$ and $N = 1$.

3.3 Classification

A linear support vector machine (SVM) is trained with training data, and then subsequently used to classify each newly-extracted EEG feature vector as being either in the target or standard class. Linear SVMs have been shown to provide good performance in similar applications [28], [29], and they are readily implementable on embedded platforms [30], [31].

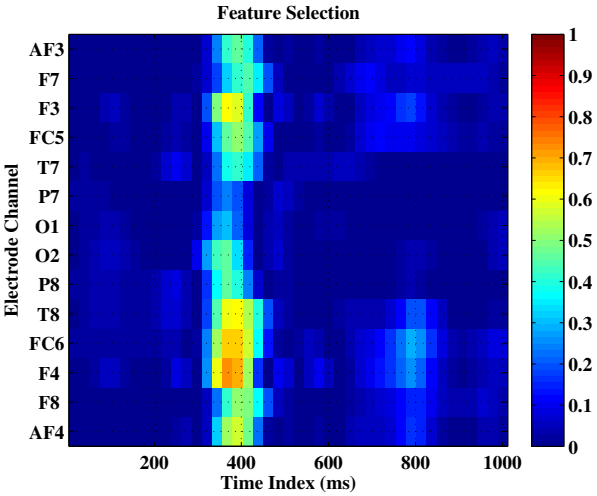

Fig. 3 Feature extraction plot generated for data obtained from a binary choice P300 classification experiment. Note, the P300 location is at approximately 400 ms. The color scale corresponds to the r^2 coefficient value.

4 Experiments

4.1 Overview

4.1.1 Equipment

We played auditory stimuli via earbud headphones and used the Emotiv EPOC headset (Emotiv Systems Inc., San Francisco, CA) to measure scalp EEG data. The EPOC headset is wireless and uses damp felt pad electrodes, which is close to the type of wearable, dry electrode EEG system that we envision for our application. The EPOC headset is a 16 electrode channel system, with a sampling rate of 128 Hz per channel, at 14 bits per sample. The active electrodes cover positions AF3/AF4, F3/F4, F7/F8, FC5/FC6, T7/T8, P3/P4, P7/P8, O1/O2 of the 10-10 positioning system, with one reference electrode behind each ear (see Fig. 4).

A Dell workstation (Dell Inc., Round Rock, TX), running MATLAB Version 7.14 (The MathWorks Inc., Natick, MA) and the BCI2000 toolbox [27], was used for central control, producing audio stimulus signals, and performing EEG signal processing.

4.1.2 Method

Two separate signal streams were output simultaneously from each of the stereo line out channels of the computer's sound card.

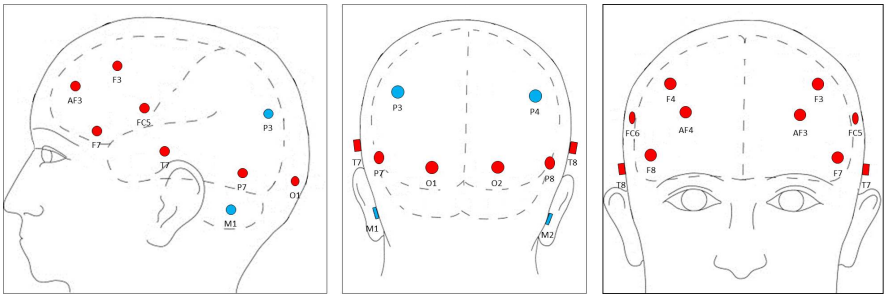

Fig. 4 Figure modified from [32], showing the standard electrode locations for the Emotiv Epoc headset. Signal electrodes are red, and reference electrodes are blue. The primary reference electrode locations are P3 and P4, but these can be used as signal electrodes, in which case the alternate reference electrode locations are over the mastoid process behind the ears (M1 and M2).

One stream was the audio stimulus that was played binaurally to the user via the headphones. The specific content of the audio stimulus stream differed for the different experiments, but in general, it consisted of a continuous signal that alternated between the target and the standard stimulus. The target stimulus was the voice that the subject was asked to attend to, while the standard stimulus was a different voice. To ensure attentiveness, the subject was asked to keep a count of how many times he heard the target stimulus. If the subject's total count of target stimulus presentations was off by more than 10%, then the EEG data for that session was discarded.

The second signal stream was a sinusoidal control signal that was part of the experimental measurement setup and was inaudible to the user. The purpose of the control signal was to label the audio stimulus. Each speaker was assigned a different label, which was encoded as the amplitude of the control signal; when there was no audio stimulus, the amplitude of the control signal was zero (please see Fig. 6). The control signal allowed for easy separation of stimulus onsets during post-processing analysis. After being output simultaneously with the audio stimulus stream, the control signal was input back to the sound card via the line-in port. It was time-aligned, recorded and saved simultaneously with the subject's scalp EEG. Using the information from the control signal, the EEG recording was parsed and labelled into target epochs and standard epochs.

After preprocessing and feature extraction, arbitrarily-selected instances of the standard-class feature vectors were discarded, so that there was an equal number of standard- and target-class instances. This balanced set of remaining feature vectors was used for leave-one-out cross validation of the linear SVM classifier. For each cross validation iteration, the receiver operator characteristic (ROC) was generated by varying the threshold used to separate the two classes from -1 to 1 (see, for example, Fig. 5). The performance of

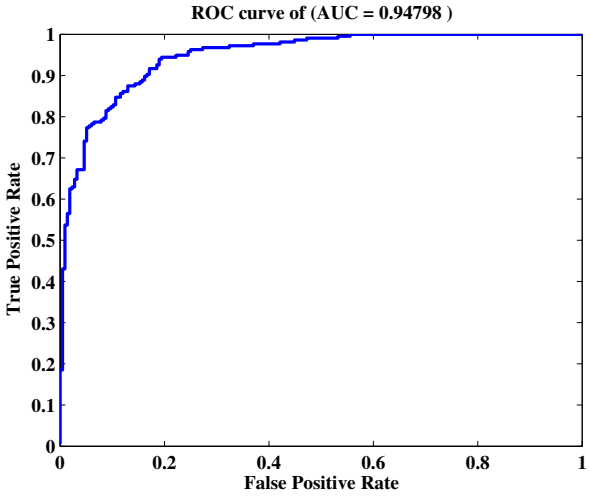

Fig. 5 A typical ROC curve that was generated by our SVM classifier. In this work, we use the area under the ROC (AUROC) as a measure of the classifier's accuracy. For a perfect classifier, AUROC= 1, while AUROC= 0.5 corresponds to random chance.

the classifier was measured as the area under the ROC (AUROC), averaged over all of the cross validation iterations.

4.2 Experiment 1: Two-Speaker/Same Word Discrimination

In this experiment, we studied whether or not it was possible to generate a P300 signal when the target/standard stimulus differentiation was based solely on the gender of the speaker.

4.2.1 Audio Stimulus

The audio stimulus stream was based on two speech samples from the TIMIT database [33], one of a male speaker, and the other of a female speaker, both saying the sentence, "She had your dark suit in greasy wash water all year." The audio stimulus stream was constructed as repetitions of the male and female speaker utterances of the word "dark" that was extracted from the sentences. Each stimulus had a duration of 227 ms with an interstimulus interval (ISI) of 500 ms, for a total stimulus period of 727 ms, as shown in Fig. 6.

For experimental runs where the target stimulus was the male voice, the audio stream consisted of sequences of 5 to 8 repetitions of the female speaker's utterance of "dark," with each sequence terminated by a single male speaker

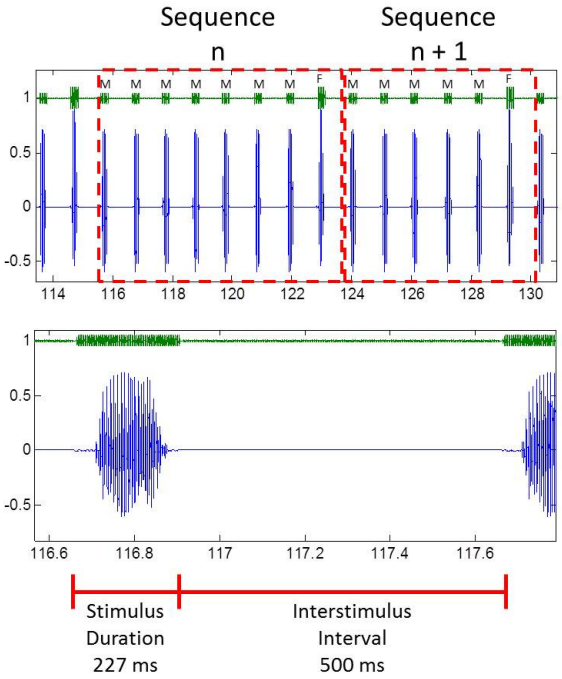

Fig. 6 (Top panel) Diagram showing a portion of a stimulus presentation stream to demonstrate the oddball presentation paradigm. In this example the target condition is the female voice, therefore, this stimulus is presented infrequently relative to the male voice. The blue signal shown here is the audio stimulus presented to the user, whereas the green signal is the control signal used to identify each stimulus. Note, the red boxes partition individual sequences, which comprise one target stimulus and 5 to 8 standard stimuli. (Bottom panel) Diagram showing the timing intervals for an individual stimulus presentation. The blue signal shown here is the audio stimulus presented to the user, whereas the green signal is the control signal used to identify this specific stimulus.

utterance of the word. This pattern was inverted for runs where the target stimulus was the female voice. The number of standard stimulus repetitions in a sequence was variable and random between 5 and 8, in order to increase the surprise facet of the P300 response, while maintaining the odd-ball paradigm.

4.2.2 EEG Data

One second of EEG data was recorded simultaneously with the presentation of each stimulus. Each of these 1 second EEG epochs was labelled as belonging to either the "target" or "standard" class, according to the stimulus type that produced it. After filtering, artifact rejection and feature extraction, the

collection of EEG epochs was divided into training and test sets; the training set was used to train the SVM, and the test set was used to quantify how accurately the trained SVM could distinguish a target-evoked EEG epoch from a standard one.

4.2.3 Recording Session Details

Data was collected during 6 separate recording sessions, which spanned the course of approximately 1 month. The breakdown of a recording session is shown in Fig. 7. Each recording session was broken into several "runs" that each lasted from 1.8 to 3.3 minutes, with a 2 minute break between runs. For any given run, the subject was presented with several sequences of varying length that were each terminated by the target stimulus. The subject was instructed to attend to the run's particular target stimulus.

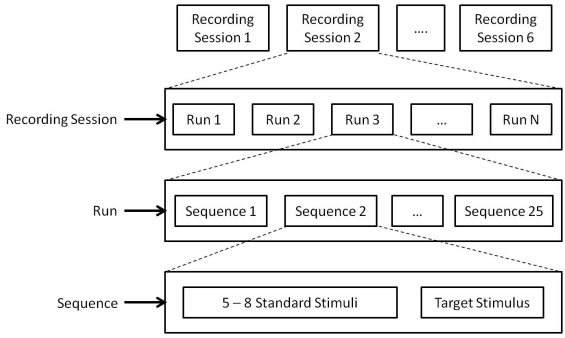

Fig. 7 Diagram showing terms as referred to in the text. For this experiment 6 recording sessions were performed. Each recording session comprises N runs. Each run comprises 25 sequences. Each sequence comprises 5 to 8 standard stimuli presentations followed by 1 target stimulus presentation. The subject is given no indication about when a sequence begins or ends.

4.2.4 Results

Figure 8 shows the AUROC numbers achieved by the SVM when it was tested and trained on data from the same recording sessions. The SVM's ability to classify a single epoch improved from 0.79 to 0.86 when data was taken from 5 versus only 1 electrode. Averaging also improved the performance of the SVM: by averaging 5 or more EEG epochs, the classification accuracy increased to 0.97 or better, using data from either 1 (AF4) or 5 electrodes. To assess the long-term robustness of the classifier, the SVM was also tested on data from a recording session that was different from the one on which it was trained. As Fig. 9 shows, the accuracy of the classifier changed only by a few percent, relative to test data from the same recording session.

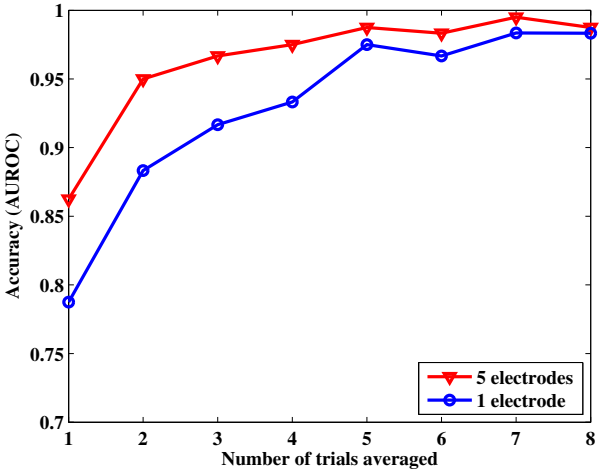

Fig. 8 Measurement results for two-speaker/single word speech experiment. The accuracy of the P300 detection algorithm is measured as the area under the receiver operator characteristic curve (AUROC). The EEG epochs that correspond to a particular stimulus type (that is, a particular speaker) are time-aligned and averaged before being input to the classifier. The EEG data used to train and test the classifier were collected from the same recording sessions. Each trial is 6 to 9 seconds long.

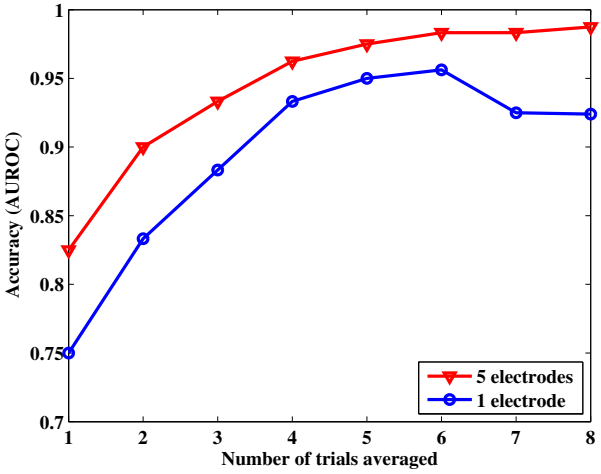

Fig. 9 Measurement results for two-speaker/single word speech experiment, time-aligned and averaged for all EEG epochs of the same stimulus type. The EEG data used to train and test the classifier were collected from different recording sessions.

4.3 Experiment 2: Two-Speaker/Streaming Speech Discrimination

Similar to Experiment 1, the purpose of this experiment was to study if it was possible to generate a P300 response when the target/standard stimulus differentiation was based on the gender of the speaker. In this experiment, however, the stimulus was not a single, repeated word, but instead an open set of words that would be encountered in natural speech.

4.3.1 Audio Stimulus

The audio stimulus stream was created from two public speeches, one female [34] and the other male [35]. The audio stimulus stream was constructed by alternating between one speech and the other, to simulate the scan mode scenario where the directional microphones are continually switching focus between two simultaneous speakers. For experimental runs where the target stimulus was the female voice, the audio stream consisted of strings of length 5 to 8 seconds of the male speaker's speech, with each string separated by a 1 second chunk of the female speaker's speech. The pattern was inverted for runs where the target stimulus was the male voice. The length of the standard string was variable and random between 5 and 8 seconds, in order to increase the surprise facet of the P300 response.

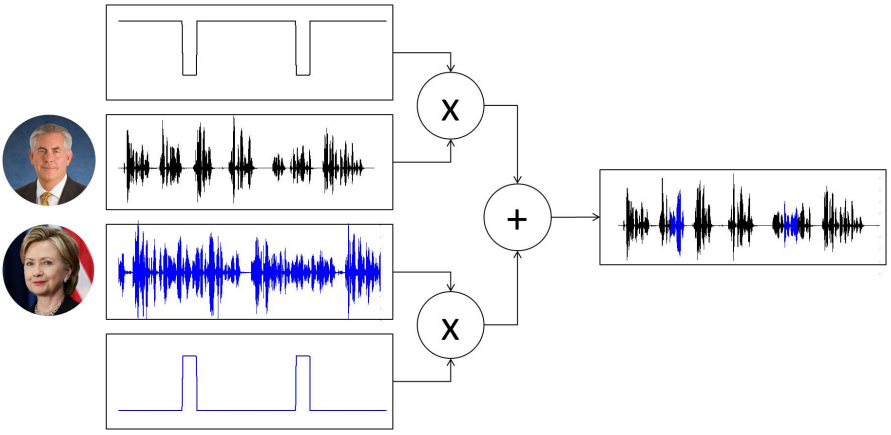

Fig. 10 Generation of audio stimulus stream for two-speaker/streaming speech experiment, where the female voice is the target stimulus. The standard stimulus (male voice) is modulated with a high duty cycle pulse train; the target stimulus (female voice) is modulated with the complementary pulse train. The audio stimulus stream is output as the combination these two modulated signals.

4.3.2 EEG Data

The first one second of EEG data that followed the presentation of each stimulus was recorded and labeled as either "target" or "standard," according to the stimulus type that produced it. After preprocessing, the EEG epochs were used as training and test sets for the SVM, as was done in Experiment 1.

4.3.3 Recording Session Details

Data was collected during 3 recording sessions, the breakdown of which is shown in Fig. 11.

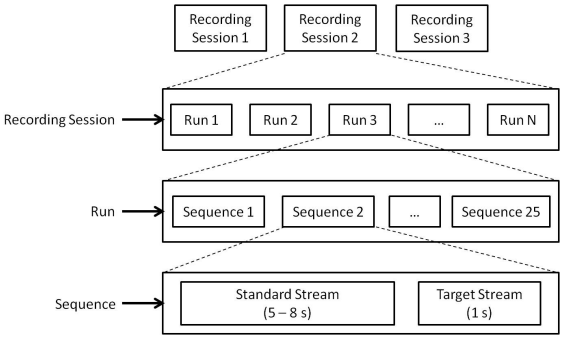

Fig. 11 Diagram showing terms as referred to in the text. For this experiment 3 recording sessions were performed. Each recording session comprises N runs. Each run comprises 25 sequences. Each sequence comprises one standard stimulus stream presentation lasting 5-8 s followed by one target stimulus stream presentation lasting 1 s.

4.3.4 Results

As with Experiment 1, Figs. 12 and 13 show that the SVM accuracy increases with number of electrodes used and number of averages taken. Using EEG data from a single electrode (AF4), and averaging over 2 epochs, the SVM accuracy is 0.75. When EEG data is taken from 5 electrodes and averaged over 5 or more epochs, the accuracy increases to over 0.95. Also, the classification accuracy drops only slightly when the SVM is trained and then tested with data from a different recording session.

4.4 Experiment 3: Multi Speaker/Streaming Speech Discrimination

The third experiment was a preliminary study of the feasibility of eliciting a P300 response from a target voice among several different possible voices.

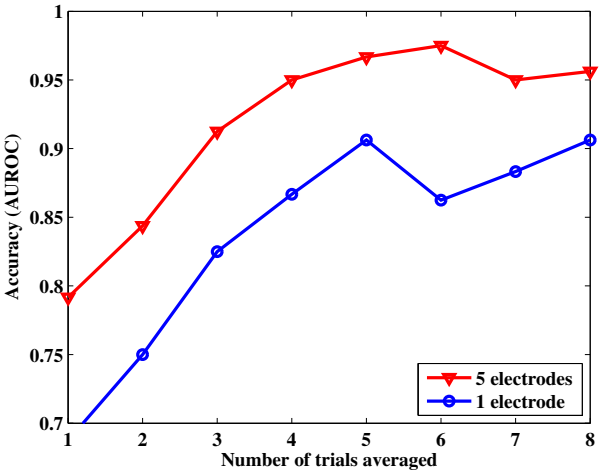

Fig. 12 Measurement results for two-speaker/streaming speech experiment. The accuracy of the P300 detection algorithm is measured as the area under the receiver operator characteristic curve (AUROC). The EEG epochs that correspond to a particular stimulus type (that is, a particular speaker) are time-aligned and averaged before being input to the classifier. The EEG data used to train and test the classifier were collected from the same recording sessions. Each trial is 6 to 9 seconds long.

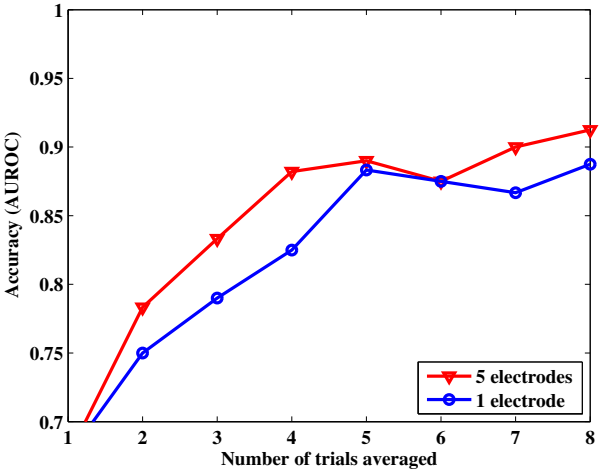

Fig. 13 Measurement results for two-speaker/streaming speech experiment, time-aligned and averaged for all EEG epochs of the same stimulus type. The EEG data used to train and test the classifier were collected from different recording sessions.

This scenario represents the actual use case of the hybrid brain/machine auditory system for a hearing aid system.

4.4.1 Audio Stimulus

The audio stimulus stream was based on the speech samples of 6 unique speakers (3 male, 3 female) from the TIMIT database. For each speaker, a single, continuous "speech" was created by arbitrarily ordering and concatenating all of the sentences that he/she had recorded. The audio stimulus stream was constructed by alternating between each of the "speeches" for durations of 1.5 seconds, each followed by 1.5 seconds of silence (the inter-stimulus interval). The ordering of speakers was random within a sequence and varied between sequences, with the same speaker never appearing twice in a row. The voice of one specific speaker, denoted as S2, was designated the target stimulus; the subject was asked to keep count of how many times the voice of speaker S2 was heard.

4.4.2 EEG Data

The first 3 seconds of EEG data that followed the presentation of each stimulus was recorded and labeled as either target or standard, according to the stimulus type that produced it. After preprocessing, the EEG epochs were separated and used as training and test sets for the SVM, as was done in the previous two experiments.

4.4.3 Recording Session Details

Data was collected in a single recording session, during which a total of 220 stimuli sequences were presented (see Fig. 14). During each sequence, 5 standard stimuli were presented and one target stimulus was presented, all in a random order. The subject did not receive any cues about the start or stop time of the sequences.

4.4.4 Results

Figures 15 and 16 show averaged EEG responses to the six stimuli, measured at the F3 and F4 locations, respectively. A clear P300 signal is visible for the response to the target stimulus, speaker S2. Figure 17 is an alternative way of visualizing the EEG data. It is a scatter plot of the three most discriminative features of a typical subset of the measured EEG responses. These three features were the ones found to have the highest r^2 values. As the scatter plot shows, the EEG responses cluster into two distinct groups, representing the target and standard classes. The plot also shows that two of the features, $F4^1$ and $F4^2$ – corresponding to the amplitude of the F4 channel, 0.97 and 1.06 seconds,

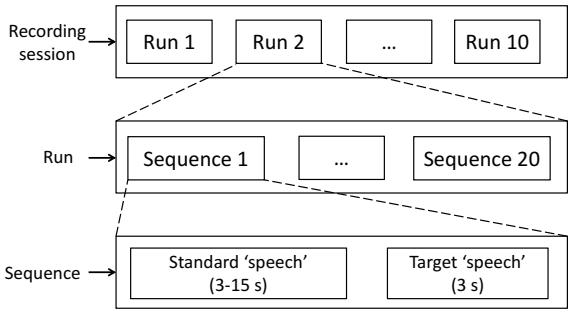

Fig. 14 Diagram showing recording procedure details. For this experiment, 1 recording sessions was performed, comprising 10 runs. Each run comprises 20 sequences, and each sequence comprises one standard stimulus stream presentation lasting 3-15 s followed by one target stimulus stream presentation lasting 3 s.

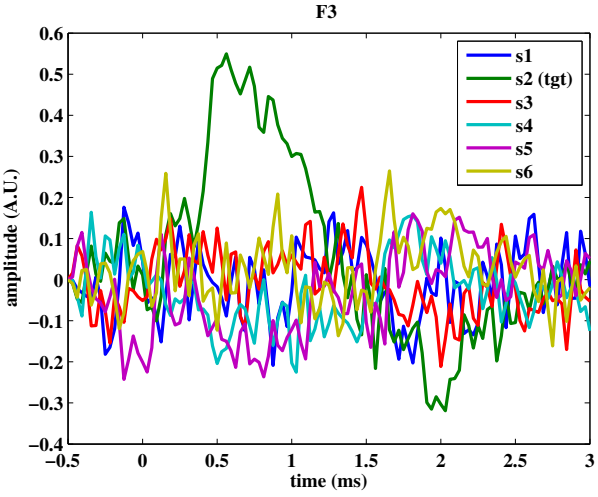

Fig. 15 Measurement results of the F3 EEG channel response for the multi speaker experiment, averaged across all trials for each of the six stimuli. The target stimulus is the voice of speaker S2.

respectively, after stimulus presentation – are highly linearly-related, implying that one does not carry much extra information in the presence of the other.

Given the redundancy of the $F4^2$ feature, we defined a new feature as the difference in amplitude of time points $t = 2$ s and $t = 0.5$ s in the F4 channel. This new feature makes use of the trough that occurs during the

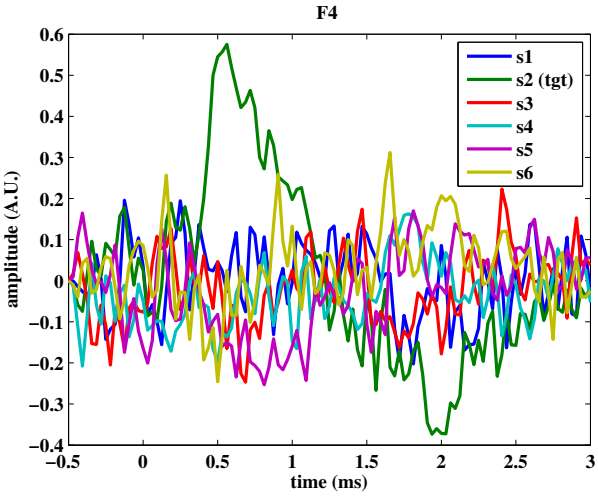

Fig. 16 Measurement results of the F4 EEG channel response for the multi speaker experiment, averaged across all trials for each of the six stimuli. The target stimulus is the voice of speaker S2.

silent interstimulus period following a target stimulus presentation, as can be seen in Figs. 15 and 16. Figure 18 shows the classification accuracy results for both single (F4) and multiple electrode data. Multiple electrode accuracy was only negligibly better (AUROC= 0.715 for 3 trial averaging) than single electrode accuracy (AUROC= 0.706 for 3 trial averaging).

5 Discussion

The experimental results show that our P300 detection algorithm can achieve better than 70% accuracy, which makes it a feasible approach for the proposed brain-controlled hearing aid [36]. However, the results also highlight some challenges that will have to be addressed before the approach can be used in a practical system.

While the minimally-obtrusive single electrode system comes with the attendant cost of degraded performance (as expected), it still achieves fairly high accuracy, which could potentially be improved with better electrode placement and better instrumentation. The P300 signal propagates with increasing amplitude from the frontal to the parietal scalp [37], but a single electrode BCI cannot take advantage of this spatio-temporal information. Instead, it must rely on single-site P300 data, which comprises some subcomponents with fairly small amplitudes and poor SNR [38]. This is particularly crucial if the electrode is not placed on the midline, where the P300 signal is largest [37]. Future studies to optimize the position of the recording

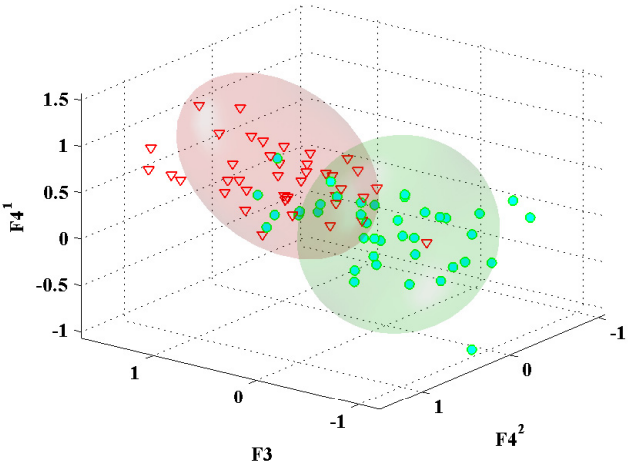

Fig. 17 Measurement results showing the three most discriminating (highest r^2 values) features that were extracted for the multi-speaker/streaming speech experiment. The feature labelled F3 corresponds to the amplitude of the F3 channel 1.19 seconds after stimulus presentation. Also, the $F4^1$ and $F4^2$ features correspond to the amplitude of the F4 channel, 0.968 and 1.06 seconds, respectively, after stimulus presentation. The ellipsoids highlight the approximate clustering of the P300 epochs (red diamonds) and the standard stimulus epochs (green dots).

site, as well as custom-designed electronics that are more sensitive to small EEG signals, are warranted.

From the results of Fig. 18, two to three trial averaging is probably necessary to obtain reliable P300 detection. This means that a six-direction scan, with a 1 second stimulus period, would take at least 12 seconds to lock onto a target. This is significantly longer than the 5 second latency that users would find acceptable [39]. Multi-trial averaging produces better results because it improves the SNR of the EEG data. To avoid averaging and its associated latency, yet maintain a useable amount of SNR, a more practical system should incorporate noise-suppression algorithms like blind source separation; single-channel versions of these algorithms have been described in [40], [41]. Also, experimentation with shorter stimulus durations and inter stimulus intervals might help to improve the system's latency.

One limitation of our experiments is that they do not include hearing-impaired subjects. However, other researchers have demonstrated that auditory-evoked EEG responses can be elicited from hearing-impaired listeners [26], [42], and used in a simple kind of BCI. These earlier works suggest that hearing-impaired listeners can effectively use our BCI, although future experiments will be needed to concretely evaluate our approach.

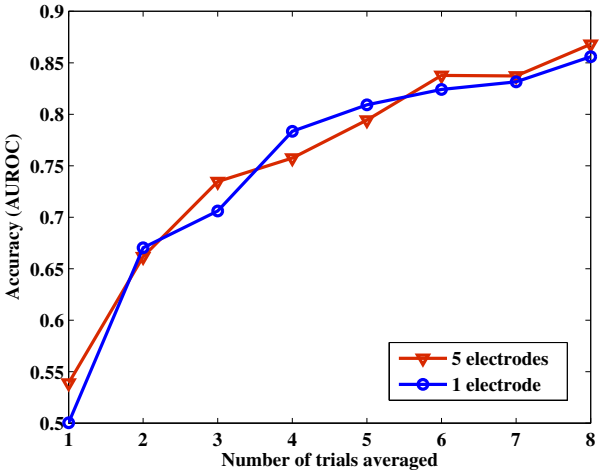

Fig. 18 Measurement results for multi-speaker/streaming speech experiment, showing AUROC for P300 classification task. For 5 electrode classification, five features were used, each taken as the amplitude of the time points with the highest r^2 value for EEG channels F3, F4 and AF3 respectively. For 1 electrode classification, the three features used were the two features in channel F4 with the highest r^2 values, as well as the difference in amplitude of the F4 channel between time points $t = 2$ s and $t = 0.5$ s. Each trial is 6 to 18 seconds long.

6 Conclusion

In this chapter, we have introduced a hybrid brain-machine system for auditory scene analysis that is based on a P300 brain computer interface, and which relies on an open set of natural, auditory stimuli. The preliminary experiments that we performed have yielded promising results, and suggest that the idea is indeed feasibile. The work has also highlighted several interesting areas for further exploration and improvement.

References

1. Jang, H., Song, J., Jeong, H.: Advanced narrow speech channeling algorithm for robot speech recognition. In: Proceedings of the 2009 International Conference on Hybrid Information Technology, pp. 130–137. ACM (2009)
2. Gravel, J.S., Fausel, N., Liskow, C., Chobot, J.: Children's speech recognition in noise using omni-directional and dual-microphone hearing aid technology. Ear and Hearing 20(1), 1–11 (1999)
3. Chung, K., Zeng, F.-G., Acker, K.N.: Effects of directional microphone and adaptive multichannel noise reduction algorithm on cochlear implant performance. The Journal of the Acoustical Society of America 120(4), 2216–2227 (2006)

4. Ricketts, T., Galster, J., Tharpe, A.M.: Directional benefit in simulated classroom environments. American Journal of Audiology 16(2), 130–144 (2007)
5. Wang, D.: Time-frequency masking for speech separation and its potential for hearing aid design. Trends in Amplification 12(4), 332–353 (2008)
6. Boldt, J., Kjems, U., Pedersen, M.S., Lunner, T., Wang, D.: Estimation of the ideal binary mask using directional systems. In: International Workshop on Acoustic Echo and Noise Control, IWAENC 2008 (2008)
7. Goetze, S., Rohdenburg, T., Hohmann, V., Kollmeier, B., Kammeyer, K.-D.: Direction of arrival estimation based on the dual delay line approach for binaural hearing aid microphone arrays. In: International Symposium on Intelligent Signal Processing and Communication Systems, ISPACS 2007, pp. 84–87. IEEE (2007)
8. Shinn-Cunningham, B.G., Best, V.: Selective attention in normal and impaired hearing. Trends in Amplification 12(4), 283–299 (2008)
9. Morla, A.: Four transformative patient demands: convenience, size, simplicity, and flexibility. Hearing Review 18(4), 36–42 (2011)
10. Witt, H., Nicolai, T., Kenn, H.: Designing a wearable user interface for hands-free interaction in maintenance applications. In: PerCom Workshops, pp. 652–655 (2006)
11. Oulasvirta, A., Bergstrom-Lehtovirta, J.: Ease of juggling: studying the effects of manual multitasking. In: Proceedings of the SIGCHI Conference on Human Factors in Computing Systems, pp. 3103–3112. ACM (2011)
12. Ng, A., Brewster, S.A., Williamson, J.: The impact of encumbrance on mobile interactions. In: Kotzé, P., Marsden, G., Lindgaard, G., Wesson, J., Winckler, M. (eds.) INTERACT 2013, Part III. LNCS, vol. 8119, pp. 92–109. Springer, Heidelberg (2013)
13. D'albis, T., Blatt, R., Tedesco, R., Sbattella, L., Matteucci, M.: A predictive speller controlled by a brain-computer interface based on motor imagery. ACM Transactions on Computer-Human Interaction (TOCHI) 19(3), 20 (2012)
14. Krusienski, D.J., Sellers, E.W., Cabestaing, F., Bayoudh, S., McFarland, D.J., Vaughan, T.M., Wolpaw, J.R.: A comparison of classification techniques for the p300 speller. Journal of Neural Engineering 3(4), 299 (2006)
15. Nijboer, F., Sellers, E.W., Mellinger, J., Jordan, M.A., Matuz, T., Furdea, A., Halder, S., Mochty, U., Krusienski, D.J., Vaughan, T.M., et al.: A p300-based brain–computer interface for people with amyotrophic lateral sclerosis. Clinical Neurophysiology 119(8), 1909–1916 (2008)
16. Iturrate, I., Antelis, J.M., Kubler, A., Minguez, J.: A noninvasive brain-actuated wheelchair based on a p300 neurophysiological protocol and automated navigation. IEEE Transactions on Robotics 25(3), 614–627 (2009)
17. Gao, S., Wang, Y., Gao, X., Hong, B.: Visual and auditory brain-computer interfaces. IEEE Transactions on Biomedical Engineering 61(5), 1436–1447 (2014)
18. Lopez-Gordo, M.A., Fernandez, E., Romero, S., Pelayo, F., Prieto, A.: An auditory brain–computer interface evoked by natural speech. Journal of Neural Engineering 9(3), 036013 (2012)
19. Klobassa, D.S., Vaughan, T.M., Brunner, P., Schwartz, N.E., Wolpaw, J.R., Neuper, C., Sellers, E.W.: Toward a high-throughput auditory p300-based brain–computer interface. Clinical Neurophysiology 120(7), 1252–1261 (2009)

20. Guo, J., Gao, S., Hong, B.: An auditory brain–computer interface using active mental response. IEEE Transactions on Neural Systems and Rehabilitation Engineering 18(3), 230–235 (2010)
21. Höller, Y., Kronbichler, M., Bergmann, J., Crone, J.S., Ladurner, G., Golaszewski, S.: Eeg frequency analysis of responses to the own-name stimulus. Clinical Neurophysiology 122(1), 99–106 (2011)
22. Hanson, V., Odame, K.: Real-time embedded implementation of the binary mask algorithm for hearing prosthetics. IEEE Transactions on Biomedical Circuits and Systems (2013)
23. Polich, J.: Habituation of p300 from auditory stimuli. Psychobiology 17(1), 19–28 (1989)
24. O'Sullivan, J.A., Power, A.J., Mesgarani, N., Rajaram, S., Foxe, J.J., Shinn-Cunningham, B.G., Slaney, M., Shamma, S.A., Lalor, E.C.: Attentional selection in a cocktail party environment can be decoded from single-trial eeg. Cerebral Cortex, bht355 (2014)
25. Ding, N., Simon, J.Z.: Emergence of neural encoding of auditory objects while listening to competing speakers. Proceedings of the National Academy of Sciences 109(29), 11854–11859 (2012)
26. Lunner, T.: Method of operating a hearing instrument based on an estimation of present cognitive load of a user and a hearing aid system. US Patent App. 12/642,345 (December 18, 2009)
27. Schalk, G., McFarland, D.J., Hinterberger, T., Birbaumer, N., Wolpaw, J.R.: Bci2000: a general-purpose brain-computer interface (bci) system. IEEE Transactions on Biomedical Engineering 51(6), 1034–1043 (2004)
28. Daubigney, L., Pietquin, O., et al.: Single-trial p300 detection with kalman ltering and svms. In: Proceedings of the European Symposium on Artificial Neural Networks, Computational Intelligence and Machine Learning, pp. 399–404 (2011)
29. Mirghasemi, H., Fazel-Rezai, R., Shamsollahi, M.B.: Analysis of p300 classifiers in brain computer interface speller. In: 28th Annual International Conference of the IEEE Engineering in Medicine and Biology Society, EMBS 2006, pp. 6205–6208. IEEE (2006)
30. Meng, H., Freeman, M., Pears, N., Bailey, C.: Real-time human action recognition on an embedded, reconfigurable video processing architecture. Journal of Real-Time Image Processing 3(3), 163–176 (2008)
31. Meng, H., Pears, N., Freeman, M., Bailey, C.: Motion history histograms for human action recognition. In: Embedded Computer Vision, pp. 139–162. Springer (2009)
32. Oostenveld, R., Praamstra, P.: The five percent electrode system for high-resolution eeg and erp measurements. Clinical Neurophysiology 112(4), 713–719 (2001)
33. Garofolo, J.S., et al.: TIMIT: acoustic-phonetic continuous speech corpus. Linguistic Data Consortium (1993)
34. Clinton, H.: Remarks on american leadership. Council on Foreign Relations (January 31, 2013)
35. Tillerson, R.: The new north american energy paradigm: Reshaping the future, Council on Foreign Relations (June 27, 2012)
36. Perelmouter, J., Birbaumer, N.: A binary spelling interface with random errors. IEEE Transactions on Rehabilitation Engineering 8(2), 227–232 (2000)

37. Johnson, R.: On the neural generators of the p300 component of the event-related potential. Psychophysiology 30(1), 90–97 (1993)
38. Polich, J.: Updating p300: an integrative theory of p3a and p3b. Clinical Neurophysiology 118(10), 2128–2148 (2007)
39. Stuermann, B.: Auto zoomcontrol-objective and subjective benefits with auto zoomcontrol. Phonak Field Study News (2011)
40. Jang, G.-J., Lee, T.-W.: A maximum likelihood approach to single-channel source separation. The Journal of Machine Learning Research 4, 1365–1392 (2003)
41. Davies, M.E., James, C.J.: Source separation using single channel ica. Signal Processing 87(8), 1819–1832 (2007)
42. Lunner, T., Neher, T.: Automatic real-time hearing aid fitting based on auditory evoked potentials. US Patent App. 13/651,032 (October 12, 2012)

Wearable Sensing for Bio-feedback in Human Robot Interaction

Yingzi Lin and David Schmidt

Intelligent Human-Machine Systems Lab
Northeastern University
Boston MA 02115, United States

Abstract. Human robot interaction is occurring more often in today's society. Robots are being developed to perform a wide variety of tasks, many of which include or even depend on HRI. The three main categories of human robot interaction are human assistance and replacement, human cooperation, and social interaction. The purpose, actions, and overall structure and dynamics of these robots will vary greatly, even within their respective categories. While the many robot designs may vary greatly, feedback is one fundamental that will always improve performance. Many designs include built-in sensors that provide feedback regarding the state of the robot and its environment, but interacting with humans presents a new challenge. Biological feedback from an interacting human can be useful for robots during human interaction. The feedback can be used to increase the effectiveness and safety of a robot's actions during interaction, which in turn will make humans more comfortable with the interaction. To achieve this, wearable sensors can be used to collect feedback. This chapter will discuss the varying types of interaction under development, and show how feedback from wearable sensors could greatly increase robot performance.

1 Introduction

Scientists have been pursuing automated machines to aid industry and manufacturing for centuries, with the first automated loom reported in the early 1800's [1]. In 1938, Devilbliss Co. introduced the first robotic arm to vehicle assembly lines, used to paint cars [2]. Today, over 700, 000 robotic arms are in use in industry. These machines all operate in a controlled environment, most commonly an assembly line. Operation in this type of environment does not require many sensors - the device has little-to no awareness of its environment. In 1948, William Grey Walter's Turtle Robots gave the world a taste of autonomous devices with environmental awareness [3]. This is the beginning of what would enable robots to leave assembly line tracks and be able to navigate the real world.

Now, companies like iRobot, Boston Dynamics, and Rethink Robotics are developing robots that can navigate a variety of environments, outdoors and indoors, without causing harm to their own form or surroundings. The robots developed can all fall under the general category of aiding in task completion, but

S.C. Mukhopadhyay (ed.), *Wearable Electronics Sensors*,
Smart Sensors, Measurement and Instrumentation 15, DOI: 10.1007/978-3-319-18191-2_14

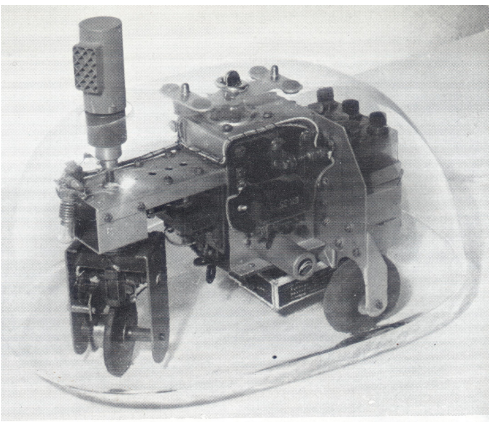

Fig. 1 William Grey Walter's Turtle Robot. One of the first autonomous robots [3]

this definition does not portray the wide variety of ways these robots will be interacting with humans. Looking at specific robot functions current research is focusing on will better express the variety of ways autonomous robots will be interacting with humans.

All HRI robots are developed to serve general purposes. Those purposes include performing repetitive tasks to replace humans, assisting humans in task performance, and socially interacting with humans. While some may do more than one of these, most robots' overall goals fall into one of these three. By looking at main goal tasks, robots can be broken down into three main categories: Human assistance and replacement, human cooperation, and social interaction. Robots within these categories can be classified into more defined subgroups based on their specific task. Human assistance/replacement robot tasks include hazardous/disaster area response and navigation, at home/elderly assistance, and rehabilitation. Human cooperation robot tasks involve working alongside humans in a busy working environment, from laboratories to hospitals. Social interaction robot tasks include entertainment, education and psychological studies. Identifying the specific tasks a robot is designed to achieve helps determine how feedback from wearable sensors can be of benefit. An overview of each category with examples for the subgroups will show how just how wearable sensors can specifically improve HRI for each category.

2 Human Assistance and Replacement

Human assistance and replacement robots are those made to replace humans performing repetitive tasks, or tasks in dangerous areas. Advancements in machine intelligence now allow robots to perform more complex tasks in the workplace that were once considered performable only by a human. While the main goal is to replace humans in task performance, not all of these robots are meant to replace

working people. A robot that can perform daily, repetitive, time consuming tasks frees the human worker to tackle more critical or complex goals, improving overall workplace efficiency. These robots will be working closely with humans on a daily basis. Information from wearable sensors could serve as an invaluable input to improve safety and productivity in a HRI workplace.

Hazardous area robots are autonomous robots designed to explore areas that would be too dangerous for humans, such as malfunctioning power plants, building failure or natural disasters. These robots have the potential to run disaster response search and rescue missions [4].

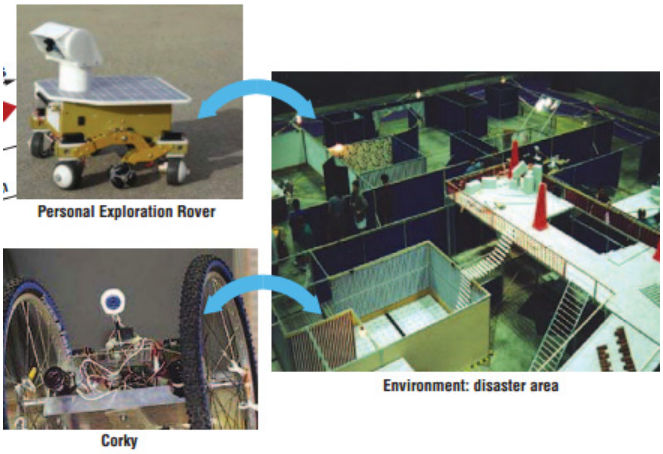

Fig. 2 Hazardous area simulation course for robot navigation [4]

If these robots will be carrying humans to safety, they will need to be able to identify humans in the environment, assess their physical condition, and handle the subject accordingly to minimize further pain or injury.

Aiding nurses in hospitals to reduce workload has been a popular subject to focus on, and for good reason. Studies have estimated that the chance of patient mortality increases by 7% for every patient added to a nurse's workload [5]. The Transition Research Corportation's HelpMate®, a hospital courier robot [6], is designed to navigate busy hospital hallways to pick up and deliver items such as meals, medications, and patient reports. Challenges in navigating busy environments include navigating around people without being distracting, and riding elevators. A series of indicator lights inform humans in the area when the robot is moving, turning, or performing a maneuver to avoid obstacles. Clara is an autonomous robot that can travel through hospital hallways, identify cardiac patients, and walk them through a spirometry exercise [7].

Fig. 3 Clara running a spirometry exercise [7]

Autonomously performing this repetitive, time consuming exercise gives nurses more time to perform more critical tasks. The task requires the robot to navigate a hospital environment, identify cardiac patients, and verbally communicate with them while monitoring the spirometer. A flow chart was designed so Clara can perform these tasks autonomously. Clara uses a camera and basic "color blob detection" to track spirometer activity during the exercise. Initial testing was performed on healthy subjects. Feedback is provided in the form of spirometer activity through visual tracking, and subjective feedback forms. From subjective feedback, most subjects had a pleasant experience working with Clara, and a majority felt she helped with the spirometry exercise.

3 Human Cooperation

Cooperation robots are very similar to assistance and replacement robots, with one key difference. They are not designed to perform a task to replace a human, but rather to aid the human with task performance. These are machines that are designed to work alongside humans to help complete a task. The most common application for cooperation robots is for assistance of the elderly and disabled, but can also include rehabilitative applications.

Elderly/Disabled assistive robots are being designed to assist humans throughout daily life in a number of ways. Some are aimed to help physically, to aid in performing day to day tasks at home, to prevent incidents and improve quality of life for the elderly living alone [8]. These autonomous robots will need to identify user intent, and decide when to intervene or assist. Information from wearable sensors could help assistance robots determine when assistance is required, either by monitoring vitals to predict health incidents, or monitoring stress/anxiety levels to determine when a subject is frustrated and could use help.

Other assistive robots are being designed to help people with disabilities. A programmable robotic arm has been tested to help people with disabled or weakened upper extremities [9]. Using a computer interface, subjects were able to program and simulate arm actions. The arm actions would pick up and manipulate objects at the desk, allowing these subjects more independence in day-to-day tasks. A mobile robot that helps the visually impaired navigate complex, indoor environments is meant to supplement a seeing-eye dog [10]. Busy environments, such as cubicle space or airports, may be too complex for a dog to learn.

Robotic Guide I (RG-I) effectively navigates an environment while safely leading a visually impaired human through it. RG-I is equipped with a Radio Frequency Identification (RFID) reader as part of the navigation system. RG-1 tracks RFID tags planted through the indoor environment in order to effectively navigate, while using a laser range finder to detect oncoming obstacles to avoid collisions.

Robotic rehabilitation devices help patients with impaired limb movement carry out the required training patterns [11]. The device provides assistance to impaired patients, ensuring the correction motion for rehabilitation training is achieved.

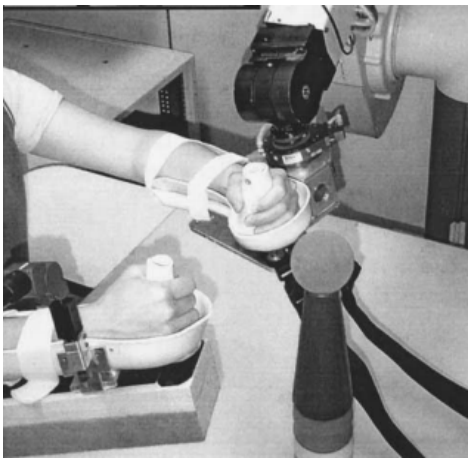

Fig. 4 Robot assisted rehabilitation exercise [11]

The device, a mirror image movement enabler (MIME), used the actions of a healthy arm to apply the right forces to the disabled arm to help perform a guided, repeated motion. Frequently performing repetitive motions such as this can improve recovery from both motor and brain injury, both of which can occur from a stroke. MIME can be used regardless of the level of impairment, making it useful during every stage of recovery. The device is meant to increase patient frequency of these exercises, to improve recovery. Assistive forces can be applied to patients recovering their range of mobility, while resistive forces can be applied to patients recovering strength. It achieves by running 4 different modes. Passive mode required the subject to relax while the robot runs the full range of movement set on its own. Active-assistive mode the patient initiates movement, and is then assisted by the robot to perform the movement set. The robot provides resistance in active-constrained mode, where the subject works against the robot forces to recover strength. The final mode is bimanual mode, where the robot reads the motion of the healthy arm, and applied the same, but mirrored motion to the injured arm. A number of redundant measures are taken to ensure patient safety. These devices receive feedback by tracking the full range of motion a patient can achieve, and how much resistance or force the patient is able to exert.

The robot was testing using patients that had decreased upper limb motor function from a single cerebrovascular accident at least six months prior, meaning they had completed outpatient therapy, but were continuing home based exercise. Subjects using the robot were tested for 2 months, and results were compared with a control group that used a physical therapist for the same number of session in a 2 month period. Improvements in function, strength, and reach were evaluated. Results evaluated by physical therapists showed that patients using MIME showed a better improvement in all aspects, making this a promising solution for at home rehabilitative exercises.

4 Social Interaction

One of the most unique and popular subjects for robot design is social interaction. While most autonomous robots are meant to interact with humans in one way or another, social interaction robots are designed specifically for that purpose. This purpose can serve a variety of means as well, other than just entertainment. Social robots can be used as tools for psychological studies, as a means for education, or to encourage a healthier lifestyle. Initially these may sound like strange objectives for a robot, and compared to the other categories, they are. Social interaction tasks present a unique challenge related to perception. A robot will be able to more effectively perform these social tasks if it is not perceived as a machine. As the following will show, the most effective social interaction robots work to be perceived not as a simple or complex machine, but as a "buddy", or a being with which people enjoy interacting.

Robots are being developed to mimic pets, as devices people can play with, watch, and even raise or train [12]. One study compared reactions to interaction with a robotic plush seal and a normal plush seal [13]. The robot seal would act and react to inputs, while the normal plush seal would not move or react at all. Physiological measurements during interaction suggest that people are more attentive when interacting with the robotic seal, and subjective questioning showed that subjects enjoyed the experience with the robotic seal more as well.

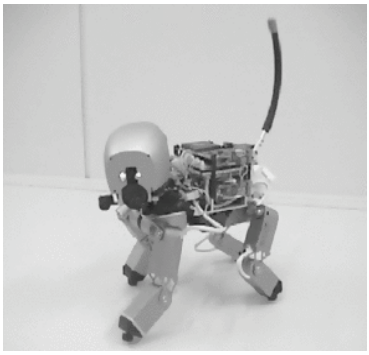

Fig. 5 MUTANT, a robotic dog for entertainment [12]

These entertainment robots are serving a practical application as well. In a world where more and more people are exposed to robots, it is hard to tell if younger children will identify these robots as living or non-living things. One study introduces young children to robots with varying degrees of performance, and then asks the children questions to see how intelligent, biological, and self motivating the children thought the robots are [14]. The three robots had the same form, but performed different actions: one would locate, approach and kick a ball, one would dance to music, and one would not do anything, just stand still. They found that a majority of tested children thought all the robots were intelligent, while only about half thought the robots were biological, or were self motivating. Very little difference in opinion was seen between the three robots.

The results from these types of studies can be used to develop social robots to aid in education. Field tests have compared robots speaking English to young Japanese students to see how much it helps the student learn the language [15]. Two humanoid robots were used over the course of two weeks to see how well interaction could help young Japanese students learn English. Essentially, they wanted to see if developing a friendly relationship with the robot would increase the amount of English learned. The robots would identify student ID tags and call them over to play speaking games in English. They found that students that continued to interact with the robots for the full two weeks had the greatest increase in English proficiency. Students that were already proficient in English tended to be the ones willing to play with the robot more, though, so they ended up benefiting more than those with a weaker understanding of the language. This suggests that through developing some sort of friendly relationship with the robot, students will be able to learn more from it, which is proof that robotic entertainment can be an important factor for education robots as well.

Other social robots have been made to explore nonverbal communication. One key example to model this after is the interaction between an infant and a caretaker. The infant cannot talk, but its emotional responses serve as cues for the caretaker to take actions for proper care. A team used this as a model to develop Kismet, a robot capable of portraying emotions through facial expressions [16].

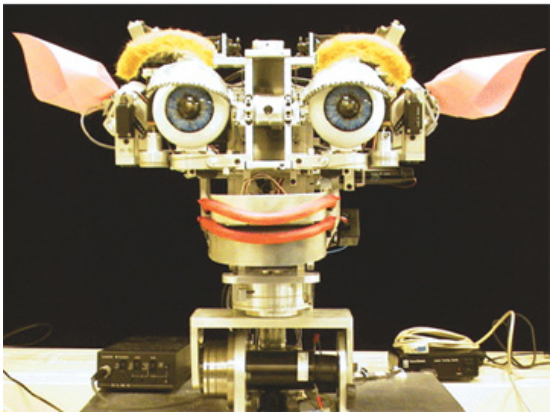

Fig. 6 Kismet, an expressive robot by MIT [16]

By defining emotional state as a collection of different systems, Kismet is able to recognize faces and expressions, and respond in a manner similar to that of an infant.

Another expressive robot is Keepon, a small robot capable of showing attention by turning and looking at faces, and expressing emotions by rocking and bobbing its body [17].

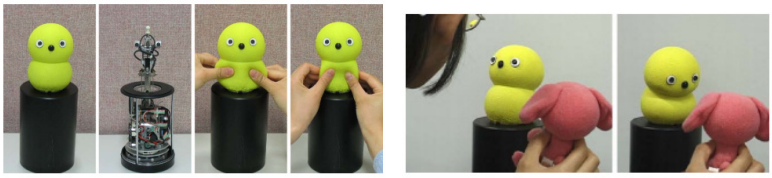

Fig. 7 Keepon, a simple robot with a soft body to engage in non-verbal social interaction [17]

During the first year of life, children develop basic capabilities for social interaction, mainly through looking at, interacting to and playing with faces of other people and toys. Toddlers with autism show a significant lack of this social activity. Keepon is capable of performing two of the main actions with toddlers; making eye contact when recognizing a face, and engaging in joint attention by looking at objects that other are looking at. Therapists can identify how toddlers pay attention to and interact with Keepon, which helps to define mental age, as well as identify potential developmental impairments. In this study, the toddler's reactions and interaction times were the relevant data collected to determine the level of attention.

As more robots are being made to work alongside humans, care must be taken to ensure the human feels safe during interaction. To analyze a subject's perception of safety, studies have measured subject measure valence/arousal of subjects as robots move autonomously [18]. The purpose of this study was to determine which robot motion would reduce anxiety during direct HRO. A robotic arm was used, and four different motions were defined by mixing two tasks with two movement plans. The tasks chosen were meant to cause direct contact with the user. The first task was to pick up a ball from the table and place it in a user's hand, and the second was to reach out, grab the ball from the user, then retract with the ball. The two paths were labelled Potential Field Planner and Safe Planner. The Potential Field Planner is a motion planning strategy that incorporates obstacle avoidance and goal attraction, based on a control scheme conceived in the 80's [19]. The Potential Field Planner pre-plans the course movement objective beforehand, and plans the details within these course objectives in real time in order to avoid obstacles. Maximum velocities are dictated by the distance between the center of mass of the arm joints and an obstacle or the goal. The safe planner is simply the Potential Field Planner with an extra strategy known as the Danger Criterion. The Danger Criterion is a feature that attempts to minimize the force of human-robot impact by dictating the inertia of the arm as a function of the distance between the center of mass of the arm joints and an obstacle [20].

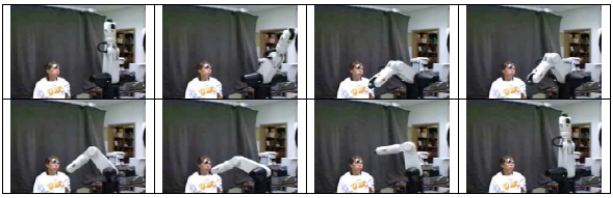

Fig. 8 Kulic and Croft's Robotic Arm Anxiety Test setup [18]

The two paths and two movement plans combine to make four Test Paths. Each Test Path was run at three different speeds; 10%, 50% and 100% of max joint velocity (3.14rad/s). This gives 12 different robot arm trajectories. Subjective and physiological data was collected. Subjective data included reporting levels of anxiety, calm, surprise, and arousal, while physiological responses were collected by measuring corrugators muscle activity, skin conductance, and heart rate. Subjective results showed that the Safe Planner induced slightly calmer reactions compared to the Potential Field planner, but slower movement speeds reduced anxiety levels significantly more. Physiological measurements determined that anxiety levels, determined from skin conductance and heart rate, were lower with slower movement speed.

A frequency domain analysis of subject heart rate data was used to determine subject anxiety levels during testing. While the subject was safe during every test run, different movement types would elicit varying levels of arousal in subjects. This type of research can be used to determine what movement types humans are most comfortable with for an optimally safe and productive workplace.

5 Discussion

Great advancements are being made in developing robots that can affectively tackle many different jobs that require HRI. It is exciting to see how much work has been done to prove that these robots can indeed perform the tasks they were developed for. These conclusions were made by observing that the robot had completed its task, or from post trial information that reported positive results. While this is helpful feedback, it is only the minimal amount needed to prove the robot has served a significant function. The health service robot, Clara, uses spyrometer tracking as the only means to monitor performance. While it can track that the exercise is running, how many breaths the patient takes, and how deep the breaths are, it cannot effectively track how much effort or strain the patient is experiencing. Also, the subjective forms listed a series of questions with possible responses being "A lot", "Somewhat", and "No". "Somewhat" is not a completely neutral response, making it easier to report a majority of positive responses from the feedback. Similarly, MIME can perform a veriety of exercises through providing either aid or resistance, but it is up to the patient to choose one of the four settings to run. This is not something the robot can track or suggest, but rather

a decision the patient needs to make. More feedback from patients can help these machines take the next step in performance. This is the type of feedback that can come from wearable sensors.

Effectively using physiological data from patients can increase robot performance from generally functional to equally effective for all subjects. During disaster response, wearable sensors would make human subjects and their vital signs easier to identify, which could save precious seconds during rescue. Hospital patients wearing physiological sensors could provide more relevant data in real time to autonomous hospital agents like Clara. This information can be used both as a measure of effort during the exercise, as well as data to supplement subjective responses during post analysis. Measuring effort during spirometry can ensure that all patients, regardless of strength, are exerting enough effort without over straining themselves, to insure testing is both rigorous and safe. Physiological data that supplements subjective data would make the reported results more believable as well.

Navigation robots like RG-1 may not need physiological sensors, subjects wearing RFID tags could help RG-1 keep track of who they are escorting, pausing if a person falls out or range, or giving verbal warnings if they stray the wrong way. Rehabilitative robot MIME could use physiological sensors to track temperature, heart rate, and muscle activity to combine two of its modes into one. By looking at muscle activity, body temperature, and heart rate, the level of effort the patient is exerting could be monitored. Combining this with the position and force data that MIME already collects, and the machine could be able to decide the level of assistance or resistance the patient can handle. Normally these are two separate modes, active-assisted and active-constrained, that the patient chooses from. Using position, force, and effort monitoring to determine between assistance or resistance, as well as the magnitude of either, could enable MIME to make better decisions that the patient can. This could result in a more rigorous workout without over straining the subject, which will lead to a healthier recovery.

In the toddler study, the reactions and interaction times with Keepon were the only relevant data collected. Physiological data from wearable sensors could provide insight onto whether reactions are positive or negative in a similar study could help determine whether toddlers found the interaction entertaining or stressful. Combined with the existing information, this could provide a more in-depth analysis for study.

These are only a few examples of how information from wearable sensors can be used to improve HRI quality. Work integrating feedback from wearable sensors with autonomous robots involved in HRI can create a more effective, personalized experience.

6 Conclusion

Robots are leaving the assembly line and are beginning to work in more complex environments. Through replacement of tasks, aide with performance and exercise,

and performing social tasks, robots are interacting with humans in a wide variety of ways. Currently, many reports state key factors that prove that interaction is successful, and that robots are performing these tasks effectively. While this is a great feat, an enhanced awareness of human state during interaction has the potential to vastly improve interaction and robot performance.

After observing recent developments in autonomous robots and human interaction, it is clear that human location and physiological data can provide essential feedback for robot interaction. Wearable sensors can provide a variety of relevant information, from location and activity tracking to monitoring physical and mental health. This information can be used in real time to help robots make more educated decisions during interaction, or stored for post analysis by developers or doctors. Because of the vast differences among people, interacting with humans is a much more dynamic task than assembling a can. Wearable sensors can be used to create a more personalized, efficiency means of human robot interaction, whether it be in the lab, at the workplace, or at home.

Acknowledgements. This work has been supported by the U.S. National Science Foundation (NSF) through the grant No. 1333524.

References

[1] Jacquard, J.M.: Newton's London Journal of Arts and Sciences (1866)
[2] Polard Jr., W.L.G.: Patent: 2213108. - United States (1940)
[3] Holland, O.: Exploration and high adventure: the legacy of Grey Walter. Philosophical Transactions of the Royal Society A, 2085–2121 (2003)
[4] Nourbakhsh, I., Sycara, K., Koes, M., Yong, M., Lewis, M., Burion, S.: Human-Robot Teaming for Search and Rescue. IEEE Pervasive Computing 4, 72–78 (2005)
[5] Aiken, L.H., Clarke, S.P., Sloane, D.M., Sochalski, J., Silber, J.H.: Hospital Nurse Staffing and Patient Mortality, Nurse Burnout, and Job Dissatisfaction. The Journal of the American Medical Association 288(16), 1987–1993 (2002)
[6] Krishnamurthy, B., Evans, J.: HelpMate(R): A Robotic Courier for Hospital Use. Autonomous Robotic Systems, 182–210, ISBN 978-1-85233-036-1998
[7] Kang, K., Freedmand, S., Mataric, M., Cunningham, M., Lopez, B.: A Hands-Off Physical Therapy Assistance Robot for Cardiac Patients. In: 9th International Conference Proceeding on Rehabilitation Robotics, Chicago IL, pp. 337–340 (2005) ISBN 0-7803-9003-2
[8] Forlizzi, J., DiSlavo, C., Gemperle, P.: Assistive Robotics and an Ecology of Elders Living Independantly in Their Homes. Human Computer Interaction 19, 25–29 (2004)
[9] Wagner, J., Wickizer, M., Michiel Van der Loos, H., Liefer, L.: User Testing and Design Iteration of the Provar User Interface. In: IEEE International Workshop on Robotic and Human Interaction, Pisa, Italy, pp. 18–22 (1999) ISBN 0-7803-5841-4
[10] Kulyukin, V., Gharpure, C., Nicholson, J., Osborne, G.: Robot-Assisted Wayfinding for the Visually Impared in Structured Indoor Environments. Auton. Robot. 21, 29–41 (2006)

[11] Lum, P., Burgar, C., Shor, P., Majmundar, M., Van der Loos, M.: Robot-Assisted Movement Training Compared with Conventional Therapy Techniques for the Rehabilitation of Upper-Limb Motor Function After Stroke. Archives of Physical Medicine and Rehabilitation 83, 952–959 (2002)
[12] Jujita, M., Kitano, M.: Development of an Autonomous Quadruped Robot for Robot Entertainment. Autonomous Robots 5, 7–18 (1998)
[13] Mitsui, T., Shibata, T., Wada, K., Touda, A., Tanie, K.: Psychophysiological Effects by Interaction with Mental Commit Robot. In: International Conference on Intelligent Robots and Systems, Maui Hawaii, vol. 3, pp. 1189–1194 (2001) ISBN 0-7803-6612-3
[14] Okita, K., Schwartz, D.: Young Children's Understanding of Animacy and Entertainment Robots. Humanoid Robotics 3, 393–412 (2006)
[15] Kanda, T., Hirano, T., Eaton, D., Ishiguro, H.: Interactive Robots as Social Partners and Peer Tutors for Children: A Field Trial. Human-Computer Interaction 19, 61–84 (2004)
[16] Breazeal, C., Scassellati, B.: Infant-Like Social Interacions Between a Robot and a Human Caretaker. Adaptive Behavior 8, 49–74 (2000)
[17] Kozima, H., Michalowski, M., Nakagawa, C.: Keepon: A Playful Robot for Research, Therapy, and Entertainment. International Journal of Social Robots 1, 3–18 (2009)
[18] Kulic, D., Croft, E.: Anxiety Detection during Human-Robot Interaction. In: International Conference on Intelligent Robotics and Systems, pp. 616–621 (2005) ISBN 0-7803-8912-3
[19] Khatib, O.: Real-Time Obstacle Avoidance for Manipulators and Mobile Robots. International Journal of Robotics Research 5, 90–98 (1986)
[20] Kulic, D., Croft, E.: Safe Planning for Human-Robot Interaction. In: International Conference on Robotics & Automation, New Orleans LA, pp. 1882–1887 (2004) ISBN 0-7803-8232-3

Author Index